Lightweight Concrete: Development of Mild Steel in Tension

January 2014

NTIS Accession No. PB2014-100627

FHWA Publication No. FHWA-HRT-14-029

U.S. Department of Transportation
Federal Highway Administration

FOREWORD

Broad-based advancements in the field of concrete materials have led to significant enhancements in the performance of lightweight concrete. Although the value of using lightweight concrete within the constructed infrastructure is clear, decades-old performance perceptions continue to raise barriers that hinder wider use of the concrete. Additionally, the lack of modern updates to structural design provisions for lightweight concrete has perpetuated additional barriers to the use of lightweight concrete. In 2007, the Federal Highway Administration (FHWA) embarked on a research program investigating the structural performance of modern lightweight concretes. This effort engaged the academic, public sector, and private sector communities to compile the body of knowledge on lightweight concrete while also conducting nearly 100 full-scale structural tests on lightweight concretes.

The American Association of State Highway and Transportation Officials (AASHTO) Subcommittee on Bridges and Structures (SCOBS) Technical Committee 10 (T-10) has expressed interest in updating the AASHTO Load and Resistance Factor Design (LRFD) Bridge Design Specifications to more accurately and consistently reflect the performance of lightweight concrete. FHWA researchers were engaged to compile the overall body of knowledge on this topic then to report back to T-10 with proposals for addressing perceived shortcomings in the current design specifications.

This report presents the results of tests on high-strength LWC splice beams as well as a compilation of data available from the literature. It develops potential revisions to the bridge design specifications, with a focus on the development length of mild steel reinforcement.

This report corresponds to the TechBrief titled "Lightweight Concrete: Development of Mild Steel in Tension" (FHWA-HRT-14-030). This report is being distributed through the National Technical Information Service for informational purposes. The content in this report is being distributed "as is" and may contain editorial or grammatical errors.

TECHNICAL REPORT DOCUMENTATION PAGE

1. Report No. FHWA-HRT-14-029	2. Government Accession No. NTIS PB2014-100627	3. Recipient's Catalog No.
4. Title and Subtitle Lightweight Concrete: Development of Mild Steel in Tension		5. Report Date January 2014
		6. Performing Organization Code:
7. Author(s) Gary G. Greene and Benjamin A. Graybeal		8. Performing Organization Report No.
9. Performing Organization Name and Address Office of Infrastructure Research & Development Federal Highway Administration 6300 Georgetown Pike McLean, VA 22101-2296		10. Work Unit No.
		11. Contract or Grant No.
12. Sponsoring Agency Name and Address Office of Infrastructure Research & Development Federal Highway Administration 6300 Georgetown Pike McLean, VA 22101-2296		13. Type of Report and Period Covered Final Report: 2010-2013
		14. Sponsoring Agency Code HRDI-40
15. Supplementary Notes This document was developed by research staff at the Turner-Fairbank Highway Research Center. Portions of the work were completed by PSI, Inc. under contract DTFH61-10-D-00017. Gary Greene of PSI, Inc. and Trine University, who is the lead contract researcher on FHWA's lightweight concrete research efforts, and Ben Graybeal of FHWA, who manages the FHWA Structural Concrete Research Program, developed this document.		

16. Abstract
Much of the fundamental basis for the current lightweight concrete provisions in the AASHTO LRFD Bridge Design Specifications is based on research of lightweight concrete (LWC) from the 1960s. The LWC that was part of this research used traditional mixes of coarse aggregate, fine aggregate, portland cement, and water. Broad-based advancement in concrete technology over the past 50 years has given rise to significant advancements in concrete mechanical and durability performance.

This document describes the results of tests on high-strength LWC splice beams that were conducted as part of an overall FHWA research project on LWC. The FHWA test results are included in a database of bond tests with over 200 tests on LWC specimens available in the literature. An analysis of the database was used to develop potential revisions to provisions related to LWC within Chapter 5 of the AASHTO LRFD Specifications. The framework for addressing LWC in the specifications that was proposed previously as a part of this research effort is applied to the design expression for development length of mild steel. The framework includes a proposed revision to the definition of LWC and a proposed modification factor relevant to LWC structural performance.

17. Key Words LWC, lightweight concrete, bridge design, LRFD design specifications, development length, splice length, bond strength	18. Distribution Statement No restrictions. This document is available through the National Technical Information Service, Springfield, VA 22161.		
19. Security Classif. (of this report) Unclassified	20. Security Classif. (of this page) Unclassified	21. No. of Pages 331	22. Price N/A

Form DOT F 1700.7 (8-72) Reproduction of completed page authorized

SI* (MODERN METRIC) CONVERSION FACTORS

APPROXIMATE CONVERSIONS TO SI UNITS

Symbol	When You Know	Multiply By	To Find	Symbol
LENGTH				
in	inches	25.4	millimeters	mm
ft	feet	0.305	meters	m
yd	yards	0.914	meters	m
mi	miles	1.61	kilometers	km
AREA				
in^2	square inches	645.2	square millimeters	mm^2
ft^2	square feet	0.093	square meters	m^2
yd^2	square yard	0.836	square meters	m^2
ac	acres	0.405	hectares	ha
mi^2	square miles	2.59	square kilometers	km^2
VOLUME				
fl oz	fluid ounces	29.57	milliliters	mL
gal	gallons	3.785	liters	L
ft^3	cubic feet	0.028	cubic meters	m^3
yd^3	cubic yards	0.765	cubic meters	m^3
NOTE: volumes greater than 1000 L shall be shown in m^3				
MASS				
oz	ounces	28.35	grams	g
lb	pounds	0.454	kilograms	kg
T	short tons (2000 lb)	0.907	megagrams (or "metric ton")	Mg (or "t")
TEMPERATURE (exact degrees)				
^{o}F	Fahrenheit	5 (F-32)/9 or (F-32)/1.8	Celsius	^{o}C
ILLUMINATION				
fc	foot-candles	10.76	lux	lx
fl	foot-Lamberts	3.426	candela/m^2	cd/m^2
FORCE and PRESSURE or STRESS				
lbf	poundforce	4.45	newtons	N
lbf/in^2	poundforce per square inch	6.89	kilopascals	kPa

APPROXIMATE CONVERSIONS FROM SI UNITS

Symbol	When You Know	Multiply By	To Find	Symbol
LENGTH				
mm	millimeters	0.039	inches	in
m	meters	3.28	feet	ft
m	meters	1.09	yards	yd
km	kilometers	0.621	miles	mi
AREA				
mm^2	square millimeters	0.0016	square inches	in^2
m^2	square meters	10.764	square feet	ft^2
m^2	square meters	1.195	square yards	yd^2
ha	hectares	2.47	acres	ac
km^2	square kilometers	0.386	square miles	mi^2
VOLUME				
mL	milliliters	0.034	fluid ounces	fl oz
L	liters	0.264	gallons	gal
m^3	cubic meters	35.314	cubic feet	ft^3
m^3	cubic meters	1.307	cubic yards	yd^3
MASS				
g	grams	0.035	ounces	oz
kg	kilograms	2.202	pounds	lb
Mg (or "t")	megagrams (or "metric ton")	1.103	short tons (2000 lb)	T
TEMPERATURE (exact degrees)				
^{o}C	Celsius	1.8C+32	Fahrenheit	^{o}F
ILLUMINATION				
lx	lux	0.0929	foot-candles	fc
cd/m^2	candela/m^2	0.2919	foot-Lamberts	fl
FORCE and PRESSURE or STRESS				
N	newtons	0.225	poundforce	lbf
kPa	kilopascals	0.145	poundforce per square inch	lbf/in^2

*SI is the symbol for the International System of Units. Appropriate rounding should be made to comply with Section 4 of ASTM E380.
(Revised March 2003)

TABLE OF CONTENTS

LIST OF FIGURES

LIST OF TABLES

LIST OF ABBREVIATIONS AND NOTATION

ABBREVIATIONS

AASHTO   American Association of State Highway and Transportation Officials

COV   coefficient of variation

FHWA   Federal Highway Administration

LRFD   load-and-resistance factor design, the design philosophy used by current AASHTO bridge design specification

LVDT   linear variable differential transformer

LWC   lightweight concrete

NCHRP   National Cooperative Highway Research Program

NWC   normal weight concrete

RC   reinforced concrete

SCOBS   Subcommittee on Bridges and Structures, a part of the overall AASHTO organizational structure

SCP   Standard Concrete Products

SDC   specified density concrete

T-10   Concrete Design technical committee in SCOBS

TFHRC   Turner-Fairbank Highway Research Center

NOTATION

A_b = area of an individual bar being developed or spliced

A_s = total area of longitudinal tension reinforcement

A_{sp} = total area of transverse reinforcement provided within the splice length

A_{sr} = 60% of the total area of spliced bars

A_{tr} = total cross-sectional area of all transverse reinforcement within spacing (s) that crosses the potential plane of splitting through the reinforcement being developed

b = width of the compression face of a rectangular member

c_b = smaller of the distance from center of a bar to nearest concrete surface and on-half the center-to-center spacing of bars being developed

c_c = bottom concrete cover for reinforcing bar being developed

c_{max} = larger of c_c and c_s

c_{min} = smaller of c_c and c_s

c_{minOJB} = smaller of c_c , c_{so}, and c_{si}

c_s = smaller of c_{so} and c_{si} + 0.25 inch

c_{si} = one-half of the bar clear spacing

c_{so} = side concrete cover for reinforcing bar

d = distance from compression face to centroid of tension reinforcement

d_b = nominal bar diameter

f_c = concrete compressive stress

f'_c = concrete compressive strength in reference to material tests values and specified compressive strength in reference to articles of the AASHTO LRFD Specification

f_{ct} = concrete splitting tensile strength

f_s = stress in developed or spliced reinforcing bar at failure

f_y = yield strength of reinforcing bars in reference to material tests values and specified minimum yield strength in reference to articles of the AASHTO LRFD Specification

f_{yt} = yield strength of transverse reinforcement

h = member height

h_r = average height of deformations on reinforcing

K_{tr} = transverse reinforcement index

$K_{tr,ACI408}$ = transverse reinforcement index defined in ACI 408-03 document

ℓ_d = development length

ℓ_{db} = basic development length for straight reinforcement to which modification factors are applied to determine the development length

ℓ_s = lap splice length

$L_{inside\ ribs}$ = inside-to-inside distance across two ribs approximately 6 inches apart, measured at the barrel of the bar

$L_{outside\ ribs}$ = outside-to-outside distance across two ribs approximately 6 inches apart, measured at the barrel of the bar

n = number of bars being developed or spliced

n_{ribs} = number of spaces between the two ribs used for determining $L_{inside\ ribs}$ and $L_{outside\ ribs}$

N = number of transverse stirrups within the development or splice length

p = nominal perimeter of a bar

R_r = relative rib area of the reinforcement

s = spacing of the transverse reinforcement

s_r = average spacing of deformations on reinforcing bar

t_d = term representing the effect of bar size on T_s

t_r = term representing the effect of relative rib area on T_s

T_b = total bond force of a developed or spliced bar

T_c = bond force of a bar not confined by transverse reinforcement

T_s = bond force of a bar attributed to the confinement provided by the transverse reinforcement

u_b = total bond strength of a bar confined by transverse reinforcement

u_c = average bond strength at failure of a bar not confined by transverse reinforcement

u_s = bond strength of a bar attributed to the confinement provided by the transverse reinforcement

α = factor used to modify development length based on reinforcement location (ACI 408-03)

β = factor used to modify development length based on reinforcement coating (ACI 408-03)

Δf_s = difference between the f_s in a specimen with stirrups and a companion specimen without stirrups

Δ_u = beam displacement at ultimate

Δ_y = beam displacement at yielding

ε_c = concrete compressive strain

ε_o = concrete strain at maximum concrete stress under uniaxial compression

λ = lightweight concrete modification factor

λ_{ACI} = factor used to modify development length based on lightweight concrete (ACI 318-11)

λ_{ACI408} = factor used to modify development length based on lightweight concrete (ACI 408-03)

μ_{target} = target displacement ductility

ϕ = resistance factor

$\Sigma gaps$ = sum of the gaps between ends of transverse deformations on reinforcing bar

Ψ_e, Ψ_s, Ψ_t = factors used to modify development length based on reinforcement coating, reinforcement size, and reinforcement location, respectively (ACI 318-11)

ω = term representing the effect of the ratio of c_{max} to c_{min} on ℓ_d

CHAPTER 1. INTRODUCTION

INTRODUCTION

Much of the fundamental basis for the current lightweight concrete provisions in the AASHTO LRFD Bridge Design Specifications (1) is based on research of lightweight concrete (LWC) from the 1960s.[2-5] The LWC that was part of this research used traditional mixes of coarse aggregate, fine aggregate, portland cement, and water. Broad-based advancement in concrete technology over the past 50 years has given rise to significant advancements in concrete mechanical and durability performance. Research during the past 30 years including the recent NCHRP studies on different aspects of high-strength concrete has resulted in revisions to the AASHTO LRFD Specifications to capitalize on the benefits of high-strength normal weight concrete (NWC). However, as described by Russell (6), many of the design equations in the AASHTO LRFD Specifications are based on data that do not include tests of LWC specimens, particularly with regard to structural members with compressive strengths in excess of 6 ksi (41 MPa).

The Federal Highway Administration (FHWA) at the Turner-Fairbank Highway Research Center (TFHRC) has executed a research program investigating the performance of LWC with concrete compressive strengths in the range of 6 to 10 ksi (41 to 69 MPa) and equilibrium densities between 0.125 kcf to 0.135 kcf (2000 to 2160 kg/m^3). The research program used LWC with three different lightweight aggregates that are intended to be representative of those available in North America. The program included tests from 27 precast/prestressed LWC girders to investigate topics including transfer length and development length of prestressing strand, the time-dependent prestress losses, and shear strength of LWC. The development and splice length of mild steel reinforcement used in girders and decks made with LWC was also investigated using 40 reinforced concrete (RC) beams. While much of the research program focused on structural behavior, it also included a material characterization component wherein the compressive strength, elastic modulus, and splitting tensile strength of the concrete mixes used in the structural testing program were assessed. One key outcome of the research program is to recommend changes to the AASHTO LRFD Bridge Design Specifications relevant to LWC.

This document describes the results of tests on 40 RC splice beams used to evaluate the bond performance of high-strength LWC. The LWC splice beams tested in this study are included in a database of bond tests on LWC and NWC specimens that was collected from test results available in the literature. This document describes the database and the analysis of the database. Design expressions in the current edition of the AASHTO LRFD Specifications are compared to the database. Potential revisions to the AASHTO LRFD Specifications relating to LWC are presented.

OBJECTIVE

There are three objectives for this document. The first objective is to describe the results of 40 tests on LWC splice beams conducted at TFHRC. The second objective is to describe a database including the TFHRC test results and to describe the analysis of the database. The third objective is to develop and present potential revisions to the AASHTO LRFD Specifications relating to the development length of mild steel reinforcement, with a focus on the performance of LWC.

OUTLINE OF DOCUMENT

Introductory material in Chapter 2 summarizes the properties of LWC, the treatment of LWC in the AASHTO LRFD Specifications, the factors affecting the bond strength of mild steel reinforcement, and the design expressions for bond strength in the AASHTO LRFD Specifications. Chapter 3 describes the LWC splice beam tests, summarizes the test results, and provides a discussion of the results. A description of the bond strength database is given in Chapter 4 and includes statistical information about the database. Chapter 5 includes an analysis of the database and comparisons of the bond strength predicted by design expressions to the bond strength determined from the tests in the database. Potential revisions to the AASHTO LRFD Specifications are included in Chapter 6. References to the paper and reports used in the bond strength database are included in Chapter 8.

The units for stress and elastic modulus are ksi and the units for unit weight are kcf for all expressions unless stated otherwise. SI units are given in parentheses for values in the text and conversion factors are provided for values in the tables.

SUMMARY OF PRELIMINARY RECOMMENDATIONS

One revision to the AASHTO LRFD Specifications is proposed in this document. This revision is related to the development length of mild steel in tension. The revision is based on the recommendations made in a previous document that is a part of this research effort.[7] The previous recommendations relate to the definition of LWC and a modification factor for LWC. The definition of LWC was proposed to include concrete with lightweight aggregates up to a unit weight of 0.135 kcf (2160 kg/m^3), which is considered the lower limit for NWC. Also the terms "sand-lightweight concrete" and "all-lightweight concrete" were removed in the proposed definition to allow other types of LWC mixtures. A LWC modification factor was proposed to potentially allow a more unified approach of accounting for the mechanical properties of LWC in the AASHTO LRFD Specifications. The proposed LWC modification factor is included in the proposed expressions for development length of mild steel. The development of the proposed revision is described in Chapter 5 and is summarized with proposed code language in Chapter 6.

CHAPTER 2. BACKGROUND

INTRODUCTION

This chapter provides background information relevant to the focus of the research effort. This information begins with a description of the mechanical properties of LWC, the gap of equilibrium densities on the AASHTO LRFD Specifications, and the LWC modification factor. The rest of the chapter covers the bond strength of mild steel reinforcement. The information on bond strength includes factors that affect bond strength, test specimens for determining bond strength, and both descriptive and design expressions for bond strength.

MECHANICAL PROPERTIES OF LWC

The aggregate in LWC can either be manufactured or natural, with a cellular pore system providing for a lower density particle. The density of lightweight aggregate is approximately half of that of normal weight rock. The reduced dead weight of the LWC has many benefits in building and bridge construction such as smaller, lighter members, longer spans, and reduced substructures and foundations requirements.[8]

As compared to NWC, LWC tends to exhibit a reduction in tensile strength. This difference is generally attributed to the characteristics of the lightweight aggregate. The performance of concrete structures is affected by the tensile strength of concrete in several significant ways. The reduced tensile strength of LWC can affect the shear strength, cracking strength at the release of prestress, and bond strength of prestressed and non-prestressed reinforcement.[8]

EQUILIBRIUM DENSITY GAP IN AASHTO LRFD

The definition for LWC in the AASHTO LRFD specifications (1) covers concrete having lightweight aggregate and an air-dry unit weight less than or equal to 0.120 kcf (1920 kg/m^3). Normal weight concrete is defined as having a unit weight from 0.135 to 0.155 kcf (2160 to 2480 kg/m^3). Concretes in the gap of densities between 0.120 and 0.135 kcf (1920 to 2160 kg/m^3) are commonly referred to as "specified density concrete" and are not directly addressed by the AASHTO LRFD Specifications. Specified density concrete (SDC) typically contains a mixture of normal weight and lightweight coarse aggregate.

Modifications to AASHTO LRFD are needed to remove the SDC-related ambiguity, to give the designer the freedom of specifying a slightly lower density than NWC, and to allow for appropriate design with SDC. The inclusion of SDC into AASHTO LRFD could take many forms, but would likely require modifications to both terminology and design expressions.

FACTOR FOR LWC TENSILE STRENGTH

The tendency for LWC to have a reduced tensile strength is not treated consistently in the AASHTO LRFD Specifications. There are many articles where the $\sqrt{f_c'}$ term is used to represent concrete tensile strength. The provisions for shear and tension development length of mild reinforcement currently include a modification for LWC. However, the tensile stress limits in prestressed concrete do not include a modification for LWC. A potential option to provide a more uniform treatment of LWC tensile strength would be to add the definition of a modification factor for LWC, such as λ, to Section 5.4 which could then be referenced in other articles. Then the factor could be added to design expressions where the $\sqrt{f_c'}$ term is used to represent concrete tensile strength.

BOND STRENGTH

This section describes factors affecting the bond strength of straight, uncoated deformed reinforcing bars in tension. The bond strength is the maximum force that is sustained by a bar. The splice strength is the bond strength of bars that are spliced, whereas the development length is the bond strength of bars that are not spliced.[9]

There are several key parameters that affect bond resistance: i) the tensile and bearing strength of the concrete; ii) the volume of concrete surrounding the bar; iii) the geometry and surface condition of the bar; and iv) the presence of transverse reinforcement.[9]

Transfer of forces from the reinforcement to the surrounding concrete occurs by chemical adhesion between bar and the concrete, friction between the bar and surrounding concrete due to the roughness of the bar, and bearing of the reinforcement ribs against the surrounding concrete. Once a bar moves with respect to the surrounding concrete, adhesion no longer contributes to the bond strength. The relative motion engages frictional resistance between the concrete and the deformations and between the concrete and the barrel of the bar. The relative motion also engages bearing resistance between the concrete and the deformations. Additional slip reduces the contribution of friction. This leaves the action of the ribs bearing against the concrete as the principal mechanism of force transfer and results in tensile stresses in the concrete and eventually radial cracking around the bar. These radial cracks can become splitting cracks if the cover is thin or the bars are closely spaced. Transverse reinforcement can delay and control crack propagation. If the cover thickness and bar spacing is sufficient, or transverse reinforcement delays a potential splitting failure, then a pullout failure can occur where the concrete shears around the bar at the edge of the bar deformations. Concrete crushing can also occur at some of the bar deformations.[9]

Bond forces occur as a result of a difference in tensile force between two sections of a member. In an uncracked flexural member, the difference in tensile force is the result of shear on the section. The actual bond stresses in a bar are also affected by flexural cracks. At the crack, the bond stresses will be zero, while the bar stress will be at a local peak. The bond stress adjacent

to the crack is high as the tensile force from the bar is transferred into the concrete. Midway between two flexural cracks in a member under uniform bending moment, the bar stresses are much lower than at a crack and the bond stresses are near zero. See Figure 1 for an illustration of bond stresses in a member under pure bending.[10]
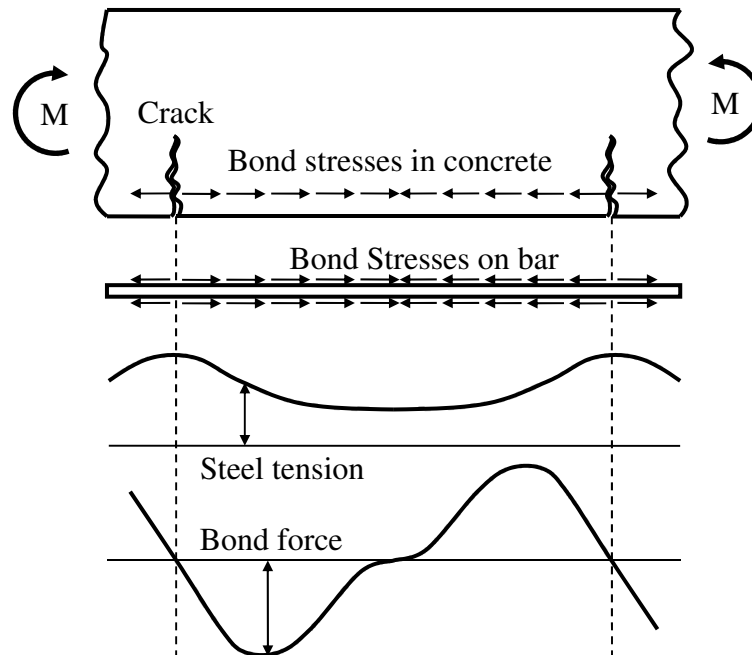
Figure 1. Illustration. Variation of Steel Stress and Bond Stress in a Member under Pure Bending (adapted from Nilson et al. (10)).

TEST SPECIMENS

The type of specimen used to measure bond strength affects the behavior of the bond response and the bond strength. The pullout specimen is small and the simplest to construct and test. As the bar is placed in tension, the concrete is placed in compression. This results in unrealistic flow of stresses in the specimen because in most reinforced concrete members, tension in the bar results in tension in the surrounding concrete. The beam end specimen provides a more realistic state of stress and is relatively simple to test. Splice specimens are larger scale, achieve a realistic stress-state in the splice, and can directly measure splice strength. Most of the data used to establish the ACI design code provisions are based on tests of splice specimens.[9] Figure 2 shows pullout, beam-end, and splice specimens.

Some less commonly used specimens are shown in Figure 3. These include specimens termed "development beams" and "tensions prisms". Development beams are equivalent to two beam-end specimens placed back-to-back. The reinforcement is shielded from the confining effects of the support reaction through the use of a bond breaker along the bar in the region of the support. Tension prisms are small specimens with tension applied to one discontinuous central bar that

makes non-contact lap splices with four perimeter bars, one in each corner of the specimen's square cross section.
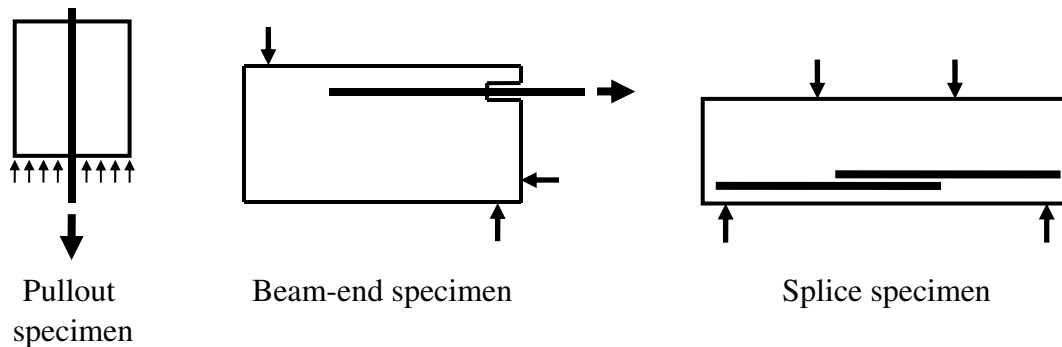
Figure 2. Illustration. Commonly used Bond Test Specimens (adapted from ACI 408-03 (9)).
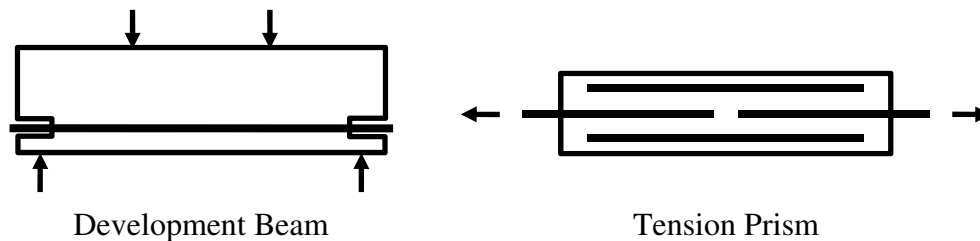
Figure 3. Illustration. Less commonly used Bond Test Specimens.

FACTORS AFFECTING BOND STRENGTH

The following section presents a summary of the factors affecting the bond strength of mild steel reinforcement in concrete with a compressive strength less than approximately 10 ksi (69 MPa). More detailed information can be found in ACI 408-03 (9). Research has shown that for compressive strengths above 10 ksi (69 MPa), the bond behavior can be different than normal strength concrete and these differences will be addressed in a separate section.

CONCRETE COVER AND BAR SPACING

Bars with thicker cover and larger bar spacing have greater bond strength. Bars with smaller cover and smaller bar spacing are likely to have a splitting failure. If the cover and bar spacing is large enough, a pullout failure can occur. The location of the splitting cracks depends on the relative thickness of the concrete cover to the tension face (c_c), the side concrete cover (c_{so}), and the distance between bars ($2c_{si}$). When c_c is less than c_{si} or c_{so}, the splitting crack forms between the bar and the tension face; however, when c_c is greater, then the splitting crack forms along the plane of the bars and through the side cover. An illustration of the terms c_c, c_{so}, and c_{si} is shown in Figure 4.

Typical Cross Section
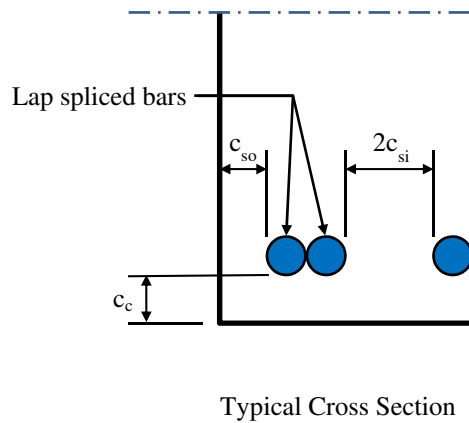
Figure 4. Illustration. Definition of Terms for Concrete Cover and Distance between Bars.

SPLICE LENGTH

Increasing the length of the splice will increase the bond strength. The relationship between bond strength and splice length is linear, however it is not proportional.[9,11,12] For example, a short splice length (i.e., near zero length) will still have some amount of bond strength because of the bearing resistance developed at each bar deformation. Doubling the splice length will cause an increase in the bond strength, but the increase will be less than twice that of the shorter splice length. This is due to the bond forces being non-uniform and bond failures being incremental. Bond stresses are also higher at the loaded end than at the non-loaded end. Bond failures are incremental because splitting cracks form at the ends of the splice where bar stresses are higher, then move toward the middle of the splice. Common relationships for design are based on bond strength being proportional to splice length. This approach tends to be conservative for short splice lengths, but unconservative for splices with longer lengths.

TRANSVERSE REINFORCEMENT

Transverse reinforcement increases the bond strength by limiting the progression of splitting cracks.[13] Increasing the amount of transverse reinforcement increases the bond strength by providing more confinement. Adding transverse reinforcement increases the bond strength until there is adequate reinforcement to cause pullout failure instead of a splitting tensile failure. Previous research has shown that confining reinforcement rarely yields.[9]

BAR SIZE

Larger bars achieve higher bond forces than smaller bars for a given bonded length. But because of their large area, they require longer bonded lengths to develop the same stress as a smaller bar. Larger bars also cause more strain in transverse reinforcement. Larger strains result in more confining force meaning that the bond strength added by transverse reinforcement increases with the size of the developed bar.[9]

7

LWC

The bond strength of concrete is dependent on its tensile strength. As LWC can have a lower tensile strength than NWC with the same compressive strength, then it follows that LWC can also exhibit lower bond strength than NWC. The AASHTO LRFD Specifications recognize this by specifying a modification factor for bond strength of LWC that is dependent on the average splitting tensile strength. In general, there is a lack of experimental data on the bond strength of LWC. Also, nearly all of the data on LWC is from pullout tests. The results of the bond tests have shown that LWC can have a bond strength that is between 65% and 100% of bond strength of NWC.[9]

CONCRETE COMPRESSIVE STRENGTH

As concrete compressive strength increases, bearing strength values increase proportionally faster than tensile strength values. The high bearing strength of high-strength concrete results in less crushing of concrete in front of the ribs and thus less local slip. The reduced slip causes high local tensile stresses in the concrete surrounding only a few ribs, resulting in a non-uniform distribution of the bond stresses.[11,14,15]

Traditionally, the effect of concrete strength on bond strength has be represented by $\sqrt{f_c'}$, which is also known to represent the tensile strength of concrete. Recent research has shown that using $\sqrt{f_c'}$ overestimates the effect of concrete strength when f_c' is above 8 ksi (55 MPa).[9,12] Some researchers have suggested using $f_c'^{0.33}$ or $f_c'^{0.25}$ to represent the effect of concrete strength.[9] Research by Darwin proposed that the reason that the tensile strength of concrete, represented by $\sqrt{f_c'}$, does not provide a good representation of high-strength concrete is because the bond strength is more directly related to the fracture energy of the aggregate.[9,12]

CONCRETE WITH COMPRESSIVE STRENGTH GREATER THAN 10 KSI

In a research study by Azizinamini, 65 splice beam specimens were tested that had compressive strengths ranging from 10.9 ksi to 16.0 ksi (75.1 MPa to 110.2 MPa).[14,15] The study showed that an increase in splice length did not necessarily increase the bond strength.

The high strength concrete used in their study had a proportionally higher bearing strength. As a result, there was less localized crushing around the outermost reinforcement deformation than in normal strength concrete. The localized crushing in normal strength concrete is the assumed mechanism that distributes load to the next deformation and allows a more uniform bond stress distribution. A uniform distribution of bond stress is assumed by the design expressions for development length in the AASHTO LRFD Specifications (1), ACI 318-11 (16), and ACI 408-03 (9). In concrete with compressive strength greater than 10 ksi (69 MPa), the higher concrete bearing stress limits the number of lugs that contribute to the bond stress. Once radial cracking develops, there is a reduction in the contribution of the outermost lugs which allows the next lugs engage at a higher bearing stress. As a result, the effective length of the splice is

limited and increasing the overall length of the splice may not cause an increase in the bond strength (i.e., force in the reinforcing bar at ultimate).

Azizinamini el al. (17) proposed that for concrete with compressive strength greater than 10 ksi (69 MPa), ductility of the spliced connection was of equal importance to bond strength. The researchers proposed that increasing the splice length was inefficient and instead a minimum amount of confining transverse reinforcement was necessary to ensure ductility of the spliced connection at ultimate.

DESCRIPTIVE EXPRESSIONS FOR BOND STRENGTH

A rational theory for predicting bond strength has not been developed. Instead, empirical equations have been developed based on comparisons with test results. The descriptive equations developed by Orangun, Jirsa, and Breen (13) and Zuo and Darwin (12) are described in this document. The expression developed by Orangun et al. was based on a limited database of tests and includes traditional parameters for predicting bond strength. The more recent expression by Zuo and Darwin is based on a much larger database, and includes additional parameters that account for bars cast in high-strength concrete, and for bars with high relative rib area.

ORANGUN, JIRSA, AND BREEN

The expressions for bond strength developed by Orangun, Jirsa, and Breen (13) were based on 62 splice beam tests (ref test). Their expression for the bond strength of splices without transverse reinforcement (u_c), given by Eq. 1, considers the tensile strength of concrete as $\sqrt{f_c'}$, and considers cover thickness (c_{minOJB}), bar diameter (d_b), and splice length (ℓ_s). For bars confined by transverse reinforcement, a term is added to account for the additional bond strength due to transverse reinforcement (u_s). The total bond strength of a bar confined by transverse reinforcement (u_b) is given by Eq. 2.

The applicability of Eq. 1 and Eq. 2 is limited to splitting failures. The inequality in Eq. 3 must be satisfied in order for Eq. 1 and Eq. 2 to be applicable.

$$\frac{u_c}{\sqrt{f_c'}} = 1.2 + 3\frac{c_{minOBJ}}{d_b} + 50\frac{d_b}{\ell_s} \qquad (\text{Eq. 1})$$

$$\frac{u_b}{\sqrt{f_c'}} = \frac{u_c}{\sqrt{f_c'}} + \frac{u_s}{\sqrt{f_c'}} = \frac{u_c}{\sqrt{f_c'}} + \frac{A_{tr}f_{yt}}{500snd_b} \qquad (\text{Eq. 2})$$

$$\frac{1}{d_b}\left(c_{minOBJ} + 0.4d_b + \frac{A_{tr}f_{yt}}{1500sn}\right) \le 2.5 \qquad (\text{Eq. 3})$$

in Eq. 1, Eq. 2, and Eq. 3, the units of stress are in psi

The expressions for bond strength developed by Zuo and Darwin (12) were based on 367 splice beam tests including tests with a compressive strength greater than 8 ksi (55 MPa). Their expression for the bond strength of splices without transverse reinforcement (T_c) is given by Eq. 4. A fundamental difference between the expression in Eq. 4 and the Orangun et al. expression in Eq. 1 is the use of $f_c'^{0.25}$ rather than $\sqrt{f_c'}$ to account for the effect of concrete strength. The use of $f_c'^{0.25}$ is intended to reflect the assumed greater dependence on the fracture energy of the aggregate for the bond strength, rather than the more commonly used $\sqrt{f_c'}$ to reflect concrete tensile strength.

The total bond strength of a bar confined by transverse reinforcement (T_b) is given by Eq. 5, and is the bond strength of an unconfined bar given by Eq. 4 plus the additional bond strength due to transverse reinforcement (T_s). The effect of concrete strength on T_s is represented by $f_c'^{0.75}$ (i.e., $f_c'^{0.25}$ multiplied by $f_c'^{0.50}$).

The Zuo and Darwin expressions include the effects of concrete cover (through c_{min} and c_{max}), reinforcement deformation size, and bar size. The reinforcement deformation size is quantified by the relative rib area (R_r). The term t_r is function of R_r and is used to quantify the effect of the reinforcement deformation size in the expression for T_s. A term for bar size (t_d) is included in the expression for T_s. The expressions for t_r and t_d are given by Eq. 6 and Eq. 7, respectively.

The applicability of Eq. 4 and Eq. 5 is limited to splitting failures. The inequality in Eq. 8 must be satisfied in order for Eq. 4 and Eq. 5 to be applicable.

$$\frac{T_c}{f_c'^{0.25}} = [59.8\ell_d(c_{min} + 0.5d_b) + 2350A_b]\left(0.1\frac{c_{max}}{c_{min}} + 0.90\right) \qquad \text{(Eq. 4)}$$

$$\frac{T_b}{f_c'^{0.25}} = \frac{T_c}{f_c'^{0.25}} + \frac{T_s}{f_c'^{0.25}} = \frac{T_c}{f_c'^{0.25}} + \left(31.14t_r t_d \frac{NA_{tr}}{n} + 4\right)f_c'^{0.5} \qquad \text{(Eq. 5)}$$

in Eq. 4 and Eq. 5, the units of stress are in psi

$$t_r = 9.6R_r + 0.28 \le 1.72 \qquad \text{(Eq. 6)}$$

$$t_d = 0.78d_b + 0.22 \qquad \text{(Eq. 7)}$$

$$\frac{1}{d_b}\left[(c_{min} + 0.5d_b)\left(0.1\frac{c_{max}}{c_{min}} + 0.90\right) + \left(\frac{0.52t_r t_d A_{tr}}{sn}\right)f_c'^{0.5}\right] \le 4.0 \qquad \text{(Eq. 8)}$$

in Eq. 8, the units of stress are in psi

DESIGN EXPRESSIONS FOR BOND STRENGTH

The two descriptive expressions for bond strength discussed in the previous section were simplified and expressed as design expressions. The Orangun, et al. descriptive expression (13)

is the basis for the design expression in the AASHTO LRFD Specifications (1). The Zuo and Darwin descriptive expression (12) is the basis for the design expression proposed by ACI Committee 408 (9). Another design expression, currently used in ACI 318-11 (16), was evaluated by NCHRP Project 12-60 (18) for high-strength concrete. The slight modifications to the ACI 318-11 expression proposed in the NCHRP Project 12-60 report is currently being reviewed by the AASHTO SCOBS T-10 committee for inclusion into the AASHTO LRFD Specifications.

This section includes design expressions for bond using two different terms. The expressions for basic development length (ℓ_{db}) have not been multiplied by factors that will increase or decrease the development length (ℓ_d). The expressions for development length (ℓ_d) include the factors in a single expression. In each case, the smallest ℓ_d allowed by the AASHTO LRFD Specifications, ACI 318-11, or ACI Committee 408 is 12 inches (305 mm). Any additional limitations on ℓ_d are stated individually.

AASHTO LRFD SPECIFICATIONS DESIGN EXPRESSION

The design expression for development length in the AASHTO LRFD Specifications was originally introduced into the Eleventh Edition of the AASHTO Standard Specifications in 1973 (19) as part of the section on Load Factor Design. The basic development length of #11 bars and smaller is given by Eq. 9. Note that the units of stress in Eq. 9 are psi. There was not a general method for considering the effect of confining reinforcement; however there was a 25% reduction in ℓ_{db} for bars enclosed inside spiral reinforcement on a 4 inch (102 mm) pitch. Other factors include an increase in ℓ_{db} for top bars, and reductions in ℓ_{db} for excess reinforcement and adequate lateral and side spacing.

The expression for ℓ_{db} in the AASHTO LRFD Specifications (1) is given by Eq. 10 and the basic form of the expression has not changed from the AASHTO Standard Specifications (19). The main difference is the use of ksi units instead of psi units and the resulting round-off in the first term. The modification factors for spiral confinement, top bars, excess reinforcement, and adequate lateral and side spacing are still in the bridge design specifications. Factors for epoxy coating and lightweight concrete have been added. The term after the inequality in Eq. 10 was included as a limit to prevent pullout failures.

$$\ell_{db} = 0.04A_b \frac{f_y}{\sqrt{f_c'}} \geq 0.0004d_b f_y \qquad \text{(Eq. 9)}$$

in Eq. 9, the units of stress are in psi

$$\ell_{db} = 1.25A_b \frac{f_y}{\sqrt{f_c'}} \geq 0.4d_b f_y \qquad \text{(Eq. 10)}$$

ACI 318-11 DESIGN EXPRESSION

The expression for ℓ_{db} has been modified more frequently than the expression in the AASHTO bridge specifications. The same expression as given in Eq. 9 was in ACI 318-77 (20). Research by Orangun et al. (13) and a document by ACI Committee 408 (21) recommended changes to the ACI 318-77 expression for ℓ_{db} as described in detail by Jirsa et al. (22). The ACI Committee 408 recommendation for ℓ_{db} is given by Eq. 11. As described by Jirsa et al., Eq. 11 is a simplification of Eq. 2, and includes the beneficial effect of confinement through the factor K_{tr}. Many of the recommendations of ACI Committee 408 (21) were included into the ACI 318-89 code (23); however Eq. 11 was not directly included. Instead the effect of confinement was included as a factor that was multiplied by ℓ_{db}.

An entirely new expression for development length ℓ_d was introduced into the ACI 318-95 code (24) and the basic form of the expression is still used in the current ACI 318-11 version (16) of the code. The ACI 318-11 expression for ℓ_d is given by Eq. 12. The Ψ_t, Ψ_e, Ψ_s, and λ_{ACI} factors in Eq. 12 account for the effects of top bars, epoxy-coating, bar size, and LWC, respectively.

The K_{tr} factor in Eq. 12 is used to account for the effects of confinement and was modified slightly from ACI 318-95 to ACI 318-11. The K_{tr} factor in the ACI 318-95 code is given by Eq. 13 and is a function of the yield strength of the confining reinforcement (f_{yt}). The confining reinforcement rarely yields so the K_{tr} term in the ACI 318-11 code, given by Eq. 14, includes an assumed f_{yt} of 60 ksi (i.e., 60,000 psi / 1500 = 40) (410 MPa).[9] In Eq. 12, the term $(c_b + K_{tr})/d_b$ is limited to a value of 2.5.

$$\ell_{db} = \frac{5500A_b}{\phi(c_b + K_{tr})\sqrt{f_c'}} \tag{Eq. 11}$$

$$\ell_d = \frac{3}{40} \frac{f_y}{\lambda_{ACI}\sqrt{f_c'}} \frac{\Psi_t \Psi_e \Psi_s}{\left(\frac{c_b + K_{tr}}{d_b}\right)} d_b \tag{Eq. 12}$$

$$K_{tr} = \frac{A_{tr}f_{yt}}{1500sn} \tag{Eq. 13}$$

in Eq. 11, Eq. 12 and Eq. 13, the units of stress are in psi

$$K_{tr} = \frac{40A_{tr}}{sn} \tag{Eq. 14}$$

The expression for ℓ_d given by Eq. 12 was evaluated as part of NCHRP Project 12-60 (18) for use with high-strength concrete. The study included 18 tests on splice beam specimens with concrete compressive strengths ranging from 12.3 ksi to 17.2 ksi (84.8 MPa to 118.5 MPa). Six splice beams were tested with top cast uncoated reinforcement and 12 were tested with top cast epoxy-coated reinforcement. The evaluation of the results from the tests on uncoated bars were

combined with the results in the ACI Committee 408 Database (9) and the authors of the NCHRP Project 12-60 report concluded that Eq. 12 could be extended for normal-weight concrete up to a compressive strength of 16 ksi (110 MPa). For epoxy-coated bars, the evaluation of the test beams were combined with the results of other tests from the literature and the authors concluded that Eq. 12 could be extended for normal-weight concrete up to a compressive strength of 17 ksi (117 MPa) if the bar size factor was removed and the epoxy coating factor was increased for some cases.

ACI COMMITTEE 408 DESIGN EXPRESSION

The expression for ℓ_d proposed by ACI Committee 408 (9) is given by Eq. 15 and is based on the work of Zuo and Darwin.[11,12] The expression includes a resistance factor (ϕ-factor) of 0.92 multiplied by the f_c' term. The descriptive expressions given by Eq. 4 and Eq. 5 were simplified to give Eq. 15. The expressions for $K_{tr,ACI408}$ and ω in Eq. 15 are given by Eq. 16 and Eq. 17, respectively. The term $(c_b\omega + K_{tr,ACI408})/d_b$ is limited to 4. In addition to a minimum ℓ_d of 12 inches (305 mm), ACI Committee 408 also requires ℓ_d to be greater than $16d_b$.

$$\ell_d = \frac{\left(\dfrac{f_y}{f_c'^{0.25}} - 2200\omega\right)\alpha\beta\lambda_{ACI408}}{70\left(\dfrac{c_b\omega + K_{tr,ACI408}}{d_b}\right)}d_b \qquad \text{(Eq. 15)}$$

$$K_{tr,ACI408} = \left(\frac{0.52t_r t_d A_{tr}}{sn}\right)f_c'^{0.5} \qquad \text{(Eq. 16)}$$

in Eq. 15 and Eq. 16, the units of stress are in psi

$$\omega = 0.1\frac{c_{max}}{c_{min}} + 0.90 \leq 1.25 \qquad \text{(Eq. 17)}$$

DIFFERENCES BETWEEN THE DESIGN EXPRESSIONS

There are several significant differences between the format of Eq. 15 proposed by ACI Committee 408 and the design expressions in the AASHTO LRFD Specifications (Eq. 10) and the ACI 318-11 specifications (Eq. 12). The first is the use of $f_c'^{0.25}$ rather than $\sqrt{f_c'}$ to account for the effect of concrete strength. Another difference is the 2200ω term in the numerator of Eq. 15. As will be discussed in a later section of this document, this term means that the predicted bar stress is a linear function of splice length, but it is not proportional to splice length. The expressions of both the AASHTO LRFD Specifications and the ACI 318-11 specifications use expressions in which the predicted bar stress is proportional to splice length.

Other differences in the expressions include the effect of confinement on ℓ_{db}. The ACI Committee 408 and ACI 318-11 expressions both include a K_{tr} term to account for confinement,

13

although the definition of K_{tr} is different in each expression. The AASHTO LRFD expression does not include a K_{tr} term. The value of the modification factor to account for the effects of top cast bars is different in the AASHTO LRFD Specifications and ACI 318-11 specification. Only ACI 318-11 includes a factor that reduces ℓ_{db} for #6 bars and smaller. AASHTO LRFD Specifications and the ACI 318-11 specifications use the same factor for epoxy coated bars. The ACI Committee 408 uses slightly different values. The factors for lightweight concrete and top cast bars are the same in ACI Committee 408 and ACI 318-11.

CHAPTER 3.   RESEARCH ON MILD STEEL DEVELOPMENT LENGTH IN LWC AT TFHRC

INTRODUCTION

This research program focused on LWC with compressive strengths in the range of 6 to 10 ksi (41 to 69 MPa) and equilibrium densities between 0.125 kcf and 0.135 kcf (2000 and 2160 kg/m^3). The research program used LWC with three different lightweight aggregates to produce 27 precast/prestressed LWC girders and 40 reinforced concrete splice beam specimens. While this research program focused on structural behavior, it also had a material characterization component that is described in another document (7) and included mechanical property tests on the concrete mixes used in the structural testing program. Mechanical tests included the compressive strength, elastic modulus, and splitting tensile strength. The concrete unit weight was determined using several methods.

This section summarizes the LWC mix design selection process, the specimen fabrication at the precaster's facility, and the material property testing. More details can be found in another document covering material properties of LWC tested by FHWA.[7] The details of the FHWA research program involving the bond performance of uncoated mild steel reinforcement in LWC is given in this section. Tests on splice beam specimens were used to evaluate the development length of mild steel reinforcement. The Russell synthesis report (6) recognized the lack of mild steel bond test data for LWC. Also, all of the bond tests for LWC referenced in ACI 213-03 (2,8) utilized a pullout test which, although easy to fabricate and simple to perform, is known to produce an unrealistic stress field within the specimen.[9] More realistic measures of bond strength can be made in beam-end specimens and splice beam specimens. Current ACI 318 design provisions for the development of mild steel bars in NWC are mostly based on tests of splice beam specimens.[9]

The test results for the 40 splice beam specimen are discussed in detail. The results include observations of specimen behavior such as test observations and load-deformation response, an analysis of the stress in the spliced bar at failure, and an assessment of specimen displacement ductility. The bar stress at failure is compared to several methods used to determine normalized splice length, two descriptive expressions for predicting bar stress, and three design expressions for predicting bar stress.

RESEARCH SIGNIFICANCE

There is a limited amount of test data on the bond between rebar and high-strength LWC. This research project includes 40 splice beam tests on this type of concrete. These tests on the bond strength of high-strength LWC will be combined with other tests on LWC and tests on NWC to determine the effect of lightweight aggregates and the bond strength. Design expressions for

development length that include a proposed modification factor for LWC are validated using the tests on LWC.

LWC MIX DESIGNS

The Expanded Shale, Clay, and Slate Institute (ESCSI) assisted FHWA in obtaining specified density mixes that had been used in production. One of the criteria for this research project was to use lightweight aggregate sources that were geographically distributed across the United States. Additional selection criteria included mixes using a large percentage of the coarse aggregate as lightweight coarse aggregate, mixes using natural sand as the fine aggregate, and mixes with a target equilibrium density between 0.125 and 0.135 kcf (2000 and 2160 kg/m^3). In order to make sure that the behavior of the concrete would be controlled by the lightweight aggregate, only mixes with greater than 50% of the coarse aggregate as lightweight aggregate were considered. The concrete density needed to be in the range of densities not currently covered by the AASHTO LRFD Bridge Design Specifications (1) because of the limited amount of test data in this density range. The literature has shown that silica fume can increase LWC compressive strength [9,25-27] and has also been shown to improve bond of mild steel reinforcement and prestressing strand.[9] As a result, mixes that included silica fume were not selected for this experimental study so that the results would be representative of mechanical properties for specified density concrete without silica fume and most likely conservative for specified density concrete with silica fume.

Three mix designs were selected with a design compressive strength greater than 6.0 ksi (41.3 MPa) to represent concrete that could be used for bridge girders. Another mix design was selected that had a design compressive strength less than 6.0 ksi (41.3 MPa) to represent concrete that could be used for a bridge deck.

The mix designs selected are shown in Table 1. Each uses partial replacement of the coarse aggregate with lightweight aggregate to achieve their reduced unit weight. The lightweight aggregates in the mixes were Haydite, an expanded shale from Ohio, Stalite, an expanded slate from North Carolina, and Utelite, an expanded shale from Utah. The normal weight coarse aggregate was No. 67 Nova Scotia granite. Natural river sand was used as the fine aggregate. Type III portland cement was used to obtain the high early strengths typically required in high-strength precast girders. Admixtures included a water reducer, an air entrainer, and a high range water reducer.

Table 1. Selected Concrete Mix Designs.

Cast Date	unit	Haydite Girder (HG)	Stalite Girder (SG)	Utelite Girder (UG)	Stalite Deck (SD)
Design 28-Day Strength	ksi	6.0	10.0	7.0	4.0
Design Release Strength	ksi	3.50	7.5	4.2	-
Target Unit Weight	kcf	0.130	0.126	0.126	0.125
Lightweight Coarse Aggregate	kips	0.80	0.88	0.74	0.51
Normal Weight Coarse	kips	0.52	0.25	0.39	0.73
Normal Weight Sand	kips	1.19	1.22	1.27	1.31
Class F Fly Ash	kips	-	-	0.15	0.12
Type III Portland Cement	kips	0.75	0.80	0.60	0.50 [†]
Water	kips	0.27	0.25	0.26	0.27
Water Reducer	oz	19	19	19	10
Air Entrainer	oz	2	2	2	4
High Range Water Reducer	oz	34	34	34	15
Water / Cementitious Materials		0.36	0.31	0.34	0.43

Note: † Mix design used Type II Portland Cement
Units: 1.0 ksi = 6.89 MPa, 0.001 kcf = 16.01 kg/m^3, 1.0 kip = 4.45 kN, 1.0 oz = 29.6 mL

EXPERIMENTAL PROGRAM

The experimental program consisted of testing to failure 40 splice beam specimens. Key test parameters include the lightweight aggregate, the bar size (#4, #6, #8, and #11), the splice length (short versus long ℓ_s/d_b ratio), and the presence of transverse reinforcement (as stirrups). Twelve splice beam designs were developed to evaluate the effect of the key parameters. A set of 12 splice beams was cast for each of three different concrete mixes intended to represent typical LWC for girders. Table 2 gives the nominal beam dimensions and reinforcement size and splice length for the 12 different specimens using girder concrete mixes. Four additional splice beam specimens were developed for a concrete mix intended to represent typical LWC for bridge deck applications. The nominal beam dimensions and reinforcement details for the specimens using the deck concrete mix are given in Table 3.

A naming scheme was developed for the 40 splice beams that included the concrete mix, bar size, relative splice length, and presence of transverse reinforcement (as stirrups). The concrete mixes were designated A through D and were SG, UG, HG, and SD, respectively. The nominal bar size was used in the naming scheme. An "S" or an "L" was used to denote a short versus long ℓ_s/d_b ratio. Beams with no transverse reinforcement had an "N" and beams with transverse reinforcement along the splice had a "T".

Table 2. Nominal Splice Beam Dimensions – Girder Concrete Mixes.

Beam	Bar Size	Splice Length (inch)	No. of Stirrups[†]	Nominal Cross Section Dimensions (width × height) (inch)	Beam Length (inch)	Support Spacing (inch)
1	#6	16	0	9 × 18	168	60
2	#6	24	0	9 × 18	168	60
3	#6	16	2	9 × 18	168	60
4	#6	24	3	9 × 18	168	60
5	#8	24	0	12 × 18	180	72
6	#8	32	0	12 × 18	180	72
7	#8	24	3	12 × 18	180	72
8	#8	32	4	12 × 18	180	72
9	#11	32	0	18 × 18	192	84
10	#11	48	0	18 × 18	192	84
11	#11	32	4	18 × 18	192	84
12	#11	48	6	18 × 18	192	84

Note: † #3 bar at 8 inch spacing
Units: 1.0 inch = 25.4 mm

Table 3. Nominal Splice Beam Dimensions – Deck Concrete Mix.

Beam	Bar Size	Splice Length (inch)	No. of Stirrups	Nominal Cross Section Dimensions (width × height) (inch)	Beam Length (inch)	Support Spacing (inch)
1	#4	12	0	9 × 18	168	60
2	#4	16	0	9 × 18	168	60
3	#6	12	0	9 × 18	168	60
4	#6	16	0	9 × 18	168	60

Units: 1.0 inch = 25.4 mm

TEST SPECIMENS

The splice beams had three adjacent bottom-cast splices. The specimens were inverted prior to testing so that the splices were at the top face, and then simply supported with ends cantilevered. Equal loads were applied at each end resulting in a constant moment region between the supports. Stirrups were placed in the cantilevered ends to prevent a shear failure. The stirrup bar size and stirrup spacing is given in Table 4 by size of the longitudinal bar. The amount of stirrups was selected to maintain a constant value of K_{tr}, as determined using Eq. 14 for specimens with smaller and larger ℓ_s/d_b ratios. The beams were proportioned so that the ends of

18

the bars at the splice were at least a distance equal to the beam height from the centerline of the support. The depth of all beams was maintained at 18 inches (457 mm). A sketch of the splice beams is shown in Figure 5.

Table 4. Stirrups in Cantilevered Ends of Splice Beams.

Longitudinal Bar Size	Stirrup Bar Size	Stirrup Spacing
#4	#3	7 spaces at 8 inches[†]
#6	#3	7 spaces at 8 inches[†]
#8	#3	7 spaces at 8 inches[‡]
#11	#4	9 spaces at 6 inches[‡]

Notes: [†] 1 stirrup per spacing; [‡] 2 stirrups per spacing
Units: 1.0 inch = 25.4 mm

(a) Plan View

(b) Elevation View

(c) Section through Splice
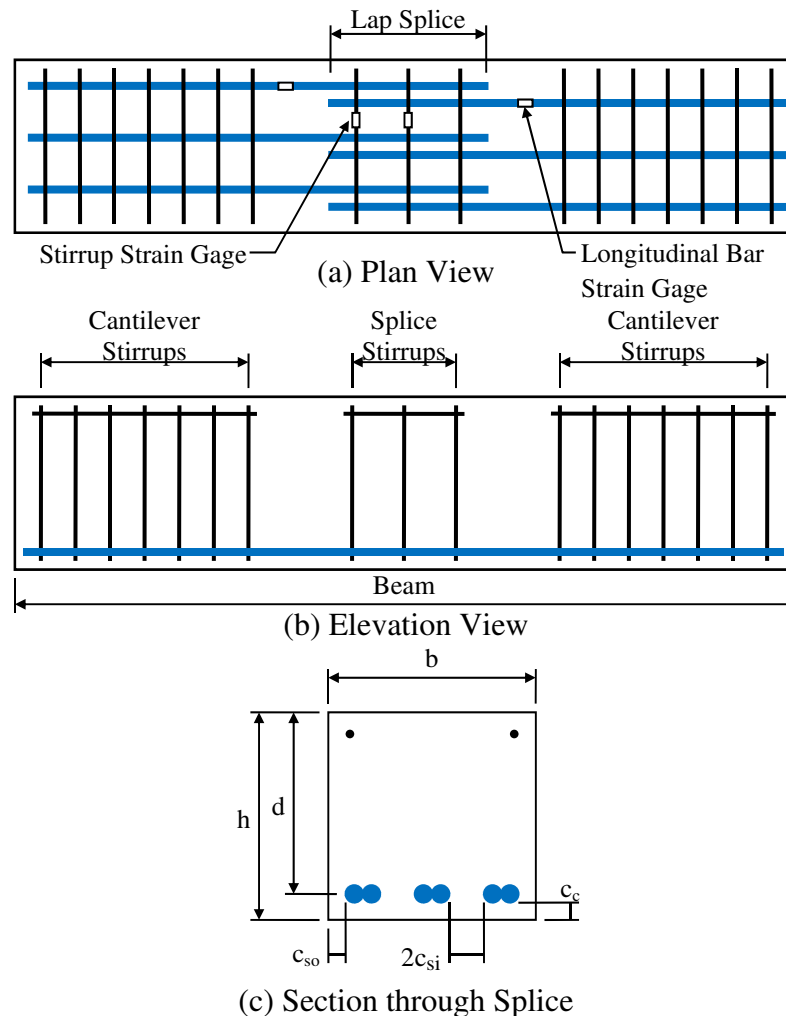
Figure 5. Illustration. Splice Beam Specimen Dimensions.

The nominal beam width, side and bottom concrete cover, and spacing between spliced bars was maintained proportional to the bar size. Side and bottom covers (c_{so} and c_c) were $1 \times d_b$, and splice spacing ($2 \times c_{si}$) was $2 \times d_b$ (approximate for the #11 bars).

SPECIMEN FABRICATION

The girders were fabricated at the Standard Concrete Products (SCP) plant in Mobile, Alabama. The fabricator was asked to prescriptively produce the concrete mixes, without trying to adjust them for target strengths or unit weight. This was intended to remove batch-to-batch variations as a variable in the study. The lightweight aggregates were stored in three piles at the plant and watered continuously using a sprinkler on each pile as shown in Figure 6.

Figure 6. Photo. Lightweight Aggregate Stockpiles at Precaster's Facility with Continuous Sprinklers.

CONCRETE PROPERTIES

Concrete for the three girder mixes and one deck mix was supplied by the precaster. After mixing, the precaster's personnel performed testing of the fresh concrete properties and produced 4 x 8 inch (102 x 203 mm) cylinders for quality control purposes. The fresh concrete properties, concrete batch weights, and compressive strength tests performed by the precaster's personnel are in another document covering material properties of the LWC tested within this research program.[7]

Independently, research staff personnel made 4 x 8 inch (102 x 203 mm) cylinders following ASTM C31 (28) for mechanical property testing and density measurements. Compression tests were performed according to ASTM C39 (29) to determine the compressive strength at 28 days, and at girder testing. Neoprene pads were used inside steel caps at each end of the cylinders. The air-dry density was calculated using the measured cylinder weight and measured cylinder lengths and diameters to calculate an average volume. The indirect tensile strength was measured using the splitting tensile test described in ASTM C 496 (30). The mechanical properties of the LWC used in the splice beams are given in Table 5. The compressive strengths, splitting tensile strengths, and air-dry densities shown are the based on the average of three cylinders.

Table 5. Splice Beam Concrete Properties.

| Mix Design | Mix Date | Compressive Strength | | 28-Day Splitting Tensile Strength (ksi) | 28-Day Air-Dry Density (kcf) |
		28 Day (ksi)	Test Day (ksi)		
HG	6/20/200	8.0	9.8	0.685	0.133
SG	5/14/200	10.6	12.2	0.716	0.126
UG	6/9/2008	9.6	10.9	0.764	0.131
SD	5/14/200	5.7	7.6	--	0.138

Units: 1.0 ksi = 6.89 MPa, 0.001 kcf = 16.01 kg/m^3

REINFORCEMENT PROPERTIES

The reinforcing bars were ASTM A615, Grade 60. The mechanical properties were tested under displacement control in a 100 kip (445 kN) testing machine. Two bars were tested for each nominal size used in the splice beams. Strain was measured with an 8 inch (203 mm) extensometer. When the extensometer reached a measured strain of 2.0% at the beginning of the assumed strain-hardening regime, the test was paused to remove the extensometer. The test was then continued until the bar fractured. The yield strength was determined using the 0.2% offset method. The average yield strength and the ultimate strength of the two bars in each size tested are given in Table 6. Test data and stress-strain relationships from individual bars are given in Appendix A.

Table 6. Reinforcing Bar Properties.

| Bar Measurement | Nominal Bar Size | | | |
	#4	#6	#8	#11
Nominal Diameter (inch)	0.50	0.75	1.00	1.41
Mass per Unit Length (lb/ft)	0.64	1.44	2.58	5.19
Rib Spacing (inch)	0.322	0.478	0.618	0.875
Rib Height (inch)	0.0290	0.049	0.0567	0.0823
Rib Angle (degrees)	60.3	60.1	60.7	61.1
Relative Rib Area	0.0771	0.0909	0.0797	0.0824
Yield Strength[†] (ksi)	65.7	67.6	73.8	66.5
Ultimate Strength (ksi)	105.3	107.1	109.3	--[‡]

Notes: [†] Calculated using 0.2% offset method; [‡] Beyond capacity of testing machine
Units: 1.0 inch = 25.4 mm, 1.0 lb/ft = 14.59 N/m, 1.0 ksi = 6.89 MPa

The reinforcing bar geometry was measured to determine the relative rib area, R_r, using the method given in ACI 408-03.[9] Two 12 inch (305 mm) long samples were measured from each nominal bar size used in the splice beams. The relative rib area was calculated using Eq. 18 which is given in ACI 408-03 (Section 6.6).

$$R_r = \frac{h_r}{s_r}\left(1 - \frac{\Sigma \text{gaps}}{p}\right)$$ (Eq. 18)

The average deformation height, h_f, was based on measurements at four typical deformations. Each deformation was measured at five locations, as shown in Figure 7, as the difference in height between the deformation and barrel of the bar using a dial gage. The dial gage used was metric with 0.01 mm divisions (0.004 inch) and was read to the nearest half division. Figure 8 shows the measurement setup using a mill table and dial gage.

The expression for calculating h_f described in ACI 408-03 is given by Eq. 19. The average rib spacing was determined using Eq. 20. Calipers with a display reading divisions of 0.0005 inches (0.013 mm) were used to measure the outside-to-side and inside-to-inside distance across two ribs that were approximately 6 inches (150 mm) apart. The average rib spacing was determined using the average of the two rib distances divided by the number of spaces between ribs.

$$h_r = 0.25\left[h_{r,\text{center}} + h_{r,\text{mid-1}} + h_{r,\text{mid-2}} + 0.5\left(h_{r,\text{end-1}} + h_{r,\text{end-2}}\right)\right]$$ (Eq. 19)

$$s_r = \frac{L_{\text{outside ribs}} - L_{\text{inside ribs}}}{n_{\text{ribs}}}$$ (Eq. 20)

The sum of the gaps in the transverse rib was determined by measuring the width of the longitudinal ribs as shown in Figure 7. The longitudinal rib width was measured at mid-height of the rib.

The angle between transverse ribs and the longitudinal axis of the bar was determined by making an imprint of the circumference of the bar. A piece of carbon paper was placed between two pieces of white paper. The bar was rolled on the top piece of paper while striking it with a hammer. The impact created an image of the transverse and longitudinal ribs on the bottom piece of paper. The image was scanned and imported in to a computer aided drafting software program. Then the angles between transverse ribs and the longitudinal rib were measured.

The weight per unit length of the sample reinforcing bars was determined by divided the weight of each bar by their length.

The average measured reinforcing bar properties of the two bars in each size is given in Table 6. Measured reinforcing bar properties from individual bars are given in Appendix A.

Cross Section
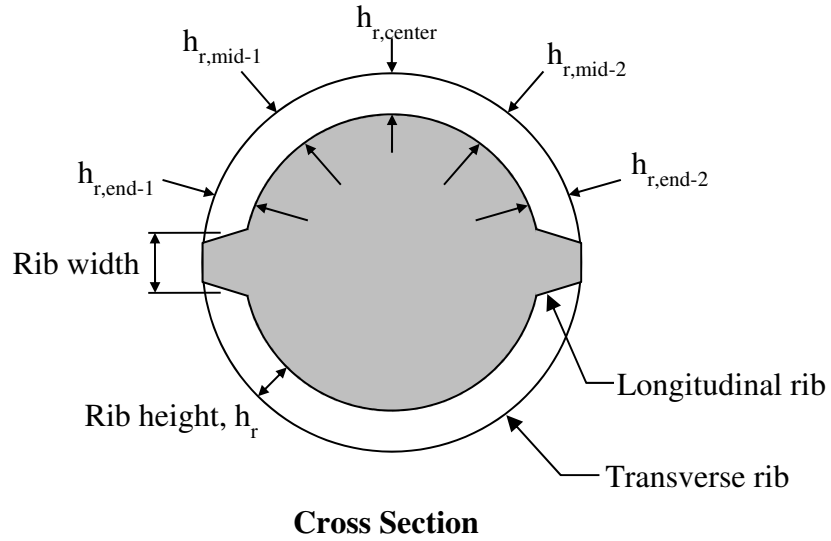
Figure 7. Illustration. Reinforcing Bar Geometry Dimensions.

(a) Mill table used for measurements   (b) Dial gage on transverse rib

Figure 8. Photos. Setup for Measuring Reinforcement Dimensions.

SPLICE BEAM TEST PROCEDURE

The splice beams were inverted so that the spliced bars were on the top face during testing. Load was applied on the top face at each cantilevered end using a 120-kip (534 kN) hydraulic jack. The load at each end was measured using a 100-kip (445 kN) loadcell. Spherical bearing plates were connected to each hydraulic jack. Another bearing plate, 1 inch (25 mm) thick, was grouted to the top face of the beam under the jack. The beams were supported on 6 inch (152 mm) diameter rollers located 4 feet (1.220 m) from the applied loads. A 6 inch (152 mm) wide bearing plate was between the roller and the bottom face of the splice beam.

Displacement measurements were taken using two string potentiometers at each end and two linear variable differential transformers (LVDTs) at mid-span as shown in Figure 9. The strain in a spliced reinforcing bar was measured using two electronic resistance strain gages, one on each side of the splice, approximately 6 inches (150 mm) from the supports (outside of the splice) as shown in Figure 5. The strain in the stirrups was also measured, with one strain gage on a stirrup near the middle of the splice and one on a stirrup near the outside of the splice. The data acquisition system recorded the jack loads, displacements, and strain measurements at a rate of 0.1 Hz.

A hand pump was used to increase the load in increments. Cracks were marked and pictures were taken during pauses in loading. The beams were incrementally loaded until near the predicted failure load. After that, the beams were loaded at a rate of about 2 kips per minute (9 kN per minute) for the smaller specimens to about 5 kips per minute (22 kN per minute) for the larger specimens until failure. A complete test took approximately 3 hours.

The cross section of each splice beam was measured at each end of the lap splice prior to beginning a test. After the test was complete, measurements of the top cover and side cover were made from pieces of concrete that had spalled off of the specimen during the test. The average cross section and cover measurements for each splice beam are given in Appendix A.
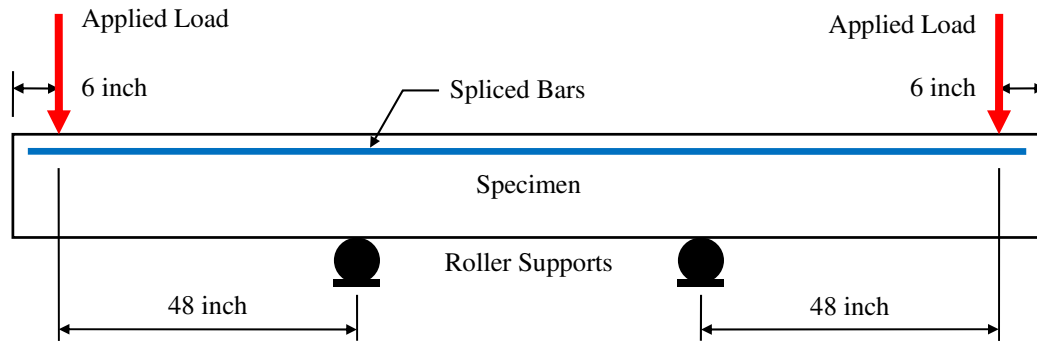
(a) Test Setup Sketch
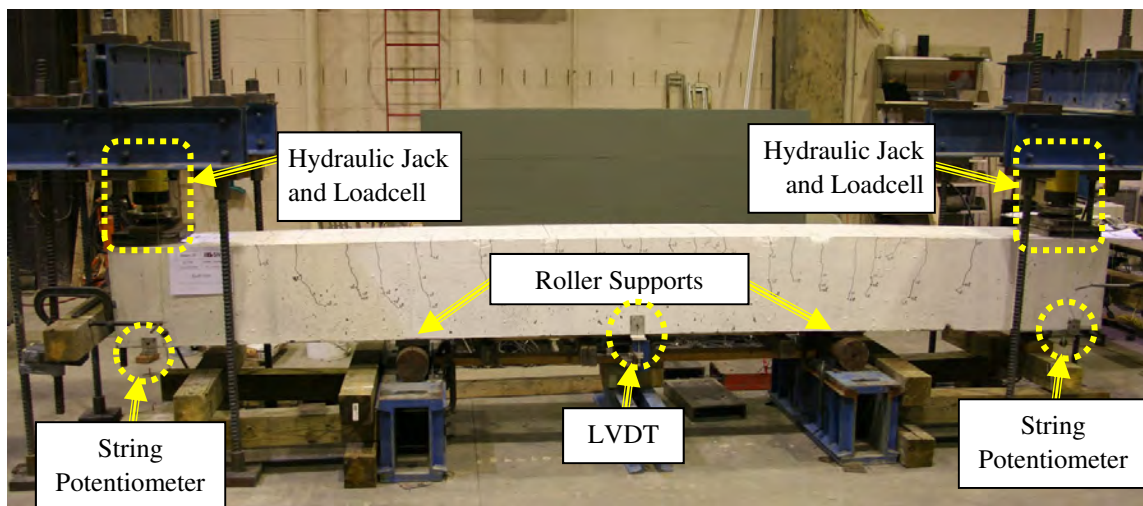
(b) Test of Specimen B11-SN

Figure 9. Illustration. Splice Beam Test Setup.

SPECIMEN BEHAVIOR AND ANALYSIS OF TEST RESULTS

This section describes trends in crack propagation and strain gage measurements that were observed during the splice beam specimen tests. This section also gives the peak load achieved and the load-deformation response of each test.

TEST OBSERVATIONS

The first flexural crack typically occurred at one end of the splice. Additional flexural cracks developed over the support before the first flexural crack opened along the length of the splice. The first splitting cracks opened directly over the spliced bars at the ends of the splice. As the load increased, the new splitting cracks opened up closer to the middle of the splice. Near failure, there was a high density of splitting cracks near the ends of the bars, and few splitting

cracks if any in the middle half of the splice. In members without transverse reinforcement (stirrups), failure was sudden and brittle.

The progression of the splitting cracks towards the middle of the splice was delayed at each stirrup. The growth of splitting cracks is shown in Figure 10 through Figure 13 for Specimen C6-LT. The photographs were taken during pauses in the loading at jack forces of 18 kips, 23 kips, 26 kips, (80 kN, 102 kN, and 116 kN) and after failure. The approximate locations of the ends of the splice and stirrups are shown by green and blue lines, respectively. The black lines in the photographs indicate cracks that were perpendicular to the rebar direction and assumed to be flexural cracks. The red lines are parallel or inclined to the rebar direction and were assumed to be splitting cracks. As the load was increased, additional splitting cracks would form closer to the middle of the splice, but would again be limited by the next stirrup (Figure 11).

Strain in the stirrups was small, sometimes even compressive, until the first splitting crack occurred through the stirrup. Additional load then caused noticeable increases in stirrup strain. The strain in a stirrup near the end of the splice ("outer") and at the middle of the splice ("inner") is shown in Figure 14 for Specimen C6-LT. As shown in the photograph of Figure 10, a splitting crack passed through the outer stirrup at approximately 16 kips (71 kN), which sharply increased in the measured strain. The strain in the middle stirrup did not experience a similar increase. Failure in the specimen occurred shortly after a splitting crack opened through the middle stirrup as indicated by a sharp increase in the middle stirrup's measured strain. The strain measured in the stirrups of Specimen B8-ST, shown in Figure 15, exhibited a similar strain behavior as that measured in the stirrups of Specimen C6-LT.

In many of the tests with stirrups, strain in the outer stirrup increased only with an increase in load until a strain of approximately 1000 microstrain was reached. After reaching this point in the test, the strain in the stirrup would slowly increase without any additional load. After this phenomenon of increasing stirrup strain without increasing load was first observed in a test, the loading rate in subsequent tests exhibiting similar behaviors was slowed and typically splitting tensile failures were observed soon thereafter.

A splitting tensile failure occurred in 36 of the splice beam tests. Yielding of the spliced bars occurred in four of the 22 specimens without transverse reinforcement and in all but two of the 18 specimens with stirrups. A flexural compression failure occurred in four specimens after significant yielding of the spliced bars was accompanied by strains in the outer stirrups greater than 1000 microstrain. The failure load and mode of failure is reported in Table 7 and Table 8 for specimens without and with stirrups, respectively. The peak load reported in the tables is the force in each hydraulic jack. Specimens indicated as yielding in Table 7 and Table 8 had a strain measured by one of the gages on a longitudinal bars exceeding 2300 microstrain, the assumed yield strain for an average yield stress of 67 ksi (462 MPa). Appendix C has photographs of the development of cracking along the splice length and figures showing the measured strain in the stirrups for all 40 splice beam specimens.
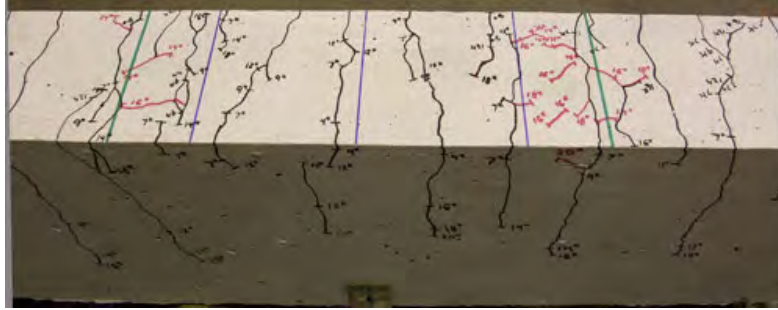
Figure 10. Photo. Crack Growth in C6-LT at 18 kips.
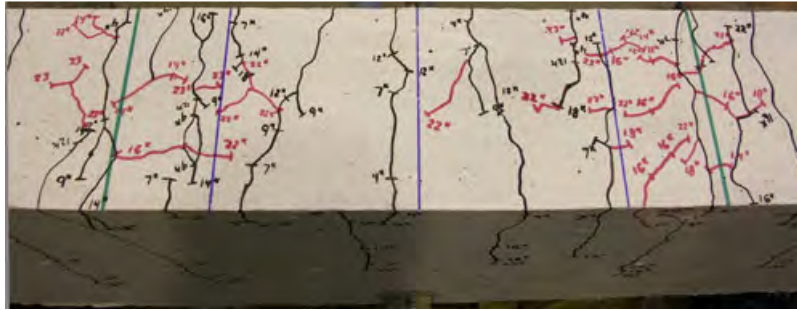
Figure 11. Photo. Crack Growth in C6-LT at 23 kips.
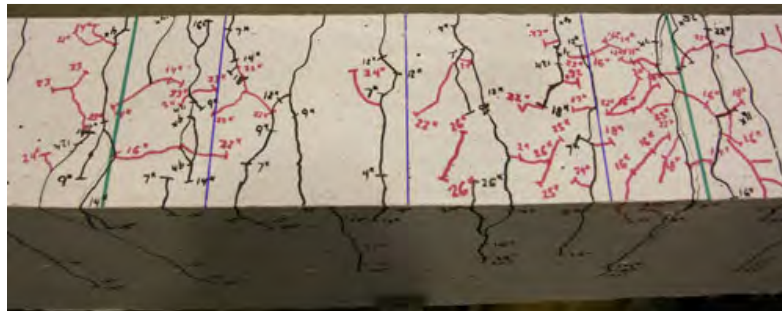
Figure 12. Photos. Crack Growth in C6-LT at 26 kips.
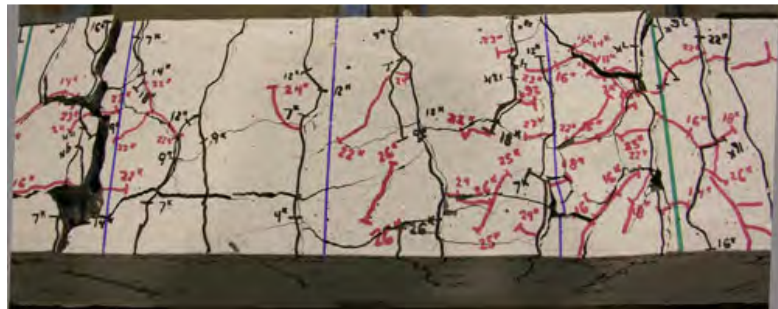
Figure 13. Photos. Crack Growth in C6-LT after failure at 32 kips.
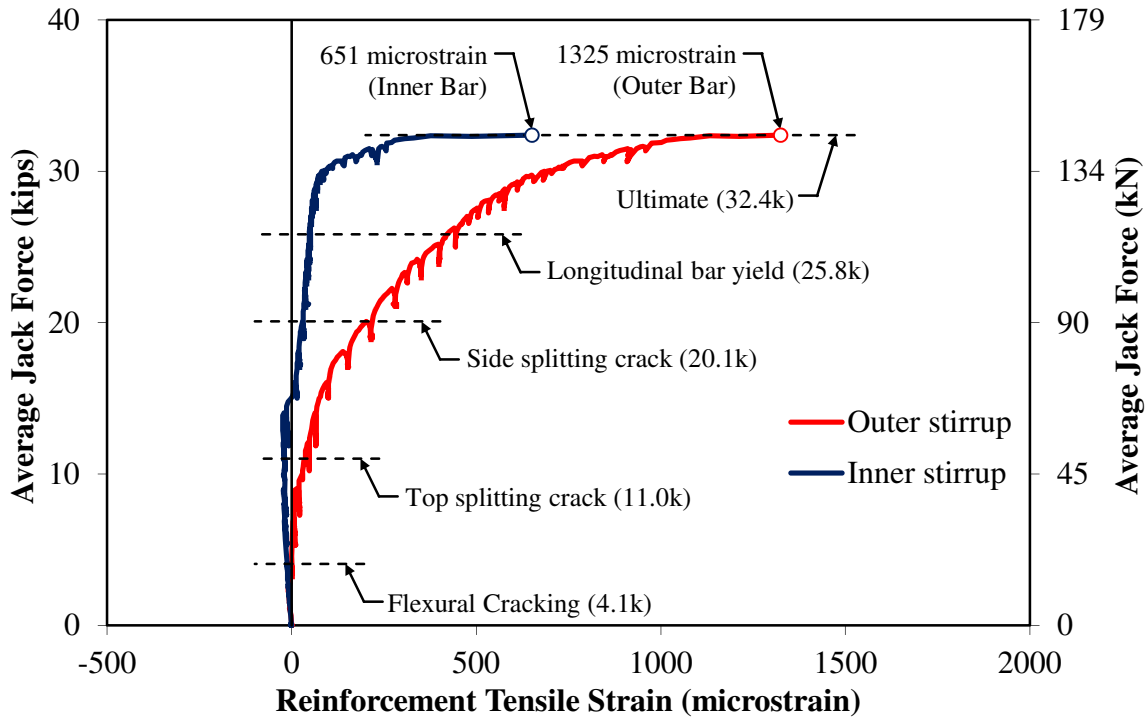
Figure 14. Graph. Strain in Transverse Reinforcement of C6-LT (HG Mix).
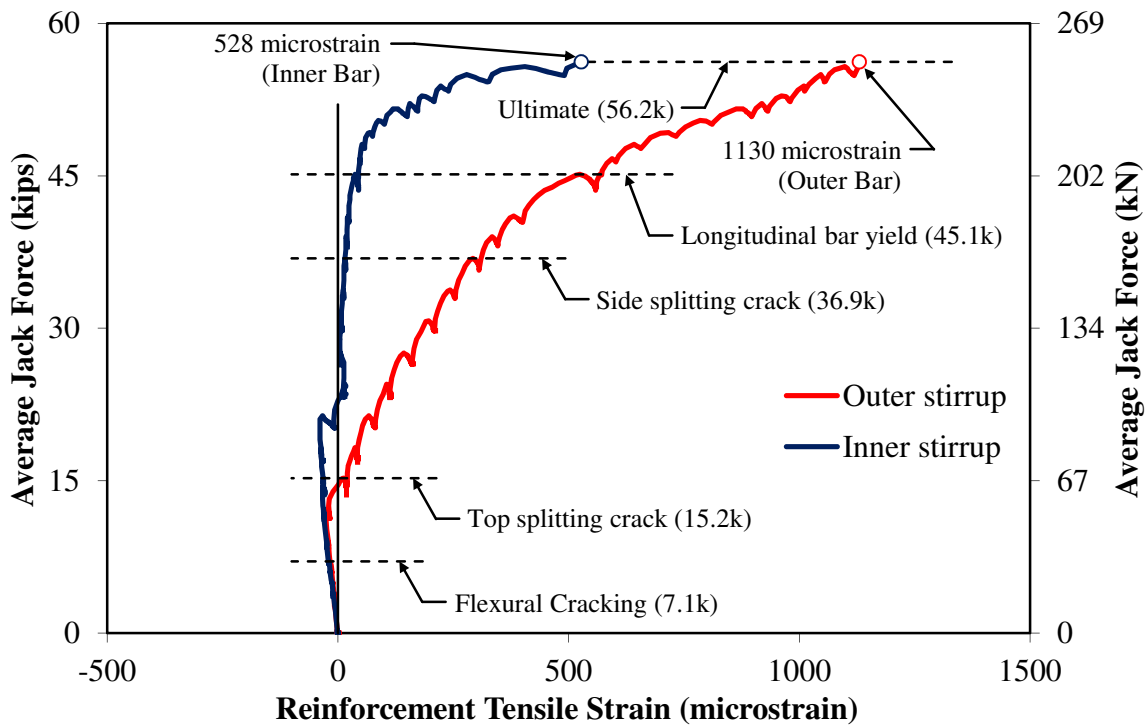
Figure 15. Graph. Strain in Transverse Reinforcement of B8-ST (UG Mix).

Table 7. Splice Beam Properties and Test Results for Specimens without Stirrups.

Specimen Name[†]	Measured Splice Length (inch)	Nominal Bar Diameter (inch)	Peak Load (kips)	Failure Mode[‡]	Calculated Failure Stress (ksi)
D4-SN	12.0	0.50	13.0	STF	65.7
D4-LN	15.9	0.50	12.9	STF w/ Yielding	65.7
D6-SN	16.0	0.75	19.8	STF	47.6
D6-LN	24.0	0.75	24.0	STF	57.3
A6-SN	16.0	0.75	19.4	STF	45.8
B6-SN	15.9	0.75	22.2	STF	51.7
C6-SN	16.0	0.75	21.2	STF	49.8
A6-LN	24.0	0.75	23.0	STF	54.1
B6-LN	24.0	0.75	25.2	STF	59.7
C6-LN	24.0	0.75	21.9	STF	51.2
A8-SN	23.8	1.00	41.0	STF	54.9
B8-SN	23.8	1.00	42.5	STF	56.8
C8-SN	23.7	1.00	39.3	STF	52.9
A8-LN	31.9	1.00	47.7	STF w/ Yielding	63.8
B8-LN	31.8	1.00	46.6	STF w/ Yielding	62.4
C8-LN	32.0	1.00	48.1	STF w/ Yielding	65.1
A11-SN	32.0	1.41	62.8	STF	44.5
B11-SN	31.9	1.41	71.5	STF	51.2
C11-SN	31.8	1.41	59.5	STF	41.7
A11-LN	47.7	1.41	70.6	STF	49.3
B11-LN	47.7	1.41	81.6	STF	57.5
C11-LN	47.8	1.41	80.4	STF	57.0

Notes:

[†] Specimen Name of form $#-%&, where: $ = Concrete Mix: A – SG, B – UG, C – HG, D – SD;
   # = Bar size; % = Relative Splice length: S – short splice (smaller ℓ_s/d_b), L – long splice (longer ℓ_s/d_b);
   & = Transverse reinforcement: N – no stirrups along splice, T – stirrups along splice

[‡] STF = Splitting tensile failure; STF w/ Yielding = STF with yielding of spliced bar; FC = flexural
   compression failure observed as crushing of concrete at bottom surface before STF

[*] Average bar stress computed based on moment curvature analysis using material properties for concrete and
   steel described in ACI 408-03

Units: 1.0 inch = 25.4 mm, 1.0 kip = 4.45 kN, 1.0 ksi = 6.89 MPa

Table 8. Splice Beam Properties and Test Results for Specimens with Stirrups.

Specimen Name[†]	Measured Splice Length (inch)	Nominal Bar Diameter (inch)	Peak Load (kips)	Failure Mode[‡]	Calculated Failure Stress[*] (ksi)
A6-ST	16.0	0.75	26.0	STF	60.97
B6-ST	15.8	0.75	28.9	STF w/ Yielding	65.98
C6-ST	16.0	0.75	26.8	STF w/ Yielding	64.26
A6-LT	23.9	0.75	32.2	STF w/ Yielding	72.90
B6-LT	23.8	0.75	31.8	STF w/ Yielding	71.45
C6-LT	24.0	0.75	32.4	STF w/ Yielding	73.89
A8-ST	24.0	1.00	50.1	STF w/ Yielding	68.74
B8-ST	24.0	1.00	56.2	STF w/ Yielding	74.10
C8-ST	24.0	1.00	57.5	STF w/ Yielding	74.52
A8-LT	32.1	1.00	56.8	STF w/ Yielding	73.96
B8-LT	32.1	1.00	62.5	FC	80.53
C8-LT	32.3	1.00	61.0	FC	78.88
A11-ST	32.0	1.41	78.9	STF	55.90
B11-ST	32.0	1.41	91.0	STF w/ Yielding	63.51
C11-ST	32.0	1.41	78.5	STF w/ Yielding	56.22
A11-LT	47.8	1.41	99.1	STF w/ Yielding	67.25
B11-LT	48.0	1.41	100.9	FC	68.67
C11-LT	48.0	1.41	102.2	FC	69.25

Notes:

[†] Specimen Name of form $#-%&, where: $ = Concrete Mix: A – SG, B – UG, C – HG, D – SD;
    # = Bar size; % = Relative Splice length: S – short splice (smaller ℓ_s/d_b), L – long splice (longer ℓ_s/d_b);
    & = Transverse reinforcement: N – no stirrups along splice, T – stirrups along splice

[‡] STF = Splitting tensile failure; STF w/ Yielding = STF with yielding of spliced bar; FC = flexural
    compression failure observed as crushing of concrete at bottom surface before STF

[*] Average bar stress computed based on moment curvature analysis using material properties for concrete and
    steel described in ACI 408-03

Units: 1.0 inch = 25.4 mm, 1.0 kip = 4.45 kN, 1.0 ksi = 6.89 MPa

LOAD-DEFORMATION RESPONSE

The load-deformation response of the 40 splice beams is shown in Figure 16 through Figure 22. Each figure shows the average measured force in the two hydraulic jacks versus the average displacement of the four string potentiometers at the ends of the beams (two at each end). The response of the 12 splice beams made from the SG, UG, and HG mixes are given in Figure 16, Figure 17, and Figure 18, respectively. The responses are then shown by bar size in Figure 19, Figure 20, and Figure 21, for bar size #6, #8, and #11, respectively. Figure 22 shows the response of the splice beams made from the SD mix compared to the response of the girder mixes with #6 bars and no stirrups.

The stiffness of the load-deformation response of splice beams with the three girder mixes was similar before yielding of the spliced bar. Yielding was indicated by large reduction in the stiffness of the load-deflection response. With the exception of one beam (C8-ST), the stiffness of the load-deformation response after yielding of the splice bar was also similar.

As expected, splice beams with an increased lap length also had an increased bond strength, as can be seen in Figure 16 through Figure 22 by comparing the failure load of the beams with shorter splices (denoted by "S" in their name) to the failure load of beams with longer splices (denoted by "L"). The addition of stirrups also caused an increase in the failure load. The addition of stirrups to the short lap length (denoted by "ST") typically caused the failure load to be greater than or equal to the failure load of a similar specimen with the longer lap length but no stirrups (denoted by "LN").

None of the beams with the shorter lap splice and no stirrups reached yielding before failure. Four of the beams with the longer lap splice and no stirrups reached the initiation of yielding (as determined from strain gages) before failure. Of the nine beams with stirrups and the shorter lap splice, one reached significant yielding before failure (C8-ST), two reached the yielding plateau before failure (B6-ST and B8-ST), and four failed shortly after reaching the initiation of yielding. All of the beams with the longer lab splice and stirrups except one (A8-LT) exhibited a significant amount of yielding before failure. Beam A8-LT just reached the yield plateau before failure, as compared to the response of B8-LT and C8-LT in Figure 20.
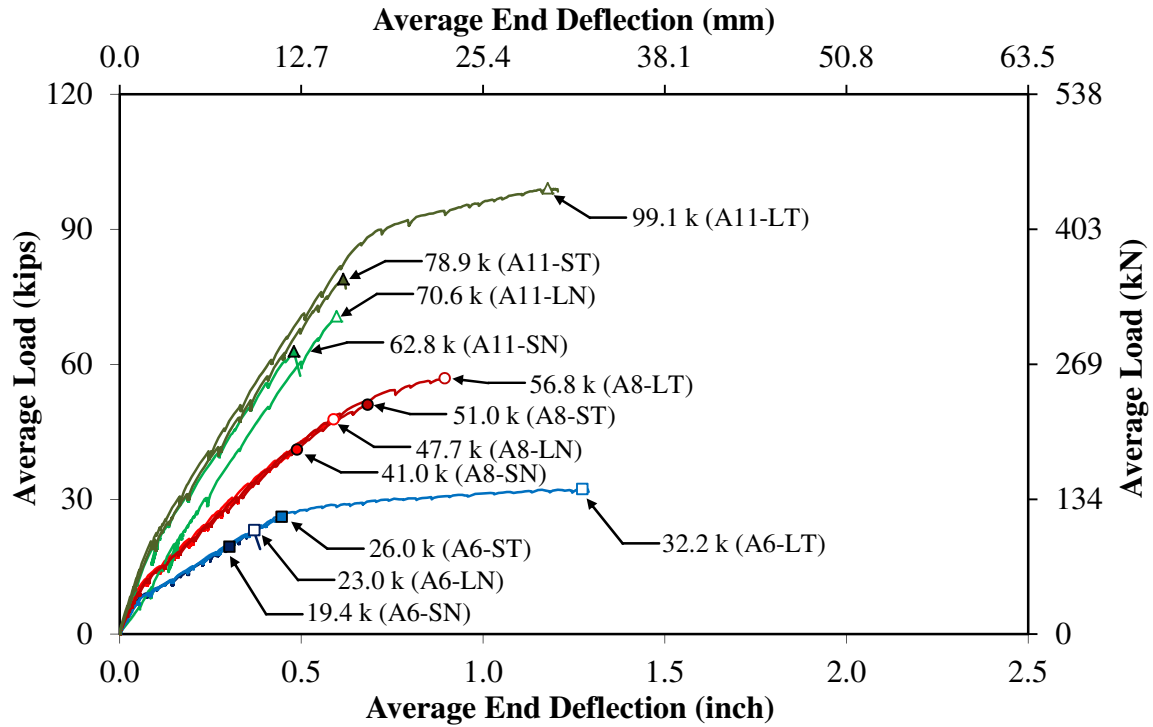
Figure 16. Graph. Load-Deformation Response of SG Mix Specimens.
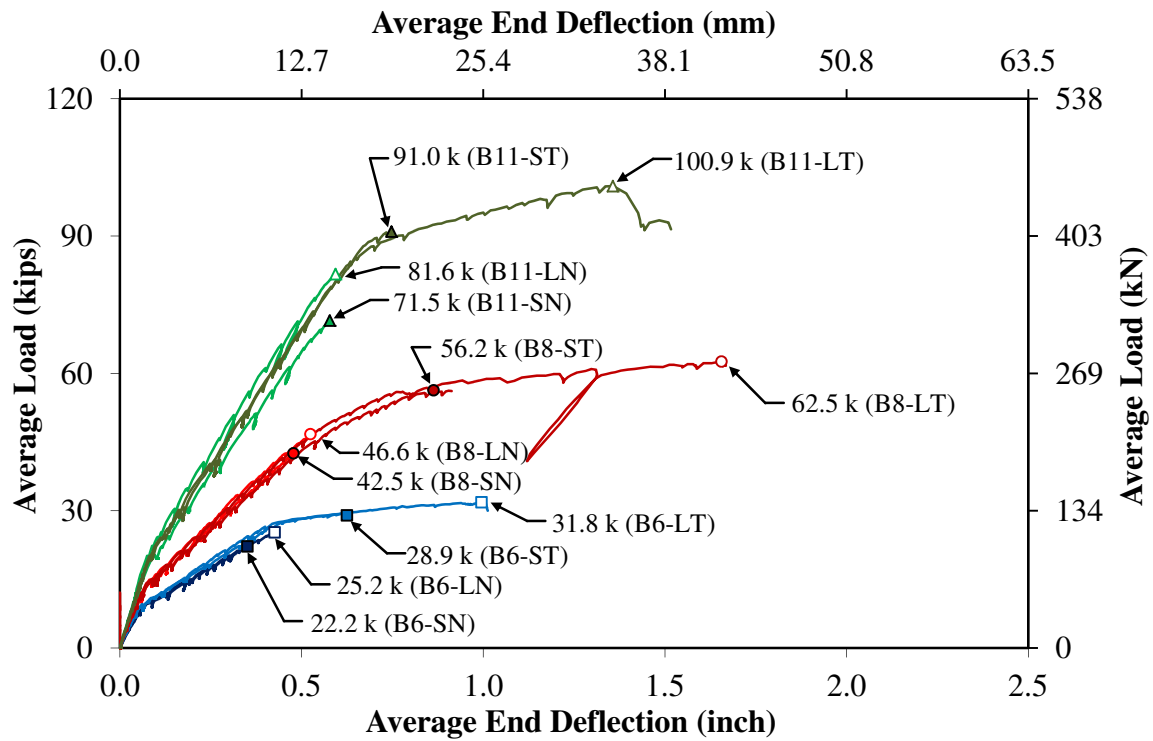
Figure 17. Graph. Load-Deformation Response of UG Mix Specimens.
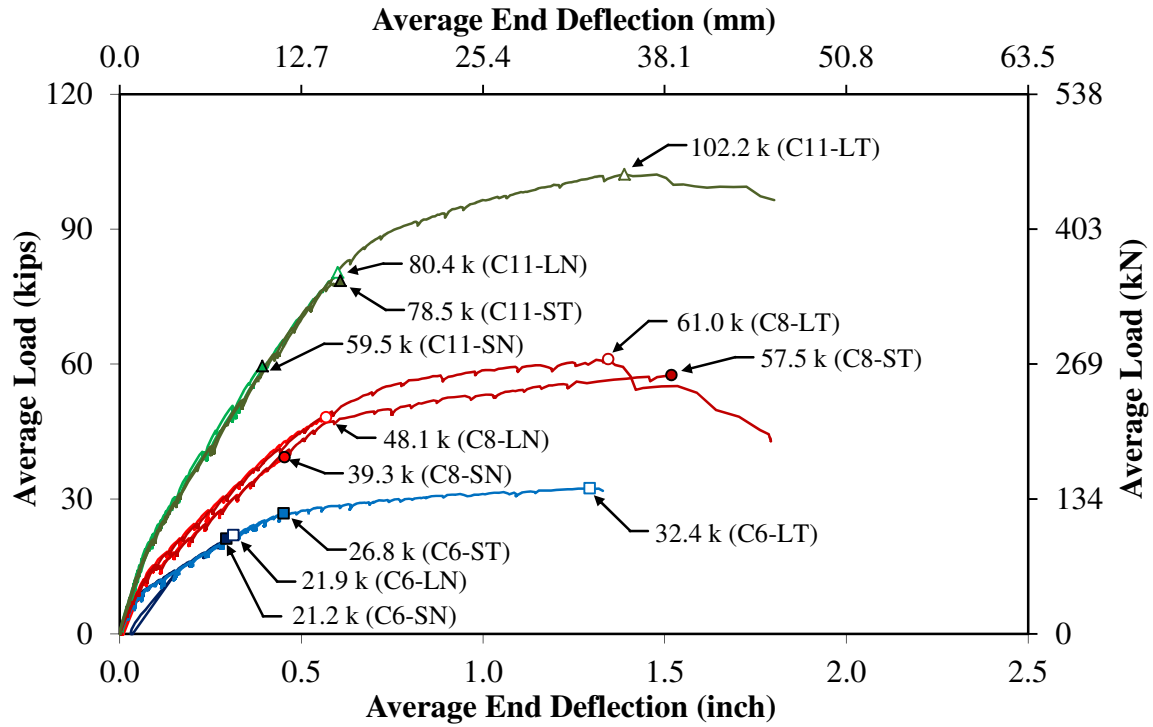
Figure 18. Graph. Load-Deformation Response of HG Mix Specimens.
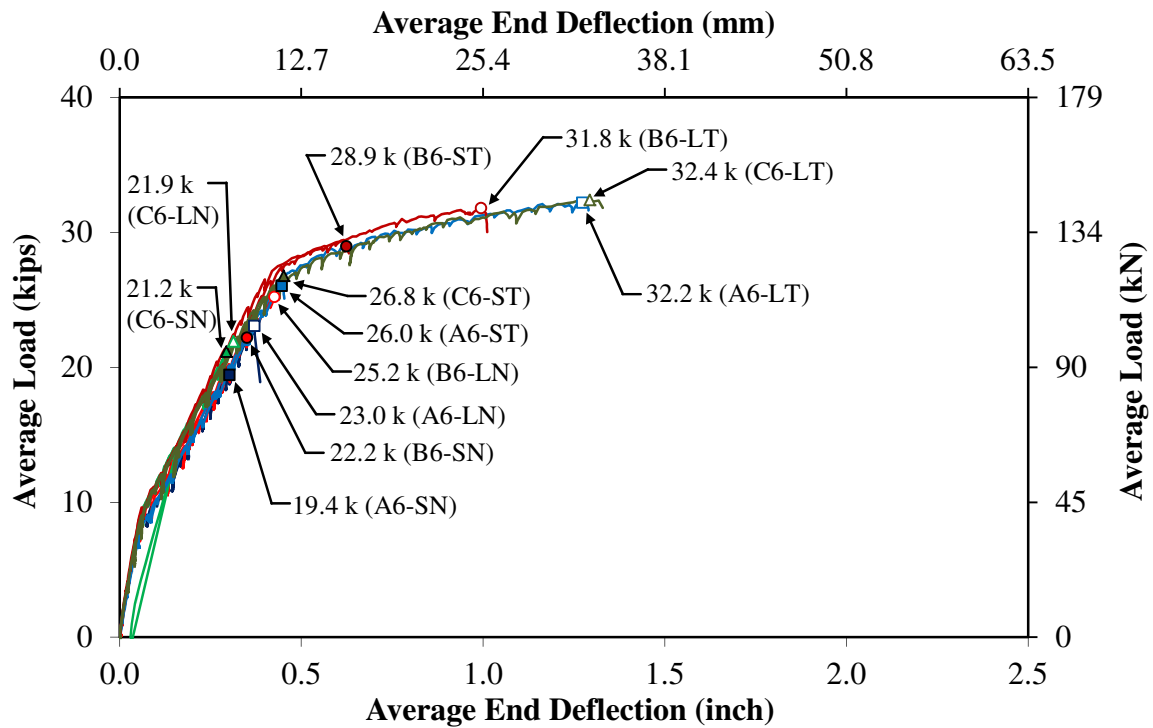
Figure 19. Graph. Load-Deformation Response of Specimens with #6 Bars.
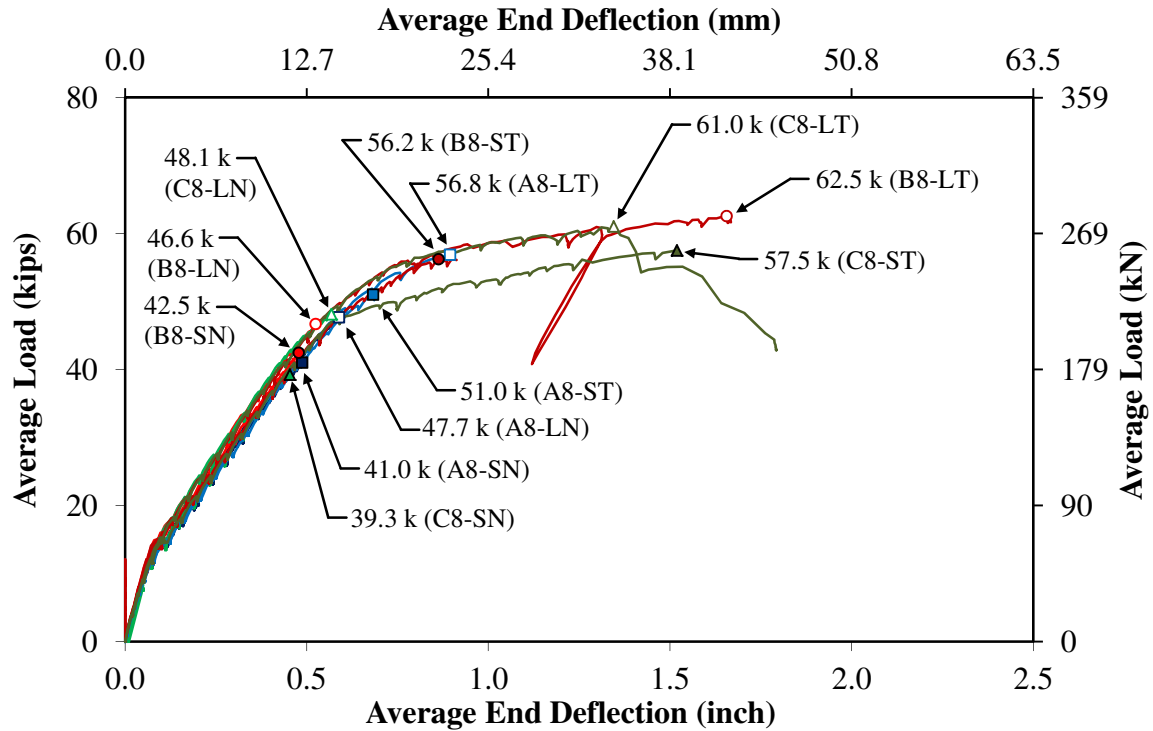
Figure 20. Graph. Load-Deformation Response of Specimens with #8 Bars.
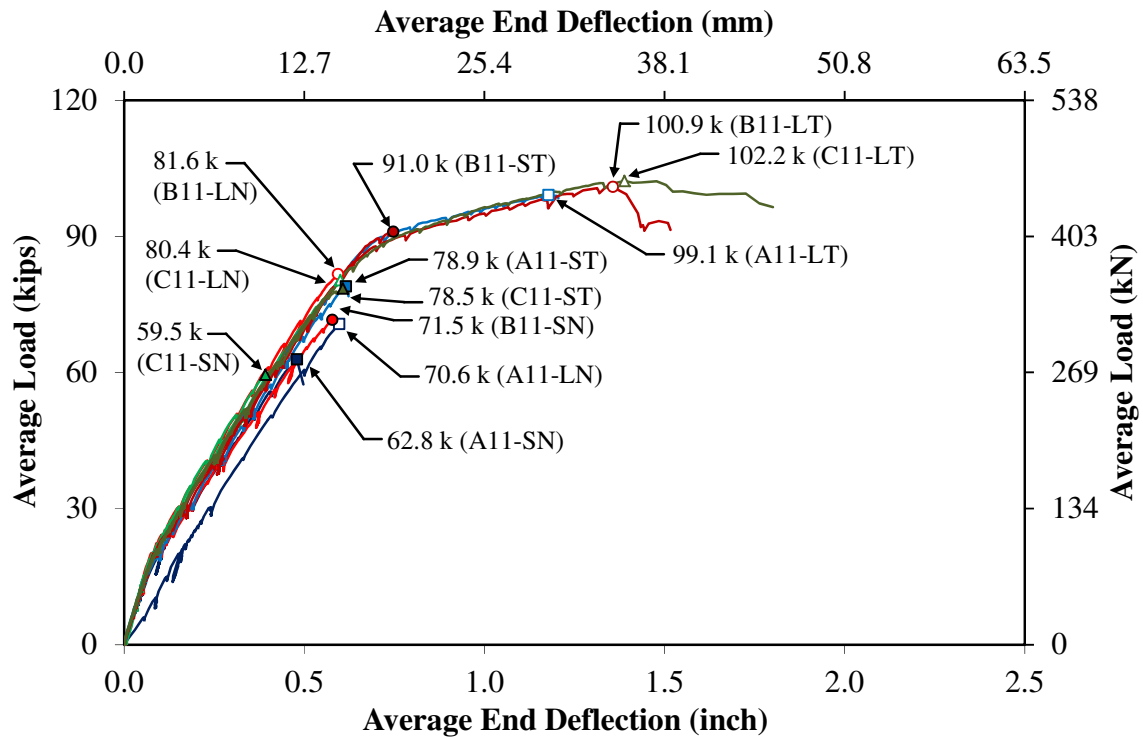
Figure 21. Graph. Load-Deformation Response of Specimens with #11 Bars.
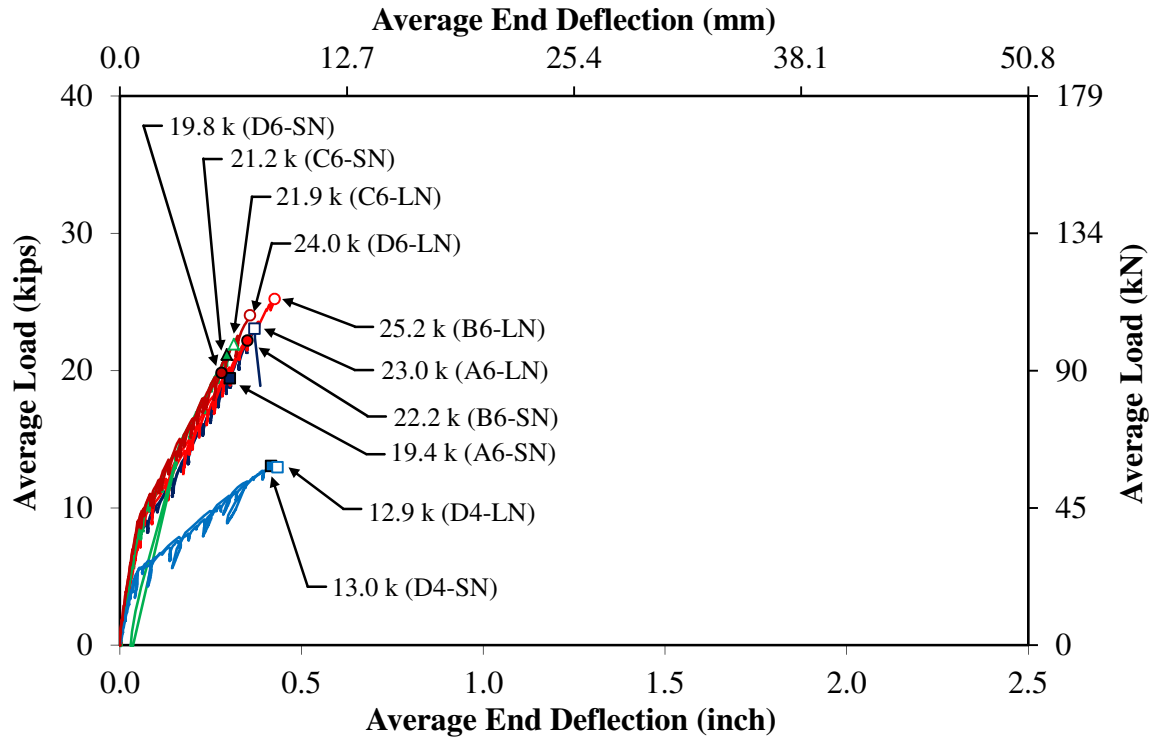
Figure 22. Graph. Load-Deformation Response of Specimens with #4 or #6 Bars and no Stirrups.

STRESS IN THE SPLICED BAR AT FAILURE

A determination of the average stress in the spliced bar at failure (f_s) is necessary for comparisons of the test results with prediction expressions (i.e., descriptive expressions for bar stress and design expressions for development length). The average bar stress at failure was calculated using the moment curvature method and idealized stress-strain curves for concrete and reinforcing bars described in ACI 408-03.[9] The parabolic stress-strain curve for concrete described in ACI 408-03 is for NWC. The following sections describe the ACI 408-03 method and the procedure used to validate the ACI 408-03 method for the 40 LWC splice beam tests that are part of this study.

The average stress in the spliced bar at failure was determined by first calculating the bending moment in the specimen at failure. A table of calculated average reinforcement stress and corresponding bending moment was determined for each specimen. The failure stress for a specimen was then determined by interpolating between failure moments in the table.

The moment in the specimen at failure included the effects of the applied load and the specimen self-weight and was determined for a section at the middle of the lap splice. The moment due to the applied load was calculated as the average of the jack forces at failure multiplied by the measured distance from the center of the jacks to the center of the roller supports. The moment

35

due to the specimen weight considered a concrete unit weight determined from the nominal unit weight of concrete cylinders measured at the time of test.

For each specimen, a table was created of average reinforcement stress and corresponding bending moment. The table was based on measurements of the test-setup, beam cross-section dimensions, concrete cylinder compressive strength and reinforcing bar yield strength. Rows in the table were calculated for the moment and corresponding average reinforcement stress at the initiation of yielding, the initiation of strain-hardening, and at seven other points. The seven points corresponded to assumed values of extreme compression fiber strain ranging from 150 microstrain to an assumed strain at concrete compressive failure of 0.003 inch/inch (0.003 mm/mm).

MOMENT CURVATURE METHOD IN ACI 408-03

The stress-strain curve for NWC in compression utilized in ACI 408-03 (9) is a simple parabola. The assumed concrete strain at maximum compressive stress, ε_o, is based on experimental curves of NWC shown by Nilson.[31] Table 5.1 in ACI 408-03 listed valves for ε_o as a function of the compressive strength, f'$_c$.

The stress-strain curve for reinforcing bars utilized in ACI 408-03 is a tri-linear model that includes a yield plateau and strain-hardening. The initiation of strain-hardening is a function of the grade of steel.

Other assumptions considered in the moment curvature method in ACI 408-03 include neglecting the tensile strength of concrete and assuming the reinforcing bars are continuous when considering their cross-sectional area.

MOMENT CURVATURE METHOD FOR LWC

Research by Wang et al. (32) has shown that ε_o for NWC does not vary substantially with the compressive strength. The ε_o of LWC, however, increases with compressive strength. At higher compressive strengths, the ε_o of LWC can be much larger than the ε_o of NWC. The effect that the larger ε_o of LWC has on the average stress in the spliced bar at failure was evaluated.

A model for the compressive stress-strain relationship of lightweight concrete (LWC) was developed by Wang et al. (32) based on tests of lightweight concrete cylinders with compressive stresses that ranged from 3 ksi to 8 ksi (21 MPa to 55 MPa). Their expression is given by Eq. 21, and has different coefficients for the ascending portion of the curve and for the descending portion of the curve. Wang et al. also developed the linear relationships for the ε_o of LWC and NWC given by Eq. 22 and Eq. 23, respectively.

$$\text{Ascending branch: } f_c = f_c' \frac{[1.325(\varepsilon_c/\varepsilon_o) - 0.808(\varepsilon_c/\varepsilon_o)^2]}{[1 - 0.675(\varepsilon_c/\varepsilon_o) + 0.192(\varepsilon_c/\varepsilon_o)^2]} \qquad \text{(Eq. 21a)}$$

$$\text{Descending branch: } f_c = f_c' \frac{[0.232(\varepsilon_c/\varepsilon_o) - 0.095(\varepsilon_c/\varepsilon_o)^2]}{[1 - 1.768(\varepsilon_c/\varepsilon_o) + 0.905(\varepsilon_c/\varepsilon_o)^2]} \qquad \text{(Eq. 21b)}$$

$$\varepsilon_o = 0.00020f_c' + 0.00217 \qquad \text{(Eq. 22)}$$

$$\varepsilon_o = 0.000125f_c' + 0.00230 \qquad \text{(Eq. 23)}$$

A comparison of the ε_o for NWC predicted by Table 5.1 in ACI 408-03, and the Wang et al. expressions for LWC and NWC (Eq. 22 and Eq. 23) are shown in Figure 23. The expression proposed by Wang et al. for NWC predicts a much larger ε_o for a given f'_c than the expression used in ACI 408-03. The Wang et al. expression for LWC predicts a slightly larger ε_o than their NWC expression, and the difference increases as f'_c increases.

A moment curvature analysis indirectly requires calculating the area and centroid under the strain-strain curve for concrete in compression. The use of a parabolic expression to approximate Eq. 21 was investigated to simplify the analysis procedure.

The stress-strain curve predicted by Eq. 21 for LWC with an f'_c of 8 ksi (55 MPa) is shown in Figure 24 along with a simple parabolic stress-strain curve using Eq. 22 for ε_o. As seen in the figure, the parabolic expression makes a reasonable approximation of Eq. 21. At strains near ε_o, there is a reasonably large difference between the area under the ACI 408-03 stress-strain curve, which is also shown in Figure 24, and the parabolic approximation of Eq. 21. The parabolic approximation should be able to show whether or not a larger ε_o for LWC has a significant effect on the calculated average bar stress.
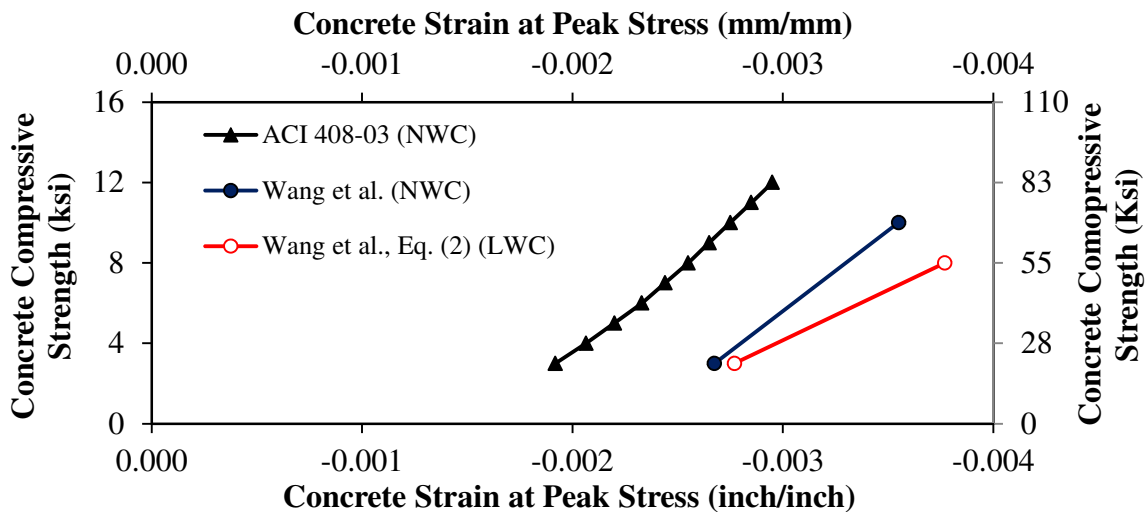
Figure 23. Graph. Expressions for Concrete Strain at Peak Stress from ACI 408-03 expression and Wang et al. expression.
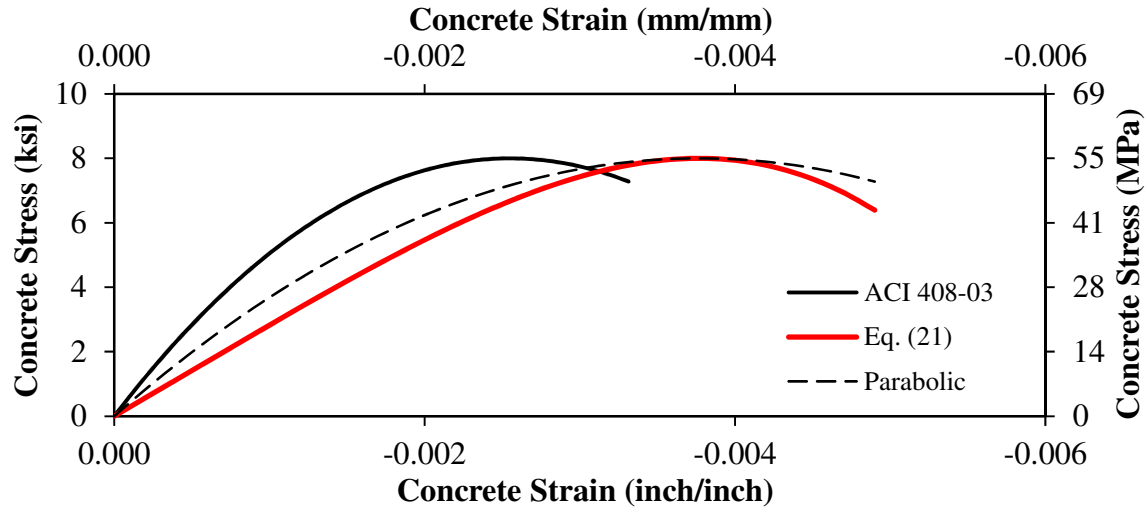
Figure 24. Graph. Expressions for Concrete Stress-Strain Curves from ACI 408-03 Expression, Wang et al., and a parabola.

VALIDATION OF THE ACI 408-03 METHOD FOR LWC

The expression for ε_o described in ACI 408-03 was developed for NWC. The f_s were calculated for the 40 LWC splice beam specimens that are a part of this study using the method described in ACI 408-03. The f_s were recalculated using the parabolic approximation of the Wang et al. stress-strain curve for LWC in compression given by Eq. 21, where ε_o was determined using Eq. 22.

The results of this comparison showed that the moment-curvature analysis using the parabolic approximation gave an f_s that was slightly larger than the f_s using the ACI 408-03 stress-strain curve, except for four beams where both methods predicted the yield stress. The average percent difference of the calculated f_s using the two curves was only 0.76%, with a maximum of 1.20%, and a minimum of 0.26%. The ACI 408-03 stress-strain curve was selected to maintain consistency with the ACI 408-03 standard, and because the influence of the larger ε_o to account for LWC did not produce a significant difference in the calculated f_s.

The f_s determined using the ACI 408-03 method for all 40 splice beam specimens is given in Table 7 and Table 8. The average bar strain predicted by moment curvature analysis is shown in Figure 25 and Figure 26 for two splice beam specimens, one with stirrups and one without stirrups. The strain measured in the spliced bar at two locations is also shown in the figure, and compares well with the predicted strain. A comparison of the predicted and measured strain for all 40 splice beams is given in Appendix C.
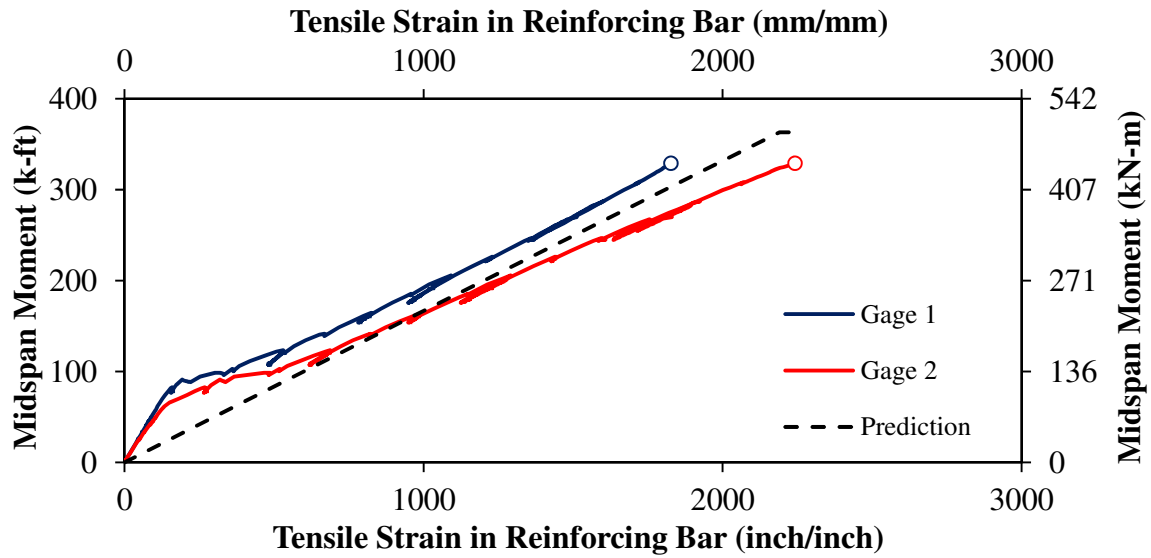
Figure 25. Graph. Measured versus Predicted Average Reinforcing Bar Strain for B11-LN
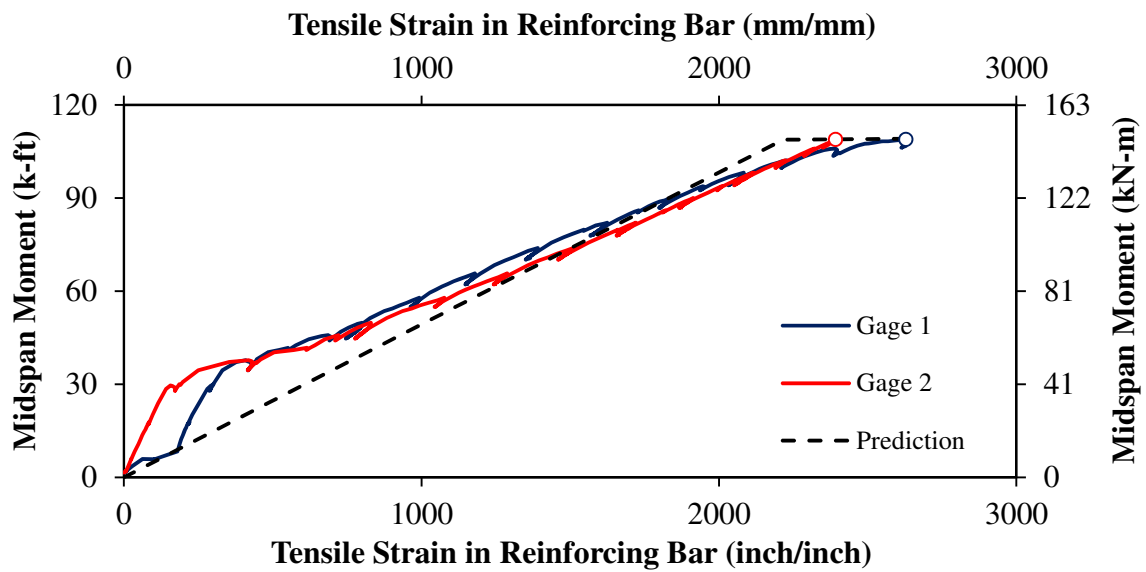
Figure 26. Graph. Measured versus Predicted Average Reinforcing Bar Strain for C6-ST.

DISPLACEMENT DUCTILITY

The average bar stress at failure (i.e., ultimate) is an important factor in determining whether or not a lap splice is long enough to achieve an adequate bond strength. Research on high-strength concrete (>10 ksi (69 MPa)) has shown that bar stress alone may be inadequate to ensure ductility in lap splices.[14,15,17] In a study by Azizinamini et al. (17), the minimum amount of confining reinforcement to achieve a defined level of displacement ductility was determined based on tests of lap spliced bars in concrete with compressive strengths ranging from 12.7 ksi to 16.5 ksi (87.5 MPa to 113.7 MPa).

This section will describe the evaluation of the displacement ductility of the 40 LWC splice beam specimens tested as part of the LWC research program at TFHRC. The procedure described by Azizinamini et al. (17) was used to determine the displacement ductility. The method proposed by Azizinamini et al. (17) for determining the target displacement ductility was also applied to the 40 LWC splice beam specimens.

DETERMINATION OF THE DISPLACEMENT DUCTILITY

Displacement ductility was defined as the ratio of the displacement at ultimate load (Δ_u) to the displacement at yielding (Δ_y). The displacement at ultimate load can be determined by using the displacement corresponding to the peak load from the load-deformation response of each test. The yield displacement is more difficult to determine and depends upon the definition of Δ_y. Possible choices for Δ_y are the displacement corresponding to the first measured strain greater than the yield strain in a spliced bar, or displacement corresponding to the first observed reduction in stiffness near the anticipated yielding on the load-deformation curve. The definition used by Azizinamini et al. (17) is the intersection of lines tangent to the load-deformation curve before and after yielding. The displacement corresponding to the intersection is defined as Δ_y.

This method was applied in this study as shown in Figure 27. Two linear regression lines were determined from the load-deformation curve. One regression line was determined on the curve before yielding across a range of loads. The load range was selected to start above cracking and below the change in slope corresponding to the onset of yielding. A different load range was selected for each nominal bar size. The load ranges for the #6, #8, and #11 bars selected for this study were 10 to 25 kips (45 to 111 kN), 15 to 40 kips (67 to 178 kN), and 25 to 60 kips (111 to 267 kN), respectively. A second regression line was determined after the onset of yielding. The range of data used in the regression was based on displacement. A default lower displacement value was based on nominal bar size and was selected to be slightly higher than the yield displacement observed from the load-displacement curve. The displacement value used as the upper limit was the displacement at ultimate load. The lower limit needed to be reduced slightly for tests failing near the yield displacement (Δ_u/Δ_y near unity). The selected lower displacement limit for the #6, #8, and #11 bars were 0.5 inch (13 mm), 0.8 inch (20 mm), and 0.8 inch (20 mm), respectively. The data ranges used to determine the regression lines for Specimen C11-LT are shown in Figure 27.
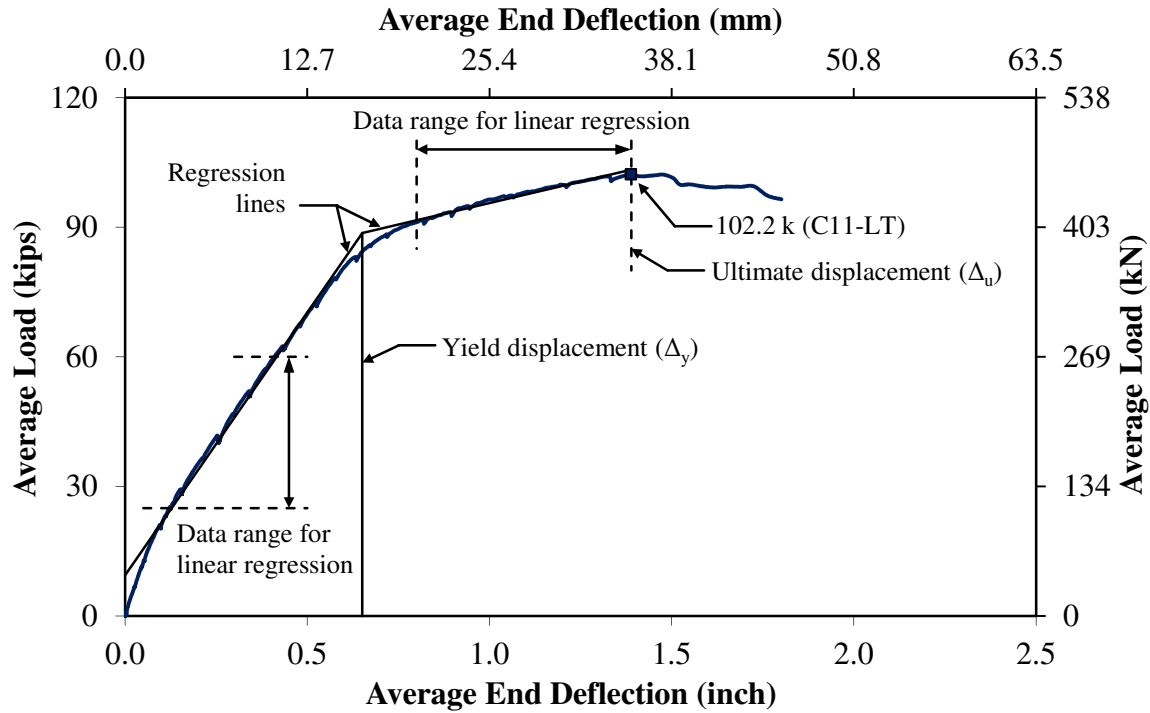
Figure 27. Graph. Determination of Yield Ductility for Specimen C11-LT.

The yield displacement (Δ_y) was determined for the 19 splice beam specimens in this study that reached yielding before ultimate load. In this analysis, a splice beam specimen that did not clearly reach yielding was defined as having yielded if its average end deflection at ultimate load was greater than or equal to the yield displacement of specimens with the same bar size. Table 9 gives the Δ_y, Δ_u, and displacement ductility (Δ_u/Δ_y) of the three specimens without stirrups and the 16 specimens with stirrups that achieved a Δ_u/Δ_y greater than unity. The only specimens without stirrups to achieve a Δ_u/Δ_y greater than unity had #8 longitudinal bars and the longer splice length (longer ℓ_s/d_b ratio). For the specimens with stirrups, two specimens with the shorter lap splice (shorter ℓ_s/d_b ratio), did not achieve a Δ_u/Δ_y greater than unity.

Approximately half of the specimens tested did not reach yielding. Of the specimens that did reach yielding, 12 did not reach a Δ_u/Δ_y greater than 2.0 and only two reached the minimum target displacement ductility of 2.7 described in the research by Azizinamini et al. (17). This result was not unexpected based on the ℓ_s/d_b ratios selected for this research study. The specimens were designed following the concept used for most of the test data in the ACI Committee 408 Database. That is, the ℓ_s/d_b ratios need to be low enough that the specimen does not yield during the test. This allows empirical expressions to be developed that predict bond strength that is controlled by splitting failure. There are 478 test results for bottom bars in the ACI Committee 408 Database.[9] Of these test results, only 15% reported an average bar stress greater than yielding, and 27% of these tests were from Azizinamini et al. (15).

In the analysis of bond strength performed by Orangun et al. (13), the result of any test that did yield was disregarded. As described by the authors, the results of tests with yielding bars were disregarded for three reasons: the failure mechanism changes after yielding, the test results they used from the literature did not distinguish between failure mechanisms after yielding, and their expression predicted bond strength and not ductility.

Table 9. Splice Beam Displacement Ductility.

Specimen Name[†]	Yield Displacement (Δ_y) (inch)	Ultimate Displacement (Δ_u) (inch)	Displacement-Ductility (Δ_u / Δ_y)	Target Displacement-Ductility[‡]	A_{sp} / A_{sr}[*]
A8-LN	0.467	0.590	1.26	3.70	--
B8-LN	0.410	0.525	1.28	3.70	--
C8-LN	0.467	0.569	1.22	3.70	--
A6-LT	0.469	1.274	2.72	5.09	0.83
B6-ST	0.449	0.625	1.39	5.09	0.56
B6-LT	0.434	0.995	2.29	5.09	0.83
C6-ST	0.327	0.452	1.38	5.09	0.56
C6-LT	0.443	1.294	2.92	5.09	0.83
A8-ST	0.549	0.683	1.24	3.70	0.46
A8-LT	0.610	0.895	1.47	3.70	0.62
B8-ST	0.669	0.864	1.29	3.70	0.46
B8-LT	0.616	1.656	2.69[$]	3.70	0.62
C8-ST	0.573	1.519	2.65	3.70	0.46
C8-LT	0.622	1.345	2.16[$]	3.70	0.62
A11-ST	0.587	0.616	1.05	2.69	0.31
A11-LT	0.656	1.178	1.80	2.69	0.47
B11-ST	0.624	0.748	1.20	2.69	0.31
B11-LT	0.686	1.357	1.98[$]	2.69	0.47
C11-LT	0.651	1.389	2.13[$]	2.69	0.47

Notes:
[†] Specimen Name of form $#-%&, where: $ = Concrete Mix: A – SG, B – UG, C – HG, D – SD;
    # = Bar size; % = Relative Splice length: S – short splice (smaller ℓ_s/d_b), L – long splice (longer ℓ_s/d_b);
    & = Transverse reinforcement: N – no stirrups along splice, T – stirrups along splice
[‡] Target displacement ductility computed based on method described in Azizinamini et al.
[*] Ratio of total area of stirrups along splice (A_{sp}) to the a quantity of 60% of the bar area spliced (A_{sr})
[$] Specimen had a flexural compression failure observed as crushing of concrete at bottom surface before STF
Units: 1.0 inch = 25.4 mm

TARGET DUCTILITY

A target ductility (μ_{target}) of 2.7 for #11 bars was determined by Azizinamini et al. (17) as the desirable minimum displacement ductility. Target displacement ductility for other bar sizes was calculated using Eq. 24. Table 9 gives the target ductility determined for the LWC splice beam specimens.

The total area of all transverse reinforcement (A_{sp}) and the value A_{sr} given by Eq. 25 were determined for each of the 19 LWC splice beams that achieved a Δ_u/Δ_y greater than unity. The ratio of A_{sp} to A_{sr} is given in Table 9. Azizinamini et al. (14,15) performed a series of tests on splice beam specimens with stirrups. The specimens had a lap splice length determined from ACI 318-95 (24) for splices with no stirrups. Each series had the same bar size, concrete cover thickness, and lap splice length, but with increasing amounts of transverse reinforcement. The ratio A_{sp}/A_{sr} was determined for the specimens and plotted versus displacement ductility. The intersection of a line passing through the A_{sp}/A_{sr} data points and μ_{target} was used to determine the required minimum amount of stirrups (through A_{sp}) for a ductile failure. The A_{sp}/A_{sr} required for #8 and #11 bars in 15 ksi (103 MPa) NWC was proposed to be 0.34 and 0.54, respectively.

$$\mu_{target} = 2.7 \frac{0.0164}{(A_s/bd)} \tag{Eq. 24}$$

$$A_{sr} = 0.60nA_b \tag{Eq. 25}$$

The A_{sp}/A_{sr} values given in Table 9 for the 19 LWC splice beam specimens are larger than the value recommended by Azizinamini et al. (17) for #8 bars and smaller than the value recommended for the #11 bars. The recommend values of A_{sp}/A_{sr} are based on the assumption that the lap splice length was equal to the ℓ_d determined using the expressions in the ACI 318-95 specifications (Eq. 12). As described previously in this document, the splice beam specimens in this study were designed with ℓ_s/d_b ratios less than that specified in ACI 318-11 (same expression as ACI 318-95) to allow the specimens to reach ultimate load before yielding. So it is expected that the LWC splice beams did not reach high levels of ductility.

The displacement ductility achieved by the LWC specimens is plotted versus lap splice length (ℓ_s) in Figure 28, Figure 29, and Figure 30 for the specimens with #6 bars, #8 bars, and #11 bars, respectively. Each figure shows the target ductility determined using Eq. 24 as a horizontal line and the development length (ℓ_d) determined using the expressions in the AASHTO LRFD Specifications (Eq. 10) and ACI 318-11 (Eq. 12) as vertical lines. Another vertical line in each figure shows the design lap length for Class C splices ($\ell_d \times 1.7$) in the AASHTO LRFD Specifications (1).
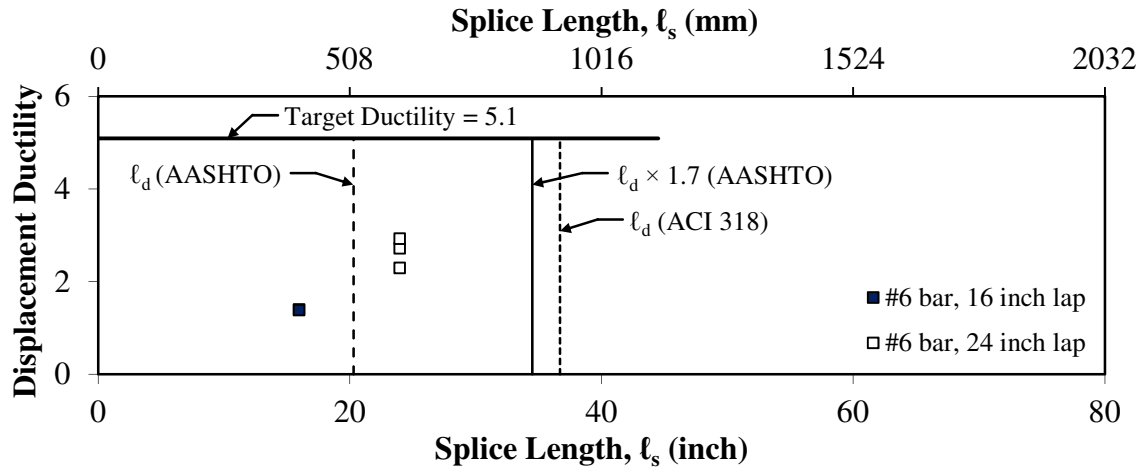
Figure 28. Graph. Displacement Ductility versus Splice Length for #6 bars.
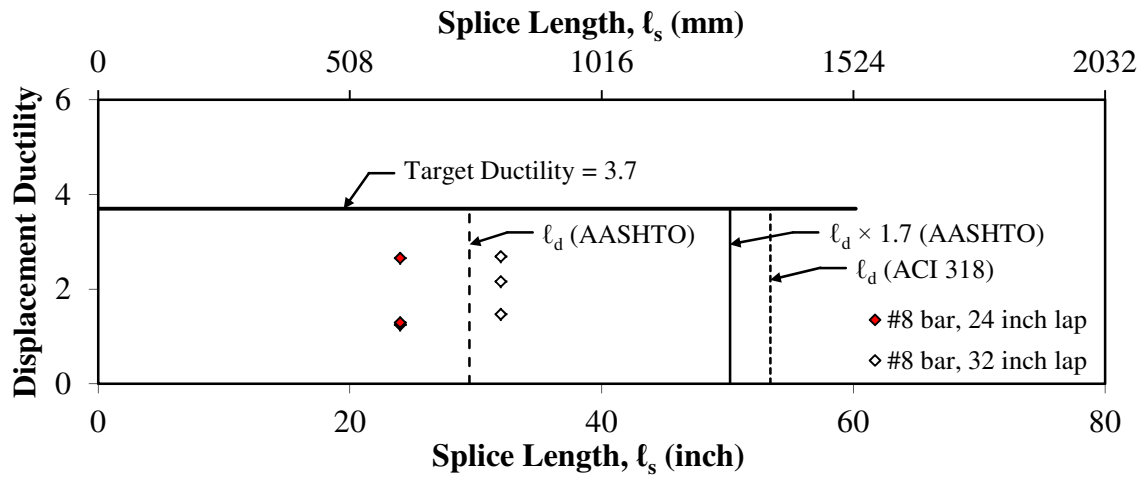
Figure 29. Graph. Displacement Ductility versus Splice Length for #8 bars.
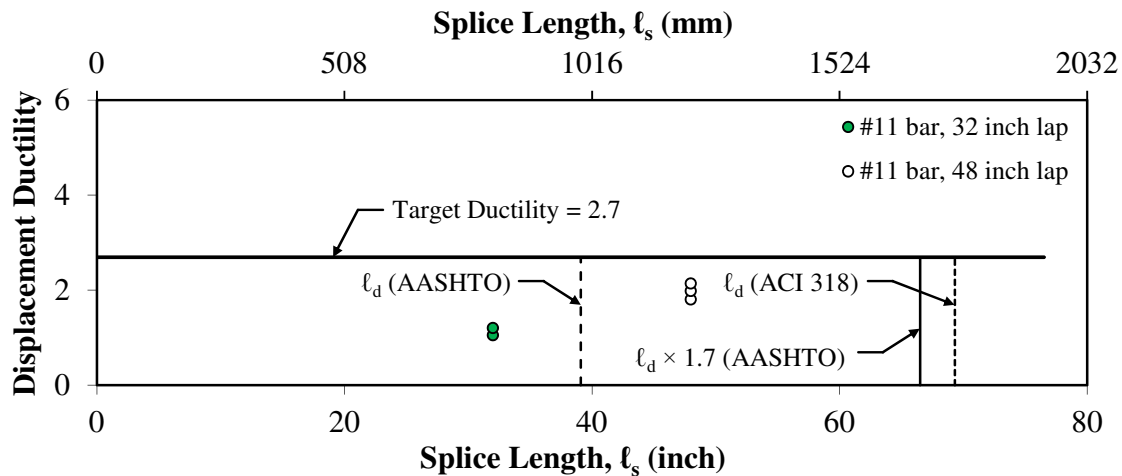
Figure 30. Graph. Displacement Ductility versus Splice Length for #11 bars.

44

In each figure, the vertical line representing the expression for ℓ_d in the AASHTO LRFD Specifications is in the middle of the data from the LWC specimens with the smaller and larger ℓ_s/d_b ratios. Also the data in each figure is below the horizontal line representing the μ_{target} proposed by Azizinamini et al. The vertical lines representing the ℓ_d proposed by ACI 318-11 and the $\ell_d \times 1.7$ specified by the AASHTO LRFD Specifications for the design of Class C splices are near each other and are approximately twice the ℓ_d specified by AASHTO LRFD Specifications for development length. It is difficult to determine from the figures whether specimens tested at the longer ℓ_s proposed by ACI 318-11 would result in a displacement ductility greater than μ_{target}.

CONCLUDING REMARKS FOR THE DISPLACEMENT DUCTILITY ANALYSIS

Nineteen LWC splice beam specimens had a displacement ductility greater than unity. None of the specimens had a displacement-ductility greater than μ_{target} given by Eq. 24, although three specimens did have a ductile flexural compression (FC) failure that included yielding of the rebar and concrete crushing. The splice lengths used in this study and the limited number of splice beam specimen tests resulting in an FC failure did not allow an experimental determination of the minimum displacement ductility for the LWC specimens in this study. The expression for μ_{target} given by Eq. 24 was developed for high-strength (up to 16 ksi (110 MPa)) NWC. The applicability of this expression for LWC needs to be considered.

The cross sections of the LWC specimens in this study were made wider for specimens with larger bar sizes in order to maintain a constant ratio of concrete cover to bar diameter and clear spacing to bar diameter. The effect was that specimens with larger bars had a slightly larger cross sectional area and a much larger rebar cross sectional area. This resulted in lower reinforcement ratios (A_s/bd) for the larger specimens.

Specimens B8-LT and C8-LT with the longer ℓ_s/d_b ratios had FC failures and achieved displacement ductilities of 2.69 and 2.16, respectively. Specimen C8-ST with the smaller ℓ_s/d_b ratio had a ductility of 2.65 but still had a splitting failure. The target ductility from Eq. 24 was 3.7 for these specimens. Two specimens with #11 bars, B11-LT and C11-LT, had displacement ductilities of 1.98 and 2.13 and had ductile FC failures. The target ductility for these specimens was 2.7 as determined from Eq. 24. Three specimens with #6 bars had displacement ductilities of 2.29, 2.72, and 2.92 and still had splitting tensile failures. The splice beams with #11 bars had larger reinforcement ratios than the specimens with #8 bars but achieved a FC failure at a lower displacement ductility. The beams with #6 bars achieved higher displacement ductility than the beams with #8 or #11 bars but still exhibited splitting tensile failures. This supports the concept proposed by Azizinamini et al. (17) that the target displacement ductility for lap splices should increase as the reinforcement ratio decreases.

The beams with #8 bars had A_{sp}/A_{sr} ratios greater than the ratio shown to cause ductile failures (17), however only two out of six LWC specimens tested with #8 bars had a ductile failure. This

indicates that a minimum A_{sp}/A_{sr} ratio alone can be inadequate to ensure a ductile failure and that a minimum lap length is also necessary.

COMPARISON OF BAR STRESS WITH SPLICE LENGTH

This section includes a comparison of the average bar stress at failure (f_s) to lap splice length (ℓ_s) and the amount of transverse reinforcement (A_{tr}) for the 40 LWC splice beam specimens. The purpose of the comparison is to examine the effect of different variables on bar stress. These variables include concrete mix, bar size, splice length, and the presence of transverse reinforcement (i.e., stirrups). The analysis includes a separate investigation of the effect of different methods commonly used to normalize bar stress and lap splice length. This separation is intended to decouple the effects of LWC and bar size from the methods used to normalize bar stress and normalize splice length.

The variables f_s, ℓ_s, and A_{tr} are commonly normalized in descriptive expressions for bar stress and design expressions for development length. In this section, the average bar stress is normalized by three factors: $\sqrt{f_c'}$, $f_c'^{0.25}$, and f_{ct}. The normalized splice length is given by a simple ℓ_s/d_b ratio, $\ell_s/d_b(c_b+K_{tr})/d_b$ based on ACI 318-11 (16), and $\ell_s(c_{min}+0.5d_b)/A_b$ based on Zuo and Darwin (12). The difference between the f_s of a specimen with stirrups to a companion specimen without stirrups is given by Δf_s. The Δf_s is compared to the normalized area of transverse reinforcement that is given by $(c_b+K_{tr})/d_b$ based on ACI 318-11 and $t_r t_d (NA_{tr}/n)/A_b$ based on Zuo and Darwin.

The normalized bar stresses and normalized splice lengths are shown in Figure 31 through Figure 37. Each figure has a left graph with groups by concrete mix (i.e., HG, SD, SG, or UG) and a right graph with groups by bar size (i.e., #4, #6, #8, or #11). The specimens with and without stirrups are separated in each figure.

Least-squares linear regression lines are shown in Figure 31 through Figure 37 by concrete mix (left figure) or bar size (right figure). Also, regression lines are shown for all specimens with stirrups (T) and all specimens without stirrups (N). The slope of the regression lines for individual mixes or bar sizes can be compared to the slope of the entire group. This can be observed in the figure as whether the regression lines are parallel or intersect. Intersecting regression lines show that the normalized bar stress of one group of concrete mixes or bar sizes was affected by an increase in the normalized splice length more or less than the other groups.

CONCRETE MIX

Table 10 gives the ratio of the mean normalized bar stress for each concrete mix to the mean normalized bar stress of the LWC specimens (mix-to-mean ratio) with the girder concrete mixes (i.e., the SD mix was not included). The normalized bar stress for the SG mix was between 3% and 9% less than the all specimen mean depending upon which factor was used for normalization

(i.e., $\sqrt{f_c'}$, $f_c'^{0.25}$, or f_{ct}). The HG mix and the UG mix had mix-to-mean ratios that were typically greater than unity and had mean-to-mix ratios that were only 4% different or less depending upon the normalizing factor. The mix-to-mean ratios were also similar for specimens with and without stirrups, with differences less than 1% for the SG mix and less than 3% for the HG and UG mixes.

In Figure 31 through Figure 35 the regression lines for the specimens without stirrups are nearly parallel. For specimens with stirrups, the slope of the regression line for the UG mix is less than the regression line for all specimens with stirrups in each figure indicating that for the same increase in normalized splice length, there was a smaller increase in normalized bar stress.

BAR SIZE

Table 10 also gives the ratio of the mean normalized bar stress for each bar size to the mean normalized bar stress of the #6, #8, and #11 bars used in the LWC specimens (bar size-to-mean ratio) with the girder concrete mixes. In Table 10, the #8 bars had bar size-to-mean ratios of 1.09 and 1.10 for specimens with and without stirrups, respectively, regardless of the factor used for normalization. The #6 bars had bar size-to-mean ratios near unity and the #11 bars had ratios between 0.92 to 0.93, regardless of the presence of stirrups or the factor used for normalization.

In Figure 31 through Figure 35 the regression lines for the specimens with stirrups (T) are nearly parallel. For specimens without stirrups (N), the slope of the regression line for the #11 bars was parallel to the average slope for all of the N-specimens. The slope of the regression line for the #8 bars was greater than the average slope and the slope of the regression line for the #6 bars was less than the average slope. There were only two tests on #4 bars using the SD mix, and the f_s for these two tests were nearly the same, resulting in a nearly horizontal line in Figure 31 through Figure 35.

FACTORS USED TO NORMALIZE BAR STRESS

The difference between the largest and smallest mix-to-mean ratio in Table 10 was 6% for specimens without stirrups when using f_{ct} as the normalizing factor. The difference increases to 9% and 14% when using $f_c'^{0.25}$ and $\sqrt{f_c'}$ as the normalizing factors, respectively. For specimens with stirrups, the difference between the mix-to-mean ratios was greater, but showed the same trend.

In Table 10, the difference between the mix-to-mean ratios determined using different normalizing factors was less than 3% and for bar size-to-mean ratio the difference was typically less than 1%. For a given normalizing factor, the difference between the largest and smallest bar size-to-mean ratio was 17% regardless of the presence of stirrups or the factor used for normalization.

Table 10. Ratio of Normalized Bar Stress by Girder Concrete Mix and Bar Size to Mean Normalized Bar Stress of Group for 36 LWC Splice Beam Specimens (18 Specimens without Stirrups (N) and 18 Specimens with Stirrups (T)).

Normalized Bar Stress	Data Group	Group Subsets	Measurement	Specimens without Stirrups (N)	Specimens with Stirrups (T)
$f_s/\sqrt{f_c'}$	Concrete Mix	All Mixes	Group Mean (μ_G)	16.31	20.89
		HG	$(f_s/\sqrt{f_c'})_{HG} / \mu_G$	1.035	1.061
		SG	$(f_s/\sqrt{f_c'})_{SG} / \mu_G$	0.915	0.914
		UG	$(f_s/\sqrt{f_c'})_{UG} / \mu_G$	1.050	1.026
	Bar Size	All Sizes	Group Mean (μ_G)	16.31	20.89
		#6	$(f_s/\sqrt{f_c'})_{\#6} / \mu_G$	1.017	0.990
		#8	$(f_s/\sqrt{f_c'})_{\#8} / \mu_G$	1.101	1.090
		#11	$(f_s/\sqrt{f_c'})_{\#11} / \mu_G$	0.933	0.920
$f_s/f_c'^{0.25}$	Concrete Mix	Group	Group Mean (μ_G)	29.63	37.94
		HG	$(f_s/f_c'^{0.25})_{HG} / \mu_G$	1.009	1.034
		SG	$(f_s/f_c'^{0.25})_{SG} / \mu_G$	0.940	0.940
		UG	$(f_s/f_c'^{0.25})_{UG} / \mu_G$	1.050	1.026
	Bar Size	Group	Group Mean (μ_G)	29.63	37.94
		#6	$(f_s/f_c'^{0.25})_{\#6} / \mu_G$	0.991	0.990
		#8	$(f_s/f_c'^{0.25})_{\#8} / \mu_G$	1.101	1.090
		#11	$(f_s/f_c'^{0.25})_{\#11} / \mu_G$	0.932	0.920
f_s/f_{ct}	Concrete Mix	Group	Group Mean (μ_G)	74.67	95.68
		HG	$(f_s/f_{ct})_{HG} / \mu_G$	1.036	1.061
		SG	$(f_s/f_{ct})_{SG} / \mu_G$	0.973	0.972
		UG	$(f_s/f_{ct})_{UG} / \mu_G$	0.991	0.967
	Bar Size	Group	Group Mean (μ_G)	74.67	95.68
		#6	$(f_s/f_{ct})_{\#6} / \mu_G$	0.970	0.990
		#8	$(f_s/f_{ct})_{\#8} / \mu_G$	1.103	1.090
		#11	$(f_s/f_{ct})_{\#11} / \mu_G$	0.931	0.920

Units: $1.0 \sqrt{ksi} = 2.63 \sqrt{MPa}$,

Table 11 gives the linear sample correlation for different factors used to normalize bar stress and different methods to normalize lap splice length. The linear sample correlation can vary between negative one and unity and represents the amount of scatter in a linear regression with unity indicating a perfect correlation. In Table 11, sample correction using f_{ct} as the normalizing factor was the largest and $\sqrt{f_c'}$ gave the smallest sample correction. This trend is observed for specimens with and without stirrups and for all specimens together.

Table 11. Linear Sample Correlation for Normalized Bar Stress versus Normalized Splice Length for 40 LWC Splice Beam Specimens (22 Specimens without Stirrups (N) and 18 Specimens with Stirrups (T)).

Expression	Linear Sample Correlation (r)		
	All Specimens (N and T)	Specimens without Stirrups (N)	Specimens with Stirrups (T)
$f_s/\sqrt{f_c'}$ versus ℓ_s/d_b (Figure 31)	0.192	0.153	0.266
$f_s/\sqrt{f_c'}$ versus $\ell_s(c_{min}+0.5d_b)/A_b$ (Figure 32)	0.266	0.280	0.265
$f_s/\sqrt{f_c'}$ versus $\ell_s/d_b \times (c_b+K_{tr})/d_b$ (Figure 33)	0.303	0.303	0.348
$f_s/(f_c'^{0.25})$ versus $\ell_s/d_b \times (c_b+K_{tr})/d_b$ (Figure 34)	0.381	0.391	0.404
f_s/f_{ct} versus $\ell_s/d_b \times (c_b+K_{tr})/d_b$ (Figure 35)	0.420	0.460	0.399
$\Delta f_s/\sqrt{f_c'}$ versus $t_r t_d(NA_{tr}/n)/A_b$ (Figure 36)	--	--	0.027
$\Delta f_s/\sqrt{f_c'}$ versus $(c_b+K_{tr})d_b$ (Figure 37)	--	--	0.053
$f_s/\sqrt{f_c'}$ versus $\ell_s(c_{min}+0.5d_b)/A_b \times (c_b+K_{tr})/d_b$	0.338	0.392	0.332
f_s/f_{ct} versus $\ell_s(c_{min}+0.5d_b)/A_b \times (c_b+K_{tr})/d_b$	0.419	0.514	0.357

In Figure 33, Figure 34, and Figure 35 the factor used to normalize bar stress is varied. The SD mix had a considerably lower compressive strength than the girder mixes (i.e., HG, SG, and UG) and had a much higher normalized bar stress as indicated by its relative position above all other N-specimens in Figure 33 through Figure 35. The SG mix has a lower normalized bar stress in Figure 33 and Figure 34 where bar stress is normalized by a function of concrete compressive strength (i.e., $\sqrt{f_c'}$ or $f_c'^{0.25}$). However, in Figure 35 where bar stress is normalized by f_{ct}, the normalized bar stress of the SG mix is comparable to the other mixes as indicated by the relative position of its regression line.

METHODS USED TO NORMALIZE SPLICE LENGTH THAT EXCLUDE THE K_{TR} TERM

Figure 31 and Figure 32 show the data with normalized splice lengths using ℓ_s/d_b and $\ell_s(c_{min}+0.5d_b)/A_b$, respectively. The trends in both figures are similar: the regression lines are parallel, the relative position of individual concrete mixes and bar sizes are similar, and the normalized bar stress data for specimens with stirrups (T-specimens) is considerably higher than the data for specimens without stirrups (N-specimens). The one exception is for the limited number of tests on the SD mix with a considerably lower compressive strength than the girder mixes.

The linear sample correlation for specimens without stirrups (N) in Table 11 for $\ell_s(c_{min}+0.5d_b)/A_b$ is larger than the correlation for ℓ_s/d_b indicating the greater scatter when using ℓ_s/d_b to normalize splice length. For specimens with stirrups (T), the sample correlations for ℓ_s/d_b and $\ell_s(c_{min}+0.5d_b)/A_b$ are nearly equal.

In Table 11, sample correction using f_{ct} as the normalizing factor was the largest and $\sqrt{f_c'}$ gave the smallest sample correction. This trend is observed for specimens with and specimens without stirrups.

METHODS USED TO NORMALIZE SPLICE LENGTH THAT INCLUDE THE K_{TR} TERM

The inclusion of the K_{tr} term in the normalized splice length results in a considerable reduction in the variability of the linear regression as observed by the increase in the linear sample correlation given in Table 11. Changing the normalized splice length from ℓ_s/d_b to $\ell_s/d_b(c_b+K_{tr})/d_b$ results in the sample correlation increasing from 0.153 to 0.303 for specimens without stirrups (N) and increasing from 0.266 to 0.348 for specimens with stirrups (T).

A comparison of Figure 31 with Figure 33 shows that the main effect of including the K_{tr} term is an increase in the normalized splice length for the specimens with stirrups (T) and is observed in Figure 33 by the T-specimens shifting to the right (i.e., to larger values of normalized splice length). The result is a decrease in the difference between the normalized bar stress of the specimens with and without stirrups.

In Figure 36 and Figure 37 the normalized increase in bar stress (Δf_s) due to the presence of stirrups is shown versus two methods for normalizing the amount of stirrups. The increase in bar stress is defined as the difference between the f_s in a specimen with stirrups and a companion specimen without stirrups. The companion specimen had the same concrete mix, bar size, and lap splice length. The normalized amount of stirrups is given by the K_{tr} term. Figure 36 shows the normalized Δf_s versus the expression for the K_{tr} term given by Zuo and Darwin.[12] Figure 37 shows a similar comparison for the K_{tr} term given by ACI 318-11.[16] The data in both figures have considerable scatter. The linear sample correlation for each K_{tr} term is given in Table 11 and shows that the ACI 318 expression ($(c_b+K_{tr})/d_b$) has a slightly higher linear sample correlation than the Zuo and Darwin expression ($t_r t_d (NA_{tr}/n)/A_b$).

Table 11 shows that there is an improvement in the sample correlation (i.e., larger value) in expressions that use $\ell_s(c_{min}+0.5d_b)/A_b$ compared to ℓ_s/d_b (0.280 versus 0.153 for N-specimens). An improvement is also observed when the K_{tr} term is included with ℓ_s/d_b (0.303 versus 0.153 for N-specimens). The use of f_{ct} instead of $\sqrt{f_c'}$ also showed an improvement (0.460 versus 0.303 for N-specimens). The composite expression given by Eq. 26 was created to evaluate the effect of combining expressions with an improvement in the sample correlation. The linear sample correlations for bar stress normalized with $\sqrt{f_c'}$ and f_{ct} compared to the normalized splice length from Eq. 26 are given in Table 11. The sample correlations show an improvement for specimens without stirrups using $\sqrt{f_c'}$ (0.392 versus 0.303) and using f_{ct} (0.514 versus 0.460). However for specimens with stirrups the sample correlations became smaller: 0.332 versus 0.348 for normalization with $\sqrt{f_c'}$ and 0.357 versus 0.399 for normalization with f_{ct}.

$$[\ell_s(c_{min} + 0.5d_b)/A_b] \times [(c_b + K_{tr})/d_b] \qquad\qquad \text{(Eq. 26)}$$
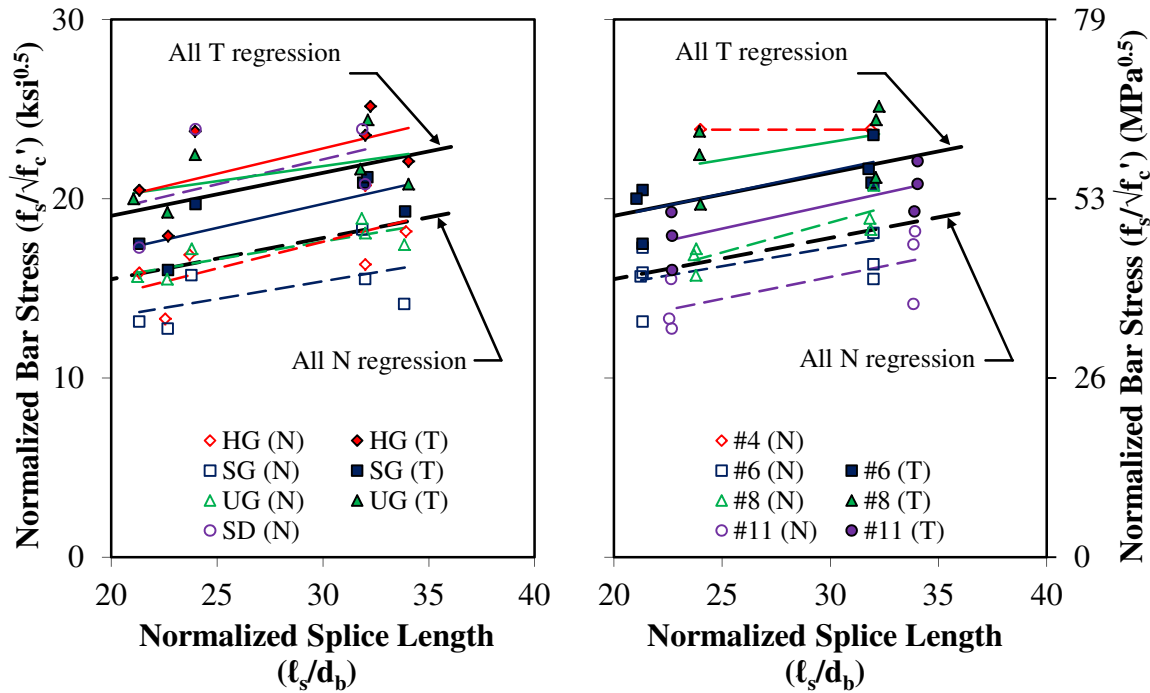
Figure 31. Graph. Normalized Bar Stress ($f_s/\sqrt{f_c'}$) versus Normalized Splice Length (ℓ_s/d_b) by Mix Design and Bar Size for Specimens without Stirrups (N) and with Stirrups (T).
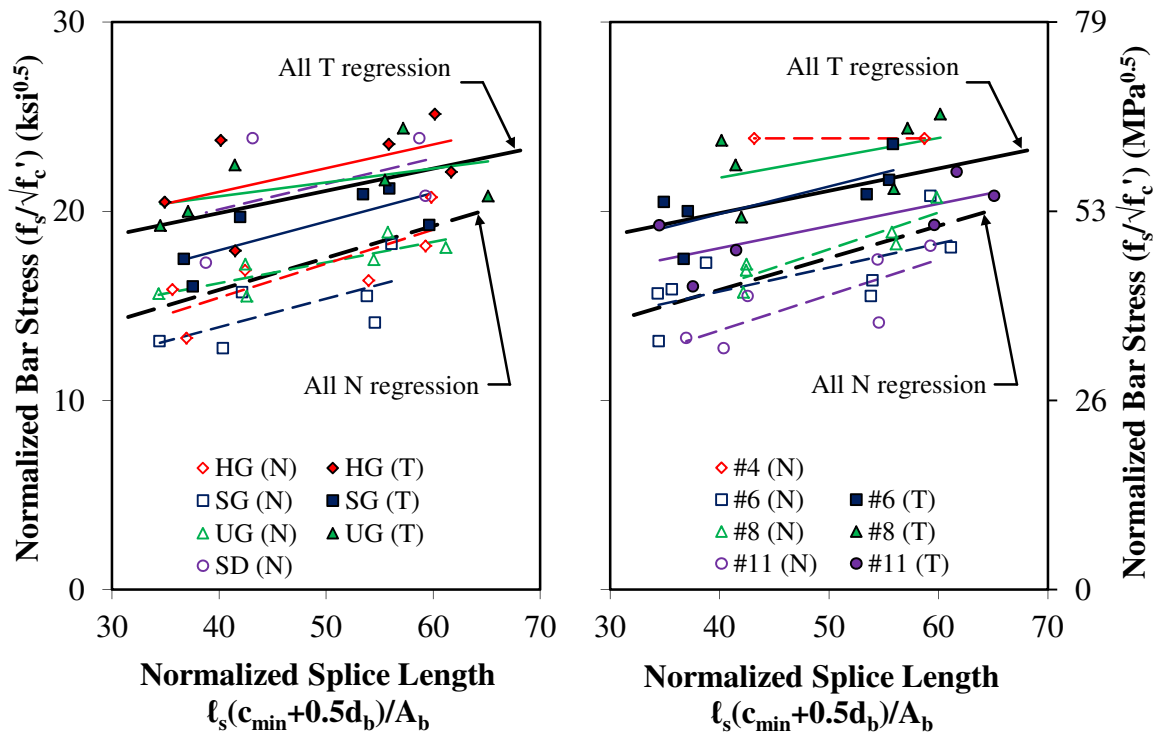
Figure 32. Graph. Normalized Bar Stress ($f_s/\sqrt{f_c'}$) versus Normalized Splice Length $\ell_s(c_{min}+0.5d_b)/A_b$ by Mix Design and Bar Size for Specimens without Stirrups (N) and with Stirrups (T).
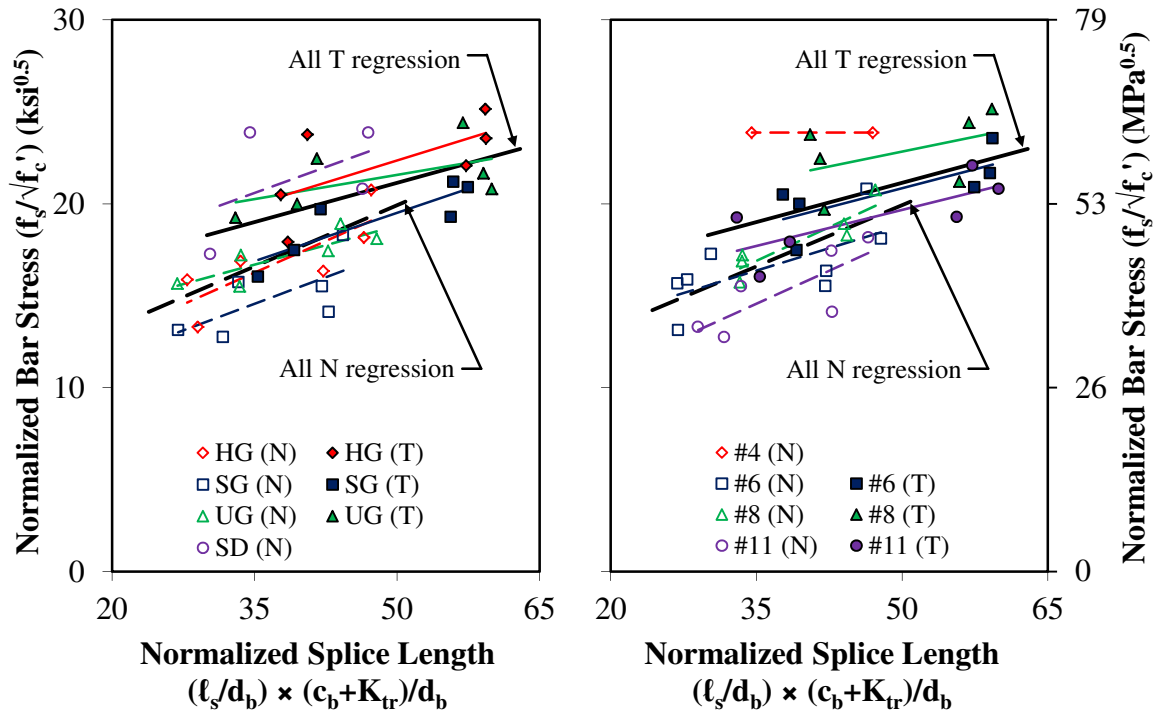
Figure 33. Graph. Normalized Bar Stress ($f_s/\sqrt{f_c'}$) versus Normalized Splice Length (ℓ_s/d_b)×(c_b+K_{tr})/d_b by Mix Design and Bar Size for Specimens without Stirrups (N) and with Stirrups (T).

SUMMARY OF ANALYSIS OF BAR STRESS WITH SPLICE LENGTH

The normalized bar stress at failure was dependent upon mix design. The higher strength SG mix had the lowest mix-to-mean bar stress ratio. The use of f_{ct} to normalize bar stress accounted for most of the reduced mix-to-mean bar stress ratio observed for the SG mix. There was very little difference between the mix-to-mean ratios for specimens with stirrups or without stirrups indicating the differences observed between concrete mixes was not dependent upon the presence of stirrups.

The bar stress at failure was dependent upon the bar size. The specimens with #8 bars consistently had a higher f_s and the specimens with #11 bars had a lower f_s. This trend was independent of the presence of stirrups or the factor used to normalize bar stress. The higher than average f_s observed in this study was likely due to the yield stress of the #8 bars being 73.8 ksi (508 MPa) versus and an average of 66.6 ksi (459 MPa) for the other bars.
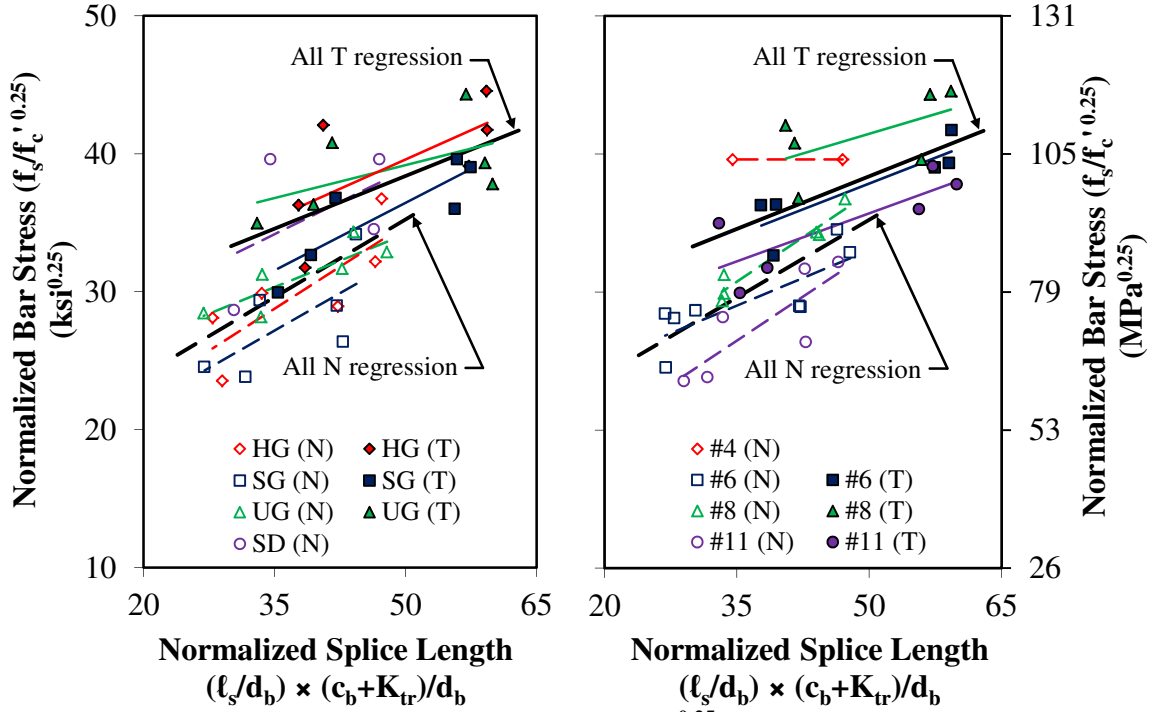
Figure 34. Graph. Normalized Bar Stress ($f_s/f_c'^{0.25}$) versus Normalized Splice Length (ℓ_s/d_b)×(c_b+K_{tr})/d_b by Mix Design and Bar Size for Specimens without Stirrups (N) and with Stirrups (T).
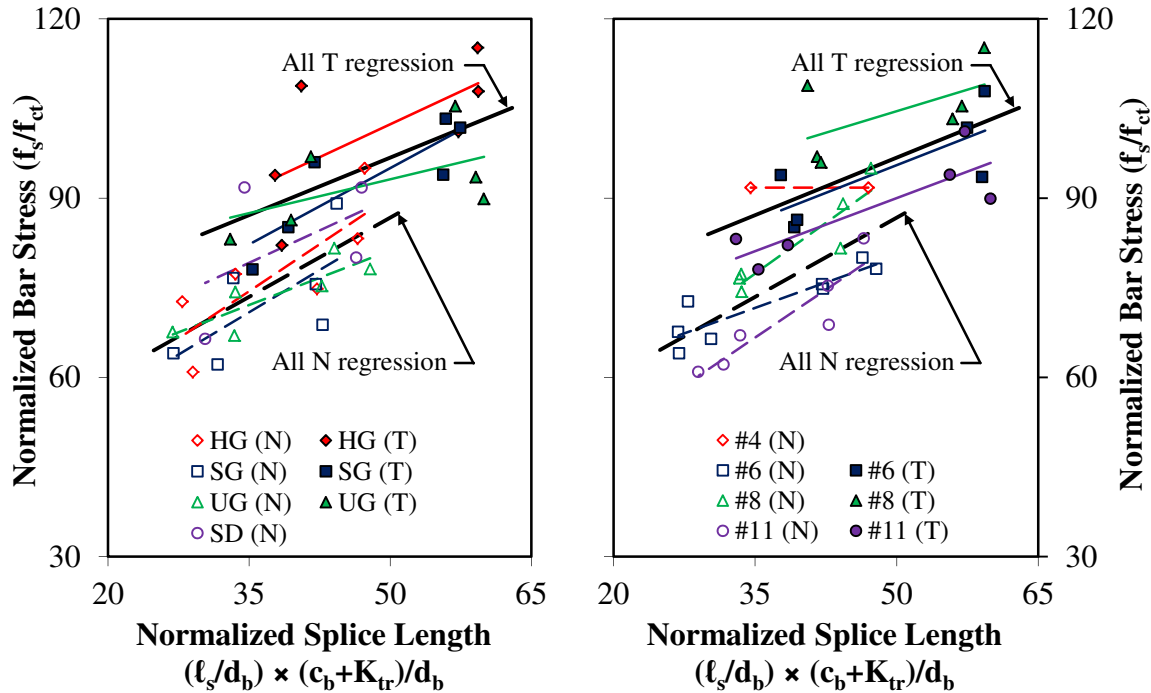
Figure 35. Graph. Normalized Bar Stress (f_s/f_{ct}) versus Normalized Splice Length (ℓ_s/d_b)×(c_b+K_{tr})/d_b by Mix Design and Bar Size for Specimens without Stirrups (N) and with Stirrups (T).
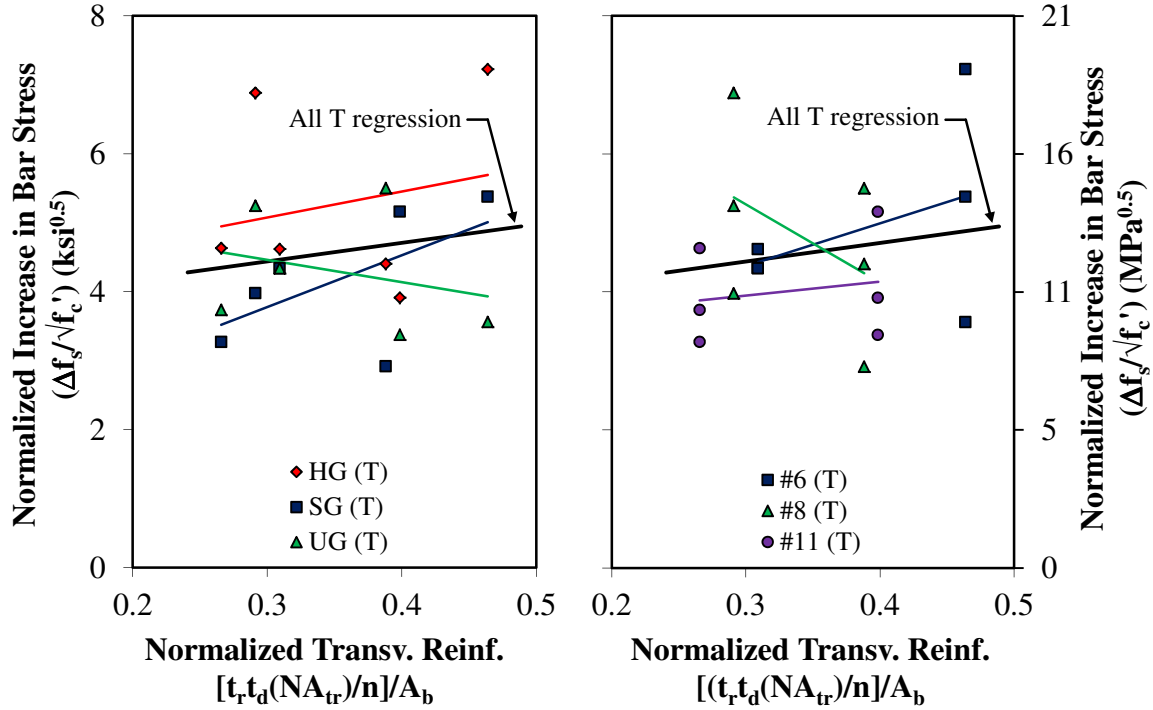
Figure 36. Graph. Normalized Increase in Bar Stress ($\Delta f_s/\sqrt{f_c'}$) versus Normalized Amount of Transverse Reinforcement $[t_r t_d (NA_{tr})/n]/A_b$ by Mix Design and Bar Size for Specimens without Stirrups (N) and with Stirrups (T).
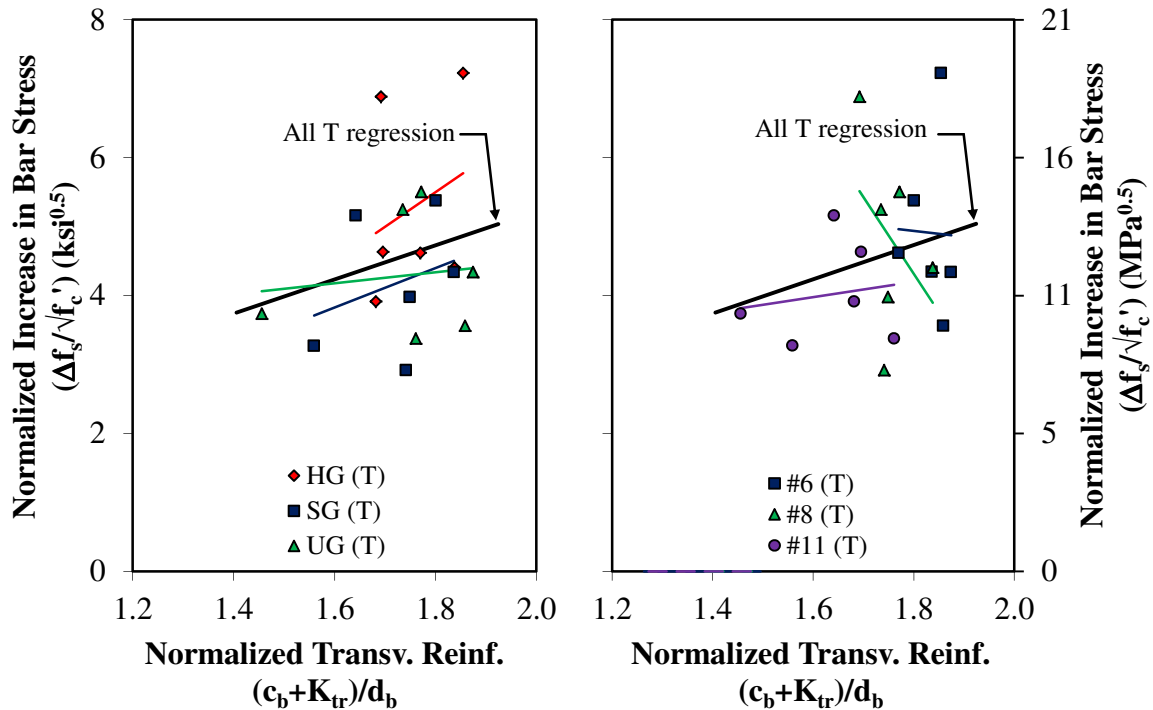
Figure 37. Graph. Normalized Increase in Bar Stress ($\Delta f_s/\sqrt{f_c'}$) versus Normalized Amount of Transverse Reinforcement $(c_b+K_{tr})/d_b$ by Mix Design and Bar Size for Specimens without Stirrups (N) and with Stirrups (T).

54

The selection of the factor used for normalizing bar stress (i.e., $\sqrt{f_c'}$, $f_c'^{0.25}$, or f_{ct}) has only a small effect on the mix-to-mean bar stress ratio and almost no effect on the bar size-to-mean bar stress ratio. This trend was observed for both specimens with stirrups and specimens without stirrups. The selection of the factor used for normalizing bar stress did have a noticeable effect on the scatter in regression lines used to fit the f_s data. The use of f_{ct} resulted in a noticeable improvement in the regression line (i.e., less scatter) over $\sqrt{f_c'}$. The use of $f_c'^{0.25}$ also resulted in an improvement in the regression line, although not as large as f_{ct}.

The use of $\ell_s(c_{min}+0.5d_b)/A_b$ instead of ℓ_s/d_b resulted in an improvement in the regression line for specimens without stirrups, but had no had no effect for specimens with stirrups. An improvement in the regression line for specimens with stirrups required the inclusion of a term for the amount of stirrups in the expression for normalized splice length. The two K_{tr} terms evaluated in this study resulted in similar levels of scatter in the data.

COMPARISON WITH DESCRIPTIVE EXPRESSIONS FOR BAR STRESS

The bar stress predicted by the descriptive expressions given by Orangun et al. (Eq. 2) and Zuo and Darwin (Eq. 5) are compared to the bar stresses determined for the 40 LWC splice beam specimens tested in this study. In this section, the method used to express Eq. 2 and Eq. 5 in terms of average bar stress (f_s) is described. Then ratios of the f_s determined from the LWC tests are compared to f_s predicted by the descriptive expressions.

EXPRESSIONS FOR BAR STRESS AND ASSUMPTIONS

The Orangun et al. expression is for the average bond stress (u_b). This relationship needs to be rearranged and given as an expression for the average bar stress at failure (f_s). The relationship between f_s and u_b is given by Eq. 27 (second and third terms). Solving Eq. 27 for u_b and recognizing that the nominal bar area (A_b) is approximately equal to $\pi/4 \times (d_b)^2$, results in Eq. 28. Substituting Eq. 28 into Eq. 2 and solving for f_s results in Eq. 29, the expression for f_s based on Orangun et al. The limit given by Eq. 3 must be satisfied in order to use Eq. 29.

The Zuo and Darwin relationship was given in terms of bar force (T_b) and also needs to be given as an expression for f_s. This is accomplished by substituting the relationship between T_b and f_s given by Eq. 27 (first and second terms) into Eq. 5 and solving for f_s. The resulting expression is given by Eq. 30, and is the expression for f_s based on Zuo and Darwin. In Eq. 30, ω, t_r, and t_d are given by Eq. 17, Eq. 6 and Eq. 7, respectively. The limit given by Eq. 8 must be satisfied in order to use Eq. 30.

$$T_b = A_b f_s = (\pi d_b \ell_s) u_b \tag{Eq. 27}$$

$$u_b = \frac{A_b f_s}{\pi d_b \ell_s} \cong \frac{\left(\frac{\pi}{4} d_b^2\right) f_s}{\pi d_b \ell_s} = \frac{1}{4}\left(\frac{d_b f_s}{\ell_s}\right) \tag{Eq. 28}$$

$$f_s = 4\left(\frac{\ell_s}{d_b}\right)\left[1.2 + 3\frac{c_{minOBJ}}{d_b} + 50\frac{d_b}{\ell_s} + \frac{A_{tr} f_{yt}}{500 s n d_b}\right]\sqrt{f_c'} \tag{Eq. 29}$$

in Eq. 29, the units of stress are in psi

$$f_s = \left(\frac{1}{A_b}\right)\left\{[59.8\ell_s(c_{min} + 0.5d_b) + 2350A_b]\omega + \left(31.14 t_r t_d \frac{NA_{tr}}{n} + 4\right)f_c'^{0.5}\right\}f_c'^{0.25} \tag{Eq. 30}$$

in Eq. 30, the units of stress are in psi

Measured values were used for the specimen geometry and material properties variables in Eq. 29 and Eq. 30. The splice length (ℓ_s), concrete cover terms (c_{min} and ω) were measured on the specimens after each test was completed. The concrete compressive strength (f_c') was measured on cylinders as described previously in this document. No limit was placed on f_c', $\sqrt{f_c'}$, or f_s. The rebar deformations were measured to calculate the relative rib area (R_r) that is used to determine t_r.

A moment curvature analysis was used to determine the f_s from the tested LWC splice beam specimens as described in a previous section of this document. In this type of analysis, the prediction of rebar yielding is possible as the stress-strain relationship used includes a yield plateau and strain-hardening. In the determination of f_s from Eq. 29 and Eq. 30, the stress is not limited to the measured yield stress of the spliced bars. The test data used to develop Eq. 29 did not contain any tests with yielding rebar.[13] The test data used to develop Eq. 30 did contain tests with yielding reinforcement.

Once the rebar begins to yield, there is only a slight increase in bar stress due to the yield plateau and strain-hardening. Expressions for predicting bar stress such as Eq. 29 and Eq. 30 do not directly account for the change in behavior from a bar in the linear-elastic range to the non-linear behavior resulting from rebar yielding. If f_s determined from tests is not limited to f_y, then not limiting the predicted bar stress to yielding would likely result in an over-estimation of f_s for specimens with yielding reinforcement and a lower test-to-prediction ratio. Likewise, limiting the bar stress to yielding would likely result in an under-estimation of f_s and a higher test-to-prediction ratio.

ANALYSIS OF TEST-TO-PREDICTION RATIOS

The results of an analysis of the test-to-prediction ratios are given in Table 12. The mean test-to-prediction ratios for the Orangun et al. expression were 0.88 and 0.90 for specimens without stirrups and with stirrups, respectively, indicating that the expression overestimated f_s. The Zuo and Darwin expression had a mean test-to-prediction ratio for all 40 specimens near unity (0.98),

with the f_s for specimens with stirrups slightly overestimated with a mean test-to-prediction ratio of 0.94.

The results of an analysis of the test-to-prediction ratios are shown graphically for the Orangun et al. expression in Figure 38 and Figure 39, and for the Zuo and Darwin expression in Figure 40 and Figure 41. For each expression, the test-to-prediction ratios are plotted versus the normalized splice length (ℓ_s/d_b), the compressive strength (f_c'), and the splitting tensile strength (f_{ct}). Each expression has two figures showing test-to-prediction ratios versus ℓ_s/d_b, one figure showing the data grouped by concrete mix (i.e., HG, SD, SG, or UG) and the other grouped by bar size (i.e., #4, #6, #8, or #11). In both figures, the specimens with and without stirrups are separated. Least-squares linear regression lines are shown for each group of concrete mix or bar size. Also, regression lines are shown for all specimens with stirrups and all specimens without stirrups. Additional figures using alternate expressions for normalized splice length ($\ell_s(c_{min}+0.5d_b)/A_b$ based on Zuo and Darwin, and $\ell_s/d_b(c_b+K_{tr})/d_b$ based on ACI 318-11) are in Appendix B.

The figures showing the Orangun et al. expression (Figure 38) and the Zuo and Darwin expression (Figure 40) both show a decrease in the test-to-prediction ratio with increases in normalized splice length. In Figure 38 for the Orangun et al. expression, the regression lines for the data grouped by concrete mix (left figure) are nearly parallel indicating that the decrease in test-to-prediction ratio was independent of the concrete mix. The regression lines for the data grouped by bar size (right figure) are slightly closer together at the higher ℓ_s/d_b ratio. This indicates that the decrease in test-to-prediction ratio may have some dependence on bar size.

The figures showing both the Orangun et al. expression (Figure 39) and the Zuo and Darwin expression (Figure 41) show a decrease in the test-to-prediction ratio with increases in compressive strength. The Zuo and Darwin expression uses $f_c'^{0.25}$ rather than $\sqrt{f_c'}$ to account for the effect of concrete strength. In the analysis of splice beam tests with NWC (12), the use of $f_c'^{0.25}$ had the effect of making the regression line horizontal (i.e., the test-to-prediction ratios were independent of compressive strength). Figure 41 indicates that the use of $f_c'^{0.25}$ did not have the same effect in the analysis of the 40 LWC splice beams that are part of this research study. Figure 39 and Figure 41 show that both the Orangun et al. expression and the Zuo and Darwin expression, respectively, gave uniform test-to-prediction ratios when compared to the concrete splitting tensile strength as shown by their horizontal regression lines.

Table 12. Test-to-Prediction Ratio of Bar Stress for Descriptive Expressions by Orangun et al. (Eq. 29) and Darwin and Zuo (Eq. 30) for 40 LWC Splice Beam Specimens (22 Specimens without Stirrups (N) and 18 Specimens with Stirrups (T)).

Data Source	Statistical Measure	Orangun et al. (Eq. 29)	Zuo and Darwin (Eq. 30)
All Specimens	mean	0.889	0.981
	COV	14.4%	12.7%
	maximum	1.304	1.408
	minimum	0.663	0.773
	Percent ≥ 1.0	17.5%	47.5%
	Percent < 1.0	82.5%	52.5%
	Percent ≥ 1.2	2.5%	2.5%
	Percent < 0.8	22.5%	5.0%
Specimens without Stirrups (N)	mean	0.882	1.017
	COV	15.6%	12.6%
	maximum	1.304	1.408
	minimum	0.663	0.798
	Percent ≥ 1.0	13.6%	59.1%
	Percent < 1.0	86.4%	40.9%
	Percent ≥ 1.2	4.5%	4.5%
	Percent < 0.8	22.7%	4.5%
Specimens without Stirrups (T)	mean	0.898	0.937
	COV	13.2%	11.6%
	maximum	1.147	1.186
	minimum	0.736	0.773
	Percent ≥ 1.0	22.2%	33.3%
	Percent < 1.0	77.8%	66.7%
	Percent ≥ 1.2	0.0%	0.0%
	Percent < 0.8	22.2%	5.6%
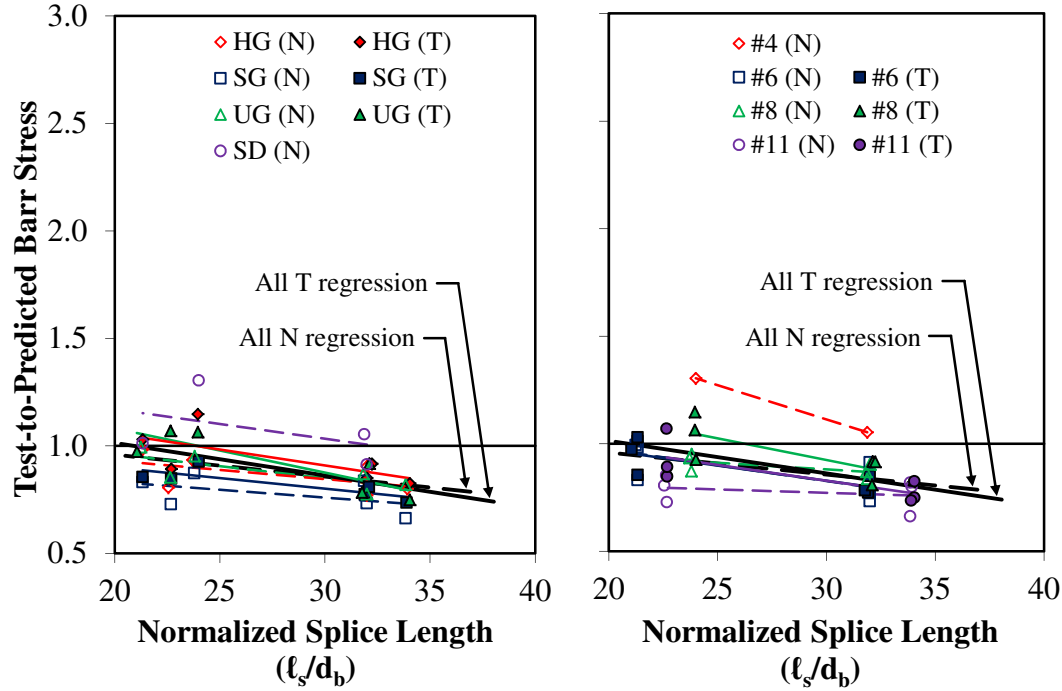
Figure 38. Graph. Bar Stress Test-to-Prediction Ratio Compared to Normalized Splice Length (ℓs/db) for Orangun et al. Expression (Eq. 29) by Mix Design and Bar Size for Specimens without Stirrups (N) and with Stirrups (T).

Figure 39. Graph. Bar Stress Test-to-Prediction Ratio Compared to Compressive Strength and Splitting Tensile Strength for Orangun et al. Expression (Eq. 29) by Mix Design and Bar Size for Specimens without Stirrups (N) and with Stirrups (T).

Figure 40. Graph. Bar Stress Test-to-Prediction Ratio Compared to Normalized Splice Length (ℓ_s/d_b) for Darwin and Zuo Expression (Eq. 30) by Mix Design and Bar Size for Specimens without Stirrups (N) and with Stirrups (T).

Figure 41. Graph. Bar Stress Test-to-Prediction Ratio Compared to Compressive Strength and Splitting Tensile Strength for Darwin and Zuo Expression (Eq. 30) by Mix Design and Bar Size for Specimens without Stirrups (N) and with Stirrups (T).

COMPARISON WITH DESIGN EXPRESSIONS FOR DEVELOPMENT LENGTH

The bar stress predicted by the design expressions in the AASHTO LRFD Specifications (Eq. 10), in ACI 318-11 (Eq. 12), and in ACI 408-03 (Eq. 15) are compared to the bar stresses determined for the 40 LWC splice beam specimens tested in this study. The method used to express Eq. 10, Eq. 12 and Eq. 15 in terms of average bar stress at failure (f_s) is described in this section. The f_s determined from the LWC tests ($f_{s,test}$) are compared to the f_s predicted by the three design expressions ($f_{s,prediction}$). The comparison is made using the ratio of $f_{s,test}$ to $f_{s,prediction}$ (i.e., test-to-prediction ratio).

EXPRESSIONS FOR BAR STRESS AND ASSUMPTIONS

The three design expressions for the development length of mild steel reinforcing bars in tension (ℓ_d or ℓ_{db}) are given in terms of the yield strength of the bar, f_y. These relationships need to be rearranged and given as expressions for (f_s) in terms of lap splice length (ℓ_s). For each design expression, f_y was replaced with f_s, ℓ_d (or ℓ_{db}) was replaced with ℓ_s, and the expressions were solved for f_s. The expression for f_s based on the AASHTO LRFD Specifications is given by Eq. 31. The ACI 318-11 and ACI 408-03 based expressions are given by Eq. 32 and Eq. 33, respectively. Note that the stress terms in Eq. 32 and Eq. 33 are in the units of psi. The expression for K_{tr} in Eq. 32 is given by Eq. 14. The term $(c_b + K_{tr})/d_b$ in Eq. 32 is limited to 2.5. The expressions for $K_{tr,ACI408}$, ω, t_r, and t_d in Eq. 33 are given by Eq. 16, Eq. 17, Eq. 6, and Eq. 7, respectively. The term $(c_b\omega + K_{tr,ACI408})/d_b$ in Eq. 33 is limited to 4.

$$f_s = \left(\frac{\ell_s}{1.25A_b}\right)\left(\frac{\lambda_{ACI}}{\psi_t\psi_e}\right)\sqrt{f_c'} \leq \left(\frac{\ell_s}{0.4d_b}\right)\left(\frac{\lambda_{ACI}}{\psi_t\psi_e}\right) \tag{Eq. 31}$$

$$f_s = \left(\frac{40}{3}\right)\left(\frac{\ell_s}{d_b}\right)\left(\frac{c_b + K_{tr}}{d_b}\right)\left(\frac{\lambda_{ACI}}{\psi_t\psi_e\psi_s}\right)\sqrt{f_c'} \tag{Eq. 32}$$

in Eq. 32, the units of stress are in psi

$$f_s = \left[70\left(\frac{\ell_s}{d_b}\right)\left(\frac{c_b\omega + K_{tr,ACI408}}{d_b}\right)\left(\frac{1}{\alpha\beta\lambda_{ACI408}}\right) + 2200\omega\right]f_c'^{0.25} \tag{Eq. 33}$$

in Eq. 33, the units of stress are in psi

Measured values were used for splice length, concrete cover terms, concrete compressive strength, and relative rib area as described previously in this document for comparisons with the descriptive expressions. No limit was placed on f_c', $\sqrt{f_c'}$, or f_s. The lightweight concrete factors (λ_{ACI} and λ_{ACI408}), top-cast bar factors (ψ_t and α), epoxy coating factors (ψ_e and β), and bar size factor (ψ_s) were taken as unity.

ANALYSIS OF TEST-TO-PREDICTION RATIOS

The results of an analysis of the test-to-prediction ratios are given in Table 13. The mean test-to-prediction ratio for all specimens was 0.94 for the AASHTO LRFD expression, 1.18 for the ACI 318-11 expression, and 1.15 for the ACI 408-03 expression. This indicates that the bar stresses were slightly overestimated by the AASHTO LRFD expression, and slightly underestimated by the ACI 318-11 expression and ACI 408-03 expression. These predictions of bar stress do not include a factor for lightweight concrete (λ taken as unity) or the safety factors applied for the design of splices.

The AASHTO LRFD expression had a mean test-to-prediction ratio of 0.84 for specimens without stirrups indicating that the expression overestimated f_s. For specimens with stirrups, the AASHTO LRFD expression slightly underestimated f_s with a mean test-to-prediction ratio of 1.06. The large change in mean test-to-prediction ratio from specimens without stirrups to specimens with stirrups is due to the AASHTO LRFD expression does not accounting for the increase in f_s due to the presence of stirrups.

The ACI 318-11 expression underestimated bar stress for specimens without stirrups and with stirrups with mean test-to-prediction ratios of 1.21 and 1.14, respectively. The decrease in test-to-prediction ratio for specimens with stirrups indicates that the ACI 318-11 overestimated the increase in bar stress due to presence of stirrups.

The ACI 408-03 expression gives a consistent underestimation of the bar stress for specimens with and without stirrups. The COV of the mean test-to-prediction ratios for the bar stresses of all specimens predicted by the ACI 408-03 expression was also noticeably less than the COV for the AASHTO LRFD expression or ACI 318-11 expression.

The results of an analysis of the test-to-prediction ratios are shown graphically for the AASHTO LRFD expression in Figure 42 and Figure 43, for the ACI 318-11 expression in Figure 44 and Figure 45, and for the ACI 408-03 expression in Figure 46 and Figure 47. For each expression, the test-to-prediction ratios are plotted versus the normalized splice length (ℓ_s/d_b), the compressive strength (f_c'), and the splitting tensile strength (f_{ct}). Similar to the figures for the descriptive expressions for f_s, the data in the figures is grouped by concrete mix and bar size, is separated for specimens with and without stirrups, and includes regressions lines by group. Additional figures using alternate expressions for normalized splice are in Appendix B.

The figures showing the test-to-predicted bar stress versus normalized bar stress for all three design expressions indicate a decrease in the test-to-prediction ratio with increases in normalized splice length. Similar to the descriptive expressions, the regression lines in Figure 42, Figure 44, and Figure 46 for the data grouped by concrete mix (left figures) are nearly parallel indicating that the decrease in test-to-prediction ratio was independent of the concrete mix.

The regression lines for the data grouped by bar size (right figure) in the figures showing the descriptive expressions were slightly closer together at the higher ℓ_s/d_b ratio. A similar trend is not observed in Figure 42, Figure 44, or Figure 46 for the three design expressions.

Table 13. Test-to-Prediction Ratio of Bar Stress for Design Expressions in AASHTO LRFD (Eq. 31), ACI 318-11 (Eq. 32), and ACI 408-03 (Eq. 33) for 40 LWC Splice Beam Specimens (22 Specimens without Stirrups (N) and 18 Specimens with Stirrups (T)).

| Data Source	Statistical Measure	AASHTO LRFD (Eq. 31)	ACI 318-11 (Eq. 32)	ACI 408-03 (Eq. 33)
All Specimens	mean	0.939	1.178	1.151
	COV	18.4%	19.3%	12.2%
	maximum	1.253	1.895	1.617
	minimum	0.617	0.836	0.891
	Percent ≥ 1.0	30.0%	80.0%	85.0%
	Percent < 1.0	70.0%	20.0%	15.0%
	Percent ≥ 1.2	15.0%	40.0%	37.5%
	Percent < 0.8	17.5%	0.0%	0.0%
Specimens without Stirrups (N)	mean	0.839	1.207	1.146
	COV	14.3%	20.3%	13.2%
	maximum	1.095	1.895	1.617
	minimum	0.617	0.836	0.891
	Percent ≥ 1.0	9.1%	86.4%	86.4%
	Percent < 1.0	90.9%	13.6%	13.6%
	Percent ≥ 1.2	0.0%	45.5%	36.4%
	Percent < 0.8	31.8%	0.0%	0.0%
Specimens without Stirrups (T)	mean	1.061	1.143	1.157
	COV	13.9%	18.0%	11.4%
	maximum	1.253	1.537	1.480
	minimum	0.841	0.876	0.973
	Percent ≥ 1.0	55.6%	72.2%	83.3%
	Percent < 1.0	44.4%	27.8%	16.7%
	Percent ≥ 1.2	33.3%	33.3%	38.9%
	Percent < 0.8	0.0%	0.0%	0.0%
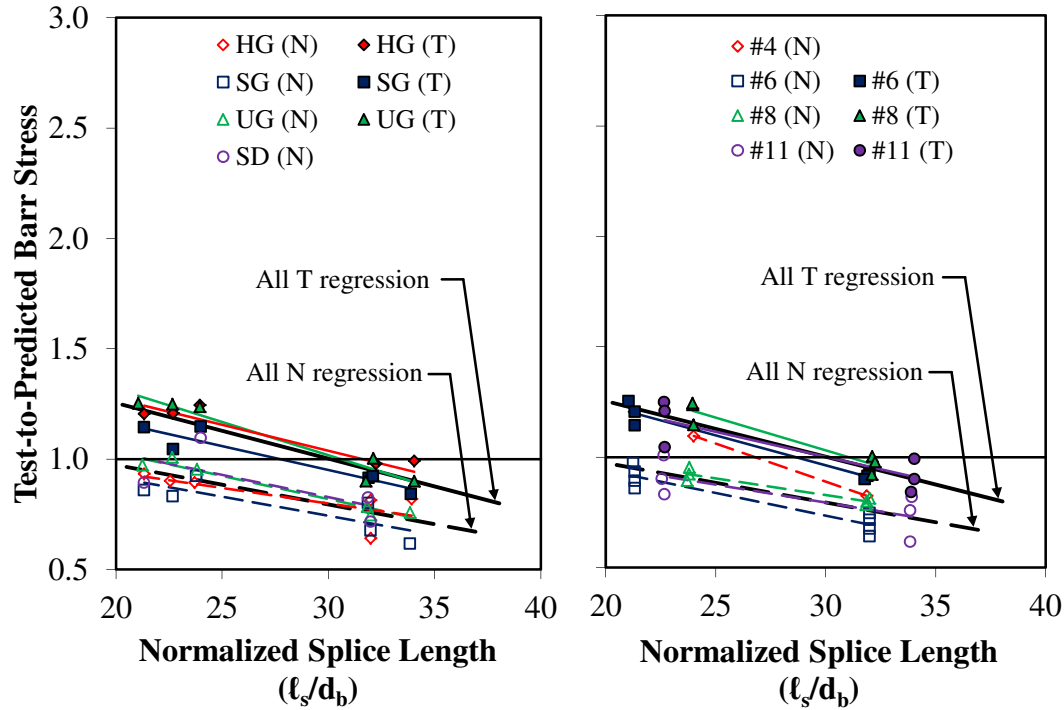
Figure 42. Graph. Bar Stress Test-to-Prediction Ratio Compared to Normalized Splice Length (ℓ_s/d_b) for AASHTO LRFD Expression (Eq. 31) by Mix Design and Bar Size for Specimens without Stirrups (N) and with Stirrups (T).
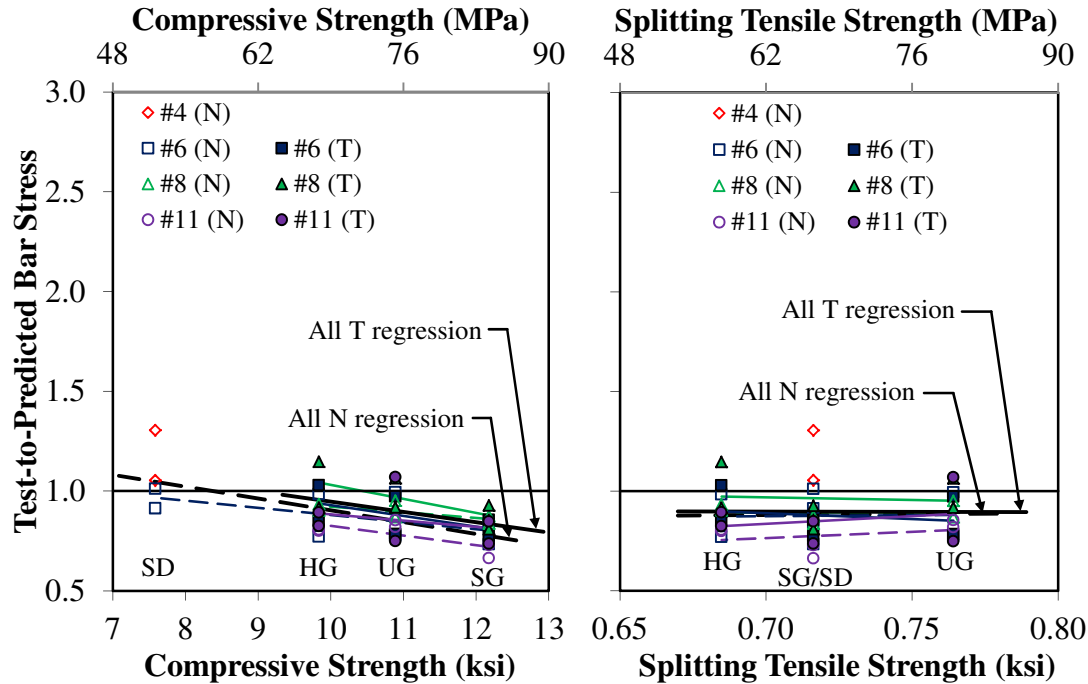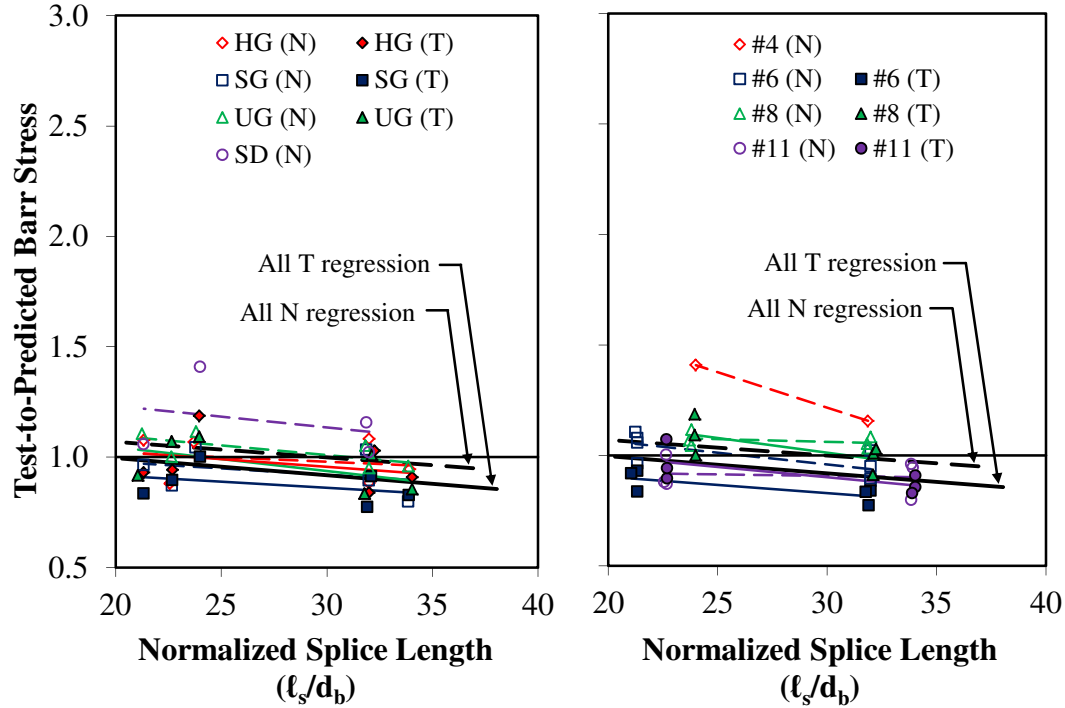

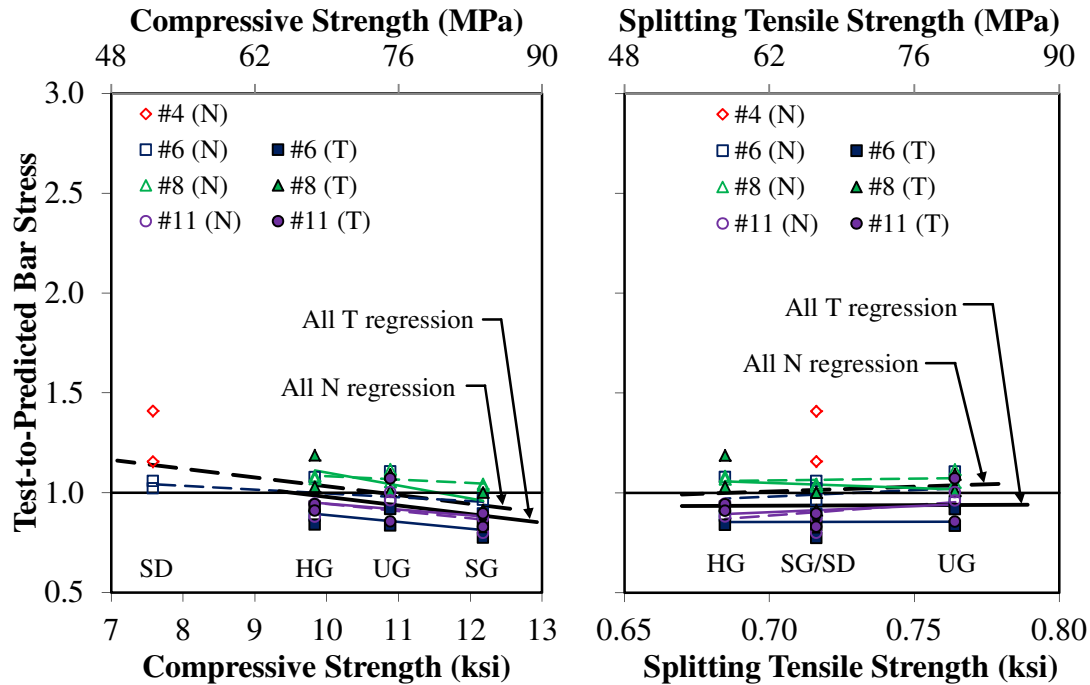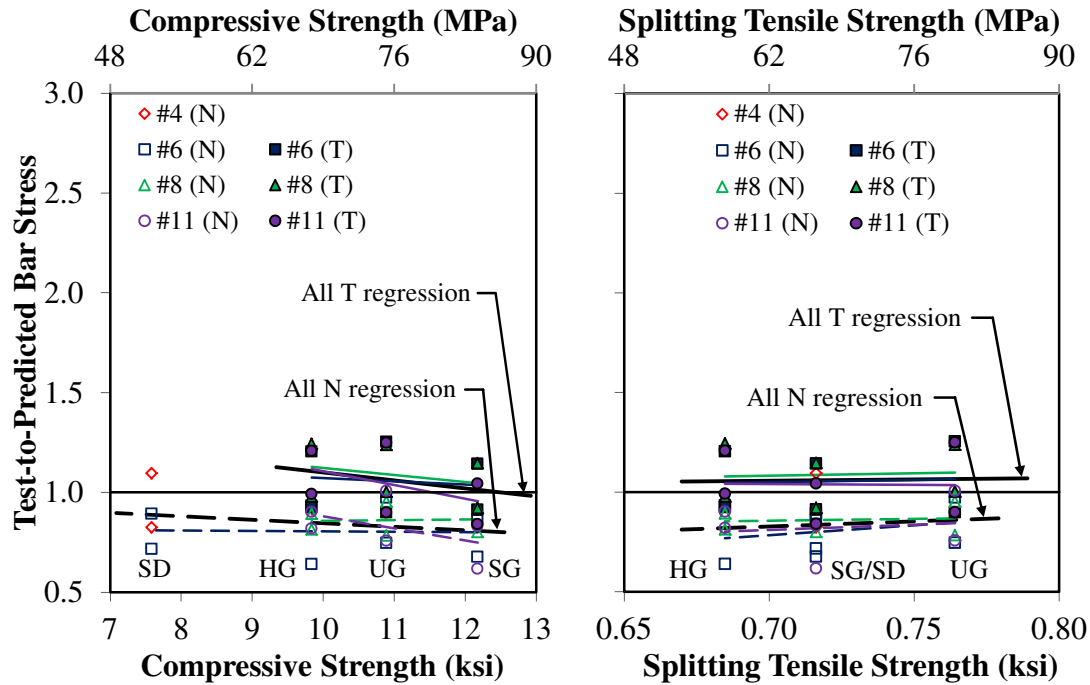**Figure 43. Graph. Bar Stress Test-to-Prediction Ratio Compared to Compressive Strength and Splitting Tensile Strength for AASHTO LRFD Expression (Eq. 31) by Mix Design and Bar Size for Specimens without Stirrups (N) and with Stirrups (T).**
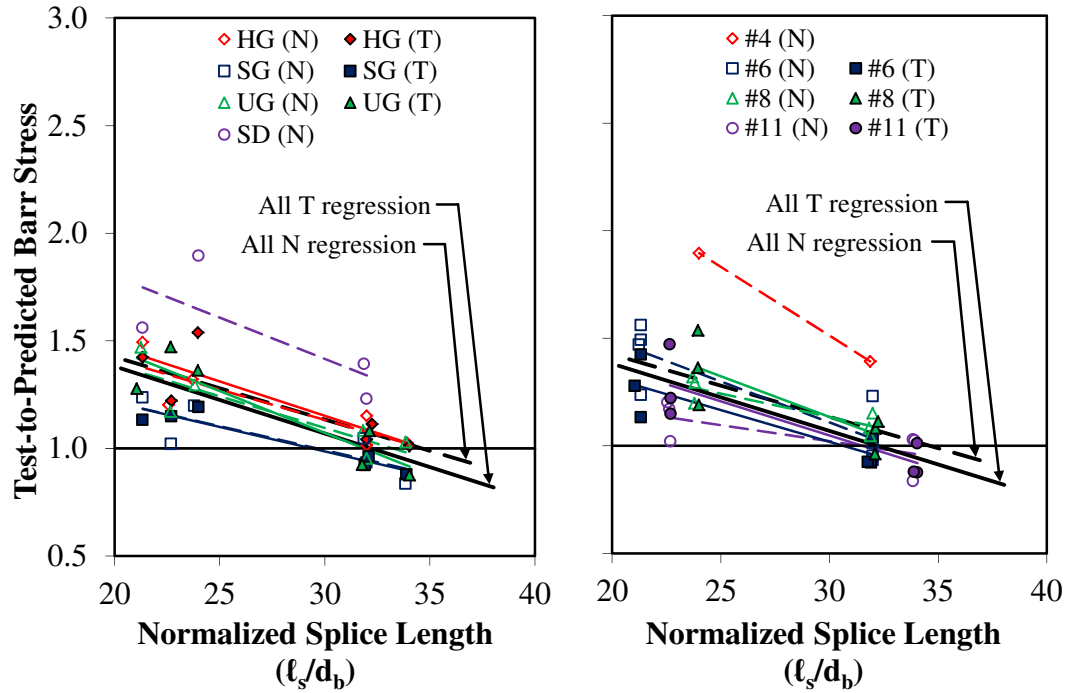
Figure 44. Graph. Bar Stress Test-to-Prediction Ratio Compared to Normalized Splice Length (ℓ_s/d_b) for ACI 318-11 Expression (Eq. 32) by Mix Design and Bar Size for Specimens without Stirrups (N) and with Stirrups (T).
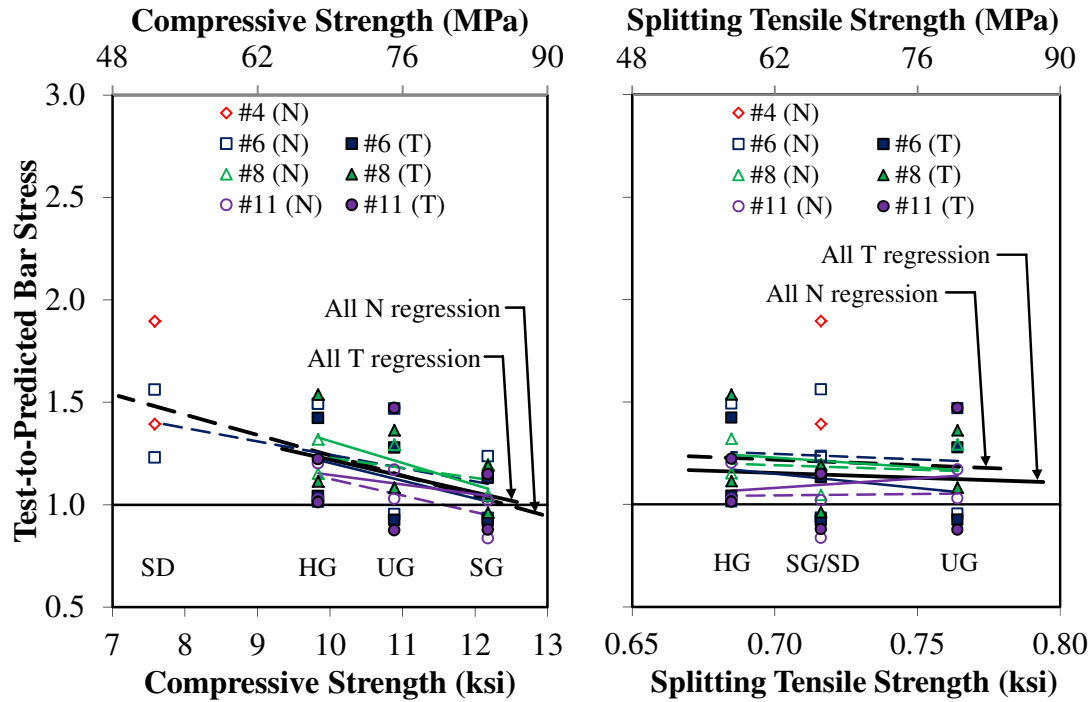
Figure 45. Graph. Bar Stress Test-to-Prediction Ratio Compared to Compressive Strength and Splitting Tensile Strength for ACI 318-11 Expression (Eq. 32) by Mix Design and Bar Size for Specimens without Stirrups (N) and with Stirrups (T).
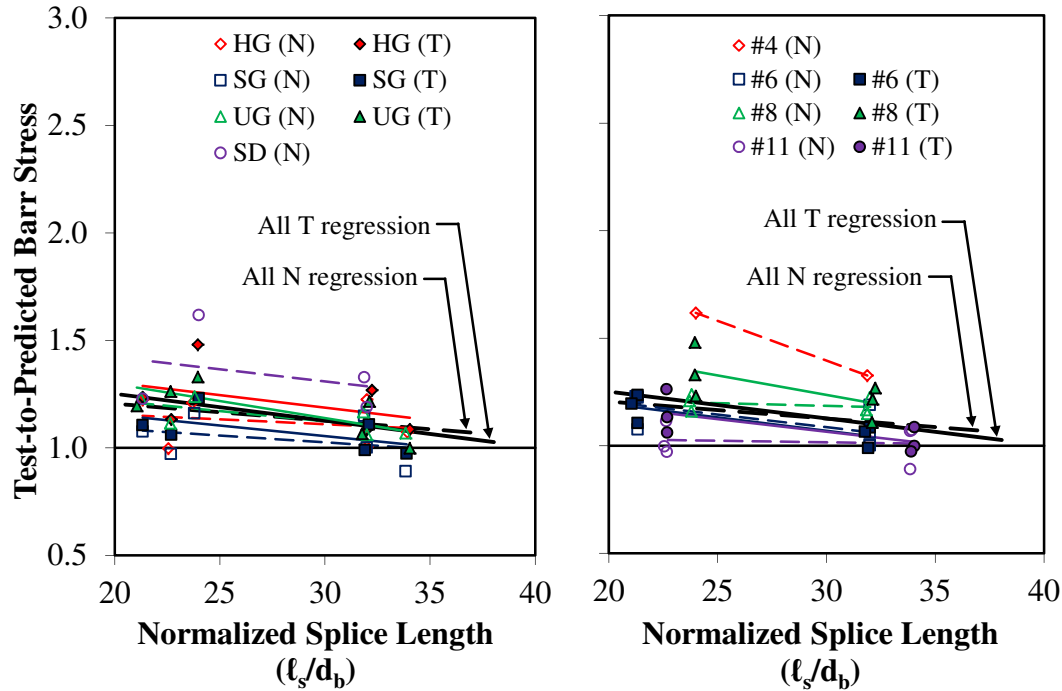
Figure 46. Graph. Bar Stress Test-to-Prediction Ratio Compared to Normalized Splice Length (ℓ_s/d_b) for ACI 408-03 Expression (Eq. 33) by Mix Design and Bar Size for Specimens without Stirrups (N) and with Stirrups (T).
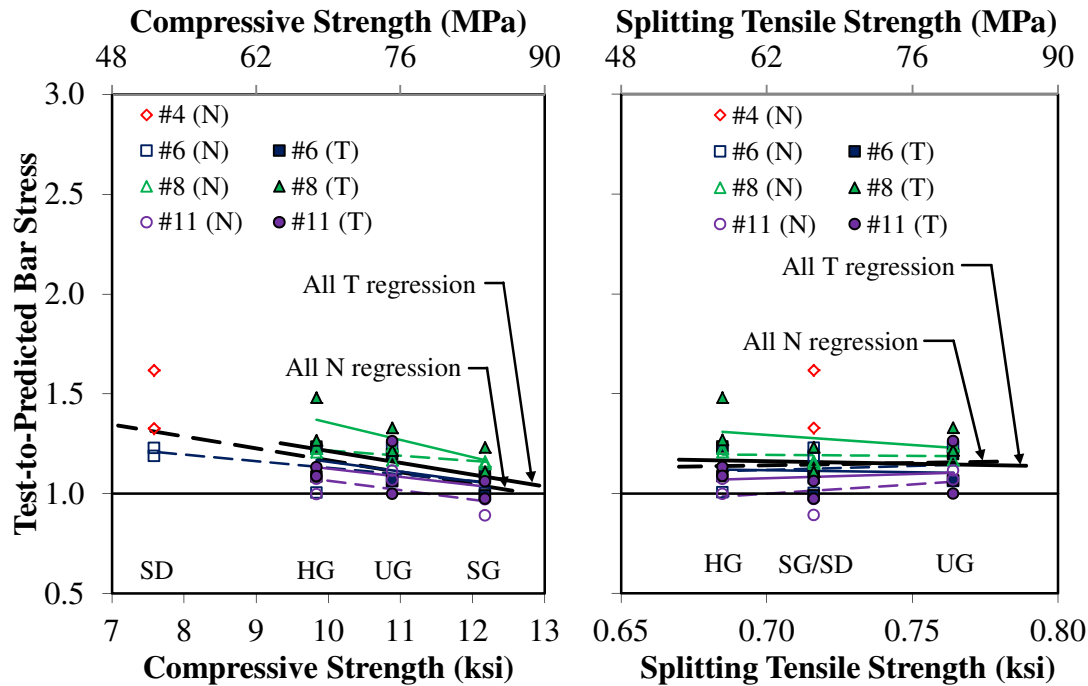
Figure 47. Graph. Bar Stress Test-to-Prediction Ratio Compared to Compressive Strength and Splitting Tensile Strength for ACI 408-03 Expression (Eq. 33) by Mix Design and Bar Size for Specimens without Stirrups (N) and with Stirrups (T).

The figures showing the AASHTO LRFD expression (Figure 43) and the ACI 408-03 expression (Figure 47) both show a slight decrease in the test-to-prediction ratio with increases in compressive strength. The rate of decrease appears slightly greater in Figure 45 for the ACI 318-11 expression.

Nearly uniform test-to-prediction ratios were observed in Figure 43, Figure 45, and Figure 47 when the design expressions are compared to the concrete splitting tensile strength as shown by their nearly horizontal regression lines.

SUMMARY OF EXPERIMENTAL RESULTS AND CONCLUDING REMARKS

The performance of 40 splice beam specimens tested to evaluate the bond strength of LWC was investigated in this research program. The splice beams had three bottom-cast splices of uncoated, mild steel bars. Bar sizes ranged from #4 to #11 and 18 beams had transverse reinforcement (stirrups) evenly spaced over the splice length. Four different concrete mix designs using three different lightweight aggregates were used. The mix designs included two expanded shales and one expanded slate. The concrete mixes used a blend of lightweight and normal-weight coarse aggregate and normal-weight sand. These mixes were prescriptively produced at the precaster's facility and used to produce the 40 splice beam specimens. For the three mix designs applicable to precast girder production, the design compressive strength ranged from 6 to 10 ksi (41 to 69 MPa) and the target unit weight ranged from 0.126 to 0.130 kcf (2020 to 2080 kg/m^3). The resulting concrete had a range in 28-day compressive strength of 8.0 to 10.6 ksi (55.1 to 73.0 MPa) and an air-dry density range of 0.126 to 0.133 kcf (2020 to 2130 kg/m^3). The one mix design applicable to field-cast bridge decks used an expanded slate and had a design compressive strength of 4 ksi (18 MPa) and a target unit weight of 0.125 kcf (2000 kg/m^3). The resulting concrete had a 28-day compressive strength of 5.7 ksi (39.3 MPa) and an air-dry density of 0.138 kcf (2210 kg/m^3).

The measured ultimate force in the hydraulic jacks was used to determine the average bar stress at failure in the splice beam specimens. The moment-curvature method described in ACI 408-03 for NWC was validated for use with the 40 LWC splice beam specimens.

The displacement ductility of the splice beam specimens was evaluated using the method described by Azizinamini et al. (17). The splice beams were designed with short-to-moderate ℓ_s/d_b ratios and as a result only 19 LWC splice beam specimens had a displacement ductility greater than unity. None of the specimens had a target displacement greater or equal to that recommended by Azizinamini et al.; however, the tests of four LWC specimens still ended in a ductile flexural-compression failure. An evaluation of the displacement ductilities of the LWC specimens do support the concept proposed by Azizinamini et al. that the target displacement ductility should increase as the reinforcement ratio decreases to ensure a ductile failure.

The normalized bar stress at failure exhibited some dependency upon the mix design. The use of f_{ct} to normalize bar stress accounted for most of the observed differences in the mix-to-mean bar

stress ratios. There was very little difference between the mix-to-mean ratios for specimens with stirrups or without stirrups indicating the differences observed between concrete mixes was not dependent upon the presence of stirrups.

The bar stress at failure was dependent upon the bar size and this trend was independent of the presence of stirrups or the factor used to normalize bar stress. The specimens with #8 bars consistently had a higher f_s than average, although this was likely due to is slightly higher yield strength.

The descriptive expression for bar stress given by Orangun et al. consistently overestimated the bar stress at failure with mean test-to-prediction ratios less than unity for specimens with stirrups and without stirrups. The descriptive expression by Zuo and Darwin gave mean test-to-prediction ratios near unity for all 40 LWC specimens. No modification of either expression was used to account for the use of LWC. Both expressions showed a decrease in the test-to-prediction ratios with an increase in compressive strength and uniform test-to-prediction ratios with an increase in splitting tensile strength.

The bar stresses at failure were also compared to expressions based on design expressions for development length of rebar. The mean test-to-prediction ratio for all specimens was 0.94 for the AASHTO LRFD expression, 1.18 for the ACI 318-11 expression, and 1.15 for the ACI 408-03 expression. This indicates that the bar stresses were slightly overestimated by the AASHTO LRFD expression, and slightly underestimated by the ACI 318-11 expression and ACI 408-03 expression. These predictions of bar stress do not include a modification factor for lightweight concrete (λ taken as unity) or the safety factors applied for the design of splices. Similar to the descriptive expressions, the design expressions showed a decrease in the test-to-prediction ratio with increases in compressive strength, and uniform test-to-prediction ratios with increases in splitting tensile strength.

CHAPTER 4.   TFHRC MILD STEEL DEVELOPMENT LENGTH DATABASE

INTRODUCTION

This chapter describes the information available in the TFHRC Mild Steel Development Length Database. The type of information included in the database for each is described. The number of each type of specimen and the types of concrete mixtures found for each specimen type is described. A large number of NWC specimens are available in the ACI Committee 408 Database. The method used to select specimens from the ACI Committee 408 Database for comparison with LWC specimen in the TFHRC Database is described. The chapter also includes statistical information by concrete mixture type and specimen type for the tests in the TFHRC Database.

TFHRC MILD STEEL DEVELOPMENT LENGTH DATABASE

A thorough literature review was performed to find published journal papers, conference papers, technical reports, and university dissertations that included tests, analysis, or discussions of LWC. Over 500 references were found in the literature that mentioned LWC. These references were reviewed for data from tests that measured the development of mild steel in tension. Tests included in the database were limited to data from beam-end specimens, splice beam specimens, tension beam specimens, and development beam specimens.[41-50] The details of the specimens in each reference are described in the following section. Only test data from published reports was included in the database.

The information collected for each test included its concrete mix, associated concrete mechanical property tests, test specimen dimensions, and test results. The recorded mechanical tests included compressive strength, modulus of elasticity, splitting tensile test, modulus of rupture, and Poisson's ratio. Up to two measures of concrete density were also recorded. Concrete mix information was recorded including the type of coarse and fine aggregate, the use of chemical admixtures, and the use of supplementary cementitious materials. Information about the mechanical tests was recorded including the specimen size, duration and type of curing, and specimen age.

In addition to data from tests on LWC, a select number of tests on NWC were also included in the database for comparison. The references containing test data on the development of mild steel in LWC also had a limited number of tests on NWC. These tests on NWC are also included. The ACI Committee 408 report (9) has data from 478 bottom-cast specimens. A subset of the ACI Committee 408 Database was selected for comparison to the LWC specimens and included in the TFHRC Database. The criteria used to select the NWC specimen from the ACI Committee 408 Database is described later in this chapter. The high-strength NWC specimens from NCHRP Project 12-60 (18) are not included in the ACI Committee 408 Database. The NWC specimens from NCHRP Project 12-60 with uncoated reinforcement are

included in the TFHRC Database. A full list of references for the tests of LWC and NWC specimens in the TFHRC Database is included in Chapter 8.

Table 14 gives a summary of the number of tests for each concrete mixture type relevant to each specimen type in the TFHRC Mild Steel Development Length Database. The definitions of different types of lightweight concrete mixtures have been traditionally based on the use of lightweight or normal weight constituent materials. The types of concrete mixtures used in the database included all-lightweight, sand-lightweight, specified density, and inverted mix. All-lightweight was defined as concrete with lightweight fine and coarse aggregate. Sand-lightweight was defined as concrete with lightweight coarse aggregate and either sand or a mixture of sand and lightweight fine aggregate. Specified density was defined as concrete with a mixture of normal weight and lightweight coarse aggregate and either sand or lightweight fine aggregate. The tests indicated as "normal weight" included those found in papers with tests on LWC specimens and the specimens from NCHRP 12-60.[18] The tests indicated as "NWC – ACI 408" are the selected tests from the ACI Committee 408 Database.[9] The tests on normal weight concrete specimens found in the literature and the specimens from NCHRP 12-60 were not repeated in the ACI Committee 408 Database.

Table 14. Summary of the Types of Specimens by Concrete Mixtures in the TFHRC Mild Steel Development Length Database.

| Expression | No. of Data Lines | | | | | |
	Total	All-Lightweight	Sand-Lightweight	Specified Density	Normal Weight	NWC - ACI408
Beam-end	72	0	64	0	8	0
Splice Beam	314	0	23	40	10	241
Tension Beam	48	0	48	0	0	0
Development Beam	40	36	0	0	4	0
Total	474	36	135	40	22	241

TEST SPECIMENS

This section describes the types of specimens included in the TFHRC Mild Steel Development Length Database. These include beam-end specimens, splice beam specimens, tension prism specimens, and development beam specimens. Illustrations of these specimen types were provided in Figure 2 and Figure 3. Many references were found that contained test data from different types of pull-out tests. For the reasons described previously in this report, no data from pull-out tests were included in the database.

There are 72 tests on beam-end specimens in the TFHRC Database. Four single-bar tests were conducted on each specimen. The data from these tests is from two references.[42,48] All of the LWC specimens were sand-lightweight and used sintered fly ash, slag, or expanded clay coarse aggregate. Eight specimens were NWC.

The TFHRC Database includes 48 tests on "tension prisms" from two references.[44,46] Tension prisms are small specimens with tension applied to one discontinuous central bar that makes non-contact lap splices with four perimeter bars, one in each corner of the specimen's square cross section. All of the specimens were made using sand-lightweight concrete with natural pumice as the coarse aggregate. An illustration of a tension prism specimen is shown in Figure 3.

Two references were found that used a flexural beam test to determine the bond strength of the reinforcement.[47,49] These tests are termed "development beams" in this document. Development beams are equivalent to two beam-end specimens placed back-to-back. The reinforcement is shielded from the confining effects of the support reaction through the use of a bond breaker along the bar in the region of the support. An illustration of a development beam specimen is shown in Figure 3. There are 36 LWC specimens and four NWC specimens in the database. All of the LWC specimens used all-lightweight concrete with expanded shale, expanded slag, or an unspecified aggregate from Japan as the coarse and fine aggregate.

As described previously in this report, splice beam specimens achieve a realistic stress-state in the splice, and can directly measure splice strength.[9] The TFHRC Database includes splice beam test data from four references in addition to the selected tests from the ACI Committee 408 Database.[9,18,41,43,45,50] The data on LWC used sand-lightweight or specified density mixes with expanded clay, expanded shale, expanded slate, and sintered fly ash as the coarse aggregate. The data from specimens with specified density concrete refer to the tests performed as part of the research program at TFHRC on LWC as described previously in this report. The data on NWC came from one of the references with LWC data, the NCHRP 12-60 report, and the ACI Committee 408 Database.[9,18,43]

The reported value for bond stress or bar stress was used for all tests expect those from two references that gave the results of splice beam tests.[18,43] The bar stress for the tests in these two references gave adequate information to allow a calculation of the bar stress at failure using the procedure from the ACI 408 Committee report as described previously in this document.[9]

SELECTION OF SPECIMENS FOR COMPARISON FROM THE ACI 408 DATABASE

The effect that lightweight aggregate has on the development of mild steel reinforcement is evaluated by comparing LWC specimens to NWC specimens. The realistic stress state in splice beam specimens and the larger number of test data from both LWC and NWC splice beam specimens make splice beam specimens a substantial part of the analysis to quantify the effect that lightweight concrete has on the development of bar stress. There is a large number of NWC splice beam tests available in the ACI Committee 408 Database. In order to determine the effect

of LWC on the development of bar stress, the LWC splice beam specimens in the TFHRC Database are compared to a subset of NWC splice beam specimens in the ACI Committee 408 Database that have similar parameters that are significant to the development of bar stress.

As shown in Table 15, the 478 NWC splice beam specimens in the ACI Committee 408 Database have a wide range of parameters such as lap splice length, bar diameter, concrete cover, concrete compressive strength, and bar yield stress.[9] The range of parameters for the specified density concrete specimens that are a part of the TFHRC LWC study described in this document are also given in Table 15. The table gives the number of specimens in the ACI Committee 408 Database that are outside the range of each parameter (i.e., greater than the maximum value or less than the minimum value from the tests at TFHRC).

Table 15. Maximum and Minimum Properties of Splice Beam Specimens in the ACI 408 Database, and the number of Specimens in the ACI 408 Database within the Property Limits of TFHRC Mild Steel Development Length Subset Databases.

Dataset	Limits	ℓ_s (inch)	d_b (inch)	ℓ_s / d_b	c_b / d_b	f_c' (ksi)	f_y (ksi)
ACI 408	Max	82.50	1.69	198.6	17.73	16.10	122.2
(478 spcmn, 286 with A_{tr})	Min	5.50	0.14	7.00	0.71	1.82	50.0
TFHRC Only	Max	48.00	1.41	34.04	1.50	10.64	73.8
(1 specimen within	Min	12.00	0.50	21.06	1.20	5.67	65.7
limits[†], 0 with A_{tr})	No > Max[‡]	23	2	52	437	93	64
	No < Min[*]	47	3	230	0	309	128
Other LWC Splice Beams	Max	39.37	1.26	50.00	3.50	8.88	81.2
(90 specimens within	Min	15.75	0.79	12.50	2.00	3.29	52.0
limits[†], 54 with A_{tr})	No > Max[‡]	59	112	8	8	120	51
	No < Min[*]	88	109	32	198	38	1
All LWC Splice Beams	Max	48.00	1.41	50.00	3.50	10.64	81.2
(241 specimens within	Min	12.00	0.50	12.50	1.20	3.29	52.0
limits[†], 155 with A_{tr})	No > Max[‡]	23	2	8	8	93	51
	No < Min[*]	47	3	32	0	38	1

Notes:
[†] No. of specimens in ACI 408 Database within maximum and minimum limits of all six parameters for the LWC datasets
[‡] No. of specimens in ACI 408 Database greater than the maximum parameter of the LWC dataset
[*] No. of specimens in ACI 408 Database less than the minimum parameter of the LWC dataset
Units: 1.0 inch = 25.4 mm, 1.0 ksi = 6.89 MPa

A NWC splice beam specimen in the ACI Committee 408 Database was assumed to be similar to the LWC splice beam specimens in the TFHRC Database if its six parameters (i.e., ℓ_s, d_b, ℓ_s/d_b, c_b/d_b, f_c', and f_y) were within the range of parameters (i.e., the maximum and minimum parameter values) in the LWC database. Only one specimen from the ACI Committee 408 Database was within the ranges of all six parameters given in Table 15 for the TFHRC splice beam specimens. For the LWC splice beams from the literature, there were 90 specimens from the ACI Committee 408 Database that were within the ranges of all six parameters. For the combined dataset consisting of both the TFHRC splice beam specimens and the LWC specimens from the literature, labeled "All LWC Splice Beams" in Table 15, there were 241 specimens from the ACI Committee 408 Database that were within the ranges of all six parameters.

In the following chapter, "Bar Stress Analysis of Specimens in the TFHRC Database" the specimens referred to as "NWC Specimens" include the selected 241 NWC specimens from the ACI Committee 408 Database combined with the NWC specimens from one of the references with LWC data and the NWC specimens from the NCHRP 12-60 report.[9,18,43]

DISTRIBUTION OF STATISTICAL PARAMETERS FOR SPECIMENS IN THE TFHRC DATABASE

A series of tables and figures were created to give statistical information on the specimens in the TFHRC Mild Steel Development Database. The statistical information is given by type of concrete mixture and then given again by type of specimen. For each type of concrete mix, Table 16 gives the mean value and range of values (i.e., maximum and minimum values) of the compressive strength, splitting tensile strength, and unit weight. Table 17 through Table 19 give the mean value and the range of values for several statistical parameters that influence bond strength by specimen type. Table 17, Table 18, and Table 19 give statistical information for all of the LWC and NWC beam-end specimens, tension prism specimens, and development beam specimens, respectively. Table 20 and Table 21 give statistical information for all of the LWC and NWC splice beam specimens, respectively. Bar stress versus splice length and bar stress versus concrete compressive strength for the specimens in the TFHRC Database is shown graphically in Figure 48 and Figure 50, respectively, by concrete mixture type and in Figure 49 and Figure 51, respectively, by specimen type.

Table 16. Distribution of Mechanical Properties by Concrete Mixtures Type in the TFHRC Mild Steel Development Length Database.

Concrete Mixture Type	Property	No. of Data Lines	Mean	COV	Max.	Min.
All-Lightweight	f_c' (ksi)	36	4.88	44.6%	8.92	2.24
	f_{ct} (ksi)	18	0.353	19.9%	0.450	0.305
	w_c (kcf)	36	0.090	13.8%	0.103	0.075
Sand-Lightweight	f_c' (ksi)	135	5.32	46.6%	10.88	1.39
	f_{ct} (ksi)	69	0.373	29.1%	0.580	0.232
	w_c (kcf)	135	0.115	6.8%	0.133	0.091
Specified Density	f_c' (ksi)	40	9.06	17.0%	10.64	5.67
	f_{ct} (ksi)	40	0.721	4.3%	0.764	0.685
	w_c (kcf)	40	0.131	2.7%	0.138	0.126
Normal Weight	f_c' (ksi)	22	8.84	50.2%	16.20	3.42
	f_{ct} (ksi)	14	0.552	47.0%	0.834	0.284
	w_c (kcf)	16	0.133	20.9%	0.150	0.075
NWC - ACI408	f_c' (ksi)	241	5.21	34.2%	10.62	3.31
	f_{ct} (ksi)	0	--	--	--	--
	w_c (kcf)	0	--	--	--	--

Units: 1.0 ksi = 6.89 MPa, 0.001 kcf = 16.01 kg/m^3

Table 17. Distribution of Properties for Beam-End Specimens in the TFHRC Mild Steel Development Length Database.

Concrete Mixture Type	Property	No. of Data Lines	Mean	COV	Max.	Min.
LWC	ℓ_s (inch)	64	6.92	32.0%	9.07	1.89
	d_b (inch)	64	0.56	19.8%	0.63	0.39
	c_b (inch)	64	1.27	32.6%	1.89	0.79
	ℓ_s / d_b	64	12.68	27.2%	14.40	3.00
	c_b / d_b	64	2.25	19.4%	3.00	2.00
	f_c' (ksi)	64	6.23	36.1%	10.88	2.81
	f_{ct} (ksi)	40	0.41	18.0%	0.54	0.23
	w_c (kcf)	64	0.12	8.9%	0.13	0.09
NWC	ℓ_s (inch)	8	4.72	47.8%	7.56	1.89
	d_b (inch)	8	0.63	0.0%	0.63	0.63
	c_b (inch)	8	1.89	0.0%	1.89	1.89
	ℓ_s / d_b	8	7.50	47.8%	12.00	3.00
	c_b / d_b	8	3.00	0.0%	3.00	3.00
	f_c' (ksi)	8	7.69	0.0%	7.69	7.69
	f_{ct} (ksi)	0	--	--	0.00	0.00
	w_c (kcf)	8	0.15	0.0%	0.15	0.15

Units: 1.0 inch = 25.4 mm, 1.0 ksi = 6.89 MPa, 0.001 kcf = 16.01 kg/m^3

Table 18. Distribution of Properties for Tension Prism Specimens in the TFHRC Mild Steel Development Length Database.

Concrete Mixture Type	Property	No. of Data Lines	Mean	COV	Max.	Min.
LWC	ℓ_s (inch)	48	12.08	34.7%	17.50	4.69
	d_b (inch)	48	0.41	14.4%	0.63	0.39
	c_b (inch)	48	2.31	17.5%	2.46	1.25
	ℓ_s / d_b	48	12.08	34.7%	17.50	4.69
	c_b / d_b	48	5.76	22.9%	6.25	1.99
	f_c' (ksi)	48	3.33	34.1%	5.37	1.39
	f_{ct} (ksi)	6	0.57	2.6%	0.58	0.55
	w_c (kcf)	48	0.11	1.9%	0.12	0.11

Units: 1.0 inch = 25.4 mm, 1.0 ksi = 6.89 MPa, 0.001 kcf = 16.01 kg/m^3

Table 19. Distribution of Properties for Development Beam Specimens in the TFHRC Mild Steel Development Length Database.

Concrete Mixture Type	Property	No. of Data Lines	Mean	COV	Max.	Min.
LWC	ℓ_s (inch)	36	23.16	28.8%	30.00	10.00
	d_b (inch)	36	0.87	14.6%	1.00	0.75
	c_b (inch)	36	1.21	24.0%	1.50	0.93
	ℓ_s / d_b	36	23.16	28.8%	30.00	10.00
	c_b / d_b	36	1.37	9.8%	1.50	1.24
	f_c' (ksi)	36	4.88	44.6%	8.92	2.24
	f_{ct} (ksi)	18	0.35	19.9%	0.45	0.30
	w_c (kcf)	36	0.09	13.8%	0.10	0.07
NWC	ℓ_s (inch)	4	26.32	0.0%	26.32	26.32
	d_b (inch)	4	0.75	0.0%	0.75	0.75
	c_b (inch)	4	0.93	0.0%	0.93	0.93
	ℓ_s / d_b	4	26.32	0.0%	26.32	26.32
	c_b / d_b	4	1.24	0.0%	1.24	1.24
	f_c' (ksi)	4	6.62	40.1%	8.92	4.32
	f_{ct} (ksi)	4	0.38	22.2%	0.45	0.30
	w_c (kcf)	4	0.09	16.5%	0.10	0.07

Units: 1.0 inch = 25.4 mm, 1.0 ksi = 6.89 MPa, 0.001 kcf = 16.01 kg/m^3

Table 20. Distribution of Properties for LWC Splice Beam Specimens in the TFHRC Mild Steel Development Length Database.

Concrete Mixture Type	Property	No. of Data Lines	Mean	COV	Max.	Min.
All LWC	ℓ_s (inch)	63	26.30	34.9%	48.00	12.00
	d_b (inch)	63	1.03	26.5%	1.41	0.50
	c_b (inch)	63	1.76	37.6%	2.76	0.72
	ℓ_s / d_b	63	25.99	27.9%	50.00	12.50
	c_b / d_b	63	1.70	31.0%	3.50	1.20
	f_c' (ksi)	63	8.28	26.5%	10.64	3.29
	f_{ct} (ksi)	63	0.55	40.7%	0.76	0.23
	w_c (kcf)	63	0.13	6.4%	0.14	0.11
TFHRC LWC	ℓ_s (inch)	40	28.04	37.0%	48.00	12.00
	d_b (inch)	40	1.01	29.2%	1.41	0.50
	c_b (inch)	40	1.39	29.3%	2.12	0.72
	ℓ_s / d_b	40	27.59	18.6%	34.04	21.06
	c_b / d_b	40	1.37	5.4%	1.50	1.20
	f_c' (ksi)	40	9.06	17.0%	10.64	5.67
	f_{ct} (ksi)	40	0.72	4.3%	0.76	0.68
	w_c (kcf)	40	0.13	2.7%	0.14	0.13
Other LWC	ℓ_s (inch)	23	23.28	24.4%	39.37	15.75
	d_b (inch)	23	1.07	21.9%	1.26	0.79
	c_b (inch)	23	2.40	20.9%	2.76	1.57
	ℓ_s / d_b	23	23.21	40.5%	50.00	12.50
	c_b / d_b	23	2.27	21.5%	3.50	2.00
	f_c' (ksi)	23	6.92	36.3%	8.88	3.29
	f_{ct} (ksi)	23	0.26	14.8%	0.35	0.23
	w_c (kcf)	23	0.12	5.6%	0.13	0.11

Units: 1.0 inch = 25.4 mm, 1.0 ksi = 6.89 MPa, 0.001 kcf = 16.01 kg/m^3

Table 21. Distribution of Properties for NWC Splice Beam Specimens in the TFHRC Mild Steel Development Length Database.

Concrete Mixture Type	Property	No. of Data Lines	Mean	COV	Max.	Min.
All NWC	ℓ_s (inch)	251	23.34	33.8%	45.00	12.00
	d_b (inch)	251	1.02	20.1%	1.41	0.50
	c_b (inch)	251	1.87	29.0%	3.44	0.75
	ℓ_s / d_b	251	22.95	27.7%	42.00	13.71
	c_b / d_b	251	1.85	25.7%	3.50	0.89
	f_c' (ksi)	251	5.42	43.2%	16.20	3.31
	f_{ct} (ksi)	10	0.62	44.3%	0.83	0.28
	w_c (kcf)	4	0.15	0.5%	0.15	0.15
ACI 408 NWC	ℓ_s (inch)	241	23.29	34.1%	45.00	12.00
	d_b (inch)	241	1.02	19.8%	1.41	0.50
	c_b (inch)	241	1.88	29.0%	3.44	0.75
	ℓ_s / d_b	241	22.82	28.1%	42.00	13.71
	c_b / d_b	241	1.85	25.5%	3.44	0.89
	f_c' (ksi)	241	5.21	34.2%	10.62	3.31
	f_{ct} (ksi)	0	--	--	--	--
	w_c (kcf)	0	--	--	--	--
Other NWC	ℓ_s (inch)	10	24.65	27.5%	36.00	16.00
	d_b (inch)	10	0.95	27.6%	1.41	0.75
	c_b (inch)	10	1.71	30.2%	2.76	1.13
	ℓ_s / d_b	10	26.17	13.7%	30.00	21.33
	c_b / d_b	10	1.86	33.2%	3.50	1.50
	f_c' (ksi)	10	10.64	56.8%	16.20	3.42
	f_{ct} (ksi)	10	0.62	44.3%	0.83	0.28
	w_c (kcf)	4	0.15	0.5%	0.15	0.15

Units: 1.0 inch = 25.4 mm, 1.0 ksi = 6.89 MPa, 0.001 kcf = 16.01 kg/m^3

Figure 48. Graph. Bar Stress Compared to Splice Length by Concrete Mixture Type in the TFHRC Mild Steel Development Length Database.

Figure 49. Graph. Bar Stress Compared to Splice Length by Specimen Type in the TFHRC Mild Steel Development Length Database.
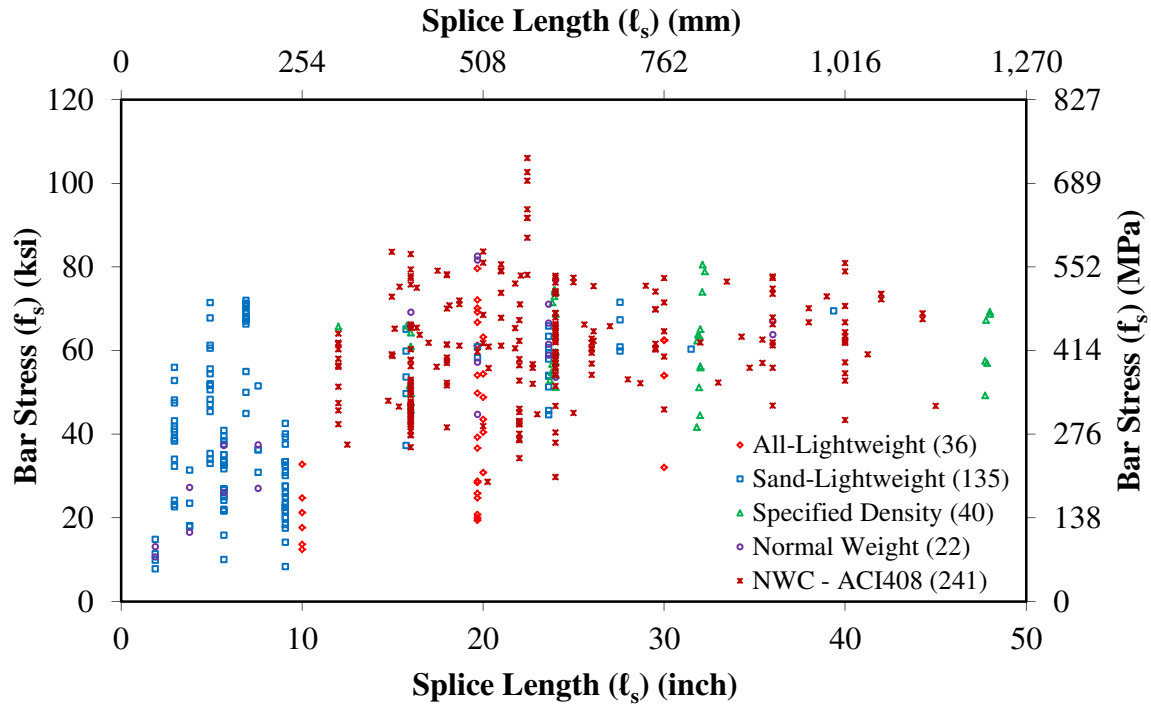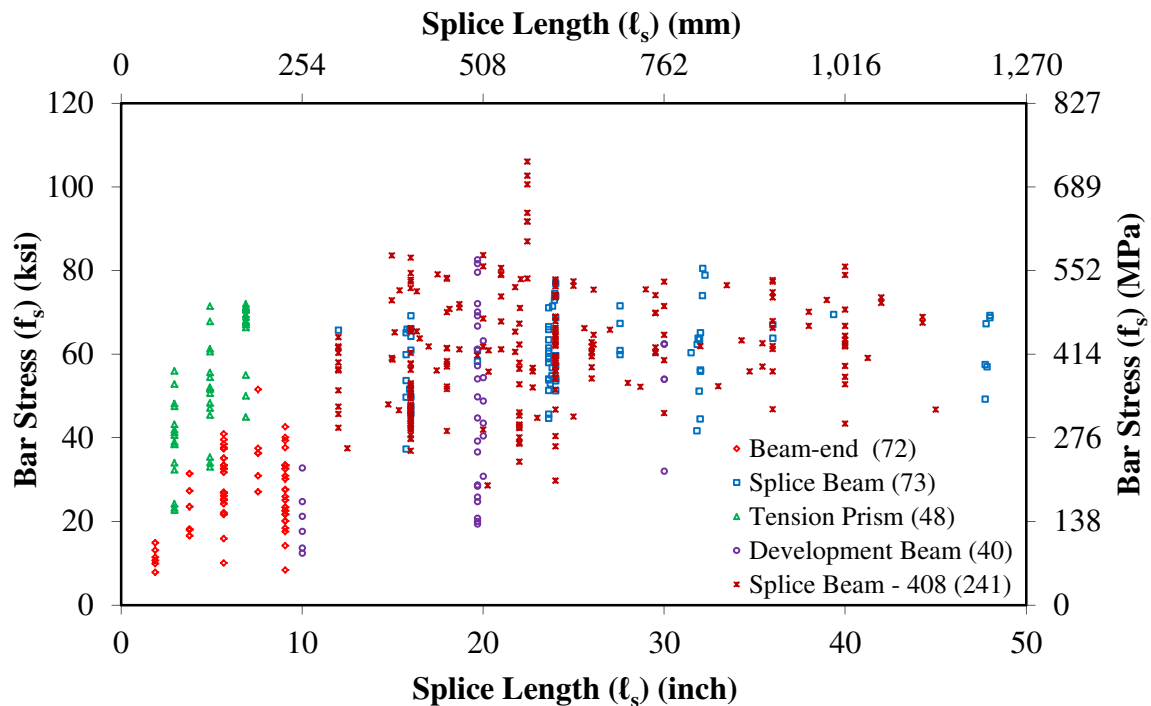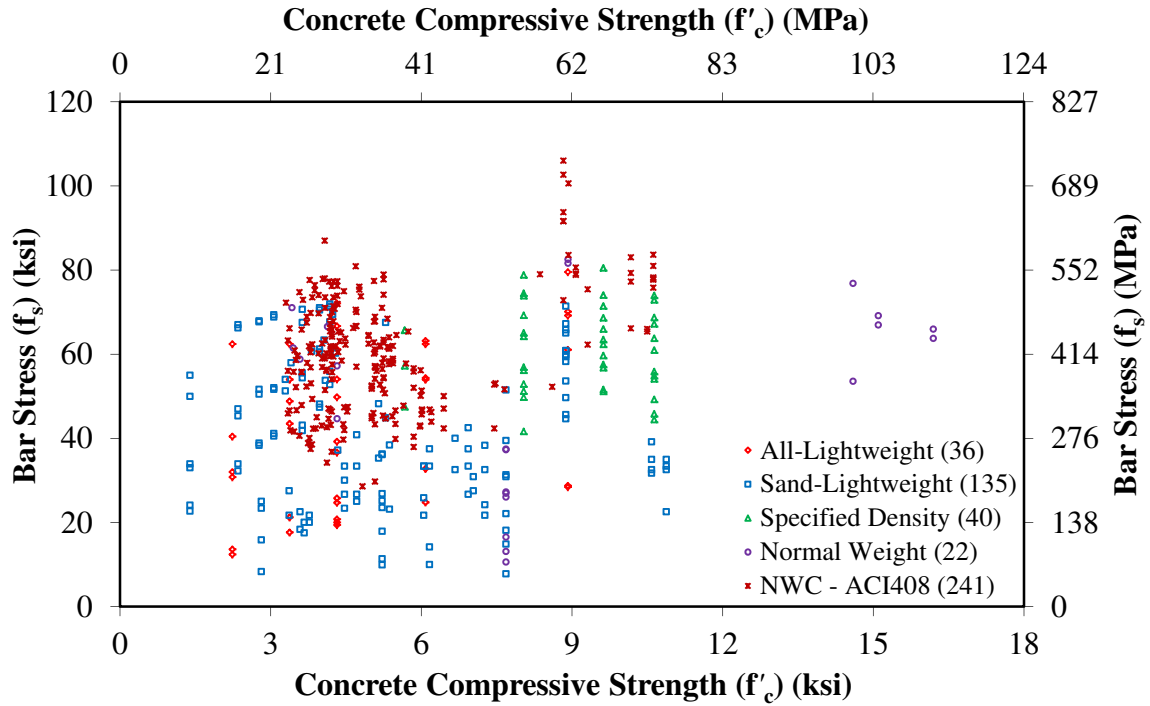
Figure 50. Graph. Bar Stress Compared to Compressive Strength by Concrete Mixture Type in the TFHRC Mild Steel Development Length Database.
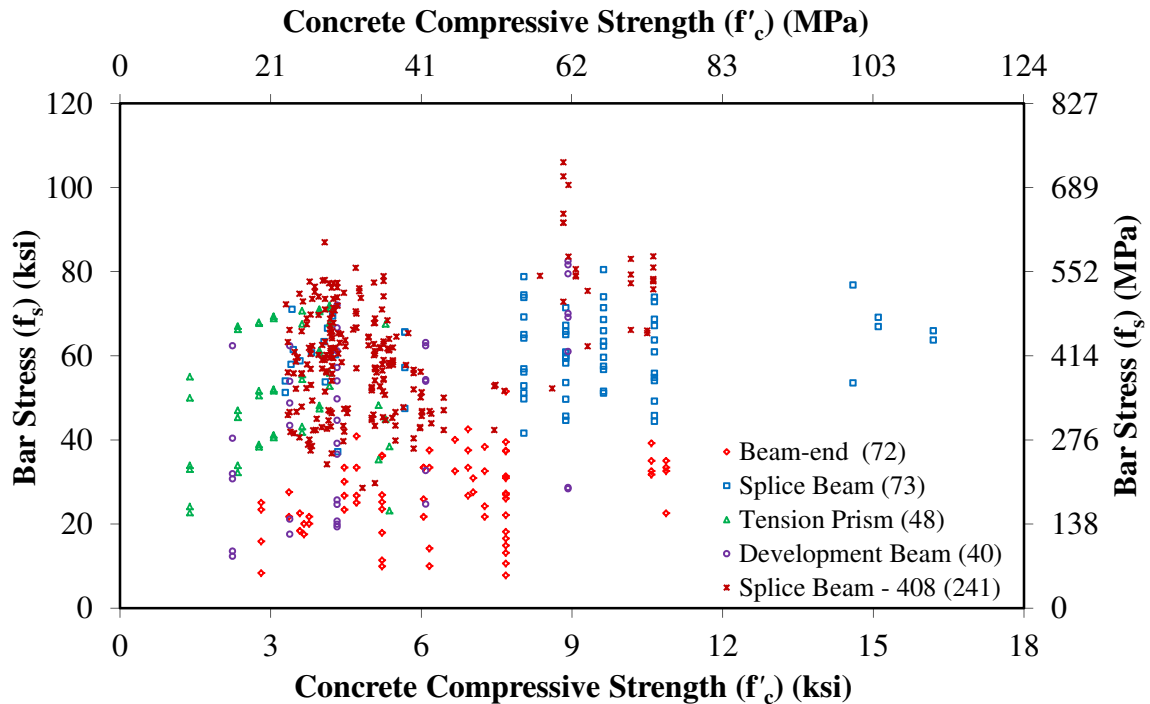

Figure 51. Graph. Bar Stress Compared to Compressive Strength by Specimen Type in the TFHRC Mild Steel Development Length Database.

CHAPTER 5.   BAR STRESS ANALYSIS OF SPECIMENS IN THE TFHRC DATABASE

INTRODUCTION

This chapter analyzes the bar stress of specimens in the TFHRC Mild Steel Development Length Database. In the first section, the bar stress is normalized by compressive strength and splitting tensile strength. This normalized stress is compared to normalized splice length to evaluate the effect of different methods used to normalized bar stress and splice length. In the second section, the bar stress predicted by design expressions without modification for LWC is analyzed. The third section evaluates the effect of a new expression for a LWC modification factor used in the design expressions. Also, a modification to one of the design expressions is proposed to improve the bar stress predicted for LWC specimens.

The quality of the prediction is given by its test-to-prediction ratio and the coefficient of variation (COV) describing the distribution of the ratios. A test-to-prediction ratio that is greater than unity indicates that the expression has under-estimated the measured value, while a ratio that is less than unity indicates an over-estimated value. The COV indicates the amount of scatter in the test-to-prediction ratio and a small COV is preferred.

The term proposed expression in the document refers to a prediction expression that is being proposed to AASHTO Subcommittee on Bridges and Structures (SCOBS) T-10 for consideration as a design expression in the AASHTO LRFD Specifications. Proposed expressions will also be included in the chapter of this document titled "Preliminary Recommendations for AASHTO LRFD Specifications".

BAR STRESS COMPARED TO SPLICE LENGTH FOR SPECIMENS IN THE TFHRC DATABASE

This section includes a comparison of the average bar stress at failure (f_s) to lap splice length (ℓ_s) for the LWC and NWC specimens in the TFHRC Database. The purpose of the comparison is to examine the effect of different parameters on bar stress. The parameters evaluated include concrete mixture type, specimen type, and different methods commonly used to normalize bar stress and lap splice length.

The bar stress and splice length are commonly normalized in design expressions for development length. In this section, the average bar stress is normalized by three factors: $\sqrt{f_c'}$, $f_c'^{0.25}$, and f_{ct}. The normalized splice length is given by a simple ℓ_s/d_b ratio, $\ell_s/d_b(c_b+K_{tr})/d_b$ based on ACI 318-11 (16), and $\ell_s(c_{min}+0.5d_b)/A_b$ based on Zuo and Darwin (12).

The linear sample correlation is used to evaluate the three factors to normalize bar stress and the three methods to normalize splice length. The linear sample correlation can vary between -1.0 and 1.0 and represents the amount of scatter in a linear regression with 1.0 indicating a perfect

correlation. Table 22 gives the sample correlations for the two methods to normalize splice length and Table 23 gives the sample correlations for the three factors to normalize bar stress. The sample correlations are given for the data as a whole and then for each concrete mixture type and specimen type.

Table 22. Linear Sample Correlation for Normalized Bar Stress ($f_s/\sqrt{f_c}$') versus Normalized Splice Length (ℓ_s/d_b and $\ell_s(c_b+0.5d_b)/A_b$) for Specimens in the TFHRC Database.

Expression	Series Label[†]	Linear Sample Correlation (r)	
		Specimens without Stirrups	Specimens with Stirrups
$f_s/\sqrt{f_c}$' versus ℓ_s/d_b	All data	0.458	0.552
(Figure 52 through Figure 55)			
	All-Lightweight (7, 29)	--	0.775
	Sand-Lightweight (127, 8)	0.382	0.470
	Specified Density (22, 18)	0.339	0.487
	Normal Weight (15, 7)	0.899	0.660
	NWC - ACI408 (86, 155)	0.759	0.690
	Beam-end (72, 0)	0.525	--
	Splice Beam (44, 29)	0.483	0.622
	Tension Prism (48, 0)	0.913	--
	Development beam (7, 33)	--	0.775
	Splice Beam - 408 (86, 155)	0.759	0.690
$f_s/\sqrt{f_c}$' versus $\ell_s(c_{min}+0.5d_b)/A_b$	All data	0.871	0.425
(Figure 56 through Figure 59)			
	All-Lightweight (7, 29)	--	0.769
	Sand-Lightweight (127, 8)	0.929	0.470
	Specified Density (22, 18)	0.477	0.491
	Normal Weight (15, 7)	0.932	-0.579
	NWC - ACI408 (86, 155)	0.818	0.364
	Beam-end (72, 0)	0.639	--
	Splice Beam (44, 29)	0.816	0.445
	Tension Prism (48, 0)	0.935	--
	Development beam (7, 33)	--	0.762
	Splice Beam - 408 (86, 155)	0.818	0.364

Notes: [†] No. of specimens with stirrups followed by No. without stirrups given in parentheses

Table 23. Linear Sample Correlation for Normalized Bar Stress ($f_s/\sqrt{f_c'}$, $f_s/f_c'^{0.25}$, and f_s/f_{ct}) versus Normalized Splice Length ($\ell_s/d_b \times (c_b+K_{tr})/d_b$) for Specimens in the TFHRC Database.

Expression	Series Label[†]	Linear Sample Correlation (r)	
		Specimens without Stirrups	Specimens with Stirrups
$f_s/\sqrt{f_c'}$ versus $\ell_s/d_b \times (c_b+K_{tr})/d_b$ (Figure 60 through Figure 63)	All data	0.872	0.428
	All-Lightweight (7, 29)	--	0.753
	Sand-Lightweight (127, 8)	0.929	0.470
	Specified Density (22, 18)	0.499	0.561
	Normal Weight (15, 7)	0.932	-0.025
	NWC - ACI 408 (86, 155)	0.817	0.600
	Beam-end (72, 1)	0.639	--
	Splice Beam (44, 29)	0.818	0.422
	Tension Prism (48, 1)	0.935	--
	Development beam (7, 33)	--	0.680
	Splice Beam - 408 (86, 155)	0.817	0.600
$f_s/(f_c'^{0.25})$ versus $\ell_s/d_b \times (c_b+K_{tr})/d_b$ (Figure 64 through Figure 67)	All data	0.820	0.383
	All-Lightweight (7, 29)	--	0.677
	Sand-Lightweight (127, 8)	0.895	0.470
	Specified Density (22, 18)	0.600	0.627
	Normal Weight (15, 7)	0.910	0.036
	NWC - ACI408 (86, 155)	0.849	0.595
	Beam-end (72, 0)	0.633	--
	Splice Beam (44, 29)	0.767	0.452
	Tension Prism (48, 0)	0.880	--
	Development beam (7, 33)	--	0.558
	Splice Beam - 408 (86, 155)	0.849	0.595
f_s/f_{ct} versus $\ell_s/d_b \times (c_b+K_{tr})/d_b$ (Figure 68 through Figure 71)	All data	0.678	0.322
	All-Lightweight (7, 11)	--	0.829
	Sand-Lightweight (61, 8)	0.651	0.470
	Specified Density (22, 18)	0.679	0.632
	Normal Weight (4, 4)	0.919	--
	Splice Beam (41, 26)	0.537	0.161
	Tension Prism (6, 0)	0.991	--
	Development beam (7, 15)	--	0.664

Notes: [†] No. of specimens with stirrups followed by No. without stirrups given in parentheses

The normalized bar stresses and normalized splice lengths are shown graphically in Figure 52 through Figure 71. The figures are given in sets of four. The first two figures show the results in groups of concrete mixture types and groups of specimen types, respectively, for specimens without stirrups. The second two figures show similar results for specimens with stirrups. The number of specimens in each group is shown in parentheses after the group label.

In each figure, the NWC specimens from the ACI Committee 408 Database are separated from the rest of the data. When the data is given by concrete mixture type, the NWC data found in references with the LWC data is labeled as "Normal Weight", while the data from the ACI Committee 408 Database is labeled "NWC – ACI 408". When the data is given by specimen type, the LWC and NWC splice beams found in references with LWC splice beam data are labeled "Splice Beam", while the data from the ACI Committee 408 Database is labeled "Splice Beam – 408".

Least-squares linear regression lines are shown in Figure 52 through Figure 71 for each group and for all specimens with stirrups (T) and all specimens without stirrups (N). The slope of the regression lines for individual groups can be compared to the slope of the entire group. This can be observed in the figure as whether the regression lines are parallel or intersect. Intersecting regression lines could indicate that the normalized bar stress of one group was affected by an increase in the normalized splice length more or less than the other groups.

Some groups of data had a limited number of tests or the data covered a limited range of splice length or bar stress. The limited data in these groups also had an effect on the slope of their regressions lines. The limited data could give the appearance of an effect of normalized splice length on normalized bar stress that would not be observed if there was additional data over a wider range of splice length or bar stress.

CONCRETE MIXTURE TYPE

A normalized splice length using an ℓ_s/d_b ratio for the specimens without stirrups gave a linear sample correlation of less than 0.40 for the LWC specimens while the sample correlation of the NWC specimens was greater than 0.75. The sample correlation improved considerably for LWC when using either $\ell_s(c_{min}+0.5d_b)/A_b$ or $\ell_s/d_b(c_b+K_{tr})/d_b$. The sample correlation for NWC improved to greater than 0.80 using either $\ell_s(c_{min}+0.5d_b)/A_b$ or $\ell_s/d_b(c_b+K_{tr})/d_b$.

In Figure 52 through Figure 67 the regression line for the NWC splice beam specimens from the ACI Committee 408 Database is above the regression line for the data as a whole. In the figures with groups by specimen type, the regression line for the NWC ACI Committee 408 Database tests is also above the regression line for the LWC and other NWC splice beam specimens in the TFHRC Database. This indicates that the bar stress for NWC is greater than the bar stress for LWC.
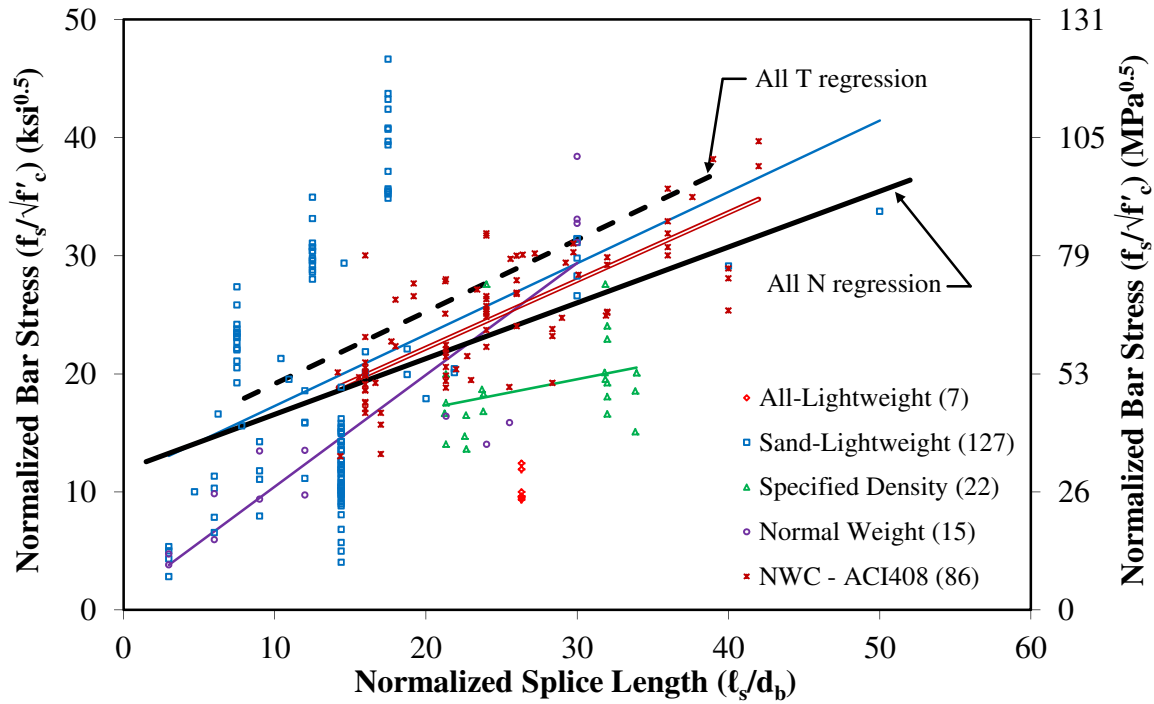
Figure 52. Graph. Normalized Bar Stress (f$_s$/√f$_c$') versus Normalized Splice Length (ℓ$_s$/d$_b$) by Concrete Mixture Type for Specimens without Stirrups (N) in the TFHRC Database.

Figure 53. Graph. Normalized Bar Stress (f$_s$/√f$_c$') versus Normalized Splice Length (ℓ$_s$/d$_b$) by Specimen Type for Specimens without Stirrups (N) in the TFHRC Database.

Figure 54. Graph. Normalized Bar Stress ($f_s/\sqrt{f_c'}$) versus Normalized Splice Length (ℓ_s/d_b) by Concrete Mixture Type for Specimens with Stirrups (T) in the TFHRC Database.
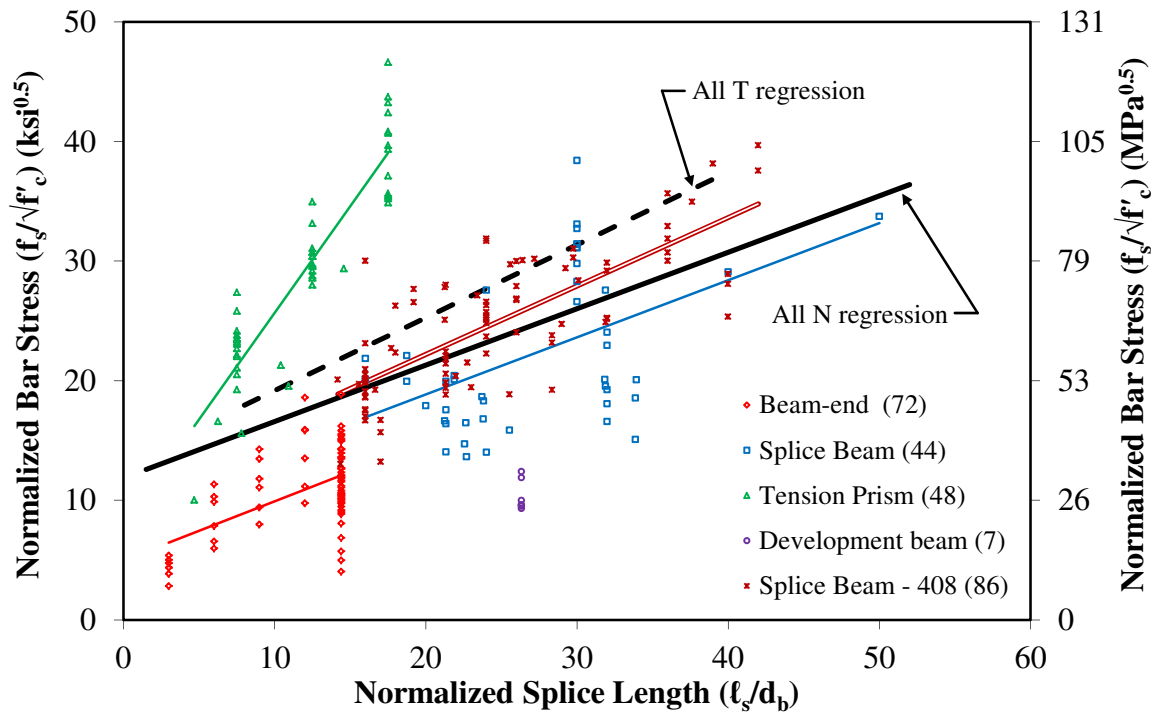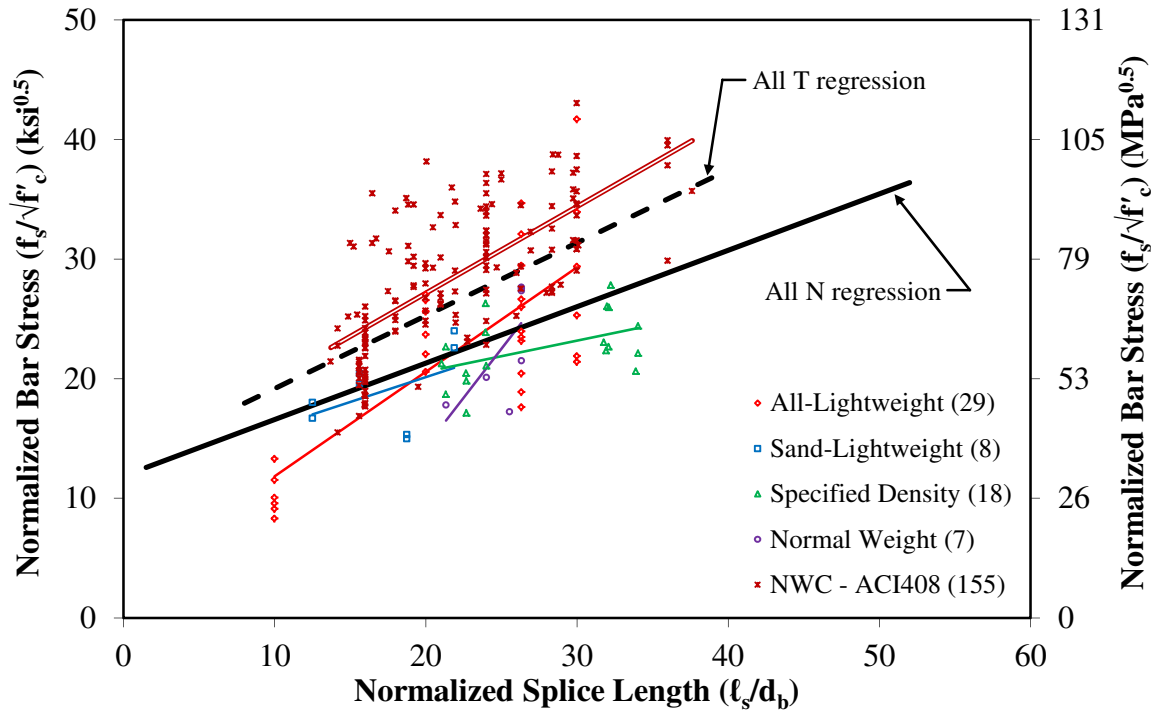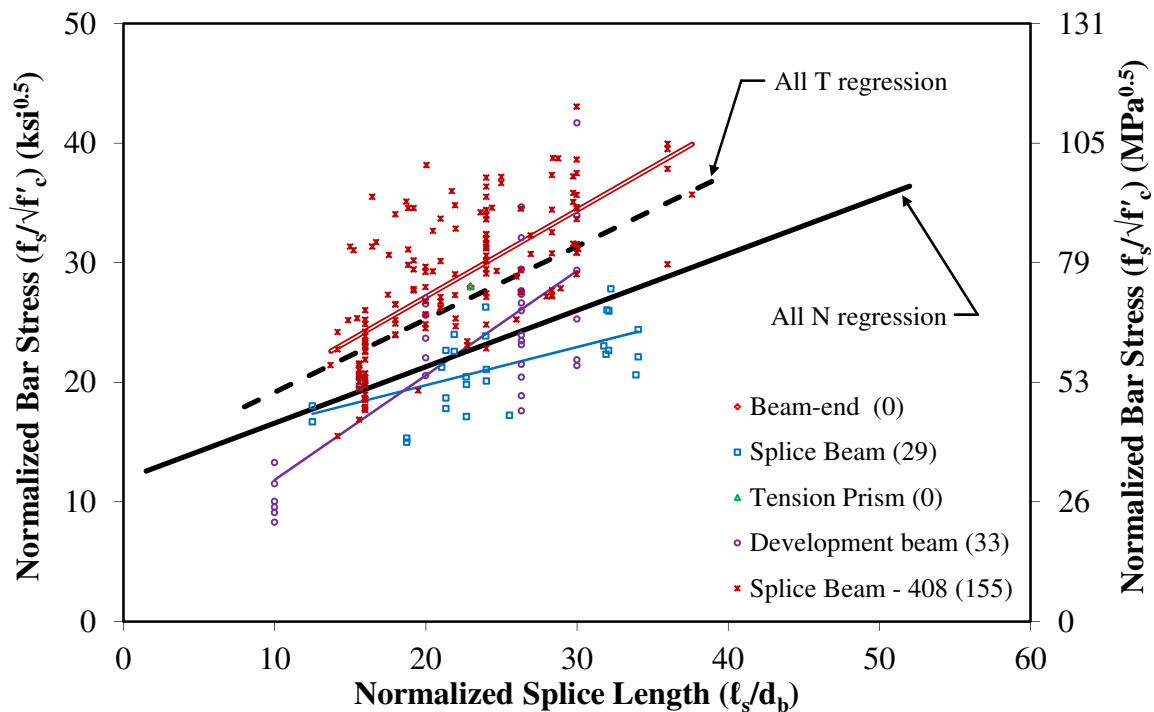

Figure 55. Graph. Normalized Bar Stress ($f_s/\sqrt{f_c'}$) versus Normalized Splice Length (ℓ_s/d_b) by Specimen Type for Specimens with Stirrups (T) in the TFHRC Database.

Figure 56. Graph. Normalized Bar Stress ($f_s/\sqrt{f'_c}$) versus Normalized Splice Length $\ell_s(c_{min}+0.5d_b)/A_b$ by Concrete Mixture Type for Specimens without Stirrups (N) in the TFHRC Database.

Figure 57. Graph. Normalized Bar Stress ($f_s/\sqrt{f'_c}$) versus Normalized Splice Length $\ell_s(c_{min}+0.5d_b)/A_b$ by Specimen Type for Specimens without Stirrups (N) in the TFHRC Database.
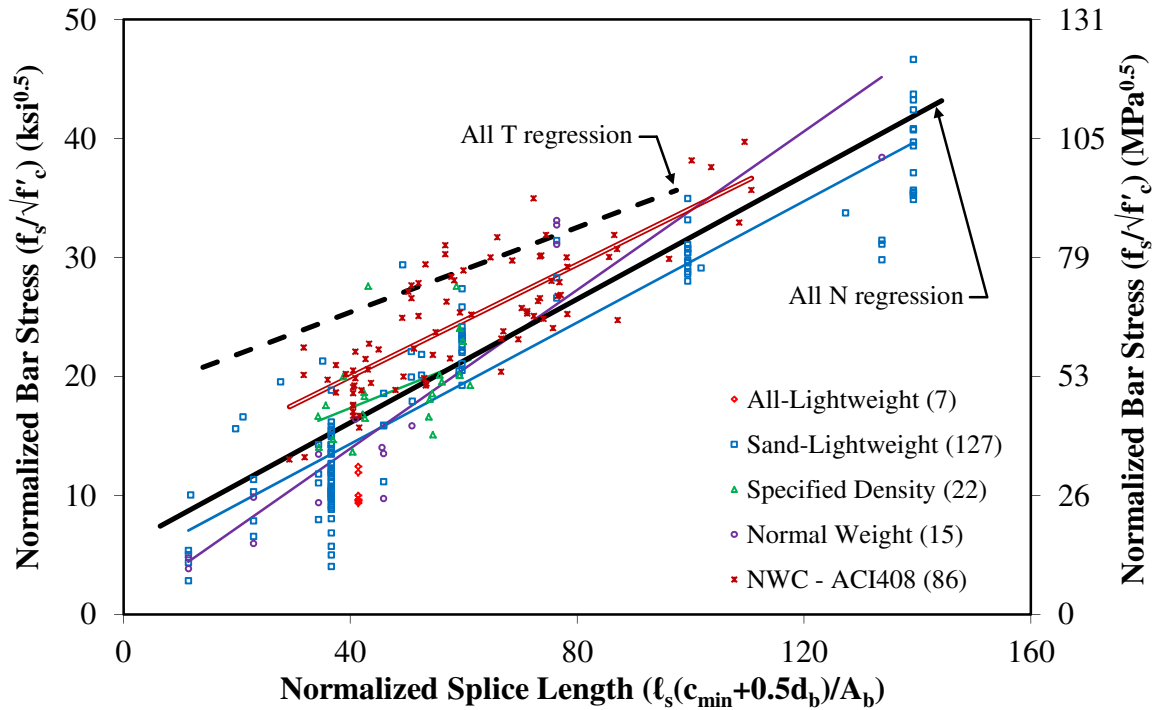
Figure 58. Graph. Normalized Bar Stress ($f_s/\sqrt{f'_c}$) versus Normalized Splice Length $\ell_s(c_{min}+0.5d_b)/A_b$ by Concrete Mixture Type for Specimens with Stirrups (T) in the TFHRC Database.
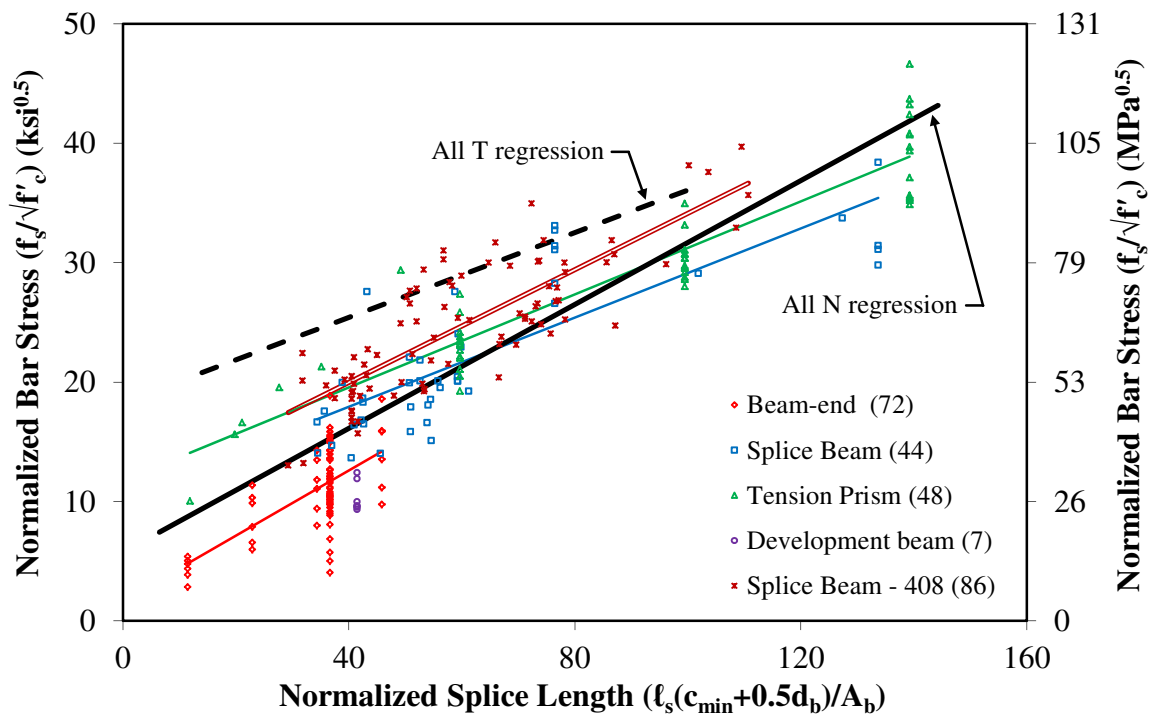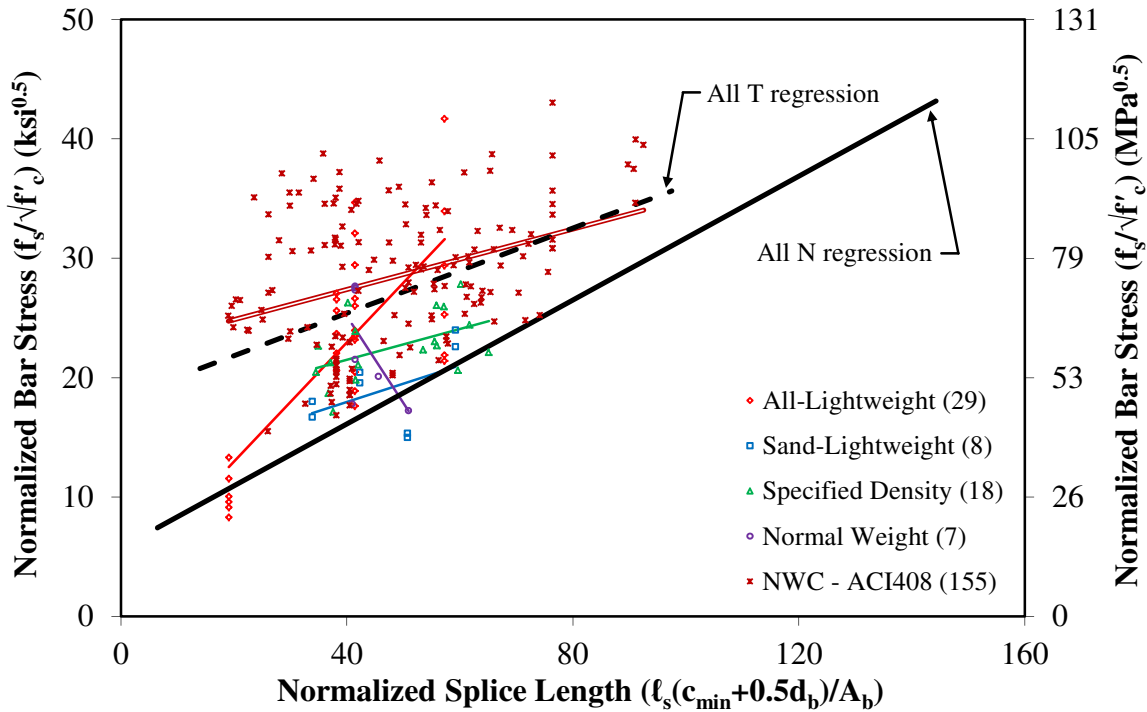

Figure 59. Graph. Normalized Bar Stress ($f_s/\sqrt{f'_c}$) versus Normalized Splice Length $\ell_s(c_{min}+0.5d_b)/A_b$ by Specimen Type for Specimens with Stirrups (T) in the TFHRC Database.

Figure 60. Graph. Normalized Bar Stress ($f_s/\sqrt{f_c'}$) versus Normalized Splice Length (ℓ_s/d_b)×(c_b+K_{tr})/d_b by Concrete Mixture Type for Specimens without Stirrups (N) in the TFHRC Database.

Figure 61. Graph. Normalized Bar Stress ($f_s/\sqrt{f_c'}$) versus Normalized Splice Length (ℓ_s/d_b)×(c_b+K_{tr})/d_b by Specimen Type for Specimens without Stirrups (N) in the TFHRC Database.

Figure 62. Graph. Normalized Bar Stress ($f_s/\sqrt{f_c'}$) versus Normalized Splice Length (ℓ_s/d_b)×(c_b+K_{tr})/d_b by Concrete Mixture Type for Specimens with Stirrups (T) in the TFHRC Database.
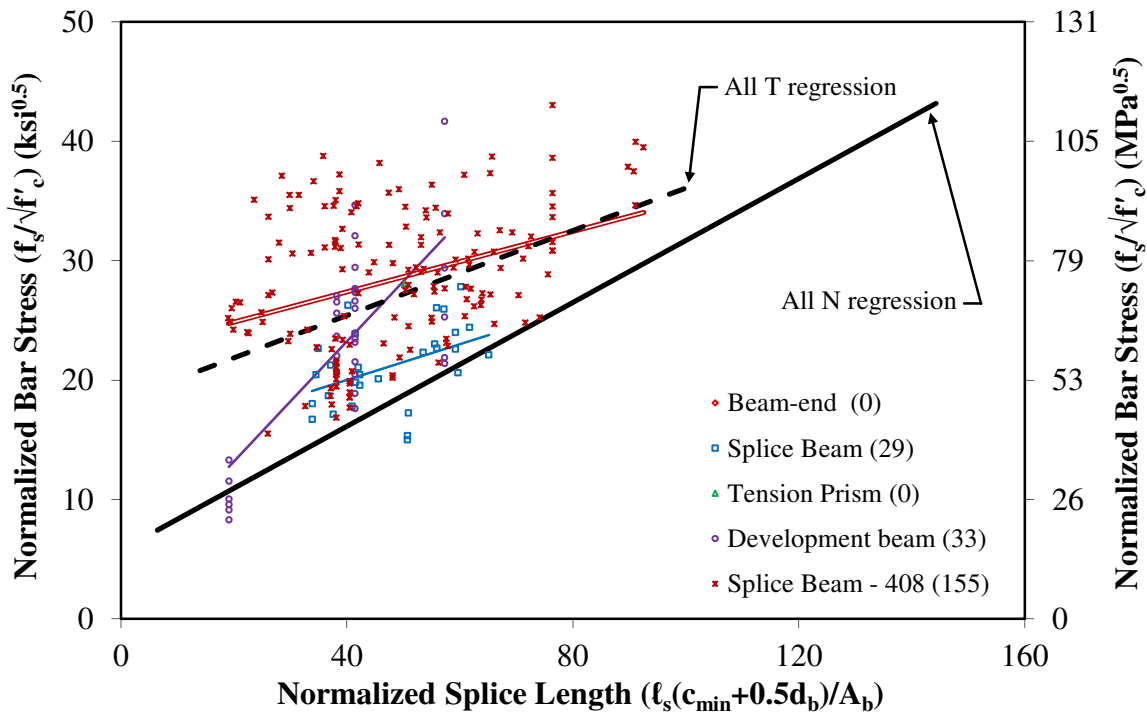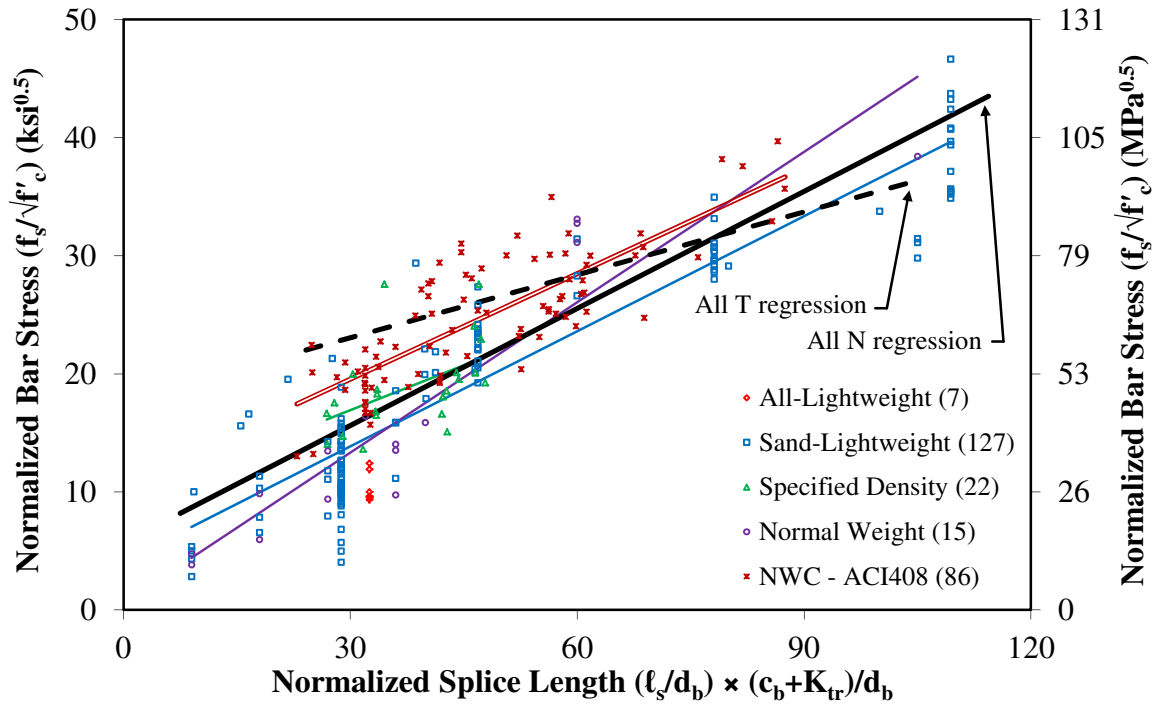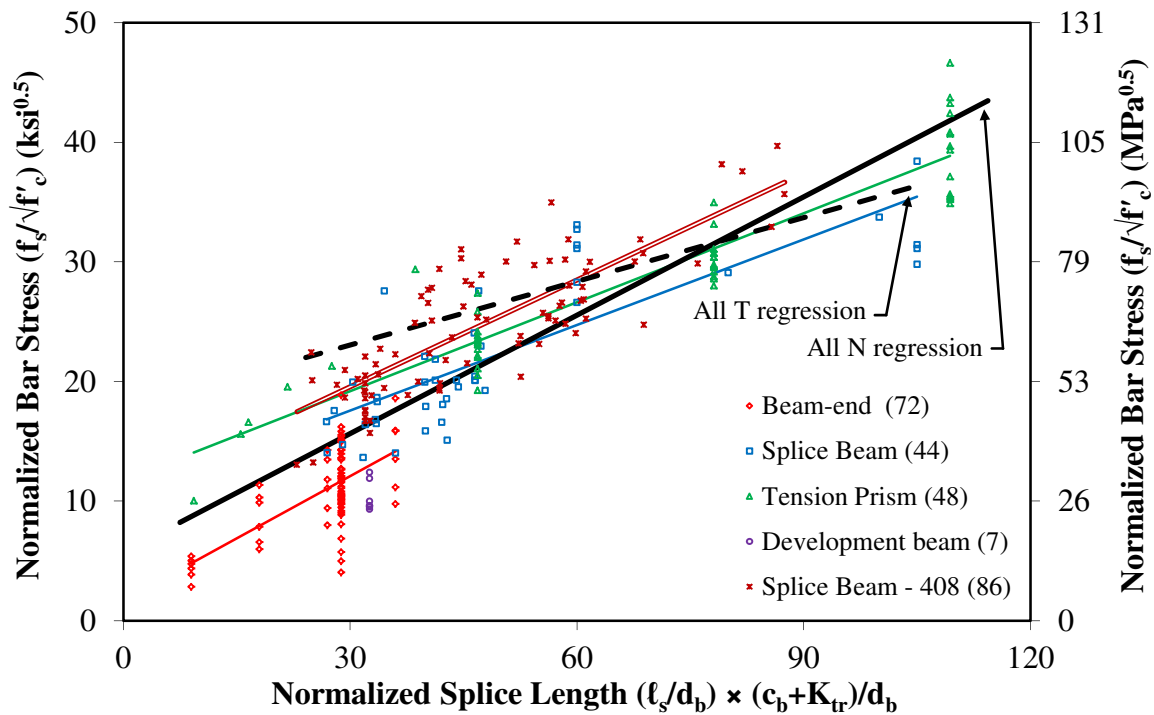

Figure 63. Graph. Normalized Bar Stress ($f_s/\sqrt{f_c'}$) versus Normalized Splice Length (ℓ_s/d_b)×(c_b+K_{tr})/d_b by Specimen Type for Specimens with Stirrups (T) in the TFHRC Database.

Figure 64. Graph. Normalized Bar Stress (f$_s$/f$_c$' $^{0.25}$) versus Normalized Splice Length (ℓ$_s$/d$_b$)×(c$_b$+K$_{tr}$)/d$_b$ by Concrete Mixture Type for Specimens without Stirrups (N) in the TFHRC Database.

Figure 65. Graph. Normalized Bar Stress (f$_s$/f$_c$' $^{0.25}$) versus Normalized Splice Length (ℓ$_s$/d$_b$)×(c$_b$+K$_{tr}$)/d$_b$ by Specimen Type for Specimens without Stirrups (N) in the TFHRC Database.

Figure 66. Graph. Normalized Bar Stress (f$_s$/f$_c$'$^{0.25}$) versus Normalized Splice Length (ℓ$_s$/d$_b$)×(c$_b$+K$_{tr}$)/d$_b$ by Concrete Mixture Type for Specimens with Stirrups (T) in the TFHRC Database.

Figure 67. Graph. Normalized Bar Stress (f$_s$/f$_c$'$^{0.25}$) versus Normalized Splice Length (ℓ$_s$/d$_b$)×(c$_b$+K$_{tr}$)/d$_b$ by Specimen Type for Specimens with Stirrups (T) in the TFHRC Database.
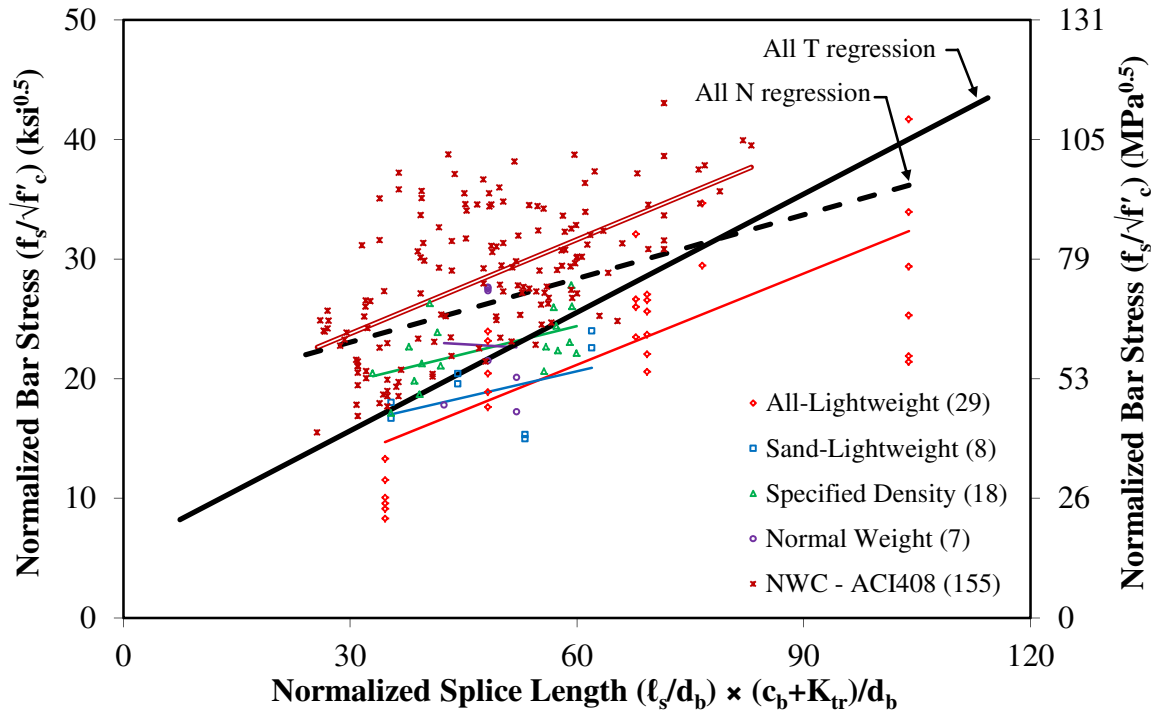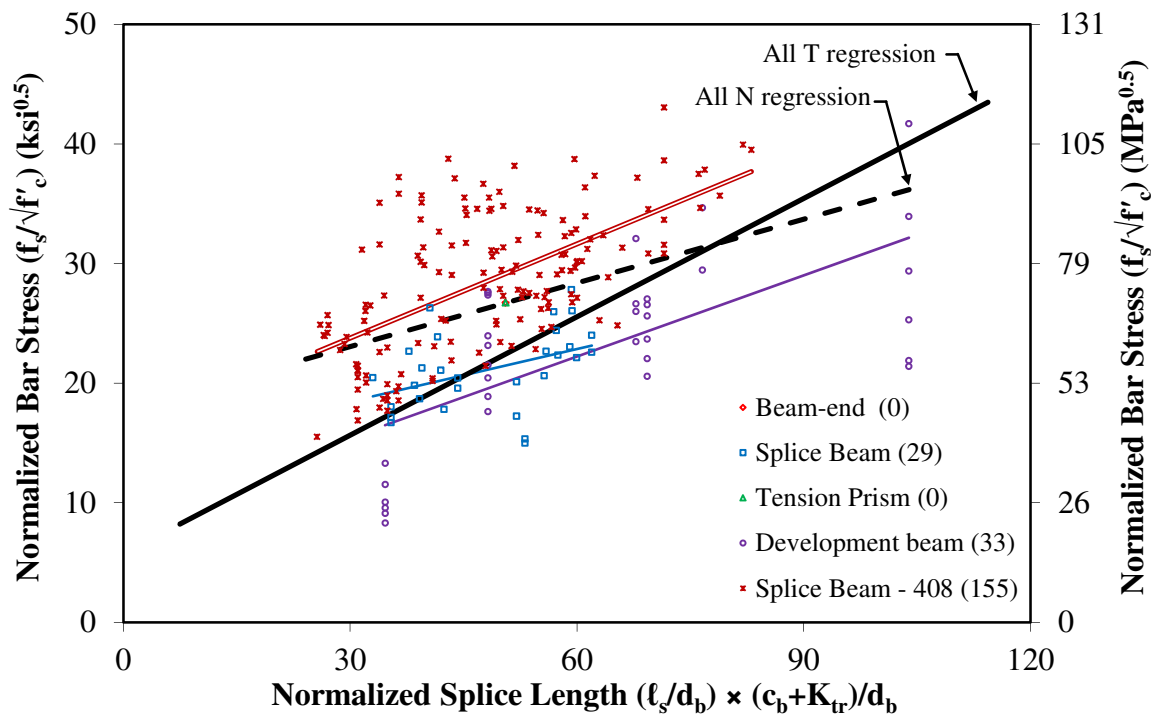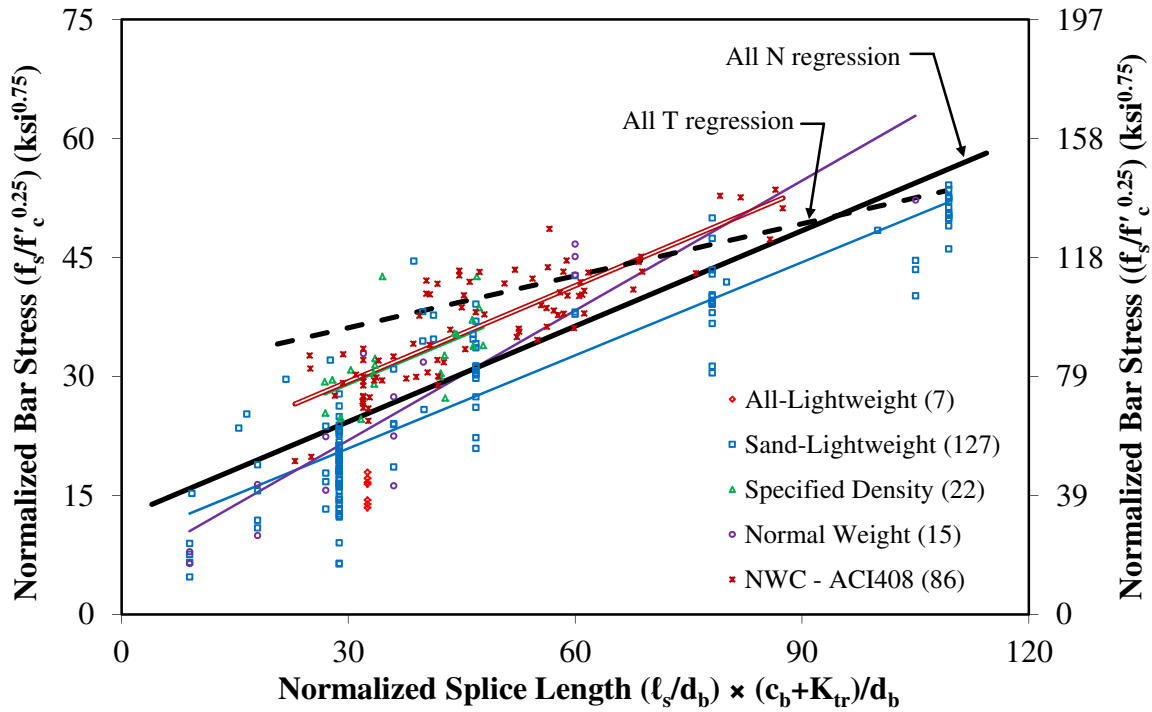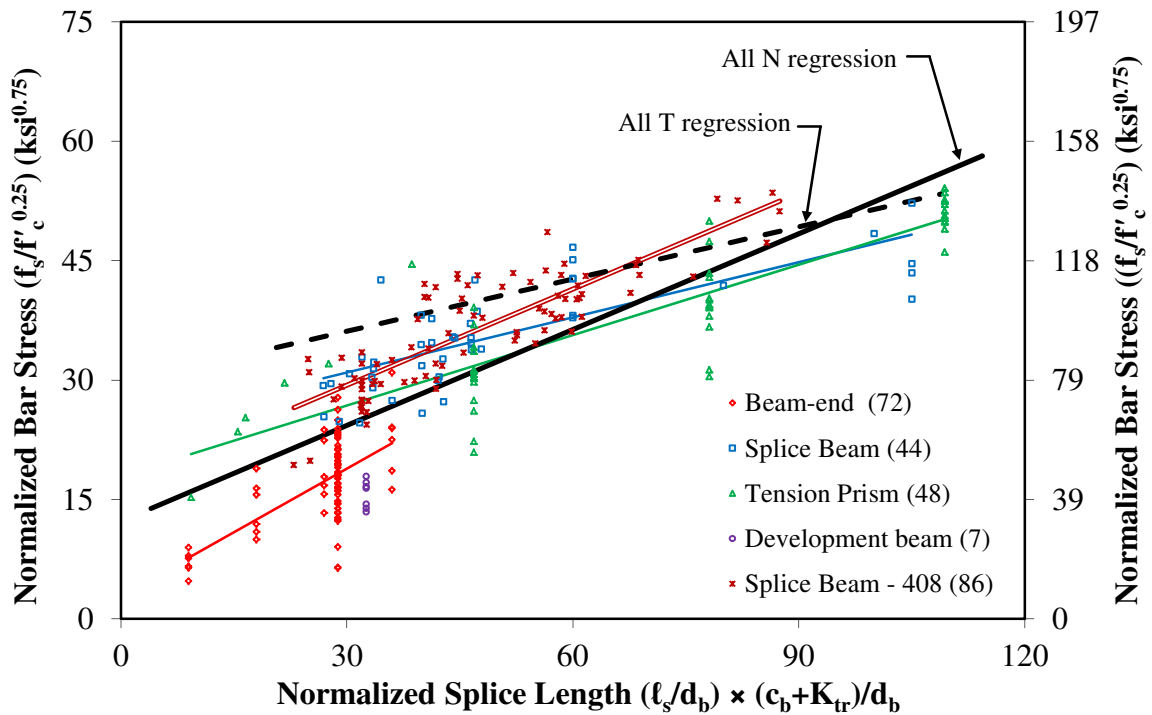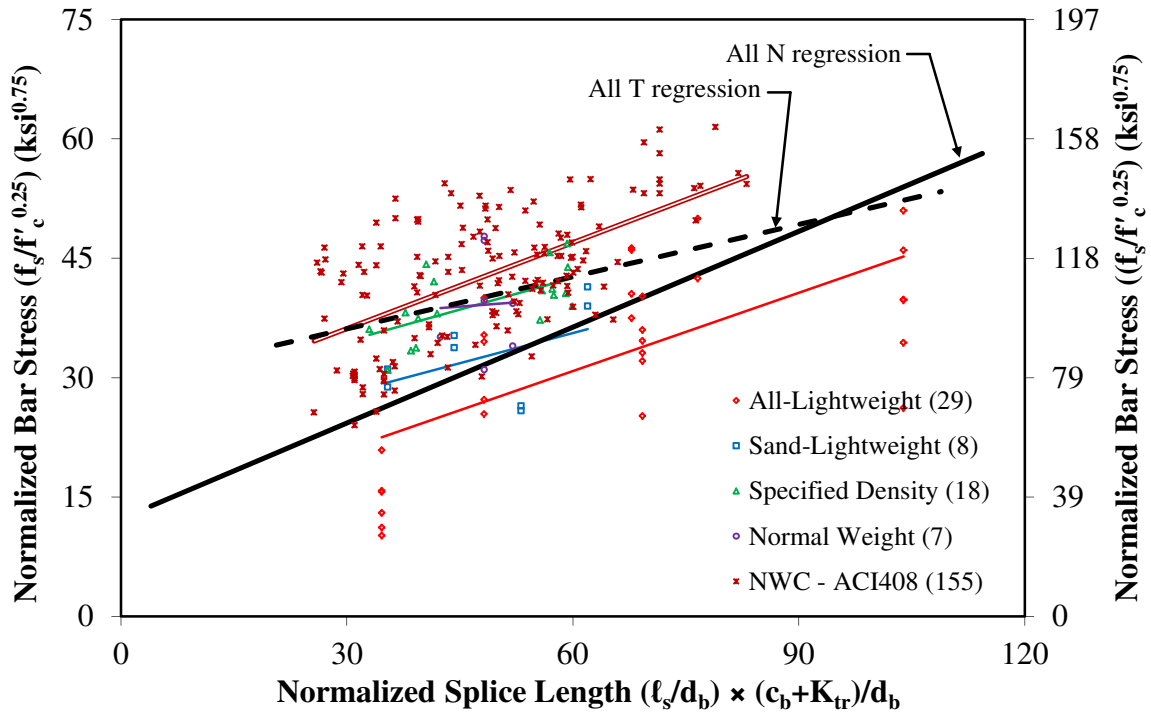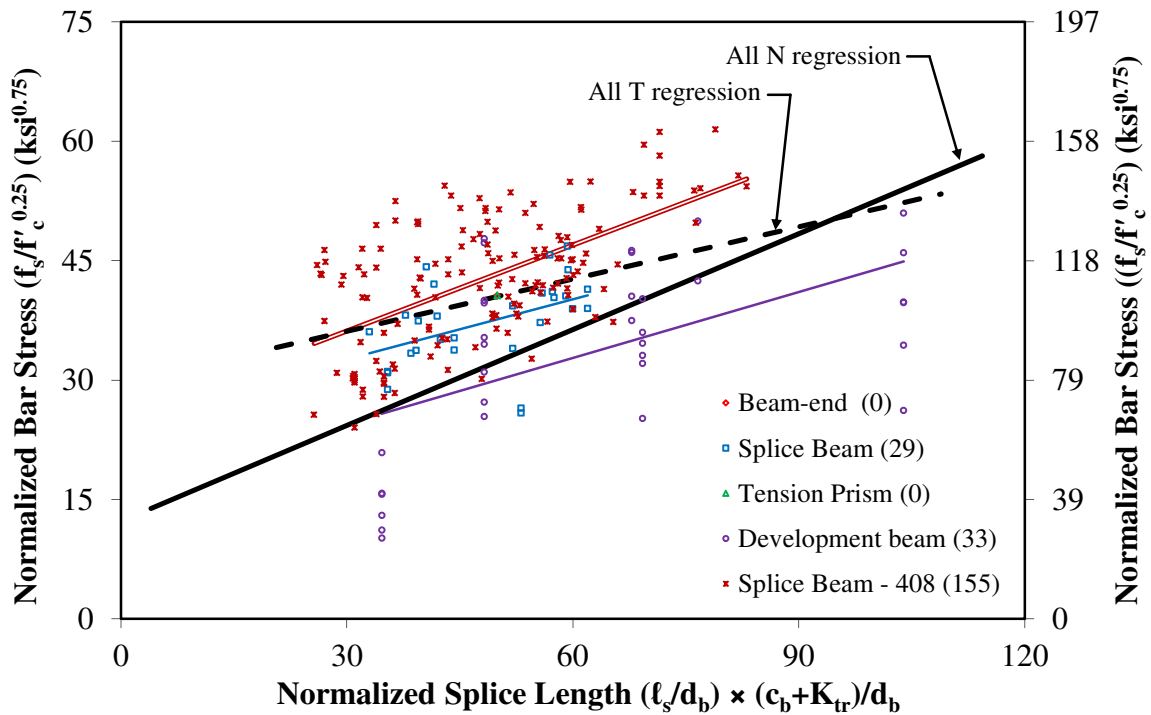
SPECIMEN TYPE

The specimens were not independent of concrete mixture type. The tension prisms had a sample correlation of greater than 0.90 regardless of the normalized splice length parameter. This is likely due to the source of the tension prism data being from only two references with all the specimens using the same natural lightweight coarse aggregate.

For specimens without stirrups, the sample correlation for the 63 LWC and 10 NWC splice beams in the TFHRC Database was 0.48 using an ℓ_s/d_b ratio. The sample correlation for the splice beams in the TFHRC Database improved to 0.82 when using either $\ell_s(c_{min}+0.5d_b)/A_b$ or $\ell_s/d_b(c_b+K_{tr})/d_b$ and is equal to the sample correlation of the NWC ACI Committee 408 splice beams.

FACTORS USED TO NORMALIZE SPLICE LENGTH

The normalized splice length using an ℓ_s/d_b ratio gave a linear sample correlation of 0.46 for specimens without stirrups and 0.55 for specimens with stirrups. The sample correction improved considerably when using either $\ell_s(c_{min}+0.5d_b)/A_b$ or $\ell_s/d_b(c_b+K_{tr})/d_b$ for specimens without stirrups with values of 0.87 for both. The value for specimens with stirrups reduced slightly to 0.43 for both.

In general, using either $\ell_s(c_{min}+0.5d_b)/A_b$ or $\ell_s/d_b(c_b+K_{tr})/d_b$ gave higher correlation values than using an ℓ_s/d_b ratio. The similarity between the correlation values of $\ell_s(c_{min}+0.5d_b)/A_b$ and $\ell_s/d_b(c_b+K_{tr})/d_b$ for specimens without stirrups is not surprising due to the similarity of the normalizing methods when K_{tr} is zero. Of the three methods to normalize splice length, only $\ell_s/d_b(c_b+K_{tr})/d_b$ includes a term to account for the amount of transverse reinforcement, but the sample correlation values for this method are similar to values for the other two methods.

In Figure 53, the normalized bar stress of the tension prism data is noticeably greater than the rest of the data. These specimens had a relatively thick concrete cover over the bars. Splice length in Figure 53 was normalized using an ℓ_s/d_b ratio. This same group of data is near the regression line for the data as a whole in Figure 57 where splice length was normalized using $\ell_s(c_{min}+0.5d_b)/A_b$ and in Figure 61 where splice length was normalized using $\ell_s/d_b(c_b+K_{tr})/d_b$.

In Figure 52 through Figure 67 the regression line for the NWC splice beam specimens from the ACI Committee 408 Database is above the regression line for the data as a whole. The method used to normalize splice length changes the relative slope between the regression lines for NWC splice beam data and the data as a whole. For specimens without stirrups, the slope of the NWC splice beams is larger than the data as a whole when using an ℓ_s/d_b ratio, and nearly equal when using $\ell_s(c_{min}+0.5d_b)/A_b$ or $\ell_s/d_b(c_b+K_{tr})/d_b$. For specimens with stirrups, the slope of the NWC splice beams is larger than the data as a whole when using an ℓ_s/d_b ratio or $\ell_s/d_b(c_b+K_{tr})/d_b$, and smaller when using $\ell_s(c_{min}+0.5d_b)/A_b$.

In Figure 54 and Figure 58 showing specimens with stirrups and the normalization of the splice length using an ℓ_s/d_b ratio or $\ell_s(c_{min}+0.5d_b)/A_b$, respectively, the regression lines for groups of concrete mixture types intersected. Normalization with $\ell_s/d_b(c_b+K_{tr})/d_b$ resulted in nearly parallel regression lines, as shown in Figure 62, indicating than an increase in normalized splice length would have a similar effect on the normalized bar stress in each group.

FACTORS USED TO NORMALIZE BAR STRESS

As shown in Table 23, the use of $\sqrt{f_c'}$ to normalize bar stress had the largest sample correlation value of 0.87 for the data from specimens without stirrups as a whole. The sample correlation using $f_c'^{0.25}$ was similar with a value of 0.82, while using f_{ct} had a sample correlation of 0.678. A similar trend was observed for specimens with stirrups.

For specimens without stirrups, the use of $\sqrt{f_c'}$ to normalize bar stress gave larger sample correlation values than $f_c'^{0.25}$ for beam-end specimens, splice beam specimens, and tension prisms. Most of these specimens were made with LWC. The splice beams from the ACI Committee 408 Database did not follow this trend and had larger sample correlation values when $f_c'^{0.25}$ rather than $\sqrt{f_c'}$ was used to normalize bar stress.

No obvious trend for specimens with stirrups was observed in Table 23 for individual groups of data that included specimens made from LWC. The NWC splice beam specimens from the ACI Committee 408 Database had a sample correlation of 0.60 using $\sqrt{f_c'}$ or $f_c'^{0.25}$ to normalize bar stress.

A comparison of the relative position and slope of the regression lines in Figure 60 through Figure 63 for bar stress normalized by $\sqrt{f_c'}$ to the equivalent plot in Figure 64 through Figure 67 for bar stress normalized by $f_c'^{0.25}$ does not indicate any significant differences between the methods of normalization.

There are significantly fewer data points with splitting tensile strength values. Figure 68 through Figure 71 show the data with bar stress normalized by f_{ct}. The data in these figures shows a large amount of scatter and obvious trends are difficult to determine.

Figure 68. Graph. Normalized Bar Stress (f_s/f_{ct}) versus Normalized Splice Length (ℓ_s/d_b)×(c_b+K_{tr})/d_b by Concrete Mixture Type for Specimens without Stirrups (N) in the TFHRC Database.

Figure 69. Graph. Normalized Bar Stress (f_s/f_{ct}) versus Normalized Splice Length (ℓ_s/d_b)×(c_b+K_{tr})/d_b by Specimen Type for Specimens without Stirrups (N) in the TFHRC Database.

95

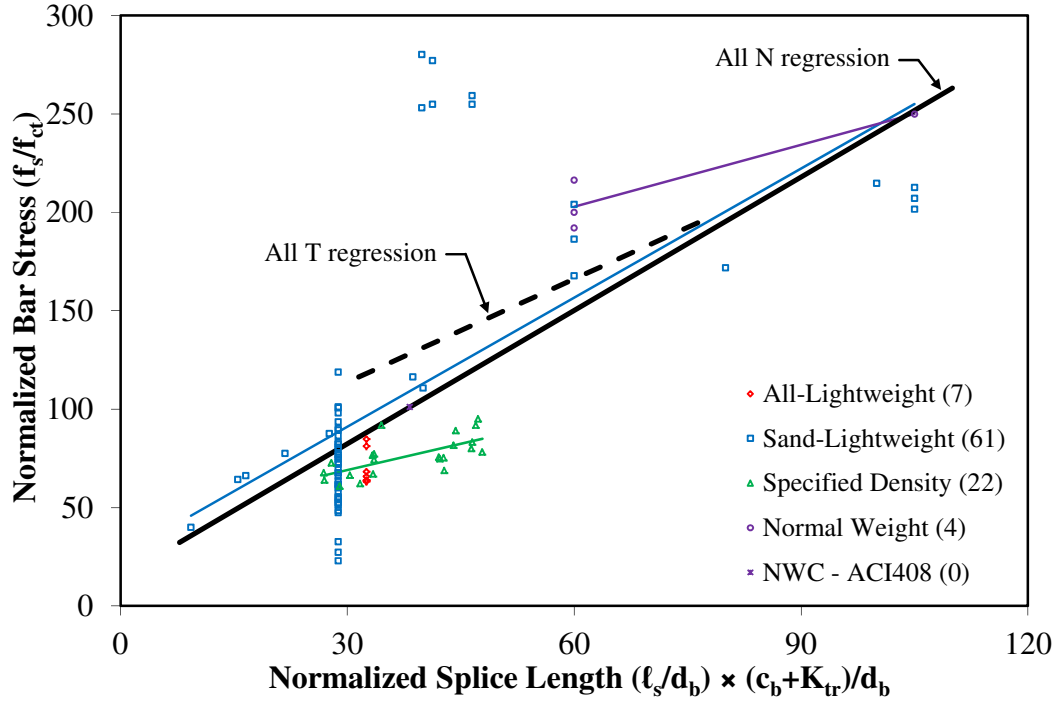**Figure 70. Graph. Normalized Bar Stress (f_s/f_{ct}) versus Normalized Splice Length $(\ell_s/d_b) \times (c_b+K_{tr})/d_b$ by Concrete Mixture Type for Specimens with Stirrups (T) in the TFHRC Database.**
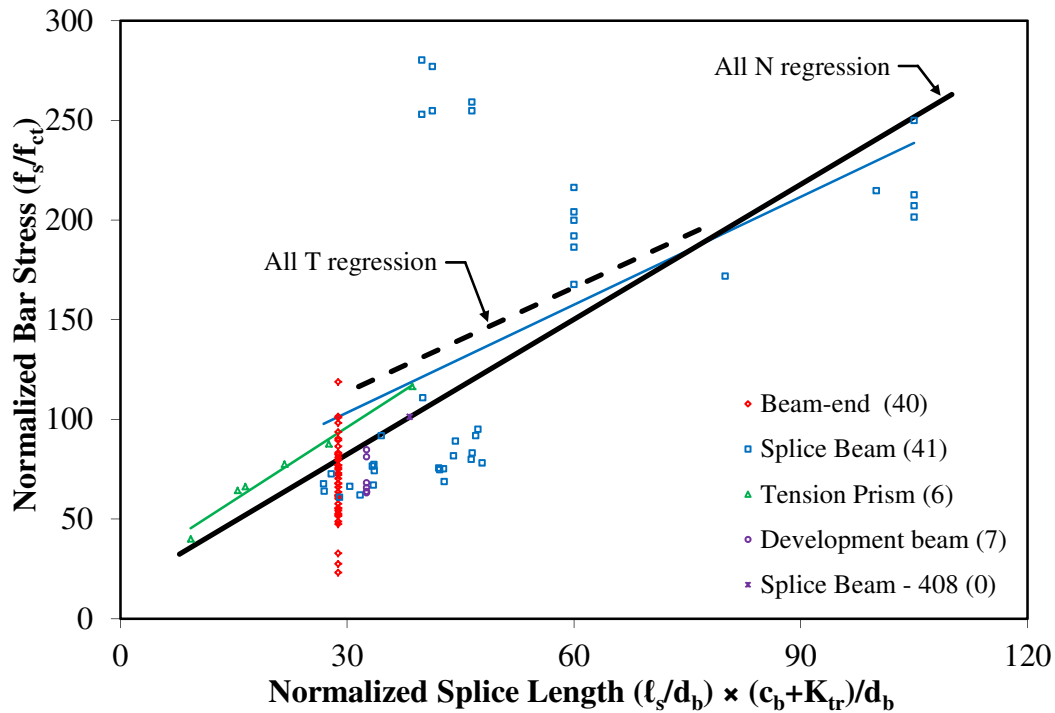

Figure 71. Graph. Normalized Bar Stress (f_s/f_{ct}) versus Normalized Splice Length $(\ell_s/d_b) \times (c_b+K_{tr})/d_b$ by Specimen Type for Specimens with Stirrups (T) in the TFHRC Database.
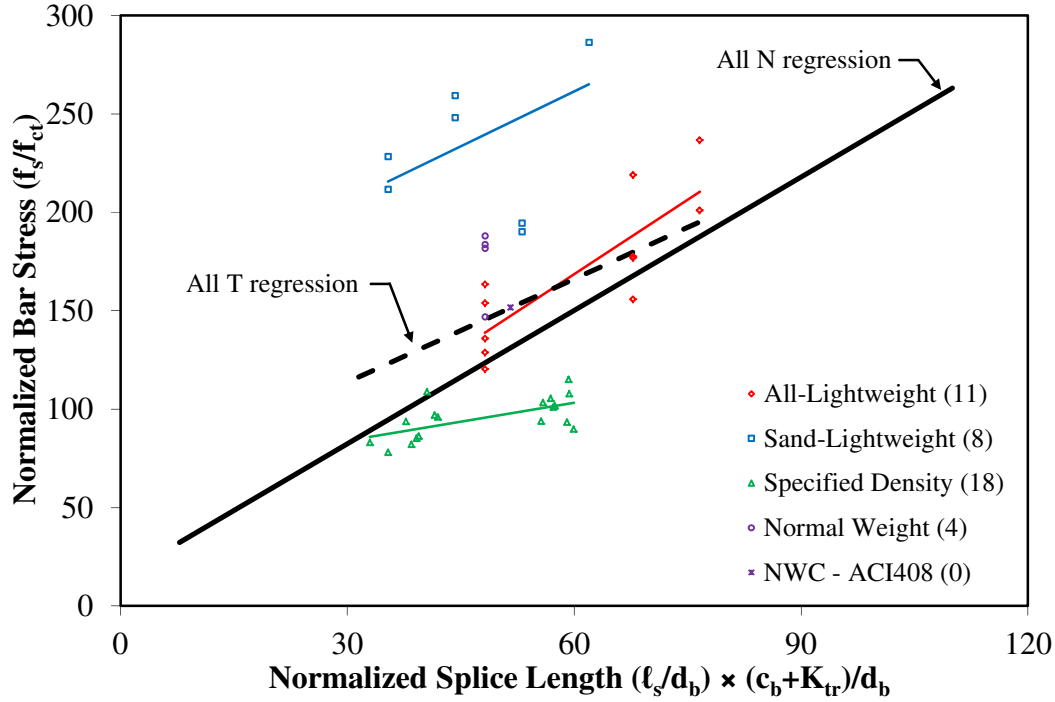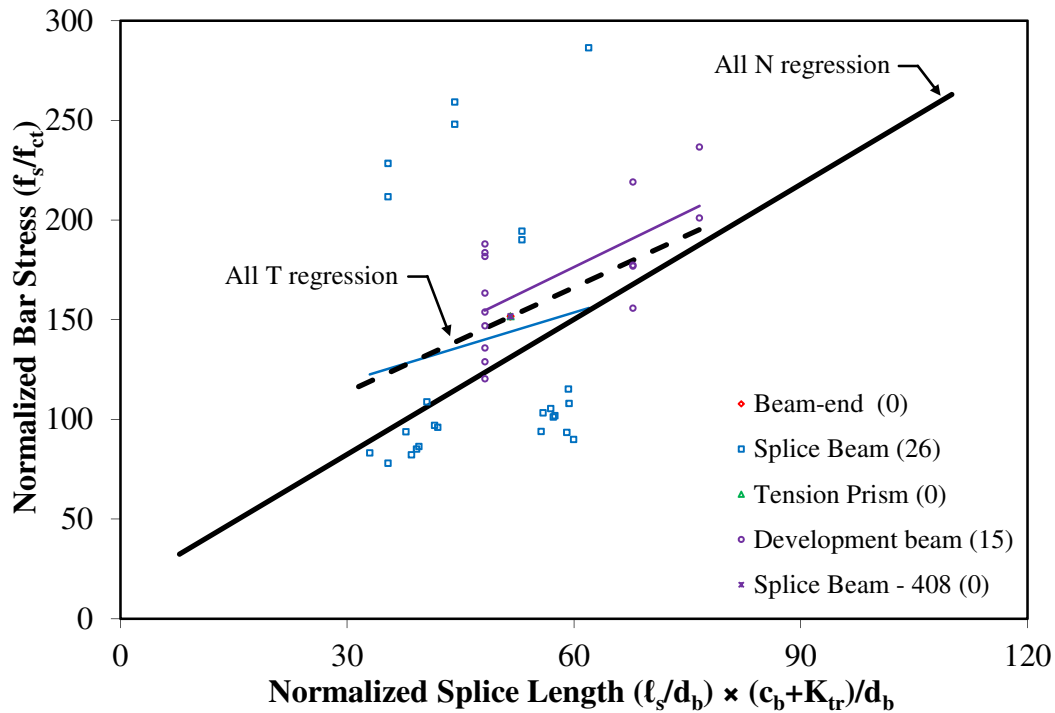
SUMMARY OF THE BAR STRESS ANALYSIS

In Figure 52 through Figure 67 the regression line for the NWC splice beam specimens from the ACI Committee 408 Database is above the regression line for the data as a whole. In the figures with groups by specimen type, the regression line for the NWC ACI Committee 408 Database tests is also above the regression line for the LWC and other NWC splice beam specimens in the TFHRC Database.

The regression line of the NWC splice beam specimens is above the regression line of the LWC splice beam specimen and above the regression line with the rest of the LWC data. This indicates that the bar stress at failure for reinforcement in NWC is greater than the bar stress at failure for reinforcement in LWC. The scatter in the data, quantified by the linear sample correlation is similar for NWC and LWC specimens without stirrups when either $\ell_s(c_{min}+0.5d_b)/A_b$ or $\ell_s/d_b(c_b+K_{tr})/d_b$ is used to normalize the splice length.

Normalization of the splice length using either $\ell_s(c_{min}+0.5d_b)/A_b$ or $\ell_s/d_b(c_b+K_{tr})/d_b$ for specimens without stirrups gave better predictions of normalized bar stress. This was indicated by the regression lines for groups by concrete mixture type or specimen type being closer to parallel and closer together in plots of normalized bar stress versus normalized splice length. Also the scatter in the data was less for normalization of the splice length using either $\ell_s(c_{min}+0.5d_b)/A_b$ or $\ell_s/d_b(c_b+K_{tr})/d_b$ as indicated by the larger linear sample correlation value.

There was less scatter in the LWC data when using $\sqrt{f_c'}$ to normalize bar stress than when using $f_c'^{0.25}$ as observed by the larger sample correlation values. For NWC splice beams, the use of $f_c'^{0.25}$ resulted in less scatter (i.e., larger sample correlation values) than when using $\sqrt{f_c'}$. The use of f_{ct} to normalize bar stress resulted in much more scatter for the limited amount of data with splitting tensile tests.

BAR STRESS PREDICTED BY DESIGN EXPRESSIONS WITHOUT MODIFICATION FOR LWC

The expressions for bar stress determined from the design expressions for development length in the AASHTO LRFD Specifications (Eq. 31), in ACI 318-11 (Eq. 32), and in ACI 408-03 (Eq. 33) are compared to the bar stresses determined from the specimens in the TFHRC Mild Steel Development Length Database. The method used to express the design expressions for development length in terms of average bar stress at failure (f_s) was described previously in this document. The f_s determined from the tests in the database are compared to the f_s predicted using the three design expressions for f_s. The comparison is made using the ratio of the f_s determined from tests to the f_s determined from the design expression (i.e., test-to-prediction ratio).

The lap splice length (or development length), concrete cover terms, concrete compressive strength, and relative rib area for each test were found in the literature. The average bar stress at

failure for splice beam specimens was determined from the ultimate moment using the method from the ACI Committee 408 report described previously in this document.[9] The average bar stress at failure for other types of specimens was taken as the reported value. No limit was placed on f_c', $\sqrt{f_c'}$, or f_s. The lightweight concrete factors (λ_{ACI} and λ_{ACI408}), top-cast bar factors (ψ_t and α), epoxy coating factors (ψ_e and β), and bar size factor (ψ_s) were taken as 1.0.

The ratio of the test-to-predicted bar stress for the three design expressions is given in Table 24 for all specimens, in Table 25 and Table 26 by concrete mixture type, and in Table 27 by specimen type. A comparison of the test-to-prediction ratios for LWC specimens to similar NWC specimens is given in Table 28 and Table 29. In each table, statistical parameters are given for the test-to-prediction ratios of each three design expression. The percent of specimens whose predicted bar stress was over-estimated (i.e., "percent < 1.0") or significantly over-estimated (i.e., "percent < 0.8") is given for each design expression.

The test-to-prediction ratios for each design expression are shown in Figure 72 through Figure 95. Eight figures are shown for each design expression. The first group of four figures shows the ratios versus the ℓ_s/d_b ratio and the second group of four figures shows the ratios versus compressive strength. In each group of four figures, the first two figures show the ratios in groups of concrete mixture types and groups of specimen types, respectively, for specimens without stirrups. The second two figures in each group of four show similar results for specimens with stirrups. The number of specimens in each group is shown in parentheses after the group label.

In each figure, the NWC specimens from the ACI Committee 408 Database are separated from the rest of the data. When the data is given by concrete mixture type, the NWC data found in references with the LWC data or in the NCHRP 12-60 report is labeled as "Normal Weight", while the data from the ACI Committee 408 Database is labeled "NWC – ACI 408". When the data is given by specimen type, the LWC and NWC splice beams found in references with LWC splice beam data are labeled "Splice Beam", while the data from the ACI Committee 408 Database is labeled "Splice Beam – 408".

Table 24. Test-to-Prediction Ratio of Bar Stress for Design Expressions in AASHTO LRFD (Eq. 31), ACI 318-11 (Eq. 32), and ACI 408-03 (Eq. 33) for Specimens in the TFHRC Database.

Concrete Mixture Type[†]	Design Expression	Mean	COV	Max.	Min.	Percent < 1.0	Percent < 0.8
All Specimens (474 total)	AASHTO	1.23	34.7%	2.98	0.23	31.6%	12.9%
	ACI 318	1.39	35.4%	3.46	0.33	18.4%	4.9%
	ACI 408	1.09	24.1%	1.78	0.27	28.7%	13.7%
All Specimens (257 without A_{tr})	AASHTO	1.14	41.5%	2.98	0.23	46.3%	21.4%
	ACI 318	1.40	41.2%	3.46	0.33	23.0%	6.2%
	ACI 408	1.01	25.2%	1.62	0.27	38.1%	19.5%
All Specimens (217 with A_{tr})	AASHTO	1.33	25.2%	2.48	0.56	14.3%	2.8%
	ACI 318	1.38	26.6%	2.45	0.68	12.9%	3.2%
	ACI 408	1.19	20.3%	1.78	0.39	17.5%	6.9%
LWC Specimens (211 total)	AASHTO	1.14	44.1%	2.98	0.23	47.9%	23.7%
	ACI 318	1.37	46.6%	3.46	0.33	32.7%	10.0%
	ACI 408	0.97	29.1%	1.62	0.27	51.2%	28.4%
LWC Specimens (156 without A_{tr})	AASHTO	1.17	48.6%	2.98	0.23	50.0%	28.8%
	ACI 318	1.48	47.6%	3.46	0.33	30.1%	9.6%
	ACI 408	0.97	30.2%	1.62	0.27	50.6%	28.8%
LWC Specimens (55 with A_{tr})	AASHTO	1.08	23.1%	1.78	0.56	41.8%	9.1%
	ACI 318	1.07	18.7%	1.54	0.68	40.0%	10.9%
	ACI 408	0.95	25.3%	1.48	0.39	52.7%	27.3%
NWC Specimens (263 total)	AASHTO	1.30	26.1%	2.48	0.63	18.6%	4.2%
	ACI 318	1.41	23.5%	2.45	0.77	6.8%	0.8%
	ACI 408	1.19	16.6%	1.78	0.40	10.6%	1.9%
NWC Specimens (101 without A_{tr})	AASHTO	1.09	24.3%	1.82	0.63	40.6%	9.9%
	ACI 318	1.28	19.4%	2.14	0.77	11.9%	1.0%
	ACI 408	1.07	15.1%	1.40	0.40	18.8%	5.0%
NWC Specimens (162 with A_{tr})	AASHTO	1.42	22.3%	2.48	0.68	4.9%	0.6%
	ACI 318	1.49	23.6%	2.45	0.79	3.7%	0.6%
	ACI 408	1.27	14.0%	1.78	0.89	5.6%	0.0%

Notes:

[†] No. of specimens without stirrups ("without A_{tr}") and with stirrups ("with A_{tr}") given in parentheses

Table 25. Test-to-Prediction Ratio of Bar Stress for Design Expressions in AASHTO LRFD (Eq. 31), ACI 318-11 (Eq. 32), and ACI 408-03 (Eq. 33) by Concrete Mixtures Type for LWC Specimens in the TFHRC Database.

Concrete Mixture Type[†]	Design Expression	Mean	COV	Max.	Min.	Percent < 1.0	Percent < 0.8
All-Lightweight (36 total)	AASHTO	0.88	36.7%	1.36	0.29	58.3%	33.3%
	ACI 318	1.02	24.6%	1.58	0.68	50.0%	25.0%
	ACI 408	0.80	34.8%	1.42	0.39	75.0%	55.6%
All-Lightweight (7 without A_{tr})	AASHTO	0.36	16.4%	0.44	0.29	100.0%	100.0%
	ACI 318	0.75	12.2%	0.90	0.68	100.0%	71.4%
	ACI 408	0.55	11.2%	0.62	0.48	100.0%	100.0%
All-Lightweight (29 with A_{tr})	AASHTO	1.00	21.8%	1.36	0.56	48.3%	17.2%
	ACI 318	1.09	21.5%	1.58	0.68	37.9%	13.8%
	ACI 408	0.86	32.2%	1.42	0.39	69.0%	44.8%
Sand-Lightweight (135 total)	AASHTO	1.27	43.9%	2.98	0.23	38.5%	23.0%
	ACI 318	1.54	47.5%	3.46	0.33	29.6%	8.9%
	ACI 408	0.97	29.8%	1.62	0.27	53.3%	29.6%
Sand-Lightweight (127 without A_{tr})	AASHTO	1.27	45.5%	2.98	0.23	40.2%	24.4%
	ACI 318	1.58	47.3%	3.46	0.33	27.6%	7.9%
	ACI 408	0.97	31.2%	1.62	0.27	53.5%	30.7%
Sand-Lightweight (8 with A_{tr})	AASHTO	1.40	21.1%	1.78	0.99	12.5%	0.0%
	ACI 318	1.08	21.1%	1.37	0.76	37.5%	25.0%
	ACI 408	0.98	15.8%	1.11	0.73	37.5%	25.0%
Specified Density (40 total)	AASHTO	0.94	18.4%	1.25	0.62	70.0%	17.5%
	ACI 318	1.18	19.3%	1.90	0.84	20.0%	0.0%
	ACI 408	1.15	12.2%	1.62	0.89	15.0%	0.0%
Specified Density (22 without A_{tr})	AASHTO	0.84	14.3%	1.10	0.62	90.9%	31.8%
	ACI 318	1.21	20.3%	1.90	0.84	13.6%	0.0%
	ACI 408	1.15	13.2%	1.62	0.89	13.6%	0.0%
Specified Density (18 with A_{tr})	AASHTO	1.06	13.9%	1.25	0.84	44.4%	0.0%
	ACI 318	1.14	18.0%	1.54	0.88	27.8%	0.0%
	ACI 408	1.16	11.4%	1.48	0.97	16.7%	0.0%

Notes:
[†] No. of specimens without stirrups ("without A_{tr}") and with stirrups ("with A_{tr}") given in parentheses

Table 26. Test-to-Prediction Ratio of Bar Stress for Design Expressions in AASHTO LRFD (Eq. 31), ACI 318-11 (Eq. 32), and ACI 408-03 (Eq. 33) by Concrete Mixtures Type for NWC Specimens in the TFHRC Database.

Concrete Mixture Type[†]	Design Expression	Mean	COV	Max.	Min.	Percent < 1.0	Percent < 0.8
Normal Weight (22 total)	AASHTO	1.15	26.6%	1.82	0.68	40.9%	4.5%
	ACI 318	1.15	19.6%	1.556	0.770	36.4%	9.1%
	ACI 408	0.97	29.4%	1.319	0.402	50.0%	22.7%
Normal Weight (15 without A_{tr})	AASHTO	1.18	28.6%	1.82	0.80	1.18	28.6%
	ACI 318	1.17	19.5%	1.56	0.77	1.17	19.5%
	ACI 408	0.90	34.0%	1.32	0.40	0.90	34.0%
Normal Weight (7 with A_{tr})	AASHTO	1.10	22.0%	1.30	0.68	28.6%	14.3%
	ACI 318	1.12	21.2%	1.36	0.79	42.9%	14.3%
	ACI 408	1.12	15.2%	1.32	0.89	28.6%	0.0%
NWC – ACI 408 (241 total)	AASHTO	1.31	25.9%	2.48	0.63	16.6%	4.1%
	ACI 318	1.43	23.0%	2.45	0.85	4.1%	0.0%
	ACI 408	1.21	14.5%	1.78	0.88	7.1%	0.0%
NWC – ACI 408 (86 without A_{tr})	AASHTO	1.08	23.2%	1.81	0.63	39.5%	11.6%
	ACI 318	1.30	19.1%	2.14	0.85	8.1%	0.0%
	ACI 408	1.10	8.8%	1.40	0.88	11.6%	0.0%
NWC – ACI 408 (155 with A_{tr})	AASHTO	1.44	21.8%	2.48	0.82	3.9%	0.0%
	ACI 318	1.50	23.1%	2.45	0.95	1.9%	0.0%
	ACI 408	1.28	13.8%	1.78	0.93	4.5%	0.0%

Notes:

[†] No. of specimens without stirrups ("without A_{tr}") and with stirrups ("with A_{tr}") given in parentheses

Table 27. Test-to-Prediction Ratio of Bar Stress for Design Expressions in AASHTO LRFD (Eq. 31), ACI 318-11 (Eq. 32), and ACI 408-03 (Eq. 33) by Specimen Type for LWC and NWC Specimens in the TFHRC Database.

Specimen Type[†]	Design Expression	Mean	COV	Max.	Min.	Percent < 1.0	Percent < 0.8
Beam-End	AASHTO	0.98	39.9%	2.10	0.23	59.7%	34.7%
(72, all without A_{tr})	ACI 318	1.06	30.8%	2.17	0.33	45.8%	15.3%
	ACI 408	0.74	28.6%	1.28	0.27	90.3%	59.7%
Splice Beam	AASHTO	1.01	26.7%	1.78	0.56	60.3%	17.8%
(73 total)	ACI 318	1.13	18.6%	1.89	0.76	28.8%	4.1%
	ACI 408	1.11	14.3%	1.62	0.73	23.3%	4.1%
Splice Beam	AASHTO	0.91	25.8%	1.63	0.56	79.5%	29.5%
(44 without A_{tr})	ACI 318	1.15	18.2%	1.89	0.80	22.7%	0.0%
	ACI 408	1.11	14.4%	1.62	0.75	22.7%	2.3%
Splice Beam	AASHTO	1.17	20.9%	1.78	0.84	31.0%	0.0%
(29 with A_{tr})	ACI 318	1.10	19.3%	1.54	0.76	37.9%	10.3%
	ACI 408	1.10	14.3%	1.48	0.73	24.1%	6.9%
Tension Prism	AASHTO	1.80	23.8%	2.98	1.06	0.0%	0.0%
(48, all without A_{tr})	ACI 318	2.42	16.0%	3.46	1.89	0.0%	0.0%
	ACI 408	1.24	13.0%	1.62	0.81	10.4%	0.0%
Development Beam	AASHTO	0.89	35.7%	1.36	0.29	57.5%	32.5%
(40 total)	ACI 318	1.05	24.2%	1.58	0.68	45.0%	22.5%
	ACI 408	0.83	35.0%	1.42	0.39	70.0%	50.0%
Development Beam	AASHTO	0.36	16.4%	0.44	0.29	100.0%	100.0%
(7 without A_{tr})	ACI 318	0.75	12.2%	0.90	0.68	100.0%	71.4%
	ACI 408	0.55	11.2%	0.62	0.47	100.0%	100.0%
Development Beam	AASHTO	1.00	22.2%	1.36	0.56	48.5%	18.2%
(33 with A_{tr})	ACI 318	1.11	20.9%	1.58	0.68	33.3%	12.1%
	ACI 408	0.89	31.9%	1.42	0.39	63.6%	39.4%

Notes:
[†] No. of specimens without stirrups ("without A_{tr}") and with stirrups ("with A_{tr}") given in parentheses

Table 28. Comparison of LWC and NWC Test-to-Prediction Ratios for Bar Stress Using Design Expressions in AASHTO LRFD (Eq. 31), ACI 318-11 (Eq. 32), and ACI 408-03 (Eq. 33) by Specimen Type for Specimens without Stirrups in the TFHRC Database.

Specimen Type[†]	Design Expression	Mean	COV	Max.	Min.	Percent < 1.0	Percent < 0.8
Beam-End - LWC	AASHTO	0.93	39.8%	2.10	0.23	65.6%	39.1%
(64 without A_{tr})	ACI 318	1.04	28.6%	1.79	0.33	50.0%	15.6%
	ACI 408	0.75	27.4%	1.17	0.27	90.6%	57.8%
Beam-End - NWC	AASHTO	1.38	24.2%	1.82	0.90	12.5%	0.0%
(8 without A_{tr})	ACI 318	1.18	24.2%	1.56	0.77	37.5%	12.5%
	ACI 408	0.67	30.1%	0.97	0.40	100.0%	62.5%
Splice Beam - LWC	AASHTO	0.90	27.6%	1.63	0.56	78.4%	35.1%
(37 without A_{tr})	ACI 318	1.15	19.1%	1.89	0.80	21.6%	0.0%
	ACI 408	1.10	14.9%	1.62	0.75	24.3%	2.7%
Splice Beam - NWC	AASHTO	0.95	15.2%	1.24	0.80	85.7%	0.0%
(7 without A_{tr})	ACI 318	1.16	13.8%	1.31	0.92	28.6%	0.0%
	ACI 408	1.17	11.3%	1.32	0.97	14.3%	0.0%
Splice Beam - ACI408	AASHTO	1.08	23.2%	1.81	0.63	39.5%	11.6%
(86 without A_{tr})	ACI 318	1.30	19.1%	2.14	0.85	8.1%	0.0%
	ACI 408	1.10	8.8%	1.40	0.88	11.6%	0.0%

Notes:
[†] No. of specimens without stirrups ("without A_{tr}") and with stirrups ("with A_{tr}") given in parentheses

Table 29. Comparison of LWC and NWC Test-to-Prediction Ratios for Bar Stress Using Design Expressions in AASHTO LRFD (Eq. 31), ACI 318-11 (Eq. 32), and ACI 408-03 (Eq. 33) by Specimen Type for Specimens with Stirrups in the TFHRC Database.

Specimen Type[†]	Design Expression	Mean	COV	Max.	Min.	Percent < 1.0	Percent < 0.8
Splice Beam - LWC	AASHTO	1.17	21.9%	1.78	0.84	34.6%	0.0%
(26 with A_{tr})	ACI 318	1.12	18.7%	1.54	0.76	30.8%	7.7%
	ACI 408	1.10	14.5%	1.48	0.73	23.1%	7.7%
Splice Beam - NWC	AASHTO	1.21	11.4%	1.30	1.05	0.0%	0.0%
(3 with A_{tr})	ACI 318	0.90	11.7%	1.00	0.79	100.0%	33.3%
	ACI 408	1.04	13.2%	1.16	0.89	33.3%	0.0%
Splice Beam - ACI408	AASHTO	1.44	21.8%	2.48	0.82	3.9%	0.0%
(155 with A_{tr})	ACI 318	1.50	23.1%	2.45	0.95	1.9%	0.0%
	ACI 408	1.28	13.8%	1.78	0.93	4.5%	0.0%
Dev. Beam - LWC	AASHTO	1.00	21.8%	1.36	0.56	48.3%	17.2%
(29 with A_{tr})	ACI 318	1.02	17.5%	1.32	0.68	48.3%	13.8%
	ACI 408	0.81	26.4%	1.15	0.39	79.3%	44.8%
Dev. Beam - NWC	AASHTO	1.01	28.1%	1.26	0.68	50.0%	25.0%
(4 with A_{tr})	ACI 318	1.28	11.5%	1.36	1.06	0.0%	0.0%
	ACI 408	1.18	15.9%	1.32	0.91	25.0%	0.0%

Notes:

[†] No. of specimens without stirrups ("without A_{tr}") and with stirrups ("with A_{tr}") given in parentheses

ANALYSIS OF TEST-TO-PREDICTION RATIOS FOR ALL LWC AND NWC SPECIMENS

The results of an analysis of the test-to-prediction ratios are given in Table 24. The mean test-to-prediction ratio for all specimens was 1.23 for the AASHTO LRFD expression, 1.39 for the ACI 318-11 expression, and 1.09 for the ACI 408-03 expression. This indicates that the bar stresses were underestimated by all three expressions with the ACI 318-11 expression giving the largest mean test-to-prediction ratio and the ACI 408-03 expression had the mean ratio closest to 1.0. The same trend was observed for all specimens without stirrups and all specimens with stirrups. These predictions of bar stress do not include a factor for lightweight concrete (λ taken as 1.0) or the safety factors applied for the design of splices.

For all LWC specimens, the ACI 318-11 expression gave the largest mean ratio (1.37) and the ACI 408-03 expression gave the smallest (0.97) and was slightly less than 1.0 (i.e., over-estimated). A similar trend was observed for LWC specimens without stirrups. For LWC specimens with stirrups, the mean ratios for the AASHTO LRFD and ACI 318-11 expressions were nearly equal at 1.08 and 1.07, respectively, and the mean ratio for the ACI 408-03 expression was 0.95.

A similar trend was also observed for NWC specimen without stirrups and with stirrups. In each case the mean ratio for the ACI 408-03 expression was the closest to 1.0 while still under-estimated the bar stress.

ANALYSIS OF TEST-TO-PREDICTION RATIOS BY CONCRETE MIXTURE TYPE

Table 25 and Table 26 give the mean test-to-prediction ratios by concrete mixture type. The ACI 318-11 expression gives mean ratios greater than 1.0 for all concrete mixture types except for the limited number of all-lightweight concrete development beam specimens without stirrups. For this small group of specimens, the maximum test-to-prediction ratios given by all three expressions were less than 1.0.

The ACI 408-03 expression gives mean ratios for the all-lightweight concrete of 0.55 for specimens without stirrups and 0.86 for specimens with stirrups. For sand-lightweight and specified density concrete specimens, the ACI 408-03 expression gave mean ratios that were near 1.0 and greater than 1.0, respectively.

For the NWC specimens not in the ACI Committee 408 Database, the AASHTO LRFD and ACI 318-11 expressions gave similar mean ratios that were 1.10 or larger. The ACI 408-03 expression over-estimated the mean ratio of the NWC specimens without stirrups and under-estimated the mean ratio for the limited number of specimens with stirrups.

The NWC specimens in the ACI Committee 408 Database followed the trend of the ACI 318-11 expression giving the largest mean ratio and the ACI 408-03 expression giving the mean ratio closest to 1.0. All three expressions gave mean ratios greater than 1.0, regardless of whether the specimens had stirrups or not.

ANALYSIS OF TEST-TO-PREDICTION RATIOS BY SPECIMEN TYPE

Table 27 gives the mean test-to-prediction ratios for all specimen types other than the splice beams in the ACI Committee 408 Database, which are given in Table 26 with the label "NWC – ACI 408". In Table 27, the mean ratios for specimens without stirrups included beam-end, splice beam, tension prism, and development beam specimens. The three design expressions gave considerably larger mean ratios for the tension prisms and considerably lower mean ratios for the development beams. The AASHTO LRFD and ACI 318-11 expressions gave similarly under-estimated mean ratios for the beam-end and splice beam specimens without stirrups. The ACI 408-03 expression gave a mean ratio for the beam-end specimens that was less than 1.0, and a mean ratio for the splice beams without stirrups that was greater than 1.0.

The mean ratios given by the ACI 318-11 and ACI 408-03 expressions for the selected splice beam specimens from the ACI Committee 408 Database are larger for the specimens with stirrups than for the specimens without stirrups. This implies that the expressions under-estimate the increase in bar stress caused by the presence of stirrups. A similar trend is observed for the development length beam specimens that are mostly LWC. The ACI 318-11 and ACI 408-03 expressions gave nearly equal mean ratios for the mostly LWC splice beam specimens, regardless of the presence of stirrups.

COMPARISON OF LWC AND NWC TEST-TO-PREDICTION RATIOS

Table 28 and Table 29 give a comparison of the mean test-to-prediction ratios of LWC specimens and similar NWC specimens. The mean ratios are grouped by specimen type and presence of stirrups. The AASHTO LRFD and ACI 318-11 expressions gave larger mean ratios for NWC than LWC for the beam-end specimens, splice beam specimens (except for the three NWC specimens not in the ACI Committee 408 Database), and development beam specimens. The ACI 408-03 expression gave mean ratios for the NWC specimens that were equal to or greater than mean ratios for LWC for all specimens except the beam-end specimens and three NWC specimens not in the ACI Committee 408 Database.

In Table 24, the mean ratios for all of the NWC specimens were larger than the mean ratios of all the LWC specimens as predicted by all three design expressions. The same trend was observed for the NWC and LWC specimens with stirrups. For the NWC and LWC specimens without stirrups, the ACI 318-11 expression gave a larger mean ratio for LWC specimens than for NWC specimens.

ANALYSIS OF TEST-TO-PREDICTION RATIOS VERSUS SPLICE LENGTH

The figures giving the test-to-prediction ratios for the AASHTO LRFD and ACI 318-11 expressions show that the regression lines have a downward trend as normalized splice length increases. The ratios for the AASHTO LRFD expression are shown in Figure 72 and Figure 73 for specimens without stirrups and in Figure 74 and Figure 75 for specimens with stirrups. The regression line for all of the specimens without stirrups and the line for all specimens with

stirrups are parallel. Figure 80 and Figure 81 show the ratios for the ACI 318-11 expression determined for specimens without stirrups, and Figure 82 and Figure 83 show the ratios for specimens with stirrups. The mean ratios determined using ACI 318-11 for the tension beam specimens are highly under-estimated (i.e., much greater than 1.0). This has the effect of reducing the slope of the regression line (i.e., making it more negative) for all specimens without stirrups (labeled "All N regression").

The figures giving the test-to-prediction ratios for the ACI 408-03 expression show that that the ratio is near 1.0. The regression lines in Figure 88 and Figure 89 for specimens without stirrups and in Figure 90 and Figure 91 for specimens with stirrups are mostly parallel and near 1.0. The mean ratios of the tension beams that were highly under-estimated by the AASHTO LRFD expression (Figure 73) and the ACI 318-11 expression (Figure 81) were near 1.0 when determined using the ACI 408-03 expression (Figure 89).

ANALYSIS OF TEST-TO-PREDICTION RATIOS VERSUS COMPRESSIVE STRENGTH

The figures giving the test-to-prediction ratios for the AASHTO LRFD and ACI 408-03 expression versus compressive strength show that the regression lines have almost no slope. This indicates that the expressions give predictions that do not begin to under-estimate or overestimate the test-to-predictions ratios for larger compressive strengths. The ratios for the AASHTO LRFD expression are shown in Figure 76 and Figure 77 for specimens without stirrups and in Figure 78 and Figure 79 for specimens with stirrups. Figure 92 and Figure 93 show the ratios for the ACI 408-03 expression determined for specimens without stirrups, and Figure 94 and Figure 95 show the ratios for specimens with stirrups. The scatter observed for the test-to-prediction ratios determined from the AASHTO LRFD expression was larger than the scatter observed for the ACI 408-03 expression, especially for the sand-lightweight tension prism specimens.

The test-to-prediction ratios for the ACI 318-11 expression decrease as compressive strength increases. The regression lines in Figure 84 and Figure 85 for specimens without stirrups and in Figure 86 and Figure 87 for specimens with stirrups have a negative slope. The slope of the regression line for all specimens without stirrups has a more negative slope than the line for all of the specimens with stirrups. This is again due to the under-estimation of bar stress for the tension prism specimens.

The mean ratios of the all-lightweight development beam specimens and the sand-lightweight beam-end specimens were significantly over-estimated by all three expressions. Recall that the test-to-prediction ratios determined for this analysis did not include any modification for LWC (i.e., λ_{ACI} and λ_{ACI408} were taken as 1.0). The amount of the over-estimation of bar stress would be reduced by using a modification factor for LWC less than 1.0.

SUMMARY OF TEST-TO-PREDICTION RATIO ANALYSIS

The bar stress at failure for the 474 LWC and NWC specimens in the TFHRC Mild Steel Development Database were compared to the bar stress determined from the AASHTO LRFD expression (Eq. 31), ACI 318-11 expression (Eq. 32), and the ACI 408-03 expression (Eq. 33). The comparison was made using test-to-prediction ratios of bar stress for each expression. The lightweight concrete modification factor was taken as 1.0 in each expression of predicted bar stress.

The AASHTO LRFD expression does not account for the presence of stirrups. The observed increase in bar stress at failure due to the presence of stirrups results in an underestimation of the test-to-prediction ratio. Also the ratio for specimens with stirrups is higher than the ratio for specimens without stirrups. The mean test-to-prediction ratio for the AASHTO LRFD expression was greater than 1.0 (i.e., under-estimated) for LWC and NWC specimens, with or without stirrups. However, the scatter in the LWC data was high, with a COV of 44%. The test-to-prediction ratio remained uniform (i.e., the slope of the regression line was near zero) with increases in concrete compressive strength. The test-to-prediction ratio was smaller for larger normalized splice lengths (i.e., the slope of the regression line was negative).

The ACI 318-11 expression under-estimated the bar stress for most of the LWC specimens and nearly all of the NWC specimens. The scatter in the predicted bar stress of LWC specimens was high, with a COV of 46%. The test-to-prediction ratio was smaller for specimens with larger normalized splice lengths and was also smaller for specimens with higher concrete compressive strengths.

The ACI 408-03 expression gave test-to-prediction ratios slightly less than unity for LWC specimens and greater than unity for NWC specimens. The COV for the LWC specimens was still high at 29%, but smaller than the COV determined using either the AASHTO LRFD or ACI 318-11 expressions. The ACI 408-03 expression gave test-to-prediction ratios that remained uniform with changes in normalized splice length or changes in compressive strength.
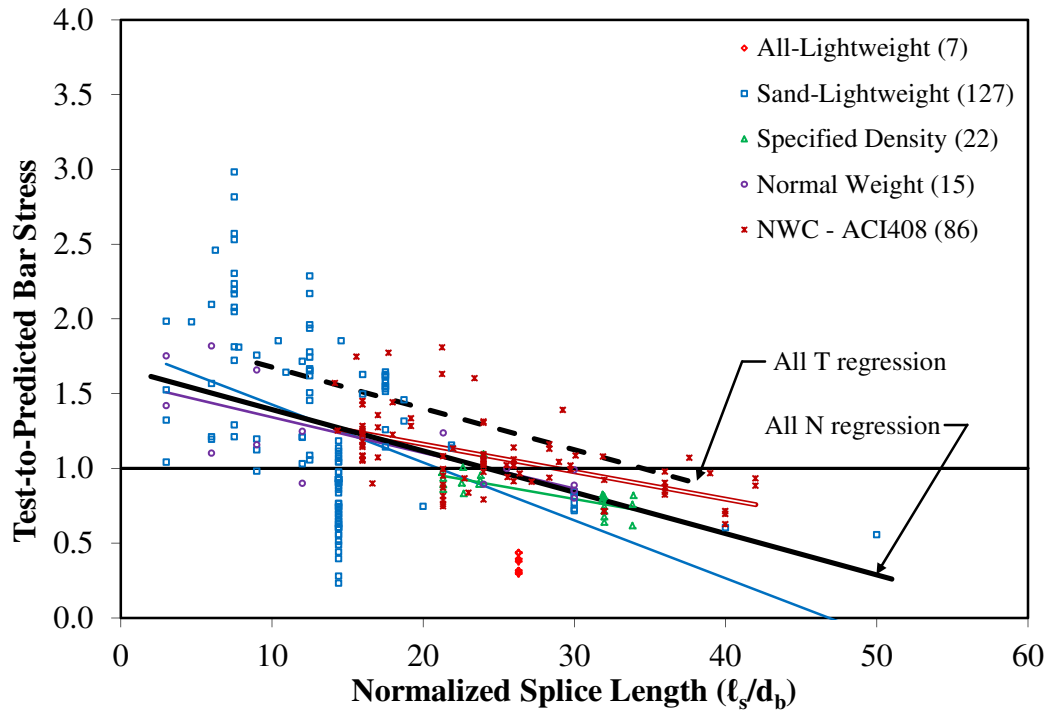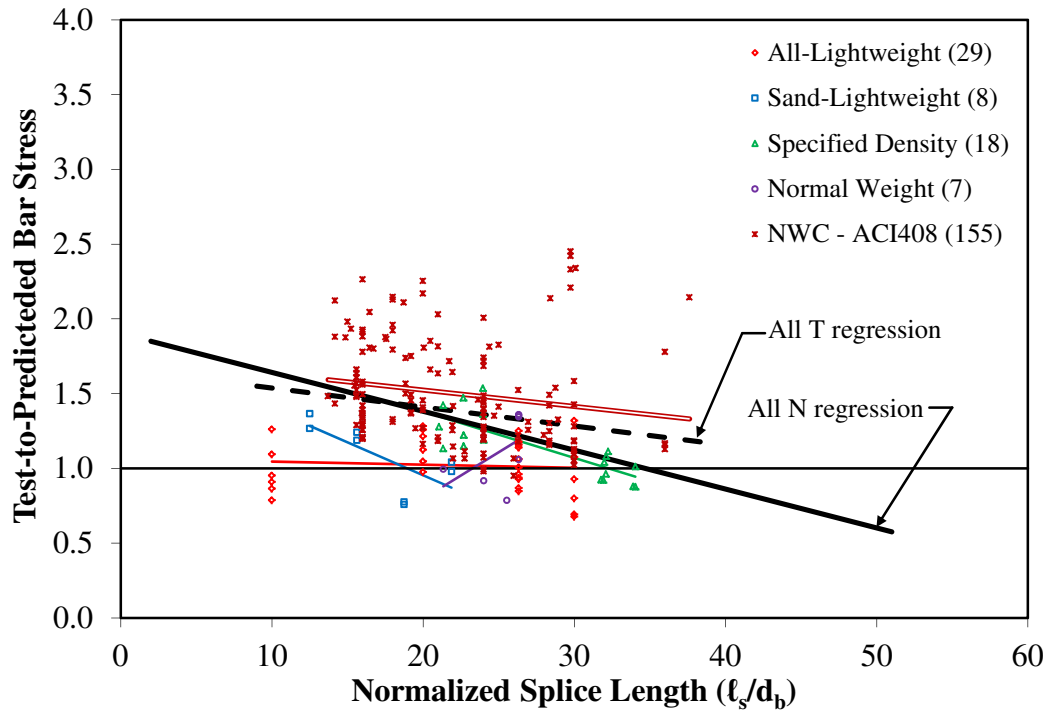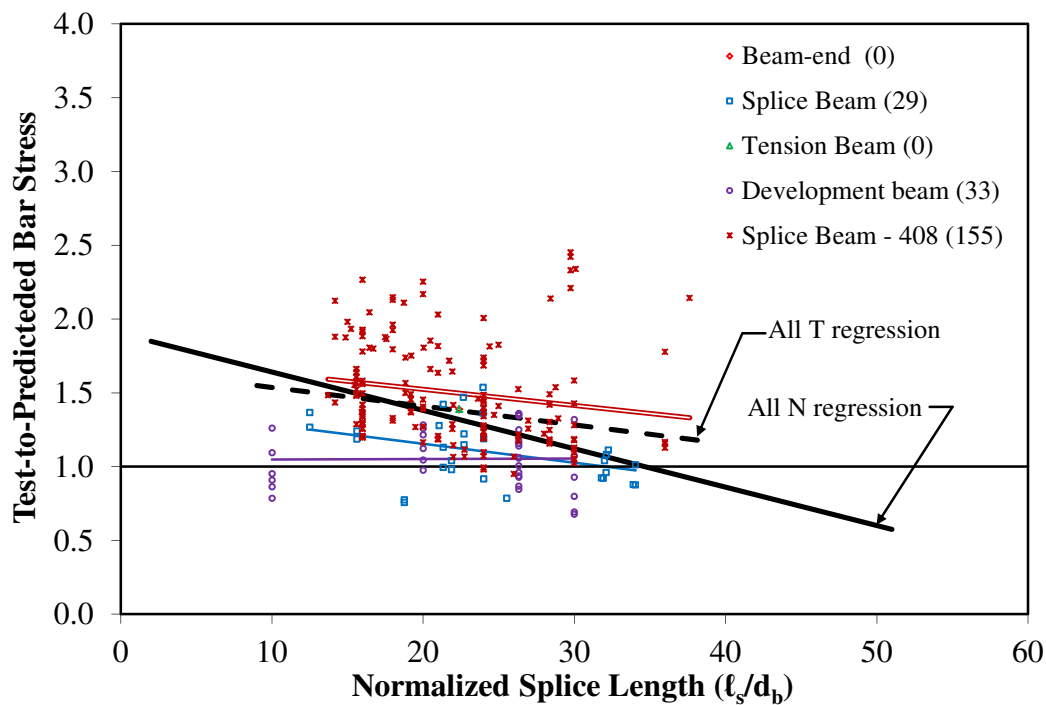
Figure 72. Graph. Bar Stress Test-to-Prediction Ratio Compared to Normalized Splice Length (ℓ_s/d_b) for AASHTO LRFD Expression (Eq. 31) by Concrete Mixture Type for Specimens without Stirrups (N) in the TFHRC Database.
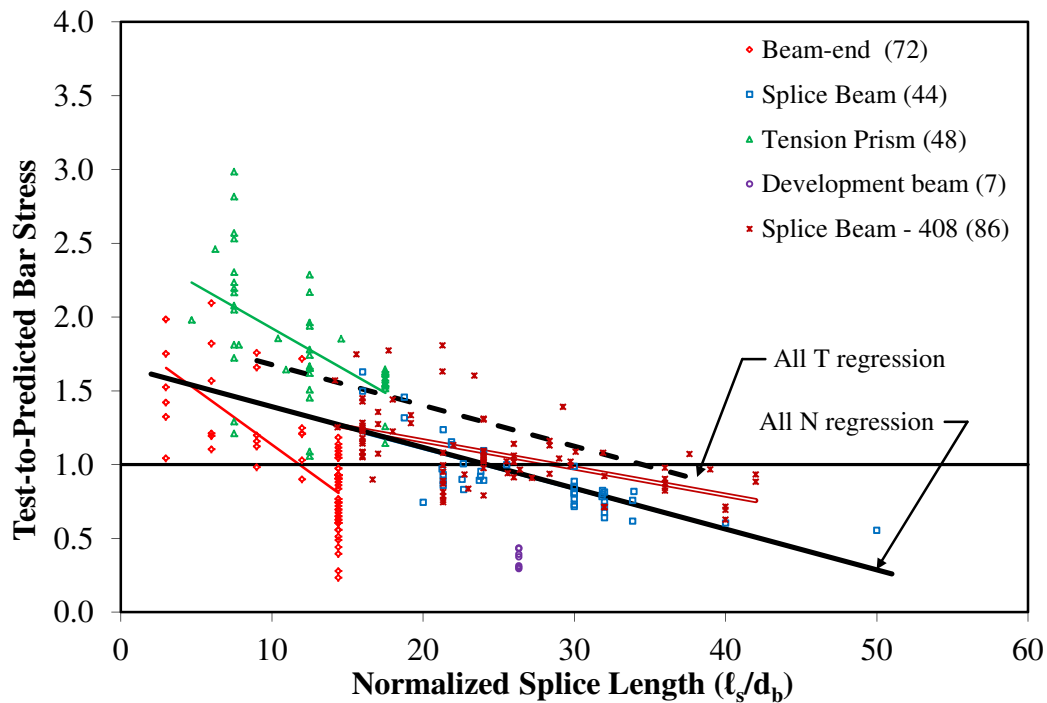
Figure 73. Graph. Bar Stress Test-to-Prediction Ratio Compared to Normalized Splice Length (ℓ_s/d_b) for AASHTO LRFD Expression (Eq. 31) by Specimen Type for Specimens without Stirrups (N) in the TFHRC Database.
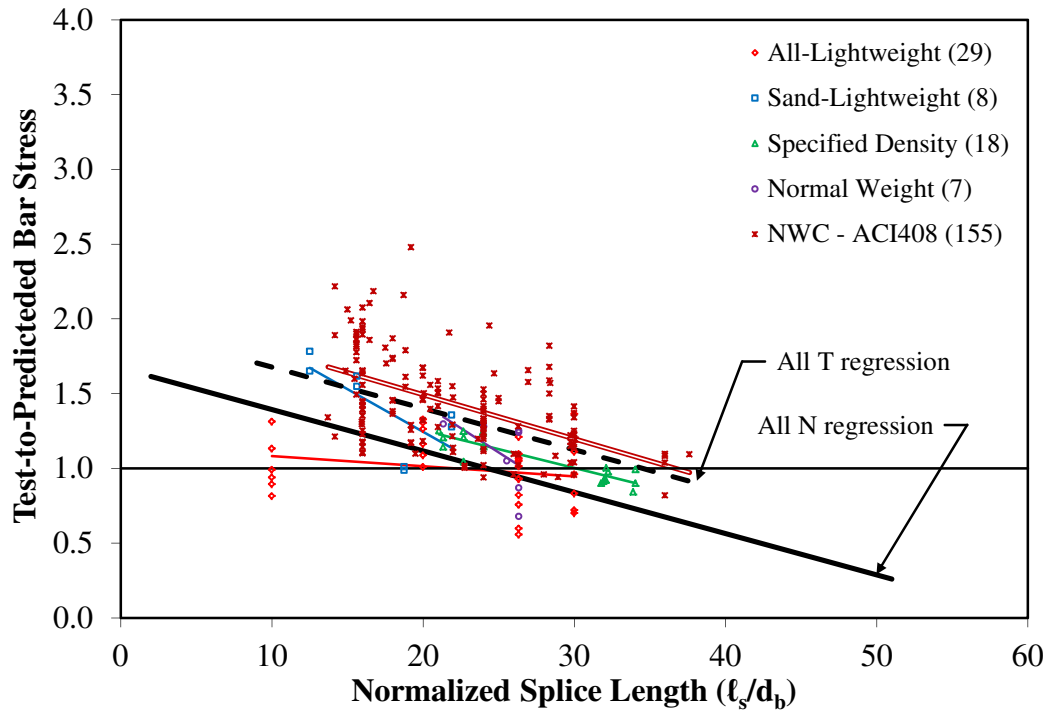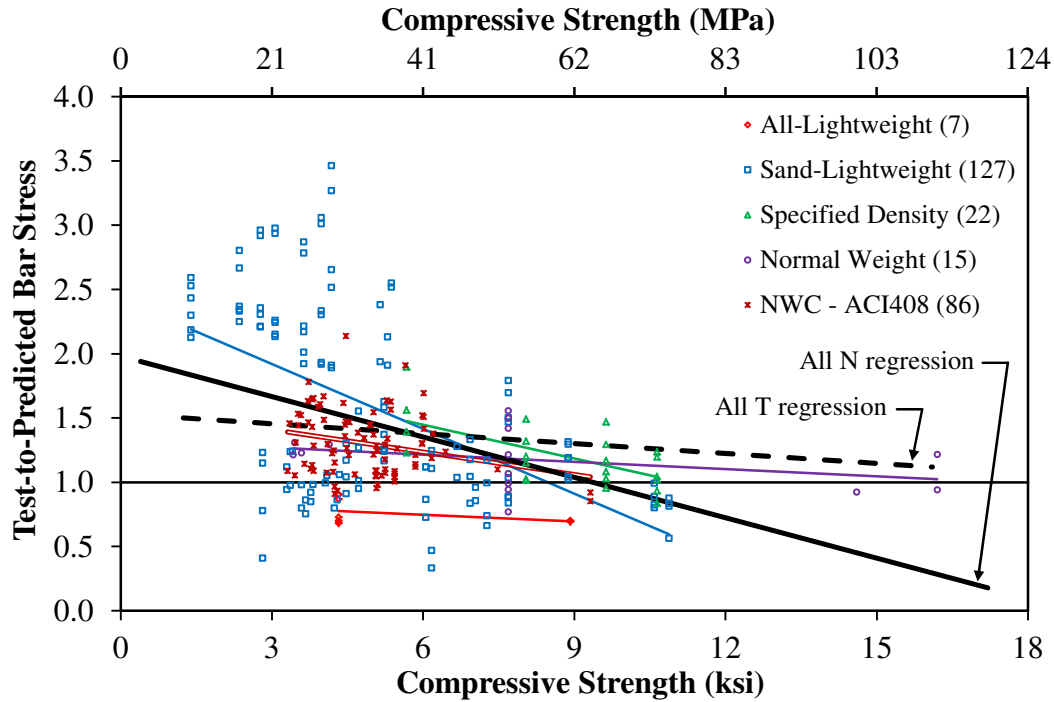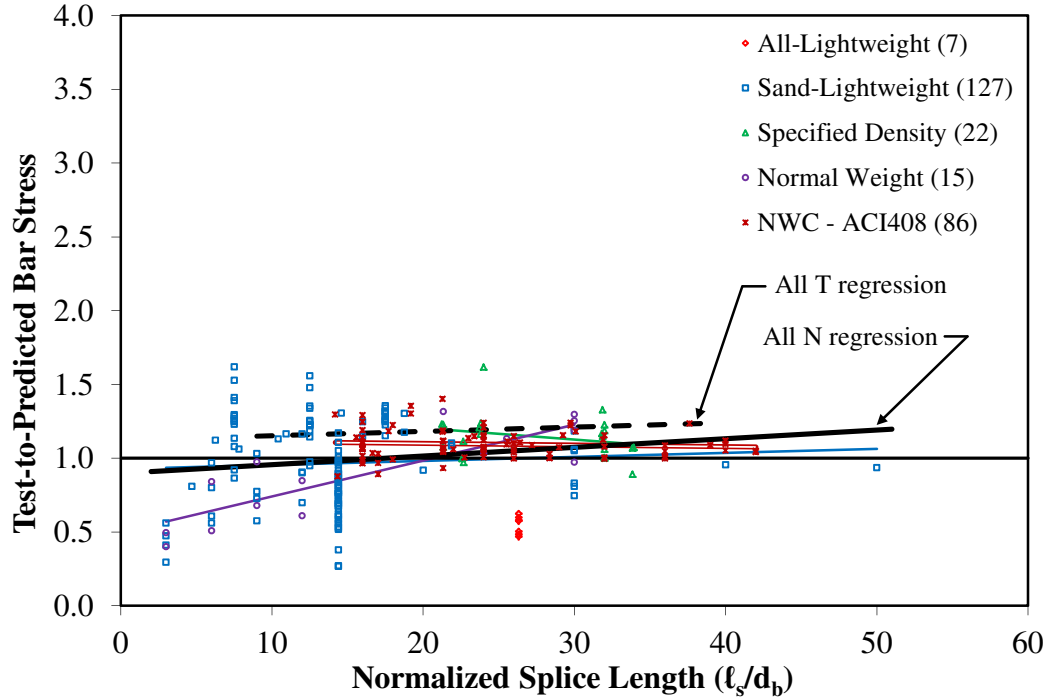
Figure 74. Graph. Bar Stress Test-to-Prediction Ratio Compared to Normalized Splice Length (ℓ_s/d_b) for AASHTO LRFD Expression (Eq. 31) by Concrete Mixture Type for Specimens with Stirrups (T) in the TFHRC Database.
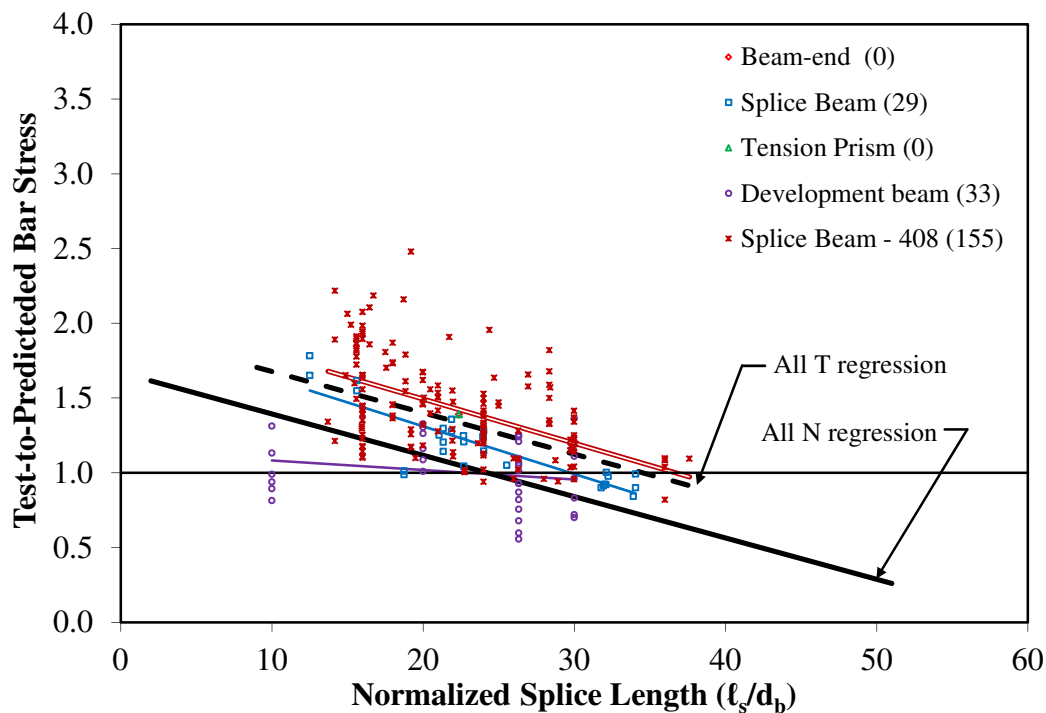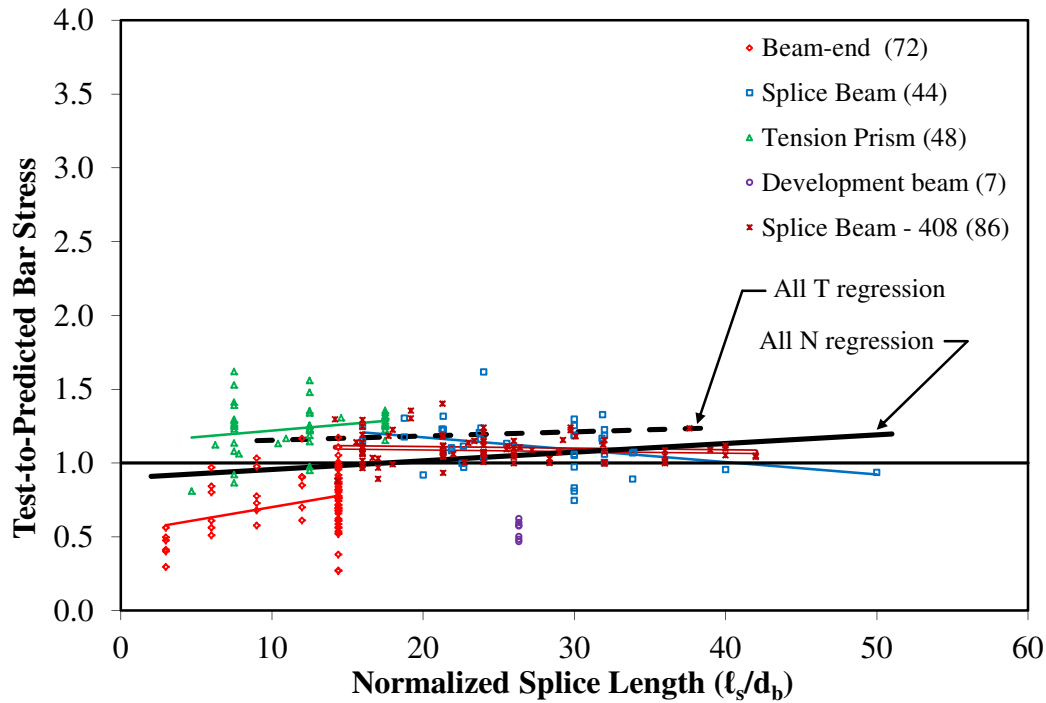

Figure 75. Graph. Bar Stress Test-to-Prediction Ratio Compared to Normalized Splice Length (ℓ_s/d_b) for AASHTO LRFD Expression (Eq. 31) by Specimen Type for Specimens with Stirrups (T) in the TFHRC Database.
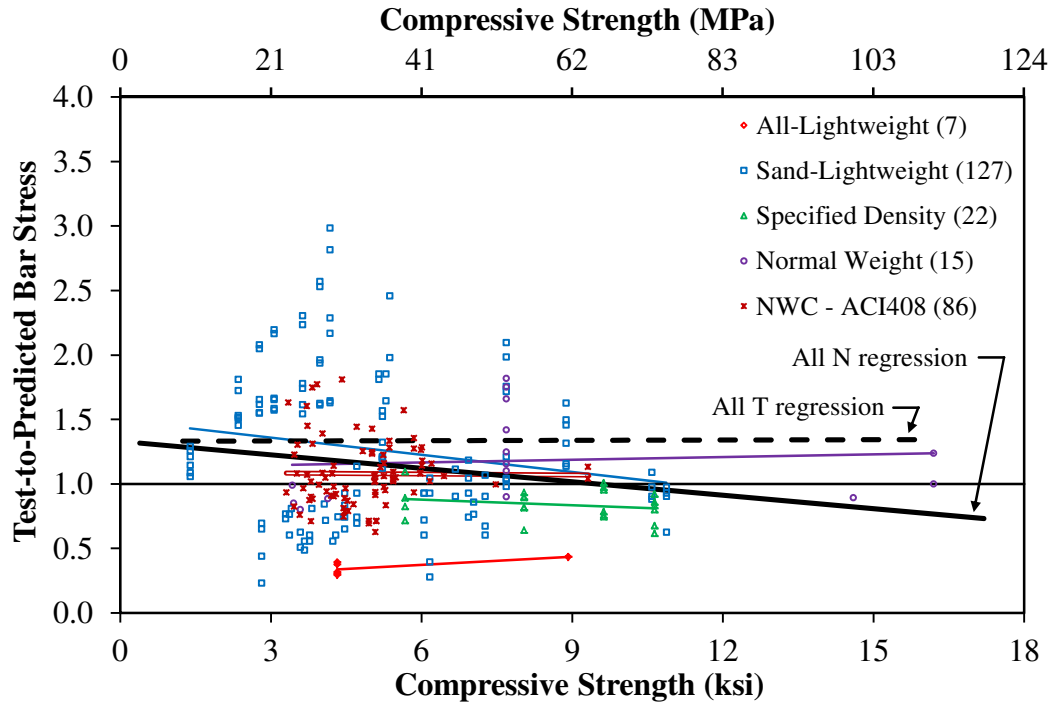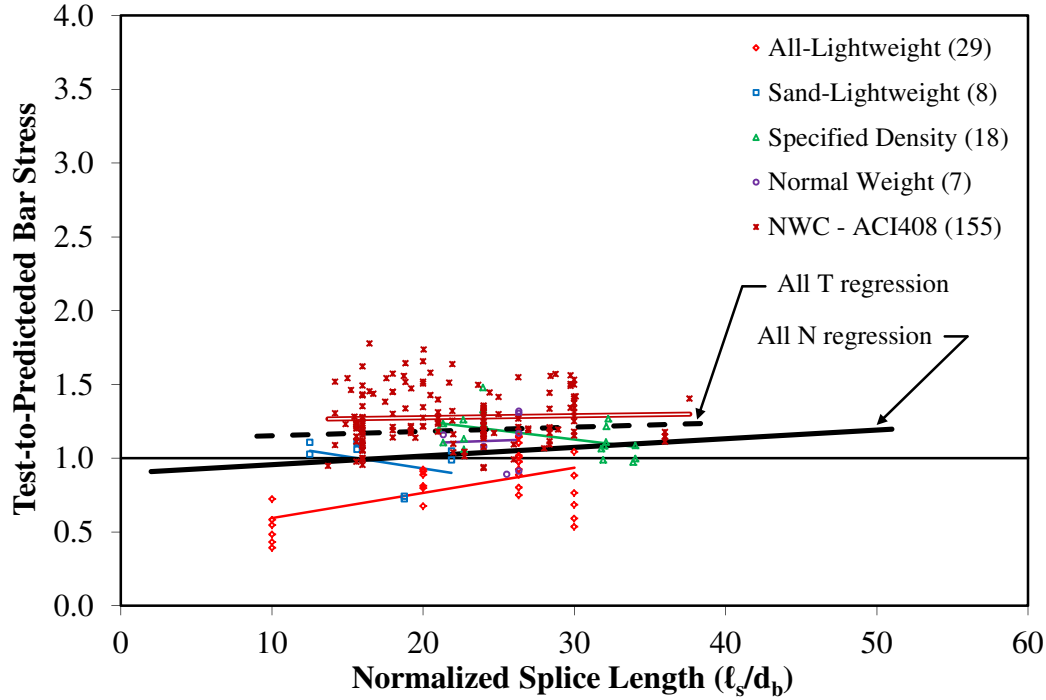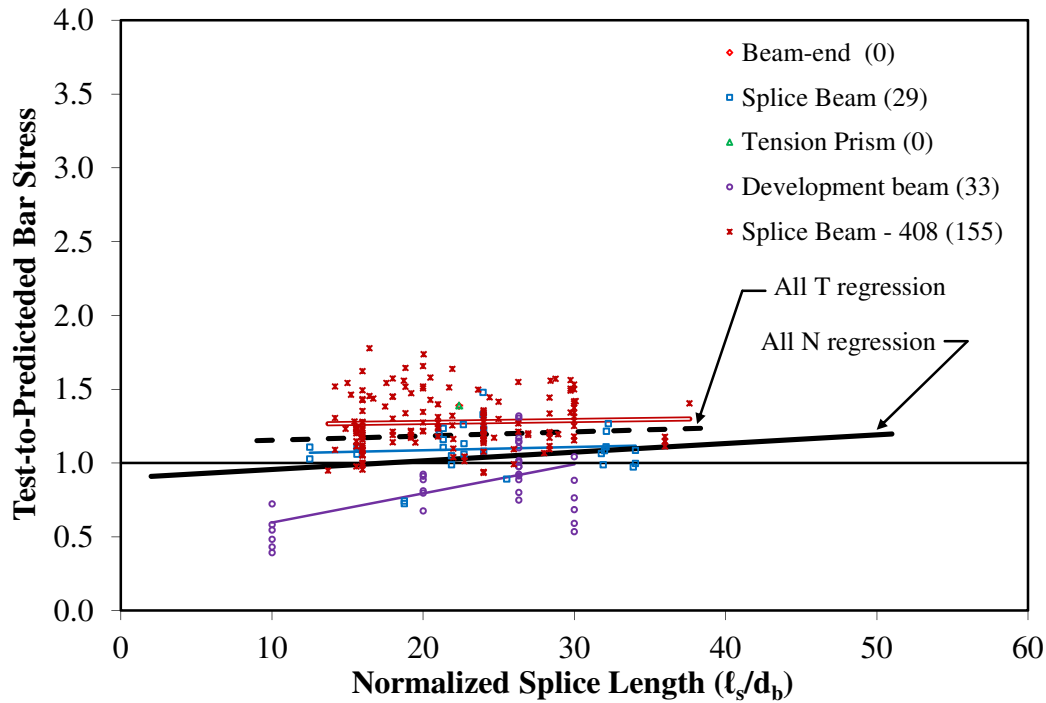
Figure 76. Graph. Bar Stress Test-to-Prediction Ratio Compared to Compressive Strength for AASHTO LRFD Expression (Eq. 31) by Concrete Mixture Type for Specimens without Stirrups (N) in the TFHRC Database.
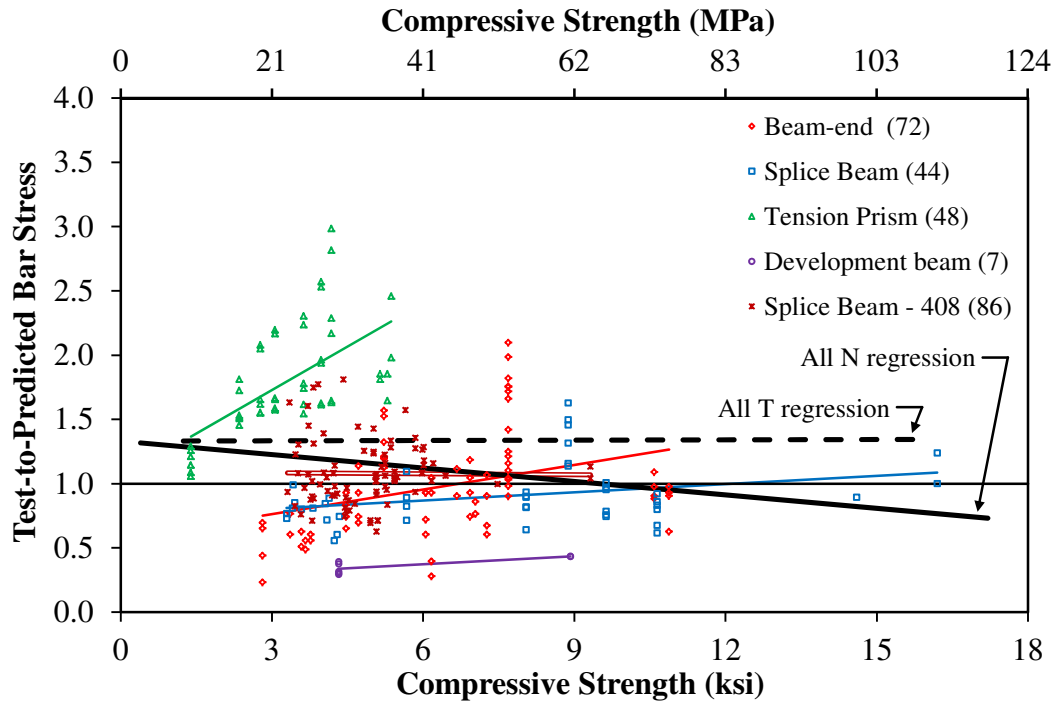
Figure 77. Graph. Bar Stress Test-to-Prediction Ratio Compared to Compressive Strength for AASHTO LRFD Expression (Eq. 31) by Specimen Type for Specimens without Stirrups (N) in the TFHRC Database.
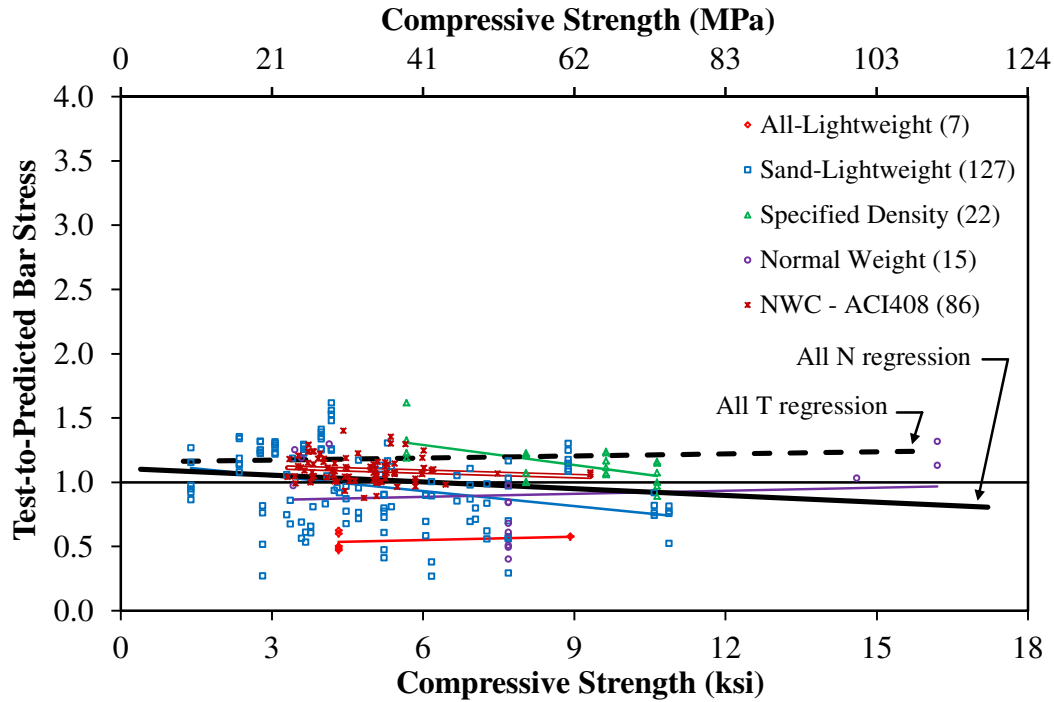
111
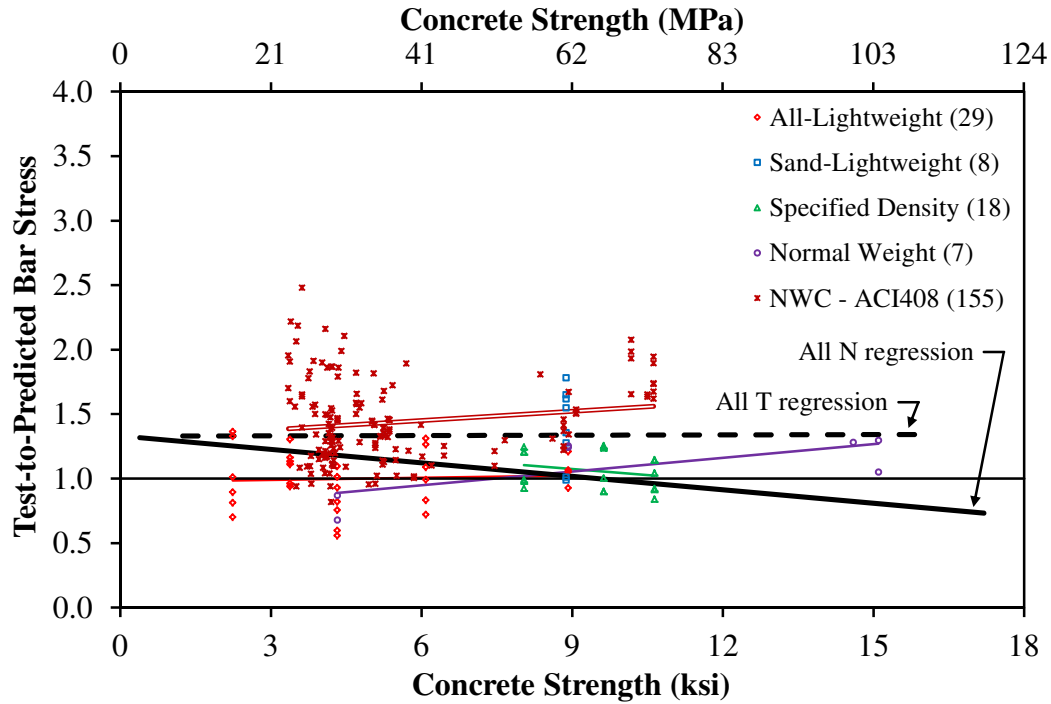
Figure 78. Graph. Bar Stress Test-to-Prediction Ratio Compared to Compressive Strength for AASHTO LRFD Expression (Eq. 31) by Concrete Mixture Type for Specimens with Stirrups (T) in the TFHRC Database.
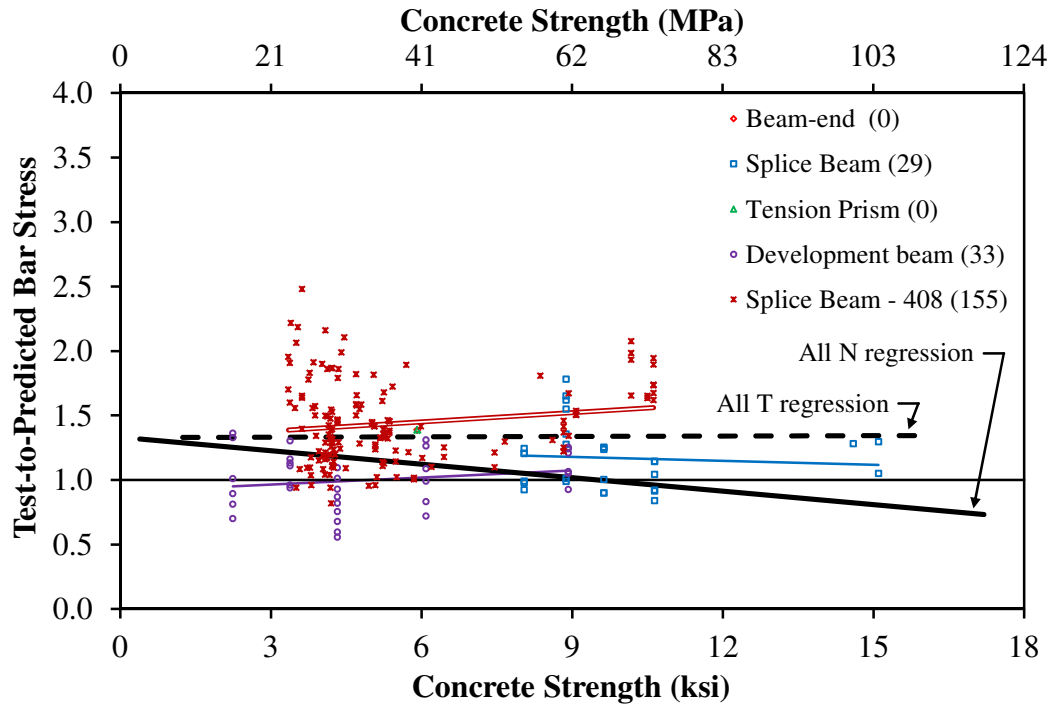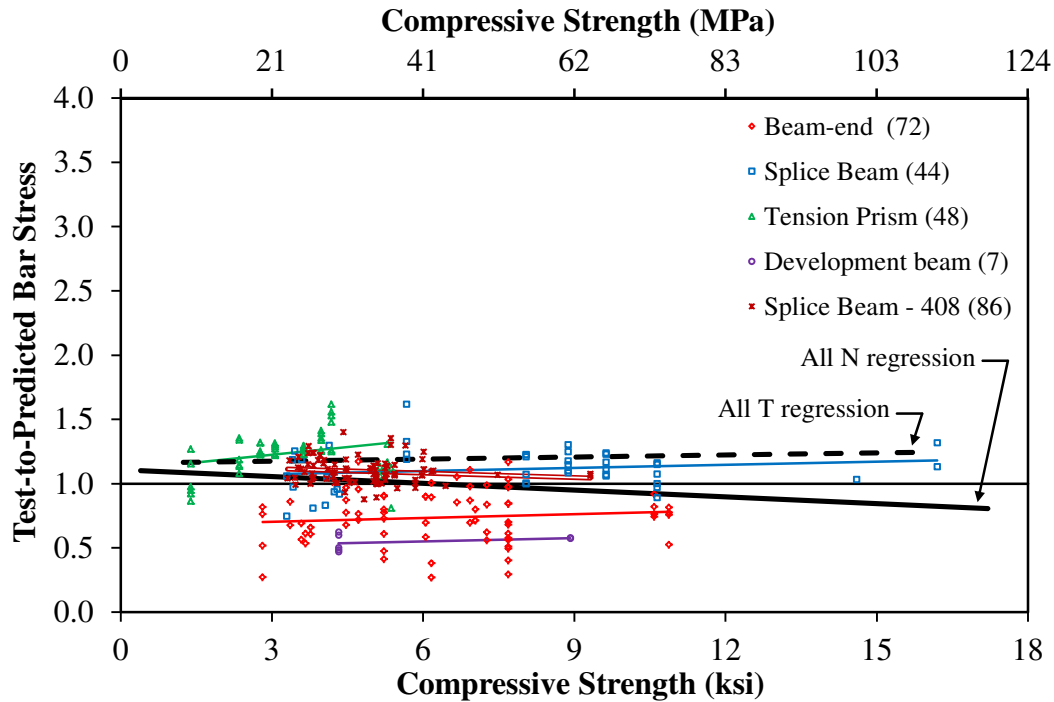

Figure 79. Graph. Bar Stress Test-to-Prediction Ratio Compared to Compressive Strength for AASHTO LRFD Expression (Eq. 31) by Specimen Type for Specimens with Stirrups (T) in the TFHRC Database.
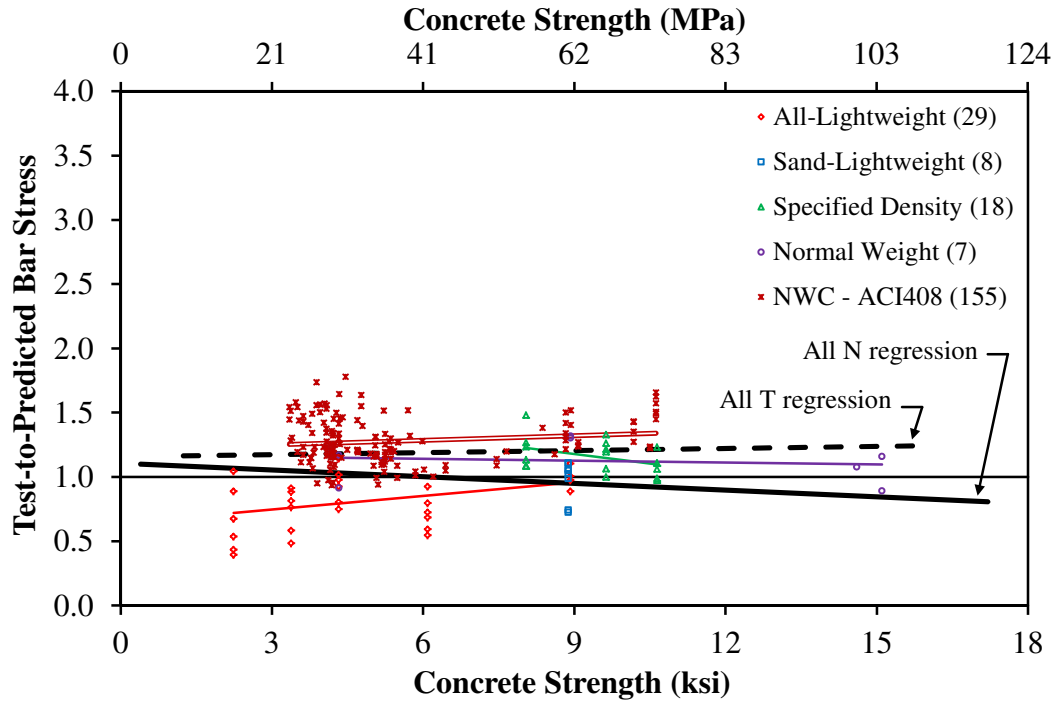
112
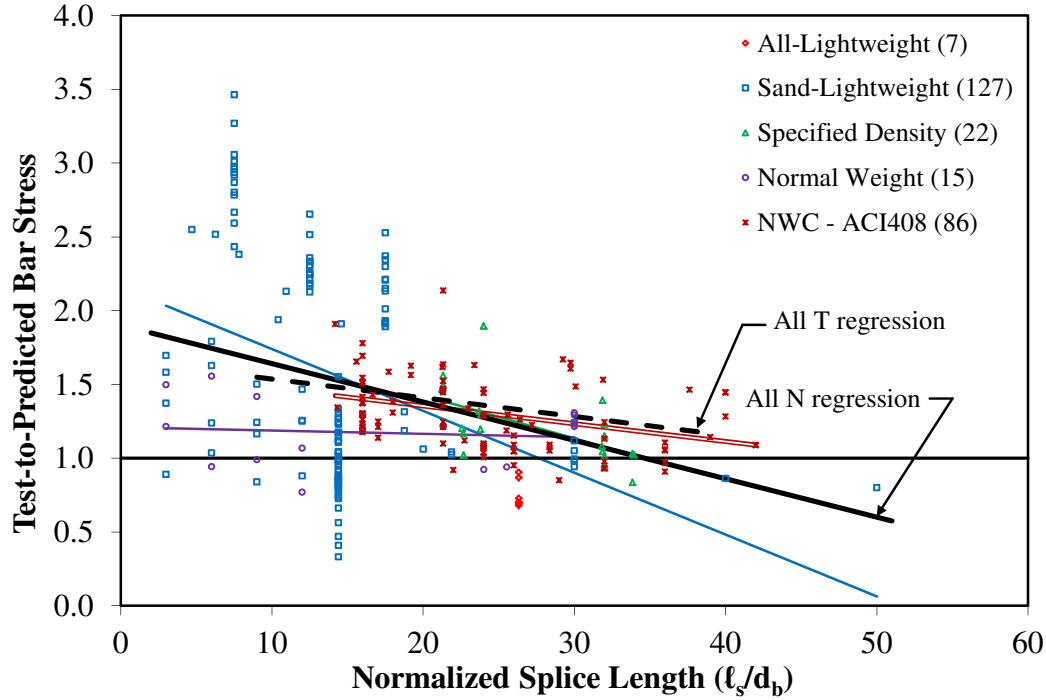
Figure 80. Graph. Bar Stress Test-to-Prediction Ratio Compared to Normalized Splice Length (ℓ_s/d_b) for ACI 318-11 Expression (Eq. 32) by Concrete Mixture Type for Specimens without Stirrups (N) in the TFHRC Database.
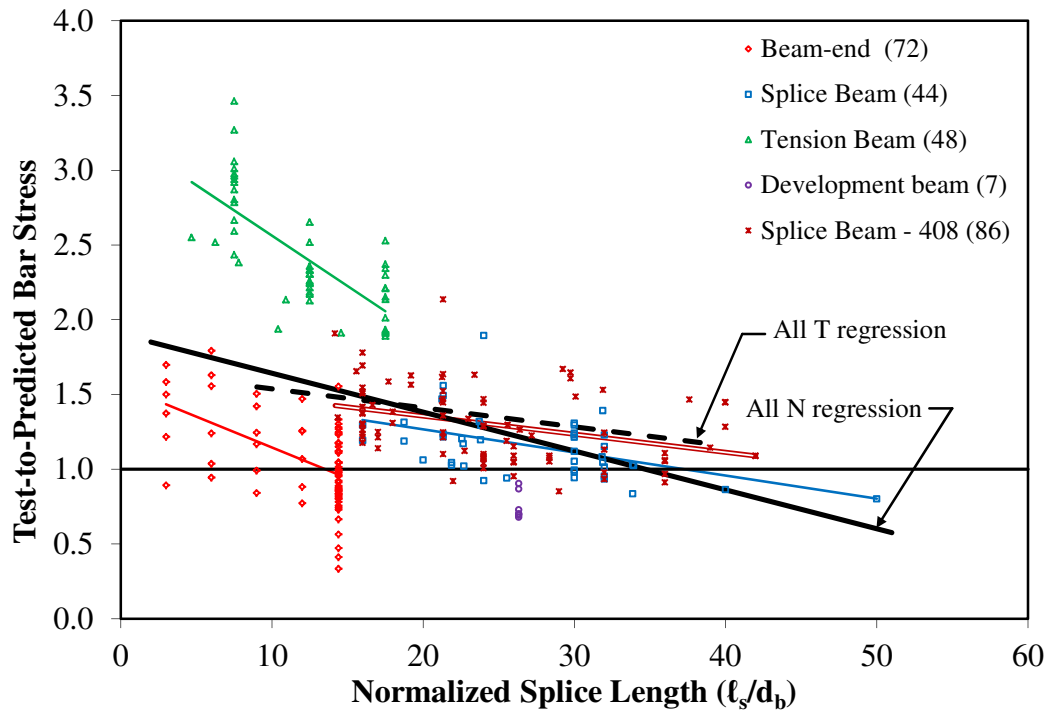
Figure 81. Graph. Bar Stress Test-to-Prediction Ratio Compared to Normalized Splice Length (ℓ_s/d_b) for ACI 318-11 Expression (Eq. 32) by Specimen Type for Specimens without Stirrups (N) in the TFHRC Database.

Figure 82. Graph. Bar Stress Test-to-Prediction Ratio Compared to Normalized Splice Length (ℓ_s/d_b) for ACI 318-11 Expression (Eq. 32) by Concrete Mixture Type for Specimens with Stirrups (T) in the TFHRC Database.

Figure 83. Graph. Bar Stress Test-to-Prediction Ratio Compared to Normalized Splice Length (ℓ_s/d_b) for ACI 318-11 Expression (Eq. 32) by Specimen Type for Specimens with Stirrups (T) in the TFHRC Database.

114

Figure 84. Graph. Bar Stress Test-to-Prediction Ratio Compared to Compressive Strength for ACI 318-11 Expression (Eq. 32) by Concrete Mixture Type for Specimens without Stirrups (N) in the TFHRC Database.
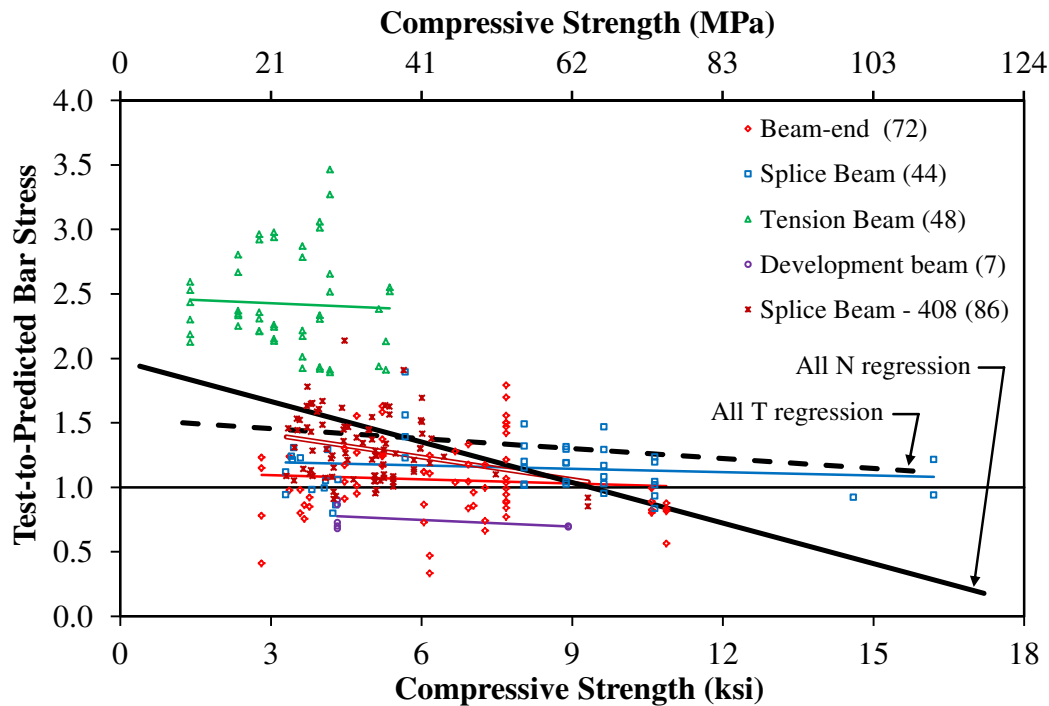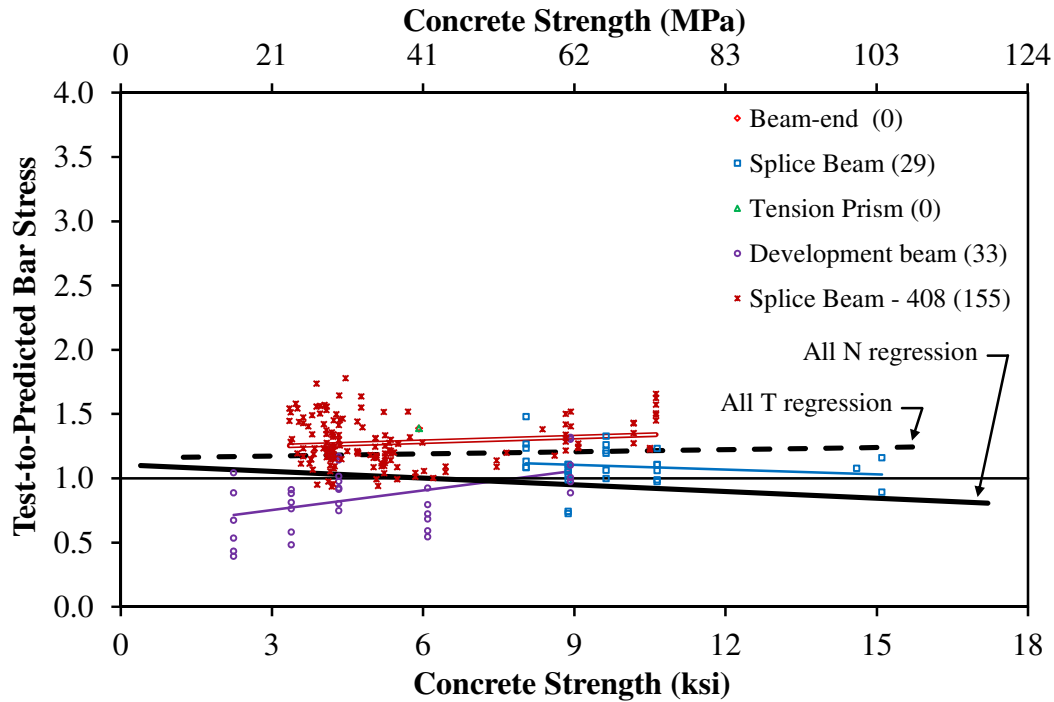

Figure 85. Graph. Bar Stress Test-to-Prediction Ratio Compared to Compressive Strength for ACI 318-11 Expression (Eq. 32) by Specimen Type for Specimens without Stirrups (N) in the TFHRC Database.
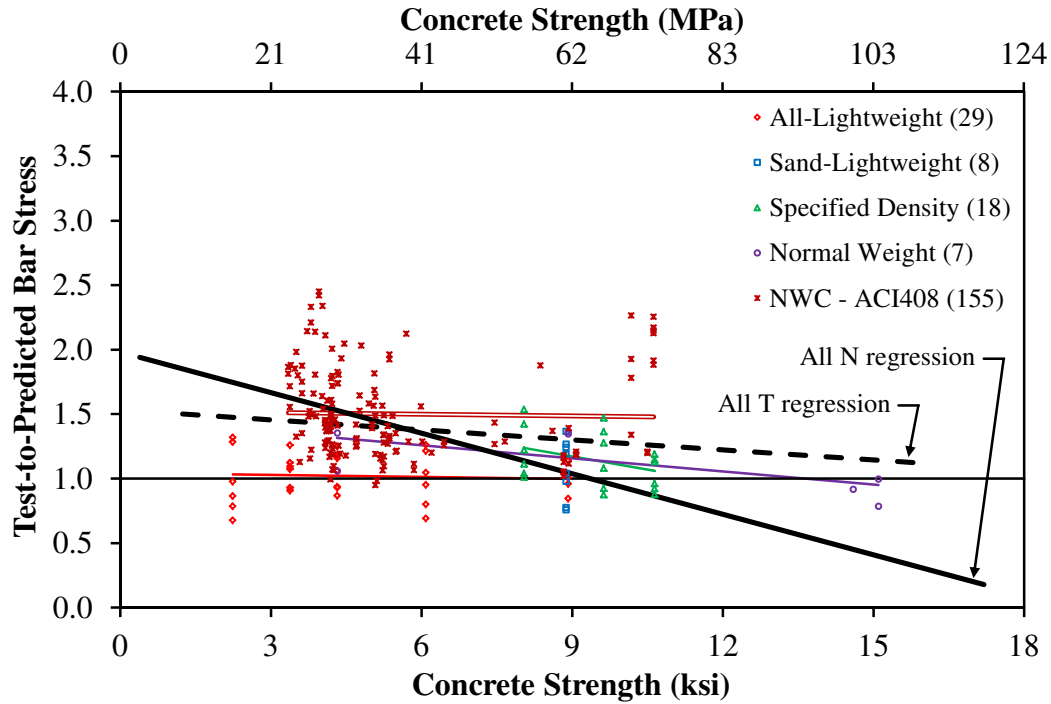
Figure 86. Graph. Bar Stress Test-to-Prediction Ratio Compared to Compressive Strength for ACI 318-11 Expression (Eq. 32) by Concrete Mixture Type for Specimens with Stirrups (T) in the TFHRC Database.
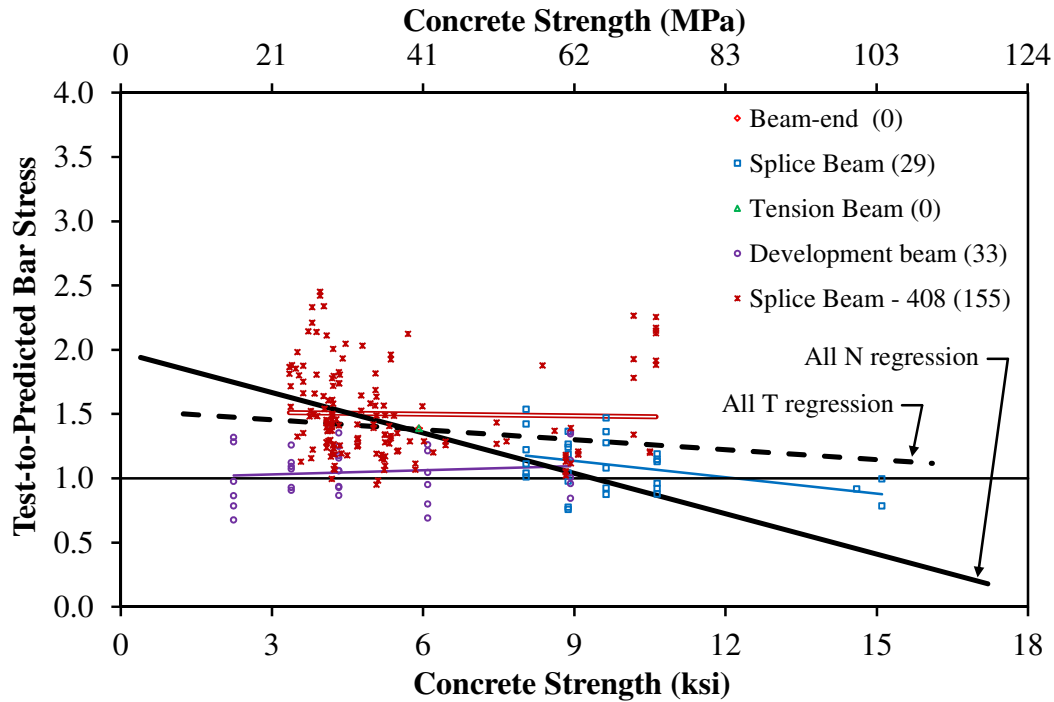
Figure 87. Graph. Bar Stress Test-to-Prediction Ratio Compared to Compressive Strength for ACI 318-11 Expression (Eq. 32) by Specimen Type for Specimens with Stirrups (T) in the TFHRC Database.

Figure 88. Graph. Bar Stress Test-to-Prediction Ratio Compared to Normalized Splice Length (ℓ_s/d_b) for ACI 408-03 Expression (Eq. 33) by Concrete Mixture Type for Specimens without Stirrups (N) in the TFHRC Database.

Figure 89. Graph. Bar Stress Test-to-Prediction Ratio Compared to Normalized Splice Length (ℓ_s/d_b) for ACI 408-03 Expression (Eq. 33) by Specimen Type for Specimens without Stirrups (N) in the TFHRC Database.

Figure 90. Graph. Bar Stress Test-to-Prediction Ratio Compared to Normalized Splice Length (ℓ_s/d_b) for ACI 408-03 Expression (Eq. 33) by Concrete Mixture Type for Specimens with Stirrups (T) in the TFHRC Database.

Figure 91. Graph. Bar Stress Test-to-Prediction Ratio Compared to Normalized Splice Length (ℓ_s/d_b) for ACI 408-03 Expression (Eq. 33) by Specimen Type for Specimens with Stirrups (T) in the TFHRC Database.

Figure 92. Graph. Bar Stress Test-to-Prediction Ratio Compared to Compressive Strength for ACI 408-03 Expression (Eq. 33) by Concrete Mixture Type for Specimens without Stirrups (N) in the TFHRC Database.

Figure 93. Graph. Bar Stress Test-to-Prediction Ratio Compared to Compressive Strength for ACI 408-03 Expression (Eq. 33) by Specimen Type for Specimens without Stirrups (N) in the TFHRC Database.

Figure 94. Graph. Bar Stress Test-to-Prediction Ratio Compared to Compressive Strength for ACI 408-03 Expression (Eq. 33) by Concrete Mixture Type for Specimens with Stirrups (T) in the TFHRC Database.

Figure 95. Graph. Bar Stress Test-to-Prediction Ratio Compared to Compressive Strength for ACI 408-03 Expression (Eq. 33) by Specimen Type for Specimens with Stirrups (T) in the TFHRC Database.

PROPOSED DESIGN EXPRESSIONS FOR BAR STRESS

The test-to-prediction ratios for the TFHRC Database previously analyzed in this chapter did not include any modification for lightweight concrete. This section will show the range of potential predicted values determined using traditional modification factors for LWC in the AASHTO LRFD expression, the ACI 318-11 expression, and the ACI 408-03 expression. Modification factors based on the unit weight and splitting tensile strength are proposed in this section. The effect of the proposed LWC modification factors on the predicted bar stress determined using the three design expressions is described and analyzed. A slight revision to the ACI 408-03 expression was made based on the analysis of the LWC test data. The effect of this revision is analyzed in this section.

COMPARISON OF PREDICTED BAR STRESS INCLUDING MODIFICATION FOR LWC

The analysis of test-to-prediction ratios given in the previous section titled "Bar Stress Predicted by Design Expressions without Modification for LWC" did not include any modification for lightweight concrete. The following shows the predictions of bar stress given by the AASHTO LRFD expression, the ACI 318-11 expression, and the ACI 408-03 expression that include modification for LWC. The predictions give an indication of the potential range of predicted bar stress using the traditional modification factors for LWC.

The prediction of the bar stress at failure, f_s, is shown for the three design expressions versus normalized splice length in Figure 96, Figure 97, Figure 98. The figures show the data for 257 LWC and NWC specimens without stirrups. The predictions are shown to a maximum f_s of 75 ksi (517 MPa), which is the limit on the design yield stress in the AASHTO LRFD Specifications.[1] As shown in Table 16, the mean concrete compressive strength for the specimens made with all-lightweight concrete and sand-lightweight is approximately 5 ksi (34 MPa). The specified density concrete specimens and the NWC specimens found in the literature had a mean concrete compressive strength of approximately 9 ksi (62 MPa). The mean concrete compressive strength for the NWC specimens in the ACI Committee 408 Database was approximately 5 ksi (34 MPa).

ACI 318-11

The predictions for f_s determined using ACI 318-11 are shown in Figure 96 for concrete with a compressive strength of 5 ksi (34 MPa) and of 9 ksi (62 MPa) assuming no modification for LWC ($\lambda = 1.0$). An additional prediction determined using ACI 318-11 is shown in the figure that assumes a compressive strength of 5 ksi (34 MPa) and an LWC modification factor of 0.75. The ACI 318-11 expression shown in Figure 96 is given by Eq. 34. The expression given by Eq. 34 is a simplification of the full expression for f_s based on ACI 318-11 that is given by Eq. 32. The specimens in Figure 96 are bottom-cast with uncoated reinforcement and no stirrups, therefore ψ_t and ψ_e are taken as 1.0 and K_{tr} is taken as zero.

$$f_s = \left[\left(\frac{\ell_s}{d_b}\right)\left(\frac{c_b}{d_b}\right)\right] \times \left(\lambda \frac{40}{3}\sqrt{f_c'}\right)$$ (Eq. 34)

in Eq. 34, the units of stress are in psi

The regression line labeled "All LWC regression" in Figure 96 includes all the data from the all-lightweight concrete specimens, the sand-lightweight concrete specimens, and the specified density concrete specimens. The data from the normal weight specimens from literature and the ACI Committee 408 Database specimens are indicated by the regression line labeled "All NWC regression". The regression line for the 156 LWC data points and the 101 NWC data points clearly cross the vertical axis above a bar stress of zero (i.e., they have a non-zero vertical axis intercept). The lines indicating the prediction given by ACI 318-11 are proportional to splice length and cross the vertical axis at the origin. The LWC and NWC regression lines support the observation made in previous research that bar stresses increase linearly with splice length but bar stress is not proportionally to splice length.[9]

A shaded region is shown in Figure 96 between the lines giving the prediction of the ACI 318-11 expression for 5 ksi (34 MPa) concrete with no modification for LWC and with a modification factor of 0.75. Modification factors for LWC have traditionally varied from 0.75 to 1.00. The shaded region indicates the range of possible predicted bar stress using the traditional LWC modification factors. For short normalized splice lengths, the LWC regression line is above the shaded region which indicates an under-estimation of bar stress. For long splice lengths, the regression line is below the shaded region which indicates an over-estimation of bar stress even if a modification factor as low as 0.75 is used.

ACI 408-03

The prediction determined using ACI 408-03 is shown in Figure 97 for the same 257 LWC and NWC specimens. The predictions determined using ACI 408-03 for assumed concrete strengths of 5 ksi (34 MPa) and 9 ksi (62 MPa) are shown in the figure, along with a shaded region indicating the range of possible predicted bar stress for 5 ksi (34 MPa) concrete with a modification factor for LWC varying from 1.00 to 0.75. The full expression for bar stress predicted by ACI 408-03 is given by Eq. 33 and was simplified by taking ω, α, and β as 1.0 and $K_{tr,ACI408}$ as zero so that it could be shown in Figure 97. The simplified expression is given by Eq. 35. The modification factor for LWC in Eq. 33 is λ_{ACI408} and is located in the denominator. The modification factor for LWC in Eq. 35, λ, is in the numerator to make the form of the equation comparable to Eq. 34 for the ACI 318-11 expression. The value of λ in Eq. 35 is approximately equal to $1/\lambda_{ACI408}$.

$$f_s = \left\{\left[\left(\frac{\ell_s}{d_b}\right)\left(\frac{c_b}{d_b}\right)\right] \times (\lambda 70) + 2200\right\} f_c'^{0.25}$$ (Eq. 35)

in Eq. 35, the units of stress are in psi

Figure 97 shows that regression lines for LWC and NWC are relatively close to the prediction lines given for the ACI 408-03 expressions. The regression line for LWC is almost entirely inside the shaded region indicating the range of possible predicted bar stress for LWC concrete. A comparison of the bar stress predictions determined using ACI 318-11 in Figure 96 and the predictions determined using ACI 408-03 in Figure 97 for the same 257 data points indicates that the ACI 408-03 expression gave a better prediction of the bar stress for both the LWC and NWC specimens.

AASHTO LRFD Specifications

The bar stress predicted by the AASHTO LRFD expression is shown in Figure 98. This figure is shown after the figures for the ACI 318-11 expression and the ACI 408-03 expression because the full expression for bar stress determined from the AASHTO LRFD Specifications does not follow the same form as the expressions given by ACI 318-11 and ACI 408-03. The full expression for bar stress is given by Eq. 31 and does not include terms for surrounding concrete thickness (c_b) or amount of transverse reinforcement (K_{tr}). The AASHTO LRFD expression also includes an inequality, which makes representing the expression more difficult. For 5 ksi (34 MPa) concrete, the right-hand term of Eq. 31 controls for bars smaller than a #8 bar. For a #8 bar and 5 ksi concrete, the right-hand and left-hand terms are nearly equal. For 9 ksi (62 MPa) concrete, the right-hand term of Eq. 31 controls for bars smaller than a #10 bar.

An equation representing the AASHTO LRFD expression in the same form as Eq. 34 and Eq. 35 for the ACI 318-11 expression and the ACI 408-03 expression is given by Eq. 36. In Eq. 36, A_b was taken as approximately equal to $\pi/4 \times (d_b)^2$, and ψ_t and ψ_e are taken as 1.0.

$$f_s = \left[\left(\frac{\ell_s}{d_b}\right)\left(\frac{c_b}{d_b}\right)\right] \times \left(\frac{\lambda}{1.25(\pi/4)c_b}\sqrt{f_c'}\right) \leq \left[\left(\frac{\ell_s}{d_b}\right)\left(\frac{c_b}{d_b}\right)\right] \times \left(\frac{\lambda}{0.4(c_b/d_b)}\right) \qquad \text{(Eq. 36)}$$

Figure 98 shows the prediction for bar stress determined using the AASHTO LRFD Specifications assuming a concrete thickness of 2 inch (i.e., c_b taken as 2 inch) (51 mm). Separate predictions were made for #4 bars and #8 bars. For bars this size, the compressive strength does not control the prediction given by the AASHTO LRFD Specifications as described previously. Lines showing no modification for LWC and a modification factor of 0.75 are shown for both bar sizes. Shaded regions indicating the range of modification for LWC are shown for both bars.

123
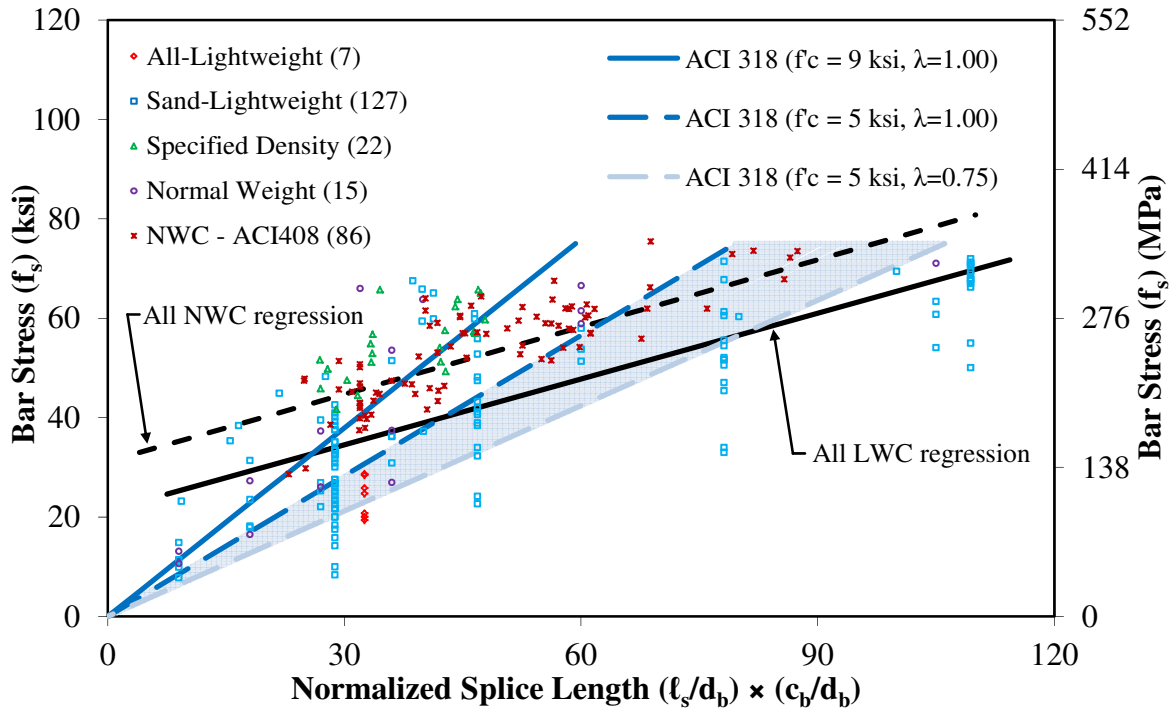
Figure 96. Graph. Bar Stress versus Normalized Splice Length (ℓ_s/d_b)×(c_b/d_b) for ACI 318-11 Expression (Eq. 34) for Specimens without Stirrups (N).
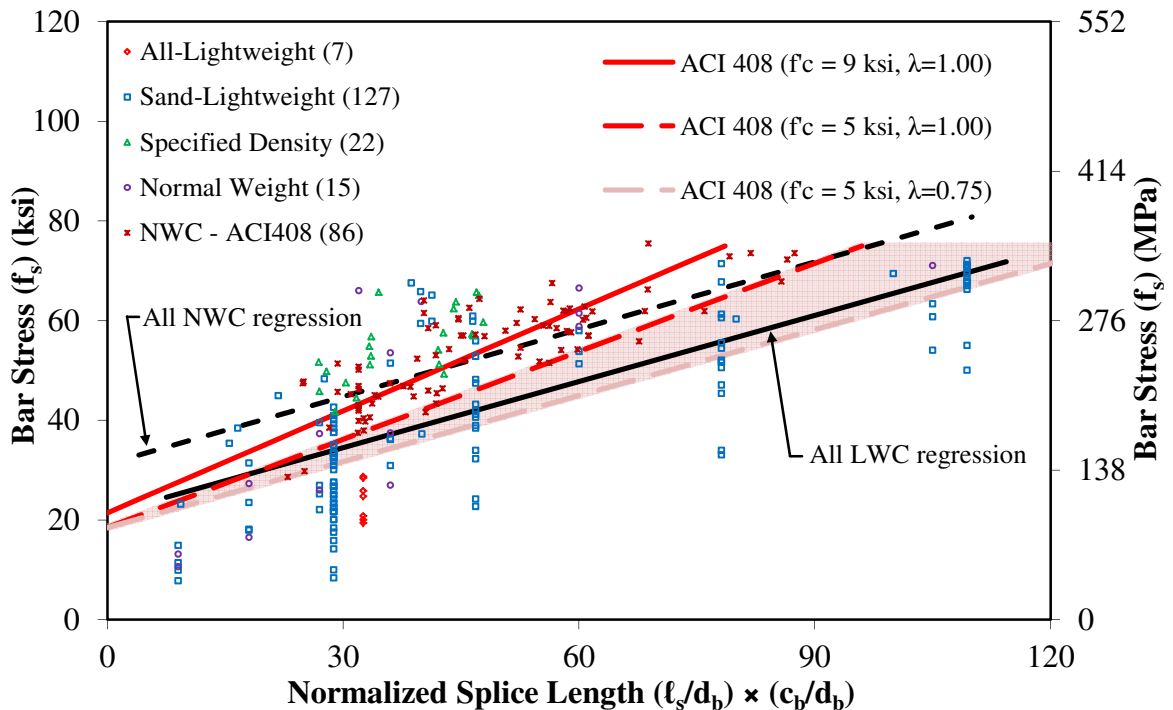
Figure 97. Graph. Bar Stress versus Normalized Splice Length (ℓ_s/d_b)×(c_b/d_b) for ACI 408-03 Expression (Eq. 35) for Specimens without Stirrups (N).
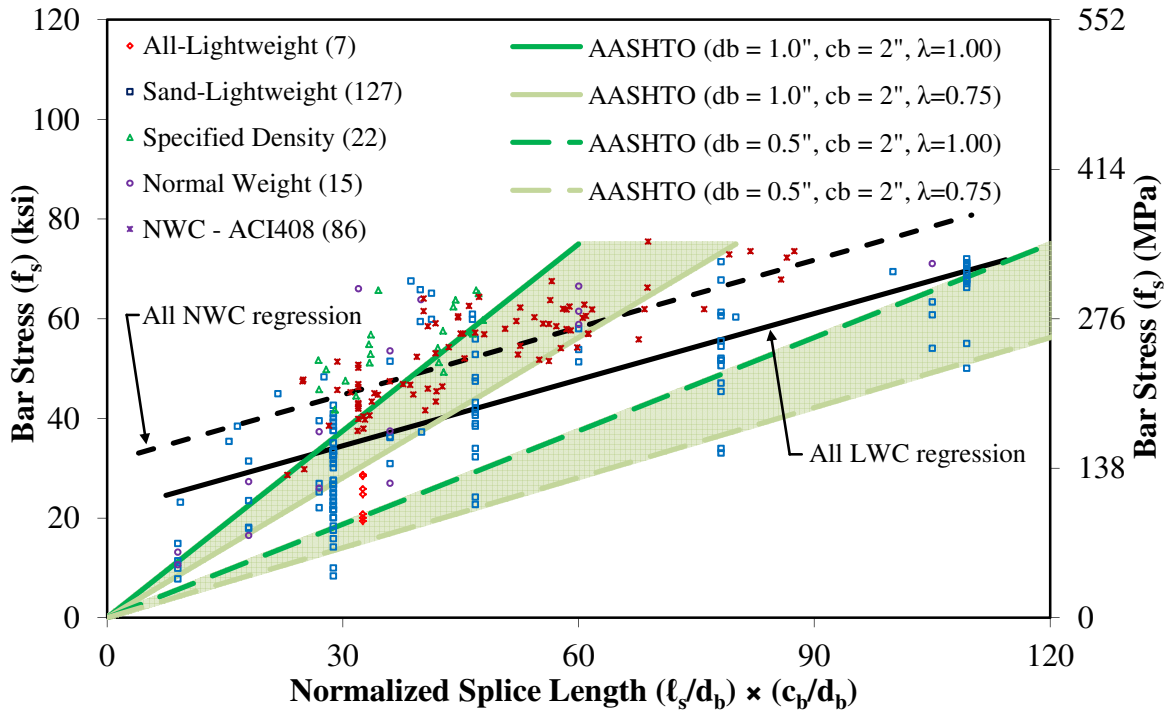
Figure 98. Graph. Bar Stress versus Normalized Splice Length (ℓ_s/d_b)×(c_b/d_b) for AASHTO LRFD Expression (Eq. 36) for Specimens without Stirrups (N).

Similar to the ACI 318-11 expression, the AASHTO LRFD expression is proportional to splice length. This results in predictions of bar stress that do not follow the regression lines for LWC or NWC shown in Figure 98. The mean bar size of the LWC beam-end specimens and tension prisms is approximately 0.5 inch (13 mm). The mean bar size of the splice beam specimens and development beam specimens is approximately 1.0 inch (25 mm). The LWC regression line passes through the shaded region for #8 bars over only a narrow region of splice lengths, and does not pass through the shaded region for #4 bars at all. Comparing the prediction of bar stress shown in Figure 98 indicates that the AASHTO LRFD expression does not predict the bar stress of the LWC specimens as well as the ACI 318-11 expression or the ACI 408-03 expression.

PROPOSED EXPRESSIONS FOR BAR STRESS BASED ON ACI 318-11 AND ACI 408-03

The proposed expressions for bar stress in this section include the modification factor for LWC previously developed for LWC.[7] The modification factor is based on the splitting tensile strength when available and the unit weight otherwise. An expression for the modification factor for LWC that is based on unit weight is convenient to designers because this is a quantity, like compressive strength, that is determined during the design phase. The expression for the modification factor for LWC (λ-factor) based on unit weight is given by Eq. 37. The expression for the λ-factor based on splitting tensile strength (f_{ct}) is given by Eq. 38.

$$\text{For } w_c \leq 0.100 \text{ kcf: } \lambda = 0.75 \tag{Eq. 37a}$$

$$\text{For } 0.100 < w_c < 0.135 \text{ kcf: } \lambda = 7.5w_c \leq 1.00 \tag{Eq. 37b}$$

$$\text{For } w_c \geq 0.135 \text{ kcf: } \lambda = 1.00 \tag{Eq. 37c}$$

$$\lambda = 4.7\frac{f_{ct}}{\sqrt{f_c'}} \leq 1.00 \tag{Eq. 38}$$

This section includes an analysis of the test-to-prediction ratios that include the λ-factor determined using Eq. 37. The test-to-prediction ratio is the ratio of the bar stress at failure (f_s) to the predicted bar stress determined using the ACI 318-11 expression given by Eq. 32 and using the ACI 408-03 expression given by Eq. 33. In Eq. 32, the λ-factor replaces the modification factor for LWC defined by ACI 318-11 (λ_{ACI}). Also, the bar size factor (ψ_s) was taken as 1.0 for all bar sizes. The modification factor for LWC in ACI 408-03 is in the denominator, so λ-factor replaces the reciprocal of λ_{ACI408} in Eq. 33 (i.e., $1/\lambda_{ACI408}$). A comparison of the test-to-prediction ratios determined using the λ-factor based on w_c from Eq. 37, the λ-factor based on f_{ct} from Eq. 38, and the λ-factor based on concrete mixture type (i.e., 0.75 for all-lightweight concrete and 0.85 for sand-lightweight concrete) is given in the subsequent section.

The test-to-prediction ratios for the ACI 318-11 and ACI 408-03 expressions with the λ-factor determined using Eq. 37 are given in Table 30 for the 211 LWC specimens. These specimens include 156 LWC specimens without stirrups, and the 55 LWC specimens with stirrups. The test-to-prediction ratios are given in Table 31 by concrete mixture type and in Table 32 by specimen type. The three tables include another equation labeled "ACI 408-rev" that is described in a later section titled "Revised Expression for Bar Stress Using ACI 408-03".

Table 30. Test-to-Prediction Ratio of Bar Stress for Design Expressions in ACI 318-11 (Eq. 32), ACI 408-03 (Eq. 33), and ACI 408-03-Revised (Eq. 39) for LWC Specimens with λ-Factor Determined Using Unit Weight (Eq. 37).

Concrete Mixture Type[†]	Design Expression	Mean	COV	Max.	Min.	Percent < 1.0	Percent < 0.8
LWC Specimens (211 total)	ACI 318	1.59	47.7%	4.10	0.38	17.5%	2.8%
	ACI 408	1.04	28.7%	1.75	0.29	40.8%	23.2%
	ACI 408-rev	1.11	28.1%	1.92	0.31	33.6%	17.1%
LWC Specimens (156 without A_{tr})	ACI 318	1.70	49.5%	4.10	0.38	18.6%	3.8%
	ACI 408	1.04	30.6%	1.75	0.29	44.2%	25.0%
	ACI 408-rev	1.11	30.3%	1.92	0.31	36.5%	18.6%
LWC Specimens (55 with A_{tr})	ACI 318	1.27	18.8%	1.76	0.85	14.5%	0.0%
	ACI 408	1.04	22.5%	1.49	0.44	30.9%	18.2%
	ACI 408-rev	1.11	21.0%	1.53	0.52	25.5%	12.7%

Notes:

[†] No. of specimens without stirrups ("without A_{tr}") and with stirrups ("with A_{tr}") given in parentheses

Table 31. Test-to-Prediction Ratio of Bar Stress for Design Expressions in ACI 318-11 (Eq. 32), ACI 408-03 (Eq. 33), and ACI 408-03-Revised (Eq. 39) by Concrete Mixture Type for LWC Specimens with λ-Factor Determined Using Unit Weight (Eq. 37).

Concrete Mixture Type[†]	Design Expression	Mean	COV	Max.	Min.	Percent < 1.0	Percent < 0.8
All-Lightweight (36 total)	ACI 318	1.28	20.1%	1.76	0.90	19.4%	0.0%
	ACI 408	0.90	30.5%	1.40	0.44	61.1%	41.7%
	ACI 408-rev	1.00	29.1%	1.53	0.52	52.8%	36.1%
All-Lightweight (7 without A_{tr})	ACI 318	1.00	12.2%	1.21	0.91	71.4%	0.0%
	ACI 408	0.64	11.2%	0.73	0.55	100.0%	100.0%
	ACI 408-rev	0.73	11.2%	0.83	0.63	100.0%	85.7%
All-Lightweight (29 with A_{tr})	ACI 318	1.35	17.5%	1.76	0.90	6.9%	0.0%
	ACI 408	0.96	27.9%	1.40	0.44	51.7%	27.6%
	ACI 408-rev	1.07	26.8%	1.53	0.52	41.4%	24.1%
Sand-Lightweight (135 total)	ACI 318	1.79	48.8%	4.10	0.38	17.0%	4.4%
	ACI 408	1.05	31.0%	1.75	0.29	45.9%	25.2%
	ACI 408-rev	1.12	31.0%	1.92	0.31	37.8%	17.0%
Sand-Lightweight (127 without A_{tr})	ACI 318	1.82	48.5%	4.10	0.38	16.5%	4.7%
	ACI 408	1.05	31.7%	1.75	0.29	47.2%	25.2%
	ACI 408-rev	1.12	31.7%	1.92	0.31	38.6%	18.1%
Sand-Lightweight (8 with A_{tr})	ACI 318	1.21	21.1%	1.54	0.85	25.0%	0.0%
	ACI 408	1.05	15.6%	1.19	0.78	25.0%	25.0%
	ACI 408-rev	1.10	15.8%	1.25	0.82	25.0%	0.0%
Specified Density (40 total)	ACI 318	1.20	18.3%	1.89	0.88	17.5%	0.0%
	ACI 408	1.17	11.7%	1.62	0.92	5.0%	0.0%
	ACI 408-rev	1.18	11.3%	1.62	0.94	2.5%	0.0%
Specified Density (22 without A_{tr})	ACI 318	1.23	19.2%	1.89	0.88	13.6%	0.0%
	ACI 408	1.16	12.6%	1.62	0.92	9.1%	0.0%
	ACI 408-rev	1.17	12.1%	1.62	0.94	4.5%	0.0%
Specified Density (18 with A_{tr})	ACI 318	1.17	17.2%	1.55	0.89	22.2%	0.0%
	ACI 408	1.18	10.8%	1.49	1.01	0.0%	0.0%
	ACI 408-rev	1.19	10.6%	1.49	1.02	0.0%	0.0%

Notes:

[†] No. of specimens without stirrups ("without A_{tr}") and with stirrups ("with A_{tr}") given in parentheses

Table 32. Test-to-Prediction Ratio of Bar Stress for Design Expressions in ACI 318-11 (Eq. 32), ACI 408-03 (Eq. 33), and ACI 408-03-Revised (Eq. 39) by Specimen Type for LWC Specimens with λ-Factor Determined Using Unit Weight (Eq. 37).

Specimen Type[†]	Design Expression	Mean	COV	Max.	Min.	Percent < 1.0	Percent < 0.8
Beam-end	ACI 318	1.19	27.2%	1.93	0.38	29.7%	9.4%
(64, all without A_{tr})	ACI 408	0.79	27.7%	1.25	0.29	84.4%	48.4%
	ACI 408-rev	0.86	28.5%	1.37	0.31	71.9%	35.9%
Splice Beam	ACI 318	1.21	17.3%	1.89	0.85	17.5%	0.0%
(63 total)	ACI 408	1.14	13.2%	1.62	0.78	11.1%	4.8%
	ACI 408-rev	1.17	13.0%	1.62	0.81	7.9%	0.0%
Splice Beam	ACI 318	1.23	16.7%	1.89	0.88	13.5%	0.0%
(37 without A_{tr})	ACI 408	1.15	13.4%	1.62	0.80	13.5%	2.7%
	ACI 408-rev	1.18	13.5%	1.62	0.81	8.1%	0.0%
Splice Beam	ACI 318	1.18	18.2%	1.55	0.85	23.1%	0.0%
(26 with A_{tr})	ACI 408	1.14	13.1%	1.49	0.78	7.7%	7.7%
	ACI 408-rev	1.16	12.5%	1.49	0.82	7.7%	0.0%
Tension Prism	ACI 318	2.85	16.4%	4.10	2.13	0.0%	0.0%
(48, all without A_{tr})	ACI 408	1.36	13.7%	1.75	0.84	6.3%	0.0%
	ACI 408-rev	1.46	13.6%	1.92	0.92	2.1%	0.0%
Development Beam	ACI 318	1.28	20.1%	1.76	0.90	19.4%	0.0%
(36 total)	ACI 408	0.90	30.5%	1.40	0.44	61.1%	41.7%
	ACI 408-rev	1.00	29.1%	1.53	0.52	52.8%	36.1%
Development Beam	ACI 318	1.00	12.2%	1.21	0.91	71.4%	0.0%
(7 without A_{tr})	ACI 408	0.64	11.2%	0.73	0.55	100.0%	100.0%
	ACI 408-rev	0.73	11.2%	0.83	0.63	100.0%	85.7%
Development Beam	ACI 318	1.35	17.5%	1.76	0.90	6.9%	0.0%
(29 with A_{tr})	ACI 408	0.96	27.9%	1.40	0.44	51.7%	27.6%
	ACI 408-rev	1.07	26.8%	1.53	0.52	41.4%	24.1%

Notes:

[†] No. of specimens without stirrups ("without A_{tr}") and with stirrups ("with A_{tr}") given in parentheses

The test-to-prediction ratios are shown graphically in Figure 99 through Figure 106. Test-to-prediction ratios for the ACI 318-11 expression are shown compared to an ℓ_s/d_b ratio in Figure 99 and Figure 100 and compared to concrete compressive strength in Figure 101 and Figure 102. Each pair of figures separates specimens without stirrups and specimens with stirrups. Figure 103 and Figure 104 show the test-to-prediction ratios for the ACI 408-03 expression compared to an ℓ_s/d_b ratio and Figure 105 and Figure 106 show the ratios compared to concrete compressive strength.

Table 30, Table 31, and Table 32 indicate that the ACI 318-11 expression gave larger test-to-prediction ratios than the ACI 408-03 expression regardless of the presence of stirrups, the concrete mixture type, or specimen type. The scatter in the test-to-prediction ratios for the ACI 318-11 expression, as indicated by the COV, is very high (50%) for all of the specimens without stirrups taken together. For the same specimens, the ACI 408-03 was still high (31%), but the scatter was still less than the ACI 318-11 expression. The COV tended to be large and varied considerably (49% and 31% for sand-lightweight specimens predicted by ACI 318-11 and ACI 408-03, respectively) when the specimens were grouped by concrete mixture type. When the specimens were grouped by specimen type, the COV were much smaller (17% and 13% for splice beam specimens predicted by ACI 318-11 and ACI 408-03, respectively).

The regression lines in Figure 99 and Figure 100 show that the test-to-prediction ratios determined using the ACI 318-11 expression are much larger than 1.0 (i.e., under-estimate bar stress) for short splice lengths and the ratios become smaller as splice length increases. Similarly, the regression lines in Figure 101 and Figure 102 show that the ratios for the ACI 318-11 expression are much larger than 1.0 for small compressive strengths and the ratios become smaller as compressive strength increases. These trends were observed for specimens without stirrups and specimens with stirrups. Very few test-to-prediction ratios were less than 1.0.

Figure 103 and Figure 104 show the regression lines for the test-to-prediction ratios determined using the ACI 408-03 expression. The regression line for the specimens without stirrups is slightly greater than 1.0 and has almost no slope. This indicates that the prediction given by ACI 408-03 slightly underestimates the bar stress over the range of splice lengths tested. The regression line for the splice beam specimens with stirrups is also slightly greater than 1.0 and has no noticeable slope. The bar stress of the all-lightweight concrete development beams with stirrups was over-estimated.
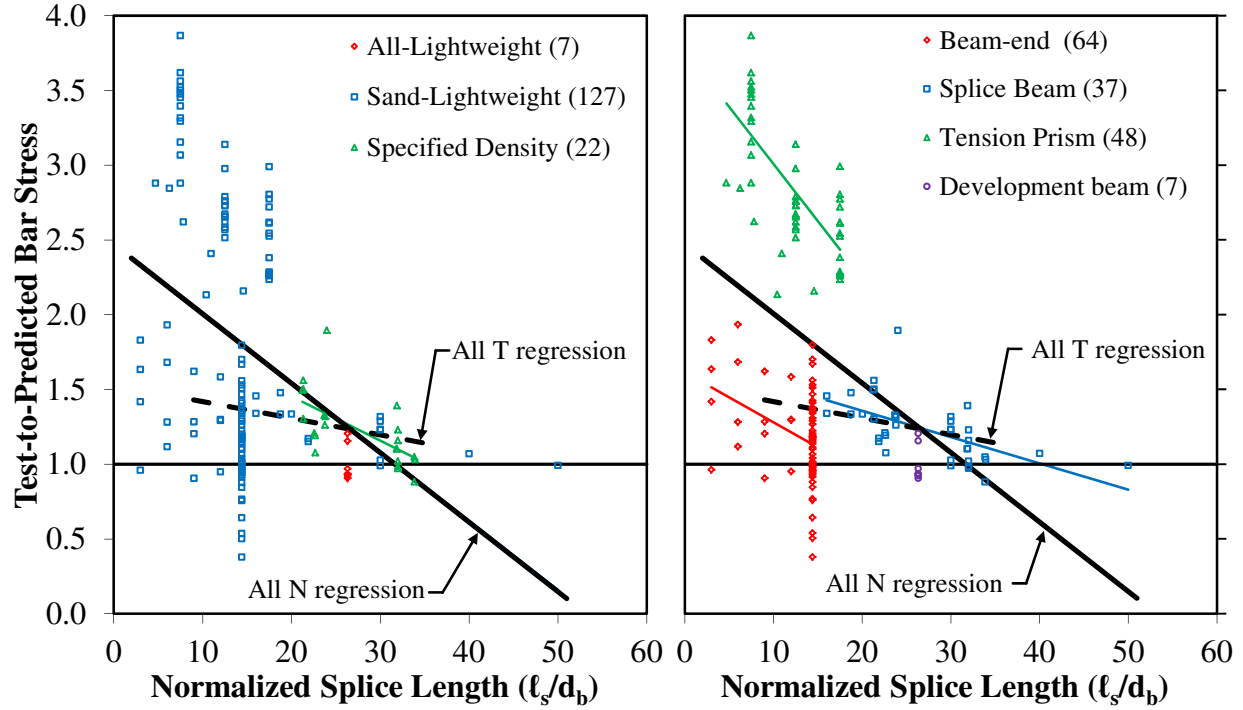
Figure 99. Graph. Bar Stress Test-to-Prediction Ratio Compared to Normalized Splice Length (ℓ_s/d_b) for ACI 318-11 Expression (Eq. 32) with Proposed Expression for λ-Factor (Eq. 37) for LWC Specimens without Stirrups (N).
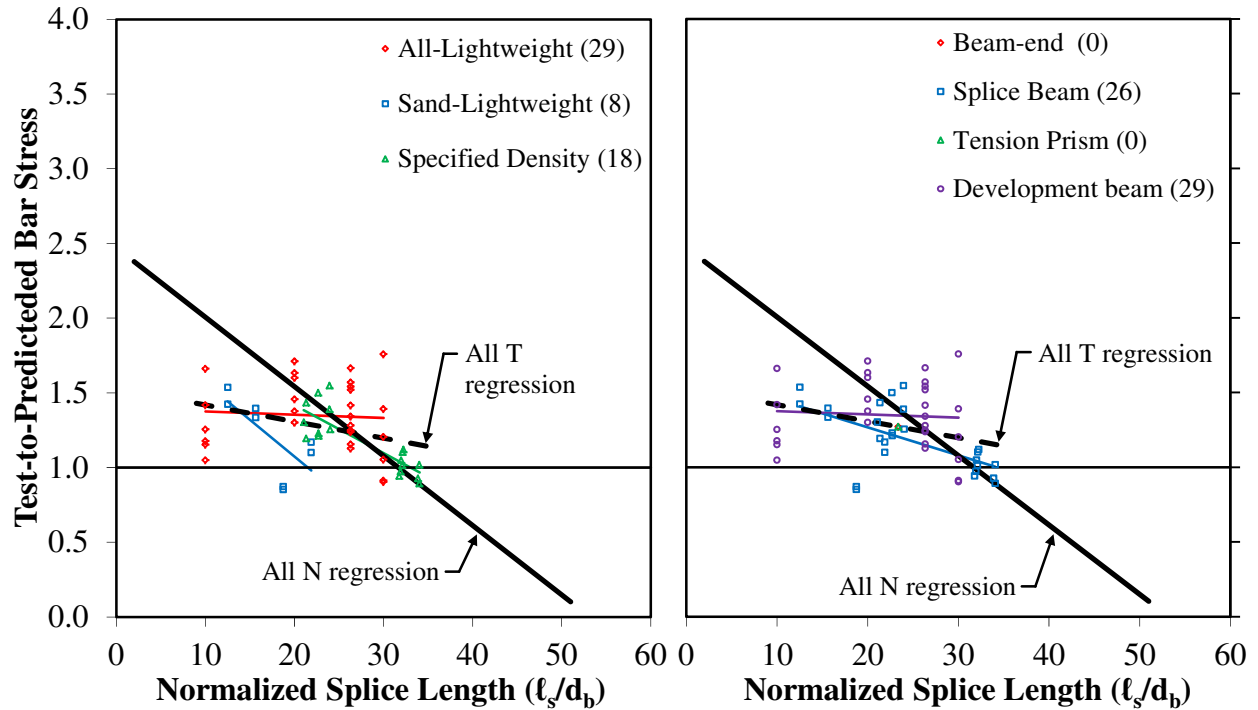
Figure 100. Graph. Bar Stress Test-to-Prediction Ratio Compared to Normalized Splice Length (ℓ_s/d_b) for ACI 318-11 Expression (Eq. 32) with Proposed Expression for λ-Factor (Eq. 37) for LWC Specimens with Stirrups (T).
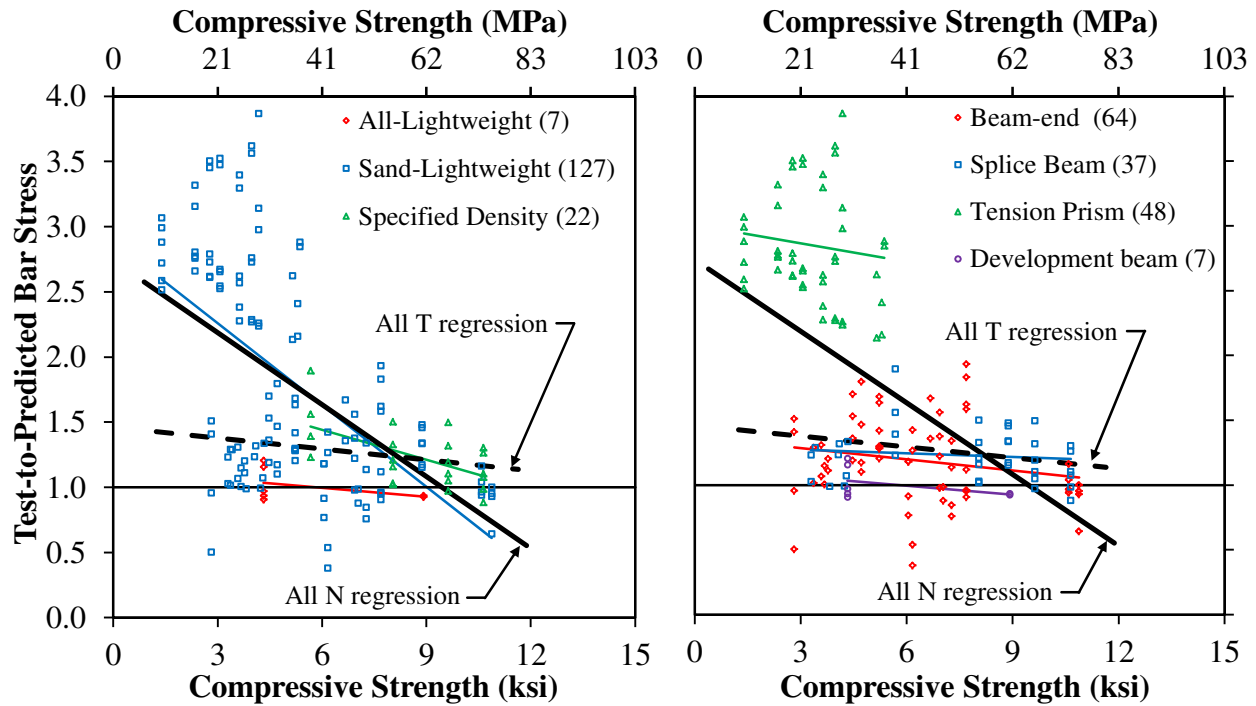
Figure 101. Graph. Bar Stress Test-to-Prediction Ratio Compared to Compressive Strength for ACI 318-11 Expression (Eq. 32) with Proposed Expression for λ-Factor (Eq. 37) for LWC Specimens with Stirrups (N).
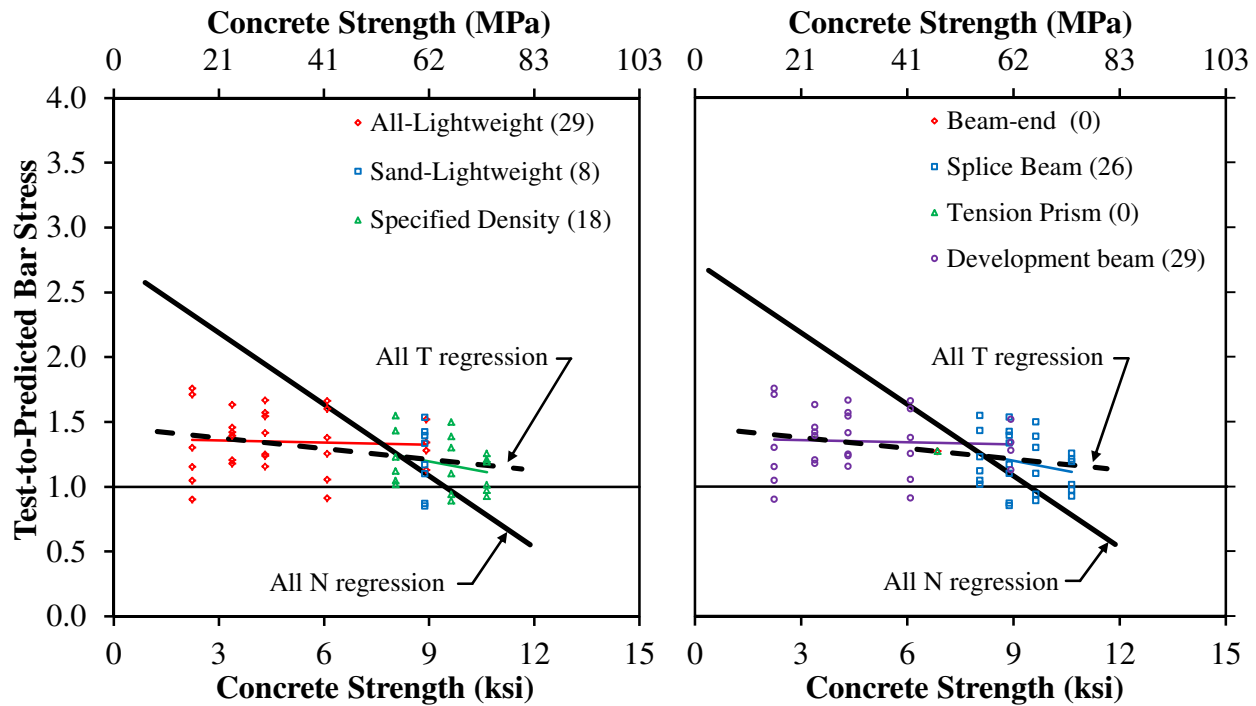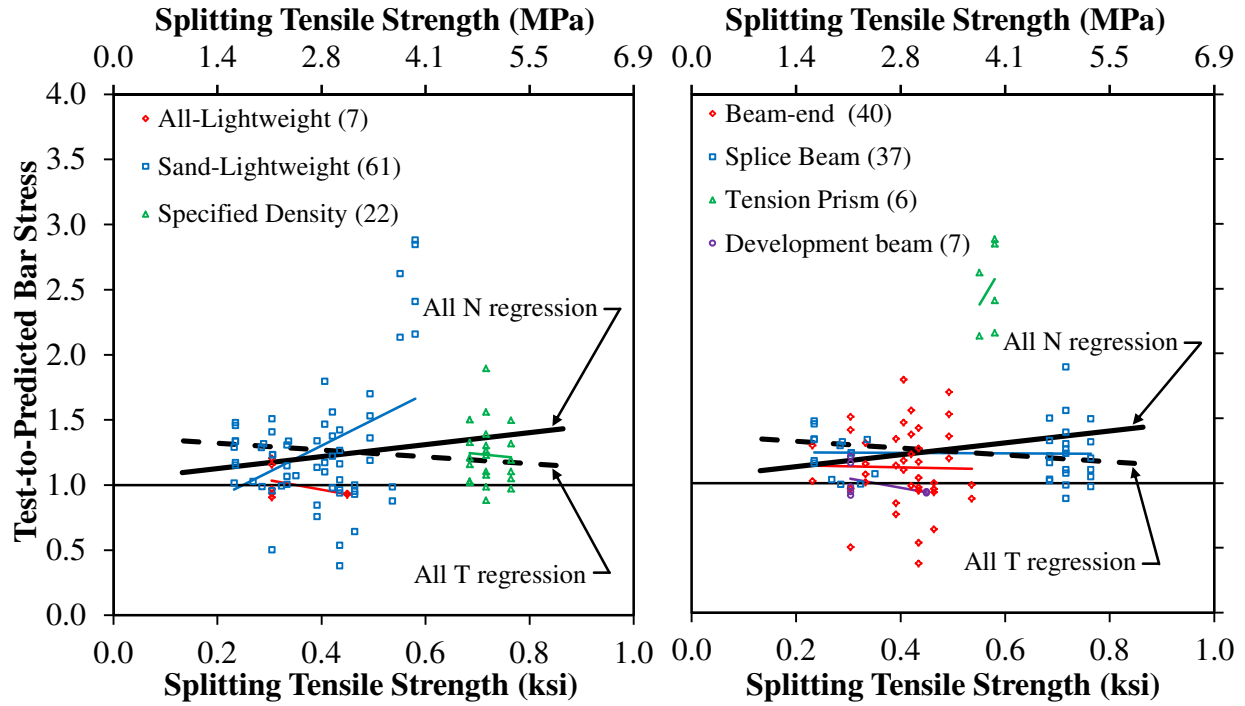

Figure 102. Graph. Bar Stress Test-to-Prediction Ratio Compared to Compressive Strength for ACI 318-11 Expression (Eq. 32) with Proposed Expression for λ-Factor (Eq. 37) for LWC Specimens with Stirrups (T).
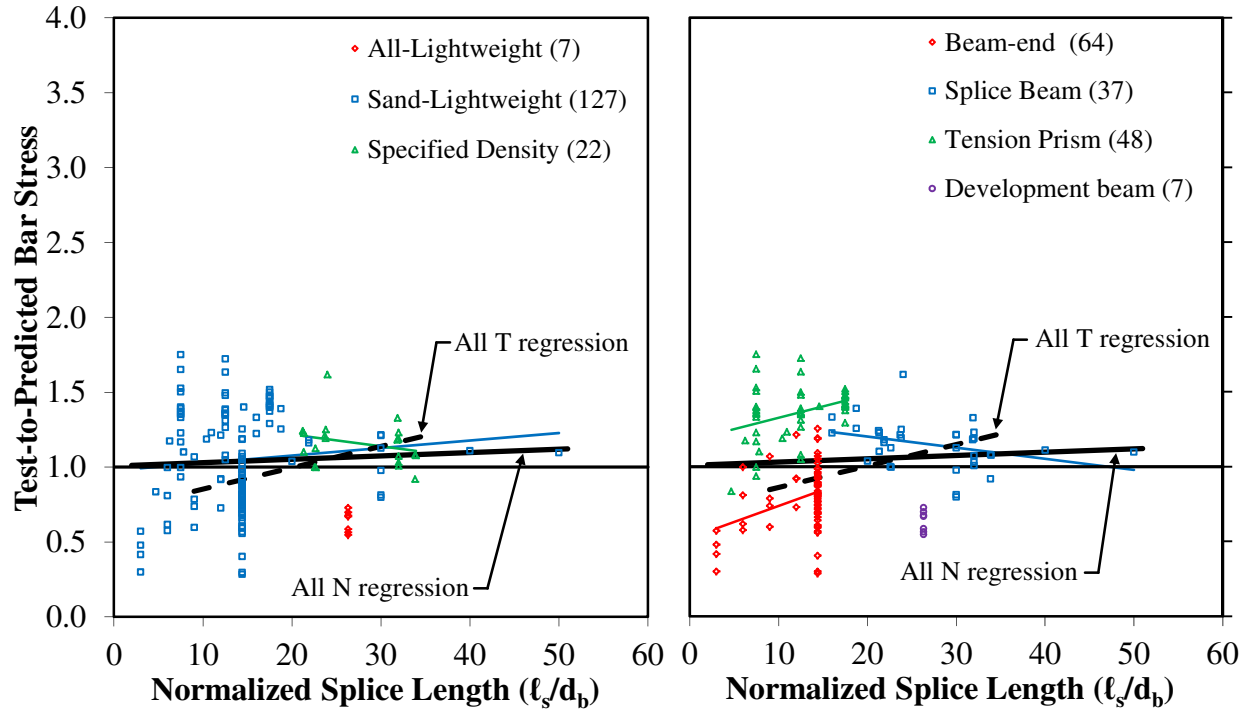
Figure 103. Graph. Bar Stress Test-to-Prediction Ratio Compared to Normalized Splice Length (ℓ_s/d_b) for ACI 408-03 Expression (Eq. 33) with Proposed Expression for λ-Factor (Eq. 37) for LWC Specimens without Stirrups (N).
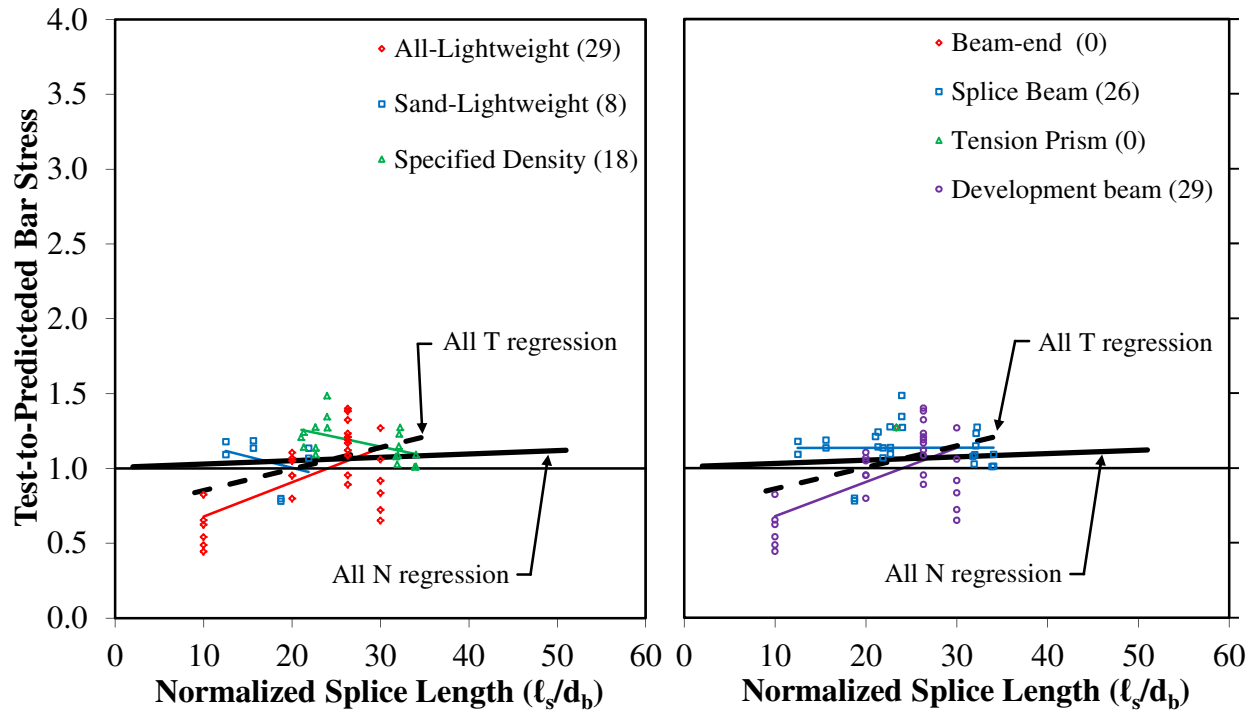
Figure 104. Graph. Bar Stress Test-to-Prediction Ratio Compared to Normalized Splice Length (ℓ_s/d_b) for ACI 408-03 Expression (Eq. 33) with Proposed Expression for λ-Factor (Eq. 37) for LWC Specimens with Stirrups (T).
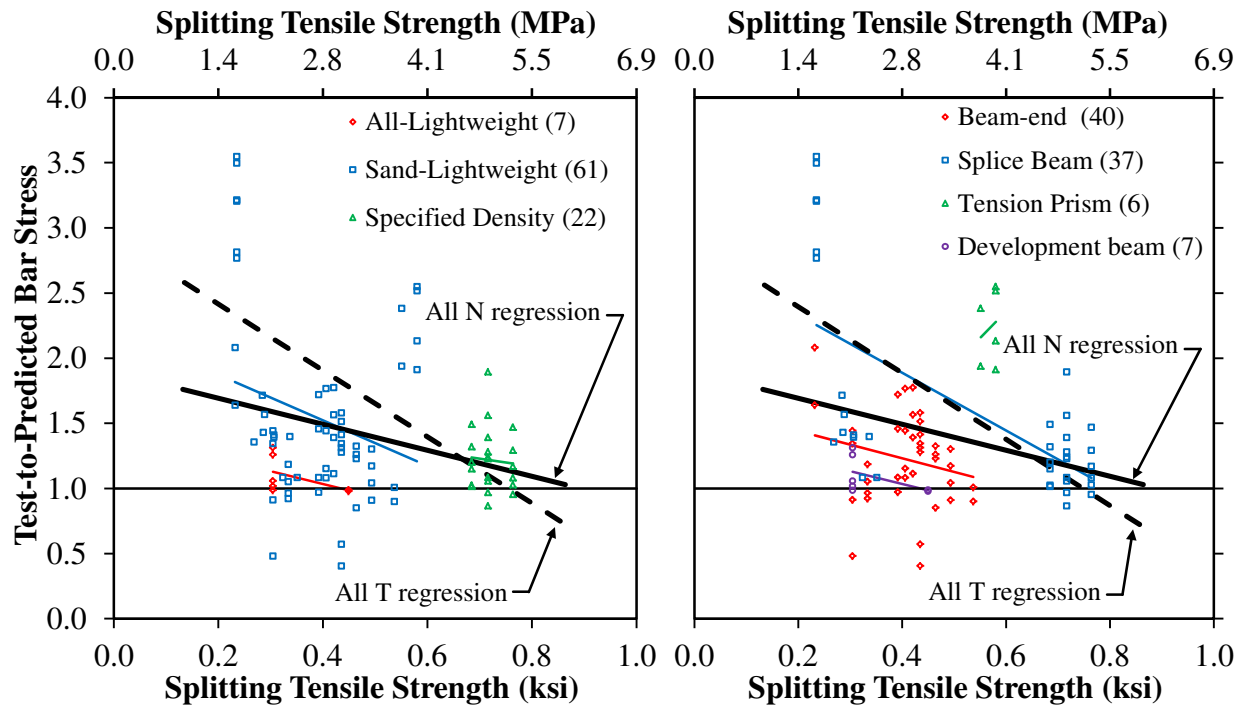
133
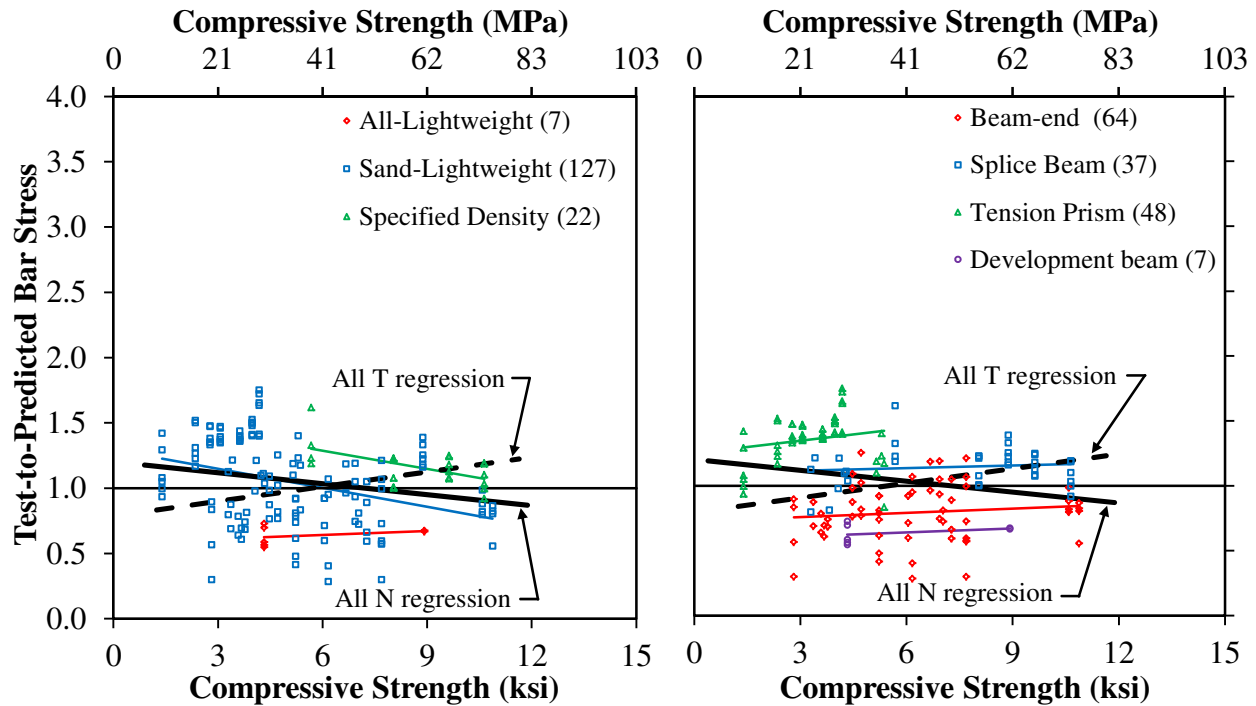
Figure 105. Graph. Bar Stress Test-to-Prediction Ratio Compared to Compressive Strength for ACI 408-03 Expression (Eq. 33) with Proposed Expression for λ-Factor (Eq. 37) for LWC Specimens with Stirrups (N).
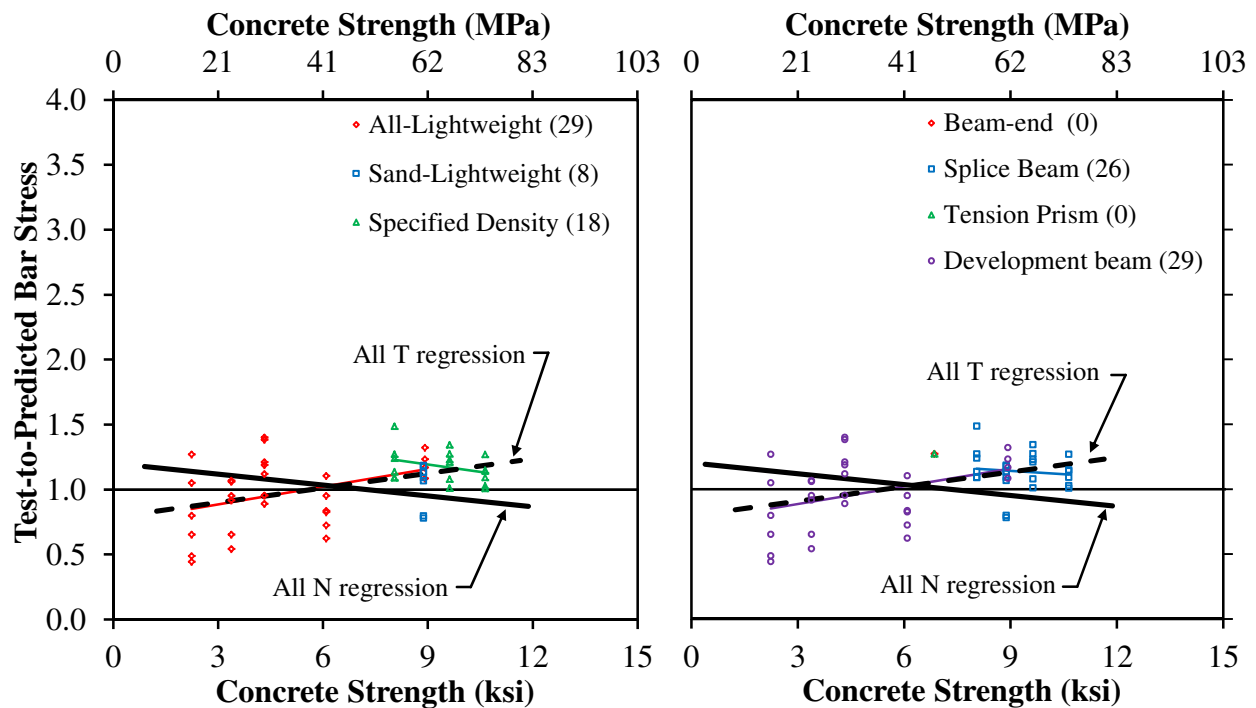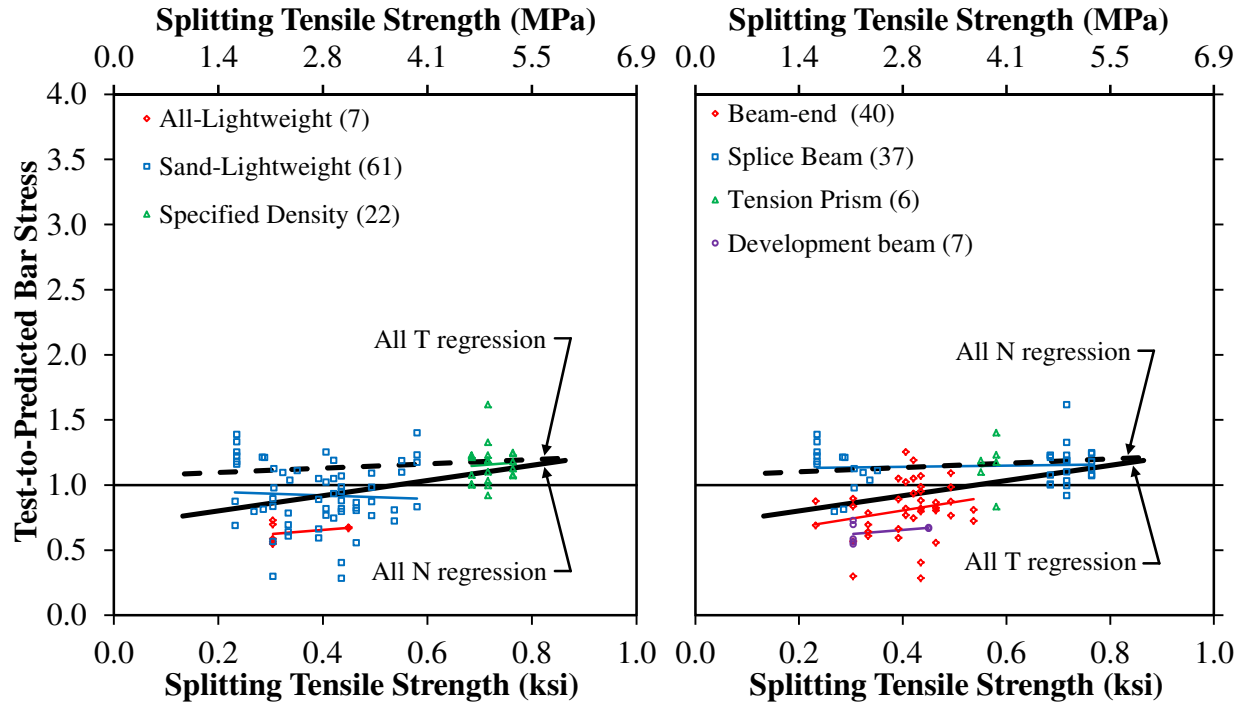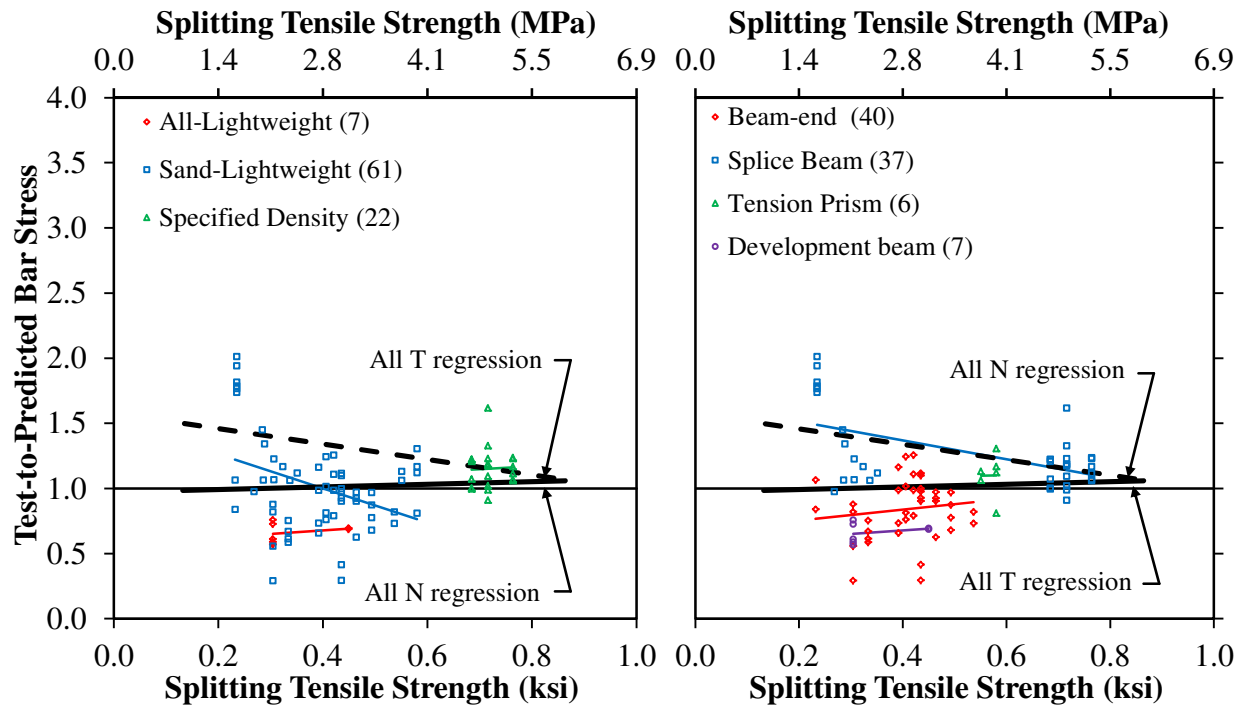

Figure 106. Graph. Bar Stress Test-to-Prediction Ratio Compared to Compressive Strength for ACI 408-03 Expression (Eq. 33) with Proposed Expression for λ-Factor (Eq. 37) for LWC Specimens with Stirrups (T).

COMPARISON OF MODIFICATION FACTOR FOR LWC DETERMINED USING UNIT WEIGHT AND SPLITTING TENSILE STRENGTH

The analysis of the proposed λ-factor in the expressions for bar stress determined from ACI 318-11 and ACI 408-03 used a λ-factor based on unit weight. A λ-factor based on unit weight was used in the preceding analysis for two reasons. The unit weight is determined during the design phase, unlike the splitting tensile strength, so a λ-factor based on unit weight is expected to be easier for a designer to use. Also, all 211 test specimens with LWC in the TFHRC Mild Steel Development Length Database included the unit weight, while the splitting tensile strength was only given for 127 test specimens.

Many of the test specimens from a few individual references recorded one set of concrete mechanical test data and applied it to multiple specimens that were tested to determine f_s. The 127 test specimens that included a value for splitting tensile strength were based on 30 actual splitting tensile strength values. Each splitting tensile strength value had a corresponding unit weight value.

The λ-factor based on f_{ct} was determined for each test using Eq. 38, and another λ-factor was determined from the corresponding w_c using Eq. 37. The λ-factor determined using f_{ct} is shown in Figure 107 compared to the λ-factor determined using w_c. Horizontal and vertical lines indicating values of the λ-factor equal to 0.75 for all-lightweight concrete, 0.85 for sand-lightweight concrete, and 1.00 for NWC are shown in the figure. The λ-factor determined using w_c has an upper limit of 1.0 and a lower limit of 0.75. The λ-factor determined using f_{ct} does not have the lower limit, which allows the λ-factor to take on much lower values. Points below the diagonal line in Figure 107 had a lower λ-factor when determined using f_{ct} (i.e., the predicted f_s would be lower than if w_c had been used to determine the λ-factor). Points above the diagonal line had a lower λ-factor when determined using w_c.

The test-to-prediction ratios determined using the ACI 318-11 expression are shown in Figure 108 and Figure 109 and are compared to the splitting tensile strength. In Figure 108, the λ-factor was determined using w_c and in Figure 109 the λ-factor was determined using f_{ct}. The effect of the two different methods to determine the λ-factor can be observed by comparing the test-to-prediction ratios of data points in Figure 109 to the ratios of the same points in Figure 108. A test where a low f_{ct} value caused an f_s value that was under-estimated by the λ-factor (determined using f_{ct}) would be indicated by an increase in test-to-prediction ratio (i.e., the data point would be higher in Figure 109 than in Figure 108). Similarly, a test where the λ-factor (determined using f_{ct}) was over-estimated by a high f_{ct} value, would be indicated by a decrease in the ratio (i.e., the data point would be lower in Figure 109).

A comparison of Figure 108 and Figure 109 indicates that the most noticeable shift was for a small number of tests with a splitting tensile strength less than 0.400 ksi (0.028 MPa). These data points had a higher test-to-prediction ratio in Figure 109 indicating that their bar stress was highly under-estimated by using the λ-factor based on f_{ct}.

135
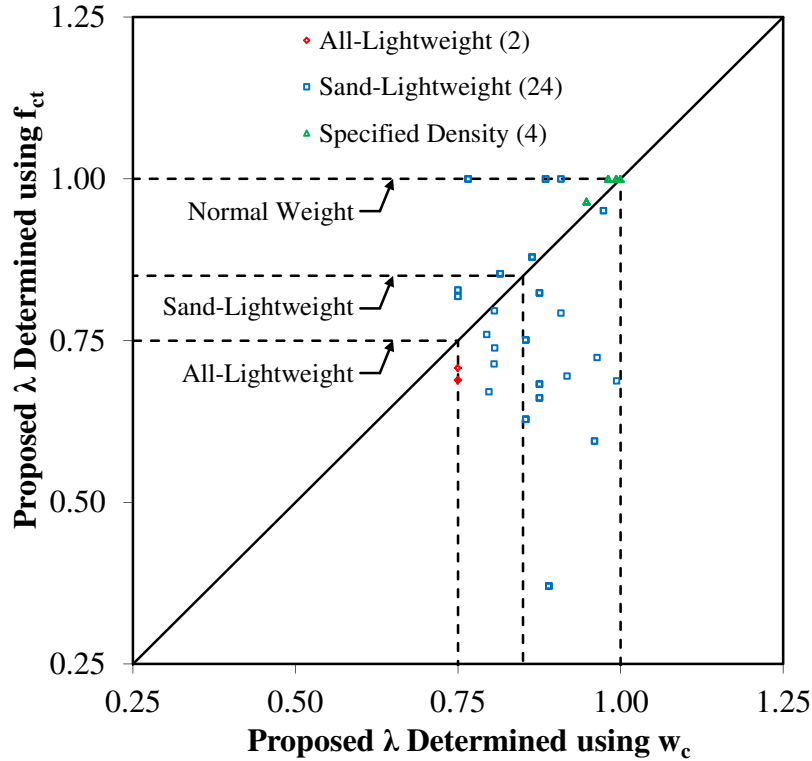
Figure 107. Graph. Proposed Expression for λ-Factor based on Unit Weight (Eq. 37) Compared to the Proposed Expression for λ-Factor based on Splitting Tensile Strength (Eq. 38).

Figure 110 and Figure 111 show the test-to-prediction ratios given by the ACI 408-03 expression versus splitting tensile strength. A comparison of these figures shows that the increase in test-to-prediction ratio for tests with a splitting tensile strength less than 0.400 ksi (0.028 MPa) was much less pronounced than for the same data points in Figure 108 and Figure 109 for the ACI 318-11 expression.

The test-to-prediction ratios determined using the λ-factor based on w_c and λ-factor based on f_{ct} is compared in Table 33, Table 34, and Table 35. Each table has ratios determined using the ACI 318-11 expression and the ACI 408-03 expression. Table 33 gives the ratios for all 127 specimens with both w_c and f_{ct} values. Table 34 and Table 35 give the ratios for these same tests by concrete mixture type and specimen type, respectively.

The test-to-prediction ratios given in Table 33 that were determined using the λ-factor based on f_{ct} were slightly larger for the ACI 408-03 expressions and much larger for the ACI 318-11 expression. The same trend was observed for the mean ratios for all-lightweight concrete and sand-lightweight concrete given in Table 34. For the specified density specimens, the ratios determined using the λ-factor based on w_c and λ-factor based on f_{ct} were similar due to the high f_{ct} values (i.e., the λ-factors were near 1.0). In Table 35 the ratios determined using the λ-factor based on f_{ct} were larger for all specimen types except for tension prisms.

136

Figure 108. Graph. Bar Stress Test-to-Prediction Ratio Compared to Splitting Tensile Strength for ACI 318-11 Expression (Eq. 32) with Proposed Expression for λ-Factor based on w_c (Eq. 37) for LWC Specimens without Stirrups (N).

Figure 109. Graph. Bar Stress Test-to-Prediction Ratio Compared to Splitting Tensile Strength for ACI 318-11 Expression (Eq. 32) with Proposed Expression for λ-Factor based on f_{ct} (Eq. 38) for LWC Specimens without Stirrups (N).

Figure 110. Graph. Bar Stress Test-to-Prediction Ratio Compared to Splitting Tensile Strength for ACI 408-03 Expression (Eq. 33) with Proposed Expression for λ-Factor based on w_c (Eq. 37) for LWC Specimens without Stirrups (N).

Figure 111. Graph. Bar Stress Test-to-Prediction Ratio Compared to Splitting Tensile Strength for ACI 408-03 Expression (Eq. 33) with Proposed Expression for λ-Factor based on f_{ct} (Eq. 38) for LWC Specimens without Stirrups (N).

Table 33. Test-to-Prediction Ratio of Bar Stress for Design Expressions in ACI 318-11 (Eq. 32), ACI 408-03 (Eq. 33), and ACI 408-03-Revised (Eq. 39) for LWC Specimens with λ-Factor Determined Using Unit Weight (Eq. 37) or Splitting Tensile Strength (Eq. 38).

LWC Specimen and λ-Factor[†]	Design Expression	Mean	COV	Max.	Min.	Percent < 1.0	Percent < 0.8
Proposed λ with w_c (127 total)	ACI 318	1.25	30.7%	2.88	0.38	23.6%	3.9%
	ACI 408	1.01	24.5%	1.62	0.29	39.4%	21.3%
	ACI 408-rev	1.07	23.0%	1.62	0.31	32.3%	13.4%
Proposed λ with w_c (90 without A_{tr})	ACI 318	1.25	34.6%	2.88	0.38	26.7%	5.6%
	ACI 408	0.96	27.1%	1.62	0.29	51.1%	27.8%
	ACI 408-rev	1.02	25.1%	1.62	0.31	42.2%	18.9%
Proposed λ with w_c (37 with A_{tr})	ACI 318	1.24	17.8%	1.67	0.85	16.2%	0.0%
	ACI 408	1.15	13.2%	1.49	0.78	10.8%	5.4%
	ACI 408-rev	1.20	13.7%	1.53	0.82	8.1%	0.0%
Proposed λ with f_{ct} (127 total)	ACI 318	1.49	44.6%	3.69	0.40	16.5%	2.4%
	ACI 408	1.09	29.9%	2.01	0.29	37.8%	18.1%
	ACI 408-rev	1.30	48.0%	3.52	0.32	26.0%	11.0%
Proposed λ with f_{ct} (90 without A_{tr})	ACI 318	1.43	42.8%	3.55	0.40	17.8%	3.3%
	ACI 408	1.02	32.5%	2.01	0.29	48.9%	25.6%
	ACI 408-rev	1.19	49.8%	3.52	0.32	35.6%	15.6%
Proposed λ with f_{ct} (37 with A_{tr})	ACI 318	1.63	46.9%	3.69	0.88	13.5%	0.0%
	ACI 408	1.28	18.3%	1.82	0.93	10.8%	0.0%
	ACI 408-rev	1.56	40.2%	2.99	1.00	2.7%	0.0%

Notes:
[†] No. of specimens without stirrups ("without A_{tr}") and with stirrups ("with A_{tr}") given in parentheses

Table 34. Test-to-Prediction Ratio of Bar Stress for Design Expressions in ACI 318-11 (Eq. 32), ACI 408-03 (Eq. 33), and ACI 408-03-Revised (Eq. 39) by Concrete Mixture Type for LWC Specimens with λ-Factor Determined Using Unit Weight (Eq. 37) or Splitting Tensile Strength (Eq. 38).

Concrete Mixture Type and λ-Factor[†]	Design Expression	Mean	COV	Max.	Min.	Percent < 1.0	Percent < 0.8
All-lightweight, Proposed λ with w_c (18 total)	ACI 318	1.23	19.7%	1.67	0.91	27.8%	0.0%
	ACI 408	0.97	31.1%	1.40	0.55	50.0%	38.9%
	ACI 408-rev	1.08	29.6%	1.53	0.63	44.4%	33.3%
All-lightweight, Proposed λ with f_{ct} (18 total)	ACI 318	1.33	19.9%	1.81	0.98	16.7%	0.0%
	ACI 408	1.01	31.4%	1.48	0.57	50.0%	38.9%
	ACI 408-rev	1.16	29.5%	1.67	0.68	38.9%	16.7%
Sand-lightweight, Proposed λ with w_c (69 total)	ACI 318	1.28	37.3%	2.88	0.38	26.1%	7.2%
	ACI 408	0.94	26.3%	1.40	0.29	56.5%	29.0%
	ACI 408-rev	1.01	25.5%	1.48	0.31	46.4%	15.9%
Sand-lightweight, Proposed λ with f_{ct} (69 total)	ACI 318	1.70	48.0%	3.69	0.40	14.5%	4.3%
	ACI 408	1.08	36.8%	2.01	0.29	49.3%	23.2%
	ACI 408-rev	1.41	57.1%	3.52	0.32	33.3%	15.9%
Specified Density, Proposed λ with w_c (40 total)	ACI 318	1.20	18.3%	1.89	0.88	17.5%	0.0%
	ACI 408	1.17	11.7%	1.62	0.92	5.0%	0.0%
	ACI 408-rev	1.18	11.3%	1.62	0.94	2.5%	0.0%
Specified Density, Proposed λ with f_{ct} (40 total)	ACI 318	1.19	18.7%	1.89	0.87	20.0%	0.0%
	ACI 408	1.16	11.8%	1.62	0.91	12.5%	0.0%
	ACI 408-rev	1.16	11.6%	1.62	0.92	7.5%	0.0%

Notes:
[†] No. of specimens given in parentheses

Table 35. Test-to-Prediction Ratio of Bar Stress for Design Expressions in ACI 318-11 (Eq. 32), ACI 408-03 (Eq. 33), and ACI 408-03-Revised (Eq. 39) by Specimen Type for LWC Specimens with λ-Factor Determined Using Unit Weight (Eq. 37) or Splitting Tensile Strength (Eq. 38).

Specimen Type and λ-Factor[†]	Design Expression	Mean	COV	Max.	Min.	Percent < 1.0	Percent < 0.8
Beam-end, Proposed λ with w_c (40 total)	ACI 318	1.12	28.1%	1.80	0.38	35.0%	12.5%
	ACI 408	0.81	26.4%	1.25	0.29	82.5%	42.5%
	ACI 408-rev	0.89	26.6%	1.36	0.31	67.5%	27.5%
Beam-end, Proposed λ with f_{ct} (40 total)	ACI 318	1.22	28.7%	2.08	0.40	25.0%	7.5%
	ACI 408	0.84	27.2%	1.26	0.29	80.0%	40.0%
	ACI 408-rev	0.98	30.8%	1.48	0.32	55.0%	27.5%
Splice Beam, Proposed λ with w_c (63 total)	ACI 318	1.21	17.3%	1.89	0.85	17.5%	0.0%
	ACI 408	1.14	13.2%	1.62	0.78	11.1%	4.8%
	ACI 408-rev	1.17	13.0%	1.62	0.81	7.9%	0.0%
Splice Beam, Proposed λ with f_{ct} (63 total)	ACI 318	1.62	50.1%	3.69	0.87	12.7%	0.0%
	ACI 408	1.28	21.6%	2.01	0.91	9.5%	0.0%
	ACI 408-rev	1.56	47.7%	3.52	0.92	4.8%	0.0%
Tension Prism, Proposed λ with w_c (6 total)	ACI 318	2.51	13.1%	2.88	2.13	0.0%	0.0%
	ACI 408	1.16	16.1%	1.40	0.84	16.7%	0.0%
	ACI 408-rev	1.23	15.1%	1.48	0.92	16.7%	0.0%
Tension Prism, Proposed λ with f_{ct} (6 total)	ACI 318	2.24	12.7%	2.55	1.91	0.0%	0.0%
	ACI 408	1.10	14.9%	1.31	0.81	16.7%	0.0%
	ACI 408-rev	1.10	14.9%	1.31	0.81	16.7%	0.0%
Development Beam Proposed λ with w_c (18 total)	ACI 318	1.23	19.7%	1.67	0.91	27.8%	0.0%
	ACI 408	0.97	31.1%	1.40	0.55	50.0%	38.9%
	ACI 408-rev	1.08	29.6%	1.53	0.63	44.4%	33.3%
Development Beam Proposed λ with f_{ct} (18 total)	ACI 318	1.33	19.9%	1.81	0.98	16.7%	0.0%
	ACI 408	1.01	31.4%	1.48	0.57	50.0%	38.9%
	ACI 408-rev	1.16	29.5%	1.67	0.68	38.9%	16.7%

Notes:

[†] No. of specimens given in parentheses

MODIFICATION FACTOR FOR LWC BASED ON CONCRETE MIXTURE TYPE

The design expressions for development length in AASHTO LRFD, ACI 318-11, and ACI 408-03 include modification factors for LWC based on concrete mixture type. In ACI 318-11 the modification factor is given by the λ-factor and has a value of 0.75 for all-lightweight concrete and 0.85 for sand-lightweight concrete. The AASHTO LRFD Specifications and ACI 408-03 use similar modification factors for all-lightweight concrete and sand-lightweight concrete.

The test-to-prediction ratios for the all-lightweight concrete specimens and the sand-lightweight concrete specimens are given in Table 36. The ratios are determined using the three design expressions and the 0.75 and 0.85 factors. The ratios are given in Table 36 for 36 all-lightweight concrete specimens and 135 sand-lightweight specimens for comparison with the ratios determined using the λ-factor based on w_c that are given in Table 31. The ratios are also given in Table 36 for the 18 all-lightweight concrete specimens and the 69 sand-lightweight concrete specimens with both w_c and f_{ct} values. The ratios for this smaller number of tests can be compared to the ratios in Table 34 determined using a λ-factor based on f_{ct}.

In Table 36 the mean test-to-prediction ratios determined for the all-lightweight concrete specimens using the AASHTO LRFD expression were the lowest and were less than 1.0, indicating over-estimation of f_s. The scatter in the ratios determined using the AASHTO LRFD expression, as indicated by the COV values, was the largest. The predictions of bar stress given by the ACI 318-11 expression and the ACI 408-03 expression for all-lightweight concrete were near or above 1.0 with a lower COV. This indicates that the ACI 318-11 and ACI 408-03 expressions gave a better prediction of bar stress than the prediction given by the AASHTO LRFD expression.

For the sand-lightweight concrete specimens, the AASHTO LRFD expression had mean ratios between the other two design expressions, although the COV was the highest or near the highest. The ACI 318-11 expression had similar mean ratios and COV values as the AASHTO LRFD expression for sand-lightweight concrete. The ACI 408-03 expression was near 1.0 with a smaller COV.

Table 36. Test-to-Prediction Ratio of Bar Stress for Design Expressions in AASHTO LRFD (Eq. 31), ACI 318-11 (Eq. 32), and ACI 408-03 (Eq. 33) Using Modification Factors for All-Lightweight Concrete and Sand-Lightweight Concrete.

Concrete Mixture Type and Factor[†]	Design Expression	Mean	COV	Max.	Min.	Percent < 1.0	Percent < 0.8
All-lightweight, 0.75 factor (36 total) [†]	AASHTO	0.88	36.7%	1.36	0.29	58.3%	33.3%
	ACI 318	1.29	20.3%	1.76	0.90	19.4%	0.0%
	ACI 408	1.01	28.9%	1.53	0.52	50.0%	36.1%
All-lightweight, 0.75 factor (18 total) [‡]	AASHTO	0.93	45.7%	1.61	0.39	50.0%	50.0%
	ACI 318	1.23	19.7%	1.67	0.91	27.8%	0.0%
	ACI 408	0.97	31.1%	1.40	0.55	50.0%	38.9%
Sand-lightweight, 0.85 factor (135 total) [†]	AASHTO	1.27	43.9%	2.98	0.23	38.5%	23.0%
	ACI 318	1.81	47.5%	4.07	0.39	14.1%	3.7%
	ACI 408	1.14	29.8%	1.90	0.32	36.3%	16.3%
Sand-lightweight, 0.85 factor (69 total) [‡]	AASHTO	1.17	44.6%	2.89	0.27	44.9%	23.2%
	ACI 318	1.30	38.7%	3.00	0.39	24.6%	7.2%
	ACI 408	0.95	27.0%	1.43	0.29	56.5%	24.6%

Notes:

[†] Data for comparison with the ratios determined using the λ factor based on w_c that are given in Table 31, No. of specimens given in parentheses

[‡] Data for comparison with the ratios determined using the λ factor based on f_{ct} that are given in Table 34, No. of specimens given in parentheses

The test-to-prediction ratios for all-lightweight concrete determined using ACI 318-11 and ACI 408-03 and an LWC factor of 0.75 were nearly equal to the ratios determined using w_c (Table 31). This is due to the low unit weight of the concrete mixtures causing the λ-factor to be at near its lower limit of 0.75. The ratios for sand-lightweight concrete determined using a factor of 0.85 and the ratios determined using w_c were also similar (Table 31). This indicates that the use of λ-factor based on w_c in the ACI 318-11 expression and the ACI 408-03 expression resulted in similar test-to-prediction ratios as those determined using the 0.75 and 0.85 factors.

REVISED EXPRESSION FOR BAR STRESS USING ACI 408-03

The bar stress predicted using the ACI 408-03 expression follows the regression lines for the tested bar stress in LWC and NWC specimens as shown in Figure 97. The mean test-to-prediction ratios determined using the ACI 408-03 are typically near 1.0, although the mean ratios for some groups of test data (i.e., all-lightweight concrete, beam-end specimens, and development beam specimens) is less than 1.0 over the range of splice lengths and concrete compressive strengths tested.
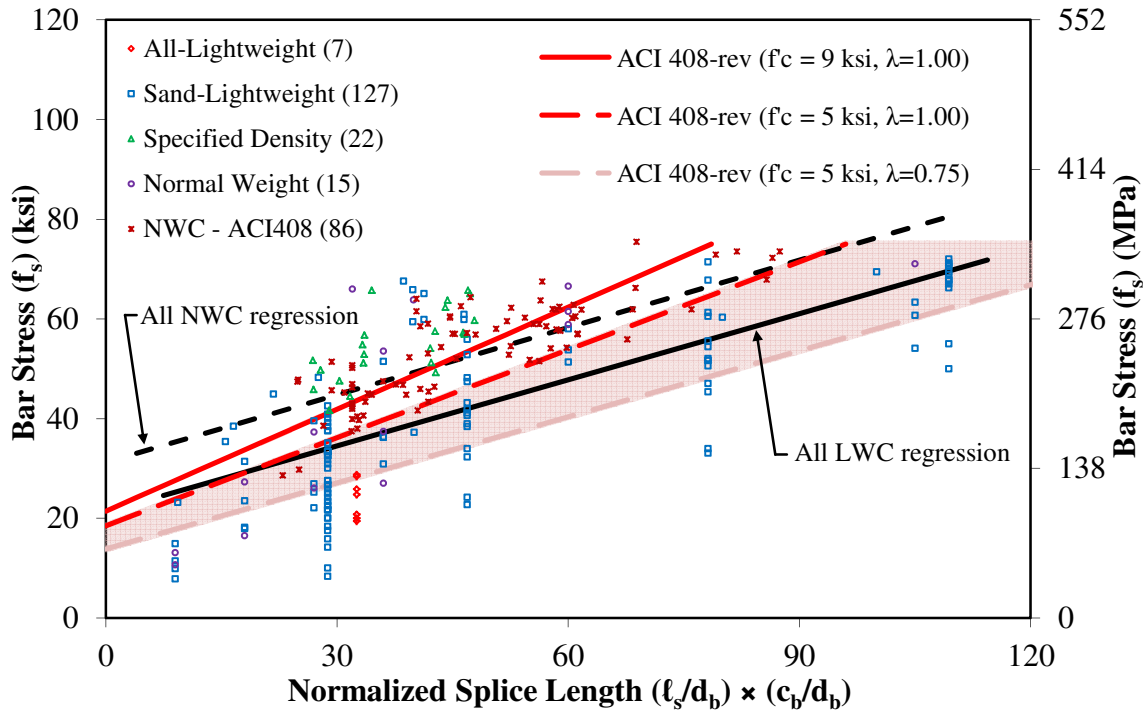
Figure 112. Graph. Bar Stress versus Normalized Splice Length $(\ell_s/d_b) \times (c_b/d_b)$ for Revised ACI 408-03 Expression (Eq. 40) for Specimens without Stirrups (N).

The form of the equation for the three design expressions can be viewed in terms of an equation of a line, that is, a slope multiplied by the independent variable plus an offset on the dependent variable. The AASHTO LRFD expression and the ACI 318-11 expressions are proportional to splice length and are in the form of a factor (i.e., slope term) multiplied by a normalized splice length term (i.e., independent variable). The ACI 408-03 expression is different in that it has a bar stress term that is added to the slope term. The bar stress term acts as an offset to the dependent variable. The offset is observed in Figure 97 as a predicted bar stress of approximately 20 ksi (138 MPa) for a normalized splice length of zero. Note that ACI 408-03 limits the minimum ℓ_s/d_b ratio to 16 for design purposes.

The λ-factor in the ACI 408-03 expression is only applied to the slope term and not to the offset term as shown in Eq. 33. Applying the λ-factor to the offset term as well would have the effect of increasing the number of LWC tests that have a test-to-prediction ratio greater than 1.0 (i.e., under-estimated). Figure 112 shows the prediction given by a revised ACI 408-03 expression that includes the λ-factor in the offset term. The revised ACI 408-03 expression is given by Eq. 39. The simplified form of the revised ACI 408-03 expression is given by Eq. 40 and is shown in Figure 112. The same assumptions used to simplify Eq. 33 were applied to Eq. 40. The line in Figure 112 showing the predicted bar stress for 5 ksi (34 MPa) concrete with a λ-factor of 0.75 is lower than the equivalent line in Figure 97 because of the revision to the ACI 408-03 expression. The lines predicting the bar stress for NWC or LWC with a λ-factor of 1.00 are the same in Figure 97 and Figure 112.

$$f_s = \left[70 \left(\frac{\ell_s}{d_b} \right) \left(\frac{c_b \omega + K_{tr,ACI408}}{d_b} \right) \left(\frac{\lambda}{\alpha \beta} \right) + 2200 \omega \lambda \right] f_c'^{0.25} \qquad \text{(Eq. 39)}$$

in Eq. 33, the units of stress are in psi

$$f_s = \left\{ \left[\left(\frac{\ell_s}{d_b} \right) \left(\frac{c_b}{d_b} \right) \right] \times (\lambda 70) + (\lambda 2200) \right\} f_c'^{0.25} \qquad \text{(Eq. 40)}$$

in Eq. 35, the units of stress are in psi

The test-to-prediction ratios determined using the revised ACI 408-03 expression are compared to normalized splice length and concrete compressive strength in Figure 113 through Figure 116. The effect of the revised ACI 408-03 expression can be seen by comparing the test-to-prediction ratios shown in these figures to their equivalent figure for the unrevised ACI 408-03 expression (i.e., Figure 103 through Figure 106). Compared to their equivalent figure the regression lines in Figure 113 through Figure 116 have shifted upward slightly (i.e., slight under-estimation) but the slopes of the regression lines remain nearly the same.

Table 30, Table 31, and Table 32 give the test-to-prediction ratios determined using the revised ACI 408-03 expression with the λ-factor based on w_c. The mean ratios given in Table 30 for all of the LWC specimens, show that the revision to the ACI 408-03 expression slightly increases the mean ratios and slightly improves the COV (i.e., reduces the value). This trend is followed in Table 31 and Table 32 where the ratios are given by concrete mixture type and specimen type.

Table 33, Table 34, and Table 35 give a comparison of the test-to-prediction ratios determined using a λ-factor based on w_c and using a λ-factor based on f_{ct}. The ratios given in these three tables were determined from a reduced number of specimens that included tests with both w_c and f_{ct} values. The ratios determined using λ-factor based on w_c followed a similar trend as the larger number of tests. The ratios determined using λ-factor based on f_{ct} had a larger mean value for the all-lightweight concrete and sand-lightweight concrete specimens, but the COV values were considerably larger than the COV values determined using the unrevised ACI 408-03 expression.
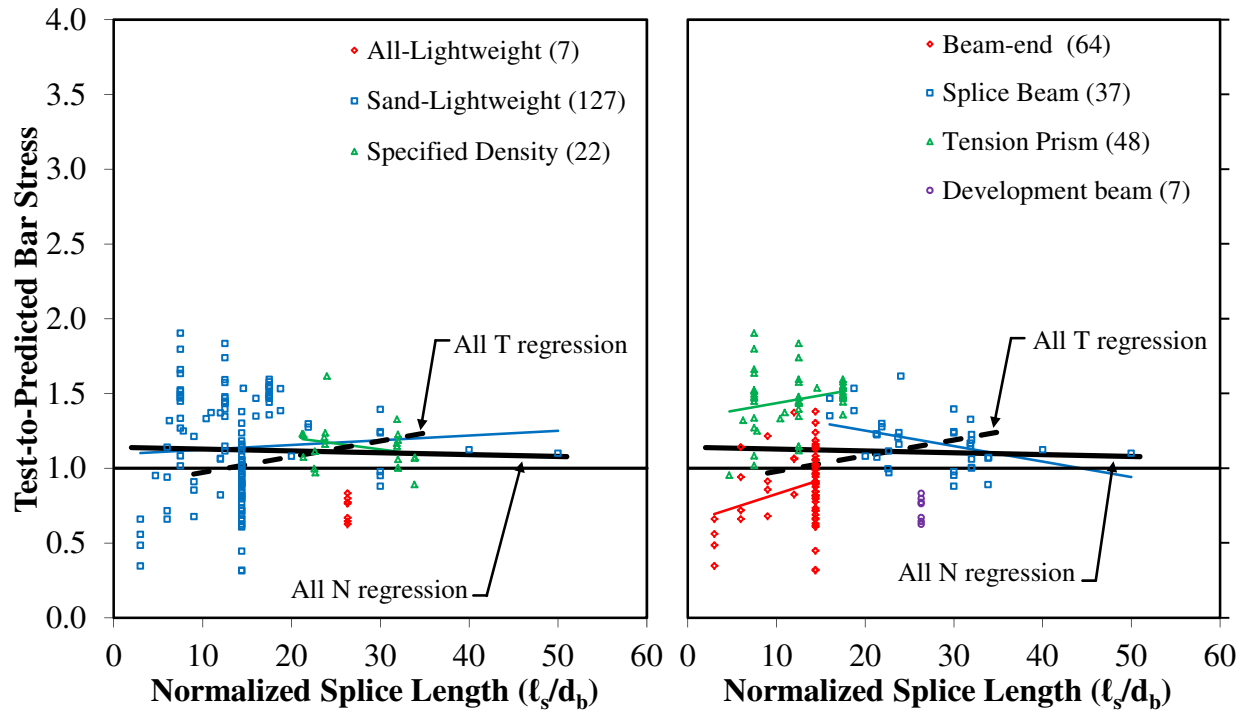
Figure 113. Graph. Bar Stress Test-to-Prediction Ratio Compared to Normalized Splice Length (ℓ_s/d_b) for Revised ACI 408-03 Expression (Eq. 39) with Proposed Expression for λ-Factor (Eq. 37) for LWC Specimens without Stirrups (N).
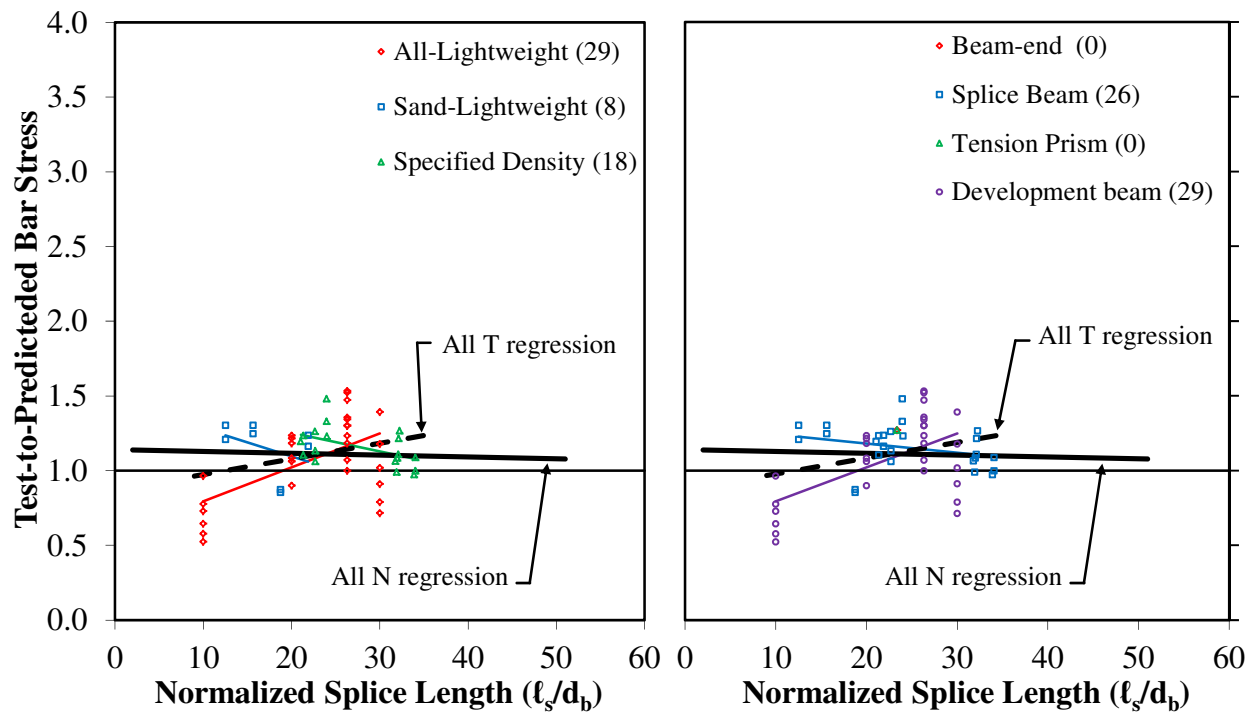
Figure 114. Graph. Bar Stress Test-to-Prediction Ratio Compared to Normalized Splice Length (ℓ_s/d_b) for Revised ACI 408-03 Expression (Eq. 39) with Proposed Expression for λ-Factor (Eq. 37) for LWC Specimens with Stirrups (T).

146
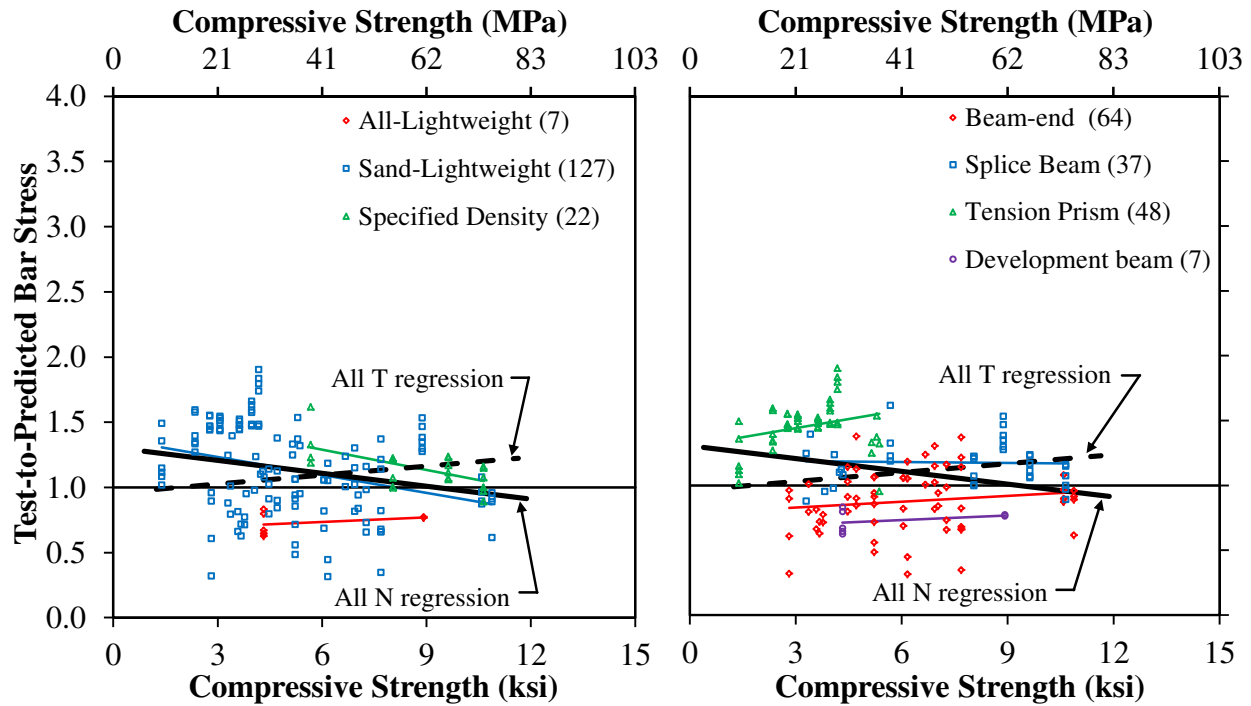
Figure 115. Graph. Bar Stress Test-to-Prediction Ratio Compared to Compressive Strength for Revised ACI 408-03 Expression (Eq. 39) with Proposed Expression for λ-Factor (Eq. 37) for LWC Specimens with Stirrups (N).
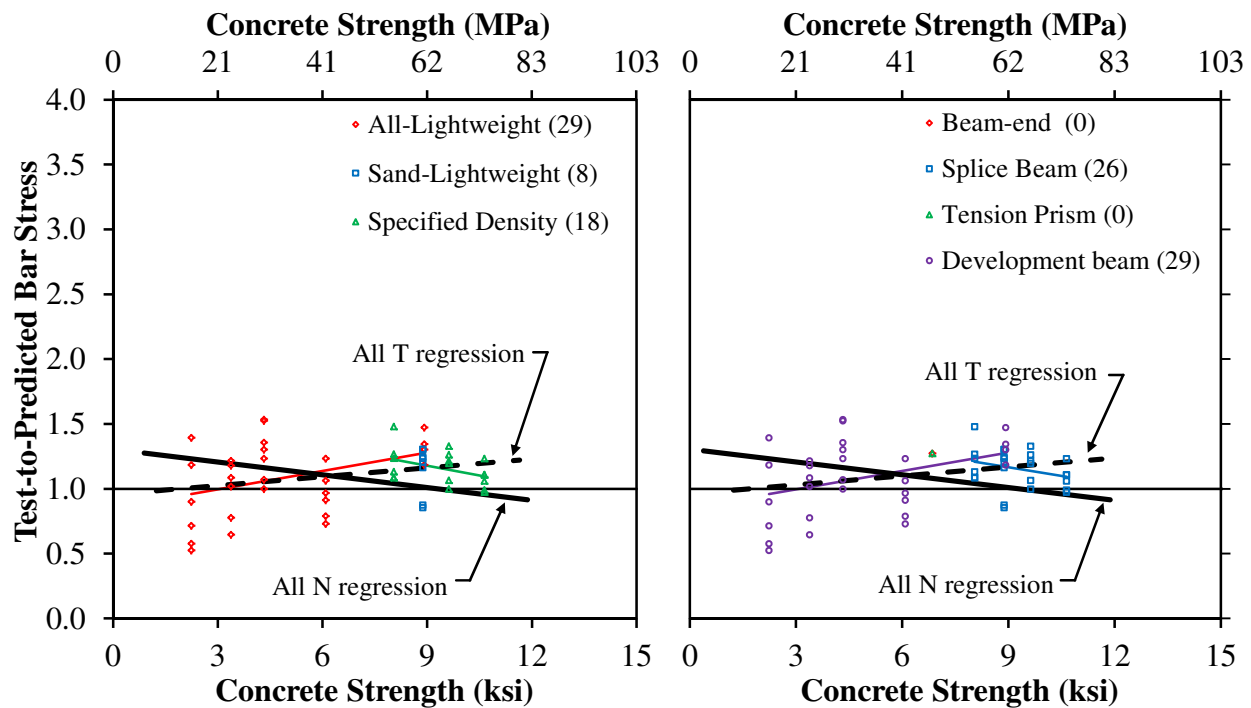
Figure 116. Graph. Bar Stress Test-to-Prediction Ratio Compared to Compressive Strength for Revised ACI 408-03 Expression (Eq. 39) with Proposed Expression for λ-Factor (Eq. 37) for LWC Specimens with Stirrups (T).

147

COMPARISON OF PREDICTED BAR STRESS FOR LWC AND NWC SPECIMENS

The test-to-prediction ratios for the NWC specimens in the ACI Committee 408 Database are given in Table 26 and the ratios for the LWC specimens that include modification for LWC are given in Table 30. The mean ratios for LWC determined using the ACI 318-11 expression are higher than the ratios for NWC for specimens without stirrups but smaller for specimens with stirrups. For the ACI 408-03 expression, the mean ratios for all of the LWC specimens is less than the ratios for NWC specimens. The revised ACI 408-03 expression had mean ratios for the LWC specimens without stirrups that were nearly equal to those for the NWC specimens, but for the specimens with stirrups the mean ratios for the LWC specimens were still smaller.

PROPOSED DESIGN EXPRESSIONS FOR DEVELOPMENT LENGTH

The expressions for bar stress evaluated previously in this chapter are given as design expressions for development length in this section. The stress terms in the expressions given in ACI 318-11 and ACI 408-03 are in pound per square inch units. The units of the stress terms are converted to kilo-pounds (kips) per square inch to be compatible with the units used in the AASHTO LRFD Specifications. Also, the terms that account for top-bar affects, confinement by stirrups, and excess reinforcement are expressed differently in ACI 318-11 and ACI 408-03 than in the AASHTO LRFD Specifications. The AASHTO LRFD terms are included in the design expressions given in this section.

ACI 318-11

The expression for bar stress given by Eq. 32 is rearranged and expressed in terms of development length in Eq. 41. This expression is similar to Eq. 12, except that the units for stress were converted to kips per square inch.

$$\ell_d = 2.37 \frac{f_y}{\lambda_{ACI}\sqrt{f_c'}} \frac{\Psi_t \Psi_e \Psi_s}{\left(\frac{c_b + K_{tr}}{d_b}\right)} d_b \qquad \text{(Eq. 41)}$$

The term $(c_b + K_{tr})/d_b$ in the denominator is expressed as a factor equal to its reciprocal in the revisions being considered by the AASHTO SCOBS T-10 committee to the AASHTO LRFD Specifications (i.e., confining factor = $d_b /(c_b + K_{tr})$). The λ-factor given by Eq. 37 or Eq. 38 replaces the λ-factor given by ACI 318-11. The factor for bar size is not used in the AASHTO LRFD Specifications. The design expression for development length based on ACI 318-11 in the form used by the AASHTO LRFD Specifications is given by Eq. 42.

$$\ell_d = \left(2.37 d_b \frac{f_y}{\sqrt{f_c'}}\right) \times \left(\frac{\Psi_t \Psi_e}{\lambda}\right) \left(\frac{d_b}{c_b + K_{tr}}\right) \qquad \text{(Eq. 42)}$$

Revised ACI 408-03

The expression for bar stress given by Eq. 39 is rearranged and expressed in terms of development length in Eq. 43. This expression is similar to Eq. 15, except for the addition of the λ-factor with the stress offset term and the conversion of the stress units to kips per square inch. The $K_{tr,ACI408}$ term to account for the confinement provided by the stirrups given by Eq. 16 was in units of pounds per square inch. The equivalent $K_{tr,ACI408}$ term in kips per square inch is given by Eq. 44.

$$\ell_d = 2.54 \frac{\left(\dfrac{f_y}{f_c'^{0.25}} - 12.37\omega\lambda\right)\alpha\beta\lambda_{ACI408}}{\left(\dfrac{c_b\omega + K_{tr,ACI408}}{d_b}\right)} d_b \qquad \text{(Eq. 43)}$$

$$K_{tr,ACI408} = \left(\frac{16.4t_r t_d A_{tr}}{sn}\right) f_c'^{0.5} \qquad \text{(Eq. 44)}$$

The term $(c_b\omega + K_{tr,ACI408})/d_b$ in the denominator is expressed as a factor equal to its reciprocal in the revisions being considered by the AASHTO SCOBS T-10 committee to the AASHTO LRFD Specifications (i.e., confining factor = $d_b/(c_b\omega + K_{tr,ACI408})$). The λ-factor given by Eq. 37 or Eq. 38 replaces the reciprocal of the λ-factor given by ACI 408-03. The design expression for development length based on ACI 408-03 in the form used by the AASHTO LRFD Specifications is given by Eq. 45.

$$\ell_d = 2.54d_b \left(\frac{f_y}{f_c'^{0.25}} - 12.37\omega\lambda\right) \times \left(\frac{\alpha\beta}{\lambda}\right)\left(\frac{d_b}{c_b\omega + K_{tr,ACI408}}\right) \qquad \text{(Eq. 45)}$$

COMPARISON OF DEVELOPMENT LENGTH DETERMINED USING PROPOSED DESIGN EXPRESSIONS

Table 37 gives the development length determined using the design expression given in the AASHTO LRFD Specifications (Eq. 10) and the development length determined using the proposed expressions. The proposed expression based on ACI 318-11 is given by Eq. 42 and the proposed expression based on ACI 408-03 is given by Eq. 45.

Table 37. Example of Development Length Determined using AASHTO LRFD Expression (Eq. 10), Proposed ACI 318-11 Expression (Eq. 42), and Proposed ACI 408-03 Expression (Eq. 45).

Expression[†]	Cases Considered[‡]	Development Length by Bar Size (inch)			
		#4	#6	#8	#11
AASHTO	NWC, f'_c = 5 ksi	6.0[*]	13.5	26.5	74.0
	LWC, f'_c = 5 ksi	8.0[*]	17.5	34.5	96.0
	NWC, f'_c = 9 ksi	6.0[*]	13.5	24.0	55.0
	NWC, f'_c = 5 ksi, & A_{tr}	6.0[*]	13.5	26.5	74.0
ACI 318	NWC, f'_c = 5 ksi	8.0[*]	18.0	32.0	63.5
	LWC, f'_c = 5 ksi	10.5[*]	24.0	42.5	84.5
	NWC, f'_c = 9 ksi	6.0[*]	13.5	23.5	47.0
	NWC, f'_c = 5 ksi, & A_{tr}	6.0[*]	13.0	23.5	46.5
Revised ACI 408 (ω = 1.00)	NWC, f'_c = 5 ksi	9.0[*]	20.0	35.5	70.0
	LWC, f'_c = 5 ksi	10.0[*]	22.0	39.0	78.0
	NWC, f'_c = 9 ksi	7.0[*]	16.0	28.5	56.0
	NWC, f'_c = 5 ksi, & A_{tr}	7.5[*]	15.5	26.5	48.5
Revised ACI 408 (ω = 1.10)	NWC, f'_c = 5 ksi	7.5[*]	17.0	30.5	61.0
	LWC, f'_c = 5 ksi	8.5[*]	19.5	34.5	68.5
	NWC, f'_c = 9 ksi	6.0[*]	13.5	24.5	48.5
	NWC, f'_c = 5 ksi, & A_{tr}	6.5[*]	14.0	23.5	43.5
Revised ACI 408 (ω = 1.25)	NWC, f'_c = 5 ksi	6.5[*]	14.0	25.0	50.0
	LWC, f'_c = 5 ksi	7.0[*]	16.5	29.0	57.5
	NWC, f'_c = 9 ksi	6.0[*]	13.0	23.5	46.5
	NWC, f'_c = 5 ksi, & A_{tr}	5.5[*]	11.5	19.5	36.5

Notes: [†] Assumes f_y = 60 ksi and c_b = 2.0 inch, term ω given by Eq. 17; [‡] A_{tr} assumes two #3 stirrups at 6.0 inch spacing and used to develop two bars, [*] 12.0 inch minimum controls

Units: 1.0 ksi = 6.89 MPa, 1.0 inch = 25.4 mm

The development lengths given in Table 37 assume the bars are Grade 60, uncoated, and bottom-cast with 2.0 inch (51 mm) of cover measured to the center of the bar. For each design expresson, four cases are considered: i) NWC with an f'$_c$ of 5.0 ksi (34 MPa), ii) LWC with an f'$_c$ of of 5.0 ksi (34 MPa), iii) high-strength NWC with an f'$_c$ of 9.0 ksi (62 MPa), iv) NWC with an f'$_c$ of 5.0 ksi (34 MPa) and confining stirrups. The cases indicated as NWC are also applicable to LWC with a λ-factor equal to 1.0 for the two proposed expressions. The case indicated as LWC uses a 1.3 factor multiplied by ℓ_d for the AASHTO LRFD expression and a λ-factor equal to 0.75 for the two proposed expressions. The case that includes confining reinforcement assumes that the stirrups are #3 bars with two legs that are spaced at 6.0 inch (152 mm) along the length of two bars being developed. Note that the development length determined for the #4 bars was less than the 12.0 inch (305 mm) minimum specified for the design expressions. The calculated values are given in Table 37 for informational purposes only.

The ACI 408-03 expression includes the term ω that accounts for some of the cover near the developed bar being much larger than the minimum cover used to define c$_b$. The term ω is dependent upon the ratio of the maximum cover dimension (c$_{max}$) to the minimum cover dimension (c$_{min}$). The ACI 408-03 expression can be simplified by assuming c$_{max}$ equals c$_{min}$ and taking ω as 1.0. When the ratio c$_{max}$ to c$_{min}$ is 2.0, then ω is 1.10 as determined using Eq. 17. The term ω has an upper limit of 1.25, which corresponds to a ratio of c$_{max}$ to c$_{min}$ of 3.5. For the c$_b$ of 2.0 inch (52 mm) used in the development lengths given in Table 37, an ω of 1.10 corresponds to a c$_{max}$ of 3.0 inch (76 mm) for #8 bars, and an ω of 1.25 corresponds to a c$_{max}$ of 5.25 inch (133 mm).

A comparison of the development lengths shown in Table 37 for the three cases without stirrups determined using the AASHTO LRFD expression and the proposed expressions based on ACI 318-11 and ACI 408 (i.e., with ω taken as 1.0) does not indicate an obvious trend. The effect that a small amount of confining stirrups have on the development length determined using the proposed expressions based on ACI 318-11 and ACI 408 is quite obvious. Also, the effect on development length of increasing the term ω from a minimum of 1.0 to a maximum of 1.25 is significant as shown in Table 37.

SUMMARY OF THE ANALYSIS OF PROPOSED DESIGN EXPRESSIONS

A comparison of the bar stress at failure to the bar stress predicted by the AASHTO LRFD expression, the ACI 318-11 expression, and the ACI 408-03 expression was made for typical values of concrete strength and bar size. The comparison showed that neither the AASHTO LRFD expression nor the ACI 318-11 expression were capable of predicting the trend of bar stress data for the LWC specimens. This is due to the bar stress in LWC specimens increasing with splice length but bar stress not increasing proportional to splice length, as was previously observed for NWC specimens.[9] The form of the ACI 408-03 expression for bar stress is better able to predict this trend.

The test-to-prediction ratios determined using the ACI 318-11 expression are much larger than 1.0 (i.e., under-estimate bar stress) for short splice lengths and the ratios become smaller as splice length increases. Similarly ratios determined using the ACI 318-11 expression are much larger than 1.0 for small compressive strengths and the ratios become smaller as compressive strength increases. The test-to-prediction ratios determined using the ACI 408-03 expression were greater than 1.0 indicating that the prediction given by ACI 408-03 slightly underestimates the bar stress over the range of splice lengths tested.

A comparison of λ-factor was determined using w_c and the λ-factor determined using f_{ct} indicated that for tests with low splitting tensile strengths, the ACI 318-11 expression highly under-estimated the bar stress when the λ-factor was based on f_{ct}. The prediction of bar stress using the ACI 408-03 expression for the same tests with low splitting tensile strengths were still under-estimated, but to a lesser extent.

A slight revision was made to the ACI 408-03 expression by adding the λ-factor to the term that causes an offset in the predicted bar stress. This had the effect of uniformly increasing the predicted bar stress of LWC specimens with a low unit weight or splitting tensile strength across the range of splice lengths tested. The result for most groups of specimens was an increase in the test-to-prediction ratio with a slight decrease in the COV when the λ-factor was based on unit weight. When the λ-factor was based on splitting tensile strength the mean test-to-prediction ratio increased, but the COV also tended to increase.

The mean test-to-prediction ratios for LWC determined using the ACI 318-11 expression are higher than the ratios for NWC specimens without stirrups but smaller for specimens with stirrups. The mean ratios determined for all of the LWC specimens using the ACI 408-03 expression is less than the ratios for NWC specimens. The revised ACI 408-03 expression gave mean ratios for the LWC specimens without stirrups that were nearly equal to the ratios for the NWC specimens, but for the specimens with stirrups the mean ratios for the LWC specimens were still smaller.

CHAPTER 6. PRELIMINARY RECOMMENDATIONS FOR AASHTO LRFD SPECIFICATIONS

INTRODUCTION

This chapter summarizes several preliminary recommended changes to the AASHTO LRFD Specifications. The first two recommended changes regarding the definition of LWC and the introduction of a LWC modification factor (λ-factor) were previously described in a related document concerning the mechanical properties of LWC and are presented again for clarity.[7] Additional recommended changes to the AASHTO LRFD Specifications are presented in this chapter that are based upon the analysis described in this document. These additional recommendations are built upon the two previous recommendations.

This document described the structural performance of 40 LWC splice beam specimens tested at TFHRC. Additional tests on the bond performance of LWC specimens were found in the literature. These tests on LWC were added to selected tests on NWC specimens found in the ACI Committee 408 Database.[9] The NWC specimens that were selected had parameters that are important to bond performance that were similar to the LWC specimens. The LWC and NWC specimens were analyzed together as the TFHRC Mild Steel Development Length Database.

The analysis of the TFHRC Database included an evaluation of design expressions for development length given in specifications other than AASHTO LRFD. The evaluation included the expression in the ACI 318-11 building code and the expression in the ACI Committee 408 report (ACI 408-03).[16,9] An additional expression based on a revision to the expression in the ACI Committee 408 report was evaluated. This chapter presents a recommended change to the AASHTO LRFD Specifications based on the revised ACI 408 expression.

AASHTO Subcommittee on Bridges and Structures (SCOBS) Technical Committee 10 (T-10) is currently considering a change to the design expression for mild steel development length in the AASHTO LRFD Specifications. This change is based on the design expression in ACI 318-11 building code as recommended by NCHRP Project 12-60.[18] The design expression based on ACI 318-11 will also be presented in this chapter as a recommended alternative.

The design expressions for development length include the recommended new expression for the λ-factor. The λ-factor is not based on the proportions of constituent materials and includes tests from types of mix designs that are not explicitly permitted by the current edition of the AASHTO LRFD Specifications.[1] These mix types include specified density LWC (typically a blend of lightweight and normal weight coarse aggregate) and inverted mixes (normal weight coarse and lightweight fine aggregate). The recommend new expression for the λ-factor is instead based on unit weight and splitting tensile strength and as a result the definitions of sand-lightweight concrete and all-lightweight concrete would no longer be needed.

PROPOSED DEFINITION FOR LWC

The definition for lightweight concrete in the AASHTO LRFD Specifications (AASHTO 2012) is in Article 5.2 and states the following:

> *Lightweight Concrete* – Concrete containing lightweight aggregate and having an air-dry unit weight not exceeding 0.120 kcf, as determined by ASTM C567. Lightweight Concrete without natural sand is termed "all-lightweight concrete" and lightweight concrete in which all of the fine aggregate consists of normal weight sand is termed "sand-lightweight concrete."

This definition limits the unit weight for LWC to 0.120 kcf (1920 kg/m^3) and includes definitions for sand-lightweight and all-lightweight concrete. The proposed definition for LWC expands the range of unit weights and eliminates the definitions for terms relating to the constituent materials in LWC. The proposed definition for LWC is as follows:

> *Lightweight Concrete* – Concrete containing lightweight aggregate and having an equilibrium density not exceeding 0.135 kcf, as determined by ASTM C567.

The term "air-dry unit weight" is used in the existing definition; however this term is not found in ASTM C567 (Standard Test Method for Determining Density of Structural Lightweight Concrete).[40] The AASHTO LRFD term "air-dry unit weight" is interpreted to be equivalent to the ASTM C567 term "equilibrium density". A statement could be added to the commentary to clarify the term "air-dry unit weight" or the term "equilibrium density" could be used in the definition for LWC.

PROPOSED EXPRESSION FOR LWC MODIFICATION FACTOR

The concept of including a modification factor for LWC in expressions for predicting nominal resistance is included in many articles of the AASHTO LRFD Specifications. However, a single unified expression or LWC modification factor is not specified. This section proposes a new term, the λ-factor, to quantify the reduction in nominal resistance that could be included in any expression for nominal resistance. The language for the LWC modification factor, or λ-factor, could be based on the existing language for the modification factor for shear in Article 5.8.2.2 which states the following:

> Where lightweight aggregate concretes are used, the following modifications shall apply in determining resistance to torsion and shear:

> Where the average splitting tensile strength of lightweight concrete, f_{ct}, is specified, the term, $\sqrt{f'_c}$ in the expressions given in Articles 5.8.2 and 5.8.3 shall be replaced by: $4.7 f_{ct} < \sqrt{f'_c}$

Where f_{ct} is not specified, the term $0.75\ \sqrt{f'_c}$ for all lightweight concrete, and 0.85 $\sqrt{f'_c}$ for sand-lightweight concrete shall be substituted for $\sqrt{f'_c}$ in the expressions given in Articles 5.8.2 and 5.8.3

Linear interpolation may be employed when partial sand replacement is used.

Article 5.8.2.2 specifically relates to torsion and shear, so a general λ-factor would not specifically reference those actions in its definition. The terms sand-lightweight concrete and all-lightweight concrete would not be used because the proposed new definition for LWC does not include them. The λ-factor relates to the material properties of structural LWC so the new Article for the definition for the λ-factor could be located in Article 5.4.2 "Normal Weight and Structural Lightweight Concrete". The λ-factor will be referred to as Article 5.4.2.8 in the present document. The proposed text for the λ-factor is as follows:

Where lightweight aggregate concretes are used, the lightweight concrete modification factor, λ, shall be determined as:

Where the average splitting tensile strength of lightweight concrete, f_{ct}, is specified, λ may be taken as: $4.7\ f_{ct}\ /\ \sqrt{f'_c}\ \leq\ 1.0$

Where f_{ct} is not specified, λ may be taken as:

$$0.75\ \leq\ \lambda = 7.5\ w_c\ \leq\ 1.0 \hspace{3cm} (5.4.2.8\text{-}1)$$

The language for the λ-factor expression when f_{ct} is not specified follows the format of the ϕ-factor for flexure for prestressed and nonprestressed members in Article 5.5.4.2.1.

The effect of using the λ-factor in expressions for the development length of mild steel is evaluated in this document. The effect of using the λ-factor in additional expressions for nominal resistance still needs to be evaluated. The proposed λ-factor could then be included in additional expressions for nominal resistance in the AASHTO LRFD Specifications. For example, the λ-factor could be added directly to design expressions for nominal shear resistance in Articles 5.8.2 and 5.8.3 and would replace the existing modification factor for LWC.

PROPOSED DESIGN EXPRESSIONS FOR DEVELOPMENT OF MILD STEEL IN TENSION

The determination of the development length of mild steel in tension consists of evaluating the expression given for basic tension development length and multiplying that length by modifications factors that either increase or decrease the development length.

The expression for basic tension development length in the AASHTO LRFD Specifications (AASHTO 2012) is in Article 5.11.2.1 and states the following:

155

The basic tension development length, ℓ_{db}, in in. shall be taken as:

For No. 11 bar and smaller: $1.25\, A_b\, f_y / \sqrt{f'_c}$

   but not less than: $0.4\, d_b\, f_y$

For No. 14 bars: $2.70\, f_y / \sqrt{f'_c}$

For No. 18 bars: $3.5\, f_y / \sqrt{f'_c}$

The modification factor that increases development length for LWC in the AASHTO LRFD Specifications (AASHTO 2012) is in Article 5.11.2.2 and states the following:

The basic development length, ℓ_{db}, shall be multiplied by the following factor or factors, as applicable:

For lightweight concrete where f_{ct} (ksi) is specified: $0.22\, \sqrt{f'_c} / f_{ct}$

For all-lightweight concrete where f_{ct} is not specified: 1.3

For sand-lightweight concrete where f_{ct} is not specified: 1.2

Linear interpolation may be used between all-lightweight and sand lightweight provisions when partial sand replacement is used.

Two proposed design expressions for development length are presented. The first expression is based on a revision to the expression in ACI 408-03. The second expression is based in ACI 318-11 and is presented as a proposed alternative.

PROPOSED DESIGN EXPRESSION FOR DEVELOPMENT LENGTH

The determination of the development length of mild steel in tension consists of evaluating an expression that includes modification factors that either increase or decrease the development length. Unlike the design expression in AASHTO 2012, the factors are not separated from an expression for basic tension development length.

The proposed design expression for development length is as follows:

The tension development length shall not be less than 12.0 in., except for lap splices specified in Article 5.11.5.3.1 and development of shear reinforcement specified in Article 5.11.2.6.

Modification factors are applied to development length to account for various effects. They are to be taken equal to 1.0 unless they are specified to increase ℓ_d in Article 5.11.2.1.2 or to decrease ℓ_d in Article 5.11.2.1.3.

The tension development length, ℓ_d, in in. shall not be less than:

$$\ell_d \;=\; 2.5\, d_b\, (f_y / f'^{0.25}_c - 12\, \lambda_{cc} \times \lambda) \times (\lambda_{rl} \times \lambda_{cf} \times \lambda_{rc} \times \lambda_{er} / \lambda)$$

where:

λ_{cc} = concrete cover factor
λ_{rl} = reinforcement location factor
λ_{cf} = coating factor
λ_{rc} = reinforcement confinement factor
λ_{er} = excess confinement factor
λ = lightweight concrete factor as specified in Article 5.4.2.8

The λ_{rl}, λ_{cf}, and λ_{er} factors are given in Article 5.11.2.1.2 and 5.11.2.1.3 of AASHTO 2012. The concrete cover factor (λ_{cc}) and the reinforcement confining factor (λ_{rc}) are new modification factors. The concrete cover factor and reinforcement confining factor can decrease development length. The proposed expressions are as follows:

The tension development length, ℓ_d, modified by the factors as specified in Article 5.11.2.1.2, may be modified by the following factors, where:

For cover to the nearest concrete surface that is not equal to the side cover or one-half the center-to-center spacing of the bars, λ_{cc} may be taken as:

$(0.1\, c_{max} / c_{min} + 0.9) \le 1.25$

In which:

c_{max} = the larger of c_c and c_s
c_{min} = the lesser of c_c and c_s
c_s = the lesser of c_{so} and c_{si} + 0.25 in.

where:

c_c = cover to the nearest concrete surface
c_{so} = side clear cover
c_{si} = one-half of the clear spacing of the bars

For reinforcement being developed in the length under consideration that is confined laterally by reinforcement spaced such that $c_b \ge 2.5$ in., regardless of existence of stirrups, $\lambda_{rc} = 0.4$

The value of the confinement factor, λ_{rc}, for the reinforcement being developed in the length under consideration satisfies the following:

$1.0 \ge \lambda_{rc} = d_b / (c_b\, \lambda_{cc} + K_{tr}) \ge 0.25$

in which:

K_{tr} = 16 t_r t_d A_{tr} $\sqrt{f'_c}$ / (s n)

t_r = 9.6 R_r + 0.28 ≤ 1.72

t_d = 0.78 d_b + 0.22

where:

K_{tr} = transverse reinforcement index

c_b = the smaller of the distance from center of bar or wire being developed to the nearest concrete surface and one-half the center-to-center spacing of the bars or wires being developed (in.)

A_{tr} = total cross-sectional area of all transverse reinforcement within spacing s that crosses the potential plane of splitting through the reinforcement being spliced or developed (in.^{2})

s = maximum center-to-center spacing of the stirrups within ℓ_d (in.)

n = number of bars or wires being spliced or developed along the plane of potential splitting

R_r = relative rib area of the reinforcement. For conventional reinforcement, t_r may be taken as 1.0

This definition of the reinforcement confinement factor includes some of the wording being considered by the SCOBS T-10 committee.

The bar stress of the specimens in the TFHRC Database without stirrups is shown in Figure 117. The prediction given by the proposed expression based on ACI 408-03 for concrete with a compressive strength of 5 ksi (34 MPa) and 9 ksi (62 MPa) is shown in the figure. The mean compressive strength of the all-lightweight concrete, sand-lightweight concrete, and NWC specimens in the ACI Committee 408 Database is 5 ksi (34 MPa). The mean compressive strength of the specified density concrete and normal weight concrete specimens found in the literature is 9 ksi (62 MPa). A prediction for 5 ksi (34 MPa) concrete and a λ-factor of 0.75 is shown in the figure. The shaded region indicates the range of possible predicted bar stress for 5 ksi (34 MPa) concrete with a modification factor for LWC varying from 1.00 to 0.75. Nearly all of the regression line for the LWC data points is within the shaded region indicating the possible range of LWC predictions.
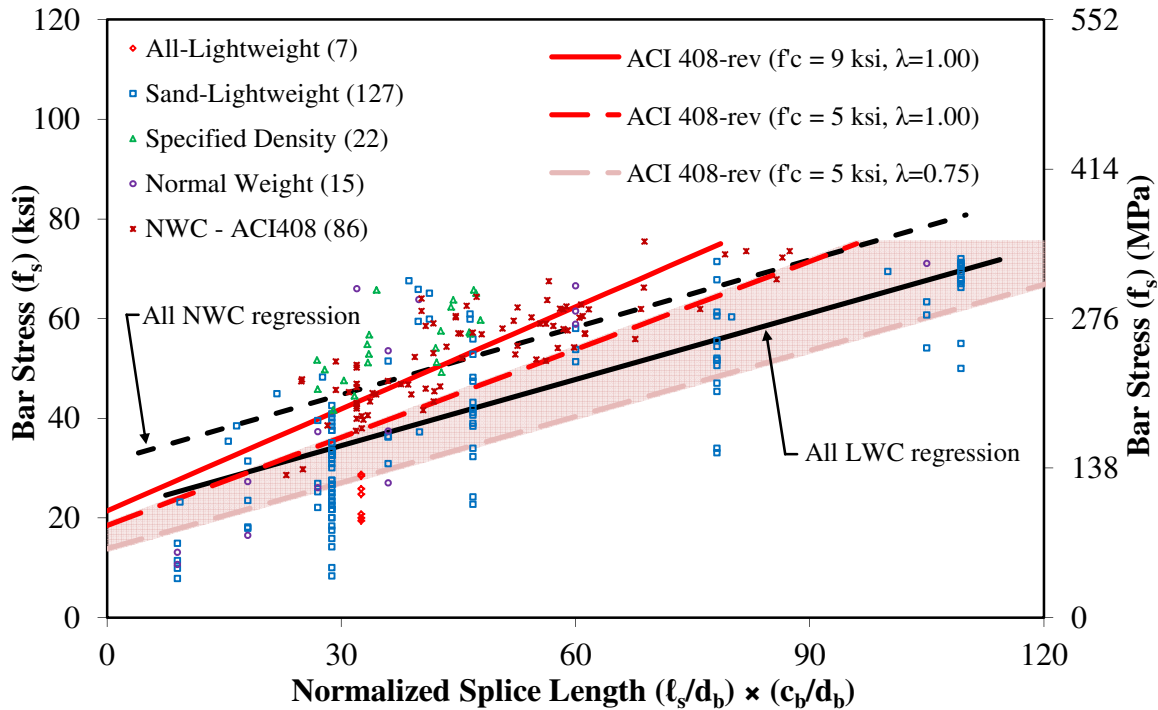
Figure 117. Graph. Bar Stress for the Proposed Expression based on ACI 408-03.

The proposed expression for development length could be simplified. After simplification, the main differences between the proposed expression given in this document and the proposed expression currently being considered by SCOBS T-10 would be expressions for ℓ_d and K_{tr}. The simplification would include eliminating λ_{cc}, the factor t_r, and the term R_r. Eliminating λ_{cc} would simplify the expressions for ℓ_d and λ_{rc}. Eliminating t_r in the expression for K_{tr} would also eliminate the need for the new term R_r that is used for reinforcing bars with large deformations.

PROPOSED ALTERNATIVE DESIGN EXPRESSION FOR DEVELOPMENT LENGTH

The proposed alternative design expression for development length is as follows:

> The tension development length, ℓ_d, shall not be less than the product of the basic tension development length, ℓ_{db}, specified herein and the modification factor or factors specified in Articles 5.11.2.1.2 and 5.11.2.1.3.

> The tension development length shall not be less than 12.0 in., except for lap splices specified in Article 5.11.5.3.1 and development of shear reinforcement specified in Article 5.11.2.6.

> The tension development length, ℓ_d, in in. shall be taken as:

$$\ell_d \quad = \quad \ell_{db} \left(\lambda_{rl} \times \lambda_{cf} \times \lambda_{rc} \times \lambda_{er} / \lambda \right)$$

in which:

ℓ_{db} = 2.4 d_b f_y / $\sqrt{f'_c}$

where:

ℓ_{db} = basic development length
λ_{rl} = reinforcement location factor
λ_{cf} = coating factor
λ_{rc} = reinforcement confinement factor
λ_{er} = excess confinement factor
λ = factor for lightweight concrete as specified in Article 5.4.2.8

The λ_{rl}, λ_{cf}, and λ_{er} factors are given in Article 5.11.2.1.2 and 5.11.2.1.3 of AASHTO 2012. The reinforcement confining factor (λ_{rc}) is a new modification factor that can decrease development length. The proposed expressions are as follows:

The basic tension development length, ℓ_{db}, modified by the factors as specified in Article 5.11.2.1.2, may be modified by the following factors, where:

Reinforcement being developed in the length under consideration is confined by concrete due to relatively wide spacing, large cover or enclosing stirrups, λ_{rc} may be taken as:

1.0 ≥ λ_{rc} = d_b / (c_b + K_{tr}) ≥ 0.4

In which:

K_{tr} = 40 A_{tr} / (s n)

where:

K_{tr} = transverse reinforcement index
c_b = the smaller of the distance from center of bar or wire being developed to the nearest concrete surface and one-half the center-to-center spacing of the bars or wires being developed (in.)

Reinforcement being developed in the length under consideration is spaced laterally not less than 5.0 in. center-to-center, with not less than 2.5 in. cover to center of bar measured in the direction of the spacing, regardless of existence of stirrups, λ_{rc} = 0.4

This definition of the reinforcement confinement factor is based on the wording being considered by the SCOBS T-10 committee.

The bar stress of the specimens in the TFHRC Database without stirrups is shown in Figure 118. The prediction given by the proposed expression based on ACI 318-11 for concrete with a

compressive strength of 5 ksi (34 MPa) and 9 ksi (62 MPa) is shown in the figure. The mean compressive strength of the all-lightweight concrete, sand-lightweight concrete, and NWC specimens in the ACI Committee 408 Database is 5 ksi (34 MPa). The mean compressive strength of the specified density concrete and normal weight concrete specimens found in the literature is 9 ksi (62 MPa). A prediction for 5 ksi (34 MPa) concrete and a λ-factor of 0.75 is shown in the figure. The shaded region indicates the range of possible predicted bar stress for 5 ksi (34 MPa) concrete with a modification factor for LWC varying from 1.00 to 0.75. The regression line for all of the NWC specimens is near the predictions given for λ-factors of 1.00. The regression line for the LWC specimens is in the central portion of the shaded region for the possible range of LWC predictions.
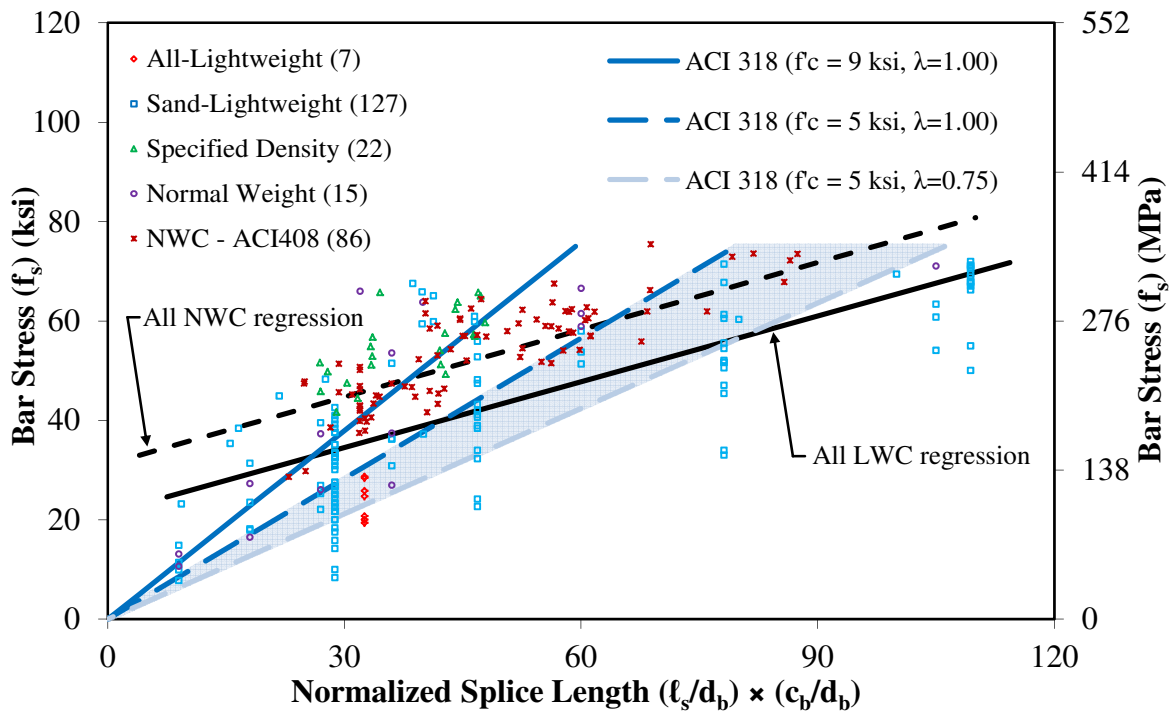
Figure 118. Graph. Bar Stress for the Proposed Expression based on ACI 318-11.

CHAPTER 7. CONCLUDING REMARKS

INTRODUCTION

This document describes tests on 40 LWC splice beam specimens, describes a bond strength database, and presents potential revisions to the AASHTO LRFD Specifications relating to the development length of mild steel reinforcement in tension. The proposed design expressions for development length were compared to tested values in a database including over 200 tests on LWC that was collected as part of this research effort. A description of the database and the development and evaluation of prediction expressions is included in this document.

Future phases of this research compilation and analysis effort will include synthesis of past work on structural performance of LWC. The test results will be compared to the prediction expressions for nominal resistance in the AASHTO LRFD Specifications incorporating appropriate proposed revisions for LWC mechanical properties.

ACKNOWLEDGEMENTS

CHAPTER 8. REFERENCES

INTRODUCTION

This chapter gives the references for the document in three parts. The first part consists of references cited in the document text. The second and third part consists of references for the bond test data used in the TFHRC Database with LWC specimens and NWC specimens, respectively.

CITED REFERENCES

1. AASHTO (2012), "AASHTO LRFD Bridge Design Specifications, Customary U.S. Units," American Association of State Highway and Transportation Officials, Sixth Edition.

2. ACI Committee 213 (1967), "Guide for Structural Lightweight Aggregate Concrete," ACI Journal, Vol. 64, No. 8, American Concrete Institute, August, pp. 433-469.

3. Hanson, J.A. (1961), "Tensile Strength and Diagonal Tension Resistance of Structural Lightweight Concrete," ACI Journal Proceedings, Vol. 58, No. 1, July 1961, pp. 1-40.

4. Ivey, D.L. and Buth, E. (1966), "Splitting Tension Test of Structural Lightweight Concrete," ASTM Journal of Materials, Vol. 1, No.4, pp. 859-871.

5. Pauw, A. (1960), "Static Modulus of Elasticity of Concrete as Affected by Density," ACI Journal, Vol. 57, No. 6, American Concrete, Institute, December, pp. 679-687.

6. Russell, H. (2007), "Synthesis of research and Provisions Regarding the Use of Lightweight concrete in Highway bridges," Report No. FHWA-HRT-07-053, Federal Highway Administration report, Washington, DC, August 2007.

7. Greene, G.G. and Graybeal, B.A. (2013), "Lightweight Concrete: Mechanical Properties," Report No. FHWA-HRT-13-062, Federal Highway Administration report, Washington, DC, June.

8. ACI Committee 213 (2003), "Guide for Structural Lightweight Aggregate Concrete," ACI 213R-03, American Concrete Institute, Farmington Hills, MI.

9. ACI Committee 408 (2003), "Bond and Development of Straight Reinforcing Bars in Tension," ACI 408R-03, American Concrete Institute, Farmington Hills, MI.

10. Nilson, A.H., Darwin, D., Dolan, C.W. (2004), *Design of Concrete Structures*, 13th Edition, McGraw-Hill, New York, 779 pp.

11. Darwin, D., Zuo, J., Tholen, M.L., Idun, E.K. (1996), "Development Length Criteria for Conventional and High Relative Rib Area Reinforcing Bars," ACI Structural Journal, Vol. 93, No. 3, May-June, pp. 1-13.

12. Zuo, J., and Darwin, D. (2000), "Splice Strength of Conventional and High Strength Relative Rib Area Bars in Normal and High-Strength Concrete," ACI Structural Journal, Vol. 97, No. 4, July-August, pp. 630-641.

13. Orangun, C.O., Jirsa, J.O., Breen, J.E. (1977), "A Reevaluation of Test Data on Development Length and Splices," ACI Journal, Vol. 74, No. 3, March, pp. 114-122.

14. Azizinamini, A., Stark, M., Roller, J.J., Ghosh, S.K. (1993), "Bond Performance of Reinforcing Bars Embedded in High-Strength Concrete," ACI Structural Journal, Vol. 90, No. 5, September-October, pp. 554-561.

15. Azizinamini, A., Pavel, R., Hatfield, E., Ghosh, S.K. (1999), "Behavior of Lap-Spliced Reinforcing Bars Embedded in High-Strength Concrete," ACI Structural Journal, Vol. 96, No. 5, September-October, pp. 826-835.

16. ACI Committee 318 (2011), "Building Code Requirements for Reinforced Concrete (ACI 318-11) and Commentary," American Concrete Institute, Farmington Hills, MI.

17. Azizinamini, A., Darwin, D., Eligehausen, R., Pavel, R., Ghosh, S.K. (1999), "Proposed Modifications to ACI 318-95 Tension Development and Lap Splice for High-Strength Concrete," ACI Structural Journal, Vol. 96, No. 6, November-December, pp. 922-927.

18. Ramirez, J.A., and Russell, B.W. (2008), "Transfer, Development and Splice Length for Strand/Reinforcement in High-Strength Concrete," NCHRP Report 603, NCHRP Project 12-60, National Cooperative Highway Research Program, Transportation Research Board, 131 pp.

19. AASHO (1973), "Standard Specifications for Highway Bridge," American Association of State Highway Officials, Eleventh Edition.

20. ACI Committee 318 (1977), "Building Code Requirements for Reinforced Concrete (ACI 318-77)," American Concrete Institute, Detroit, MI, 102 pp.

21. ACI Committee 408 (1979), "Suggested Development, Splice and Standard Hook Provisions for Deformed Bars in Tension," Concrete International, July, pp. 44-46.

22. Jirsa, J.O, Lutz, L.A., Gergely, P. (1979), "Rationale for Suggested Development, Splice and Standard Hook Provisions for Deformed Bars in Tension," Concrete International, July, pp. 47-61.

23. ACI Committee 318 (1989), "Building Code Requirements for Reinforced Concrete (ACI 318-89) and Commentary – ACI 318R-89," American Concrete Institute, Detroit, MI, 353 pp.

24. ACI Committee 318 (1995), "Building Code Requirements for Structural Concrete (ACI 318-95) and Commentary (ACI 318R-95)," American Concrete Institute, Farmington Hills, MI, 369 pp.

25. Burge, T.A. (1983), "High-Strength Lightweight Concrete with Silica Fume," SP79, Fly Ash, Silica Fume, Slag and Other Mineral By-Products in Concrete, V.M. Malhotra editor, ACI, pp. 731-745.

26. Seabrook, P.I. and Wilson, H.S. (1988), "High Strength Lightweight Concrete for use in Offshore Structures: Utilization of Fly Ash and Silica Fume," International Journal of Cement Composites and Lightweight Concrete, Vol. 10, No. 3, August, pp. 183-192.

27. Yeginobali, A., Sobolev, K.G., Soboleva, S.V., Tokyay, M. (1998), "High Strength Natural Lightweight Aggregate Concrete with Silica Fume," ACI SP 178-38, ACI, May, 739-758.

28. ASTM C31 (2006), "Standard Practice for Making and Curing Concrete Test Specimens in the Field," American Society for Testing and Materials Standard Practice C39, Philadelphia, PA.

29. ASTM C39 (2001), "Standard Test Method for Compressive Strength of Cylindrical Concrete Specimens," American Society for Testing and Materials Standard Practice C39, Philadelphia, PA.

30. ASTM C496 (2002), "Standard Test Method for Splitting Tensile Strength of Cylindrical Concrete Specimens," American Society for Testing and Materials Standard Practice C496, Philadelphia, PA.

31. Nilson, A.H. (1997), *Design of Concrete Structures*, 12th Edition, McGraw-Hill, New York, 780 pp.

32. Wang, P.T., Shah, S. P., Naaman, A.E. (1978), "Stress-Strain Curves of Normal and Lightweight Concrete in Compression," ACI Journal, Vol. 75, No. 11, November, pp. 603-611.

33. Rizkalla, S., Mirmiran, A., Zia, P., Russell, H., Mast, R. (2007), "Application of the LRFD Bridge Design Specifications to High-Strength Structural Concrete: Flexure and Compression Provisions, NCHRP Report 595," NCHRP Project 12-64, Transportation Research Board.

34. ACI Committee 363 (2010), "Report on High-Strength Concrete," ACI 363R-10, American Concrete Institute Committee 363, Farmington Hills, MI.

35. ACI Committee 318 (1962), "Building Code Requirements for Reinforced Concrete (ACI 318-56)," ACI Journal Proceedings, American Concrete Institute, Vol. 59, No. 12, pp. 1821-1848.

36. Slate, F.O., Nilson, A.H., and Martinez, S. (1986), "Mechanical Properties of High-Strength Lightweight Concrete," ACI Journal, Vol. 83, July-August, pp. 606-613.

37. Jones, T.R., and Stephenson, H.K. (1957), "Properties of Lightweight Concrete Related to Prestressing," Proceedings: World Conference on Prestressed Concrete, San Francisco, California, July, 12 pp.

38. Morales, S.M. (1982), "Short-Term Mechanical Properties of High-Strength Light-Weight Concrete," Cornell University, Report No. 82-9, NSF Grant No. ENG78-05124, Ithaca, NY, August, 98 pp.

39. Ryan, W.G. (1968), "The Production and Properties of Structural Lightweight Concrete in Australia," Session A, Paper 2, Proceedings First International Congress on Lightweight Concrete," Vol. 1, London, May, pp. 17-21.

40. ASTM C496 (2002), "Standard Test Method for Splitting Tensile Strength of Cylindrical Concrete Specimens," American Society for Testing and Materials Standard Practice C496, Philadelphia, PA.

LWC REFERENCES FOR TFHRC MILD STEEL DEVELOPMENT LENGTH DATABASE

41. Bjerkeli, L., Hansen, E.A., Thorenfeldt, E. (1995), "Tension Lap Splices in High Strength LWA Concrete," International Symposium on Structural Lightweight Aggregate Concrete, Sandefjord, Norway, June, pp. 131-142.

42. Clarke, J.L., and Birjandi, F.K. (1993), "Bond Strength Tests for Ribbed Bars in Lightweight Aggregate Concrete," Magazine of Concrete Research, Vol. 45, No. 163, pp. 79-87.

43. CUR Research Committee C75 (1995), "Structural Behaviour of Concrete with Coarse Lightweight Aggregates," CUR Report 173, Centre for Civil Engineering Research and Codes, CUR, Gouda, 76 pp.

44. Green, S.M.F., Brooke, N.J. McSaveney, L.G., Ingham, J.M. (2011), "Mixture Design Development and Performance Verification of Structural Lightweight Pumice Aggregate Concrete," Journal of Materials in Civil Engineering, ASCE, Vol. 23, No. 8, August, pp. 1211-1219.

45. Greene, G. and Graybeal, B., "FHWA Research Program on Lightweight High-Performance Concrete – Development Length of Uncoated Mild Steel in Tension," Third International fib Congress and PCI National Bridge Conference, Washington, D.C., May 29-June 2, 2010, 19 pp.

46. Hossain, K.M.A. (2008), "Bond Characteristics of Plain and Deformed Bars in Lightweight Pumice Concrete," Construction and Building Materials, Vol. 22, pp. 1491-1499.

47. Kobayashi, K., Matsuzaki, Y., Fukuyama, H., and Hakuto, S. (2000), "Performance Evaluation of RC Elements with Ultra Lightweight Concrete," Composite and Hybrid Structures: Proceedings of the 6th ASCCS International Conference on Steel-Concrete Composite Structures, Xiao, Y., and Mahin, S.A., editors, March, pp. 977-984.

48. Ofori-Darko, F.K. (2000), "Bond Properties of Lightweight Aggregate Concrete," Second International Symposium on Structural Lightweight Aggregate Concrete, Kristiansand, Norway, June, pp. 650-659.

49. Petersen, P.H., (1948), "Properties of Some Lightweight-Aggregate Concretes With and With an Air-Entraining Admixture," Building Materials and Structures Report BMS112, U.S. Department of Commerce, National Bureau of Standards, August, 7 pp.

50. Stroband, J. (1992), "Experimenteel Onderzoek naar de Sterkte van Overlappingslassen in Lichtbeton," (Investigation of the Strength of Lap Joints in Lightweight Concrete) TU Delft/TNO Douw, Technische Universiteit Delft (Delft University of Technology), Report No. 25.5-92-5, July, 53 pp.

NWC REFERENCES FOR TFHRC MILD STEEL DEVELOPMENT LENGTH DATABASE

51. Chamberlin, S.J. (1956), "Spacing of Reinforcement in Beams," ACI Journal, Proceedings, Vol. 53, No. 1, July, pp. 113-134.

52. Chinn, J., Ferguson, P.M., Thompson, J.N. (1955), "Lapped Splices in Reinforced Concrete Beams," ACI Journal, Proceedings, Vol. 52, No. 2, October, pp. pp. 201-213.

53. Choi, O.C., Hadje-Ghaffari, H., Darwin, D., and McCabe, S.L. (1990), "Bond of Epoxy-Coated Reinforcement to Concrete: Bar Parameters," SM Report No. 25, University of Kansas Center for Research, Lawrence, Kansas, July, 217 pp.

54. Choi, O.C., Hadje-Ghaffari, H., Darwin, D., and McCabe, S.L. (1991), "Bond of Epoxy-Coated Reinforcement to Concrete: Bar Parameters," ACI Materials Journal, Vol. 88, No. 2, March-April, pp. 207-217.

55. Defries, R.A., Moehle, J.P., Hester, W. (1991), "Lap Splice of Plain and Epoxy-Coated Reinforcements: An Experimental Study Considering Concrete Strength, Casting Position, and Anti-Bleeding Additives," Report No. UCB/SEMM-91/02 Structural Engineering Mechanics and Materials, University of California, Berkley, California, January, 86, pp.

56. Ferguson, P.M., and Breen, J.E. (1965), "Lapped Splices for High-Strength Reinforcing Bars," ACI Journal, Proceedings, Vol. 62, No. 9, September, pp. 1063-1078.

57. Hasan, H.O., Cleary, D.B., Ramirez, J.A. (1996), "Performance of Concrete Bridge Decks and Slabs Reinforced with Epoxy-Coated Steel under Repeated Loadings," ACI Structural Journal, Vol. 93, No. 4, July-August, pp. 397-403.

58. Hester, C.J., Salamizavaregh, S., Darwin, D., McCabe, S.L. (1991), "Bond of Epoxy-Coated Reinforcement to Concrete: Splices," SL Report 91-1, University of Kansas Center for Research, Lawrence, Kansas, May, 66 pp.

59. Hester, C.J., Salamizavaregh, S., Darwin, D., McCabe, S.L. (1993), "Bond of Epoxy-Coated Reinforcement to Concrete: Splices," ACI Structural Journal, V. 90, No. 1, January-February, pp. 89-102.

60. Kadoriku, J. (1994), "Study on Behavior of Lap Splices in High-Strength Reinforced Concrete Members," Doctorate thesis, Kobe University, March, Japan, 201 pp.

61. Rezansoff, T., Akanni, A., and Sparling, B. (1993), "Tensile Lap Splices under Static Loading: A Review of the Proposed ACI 318 Code Provisions," ACI Structural Journal, Vol. 90, No. 4, July-August, pp. 374-384.

62. Resansoff, T., Konkankar, U.S., and Fu, Y.C. (1991), "Confinement Limits for Tension Lap Splices under Static Loading," Report No. S7N 0W0, University of Saskatchewan, August.

63. Thompson, M.A., Jirsa, J.O., Breen, J.E., Meinheit, D.F. (1975), "The Behavior of Multiple Lap Splices in Wide Sections," Research Report No. 154-1, Center for Highway Research, University of Texas at Austin, Texas, February, 75 pp.

64. Zekany, A.J., Neumann, S., Jirsa, J.O., Breen, J.E. (1981), "The Influence of Shear on Lapped Splices in Reinforced Concrete," Research Report 242-2, Center for Transportation Research, Bureau of Engineering Research, University of Texas at Austin, Texas, July, 88 pp.

65. Zuo, J., and Darwin, D. (1998), "Bond Strength of High Relative Rib Area Reinforcing Bars," SM Report No. 46, University of Kansas Center for Research, Lawrence, Kansas, 350 pp.

APPENDIX A

This appendix contains tables with data from the reinforcing bars used in the LWC splice beams tested at TFHRC. The data includes the results of mechanical tests, measurements of bar geometric properties, and the maximum strain measured in the reinforcement during the splice beams tests.

Table 38. Spliced Longitudinal Reinforcing Bar Mechanical Properties.

Tensile Test	Bar Size	Yield Strength[†] (ksi)	Ultimate Strength (ksi)
SB4-A	4	64.6	105.2
SB4-B	4	66.9	105.3
SB6-A1	6	64.8	107.0
SB6-A2	6	63.7	104.7
SB6-B1	6	71.3	108.0
SB6-B2	6	70.7	108.6
SB8-A1	8	72.8	109.3
SB8-A2	8	72.6	108.7
SB8-B1	8	75.5	109.9
SB8-B2	8	74.4	109.4
SB11-A1	11	70.7	-- ‡
SB11-A2	11	68.2	-- ‡
SB11-B1	11	63.7	-- ‡
SB11-B2	11	63.4	-- ‡

Notes: † Calculated using 0.2% offset method;
    ‡ Beyond capacity of testing machine
Units: 1.0 ksi = 6.89 MPa

Table 39. Spliced Longitudinal Reinforcing Bar Geometric Properties.

Rebar Sample	Nominal Diameter (inch)	Weight (lb/ft)	Rib Height, h_f (inch)	Rib Spacing, s_r (inch)	Sum of Gaps, $\Sigma gaps$ (inch)	Relative Rib Area, R_r	Transverse Rib Angle, β (degrees)
SB4-A	0.50	0.64	0.0282	0.322	0.209	0.0759	60.4
SB4-B	0.50	0.64	0.0298	0.323	0.209	0.0800	60.2
SB6-A1	0.75	1.47	0.0506	0.480	0.288	0.0924	60.7
SB6-A2	0.75	1.47	0.0517	0.479	0.309	0.0937	60.9
SB6-B1	0.75	1.44	0.0518	0.478	0.261	0.0963	60.2
SB6-B2	0.75	1.44	0.0480	0.479	0.273	0.0886	60.0
SB8-A1	1.00	2.57	0.0556	0.619	0.390	0.0787	61.6
SB8-A2	1.00	2.59	0.0578	0.618	0.377	0.0823	59.7
SB8-B1	1.00	2.59	0.0584	0.630	0.355	0.0822	60.2
SB8-B2	1.00	2.59	0.0588	0.629	0.347	0.0831	60.1
SB11-A1	1.41	5.13	0.0847	0.872	0.447	0.0874	56.8
SB11-A2	1.41	5.13	0.0797	0.866	0.462	0.0824	57.4
SB11-B1	1.41	5.18	0.0814	0.875	0.513	0.0823	60.8
SB11-B2	1.41	5.19	0.0831	0.876	0.517	0.0838	61.3

Units: 1.0 inch = 25.4 mm, 1.0 lb/ft = 14.59 N/m
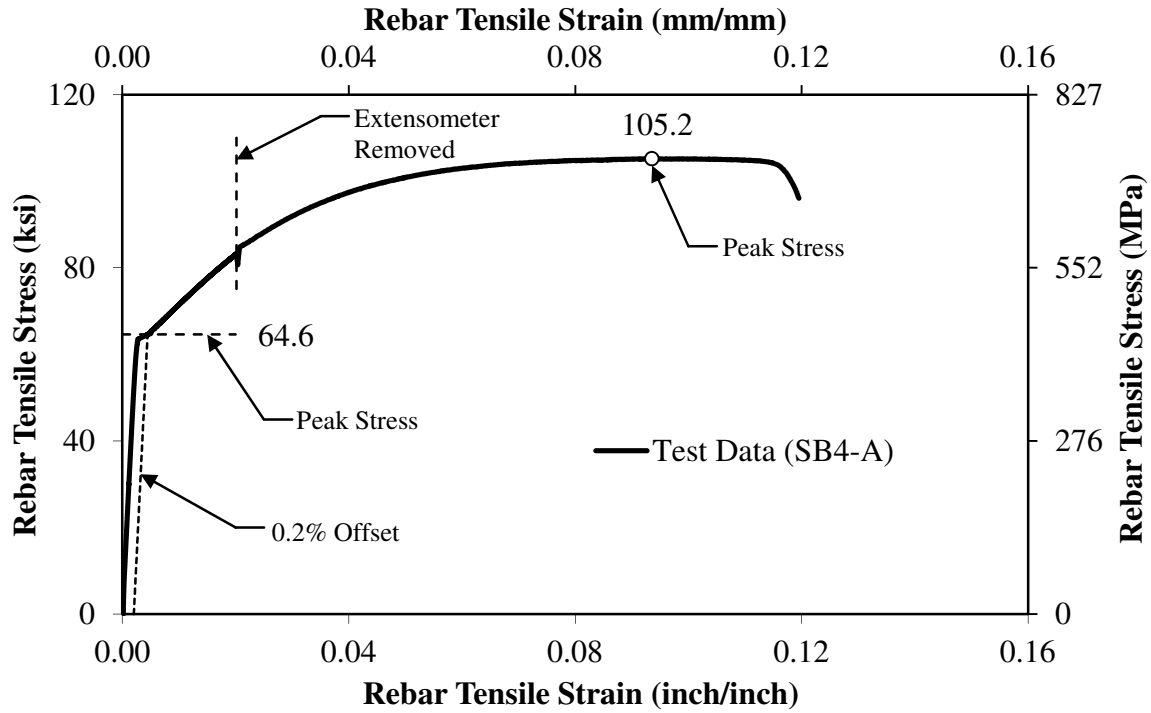
Figure 119. Graph. Measured Stress-Strain Relationship for #4 Longitudinal Splice Beam Specimen Reinforcing Bar – Coupon 1.
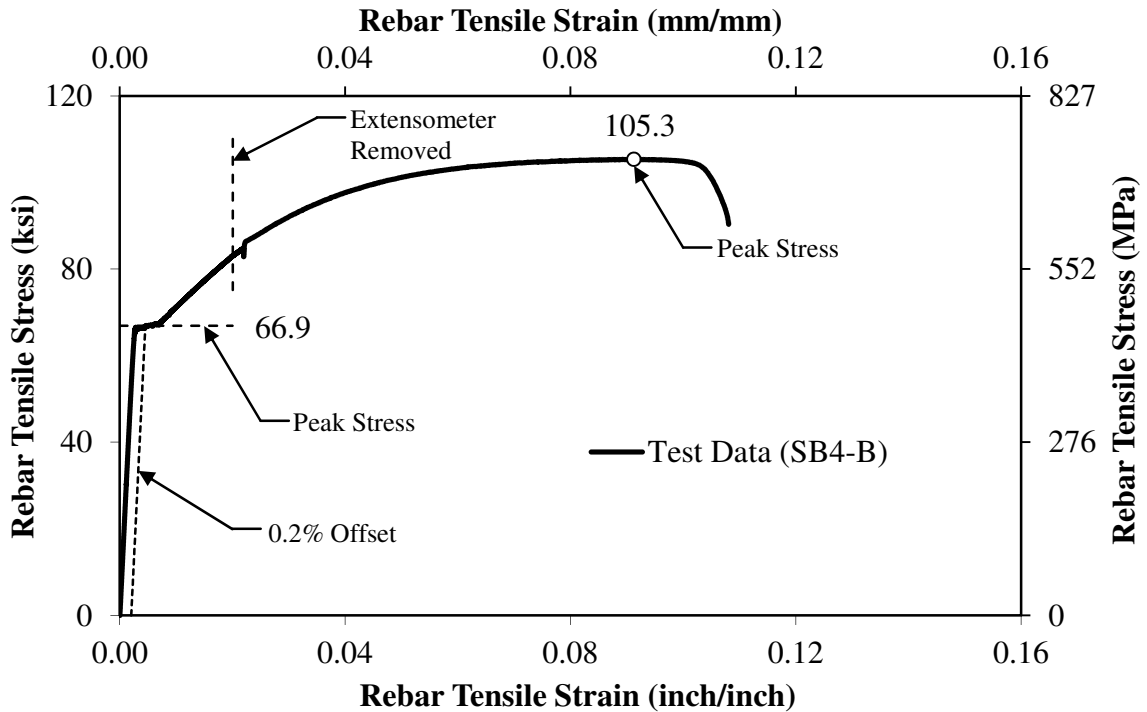
Figure 120. Graph. Measured Stress-Strain Relationship for #4 Longitudinal Splice Beam Specimen Reinforcing Bar – Coupon 2.
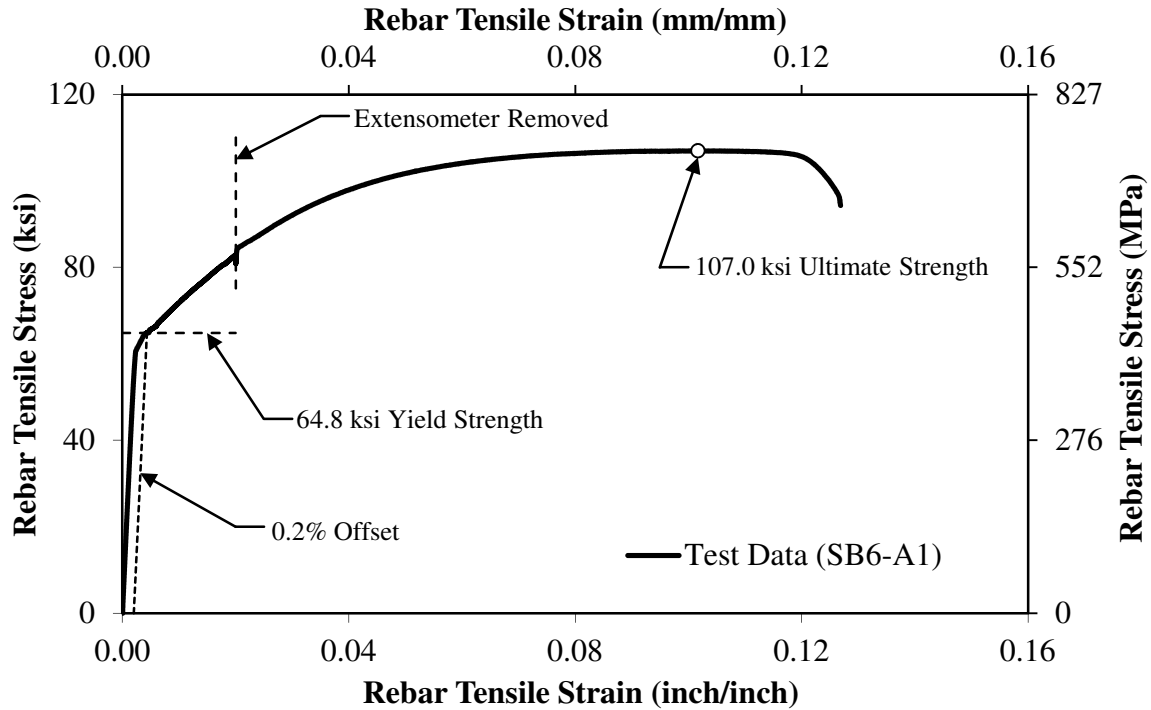
Figure 121. Graph. Measured Stress-Strain Relationship for #6 Longitudinal Splice Beam Specimen Reinforcing Bar – Sample 1, Coupon 1.
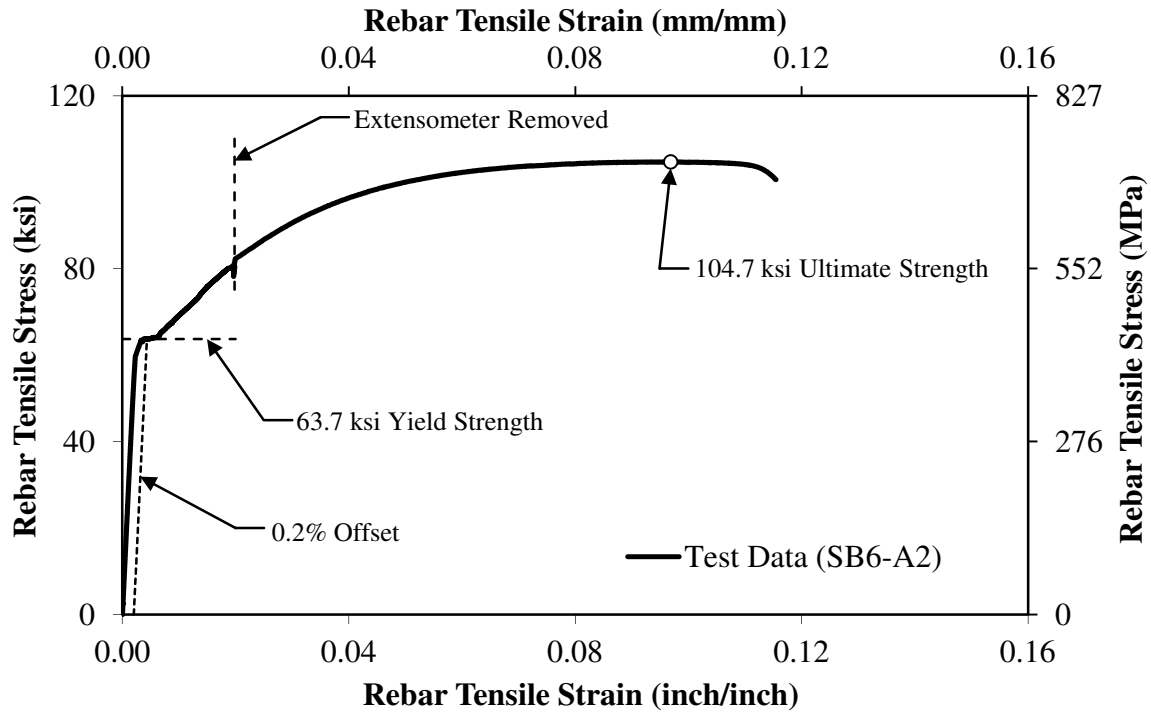
Figure 122. Graph. Measured Stress-Strain Relationship for #6 Longitudinal Splice Beam Specimen Reinforcing Bar – Sample 1, Coupon 2.
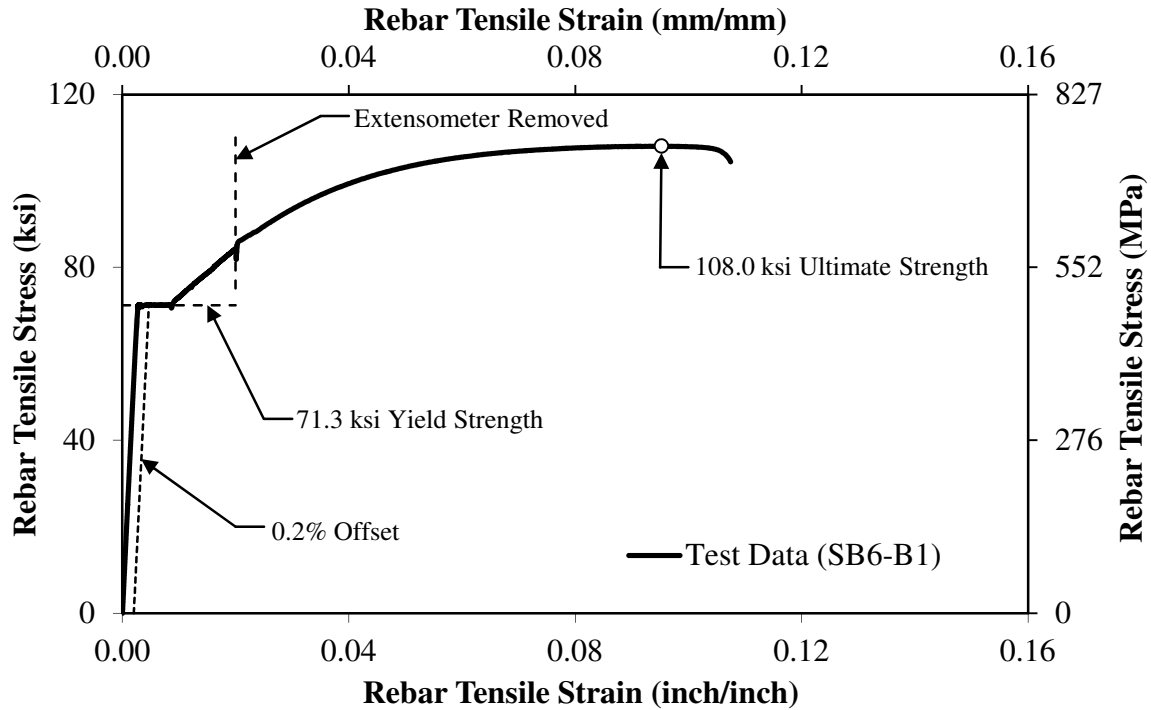
Figure 123. Graph. Measured Stress-Strain Relationship for #6 Longitudinal Splice Beam Specimen Reinforcing Bar – Sample 2, Coupon 1.
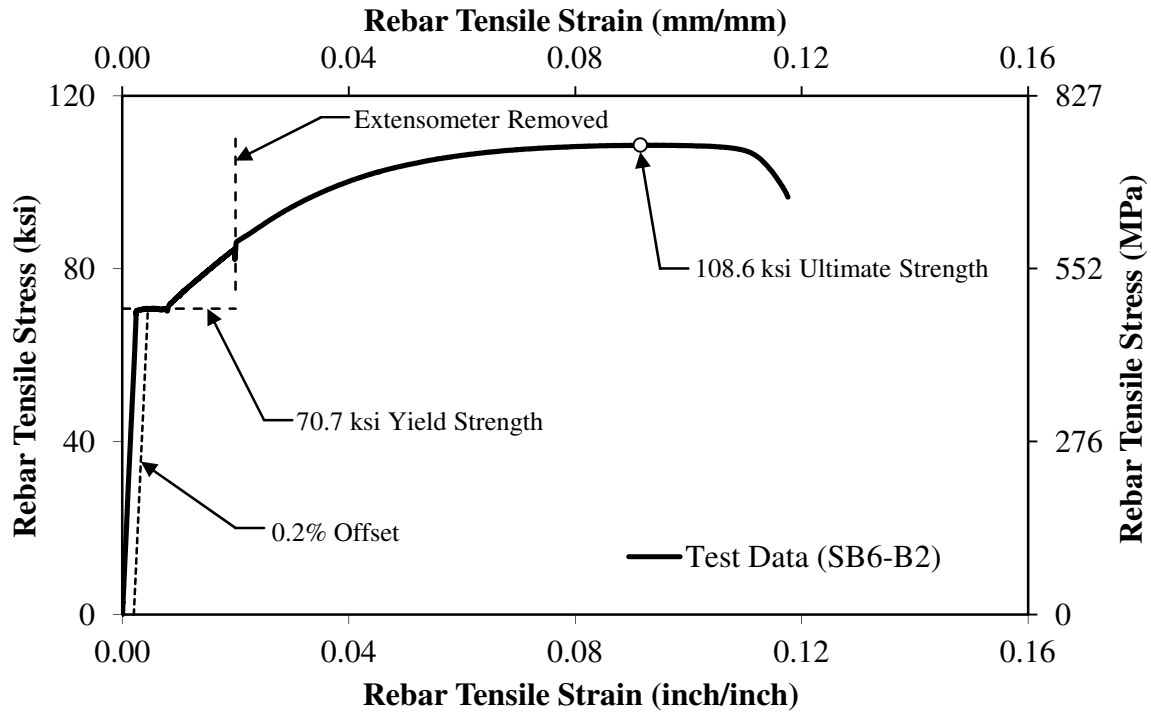
Figure 124. Graph. Measured Stress-Strain Relationship for #6 Longitudinal Splice Beam Specimen Reinforcing Bar – Sample 2, Coupon 2.
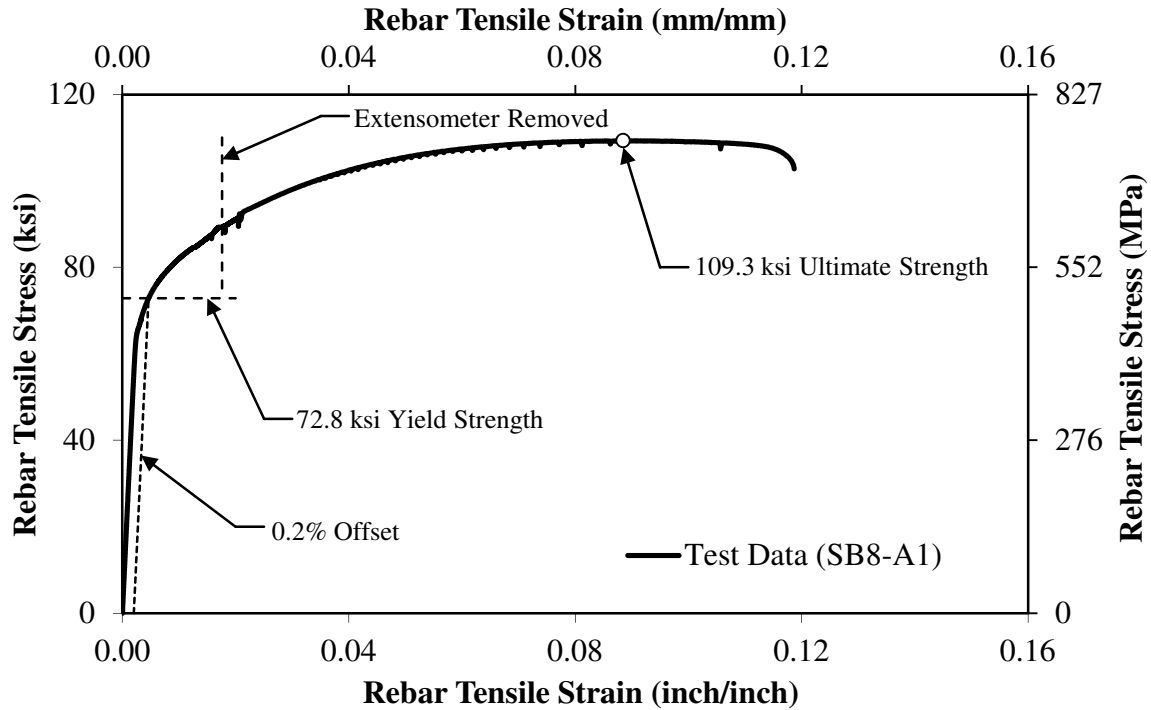
Figure 125. Graph. Measured Stress-Strain Relationship for #8 Longitudinal Splice Beam Specimen Reinforcing Bar – Sample 1, Coupon 1.
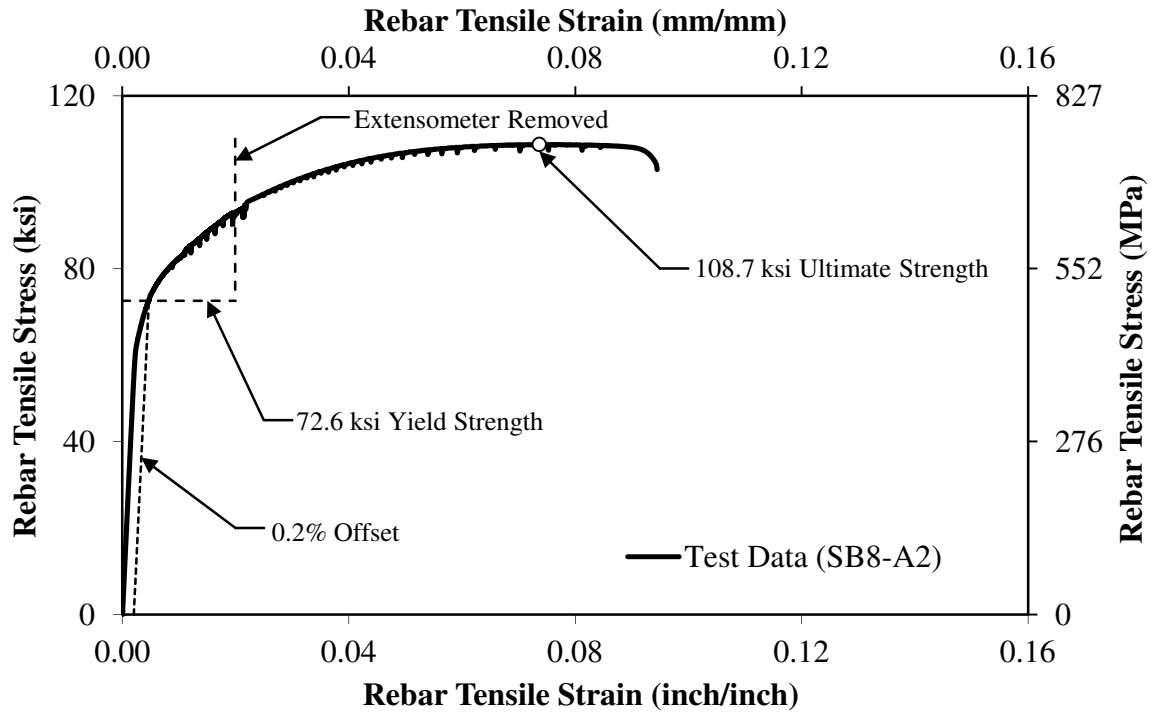
Figure 126. Graph. Measured Stress-Strain Relationship for #8 Longitudinal Splice Beam Specimen Reinforcing Bar – Sample 1, Coupon 2.
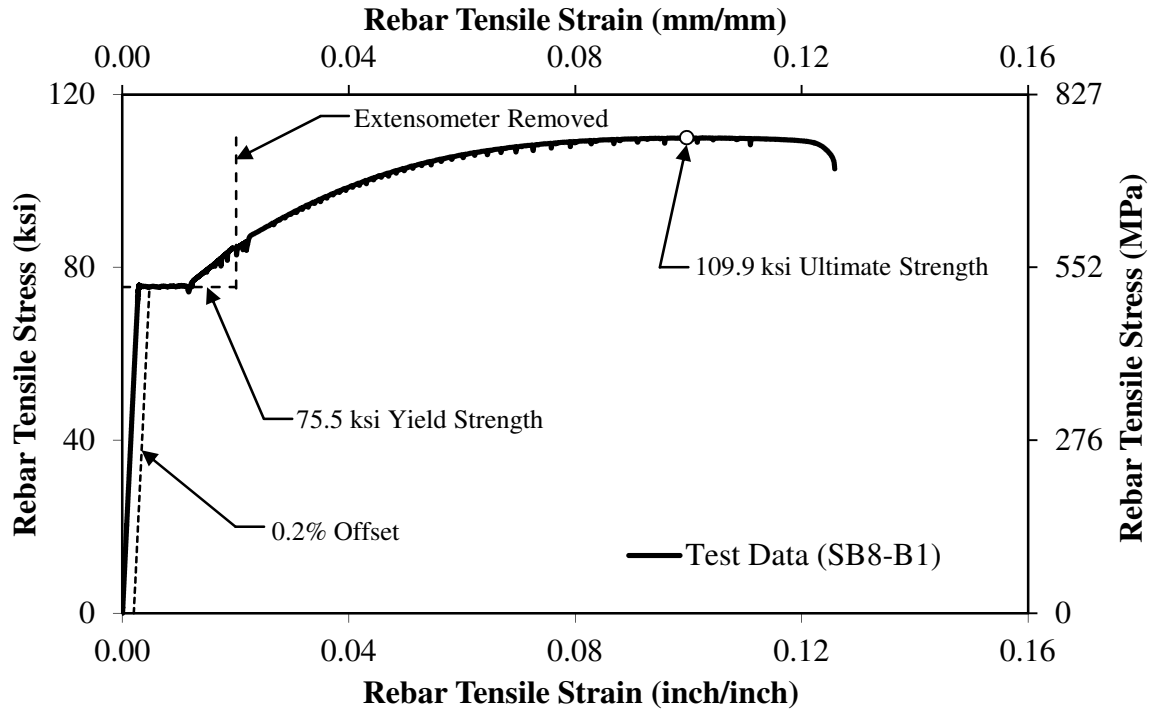
Figure 127. Graph. Measured Stress-Strain Relationship for #8 Longitudinal Splice Beam Specimen Reinforcing Bar – Sample 2, Coupon 1.
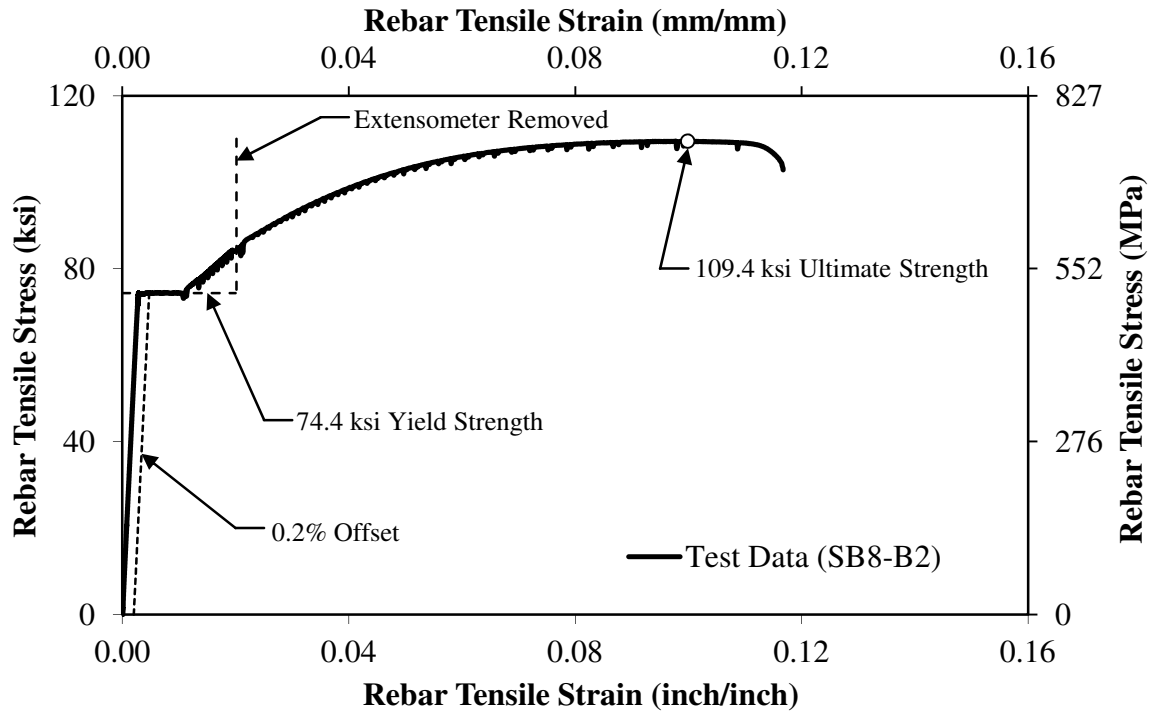
Figure 128. Graph. Measured Stress-Strain Relationship for #8 Longitudinal Splice Beam Specimen Reinforcing Bar – Sample 2, Coupon 2.
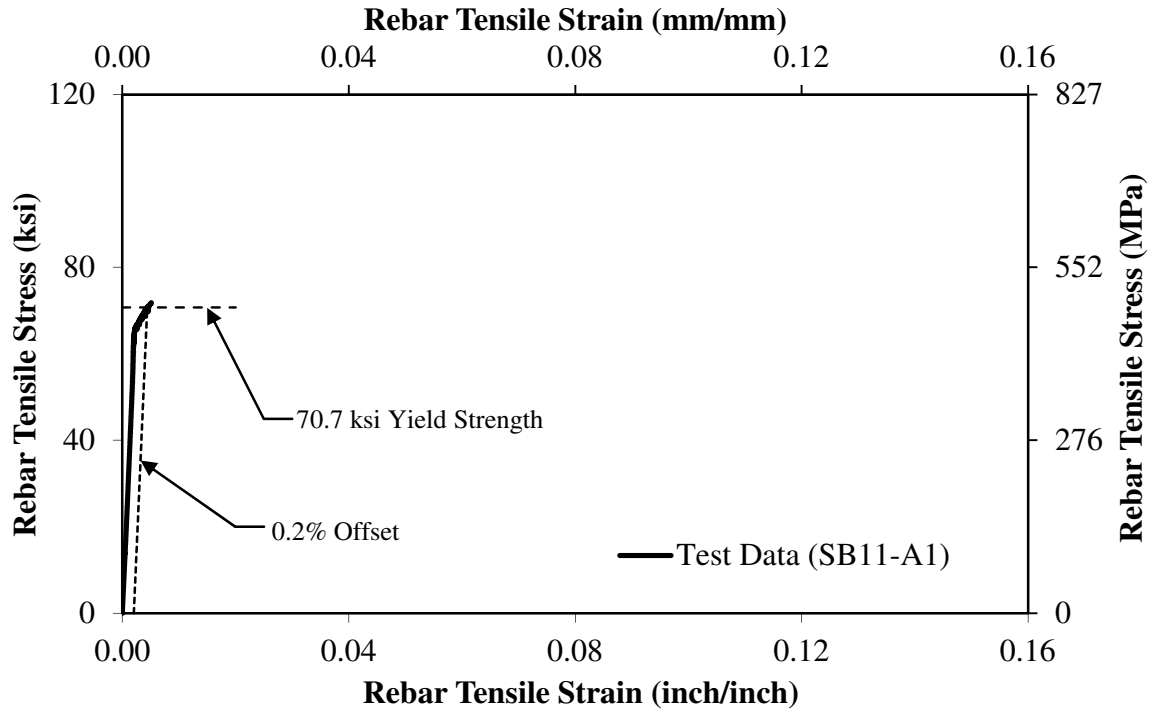
Figure 129. Graph. Measured Stress-Strain Relationship for #11 Longitudinal Splice Beam Specimen Reinforcing Bar – Sample 1, Coupon 1.
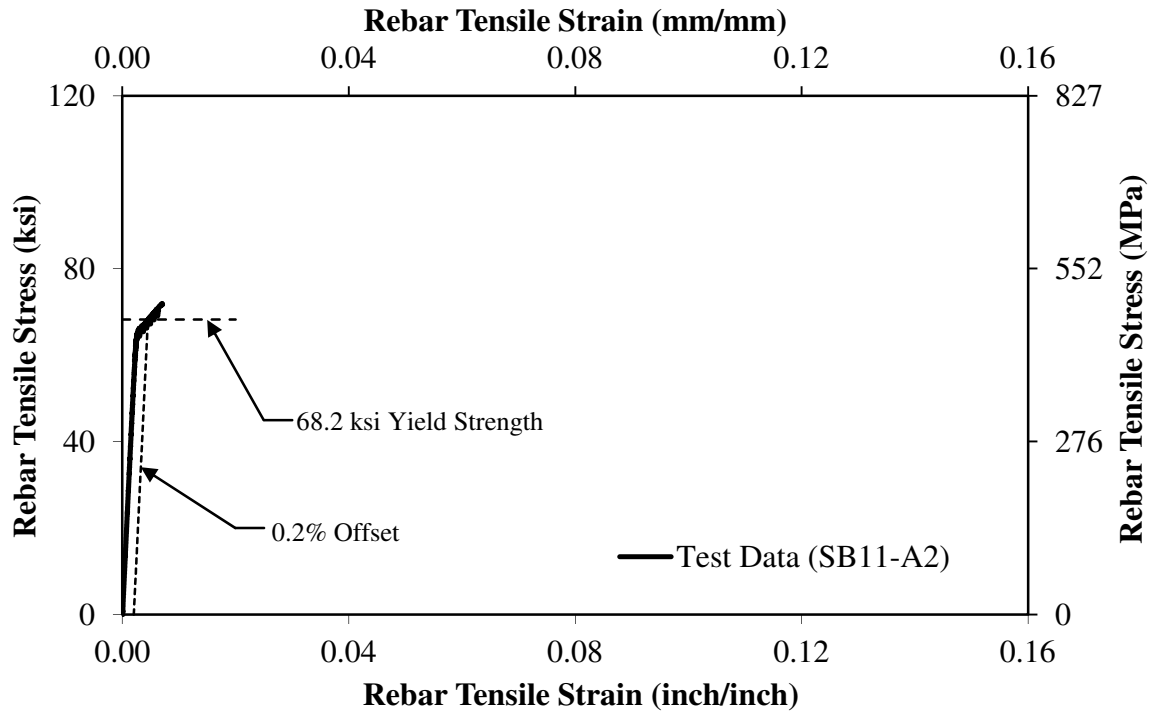
Figure 130. Graph. Measured Stress-Strain Relationship for #11 Longitudinal Splice Beam Specimen Reinforcing Bar – Sample 1, Coupon 2.
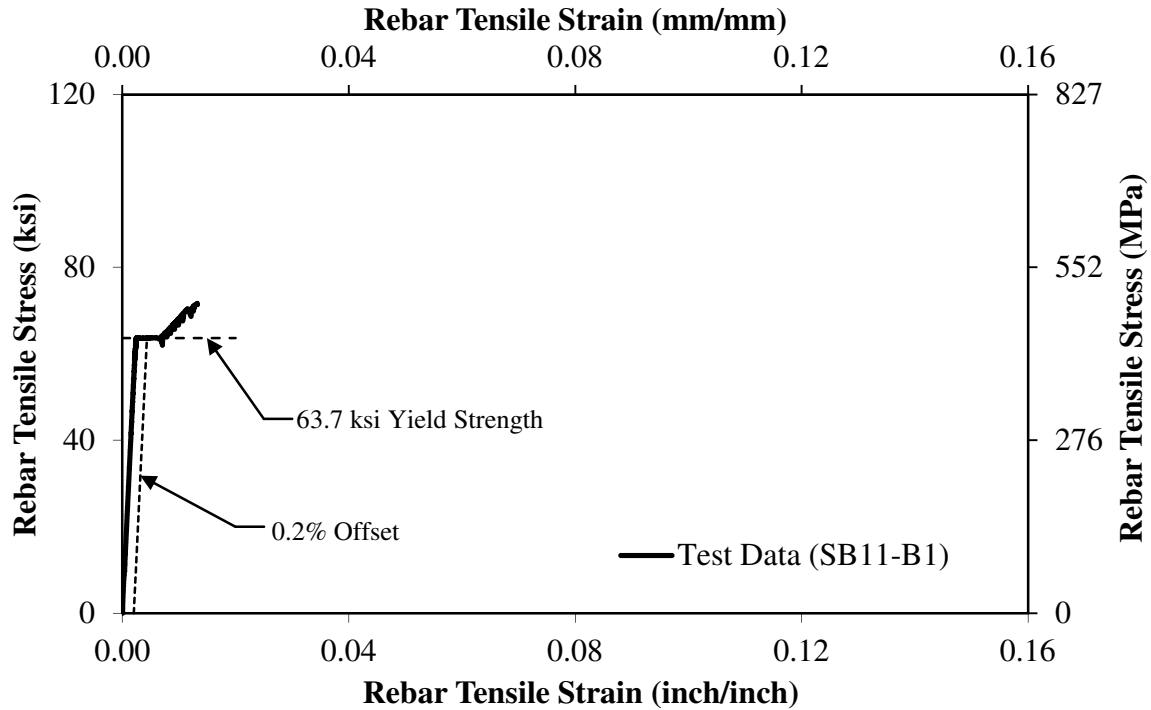
Figure 131. Graph. Measured Stress-Strain Relationship for #11 Longitudinal Splice Beam Specimen Reinforcing Bar – Sample 2, Coupon 1.
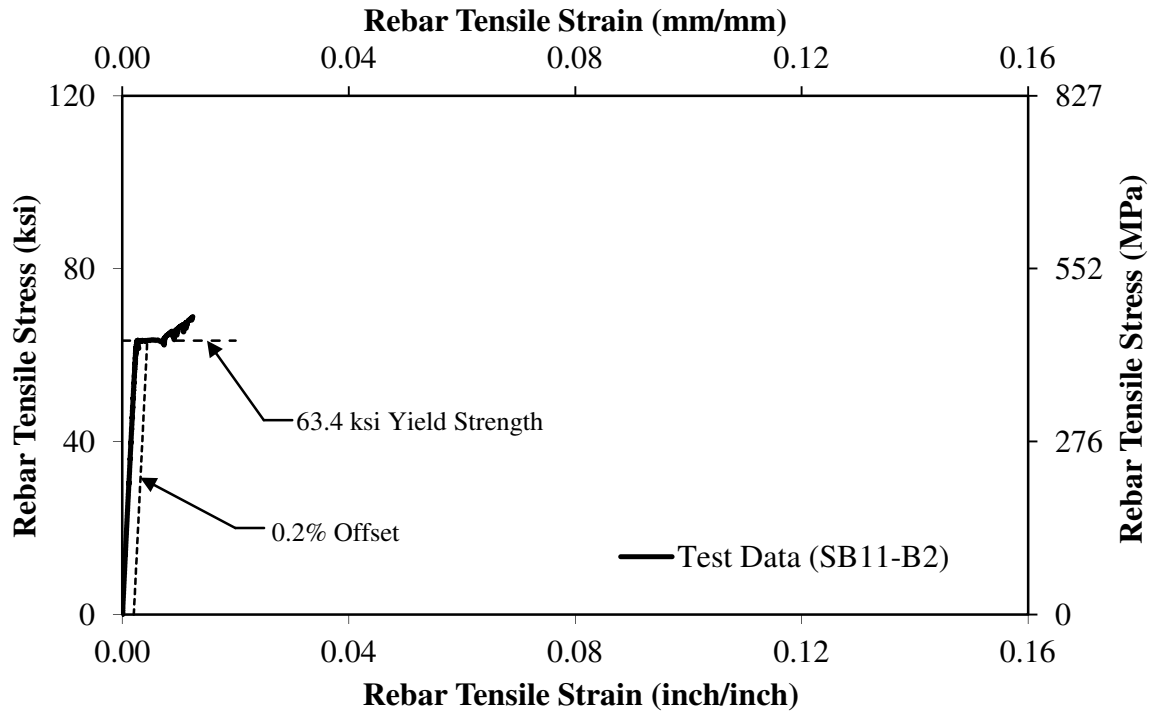
Figure 132. Graph. Measured Stress-Strain Relationship for #11 Longitudinal Splice Beam Specimen Reinforcing Bar – Sample 2, Coupon 2.

Table 40. Measured Splice Beam Specimen Geometry and Reinforcement Strain.

Specimen Name	ℓ_s (inch)	d_b (inch)	c_{so} (inch)	c_{si} (inch)	c_b (inch)	b (inch)	h (inch)	L_c (inch)	$\varepsilon_{sL,max}$[†]	$\varepsilon_{sT,max}$[†]
D4-SN	12.00	0.50	0.536	0.471	0.469	5.90	18.16	60.00	2489	--
D4-LN	15.94	0.50	0.540	0.487	0.534	5.92	18.14	59.25	7249	--
D6-SN	16.00	0.75	0.791	0.692	0.748	8.85	18.07	60.00	1589	--
D6-LN	24.00	0.75	0.719	0.712	0.834	8.86	18.08	60.75	1995	--
A6-SN	16.00	0.75	0.724	0.734	0.573	8.98	17.94	59.88	1646	--
B6-SN	15.94	0.75	0.797	0.679	0.574	8.98	18.24	59.50	2018	--
C6-SN	16.00	0.75	0.818	0.682	0.606	8.95	18.20	59.38	1751	--
A6-LN	24.00	0.75	0.820	0.726	0.612	9.05	18.19	58.88	2174	--
B6-LN	24.00	0.75	0.777	0.746	0.833	9.04	18.14	59.81	2338	--
C6-LN	24.00	0.75	0.917	0.638	0.615	9.02	18.14	60.25	1840	--
A6-ST	16.00	0.75	0.928	0.636	0.751	9.01	18.16	60.00	2630	1338
B6-ST	15.79	0.75	0.876	0.659	0.969	9.04	18.31	59.63	11424	1592
C6-ST	16.00	0.75	1.015	0.586	1.004	9.00	18.16	59.75	2639	523
A6-LT	23.94	0.75	0.944	0.608	0.884	9.07	18.13	59.63	16422	1294
B6-LT	23.83	0.75	0.940	0.650	0.669	9.09	18.06	59.81	14390	1037
C6-LT	24.00	0.75	0.951	0.649	0.905	9.04	18.17	59.25	14965	1835
A8-SN	23.79	1.00	1.141	0.943	0.901	12.06	18.19	71.75	2219	--
B8-SN	23.81	1.00	1.075	0.919	0.909	12.05	18.27	71.75	2250	--
C8-SN	23.71	1.00	1.076	0.965	0.915	12.01	18.29	71.25	1943	--
A8-LN	31.88	1.00	1.159	0.929	0.891	12.04	18.18	71.75	3138	--
B8-LN	31.83	1.00	1.070	0.968	0.884	12.01	18.22	71.88	2397	--
C8-LN	32.00	1.00	1.040	0.977	1.015	11.99	18.27	71.63	2854	--
A8-ST	24.00	1.00	1.099	0.887	0.883	12.01	18.06	71.63	3670	1445
B8-ST	23.96	1.00	1.127	0.868	1.031	11.98	18.21	71.38	2880	1190
C8-ST	23.96	1.00	1.092	0.877	0.825	11.98	18.23	71.88	13291	1136
A8-LT	32.10	1.00	1.077	1.444	0.876	12.01	18.17	71.75	4534	986
B8-LT	32.13	1.00	1.177	0.907	0.959	11.98	18.16	71.94	19157	1457
C8-LT	32.25	1.00	1.049	0.976	0.974	12.00	18.26	71.63	24409	1060
A11-SN	31.98	1.41	1.529	1.591	1.265	17.88	18.20	83.88	1743	--
B11-SN	31.94	1.41	1.667	1.540	1.376	17.96	18.26	83.63	2037	--
C11-SN	31.81	1.41	1.594	1.569	1.108	17.93	18.34	83.88	1387	--
A11-LN	47.73	1.41	1.586	1.602	1.079	18.04	18.26	83.75	1877	--
B11-LN	47.73	1.41	1.579	1.608	1.075	18.05	18.16	83.75	2243	--
C11-LN	47.83	1.41	1.569	1.607	1.229	18.03	18.28	83.75	2022	--
A11-ST	32.00	1.41	1.500	1.610	1.127	17.90	18.10	83.63	2333	1353
B11-ST	31.96	1.41	1.559	1.586	0.981	17.92	18.15	83.88	5180	1056
C11-ST	32.00	1.41	1.559	1.582	1.320	17.91	18.23	83.75	2155	1221
A11-LT	47.79	1.41	1.584	1.589	1.242	17.99	18.03	83.88	8674	1379
B11-LT	48.00	1.41	1.538	1.604	1.411	17.95	18.22	83.75	15227	1369
C11-LT	48.00	1.41	1.583	1.575	1.300	17.93	18.21	84.00	5325	1430

Units: 1.0 inch = 25.4 mm

Note: [†] Maximum measured strain in longitudinal reinforcement ($\varepsilon_{sL,max}$) in microstrain, and maximum measured strain in stirrups ($\varepsilon_{sT,max}$) in microstrain

APPENDIX B

This appendix contains figures showing the test-to-prediction ratios determined using descriptive and design expressions for bar stress that are compared to two expressions for normalized splice length. The descriptive expressions include the Orangun et al. Expression (Eq. 29) and Darwin and Zuo Expression (Eq. 30). The design expressions include the AASHTO LRFD Expression (Eq. 31), the ACI 318-11 Expression (Eq. 32), and the ACI 408-03 Expression (Eq. 33). The test-to-prediction ratios are compared to normalized splice length given by $\ell_s(c_{min}+0.5d_b)/A_b$ based on Zuo and Darwin, and $\ell_s/d_b(c_b+K_{tr})/d_b$ based on ACI 318-11.
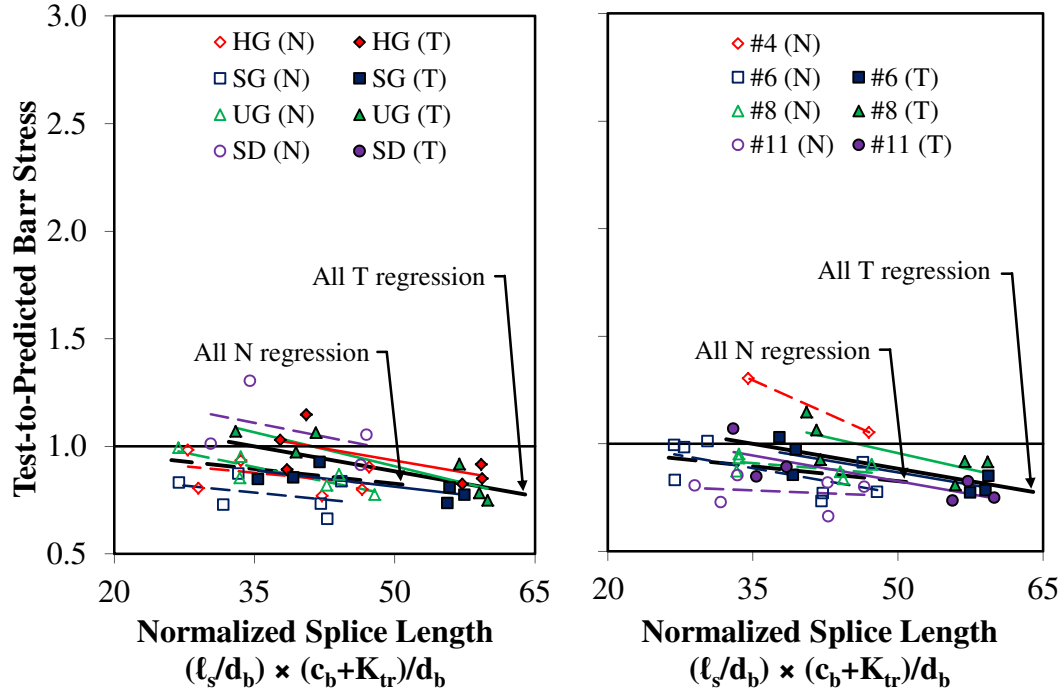
Figure 133. Graph. Bar Stress Test-to-Prediction Ratio Compared to Normalized Splice Length $(\ell_s/d_b) \times (c_b+K_{tr})/d_b$ for Orangun et al. Expression (Eq. 29) by Mix Design and Bar Size for Specimens without Stirrups (N) and with Stirrups (T).
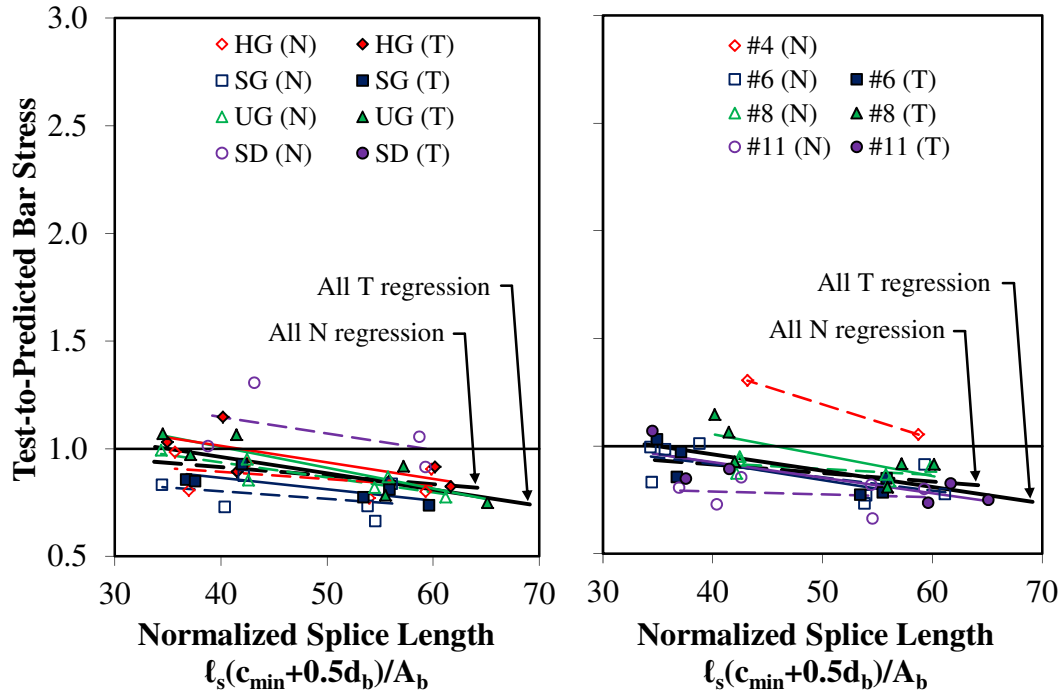
Figure 134. Graph. Bar Stress Test-to-Prediction Ratio Compared to Normalized Splice Length $\ell_s(c_{min}+0.5d_b)/A_b$ for Orangun et al. Expression (Eq. 29) by Mix Design and Bar Size for Specimens without Stirrups (N) and with Stirrups (T).
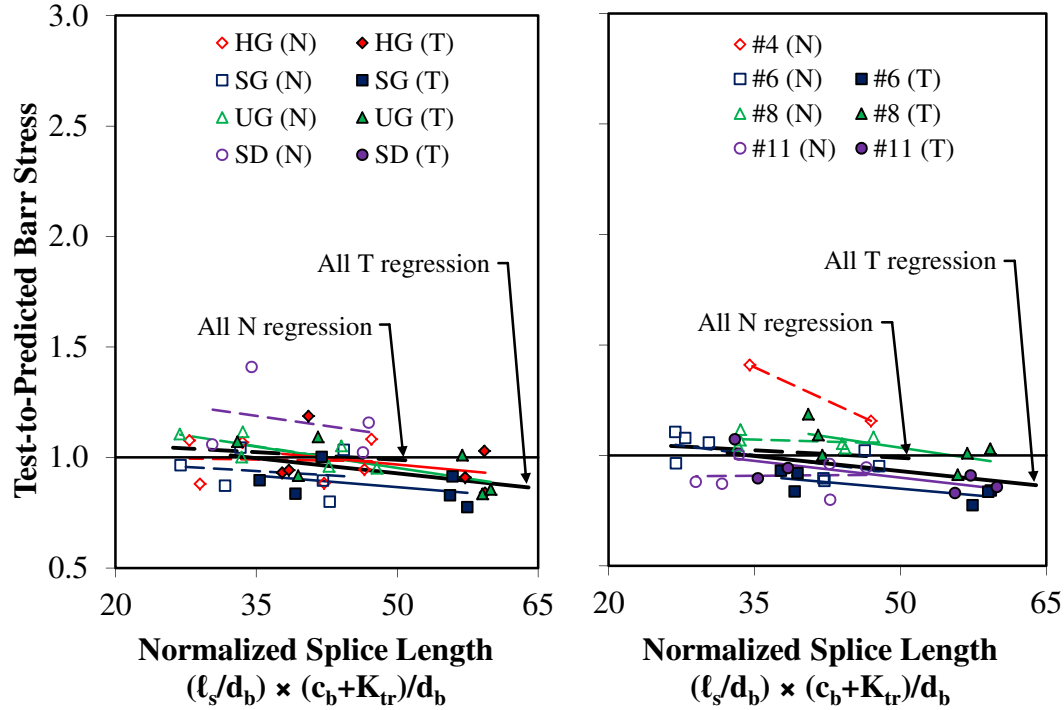
Figure 135. Graph. Bar Stress Test-to-Prediction Ratio Compared to Normalized Splice Length $(\ell_s/d_b) \times (c_b+K_{tr})/d_b$ for Darwin and Zuo Expression (Eq. 30) by Mix Design and Bar Size for Specimens without Stirrups (N) and with Stirrups (T).
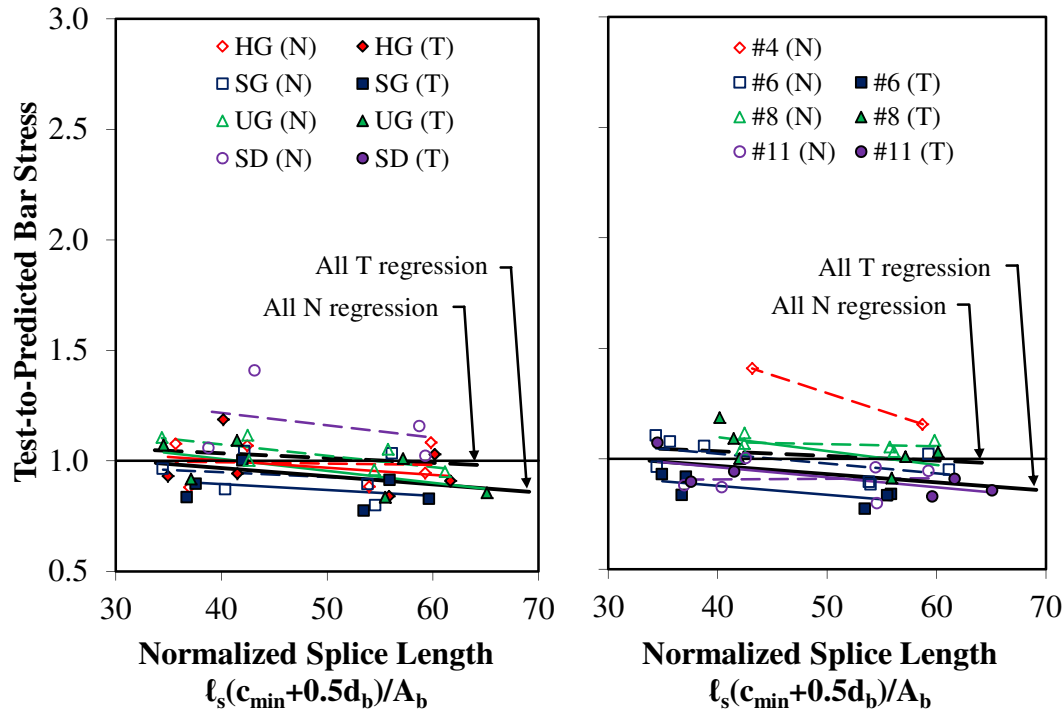
Figure 136. Graph. Bar Stress Test-to-Prediction Ratio Compared to Normalized Splice Length $\ell_s(c_{min}+0.5d_b)/A_b$ for Darwin and Zuo Expression (Eq. 30) by Mix Design and Bar Size for Specimens without Stirrups (N) and with Stirrups (T).
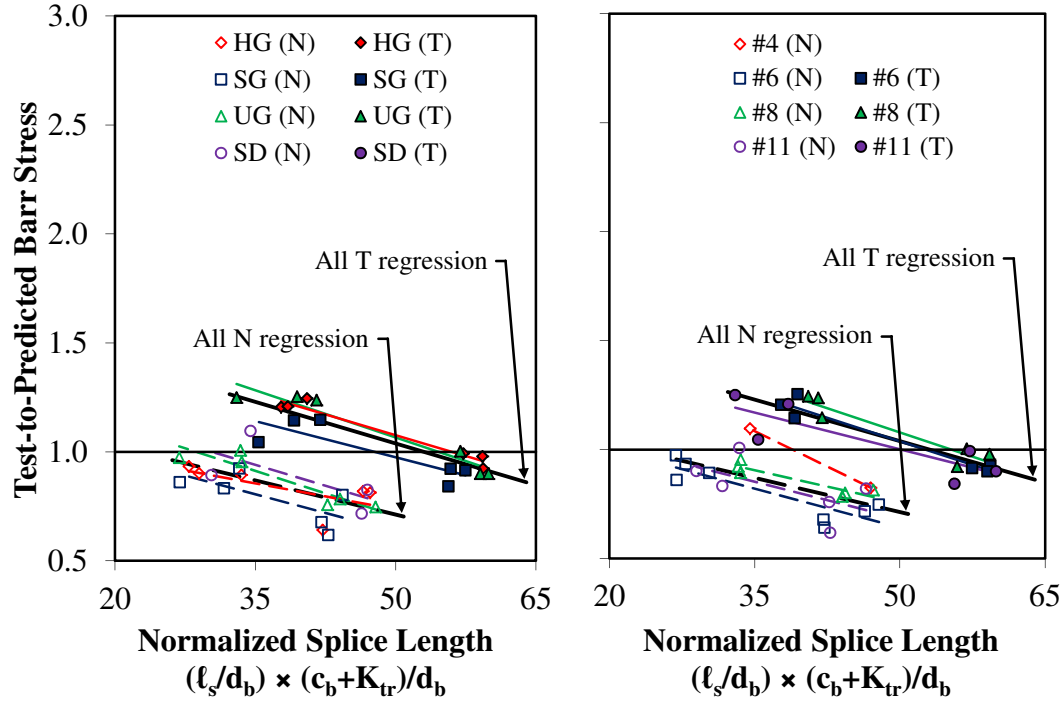
Figure 137. Graph. Bar Stress Test-to-Prediction Ratio Compared to Normalized Splice Length $(\ell_s/d_b) \times (c_b+K_{tr})/d_b$ for AASHTO LRFD Expression (Eq. 31) by Mix Design and Bar Size for Specimens without Stirrups (N) and with Stirrups (T).
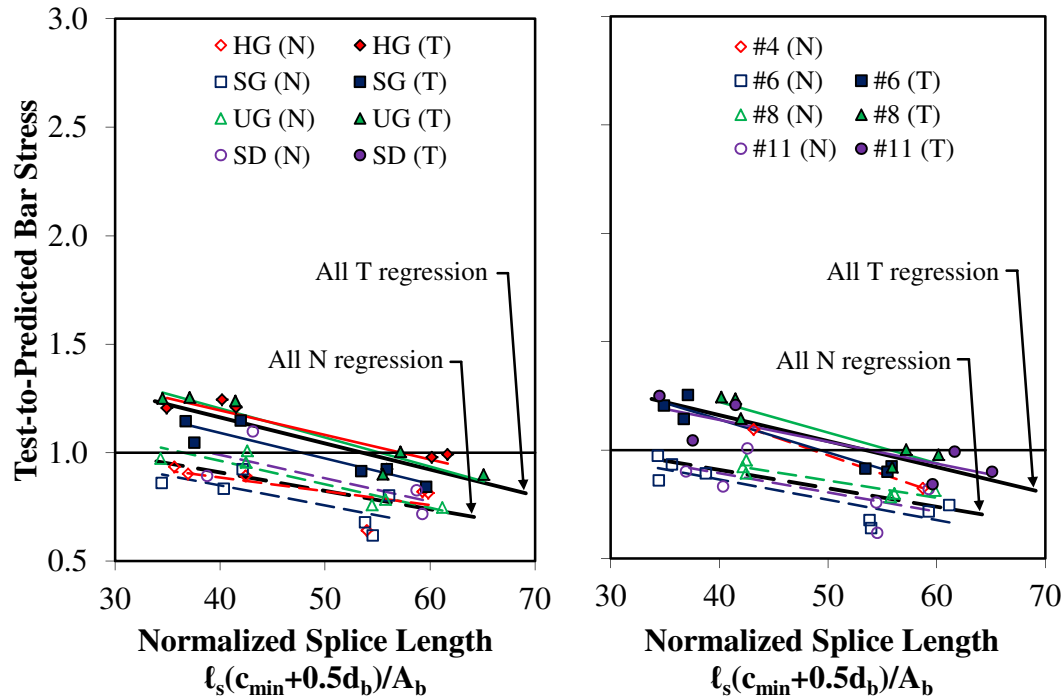
Figure 138. Graph. Bar Stress Test-to-Prediction Ratio Compared to Normalized Splice Length $\ell_s(c_{min}+0.5d_b)/A_b$ for AASHTO LRFD Expression (Eq. 31) by Mix Design and Bar Size for Specimens without Stirrups (N) and with Stirrups (T).
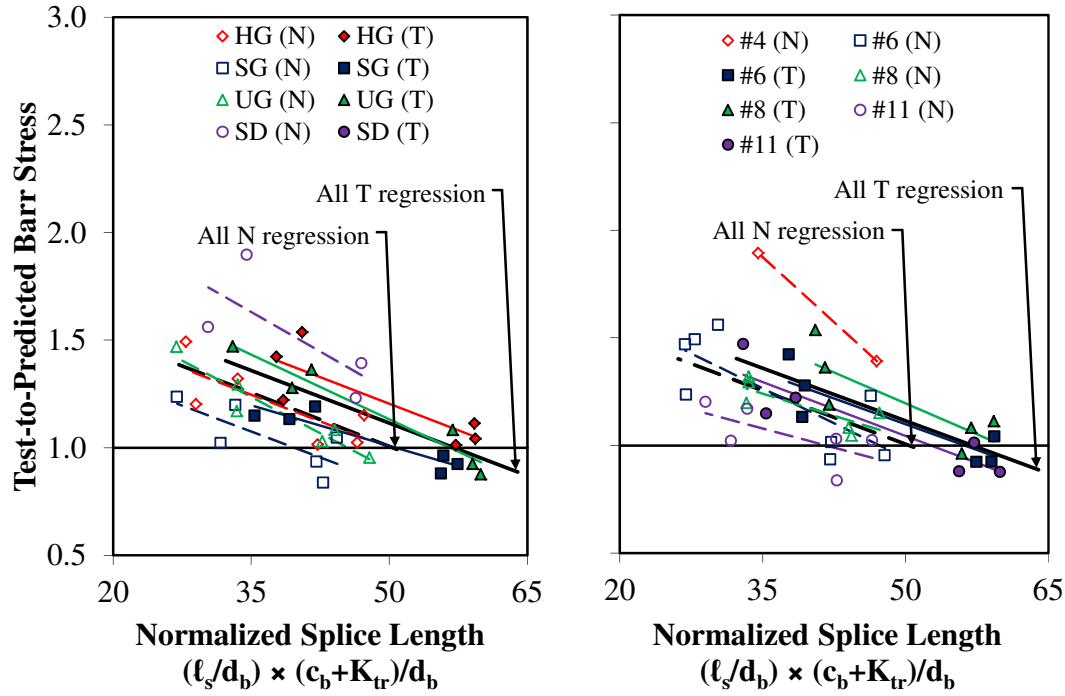
Figure 139. Graph. Bar Stress Test-to-Prediction Ratio Compared to Normalized Splice Length $(\ell_s/d_b) \times (c_b+K_{tr})/d_b$ for ACI 318-11 Expression (Eq. 32) by Mix Design and Bar Size for Specimens without Stirrups (N) and with Stirrups (T).
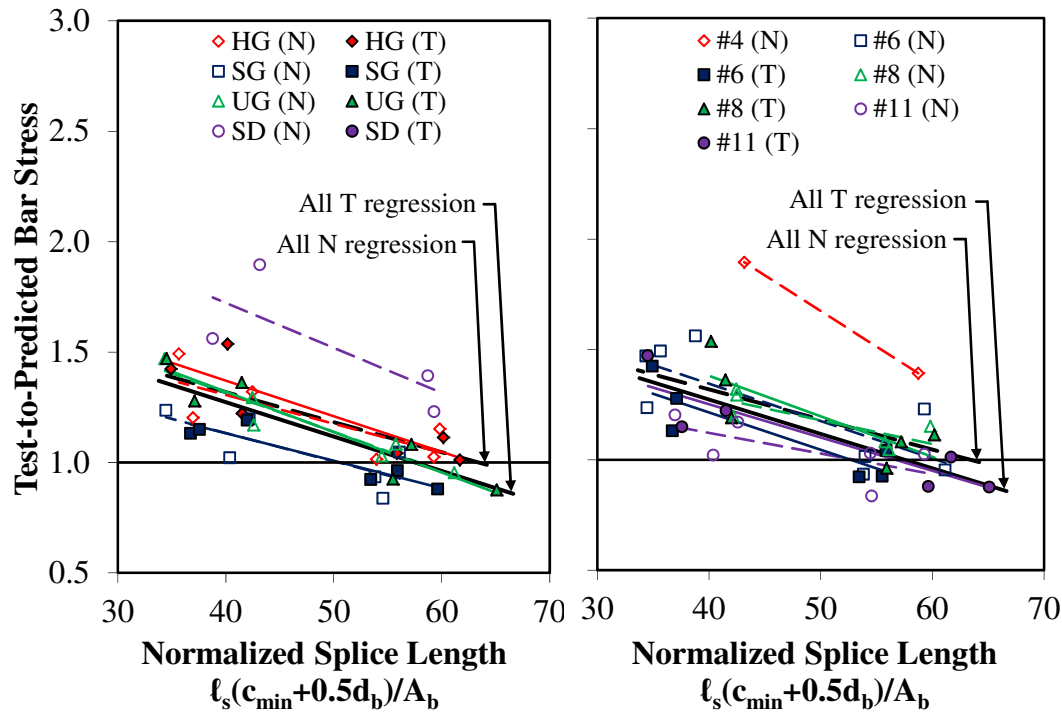
Figure 140. Graph. Bar Stress Test-to-Prediction Ratio Compared to Normalized Splice Length $\ell_s(c_{min}+0.5d_b)/A_b$ for ACI 318-11 Expression (Eq. 32) by Mix Design and Bar Size for Specimens without Stirrups (N) and with Stirrups (T).
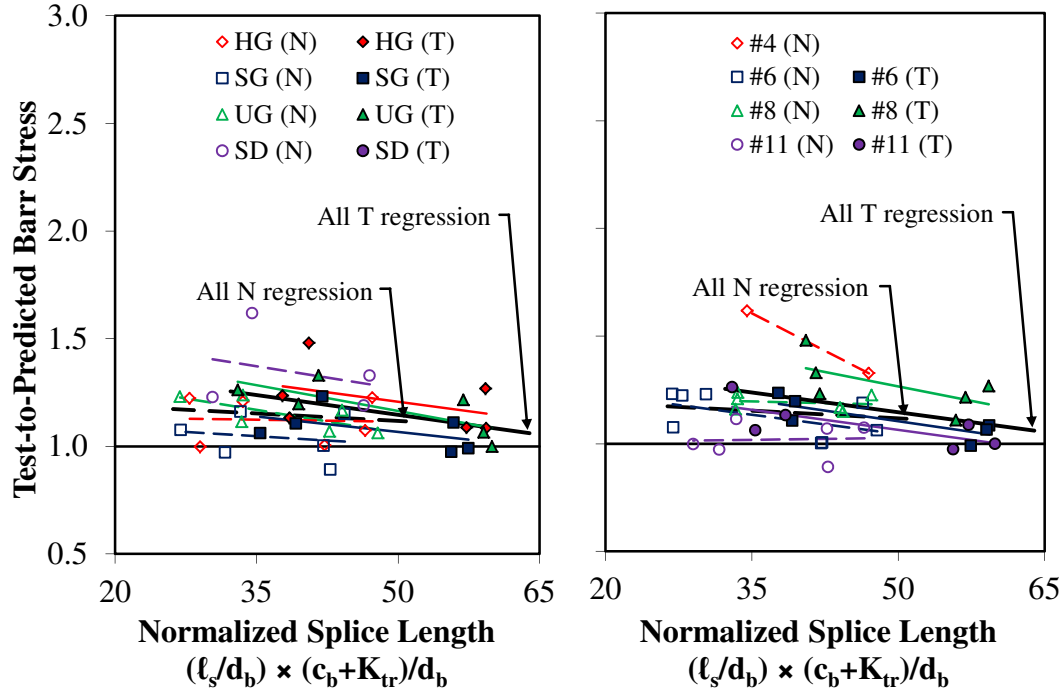
Figure 141. Graph. Bar Stress Test-to-Prediction Ratio Compared to Normalized Splice Length $(\ell_s/d_b)\times(c_b+K_{tr})/d_b$ for ACI 408-03 Expression (Eq. 33) by Mix Design and Bar Size for Specimens without Stirrups (N) and with Stirrups (T).
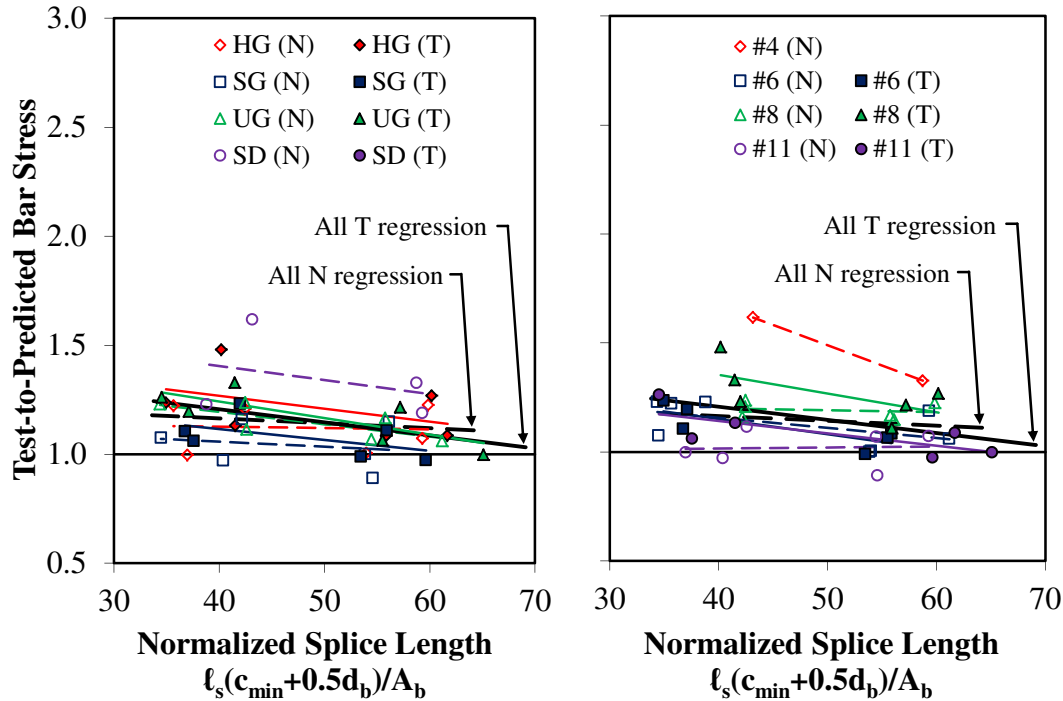
Figure 142. Graph. Bar Stress Test-to-Prediction Ratio Compared to Normalized Splice Length $\ell_s(c_{min}+0.5d_b)/A_b$ for ACI 408-03 Expression (Eq. 33) by Mix Design and Bar Size for Specimens without Stirrups (N) and with Stirrups (T).

APPENDIX C

In order to determine the effect of LWC on the development of bar stress, the LWC splice beam specimens in the TFHRC Database are compared to a subset of NWC splice beam specimens in the ACI Committee 408 Database that have similar parameters that are significant to the development of bar stress. This appendix contains a list of the selected specimens from the ACI Committee 408 Database that are used in the TFHRC Database.

Table 41. List of Selected NWC Splice Beam Specimens from the ACI Committee 408 Database in the TFHRC Mild Steel Development Length Database.

Reference	Specimen Names
Azizinamini, Pavel, Hatfield and Ghosh 1999 [15]	7, 39, 43, 46
Chamberlin 1956 [51]	SIV53, SIII23
Chinn, Ferguson, and Thompson 1955 [52]	D34, D12, D17, D19, D23, D24, D30, D4, D40, D25, D26, D35, D33
Choi, Hadje-Ghaffari, Darwin, and McCabe 1990 & 1991 [53,54]	1-5N0-12-0-U, 1-5N0-12-0-U, 2-6C0-12-0-U, 2-6S0-12-0-U, 3-8N0-16-0-U, 3-8S0-16-0-U, 4-11C0-24-0-U, 4-11S0-24-0-U
Darwin, Tholen, Idun, and Zuo 1996 [11]	1.1, 1.2, 1.3, 2.4, 2.5, 4.5, 6.5, 8.3, 10.2, 13.4, 14.3, 15.5, 16.2, 13.1, 13.2, 14.5, 14.6, 1.5, 1.6, 2.1, 2.2, 2.3, 3.4, 3.5, 4.1, 4.2, 4.4, 5.1, 5.2, 5.3, 5.4, 5.5, 5.6, 6.1, 6.2, 6.3, 6.4, 7.1, 7.6, 8.4, 9.1, 9.2, 9.3, 9.4, 10.3, 11.4, 14.1, 15.3, 15.4, 16.3, 16.4, 17.3, 17.4, 18.1, 18.3, 18.4
DeVries, Moehle, and Hester 1991 [55]	8G-22B-P9, 8N-18B-P9, 8G-16B-P9, 8G-18B-P9
Freguson and Breen 1965 [56]	8F36d, 8F36e, 8F36f, 8R18a, 8R24a, 8F36a, 8F36b, 8F36k, 8F39a, 8F42b, 8R42a, 11R24a, 11R30a
Hasan, Cleary, and Ramirez 1996 [57]	U7STAT
Hester, Salamizavaregh, Darwin, and McCabe 1991 & 1993 [58,59]	7-8C3-16-3-U, 4-8S3-16-2-U, 4-8S3-16-3-U, 5-8C3-16-2-U, 6-8C3-22 3/4-3-U, 1-8N3-16-2-U, 6-8C3-22 3/4-4-U, 5-8C3-16-3-U, 3-8S3-16-2-U, 2-8C3-16-2-U, 1-8N3-16-0-U, 2-8C3-16-0U, 3-8S3-16-0-U, 4-8S3-16-0-U, 5-8C3-16-0-U, 7-8C3-16-0-U, 6-8C3-22-0-U
Kadoriku 1994 [60]	PB-01, PB-02, PB-16, PB-19, PB-20, PB-21, PB-27, PB-31, PB-10, PB-16, PB-11
Rezansoff, Akanni, and Sparling 1993 [61]	1b, 1a, 7, 3a, 3b, 4b, 9, 10, 4a, 2a, 2b, 5a, 5b
Rezansoff, Konkankar and Fu 1991 [62]	20-6-2, 20-6-3, 20-6-1, 20-8-11, 20-8-9, 20-8-10, 20-8-1, 20-8-12, 20-8-2, 20-8-3, 20-8-6, 20-8-7, 20-8-8, 20-8-5, 20-8-4, 20-8-21, 20-8-13, 20-8-15, 20-8-18, 20-8-17, 20-11-8, 20-11-5, 20-11-6, 20-9-1, 20-9-2
Thompson, Jirsa, Breen, and Meinheit 1975 [63]	11-20-4/2/2-6/6-S5, 8-15-4/2/2-6/6-S5, 6-12-4/2/2-6/6, 8-18-4/3/2-6/6, 11-25-6/2/3-5/5, 11-30-4/2/4-6/6, 11-30-4/2/2.7/4/6, 11-45-4/1/2-6/6
Zekany, Neumann, Jirsa, and Breen 1981 [64]	11-40-B-A, 2-4.5-80-B, 2-5-40-B(4), 3-5-53-B, 2-4.5-53-B, 11-53-B, 11-40-B, 11-53-B-D, 3-5-40-B, 9-53-B, 9-53-B-N, N-N-80-B
Zuo and Darwin 1998 & 2000 [65,12]	19.1-B-S-U, 19.2-B-N-U, 20.6-B-S-U, 23a.5-B-S-U, 23a.6-B-S-U, 24.1-B-S-U, 25.1-B-S-U, 26.3-B-S-U, 26.5-B-S-U, 34.1-B-S-U, 34.2-B-N-U, 34.3-B-S-U, 34.4-B-N-U, 36.3-B-S-U, 36.4-B-N-U, 38.1-B-N-U, 38.2-B-S-U, 19.3-B-S-U, 19.4-B-N-U, 21.1-B-S-U, 21.3-B-S-U, 21.5-B-S-U, 23a.1-B-S-U, 23a.3-B-N-U, 23a.4-B-S-U, 23b.1-B-S-U, 26.1-B-S-U, 29.1-B-S-U, 29.2-B-S-U, 29.3-B-S-U, 29.4-B-S-U, 29.5-B-S-U, 29.6-B-S-U, 33.1-B-S-U, 33.2-B-S-U, 33.3-B-S-U, 33.4-B-S-U, 33.5-B-S-U, 33.6-B-S-U, 35.1-B-S-U, 35.3-B-S-U, 36.1-B-S-U, 36.2-B-S-U, 37.4-B-S-U, 38.3-B-S-U, 38.4-B-S-U, 38.5-B-S-U, 38.6-B-S-U, 41.1-B-S-U, 41.2-B-S-U, 41.3-B-S-U, 41.4-B-S-U, 41.5-B-N-U, 41.6-B-S-U

APPENDIX D

This appendix contains detailed tests results of the 40 high-strength LWC splice beams tested at TFHRC. Tables give the bar size, lap length, and size and spacing of stirrups along the splice. Tables also give the applied load, measured deflection, and measured reinforcement strain at cracking, yielding, and ultimate. Figures show the applied load versus measured deflection and measured reinforcement strain. Photographs show the progression of cracking along the splice at different levels of applied load and after failure.

Splice Beam A6-SN

Table 42. Test parameters for Splice Beam A6-SN.

Concrete Mix	Spliced Bar Size	Lap Length, inch (mm)	#3 (10M) Bar Transverse Reinforcement	Nominal Beam Cross-Section Dimensions (Width by Height), inch (mm)
Stalite	#6 (19M)	16 (410)	None	18 by 18 (460 by 460)

Table 43. Test data for Splice Beam A6-SN.

| Event	Average Jack Load, kips (kN)	Average Beam End Deflection, inch (mm)	Longitudinal Rebar Strain, microstrain		Transverse Rebar Strain, microstrain	
			Gage 1	Gage 2	Gage 1	Gage 2
Flexural cracking	7.1 (31)	0.05 (1.2)	167	178	N/A	N/A
Top splitting crack	12.1 (54)	0.15 (3.7)	855	913	N/A	N/A
Side splitting crack	N/A	N/A	N/A	N/A	N/A	N/A
Long. rebar yield	N/A	N/A	N/A	N/A	N/A	N/A
Ultimate	19.4 (86)	0.3 (7.7)	1599	1646	N/A	N/A

Notes:
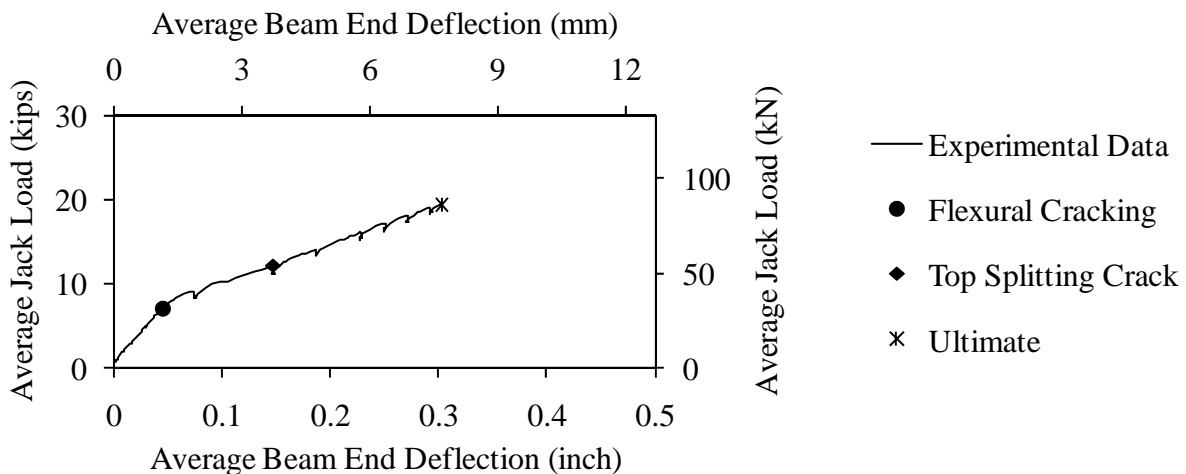
Figure 143. Graph. Load versus deflection for Beam A6-SN.
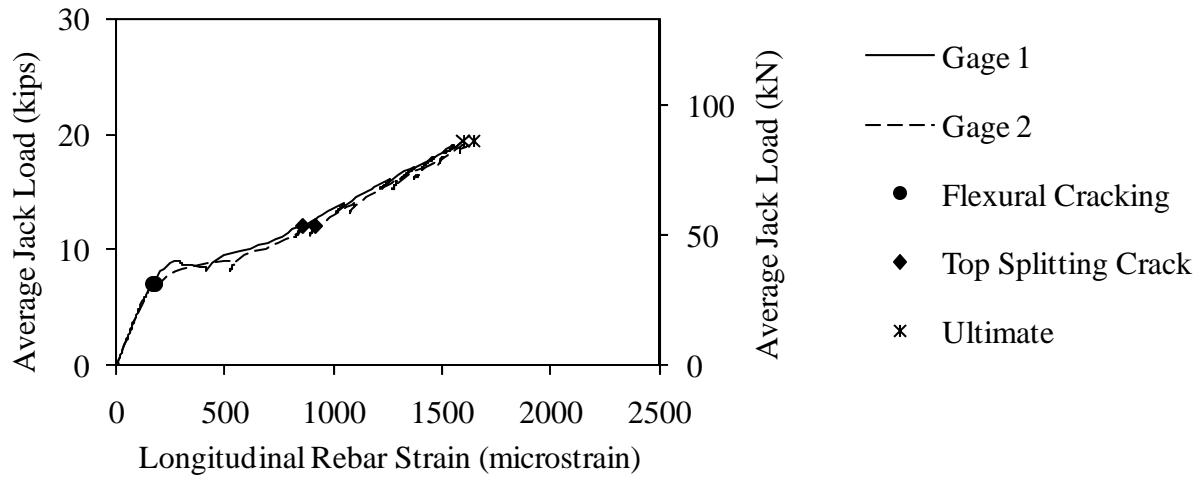
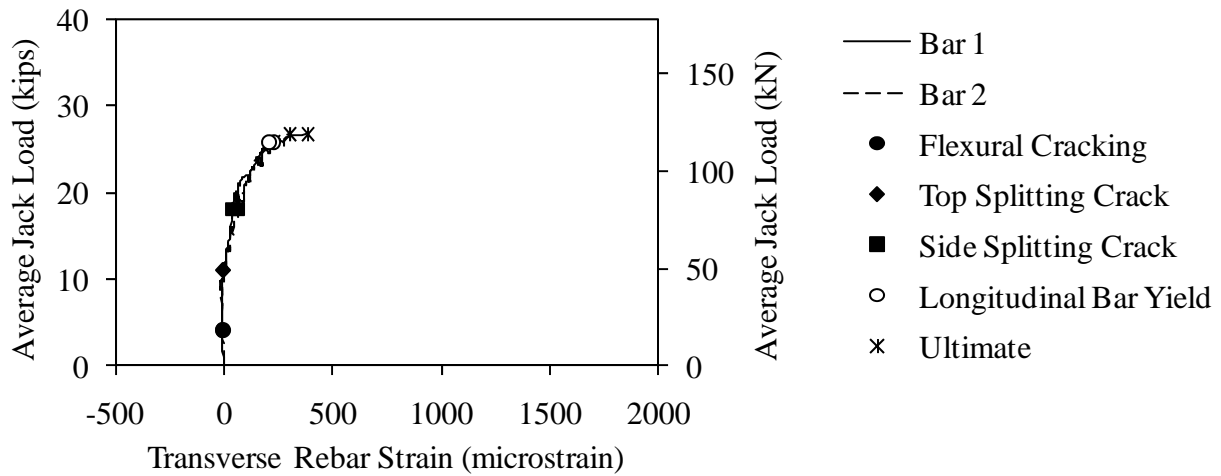**Figure 144. Graph. Load versus longitudinal rebar strain for Beam A6-SN.**
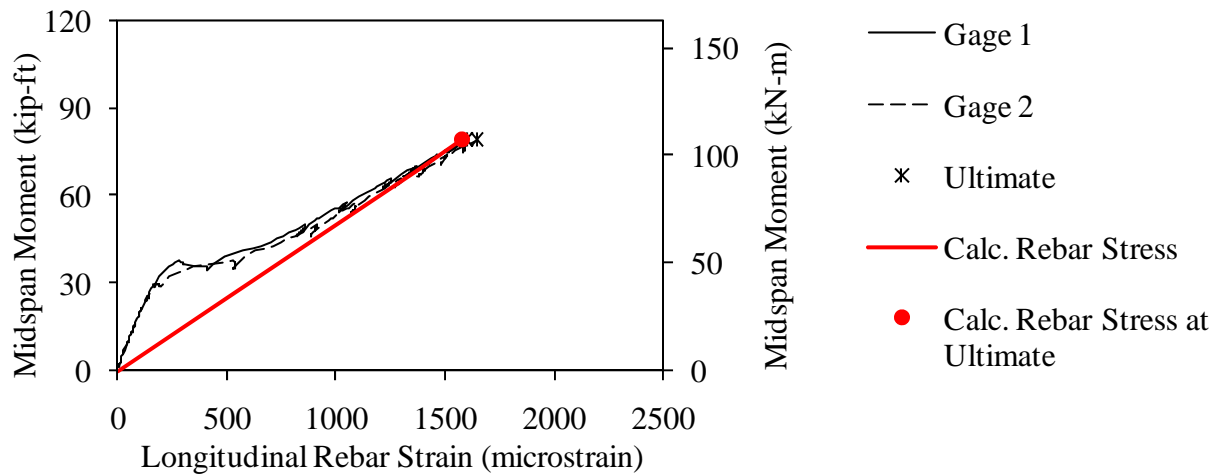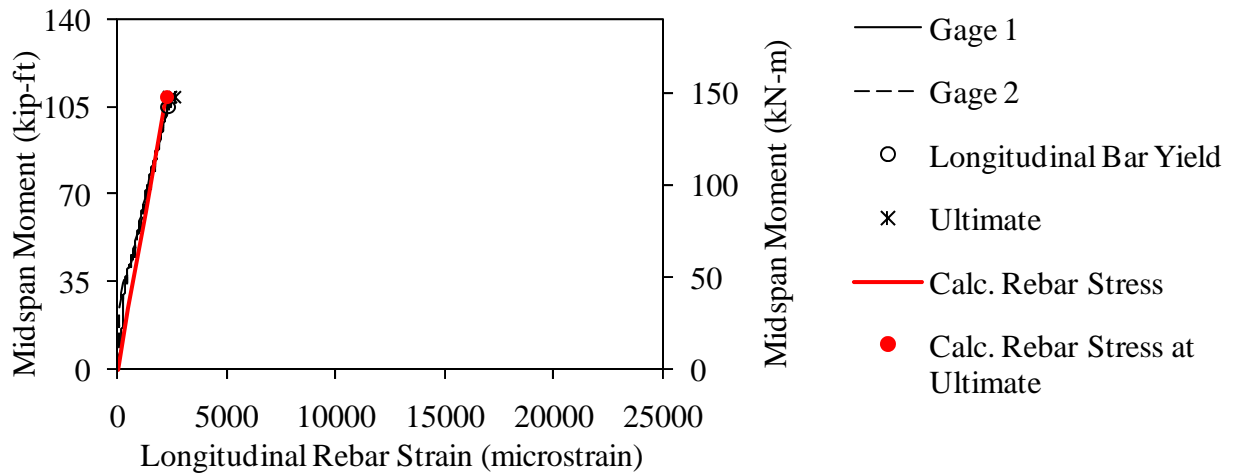

**Figure 145. Graph. Measured and predicted midspan moment versus longitudinal rebar strain for Beam A6-SN.**
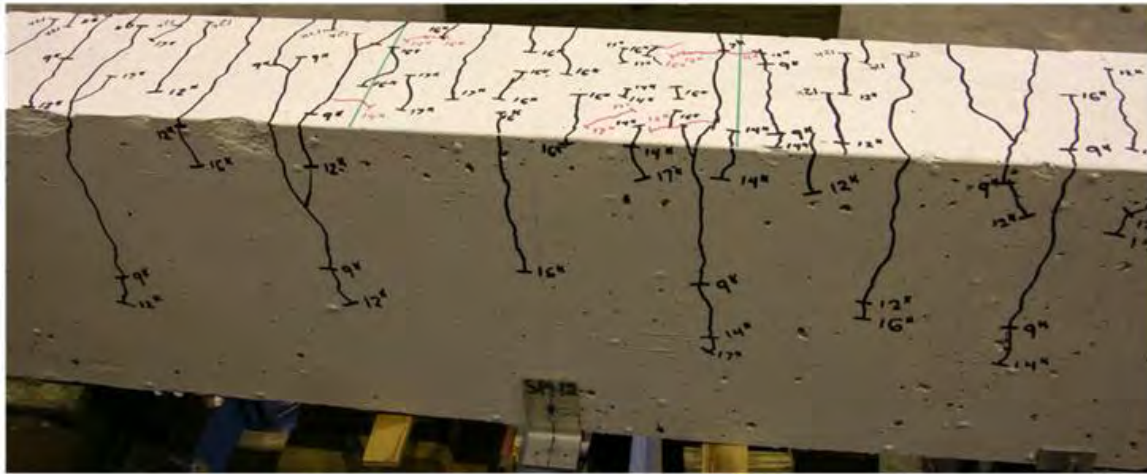
**Figure 146. Photo. Side face of Beam A6-SN before failure.**
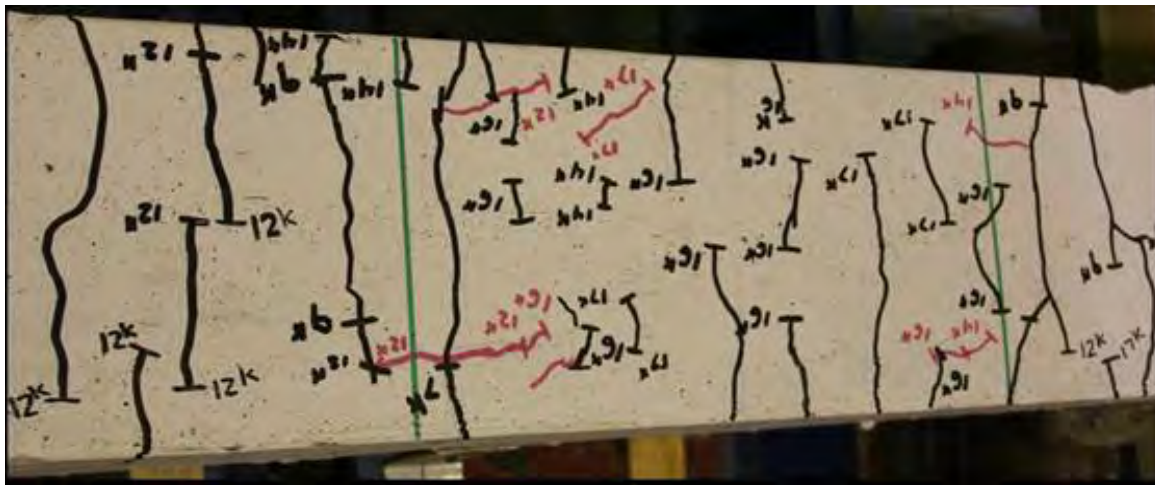
**Figure 147. Photo. Top face of Beam A6-SN before failure.**

Figure 148. Photo. Beam A6-SN after failure.

Splice Beam B6-SN

<div align="center">

Table 44. Test parameters for Splice Beam B6-SN.

</div>

Concrete Mix	Spliced Bar Size	Lap Length, inch (mm)	#3 (10M) Bar Transverse Reinforcement	Nominal Beam Cross-Section Dimensions (Width by Height), inch (mm)
Utelite	#6 (19M)	16 (410)	None	18 by 18 (460 by 460)

<div align="center">

Table 45. Test data for Splice Beam B6-SN.

</div>

| Event	Average Jack Load, kips (kN)	Average Beam End Deflection, inch (mm)	Longitudinal Rebar Strain, microstrain		Transverse Rebar Strain, microstrain	
			Gage 1	Gage 2	Gage 1	Gage 2
Flexural cracking	8.1 (36)	0.06 (1.4)	207	279	N/A	N/A
Top splitting crack	14.2 (63)	0.18 (4.5)	1150	1121	N/A	N/A
Side splitting crack	N/A	N/A	N/A	N/A	N/A	N/A
Long. rebar yield	N/A	N/A	N/A	N/A	N/A	N/A
Ultimate	22.2 (99)	0.35 (8.9)	2018	1934	N/A	N/A

Notes:
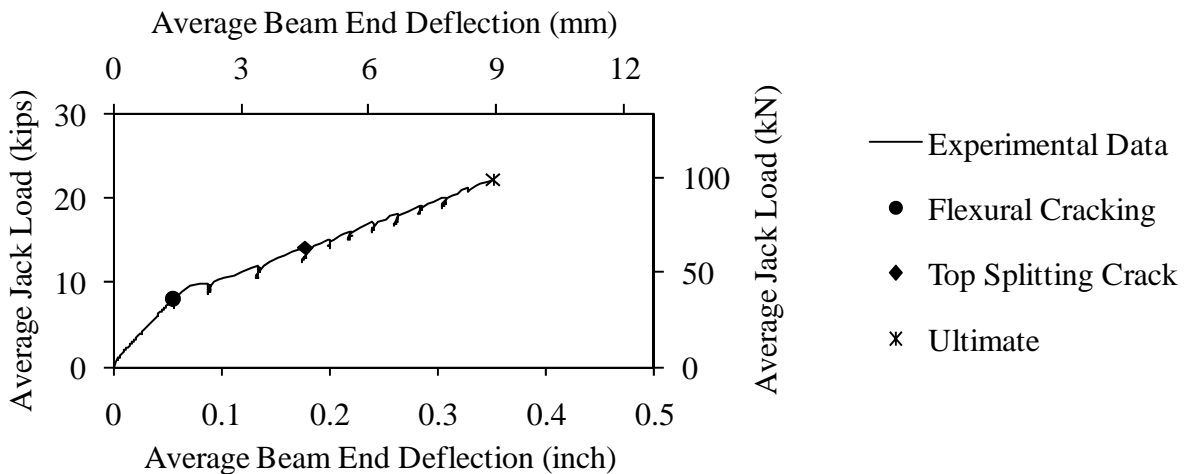
Figure 149. Graph. Load versus deflection for Beam B6-SN.
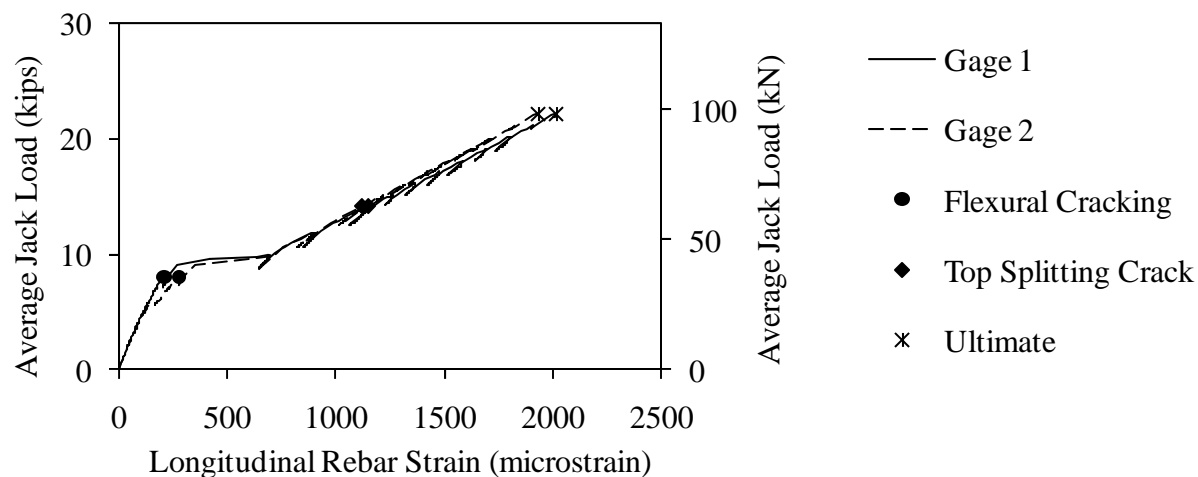
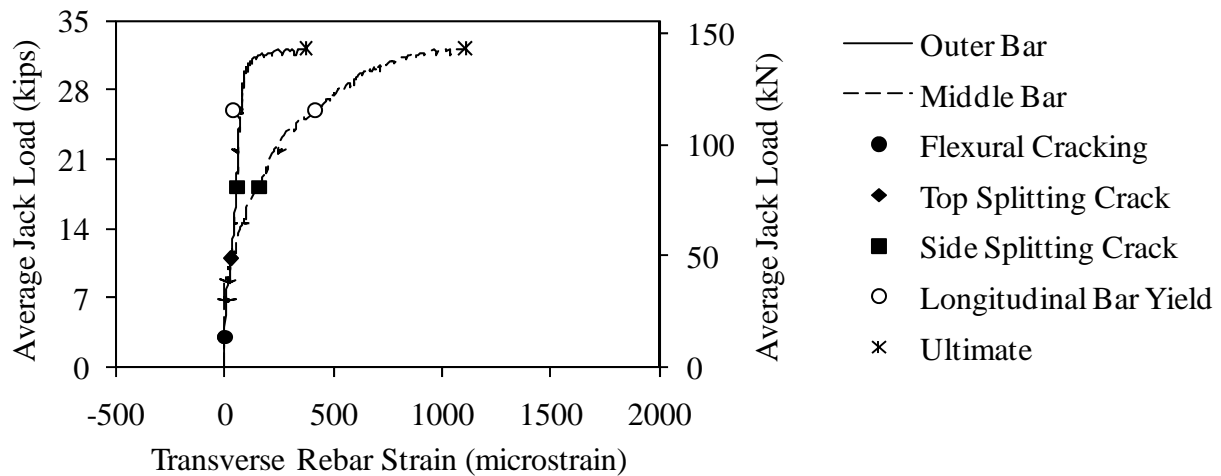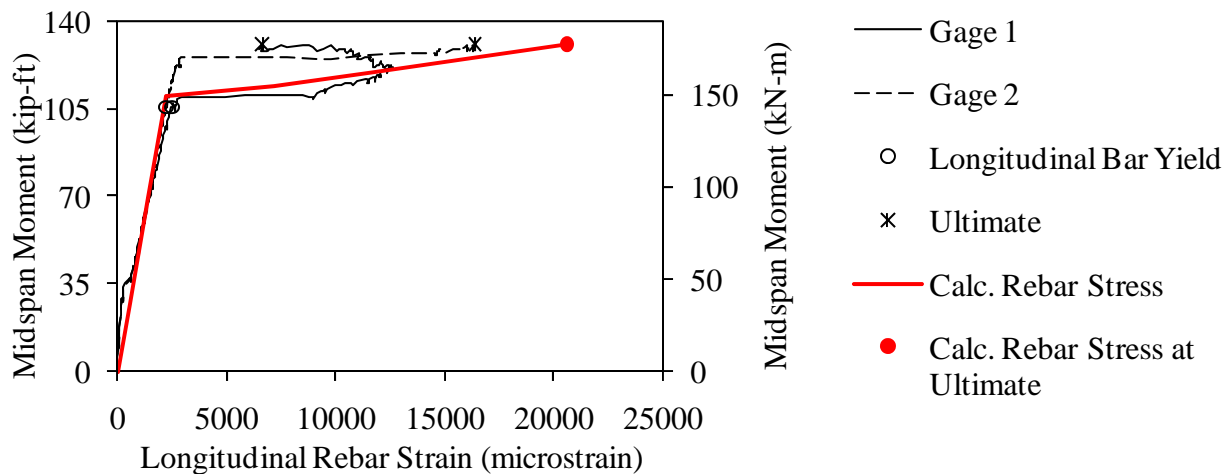**Figure 150. Graph. Load versus longitudinal rebar strain for Beam B6-SN.**
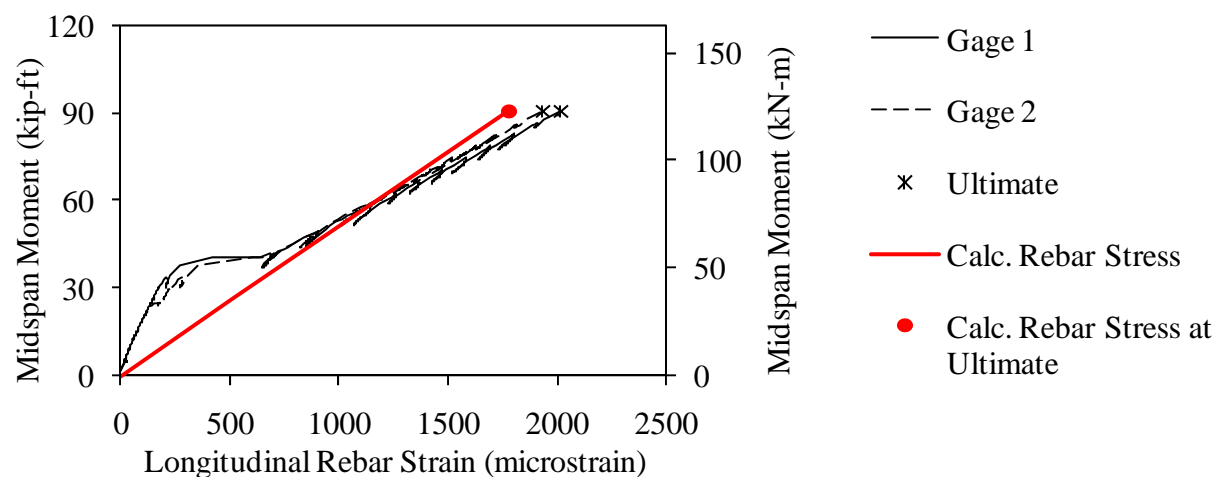
Figure 151. Graph. Measured and predicted midspan moment versus longitudinal rebar strain for Beam B6-SN.
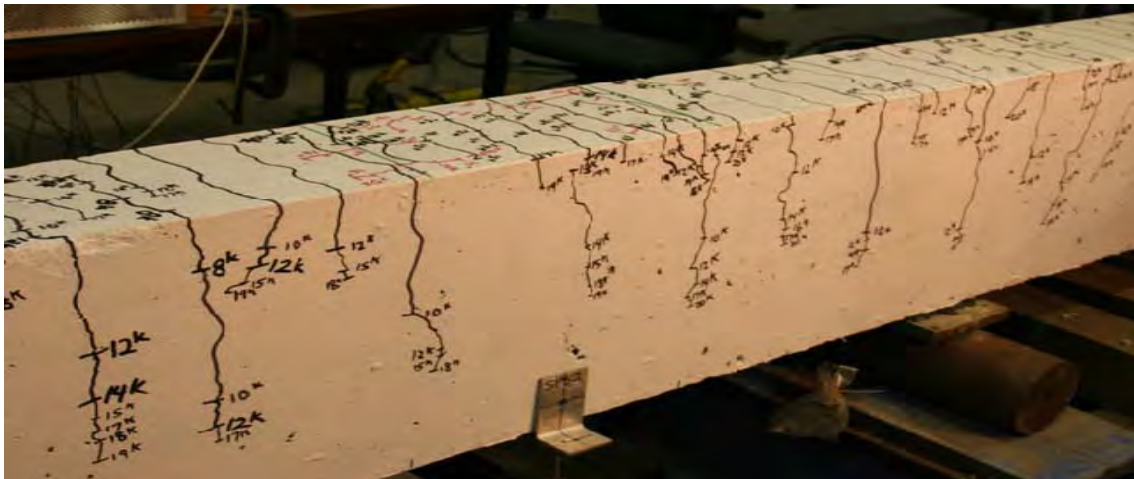
Figure 152. Photo. Side face of Beam B6-SN before failure.
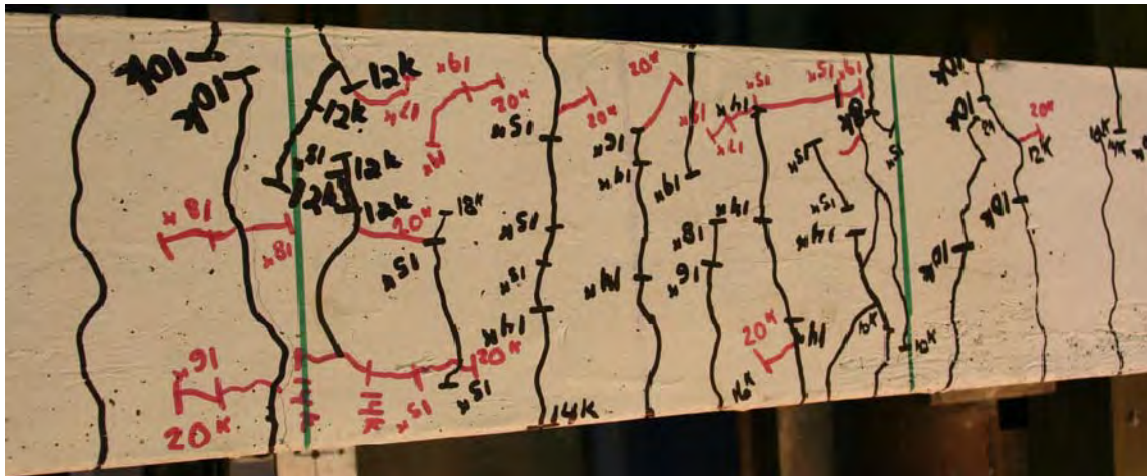
Figure 153. Photo. Top face of Beam B6-SN before failure.
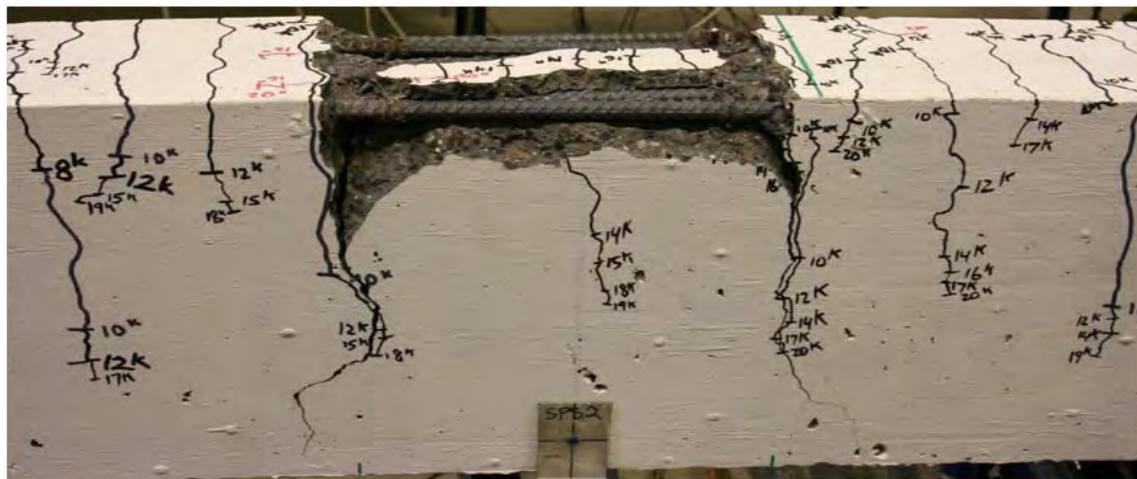
Figure 154. Photo. Beam B6-SN after failure.

Splice Beam C6-SN

Table 46. Test parameters for Splice Beam C6-SN.

Concrete Mix	Spliced Bar Size	Lap Length, inch (mm)	#3 (10M) Bar Transverse Reinforcement	Nominal Beam Cross-Section Dimensions (Width by Height), inch (mm)
Haydite	#6 (19M)	16 (410)	None	18 by 18 (460 by 460)

Table 47. Test data for Splice Beam C6-SN.

Event	Average Jack Load, kips (kN)	Average Beam End Deflection, inch (mm)	Longitudinal Rebar Strain, microstrain		Transverse Rebar Strain, microstrain	
			Gage 1	Gage 2	Gage 1	Gage 2
Flexural cracking	6.1 (27)	0.04 (0.9)	0	122	N/A	N/A
Top splitting crack	11.1 (50)	0.1 (2.4)	0	672	N/A	N/A
Side splitting crack	N/A	N/A	N/A	N/A	N/A	N/A
Long. rebar yield	N/A	N/A	N/A	N/A	N/A	N/A
Ultimate	21.2 (94)	0.29 (7.5)	0	1751	N/A	N/A

Notes:
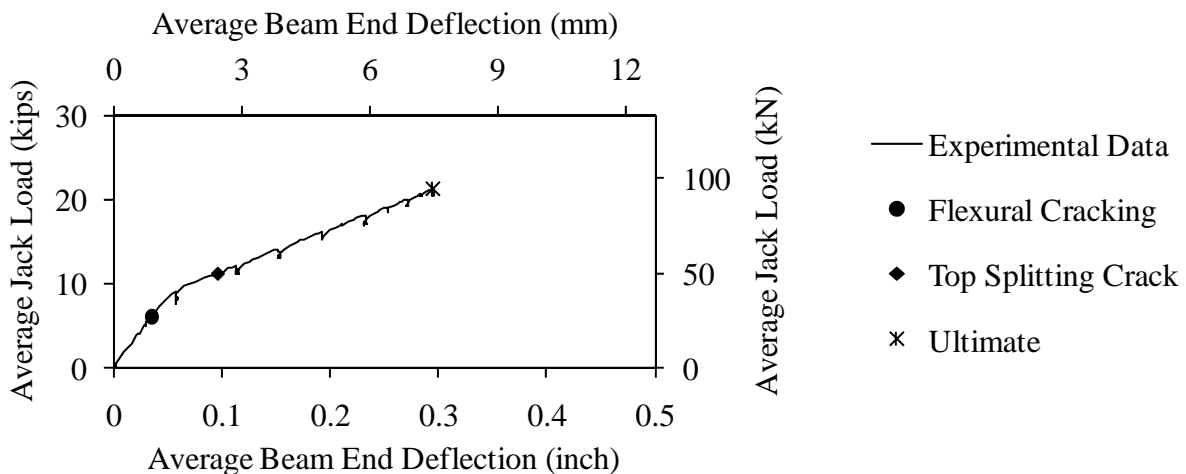
Figure 155. Graph. Load versus deflection for Beam C6-SN.
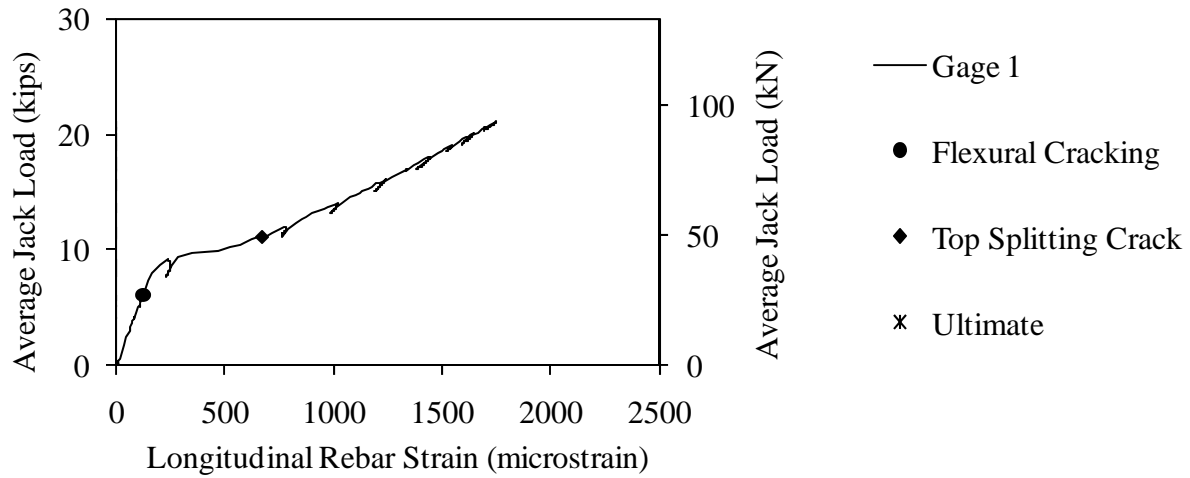
Figure 156. Graph. Load versus longitudinal rebar strain for Beam C6-SN.
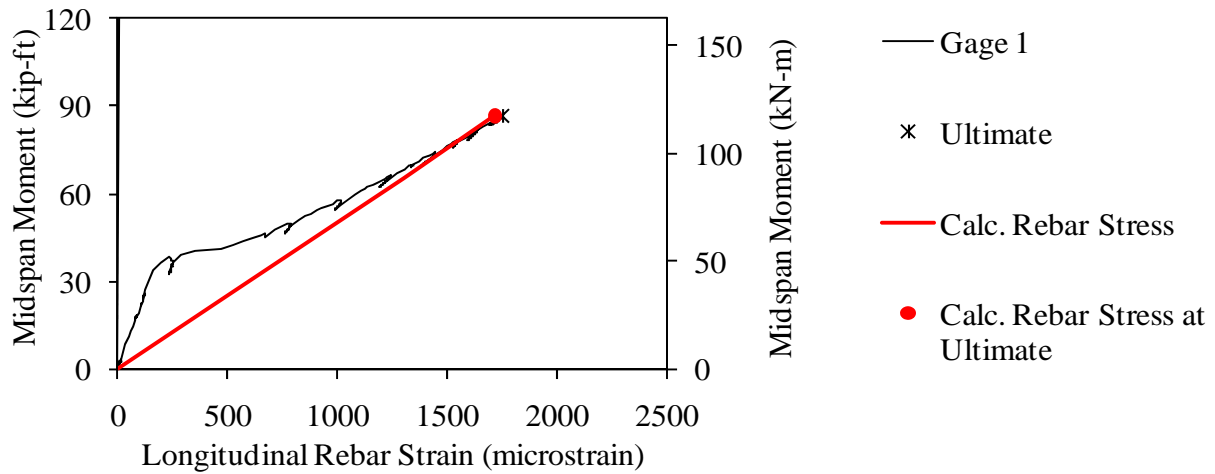
**Figure 157. Graph. Measured and predicted midspan moment versus longitudinal rebar strain for Beam C6-SN.**
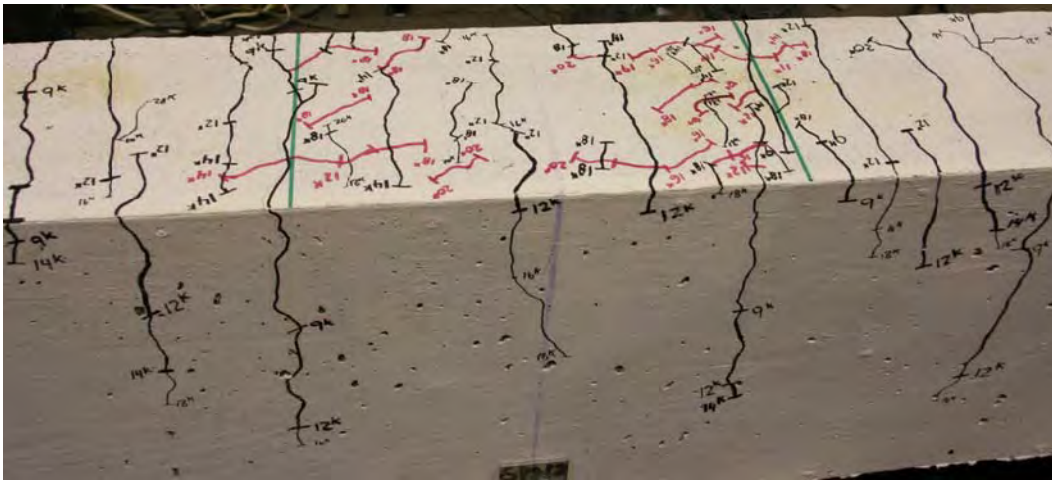
**Figure 158. Photo. Side face of Beam C6-SN before failure.**
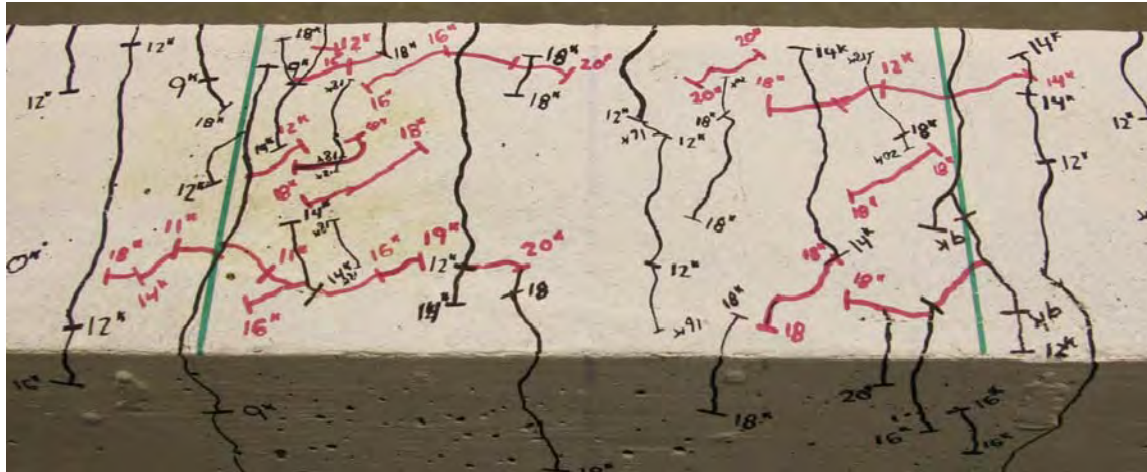
**Figure 159. Photo. Top face of Beam C6-SN before failure.**
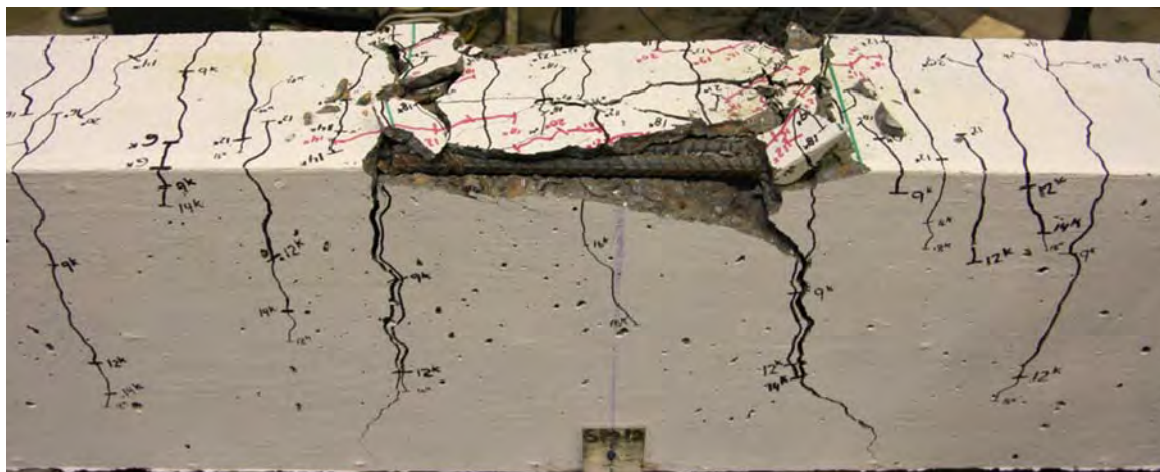
Figure 160. Photo. Beam C6-SN after failure.

Splice Beam A6-LN

Table 48. Test parameters for Splice Beam A6-LN.

Concrete Mix	Spliced Bar Size	Lap Length, inch (mm)	#3 (10M) Bar Transverse Reinforcement	Nominal Beam Cross-Section Dimensions (Width by Height), inch (mm)
Stalite	#6 (19M)	24 (610)	None	18 by 18 (460 by 460)

Table 49. Test data for Splice Beam A6-LN.

| Event	Average Jack Load, kips (kN)	Average Beam End Deflection, inch (mm)	Longitudinal Rebar Strain, microstrain		Transverse Rebar Strain, microstrain	
			Gage 1	Gage 2	Gage 1	Gage 2
Flexural cracking	6.5 (29)	0.04 (1.1)	189	204	N/A	N/A
Top splitting crack	13 (58)	0.17 (4.2)	1062	1127	N/A	N/A
Side splitting crack	N/A	N/A	N/A	N/A	N/A	N/A
Long. rebar yield	N/A	N/A	N/A	N/A	N/A	N/A
Ultimate	23 (102)	0.37 (9.4)	2049	2174	N/A	N/A

Notes:
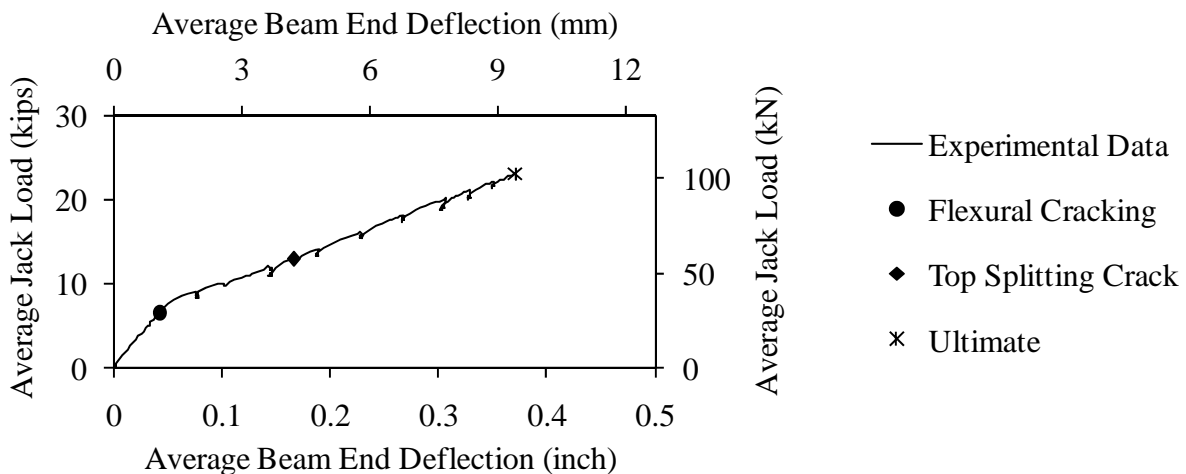
Figure 161. Graph. Load versus deflection for Beam A6-LN.
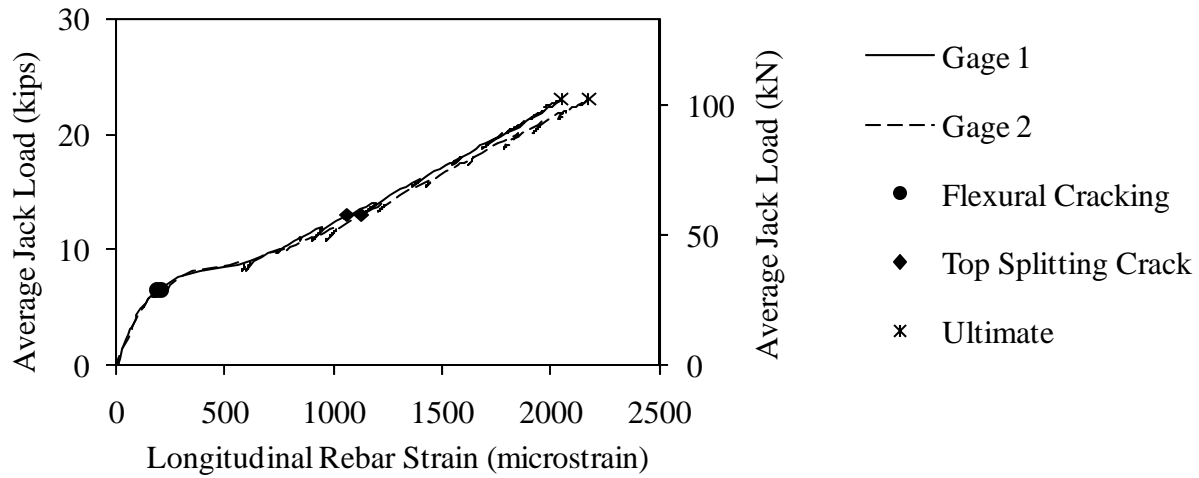
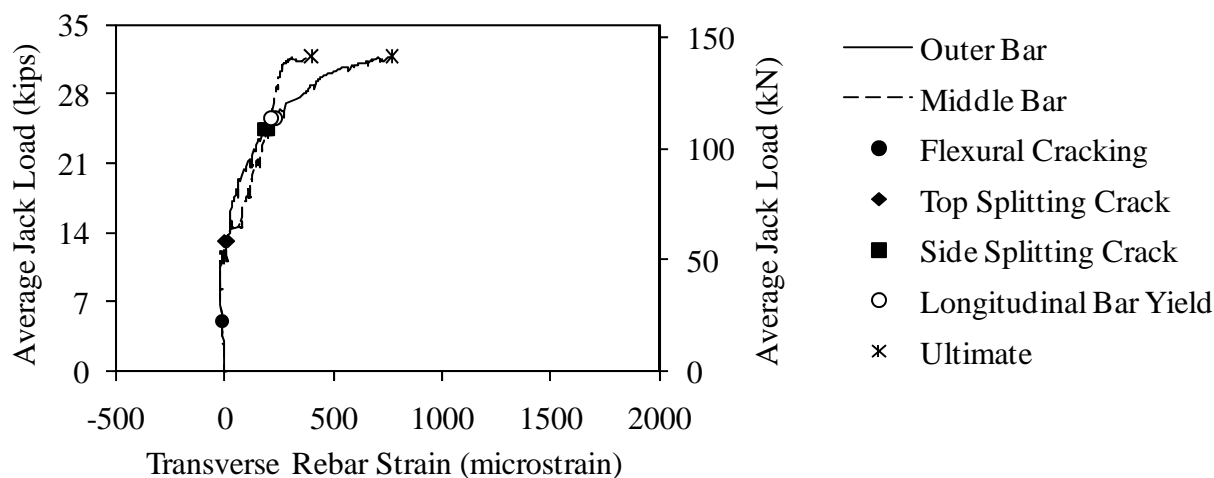**Figure 162. Graph. Load versus longitudinal rebar strain for Beam A6-LN.**
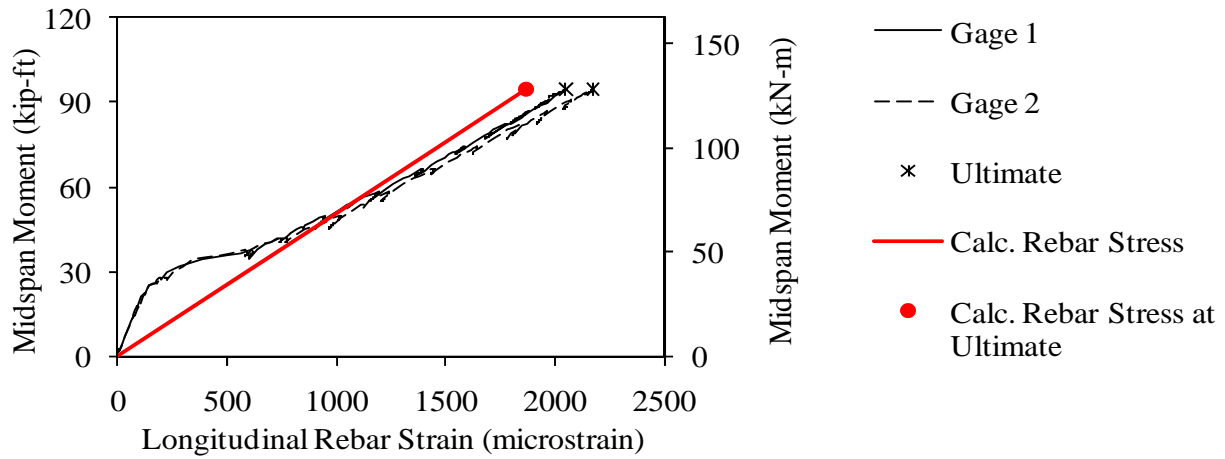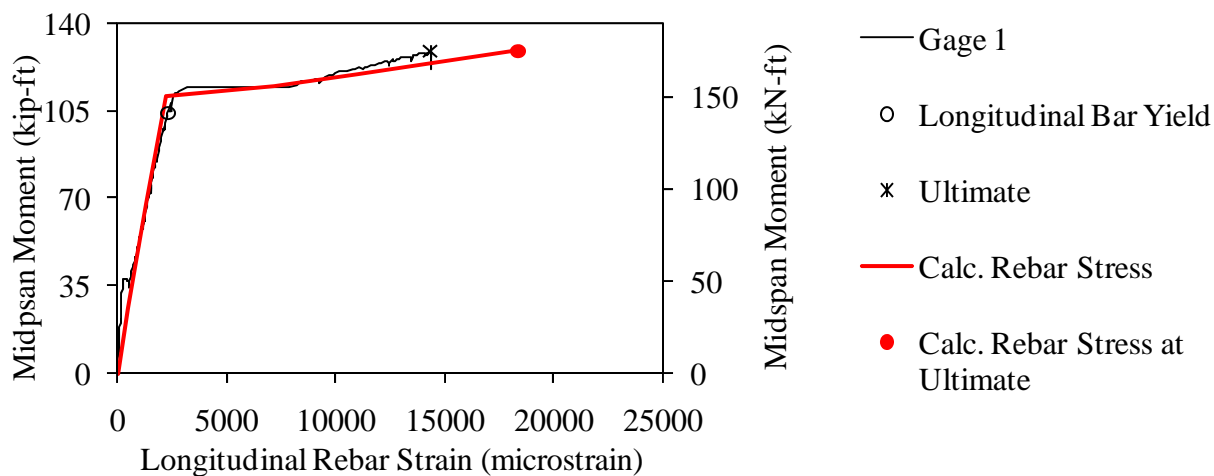

**Figure 163. Graph. Measured and predicted midspan moment versus longitudinal rebar strain for Beam A6-LN.**
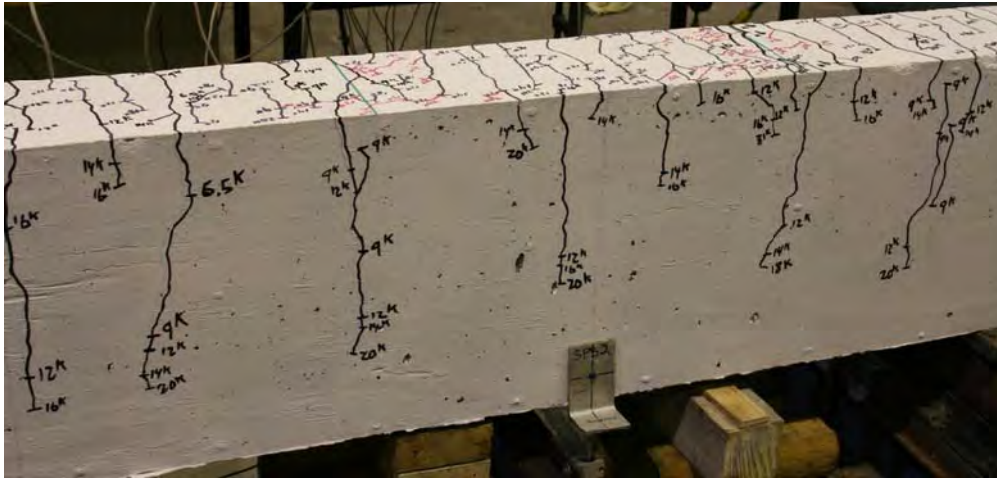
**Figure 164. Photo. Side face of Beam A6-LN before failure.**
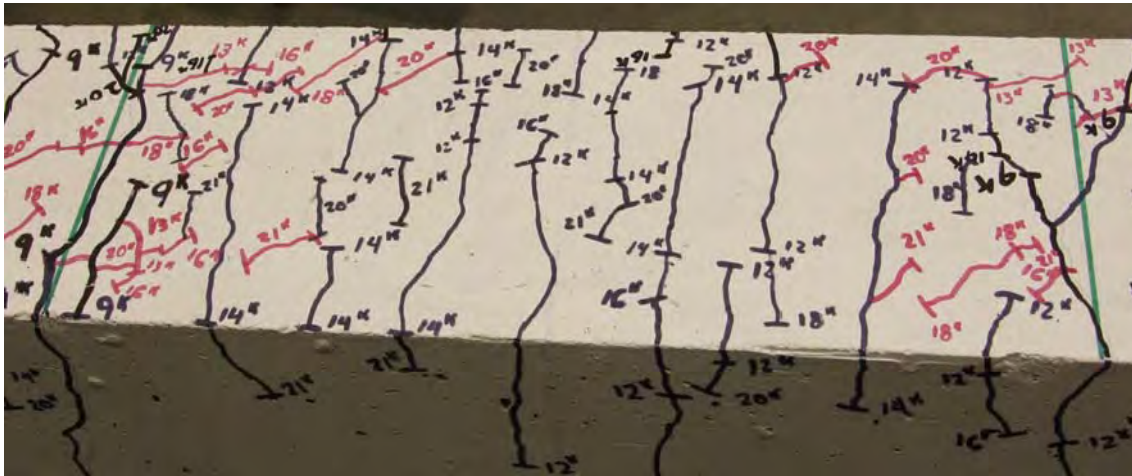
**Figure 165. Photo. Top face of Beam A6-LN before failure.**
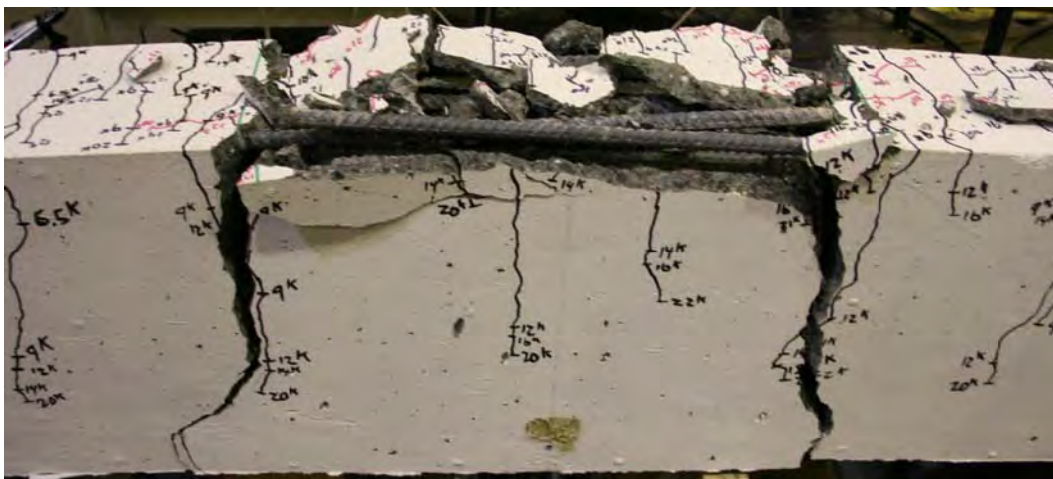
Figure 166. Photo. Beam A6-LN after failure.

Splice Beam B6-LN

<div align="center">

Table 50. Test parameters for Splice Beam B6-LN.

</div>

Concrete Mix	Spliced Bar Size	Lap Length, inch (mm)	#3 (10M) Bar Transverse Reinforcement	Nominal Beam Cross-Section Dimensions (Width by Height), inch (mm)
Utelite	#6 (19M)	24 (610)	None	18 by 18 (460 by 460)

<div align="center">

Table 51. Test data for Splice Beam B6-LN.

</div>

| Event	Average Jack Load, kips (kN)	Average Beam End Deflection, inch (mm)	Longitudinal Rebar Strain, microstrain		Transverse Rebar Strain, microstrain	
			Gage 1	Gage 2	Gage 1	Gage 2
Flexural cracking	7.5 (34)	0.05 (1.3)	197	215	N/A	N/A
Top splitting crack	15 (67)	0.19 (4.9)	1197	1223	N/A	N/A
Side splitting crack	22.4 (100)	0.35 (8.9)	1931	1961	N/A	N/A
Long. rebar yield	N/A	N/A	N/A	N/A	N/A	N/A
Ultimate	25.2 (112)	0.43 (10.8)	2338	2279	N/A	N/A

Notes:
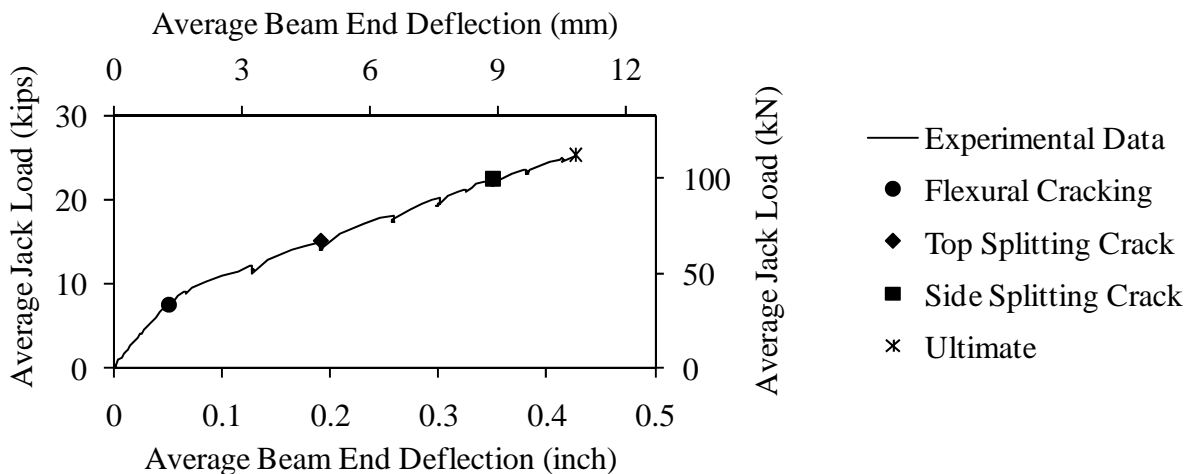
Figure 167. Graph. Load versus deflection for Beam B6-LN.
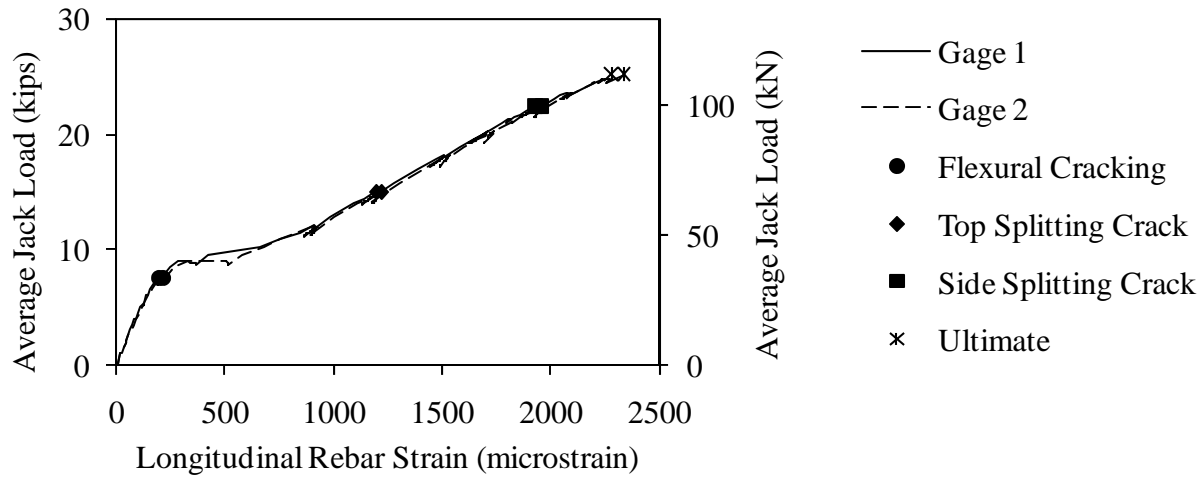
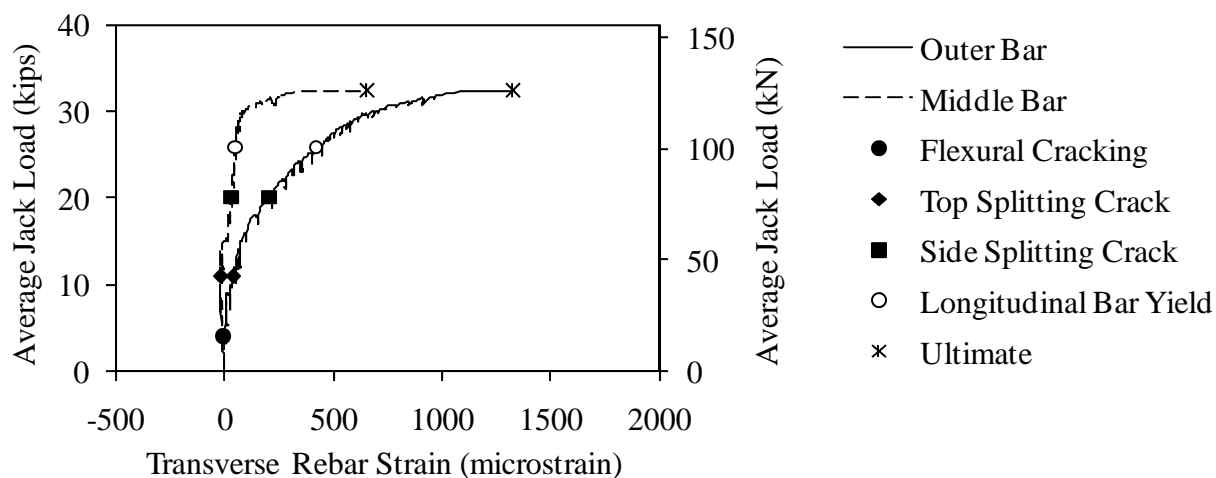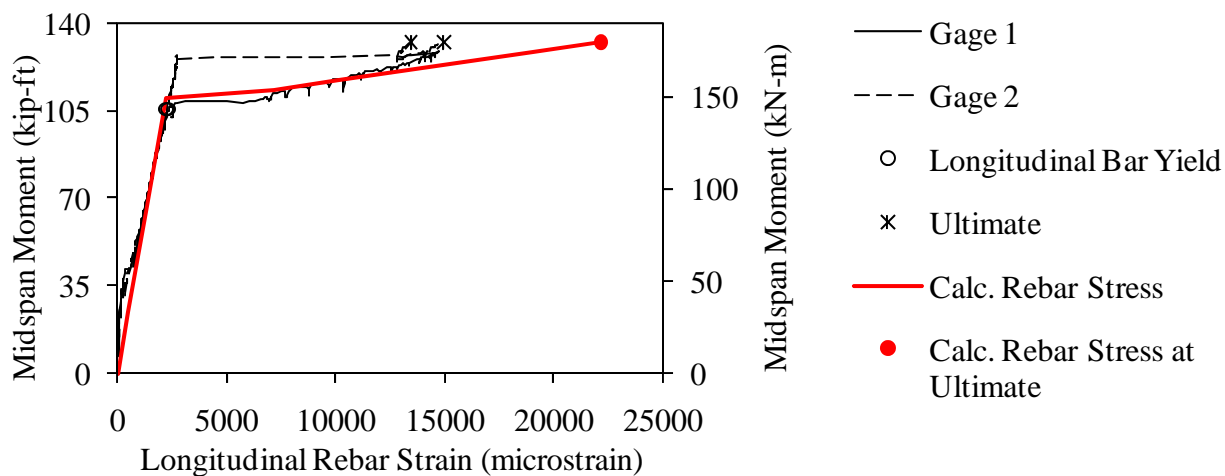**Figure 168. Graph. Load versus longitudinal rebar strain for Beam B6-LN.**
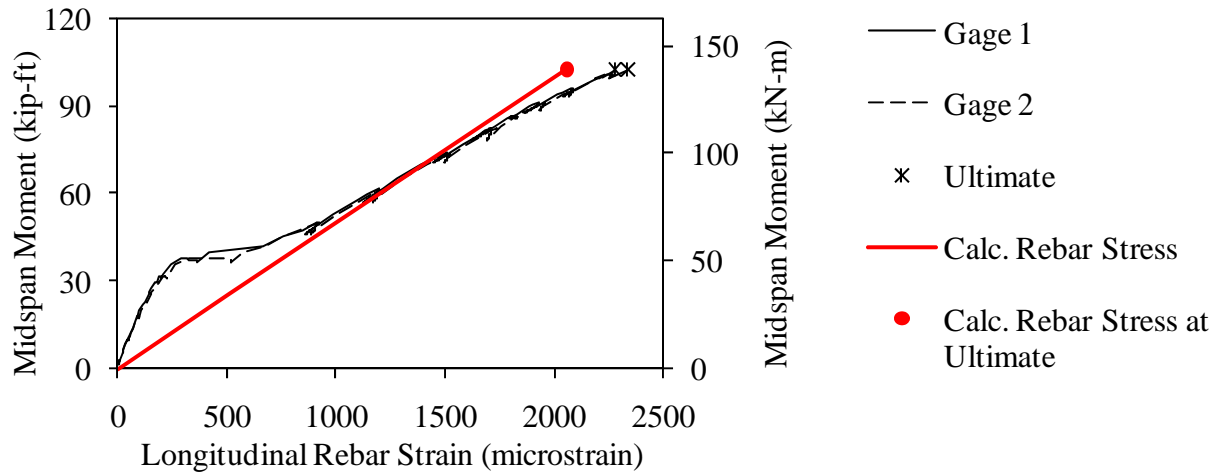
**Figure 169. Graph. Measured and predicted midspan moment versus longitudinal rebar strain for Beam B6-LN.**
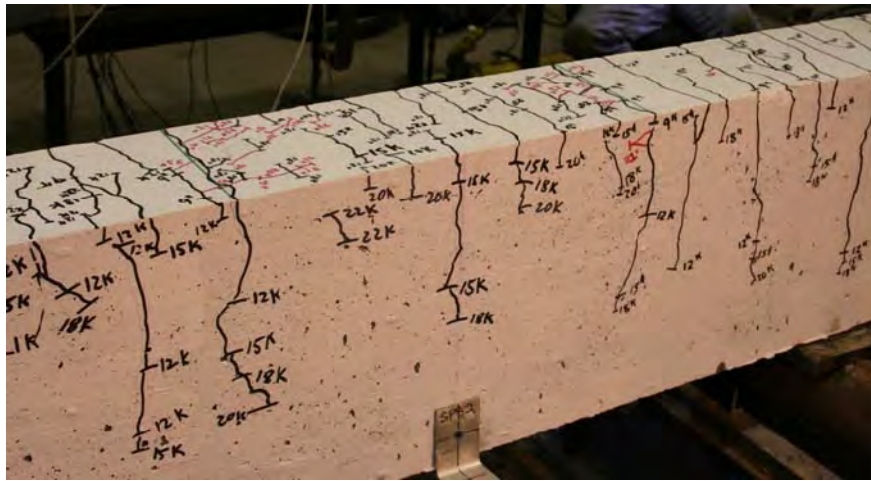
Figure 170. Photo. Side face of Beam B6-LN before failure.

Figure 171. Photo. Top face of Beam B6-LN before failure.

Figure 172. Photo. Beam B6-LN after failure.

Splice Beam C6-LN

Table 52. Test parameters for Splice Beam C6-LN.

Concrete Mix	Spliced Bar Size	Lap Length, inch (mm)	#3 (10M) Bar Transverse Reinforcement	Nominal Beam Cross-Section Dimensions (Width by Height), inch (mm)
Haydite	#6 (19M)	24 (610)	None	18 by 18 (460 by 460)

Table 53. Test data for Splice Beam C6-LN.

Event	Average Jack Load, kips (kN)	Average Beam End Deflection, inch (mm)	Longitudinal Rebar Strain, microstrain		Transverse Rebar Strain, microstrain	
			Gage 1	Gage 2	Gage 1	Gage 2
Flexural cracking	5.1 (23)	0.03 (0.8)	102	100	N/A	N/A
Top splitting crack	11.1 (49)	0.09 (2.4)	419	808	N/A	N/A
Side splitting crack	N/A	N/A	N/A	N/A	N/A	N/A
Long. rebar yield	N/A	N/A	N/A	N/A	N/A	N/A
Ultimate	21.9 (97)	0.31 (8)	1703	1840	N/A	N/A

Notes:
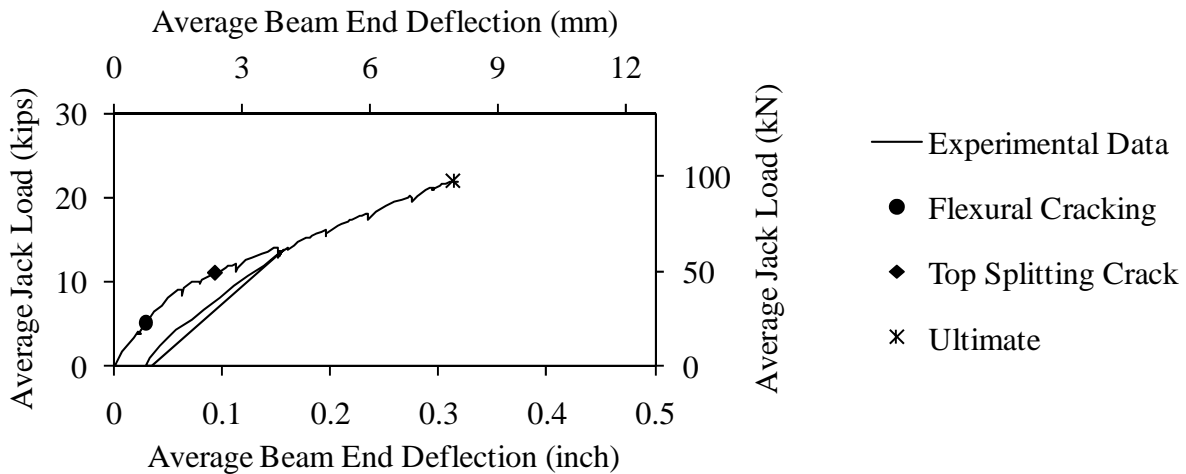
Figure 173. Graph. Load versus deflection for Beam C6-LN.
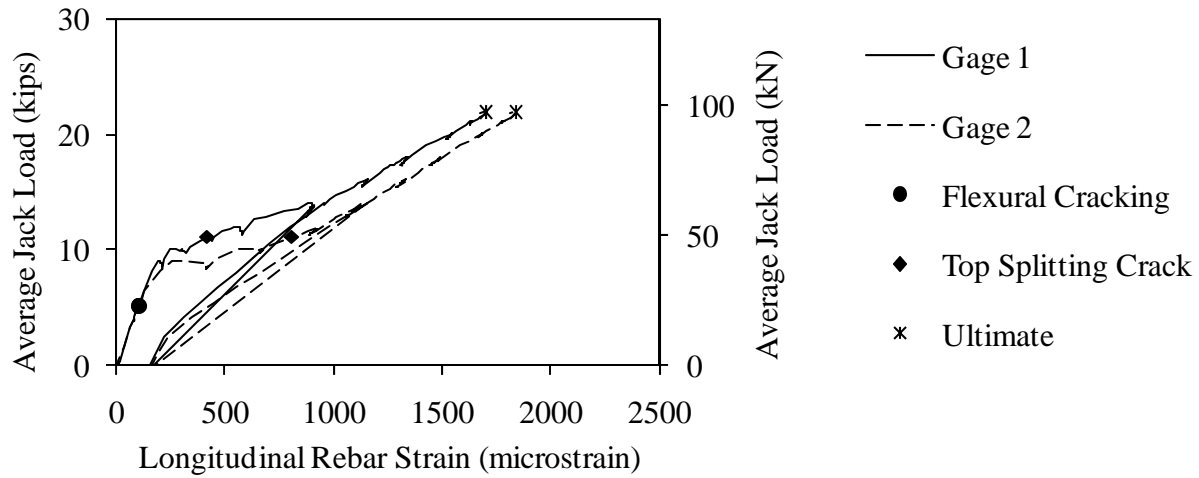
Figure 174. Graph. Load versus longitudinal rebar strain for Beam C6-LN.
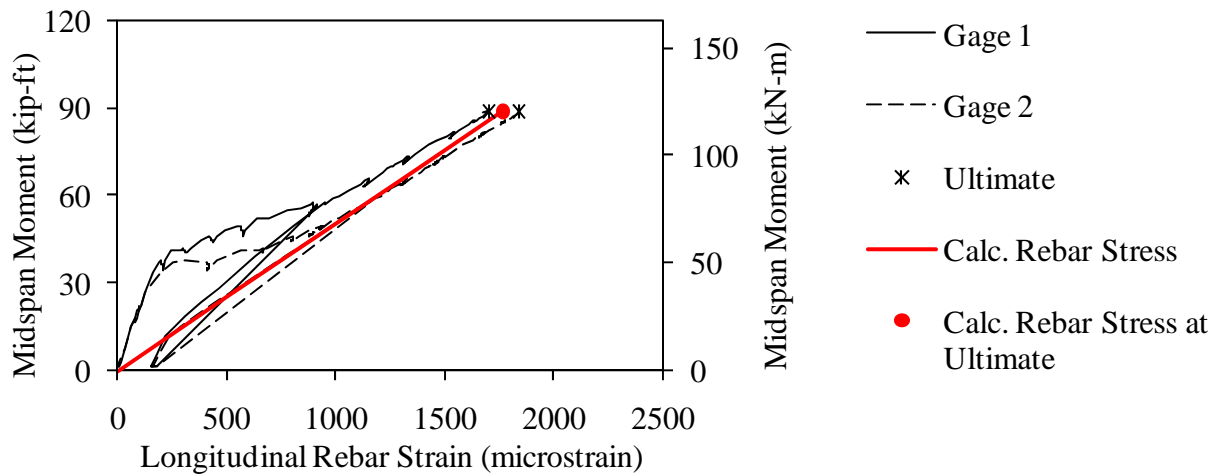
Figure 175. Graph. Measured and predicted midspan moment versus longitudinal rebar strain for Beam C6-LN.
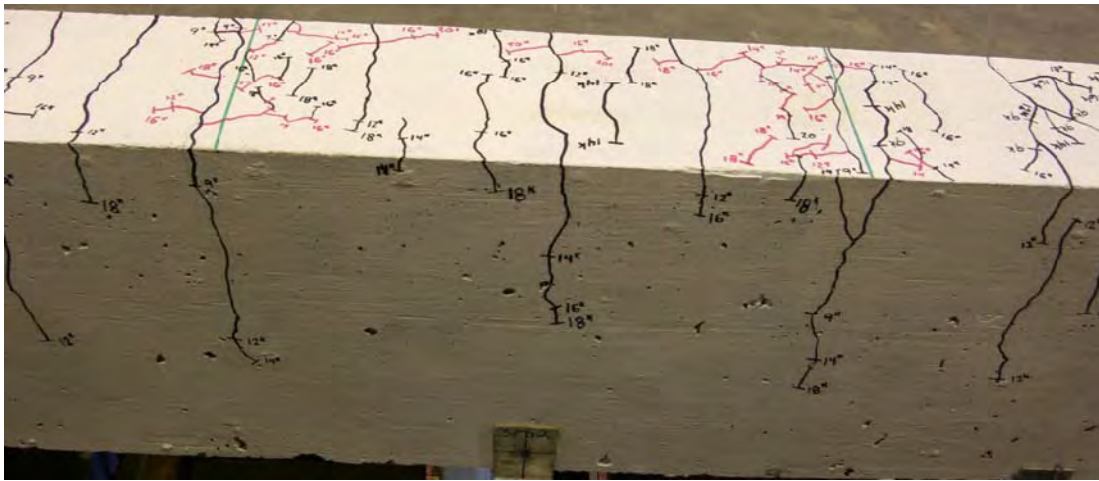
Figure 176. Photo. Side face of Beam C6-LN before failure.
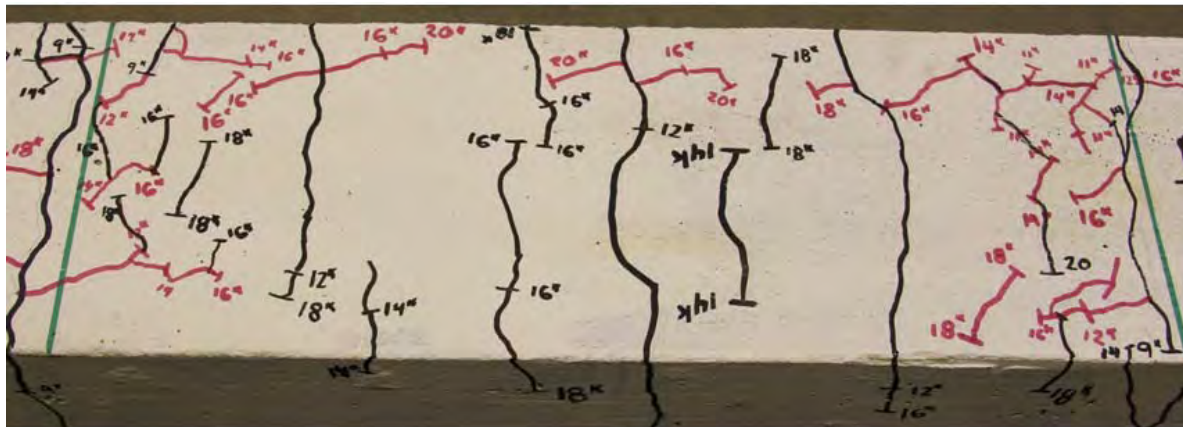
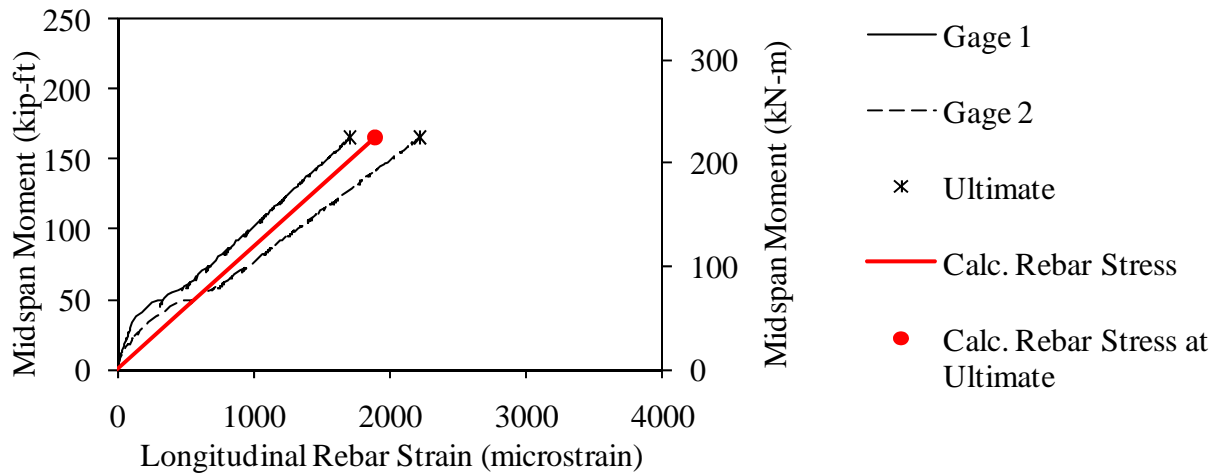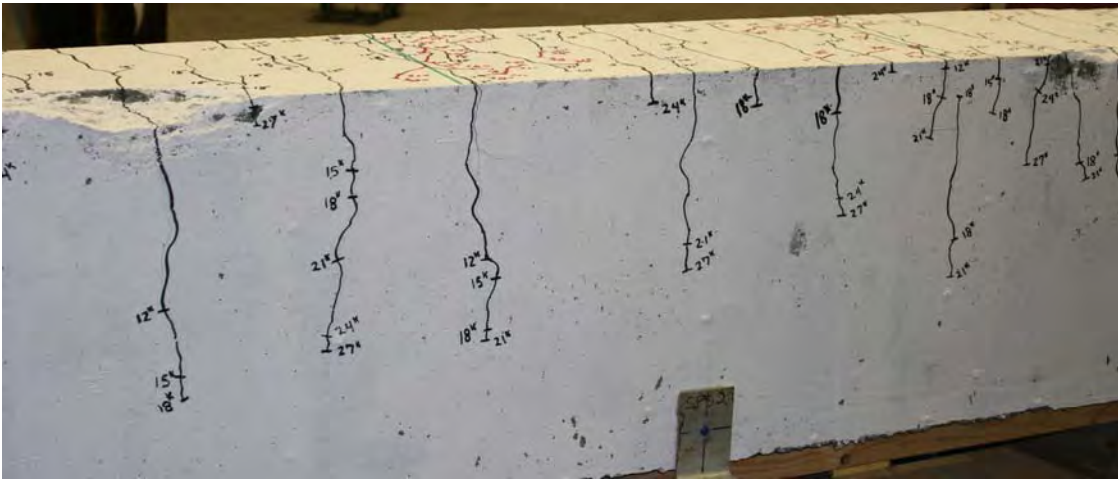**Figure 177. Photo. Top face of Beam C6-LN before failure.**

Figure 178. Photo. Beam C6-LN after failure.

Splice Beam A6-ST

<div align="center">Table 54. Test parameters for Splice Beam A6-ST.</div>

Concrete Mix	Spliced Bar Size	Lap Length, inch (mm)	#3 (10M) Bar Transverse Reinforcement	Nominal Beam Cross-Section Dimensions (Width by Height), inch (mm)
Stalite	#6 (19M)	16 (410)	(2) at 8 in. (200mm)	18 by 18 (460 by 460)

<div align="center">Table 55. Test data for Splice Beam A6-ST.</div>

Event	Average Jack Load, kips (kN)	Average Beam End Deflection, inch (mm)	Longitudinal Rebar Strain, microstrain		Transverse Rebar Strain, microstrain	
			Gage 1	Gage 2	Gage 1	Gage 2
Flexural cracking	5 (22)	0.03 (0.8)	122	119	2	-7
Top splitting crack	9.1 (40)	0.08 (2)	606	671	6	-9
Side splitting crack	24.2 (108)	0.4 (10.2)	2304	2341	169	382
Long. rebar yield	24.1 (107)	0.4 (10.1)	2283	2327	163	371
Ultimate	26 (116)	0.45 (11.3)	2617	2516	333	606

Notes:
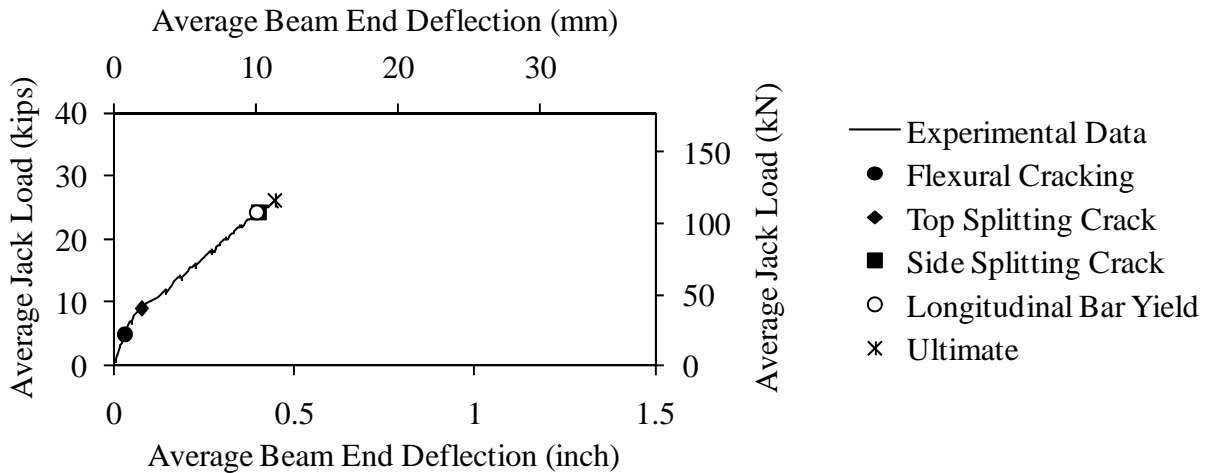
Figure 179. Graph. Load versus deflection for Beam A6-ST.
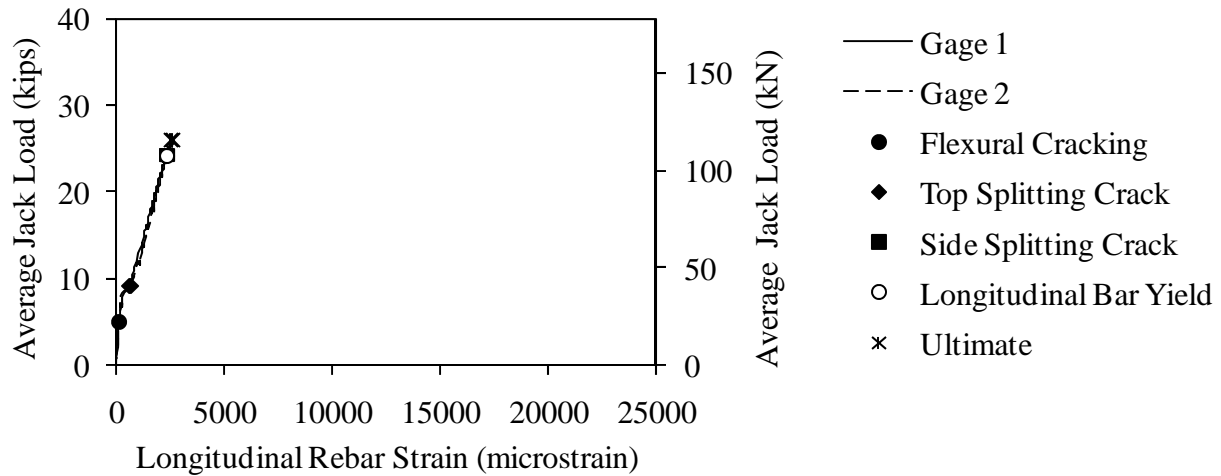
Figure 180. Graph. Load versus longitudinal rebar strain for Beam A6-ST.
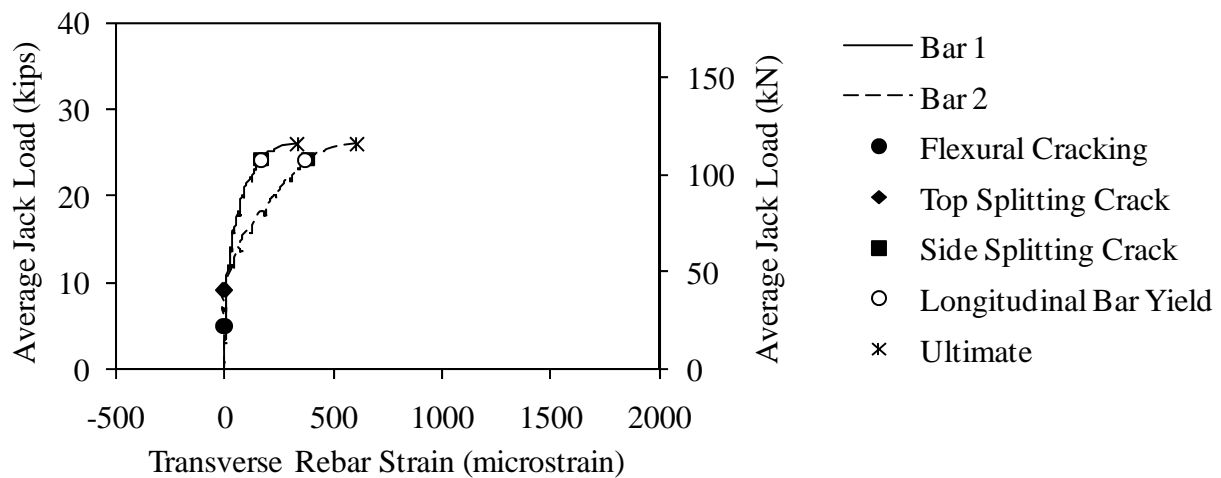
Figure 181. Graph. Load versus transverse rebar strain for Beam A6-ST.
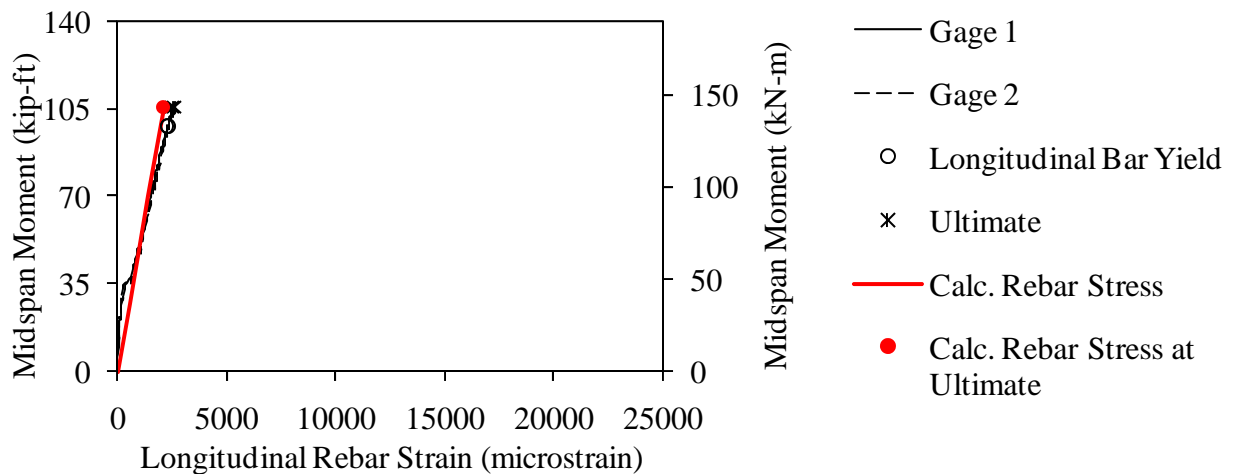
Figure 182. Graph. Measured and predicted midspan moment versus longitudinal rebar strain for Beam A6-ST.

Figure 183. Photo. Side face of Beam A6-ST before failure.
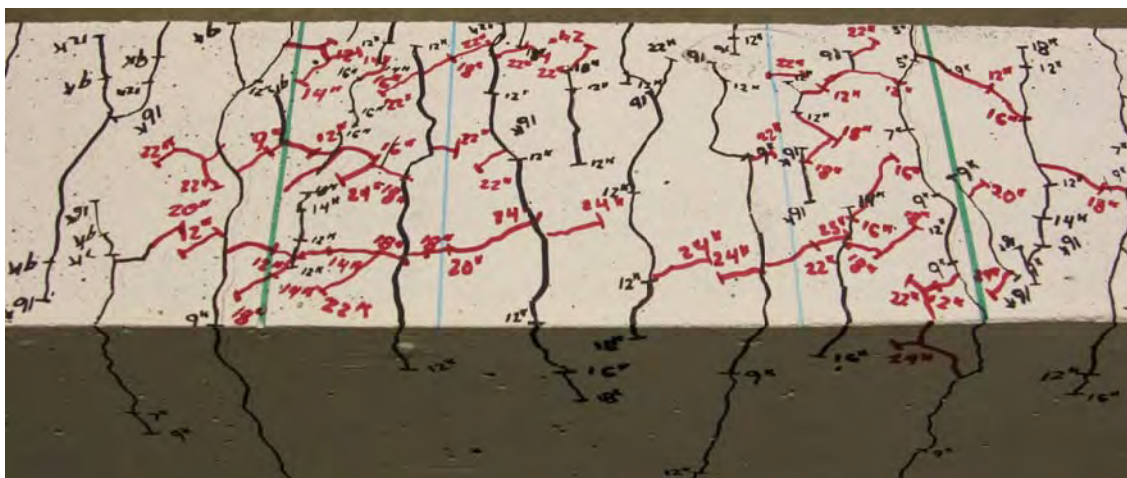
Figure 184. Photo. Top face of Beam A6-ST before failure.

Figure 185. Photo. Beam A6-ST after failure.

Splice Beam B6-ST

<p style="text-align:center">Table 56. Test parameters for Splice Beam B6-ST.</p>

Concrete Mix	Spliced Bar Size	Lap Length, inch (mm)	#3 (10M) Bar Transverse Reinforcement	Nominal Beam Cross-Section Dimensions (Width by Height), inch (mm)
Utelite	#6 (19M)	16 (410)	(2) at 8 in. (200mm)	18 by 18 (460 by 460)

<p style="text-align:center">Table 57. Test data for Splice Beam B6-ST.</p>

| Event	Average Jack Load, kips (kN)	Average Beam End Deflection, inch (mm)	Longitudinal Rebar Strain, microstrain		Transverse Rebar Strain, microstrain	
			Gage 1	Gage 2	Gage 1	Gage 2
Flexural cracking	4.1 (18)	0.02 (0.5)	102	102	0	-7
Top splitting crack	11.1 (50)	0.09 (2.4)	767	827	-8	-20
Side splitting crack	18.2 (81)	0.24 (6.2)	1556	1575	57	83
Long. rebar yield	25.3 (112)	0.39 (9.9)	2326	2289	133	254
Ultimate	28.9 (129)	0.62 (15.9)	11423	2690	878	1072

Notes:
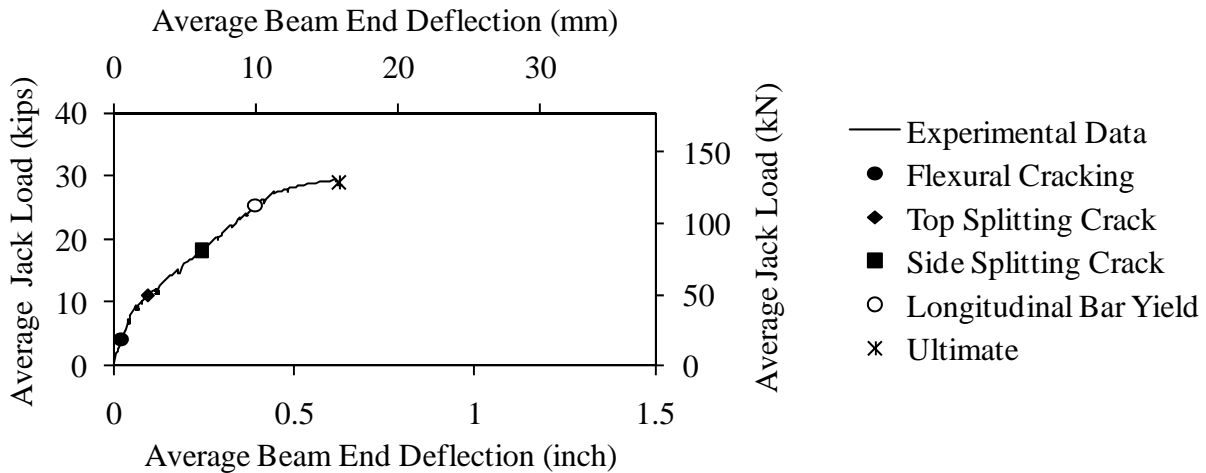
Figure 186. Graph. Load versus deflection for Beam B6-ST.
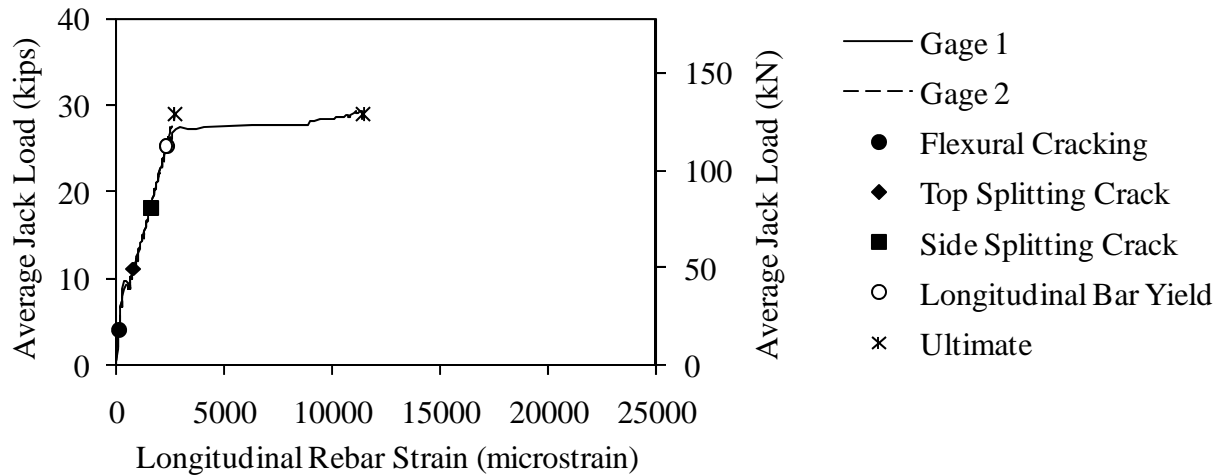
Figure 187. Graph. Load versus longitudinal rebar strain for Beam B6-ST.
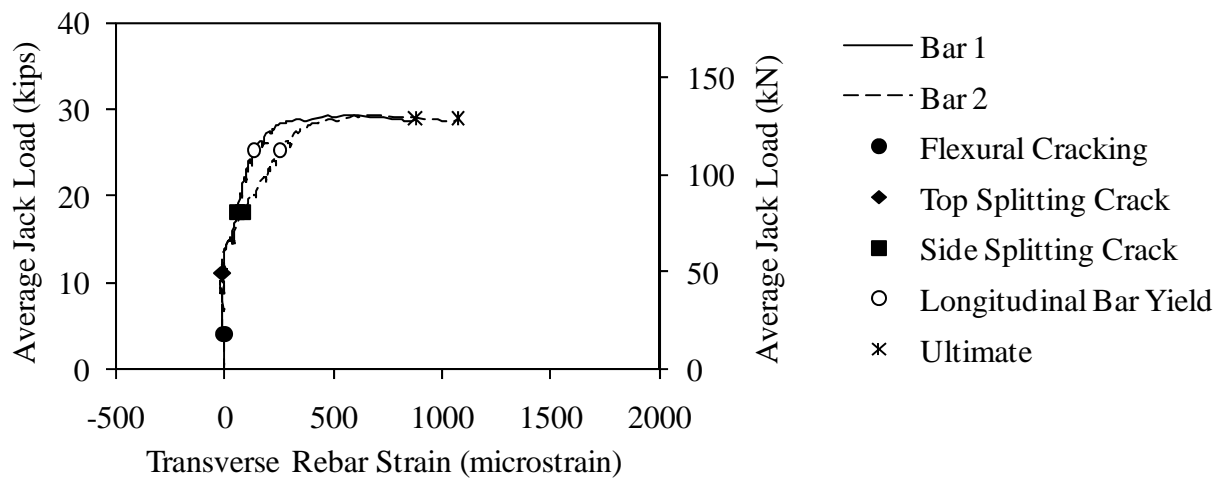
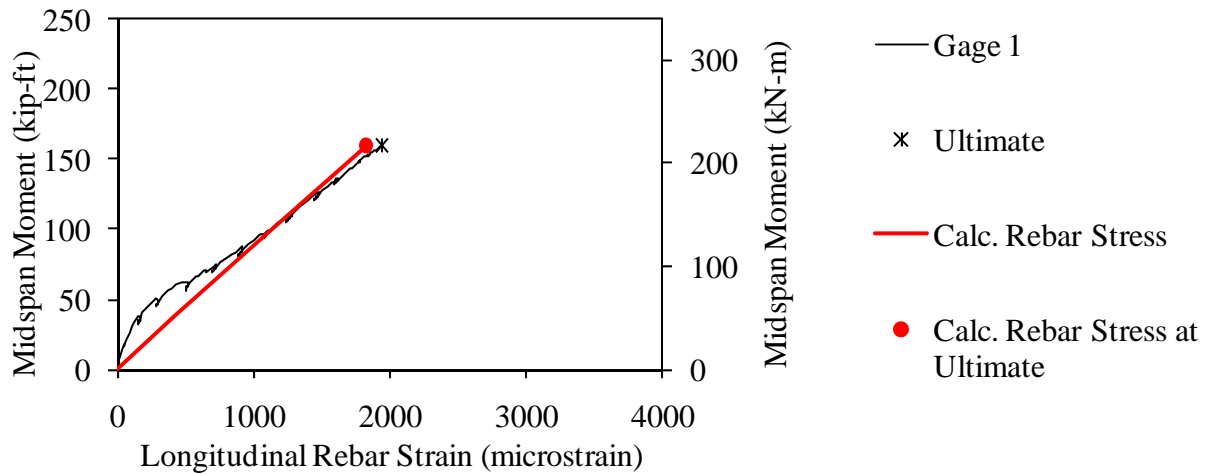**Figure 188. Graph. Load versus transverse rebar strain for Beam B6-ST.**
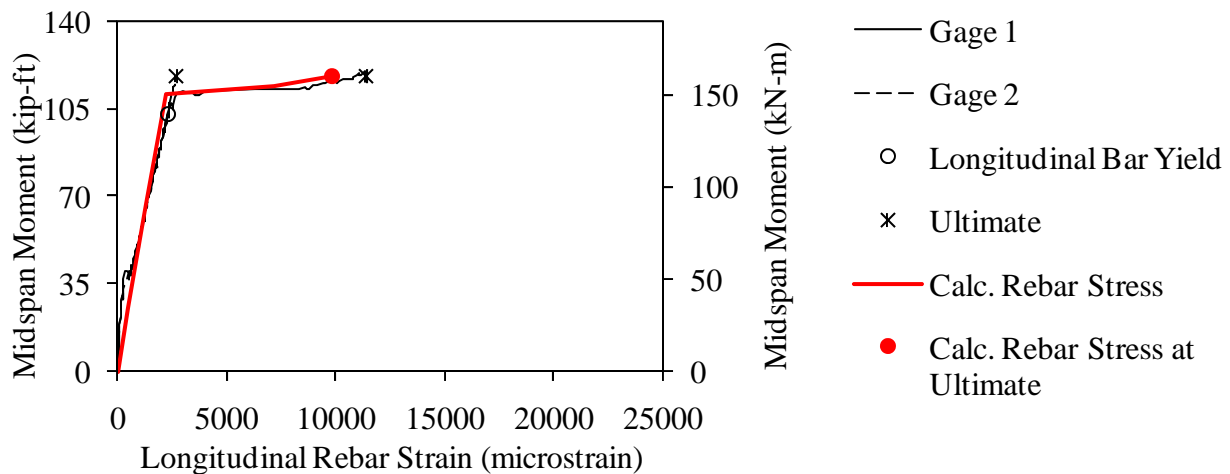
**Figure 189. Graph. Measured and predicted midspan moment versus longitudinal rebar strain for Beam B6-ST.**

**Figure 190. Photo. Side face of Beam B6-ST before failure.**
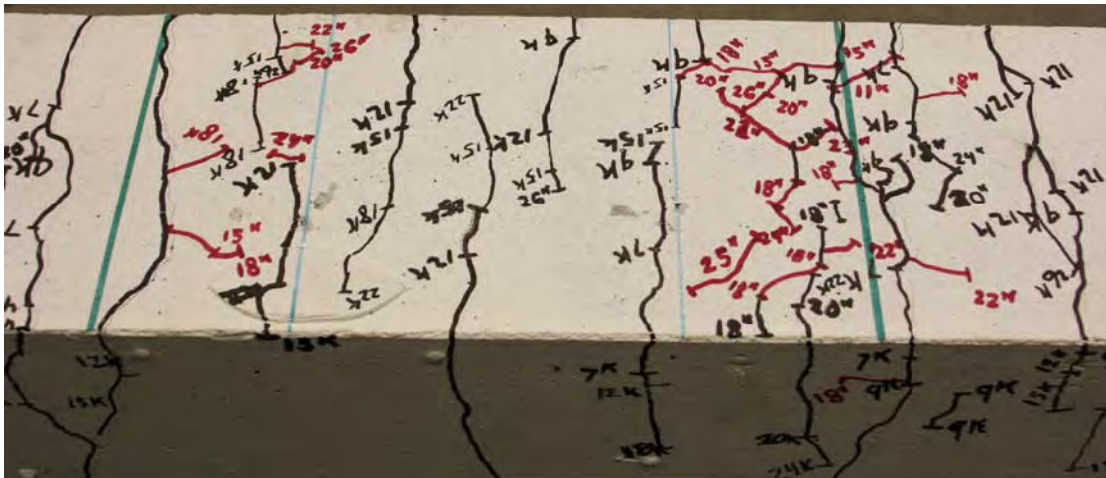
**Figure 191. Photo. Top face of Beam B6-ST before failure.**
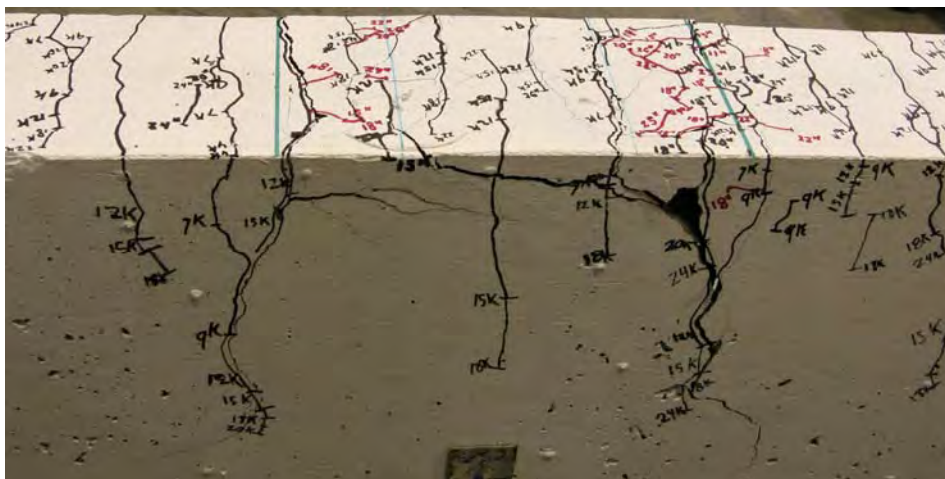
Figure 192. Photo. Beam B6-ST after failure.

Splice Beam C6-ST

<div align="center">

Table 58. Test parameters for Splice Beam C6-ST.

</div>

Concrete Mix	Spliced Bar Size	Lap Length, inch (mm)	#3 (10M) Bar Transverse Reinforcement	Nominal Beam Cross-Section Dimensions (Width by Height), inch (mm)
Haydite	#6 (19M)	16 (410)	(2) at 8 in. (200mm)	18 by 18 (460 by 460)

<div align="center">

Table 59. Test data for Splice Beam C6-ST.

</div>

| Event	Average Jack Load, kips (kN)	Average Beam End Deflection, inch (mm)	Longitudinal Rebar Strain, microstrain		Transverse Rebar Strain, microstrain	
			Gage 1	Gage 2	Gage 1	Gage 2
Flexural cracking	4.1 (18)	0.02 (0.6)	220	85	-9	-6
Top splitting crack	11.1 (49)	0.1 (2.5)	687	721	1	-4
Side splitting crack	18.1 (80)	0.24 (6.2)	1391	1513	38	63
Long. rebar yield	25.8 (115)	0.42 (10.5)	2327	2290	229	208
Ultimate	26.8 (119)	0.45 (11.5)	2628	2392	387	305

Notes:

<div align="center">
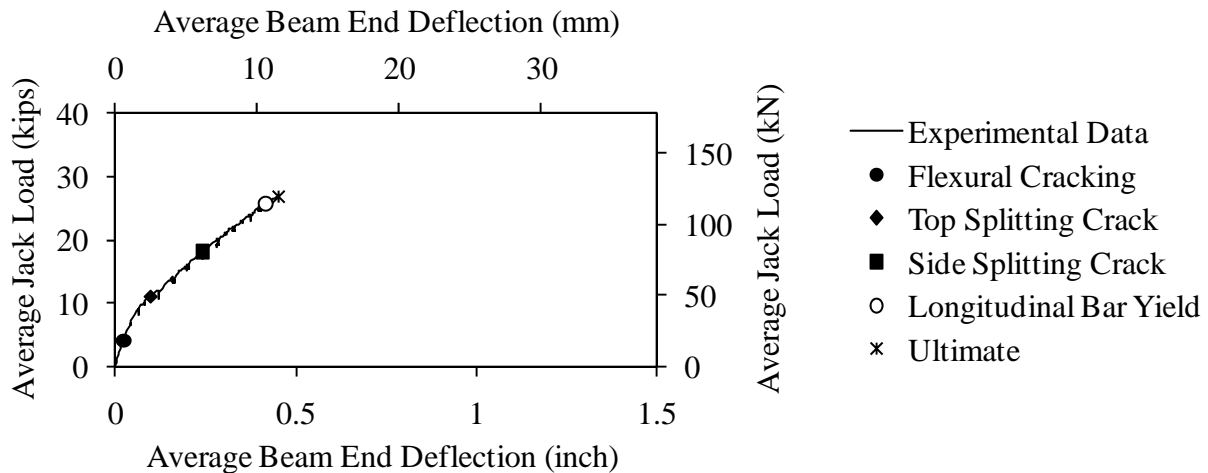
Figure 193. Graph. Load versus deflection for Beam C6-ST.

</div>
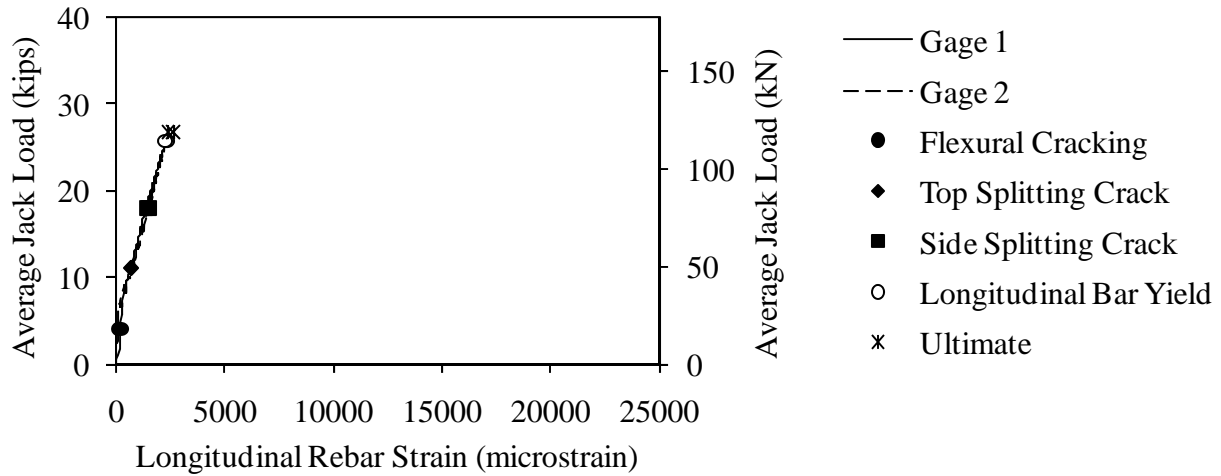
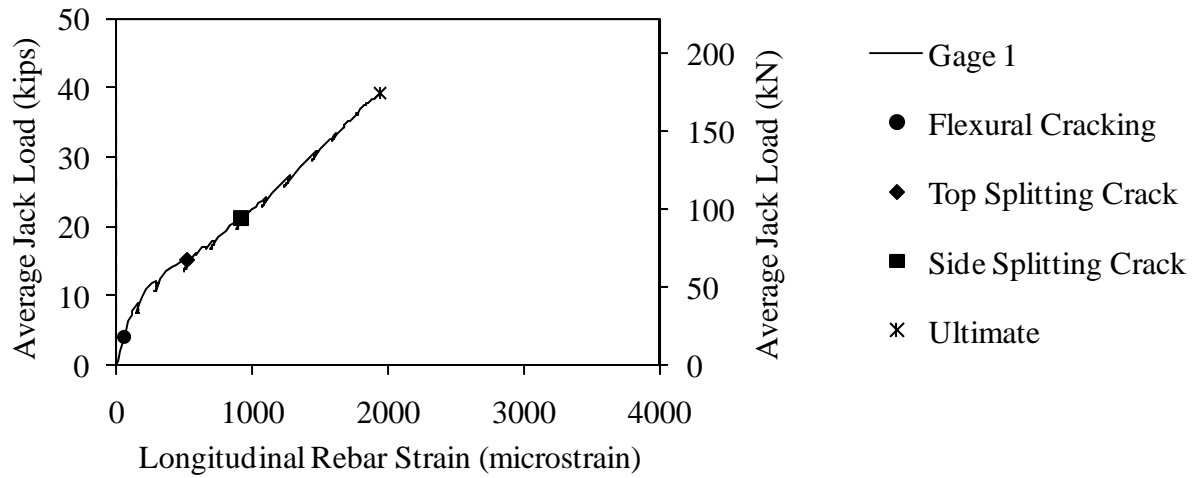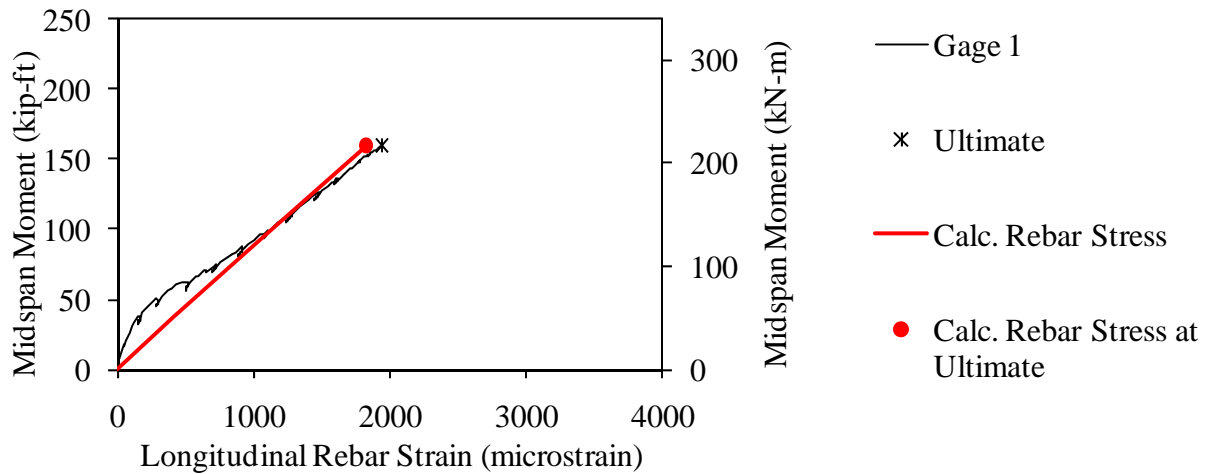**Figure 194. Graph. Load versus longitudinal rebar strain for Beam C6-ST.**

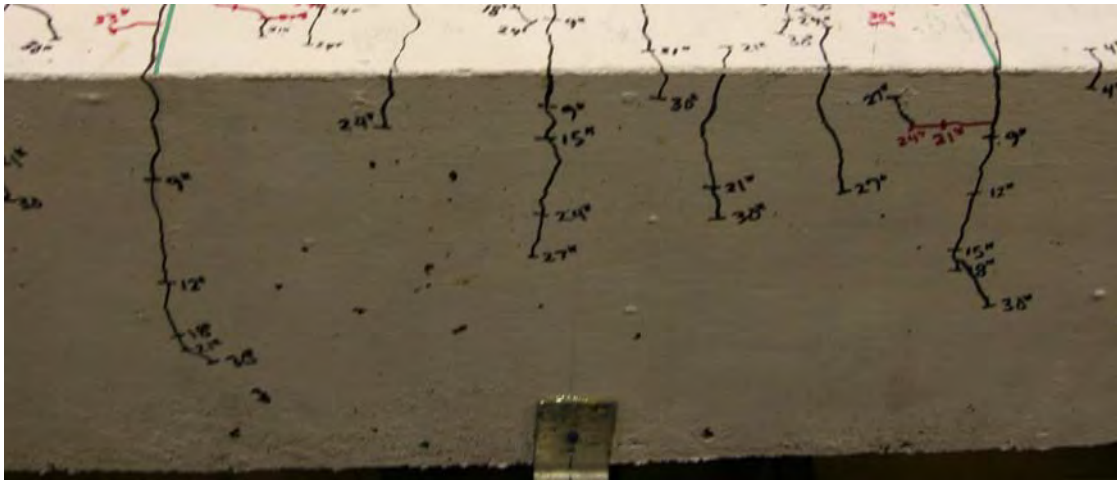**Figure 195. Graph. Load versus transverse rebar strain for Beam C6-ST.**

Figure 196. Graph. Measured and predicted midspan moment versus longitudinal rebar strain for Beam C6-ST.

D-27
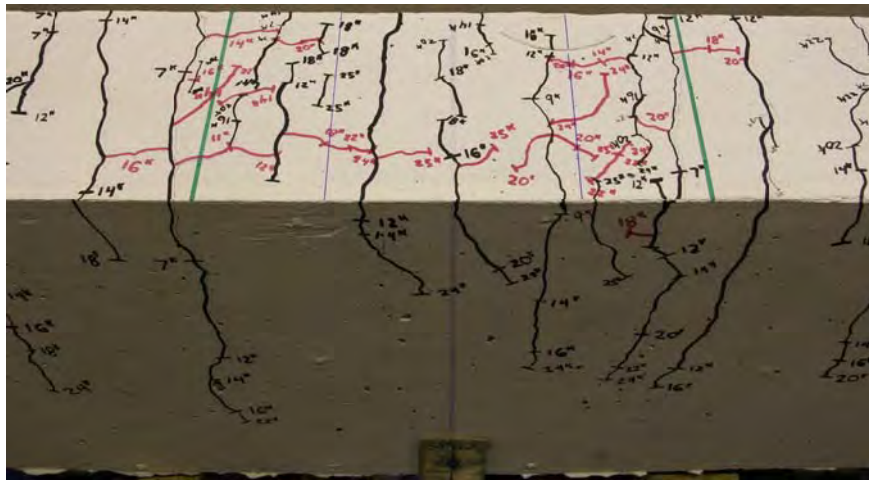
Figure 197. Photo. Side face of Beam C6-ST before failure.
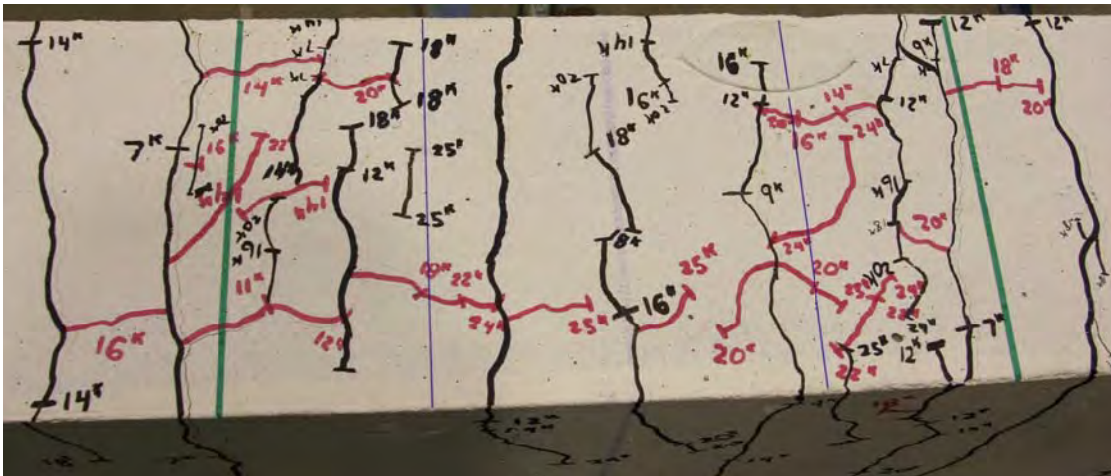
Figure 198. Photo. Top face of Beam C6-ST before failure.
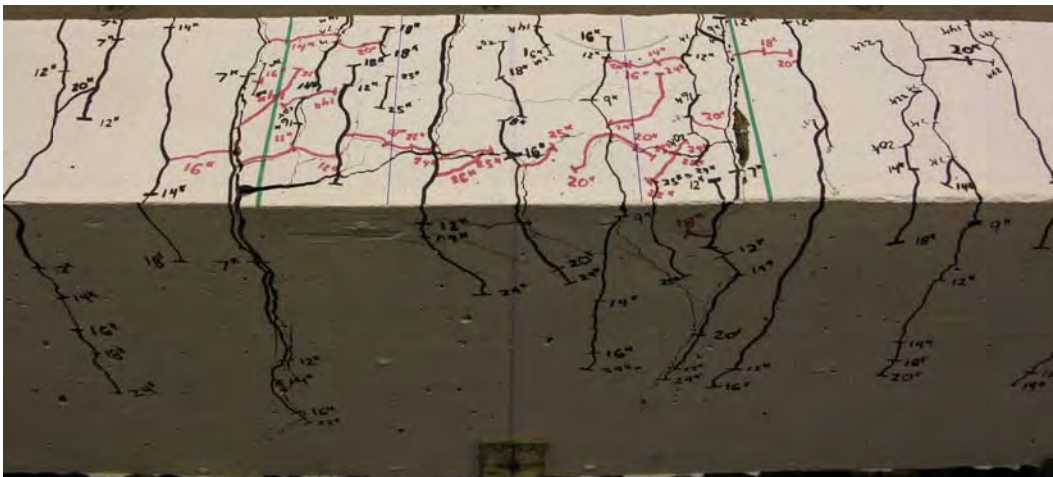
Figure 199. Photo. Beam C6-ST after failure.

Splice Beam A6-LT

<p style="text-align: center;">Table 60. Test parameters for Splice Beam A6-LT.</p>

Concrete Mix	Spliced Bar Size	Lap Length, inch (mm)	#3 (10M) Bar Transverse Reinforcement	Nominal Beam Cross-Section Dimensions (Width by Height), inch (mm)
Stalite	#6 (19M)	24 (610)	(3) at 8 in. (200mm)	18 by 18 (460 by 460)

<p style="text-align: center;">Table 61. Test data for Splice Beam A6-LT.</p>

| Event	Average Jack Load, kips (kN)	Average Beam End Deflection, inch (mm)	Longitudinal Rebar Strain, microstrain		Transverse Rebar Strain, microstrain	
			Gage 1	Gage 2	Gage 1	Gage 2
Flexural cracking	3.1 (14)	0.02 (0.5)	72	65	-1	-6
Top splitting crack	11 (49)	0.12 (3.1)	854	825	30	26
Side splitting crack	18.2 (81)	0.26 (6.7)	1609	1508	54	155
Long. rebar yield	25.9 (115)	0.43 (10.8)	2481	2225	39	416
Ultimate	32.2 (143)	1.27 (32.4)	6658	16387	374	1108

Notes:
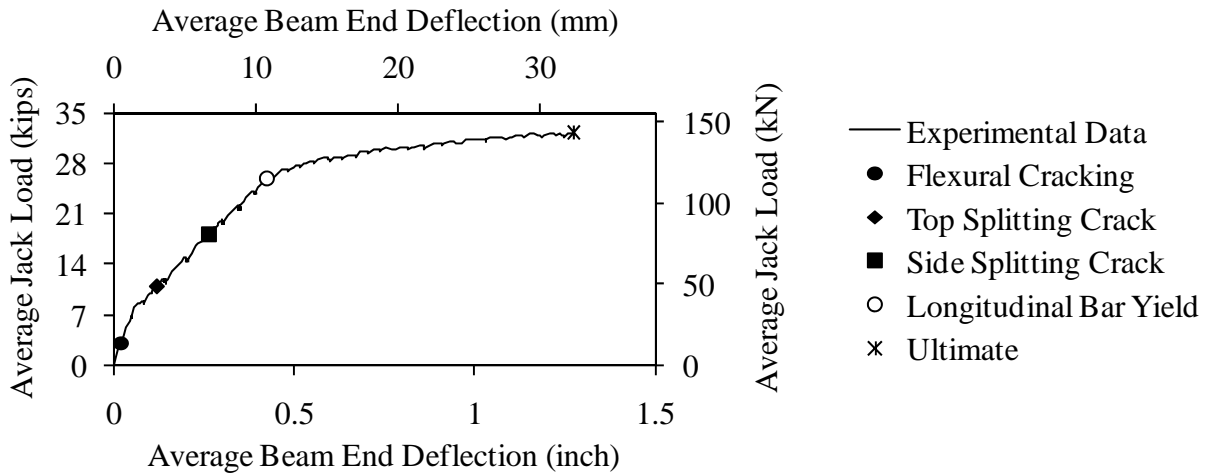
Figure 200. Graph. Load versus deflection for Beam A6-LT.
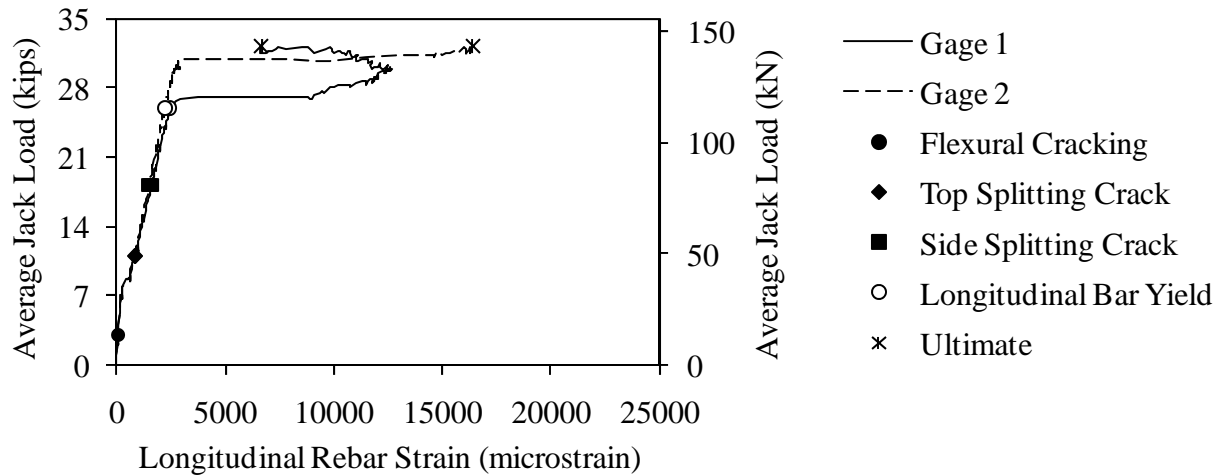
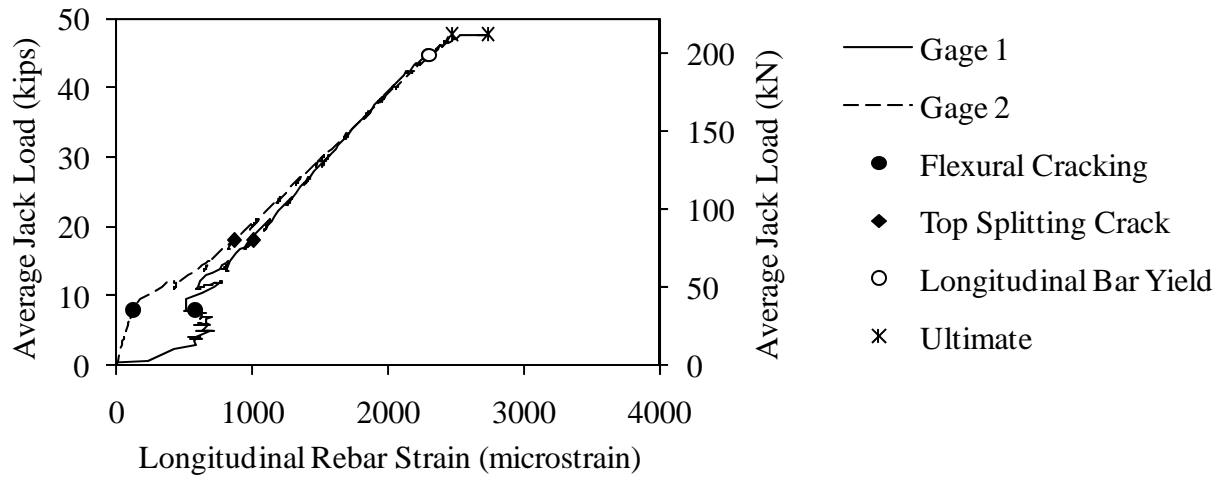**Figure 201. Graph. Load versus longitudinal rebar strain for Beam A6-LT.**

Figure 202. Graph. Load versus transverse rebar strain for Beam A6-LT.
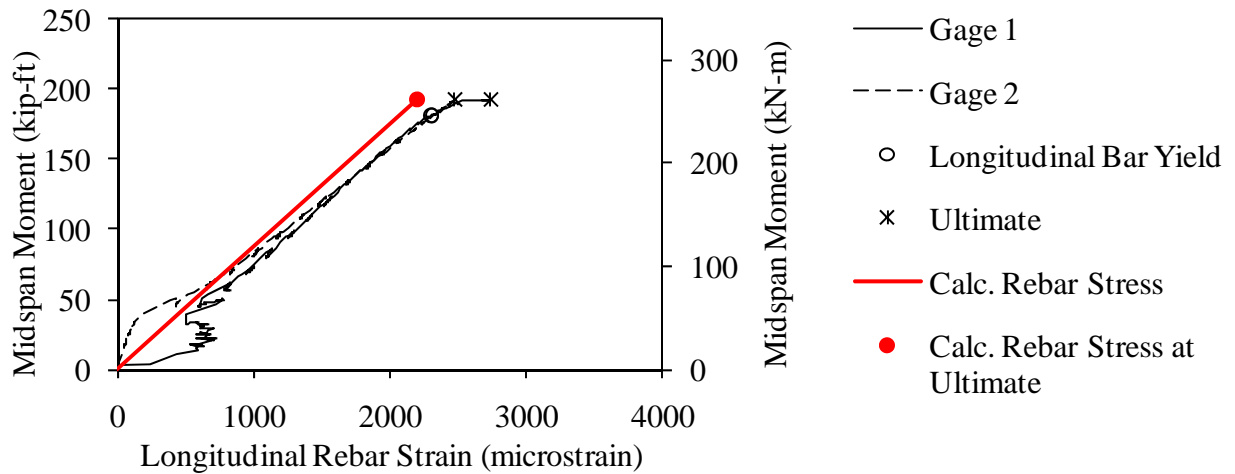

Figure 203. Graph. Measured and predicted midspan moment versus longitudinal rebar strain for Beam A6-LT.
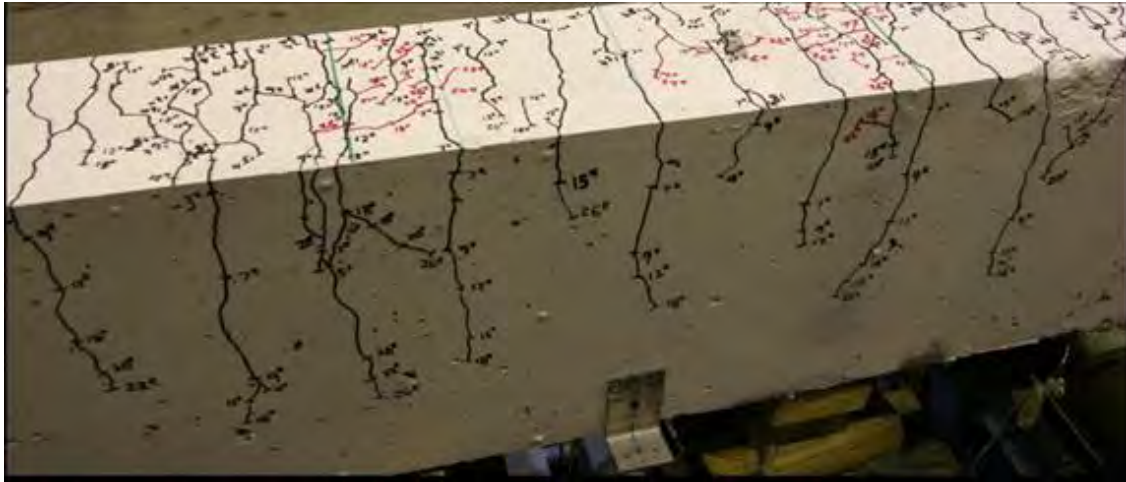
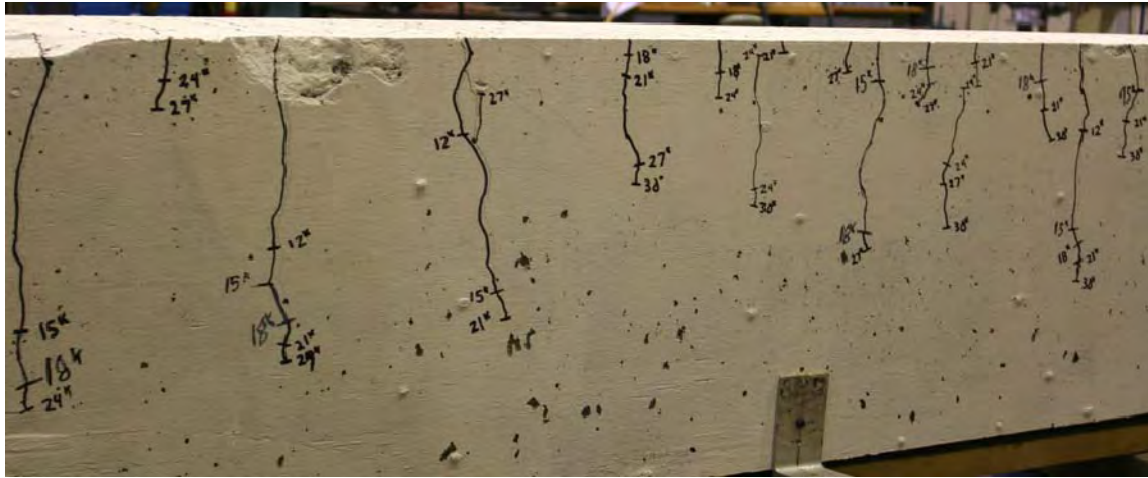**Figure 204. Photo. Side face of Beam A6-LT before failure.**
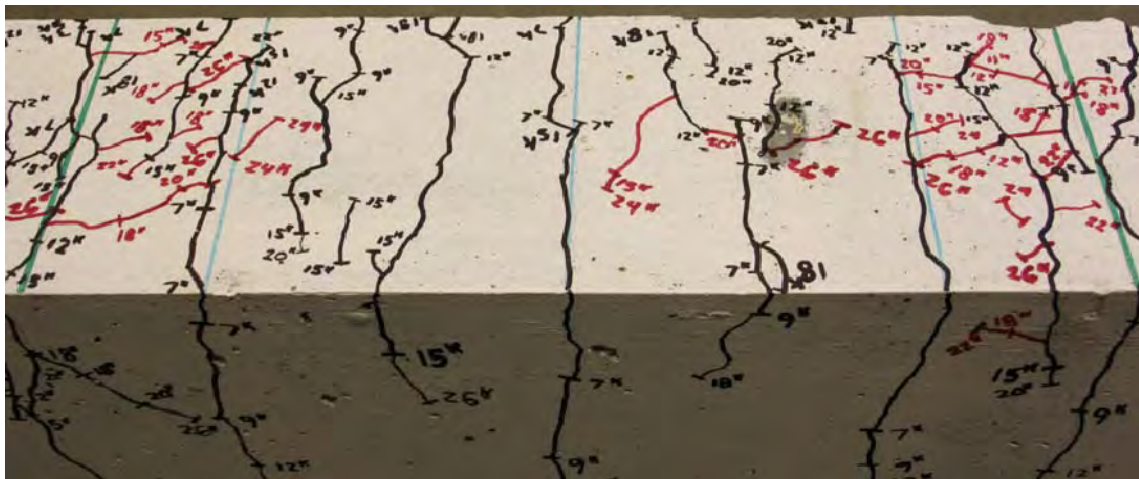
**Figure 205. Photo. Top face of Beam A6-LT before failure.**
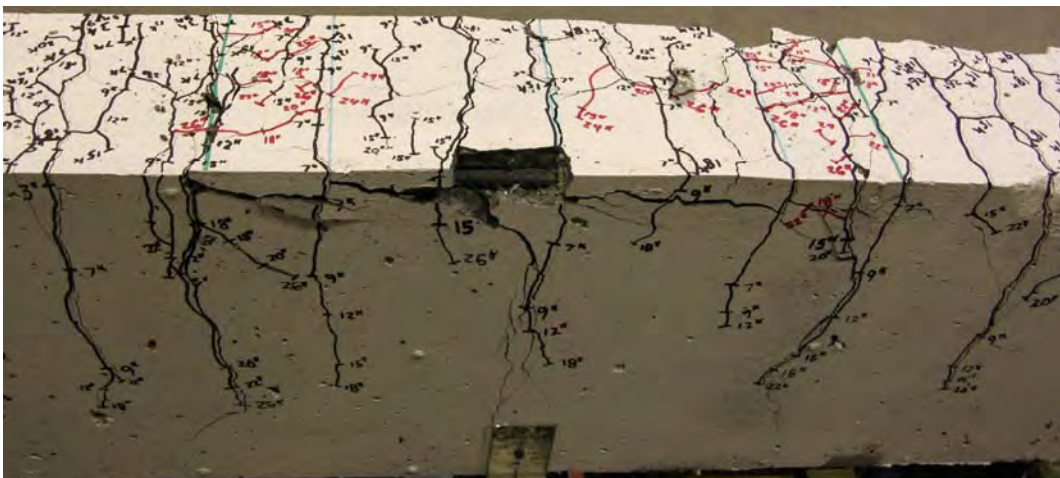
Figure 206. Photo. Beam A6-LT after failure.

Splice Beam B6-LT

Table 62. Test parameters for Splice Beam B6-LT.

Concrete Mix	Spliced Bar Size	Lap Length, inch (mm)	#3 (10M) Bar Transverse Reinforcement	Nominal Beam Cross-Section Dimensions (Width by Height), inch (mm)
Utelite	#6 (19M)	24 (610)	(3) at 8 in. (200mm)	18 by 18 (460 by 460)

Table 63. Test data for Splice Beam B6-LT.

| Event	Average Jack Load, kips (kN)	Average Beam End Deflection, inch (mm)	Longitudinal Rebar Strain, microstrain		Transverse Rebar Strain, microstrain	
			Gage 1	Gage 2	Gage 1	Gage 2
Flexural cracking	5.1 (23)	0.03 (0.7)	130	0	-13	-15
Top splitting crack	13.1 (58)	0.13 (3.4)	1028	0	13	-4
Side splitting crack	24.4 (109)	0.35 (9)	2155	0	185	193
Long. rebar yield	25.6 (114)	0.38 (9.7)	2314	0	232	209
Ultimate	31.8 (141)	1 (25.3)	14360	0	768	399

Notes:
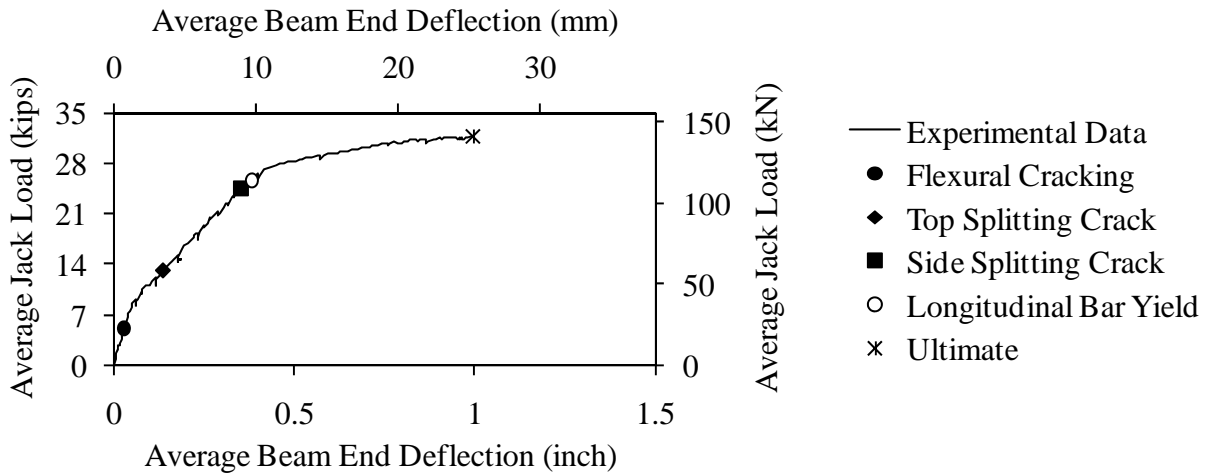
Figure 207. Graph. Load versus deflection for Beam B6-LT.
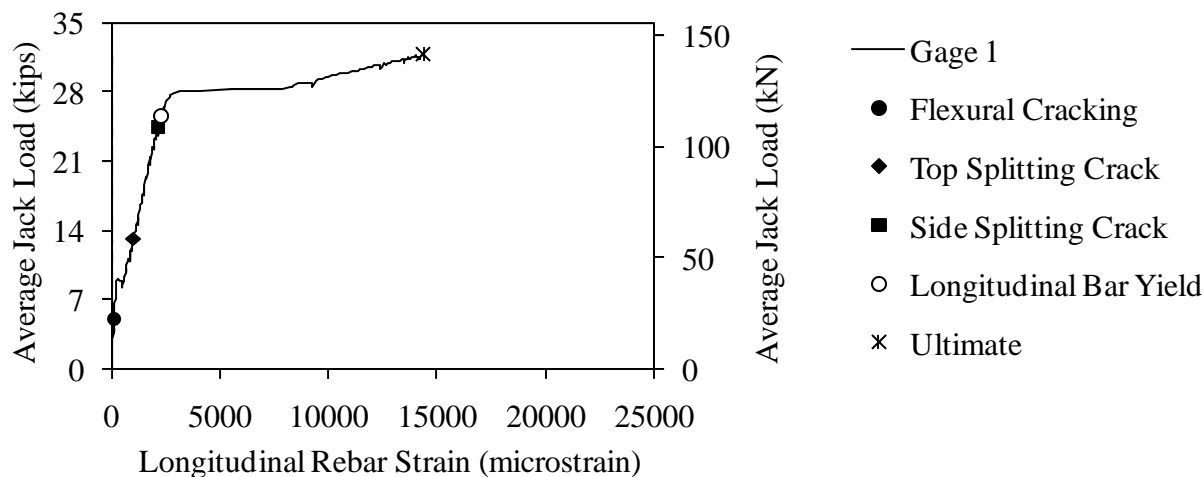
Figure 208. Graph. Load versus longitudinal rebar strain for Beam B6-LT.
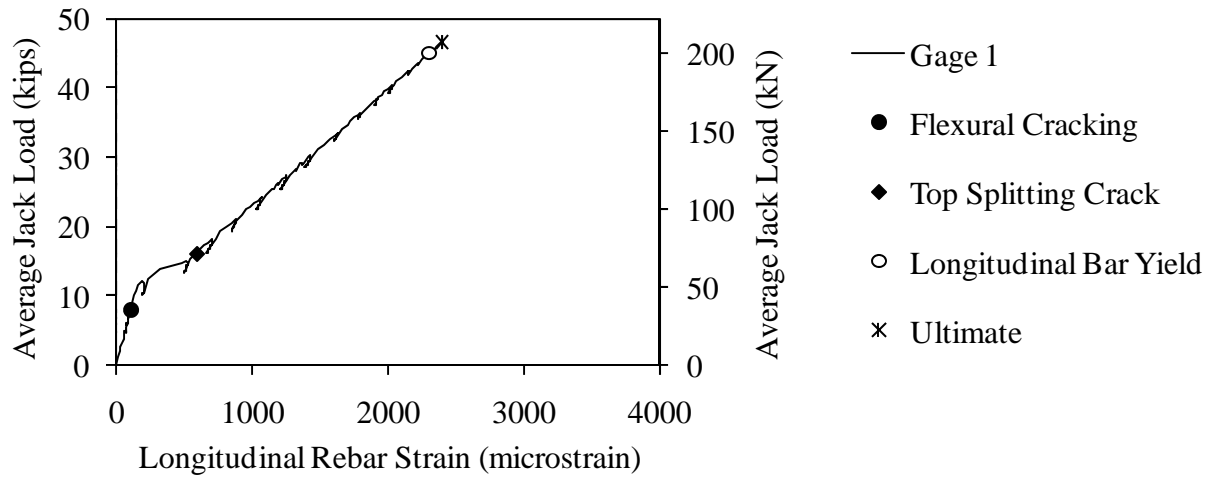

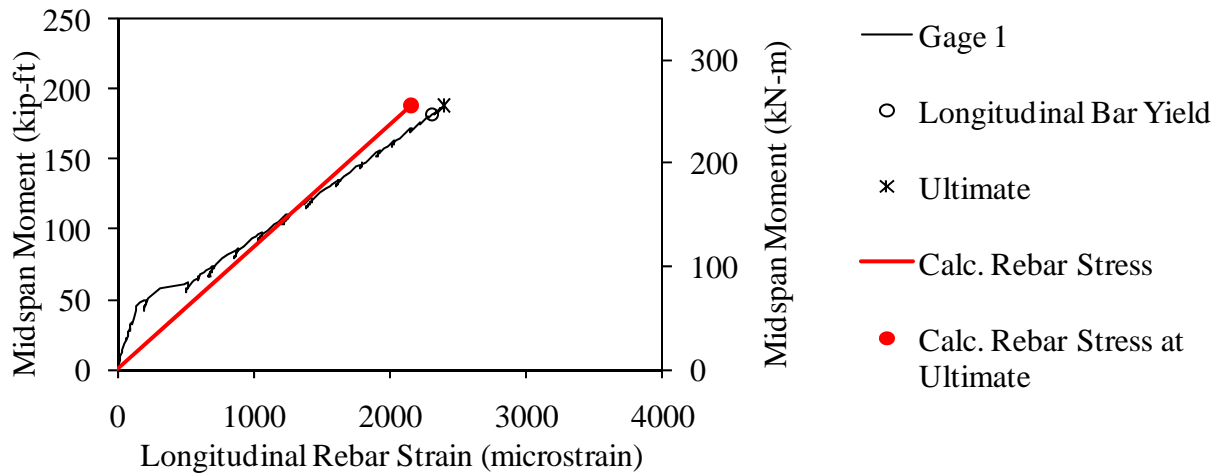**Figure 209. Graph. Load versus transverse rebar strain for Beam B6-LT.**

Figure 210. Graph. Measured and predicted midspan moment versus longitudinal rebar strain for Beam B6-LT.
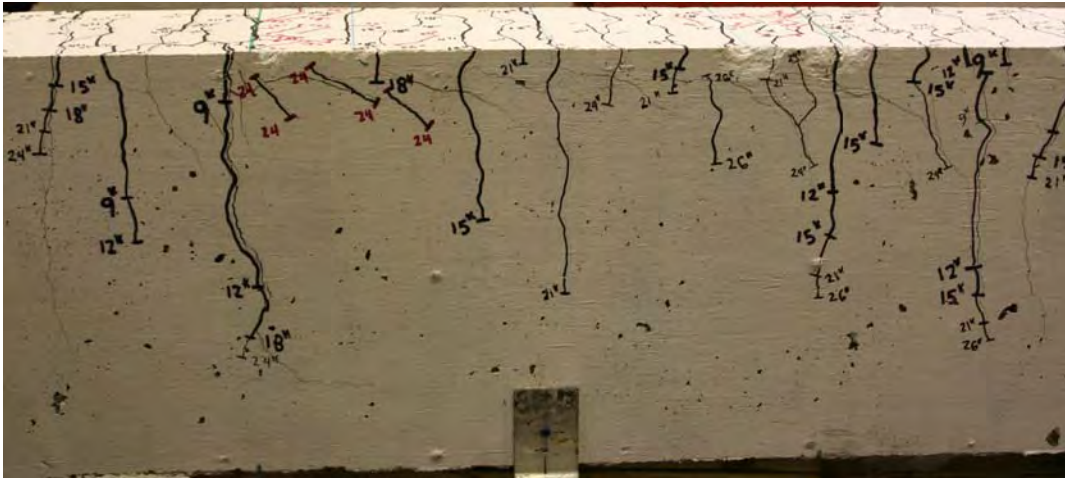
**Figure 211. Photo. Side face of Beam B6-LT before failure.**
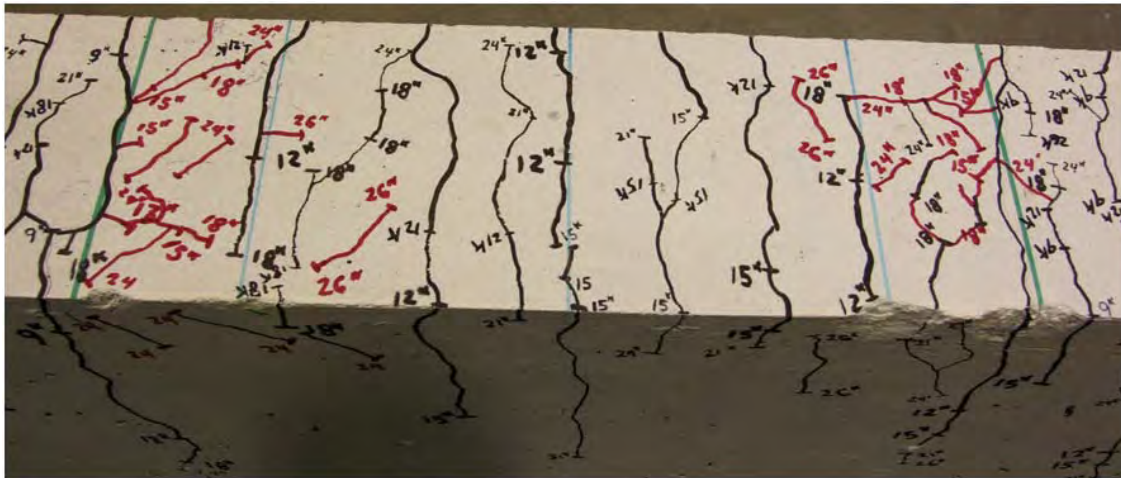
**Figure 212. Photo. Top face of Beam B6-LT before failure.**
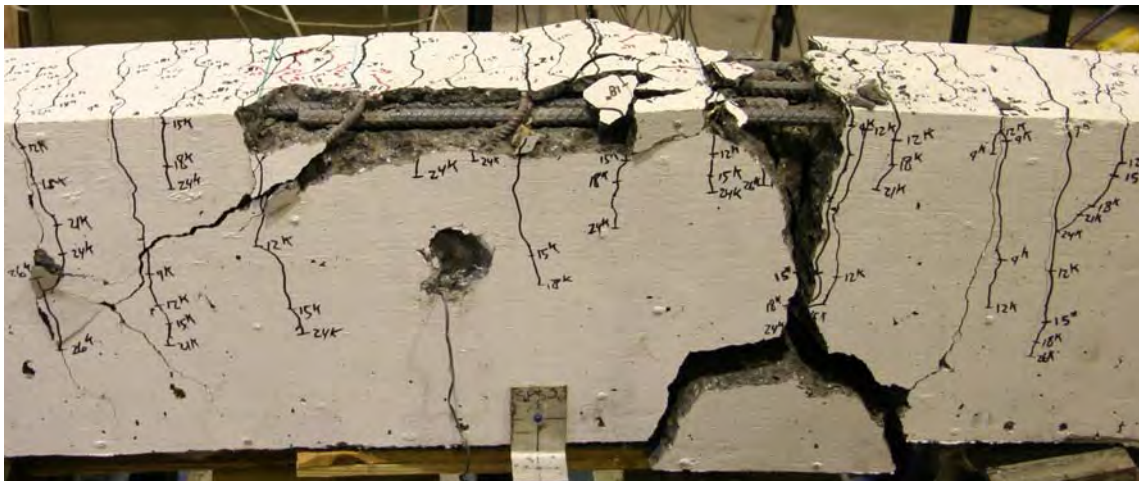
Figure 213. Photo. Beam B6-LT after failure.

Splice Beam C6-LT

Table 64. Test parameters for Splice Beam C6-LT.

Concrete Mix	Spliced Bar Size	Lap Length, inch (mm)	#3 (10M) Bar Transverse Reinforcement	Nominal Beam Cross-Section Dimensions (Width by Height), inch (mm)
Haydite	#6 (19M)	24 (610)	(3) at 8 in. (200mm)	18 by 18 (460 by 460)

Table 65. Test data for Splice Beam C6-LT.

| Event	Average Jack Load, kips (kN)	Average Beam End Deflection, inch (mm)	Longitudinal Rebar Strain, microstrain		Transverse Rebar Strain, microstrain	
			Gage 1	Gage 2	Gage 1	Gage 2
Flexural cracking	4.1 (18)	0.02 (0.6)	78	82	-4	-14
Top splitting crack	11 (49)	0.09 (2.4)	767	673	37	-21
Side splitting crack	20.1 (89)	0.28 (7.1)	1627	1667	202	29
Long. rebar yield	25.8 (115)	0.42 (10.8)	2344	2258	421	48
Ultimate	32.4 (144)	1.29 (32.9)	13465	14953	1325	651

Notes:
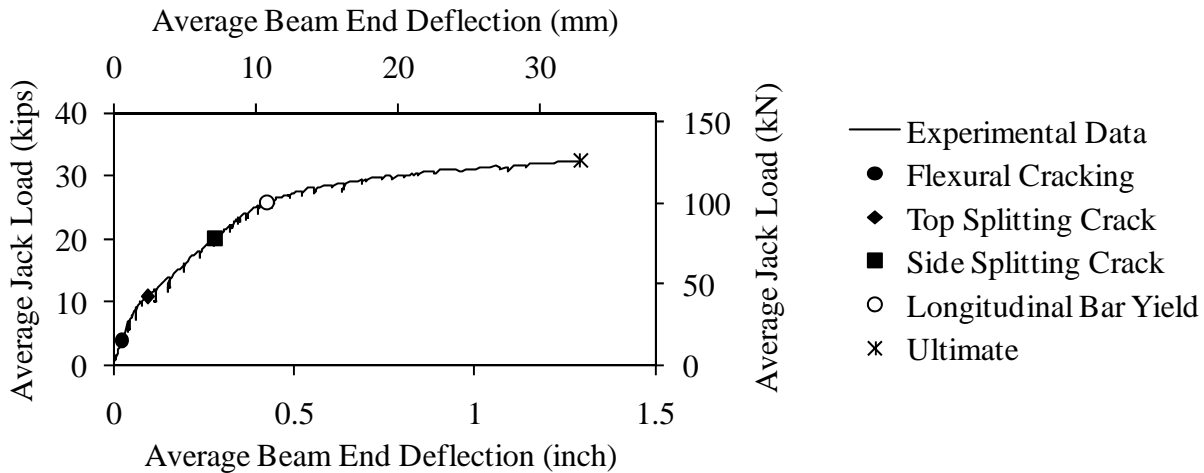
Figure 214. Graph. Load versus deflection for Beam C6-LT.
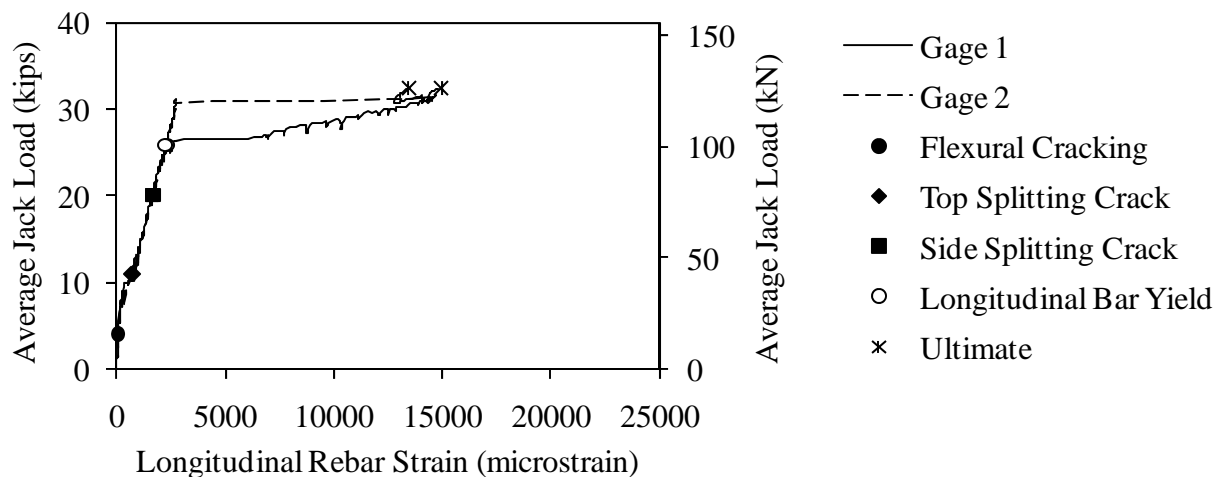
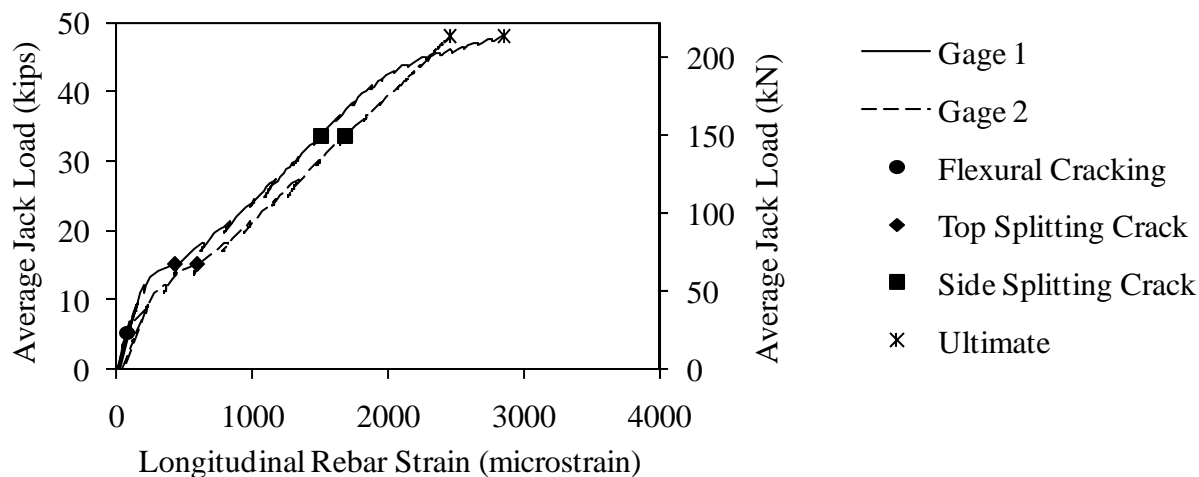**Figure 215. Graph. Load versus longitudinal rebar strain for Beam C6-LT.**

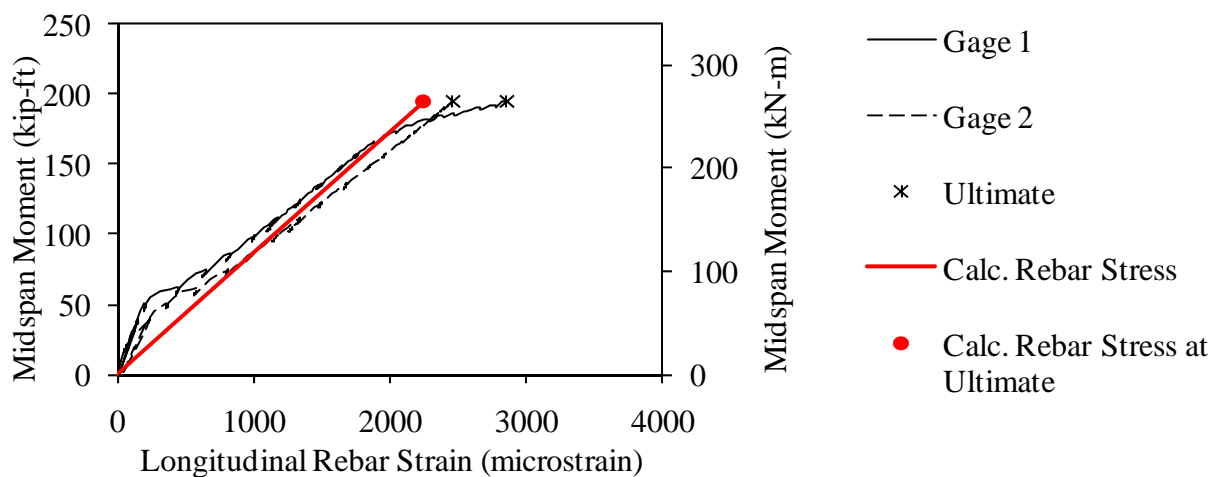**Figure 216. Graph. Load versus transverse rebar strain for Beam C6-LT.**

**Figure 217. Graph. Measured and predicted midspan moment versus longitudinal rebar strain for Beam C6-LT.**
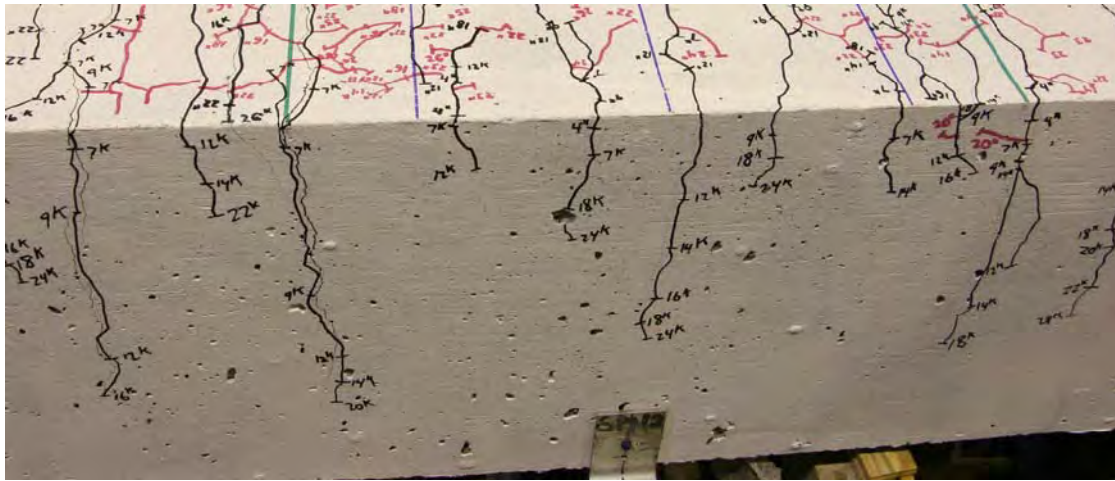
**Figure 218. Photo. Side face of Beam C6-LT before failure.**

**Figure 219. Photo. Top face of Beam C6-LT before failure.**
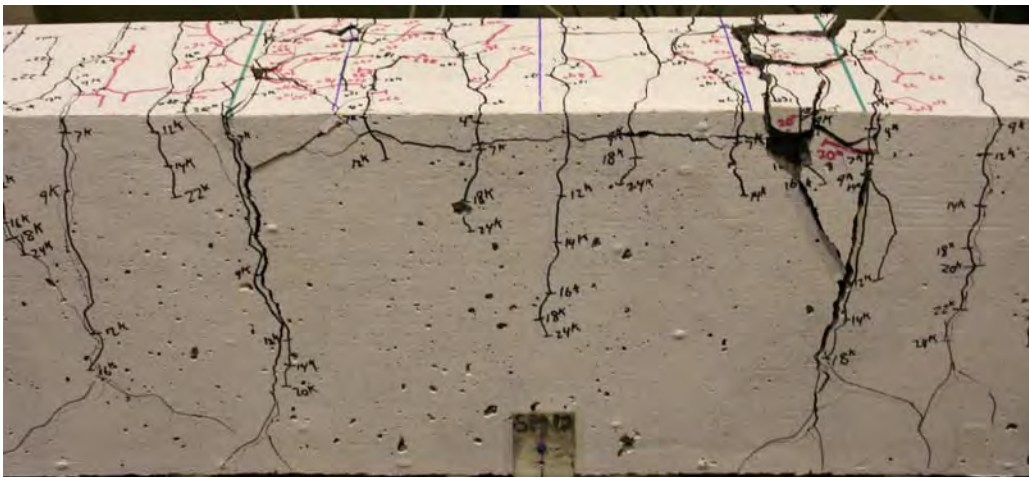
Figure 220. Photo. Beam C6-LT after failure.

Splice Beam A8-SN

Table 66. Test parameters for Splice Beam A8-SN.

Concrete Mix	Spliced Bar Size	Lap Length, inch (mm)	#3 (10M) Bar Transverse Reinforcement	Nominal Beam Cross-Section Dimensions (Width by Height), inch (mm)
Stalite	#8 (25M)	24 (610)	None	18 by 18 (460 by 460)

Table 67. Test data for Splice Beam A8-SN.

| Event	Average Jack Load, kips (kN)	Average Beam End Deflection, inch (mm)	Longitudinal Rebar Strain, microstrain		Transverse Rebar Strain, microstrain	
			Gage 1	Gage 2	Gage 1	Gage 2
Flexural cracking	7 (31)	0.04 (0.9)	94	184	N/A	N/A
Top splitting crack	16.1 (72)	0.13 (3.3)	581	841	N/A	N/A
Side splitting crack	N/A	N/A	N/A	N/A	N/A	N/A
Long. rebar yield	N/A	N/A	N/A	N/A	N/A	N/A
Ultimate	41 (182)	0.49 (12.4)	1707	2219	N/A	N/A

Notes:
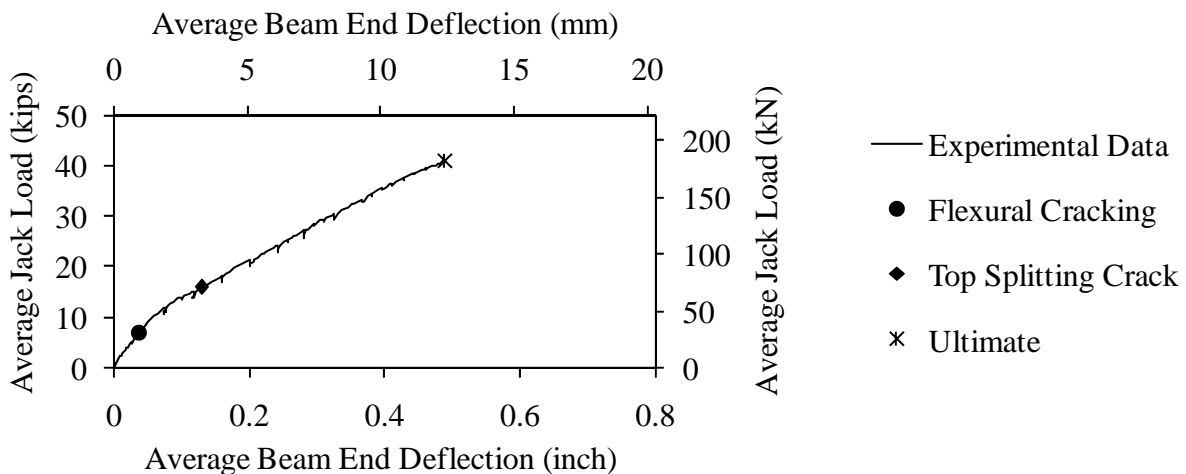
Figure 221. Graph. Load versus deflection for Beam A8-SN.
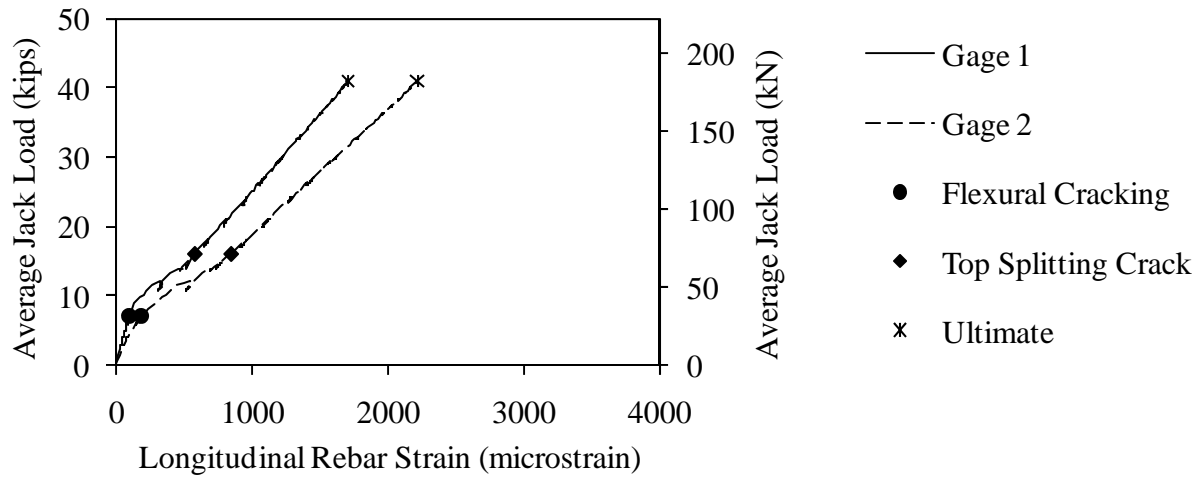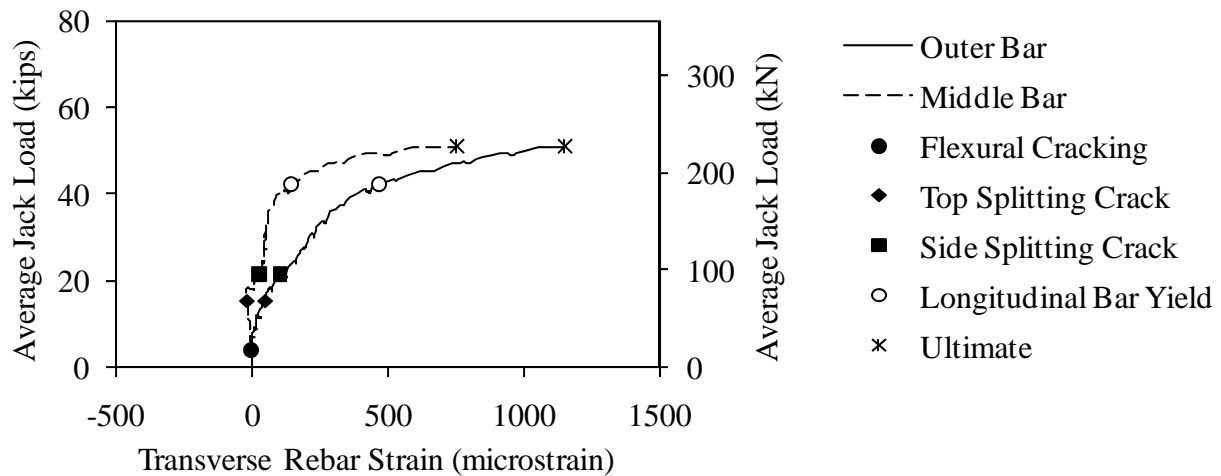
Figure 222. Graph. Load versus longitudinal rebar strain for Beam A8-SN.

Figure 5. Graph. Measured and predicted midspan moment versus longitudinal rebar strain for Beam A8-SN.

Figure 223. Photo. Side face of Beam A8-SN before failure.
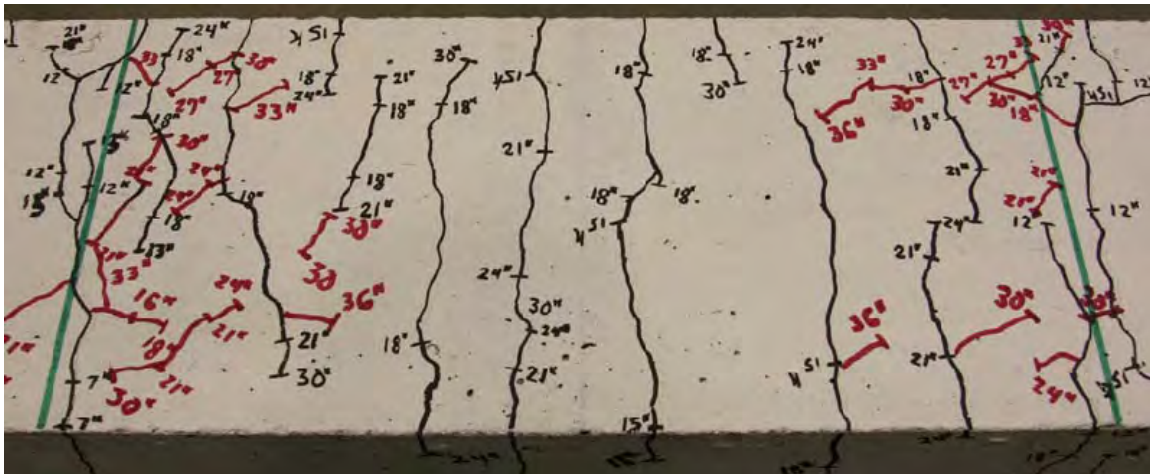
Figure 224. Photo. Top face of Beam A8-SN before failure.

Figure 225. Photo. Beam A8-SN after failure.

Splice Beam B8-SN

Table 68. Test parameters for Splice Beam B8-SN.

Concrete Mix	Spliced Bar Size	Lap Length, inch (mm)	#3 (10M) Bar Transverse Reinforcement	Nominal Beam Cross-Section Dimensions (Width by Height), inch (mm)
Utelite	#8 (25M)	24 (610)	None	18 by 18 (460 by 460)

Table 69. Test data for Splice Beam B8-SN.

Event	Average Jack Load, kips (kN)	Average Beam End Deflection, inch (mm)	Longitudinal Rebar Strain, microstrain		Transverse Rebar Strain, microstrain	
			Gage 1	Gage 2	Gage 1	Gage 2
Flexural cracking	8.2 (36)	0.04 (1)	108	123	N/A	N/A
Top splitting crack	17.2 (76)	0.13 (3.2)	626	793	N/A	N/A
Side splitting crack	25.3 (113)	0.24 (6)	1127	1282	N/A	N/A
Long. rebar yield	N/A	N/A	N/A	N/A	N/A	N/A
Ultimate	42.5 (189)	0.48 (12.2)	2113	2250	N/A	N/A

Notes:
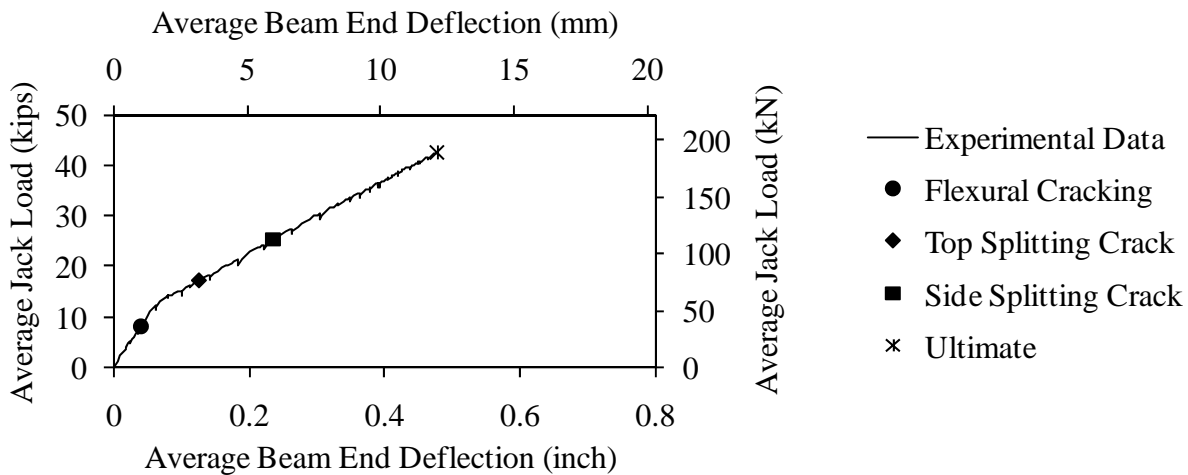
Figure 226. Graph. Load versus deflection for Beam B8-SN.
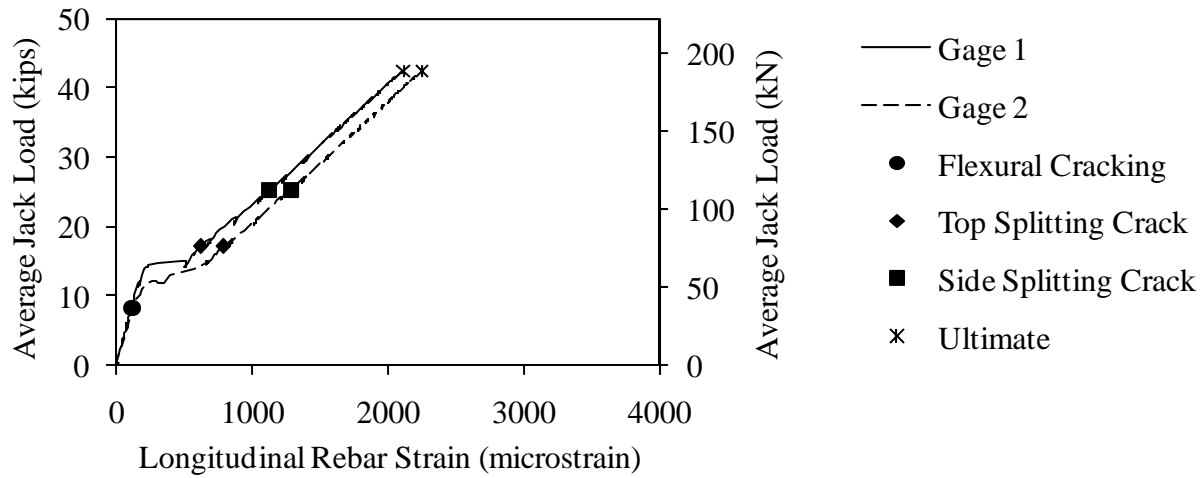
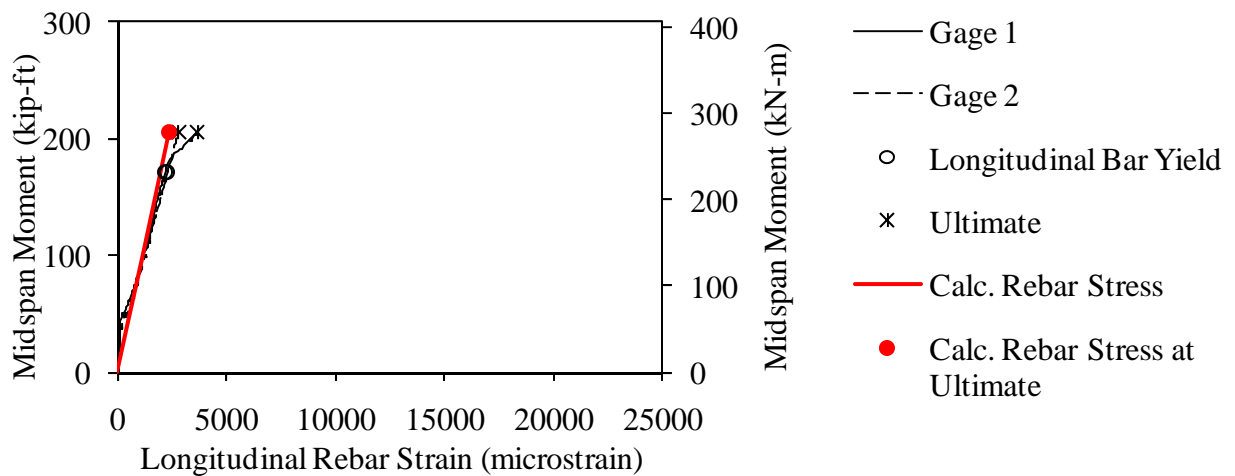**Figure 227. Graph. Load versus longitudinal rebar strain for Beam B8-SN.**

**Figure 5. Graph. Measured and predicted midspan moment versus longitudinal rebar strain for Beam B8-SN.**
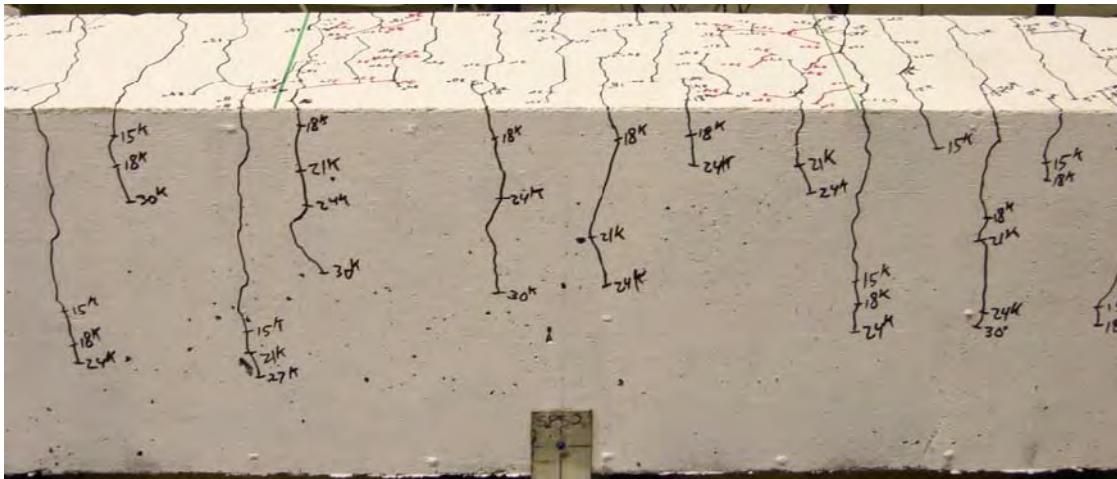
**Figure 228. Photo. Side face of Beam B8-SN before failure.**
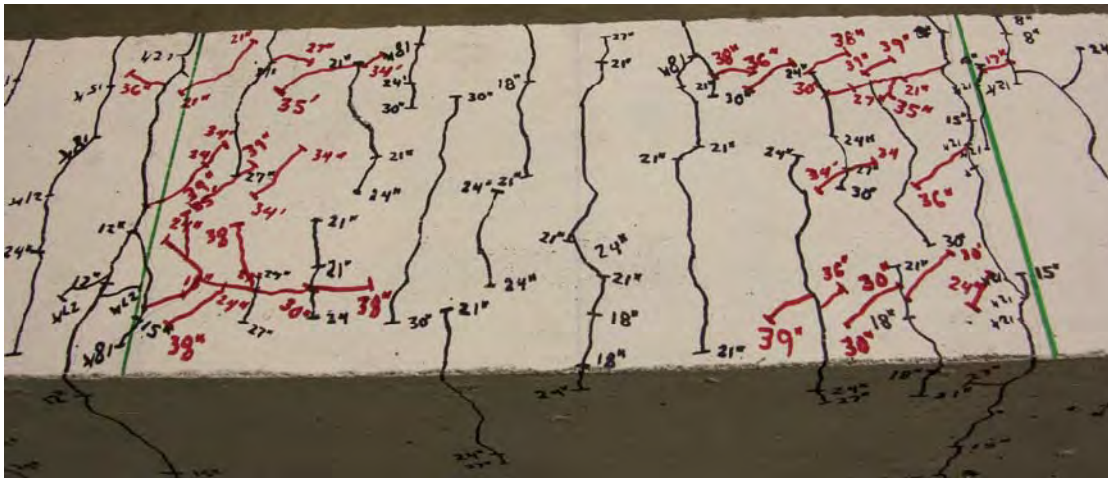
**Figure 229. Photo. Top face of Beam B8-SN before failure.**
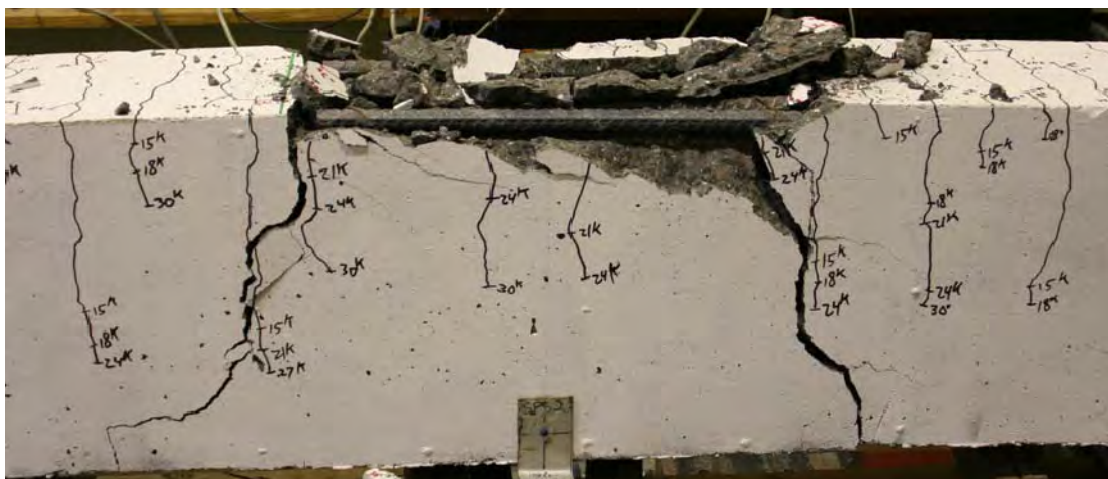
Figure 230. Photo. Beam B8-SN after failure.

Splice Beam C8-SN

Table 70. Test parameters for Splice Beam C8-SN.

Concrete Mix	Spliced Bar Size	Lap Length, inch (mm)	#3 (10M) Bar Transverse Reinforcement	Nominal Beam Cross-Section Dimensions (Width by Height), inch (mm)
Haydite	#8 (25M)	24 (610)	None	18 by 18 (460 by 460)

Table 71. Test data for Splice Beam C8-SN.

| Event	Average Jack Load, kips (kN)	Average Beam End Deflection, inch (mm)	Longitudinal Rebar Strain, microstrain		Transverse Rebar Strain, microstrain	
			Gage 1	Gage 2	Gage 1	Gage 2
Flexural cracking	4.1 (18)	0.02 (0.5)	54	0	N/A	N/A
Top splitting crack	15.1 (67)	0.11 (2.9)	522	0	N/A	N/A
Side splitting crack	21.2 (94)	0.19 (4.8)	918	0	N/A	N/A
Long. rebar yield	N/A	N/A	N/A	N/A	N/A	N/A
Ultimate	39.3 (175)	0.45 (11.5)	1943	0	N/A	N/A

Notes:
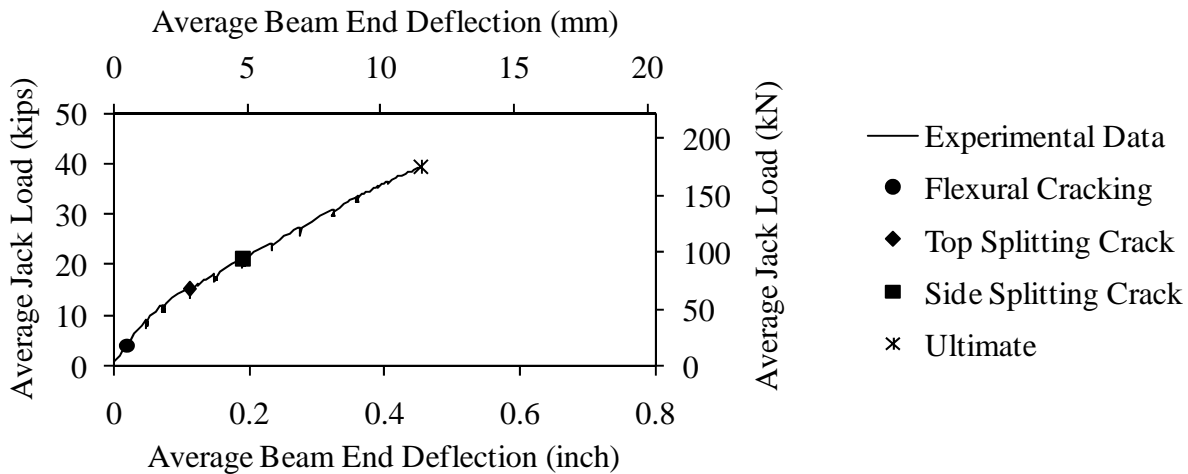
Figure 231. Graph. Load versus deflection for Beam C8-SN.

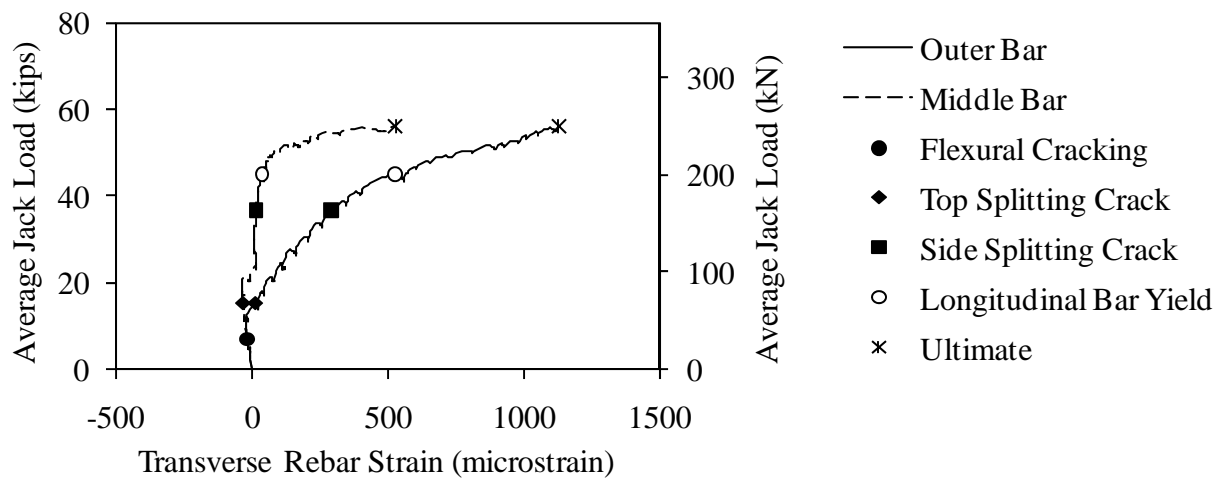**Figure 232. Graph. Load versus longitudinal rebar strain for Beam C8-SN.**
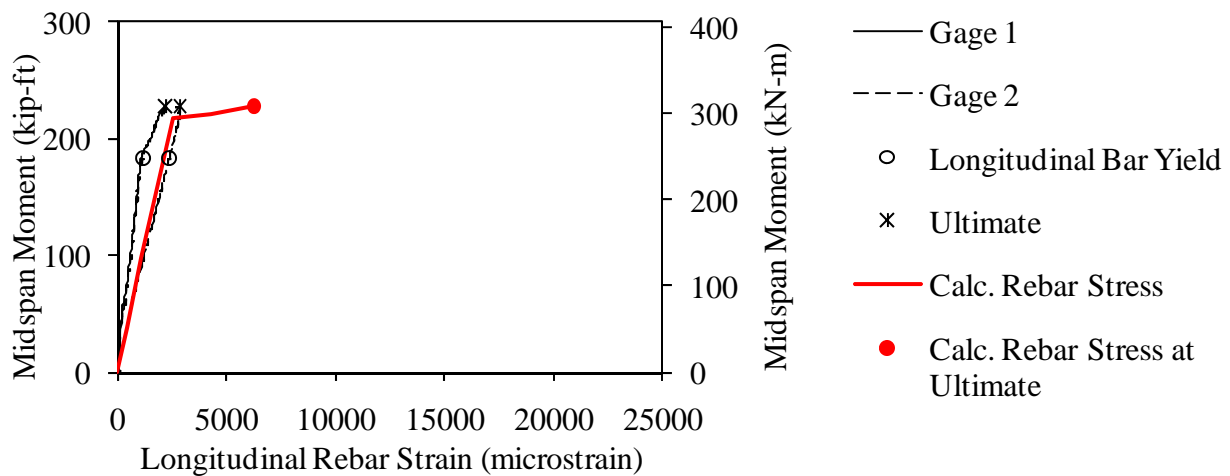

**Figure 233. Graph. Measured and predicted midspan moment versus longitudinal rebar strain for Beam C8-SN.**

**Figure 234. Photo. Side face of Beam C8-SN before failure.**

**Figure 235. Photo. Top face of Beam C8-SN before failure.**

Figure 236. Photo. Beam C8-SN after failure.

Splice Beam A8-LN

Table 72. Test parameters for Splice Beam A8-LN.

Concrete Mix	Spliced Bar Size	Lap Length, inch (mm)	#3 (10M) Bar Transverse Reinforcement	Nominal Beam Cross-Section Dimensions (Width by Height), inch (mm)
Stalite	#8 (25M)	32 (810)	None	18 by 18 (460 by 460)

Table 73. Test data for Splice Beam A8-LN.

| Event	Average Jack Load, kips (kN)	Average Beam End Deflection, inch (mm)	Longitudinal Rebar Strain, microstrain		Transverse Rebar Strain, microstrain	
			Gage 1	Gage 2	Gage 1	Gage 2
Flexural cracking	8 (36)	0.04 (1)	978	121	N/A	N/A
Top splitting crack	18.1 (80)	0.15 (3.8)	1410	864	N/A	N/A
Side splitting crack	N/A	N/A	N/A	N/A	N/A	N/A
Long. rebar yield	44.7 (199)	0.53 (13.6)	2696	2308	N/A	N/A
Ultimate	47.7 (212)	0.59 (15)	3138	2475	N/A	N/A

Notes:
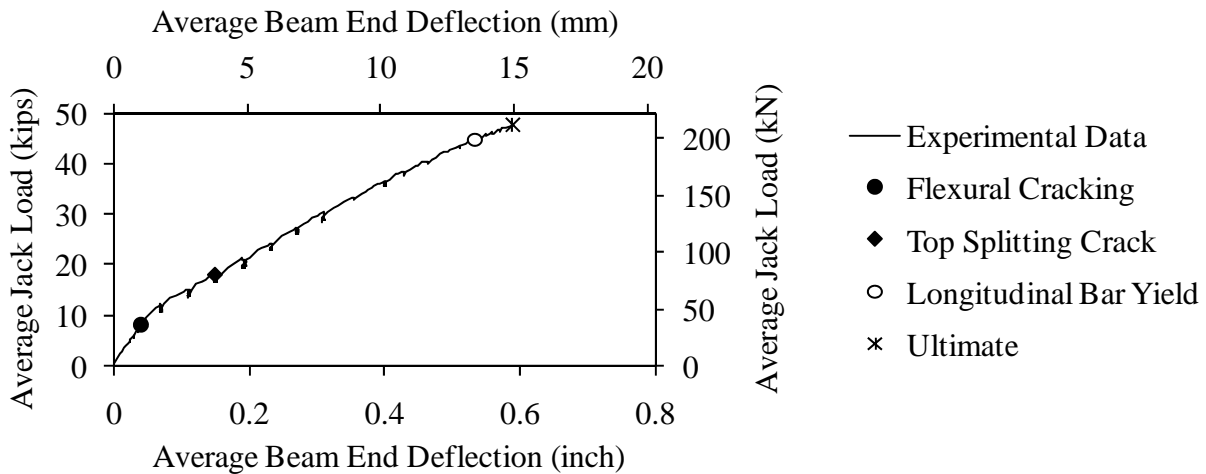
Figure 237. Graph. Load versus deflection for Beam A8-LN.

Figure 238. Graph. Load versus longitudinal rebar strain for Beam A8-LN.

Figure 239. Graph. Measured and predicted midspan moment versus longitudinal rebar strain for Beam A8-LN.

Figure 240. Photo. Side face of Beam A8-LN before failure.
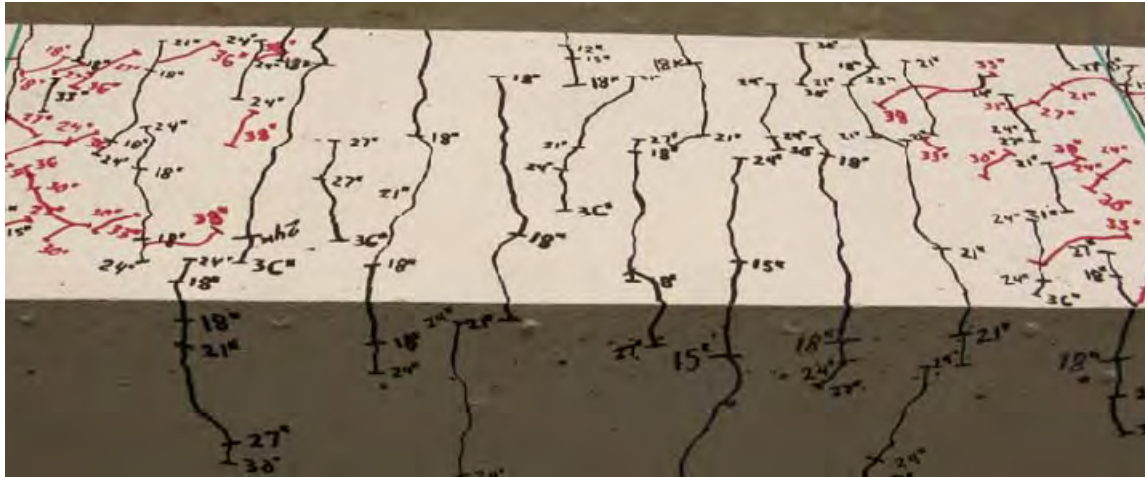
Figure 241. Photo. Top face of Beam A8-LN before failure.
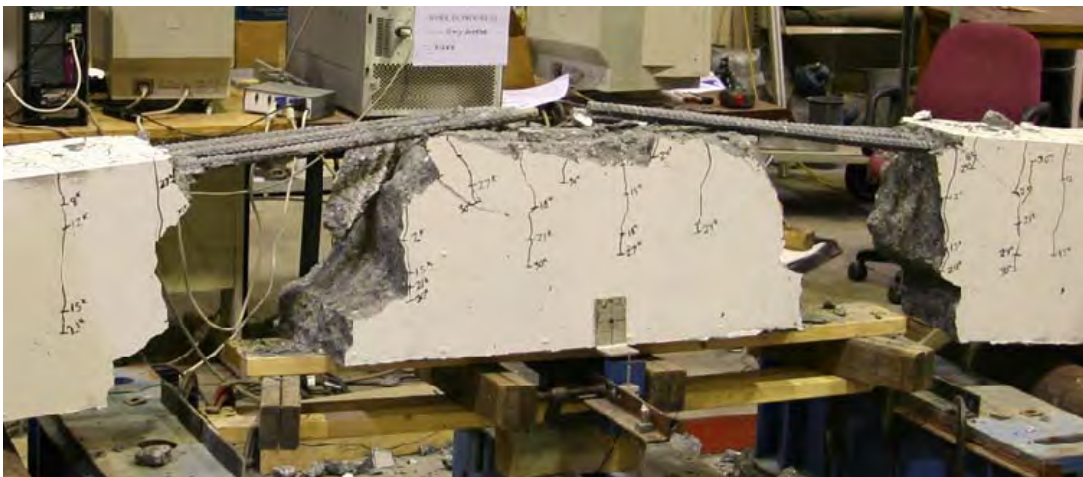
Figure 242. Photo. Beam A8-LN after failure.

D-49

Splice Beam B8-LN

<div align="center">

Table 74. Test parameters for Splice Beam B8-LN.

Concrete Mix	Spliced Bar Size	Lap Length, inch (mm)	#3 (10M) Bar Transverse Reinforcement	Nominal Beam Cross-Section Dimensions (Width by Height), inch (mm)
Utelite	#8 (25M)	32 (810)	None	18 by 18 (460 by 460)

</div>

<div align="center">

Table 75. Test data for Splice Beam B8-LN.

Event	Average Jack Load, kips (kN)	Average Beam End Deflection, inch (mm)	Longitudinal Rebar Strain, microstrain Gage 1	Longitudinal Rebar Strain, microstrain Gage 2	Transverse Rebar Strain, microstrain Gage 1	Transverse Rebar Strain, microstrain Gage 2
Flexural cracking	8.1 (36)	0.04 (1)	0	106	N/A	N/A
Top splitting crack	16.1 (71)	0.1 (2.5)	0	593	N/A	N/A
Side splitting crack	N/A	N/A	N/A	N/A	N/A	N/A
Long. rebar yield	45 (200)	0.5 (12.6)	0	2306	N/A	N/A
Ultimate	46.6 (207)	0.53 (13.3)	0	2397	N/A	N/A

</div>

Notes:
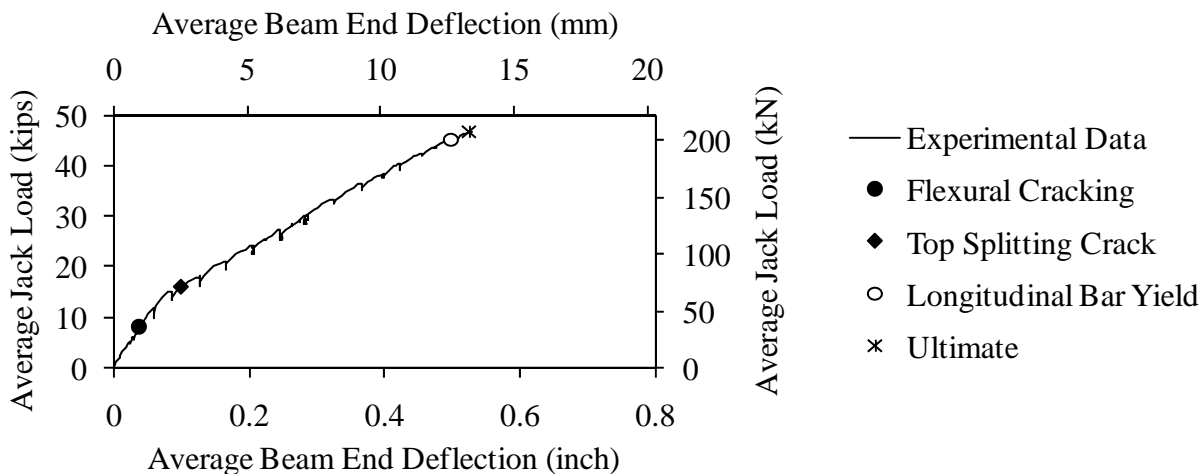
Figure 243. Graph. Load versus deflection for Beam B8-LN.

Figure 244. Graph. Load versus longitudinal rebar strain for Beam B8-LN.
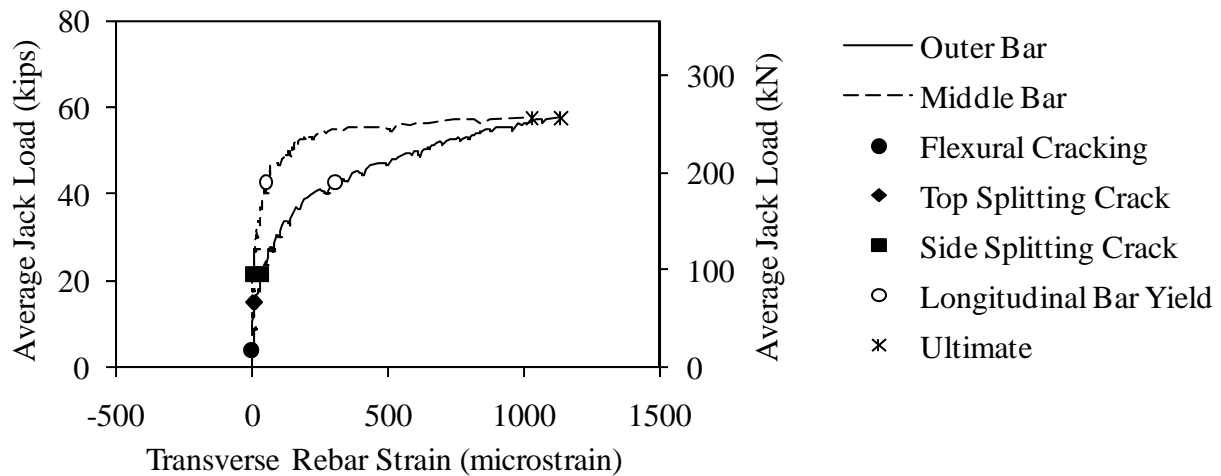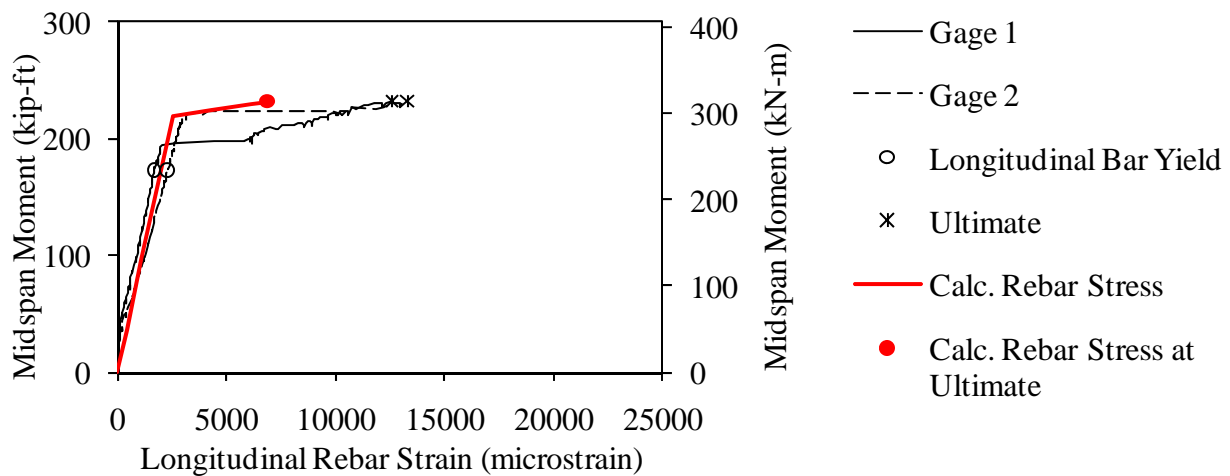

Figure 245. Graph. Measured and predicted midspan moment versus longitudinal rebar strain for Beam B8-LN.

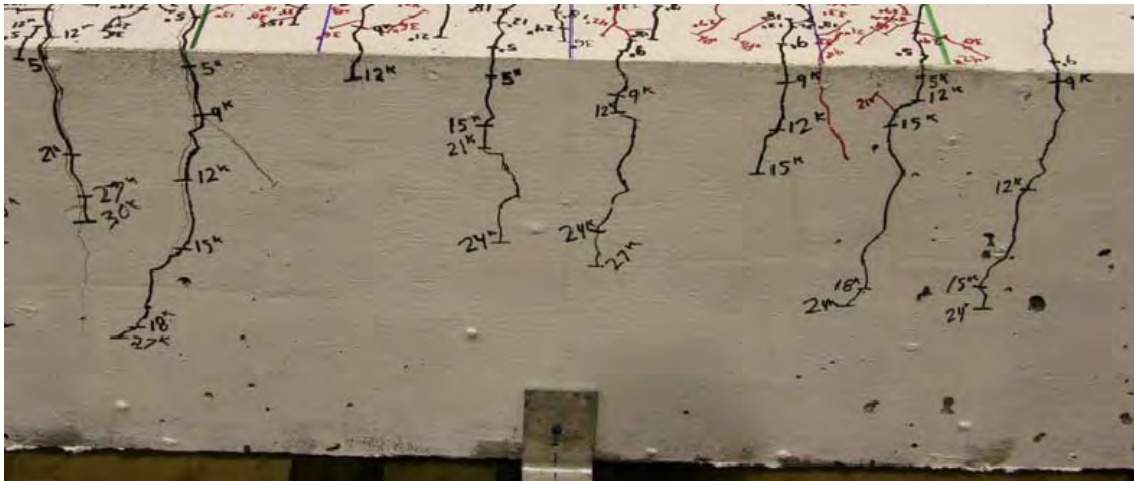**Figure 246. Photo. Side face of Beam B8-LN before failure.**
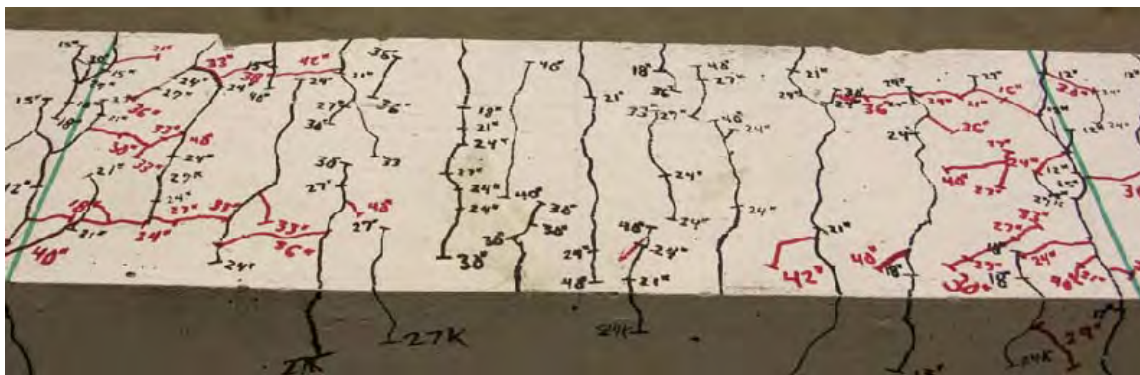

Figure 247. Photo. Top face of Beam B8-LN before failure.
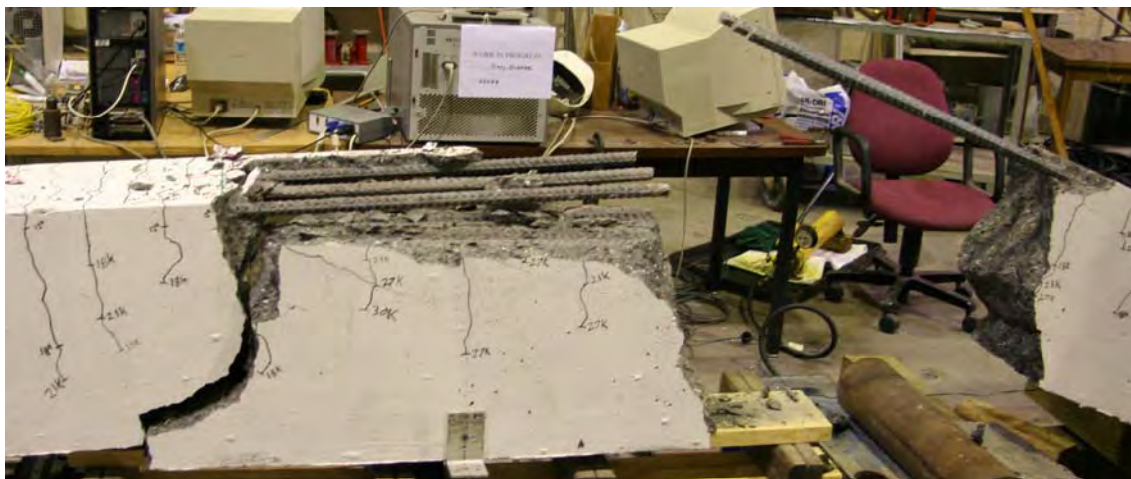
Figure 248. Photo. Beam B8-LN after failure.

Splice Beam C8-LN

Table 76. Test parameters for Splice Beam C8-LN.

Concrete Mix	Spliced Bar Size	Lap Length, inch (mm)	#3 (10M) Bar Transverse Reinforcement	Nominal Beam Cross-Section Dimensions (Width by Height), inch (mm)
Haydite	#8 (25M)	32 (810)	None	18 by 18 (460 by 460)

Table 77. Test data for Splice Beam C8-LN.

| Event	Average Jack Load, kips (kN)	Average Beam End Deflection, inch (mm)	Longitudinal Rebar Strain, microstrain		Transverse Rebar Strain, microstrain	
			Gage 1	Gage 2	Gage 1	Gage 2
Flexural cracking	5.2 (23)	0.03 (0.6)	74	74	N/A	N/A
Top splitting crack	15.2 (68)	0.09 (2.3)	435	593	N/A	N/A
Side splitting crack	33.7 (150)	0.33 (8.4)	1504	1689	N/A	N/A
Long. rebar yield	N/A	N/A	N/A	N/A	N/A	N/A
Ultimate	48.1 (214)	0.57 (14.4)	2854	2461	N/A	N/A

Notes:
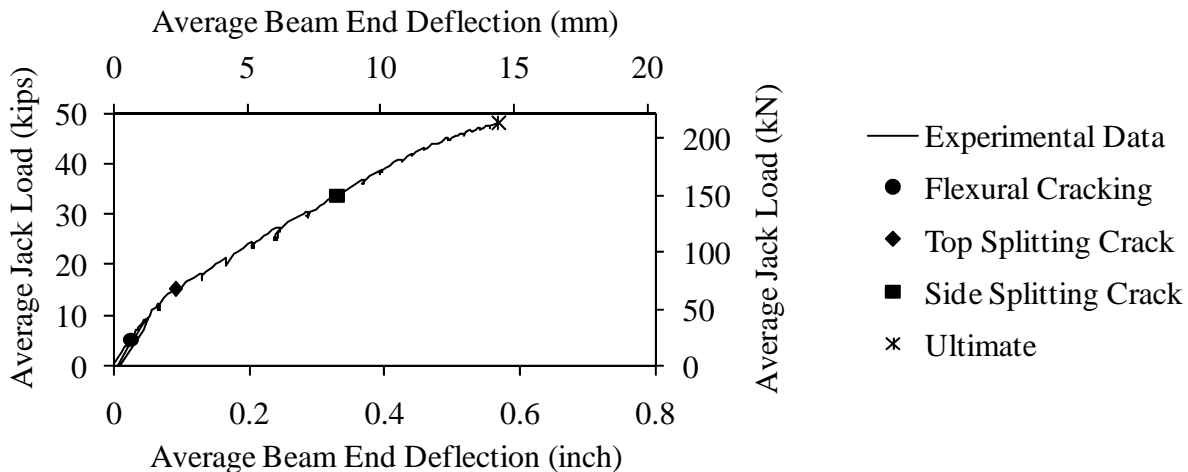
Figure 249. Graph. Load versus deflection for Beam C8-LN.

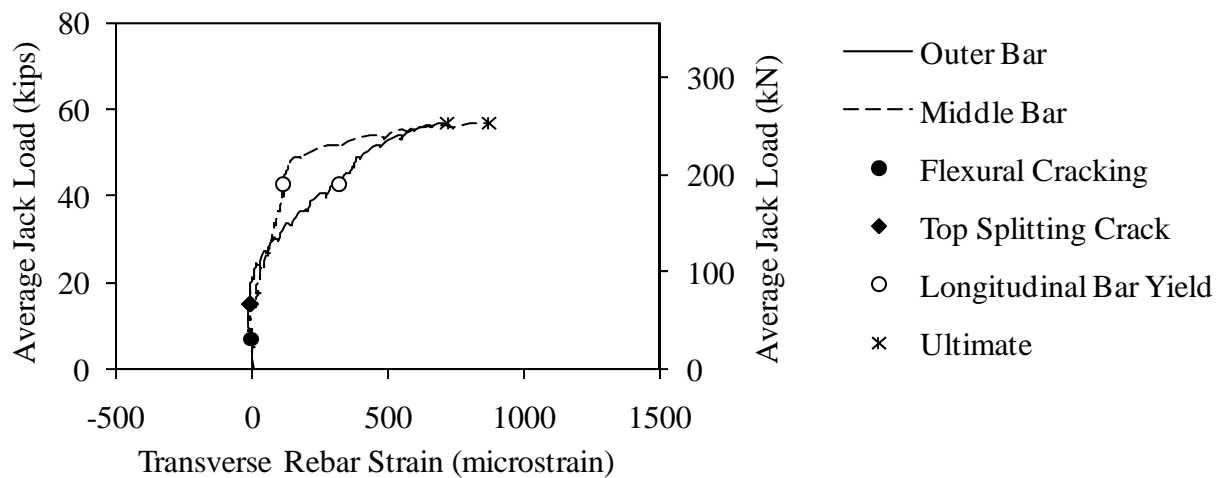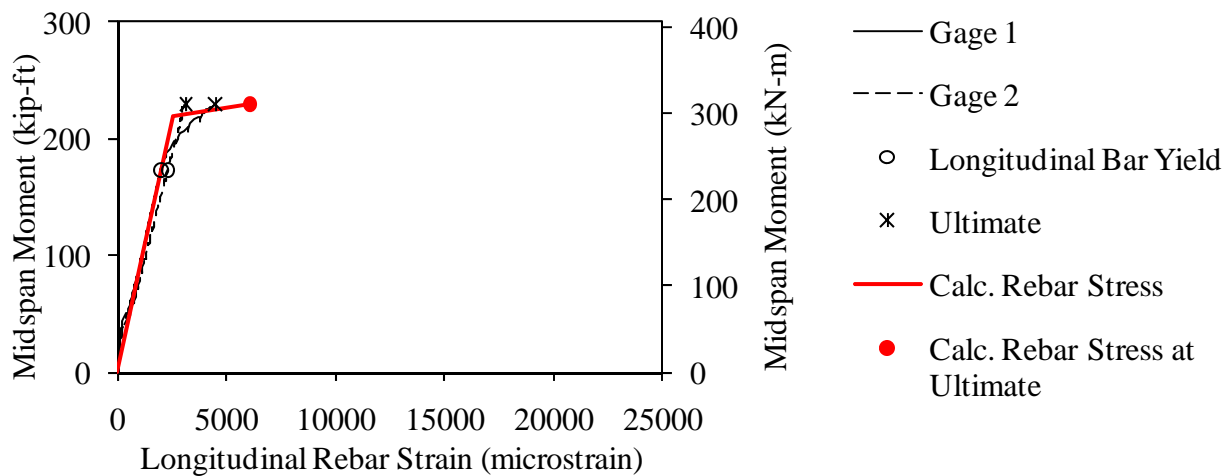**Figure 250. Graph. Load versus longitudinal rebar strain for Beam C8-LN.**

**Figure 251. Graph. Measured and predicted midspan moment versus longitudinal rebar strain for Beam C8-LN.**
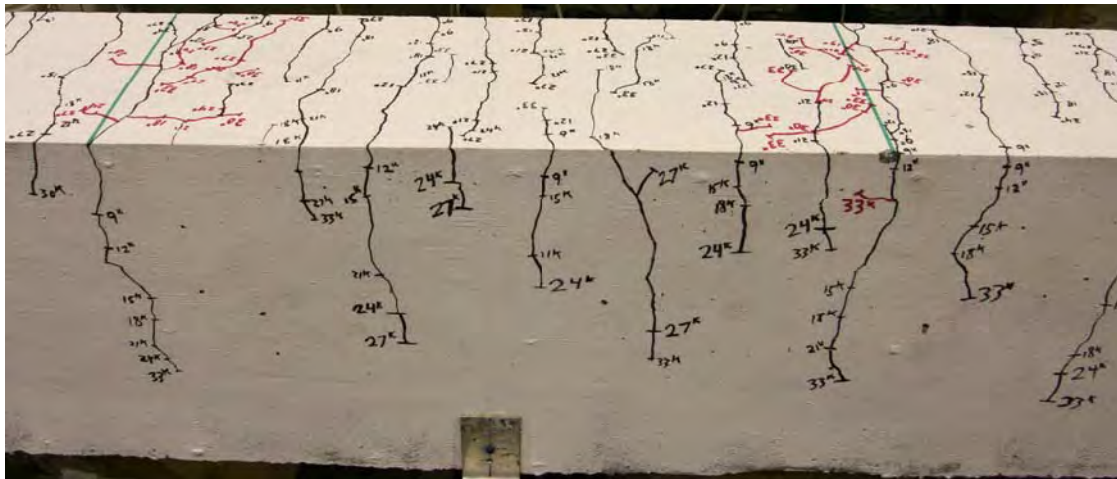
**Figure 252. Photo. Side face of Beam C8-LN before failure.**
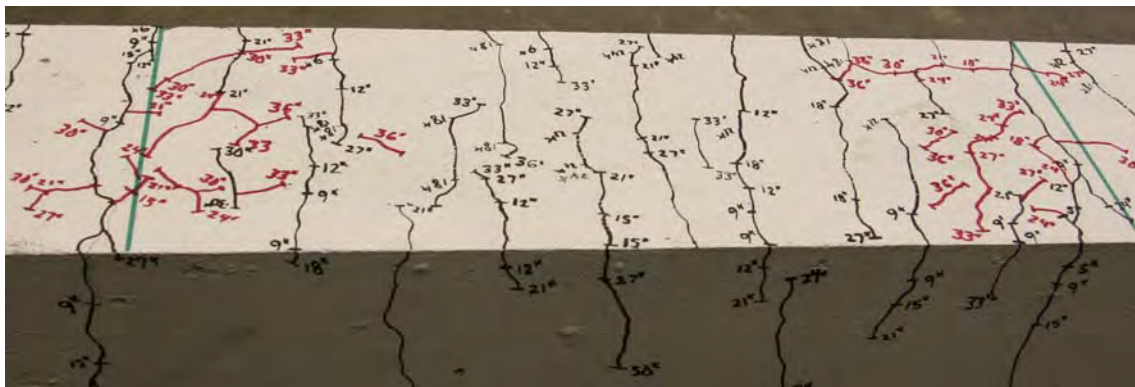
**Figure 253. Photo. Top face of Beam C8-LN before failure.**
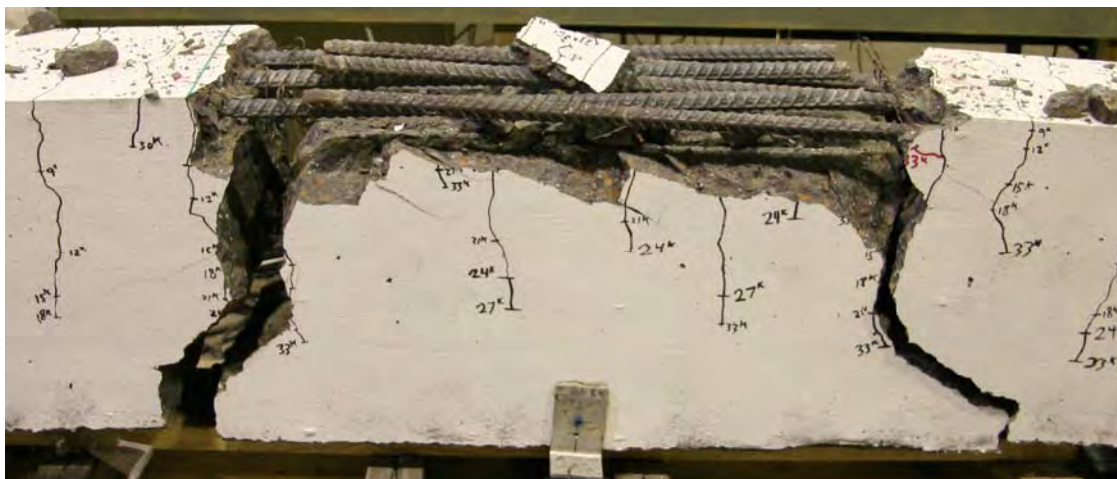
Figure 254. Photo. Beam C8-LN after failure.

Splice Beam A8-ST

Table 78. Test parameters for Splice Beam A8-ST.

Concrete Mix	Spliced Bar Size	Lap Length, inch (mm)	#3 (10M) Bar Transverse Reinforcement	Nominal Beam Cross-Section Dimensions (Width by Height), inch (mm)
Stalite	#8 (25M)	24 (610)	(3) at 8 in. (200mm)	18 by 18 (460 by 460)

Table 79. Test data for Splice Beam A8-ST.

| Event	Average Jack Load, kips (kN)	Average Beam End Deflection, inch (mm)	Longitudinal Rebar Strain, microstrain		Transverse Rebar Strain, microstrain	
			Gage 1	Gage 2	Gage 1	Gage 2
Flexural cracking	4.1 (18)	0.02 (0.5)	56	63	-2	-4
Top splitting crack	15.3 (68)	0.12 (3.1)	587	709	45	-20
Side splitting crack	21.5 (95)	0.21 (5.3)	1013	1083	104	27
Long. rebar yield	42.4 (188)	0.51 (12.9)	2191	2304	466	141
Ultimate	51 (227)	0.68 (17.4)	3670	2800	1151	753

Notes:
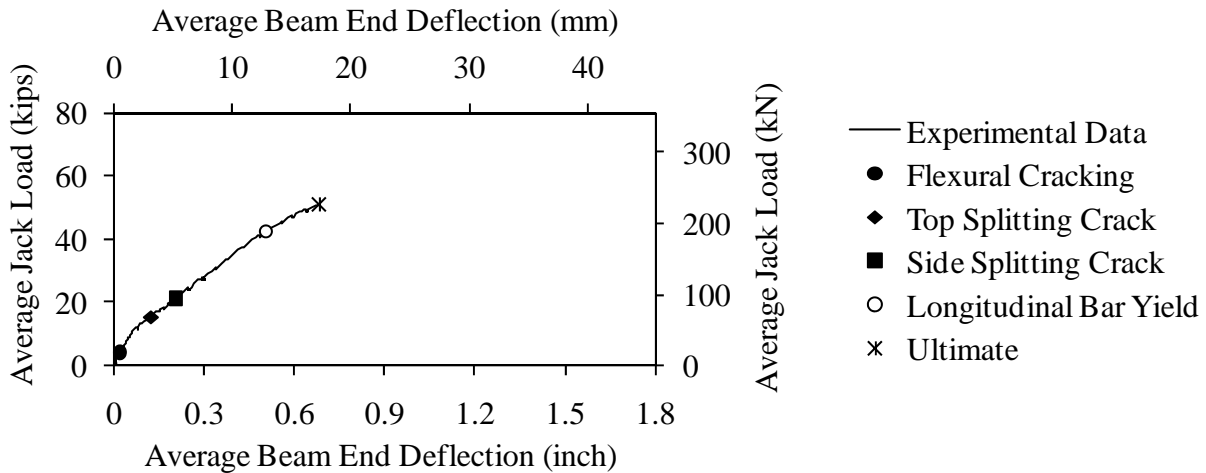
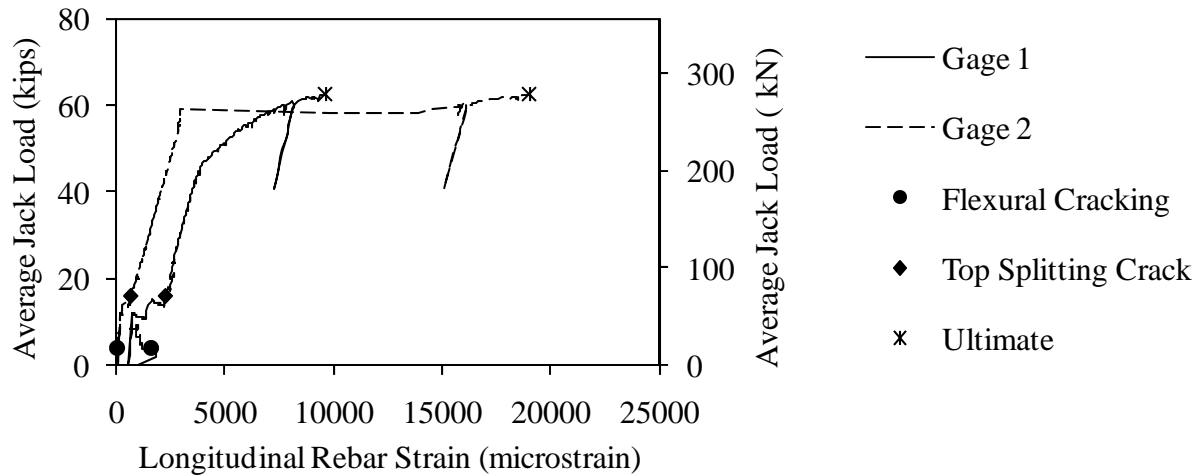**Figure 255. Graph. Load versus deflection for Beam A8-ST.**
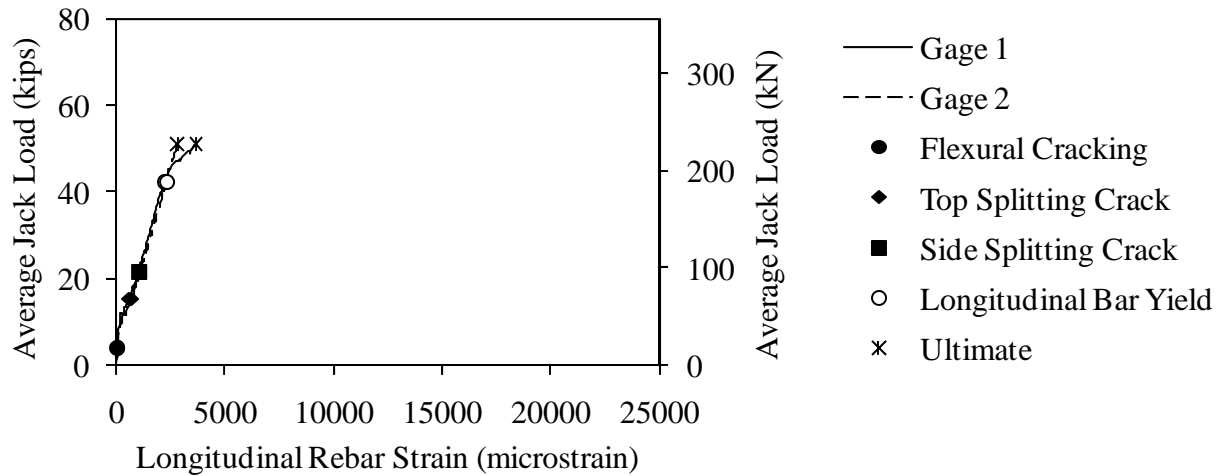
Figure 256. Graph. Load versus longitudinal rebar strain for Beam A8-ST.
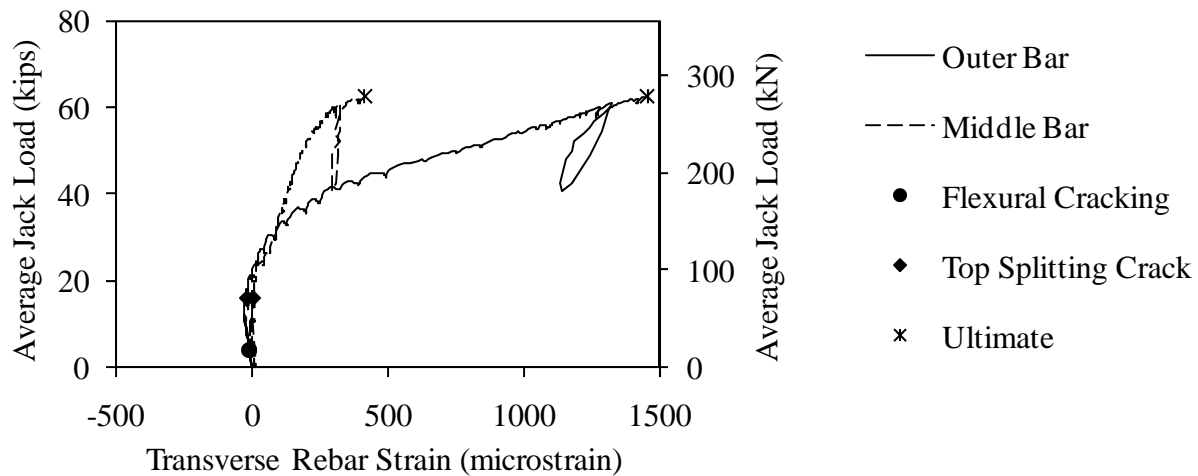

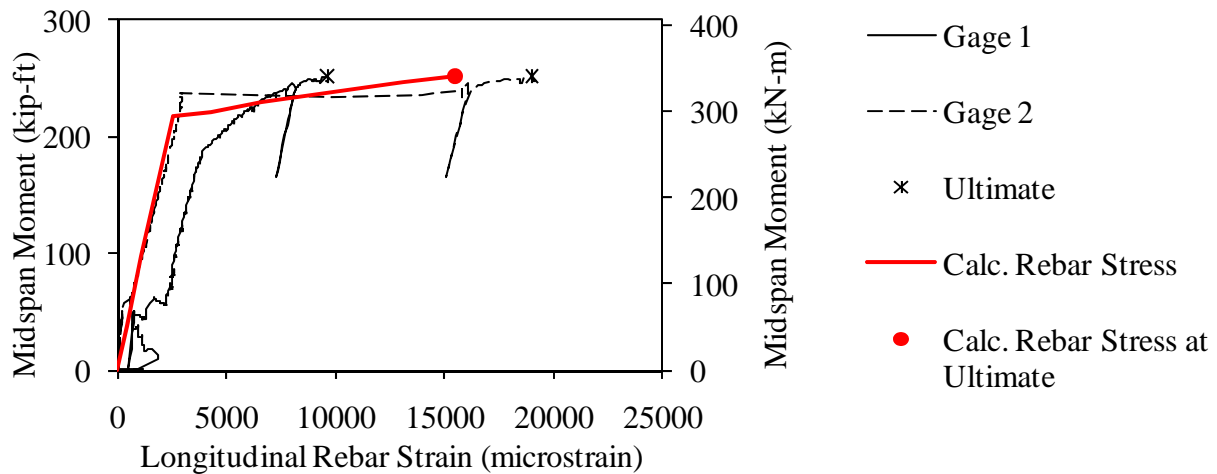**Figure 257. Graph. Load versus transverse rebar strain for Beam A8-ST.**

Figure 258. Graph. Measured and predicted midspan moment versus longitudinal rebar strain for Beam A8-ST.
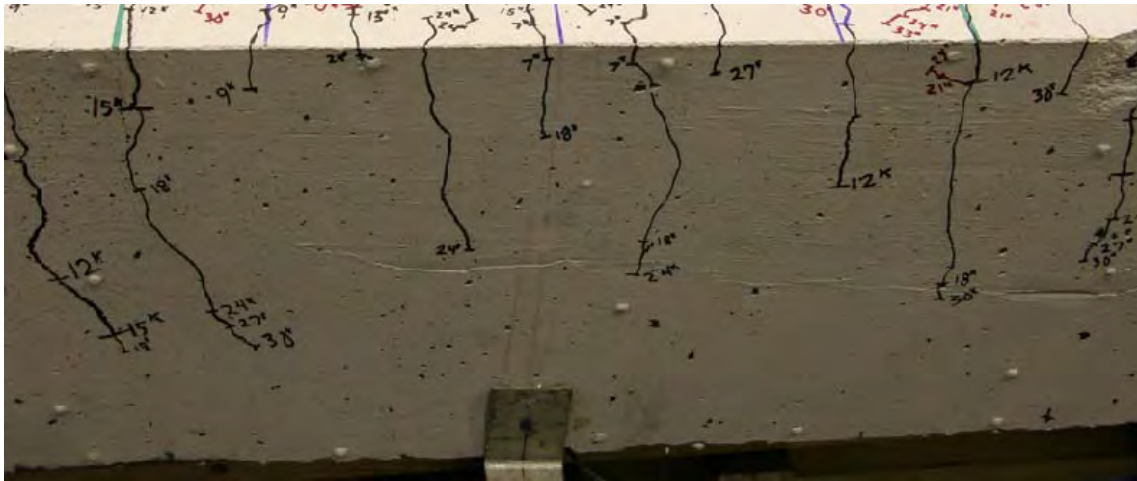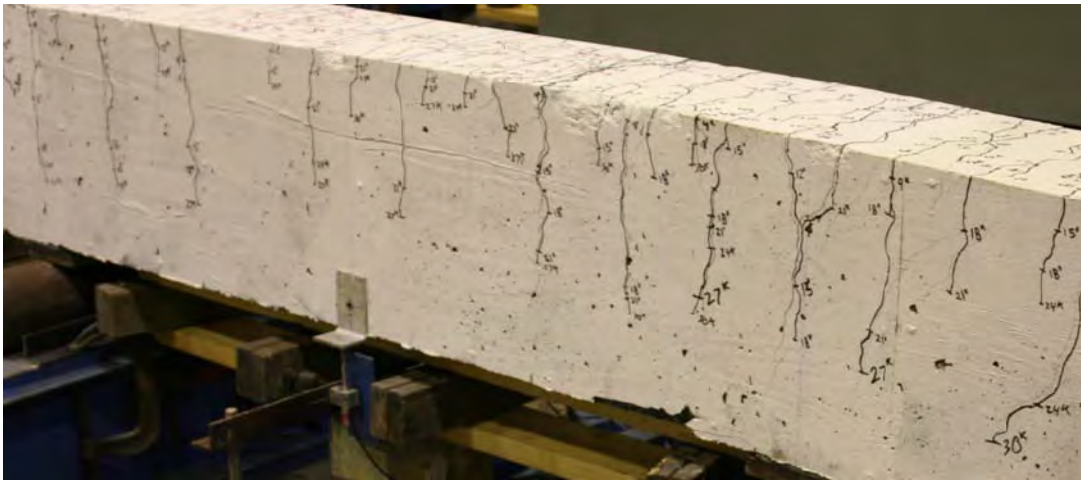
Figure 259. Photo. Side face of Beam A8-ST before failure.
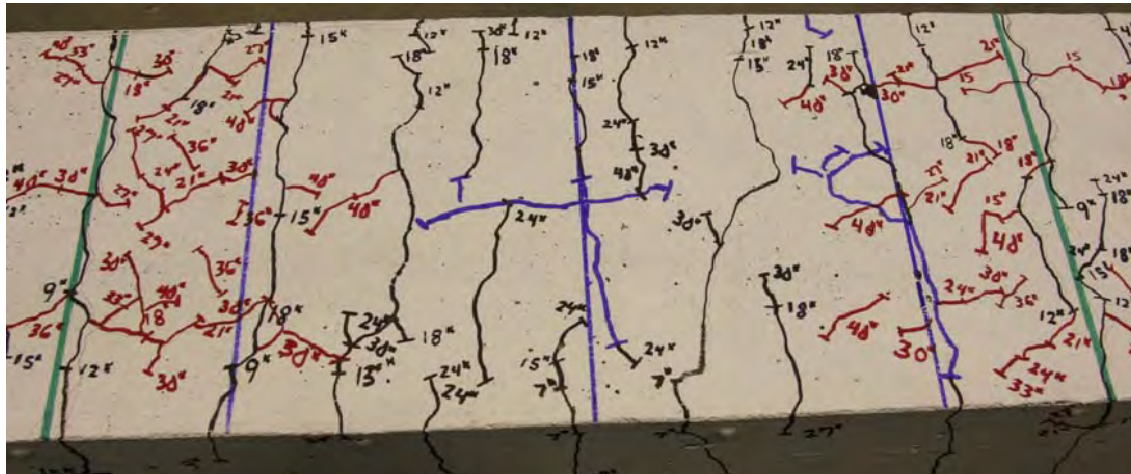
Figure 260. Photo. Top face of Beam A8-ST before failure.
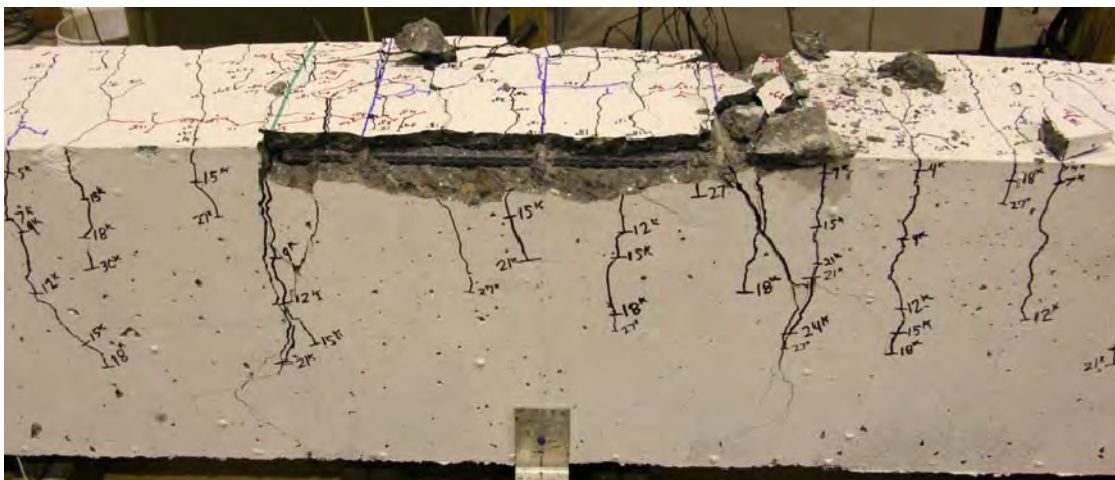
Figure 261. Photo. Beam A8-ST after failure.

Splice Beam B8-ST

Table 80. Test parameters for Splice Beam B8-ST.

Concrete Mix	Spliced Bar Size	Lap Length, inch (mm)	#3 (10M) Bar Transverse Reinforcement	Nominal Beam Cross-Section Dimensions (Width by Height), inch (mm)
Utelite	#8 (25M)	24 (610)	(3) at 8 in. (200mm)	18 by 18 (460 by 460)

Table 81. Test data for Splice Beam B8-ST.

Event	Average Jack Load, kips (kN)	Average Beam End Deflection, inch (mm)	Longitudinal Rebar Strain, microstrain		Transverse Rebar Strain, microstrain	
			Gage 1	Gage 2	Gage 1	Gage 2
Flexural cracking	7.1 (31)	0.04 (0.9)	133	107	-17	-20
Top splitting crack	15.2 (68)	0.1 (2.6)	421	678	13	-31
Side splitting crack	36.9 (164)	0.41 (10.3)	924	1920	293	15
Long. rebar yield	45.1 (201)	0.54 (13.6)	1177	2370	525	37
Ultimate	56.2 (250)	0.86 (21.9)	2191	2880	1130	528

Notes:
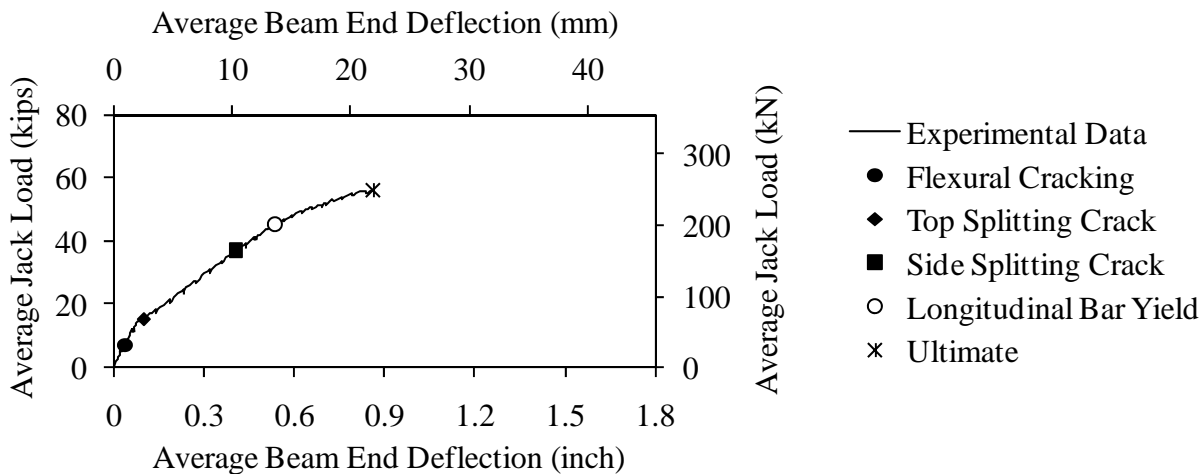
Figure 262. Graph. Load versus deflection for Beam B8-ST.
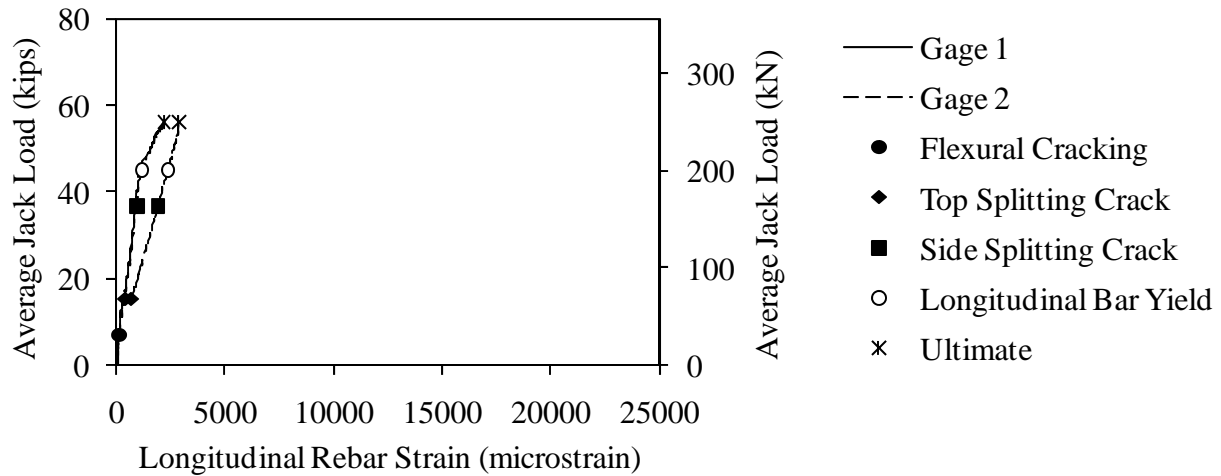
Figure 263. Graph. Load versus longitudinal rebar strain for Beam B8-ST.

Figure 264. Graph. Load versus transverse rebar strain for Beam B8-ST.

Figure 265. Graph. Measured and predicted midspan moment versus longitudinal rebar strain for Beam B8-ST.
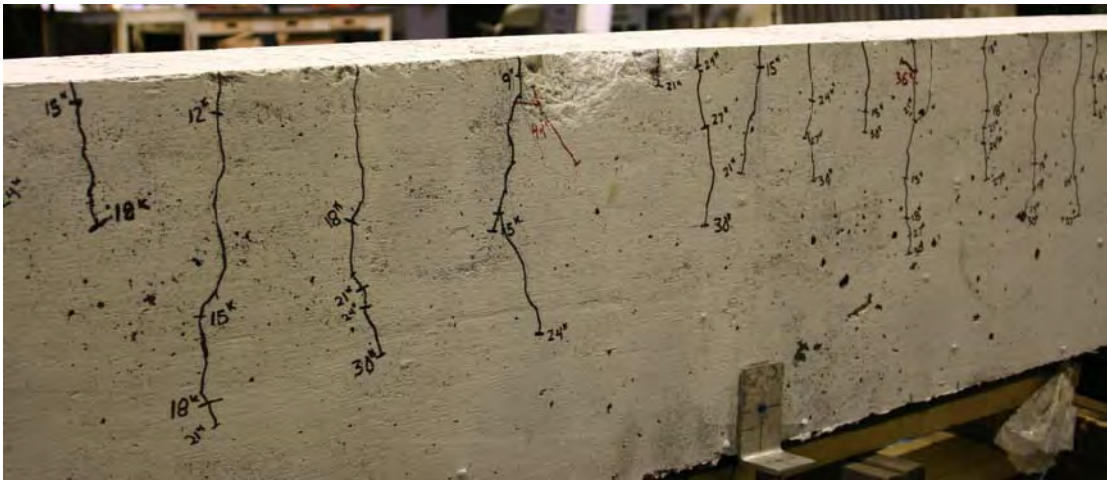
**Figure 266. Photo. Side face of Beam B8-ST before failure.**
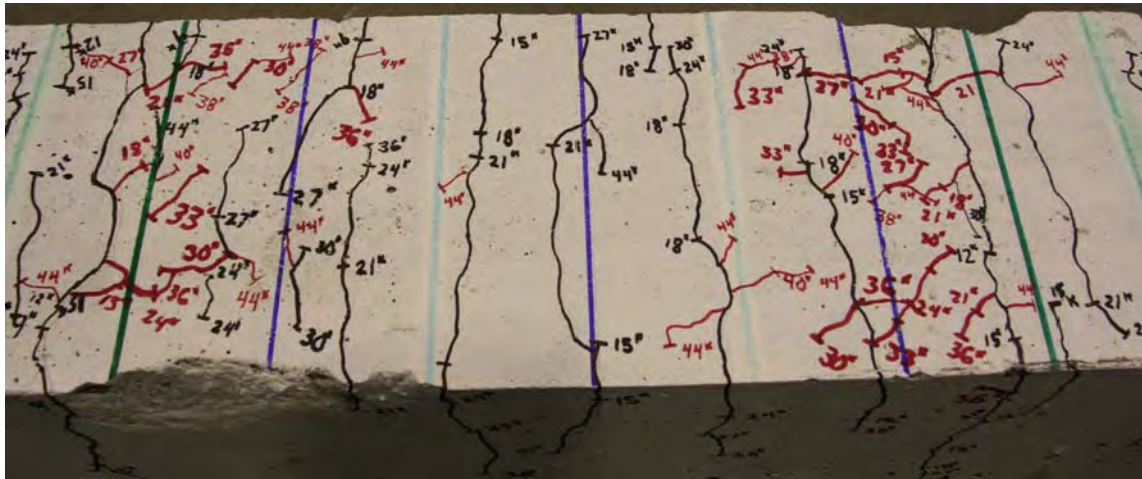

Figure 267. Photo. Top face of Beam B8-ST before failure
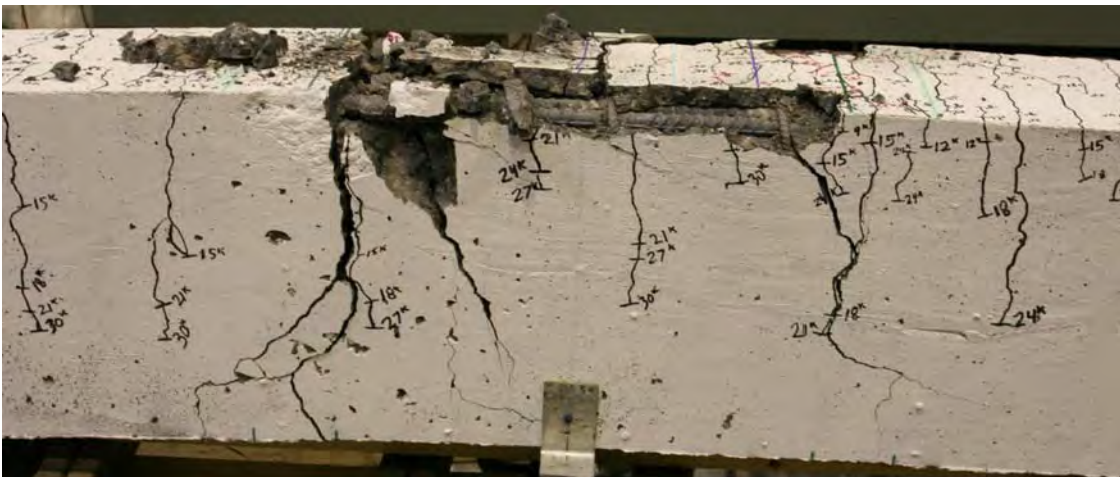
Figure 268. Photo. Beam B8-ST after failure.

Splice Beam C8-ST

Table 82. Test parameters for Splice Beam C8-ST.

Concrete Mix	Spliced Bar Size	Lap Length, inch (mm)	#3 (10M) Bar Transverse Reinforcement	Nominal Beam Cross-Section Dimensions (Width by Height), inch (mm)
Haydite	#8 (25M)	24 (610)	(3) at 8 in. (200mm)	18 by 18 (460 by 460)

Table 83. Test data for Splice Beam C8-ST.

| Event	Average Jack Load, kips (kN)	Average Beam End Deflection, inch (mm)	Longitudinal Rebar Strain, microstrain		Transverse Rebar Strain, microstrain	
			Gage 1	Gage 2	Gage 1	Gage 2
Flexural cracking	4 (18)	0.02 (0.5)	48	51	0	-2
Top splitting crack	15.2 (68)	0.11 (2.7)	387	647	11	0
Side splitting crack	21.4 (95)	0.2 (5)	713	1044	35	2
Long. rebar yield	42.7 (190)	0.5 (12.6)	1688	2305	304	52
Ultimate	57.5 (256)	1.52 (38.6)	12589	13291	1136	1032

Notes:
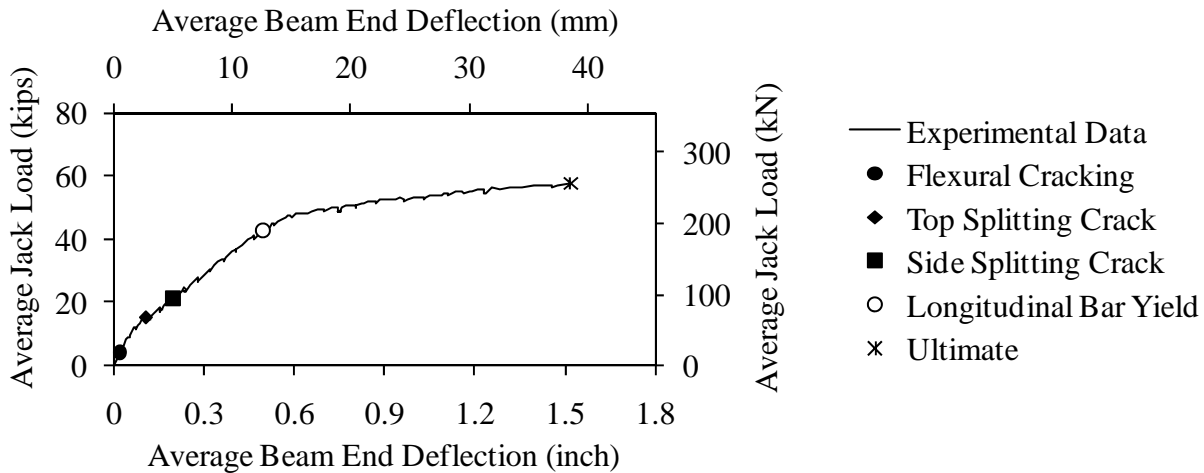
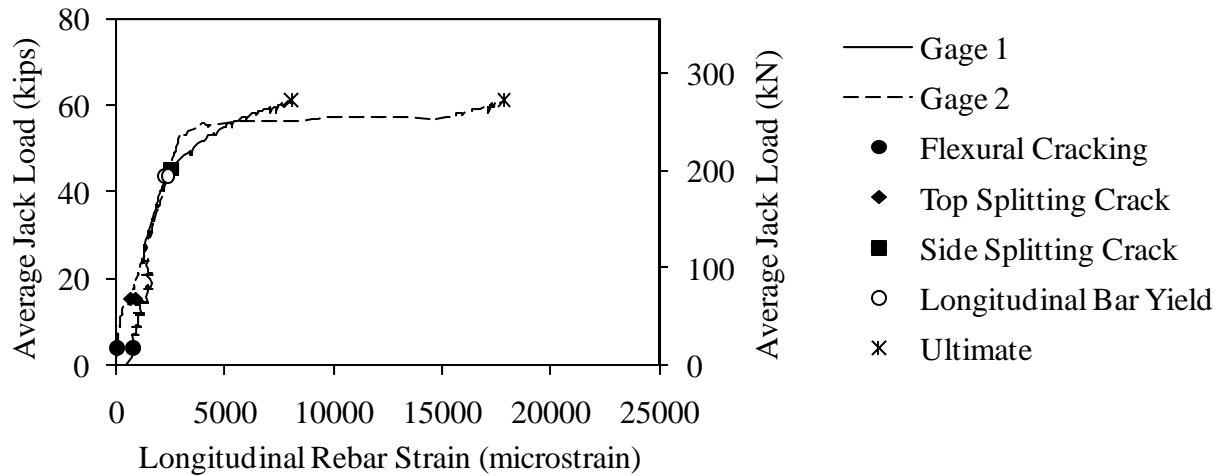**Figure 269. Graph. Load versus deflection for Beam C8-ST.**
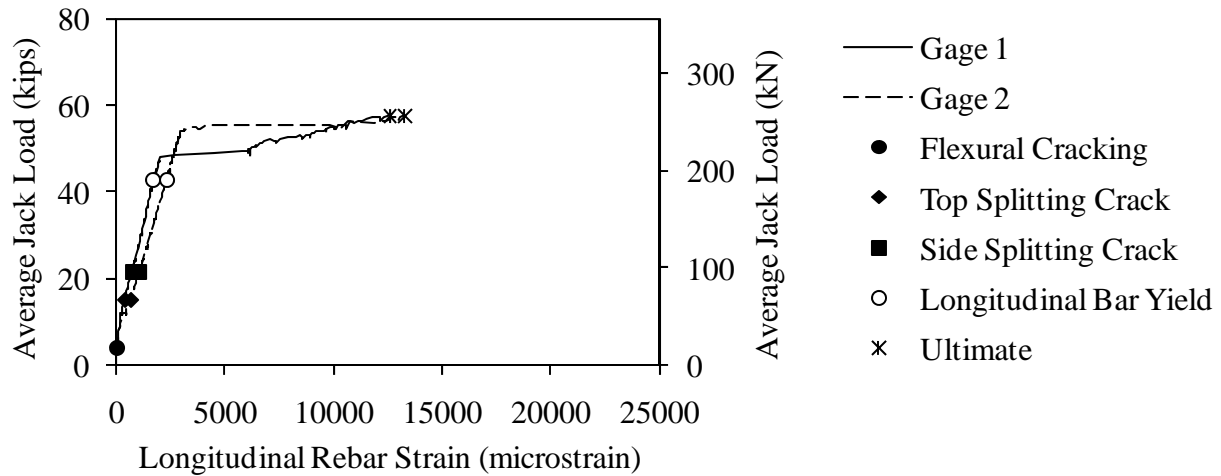
Figure 270. Graph. Load versus longitudinal rebar strain for Beam C8-ST.
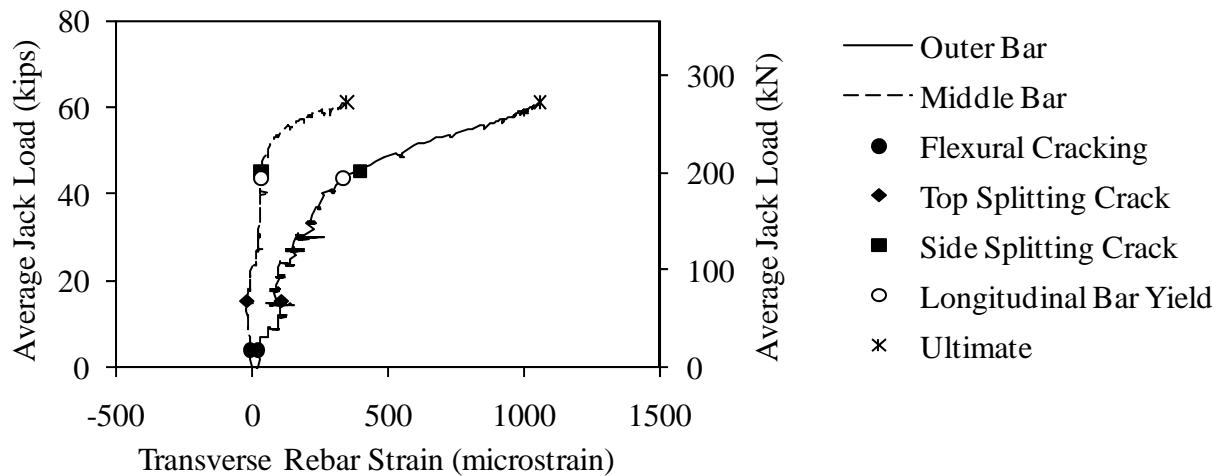

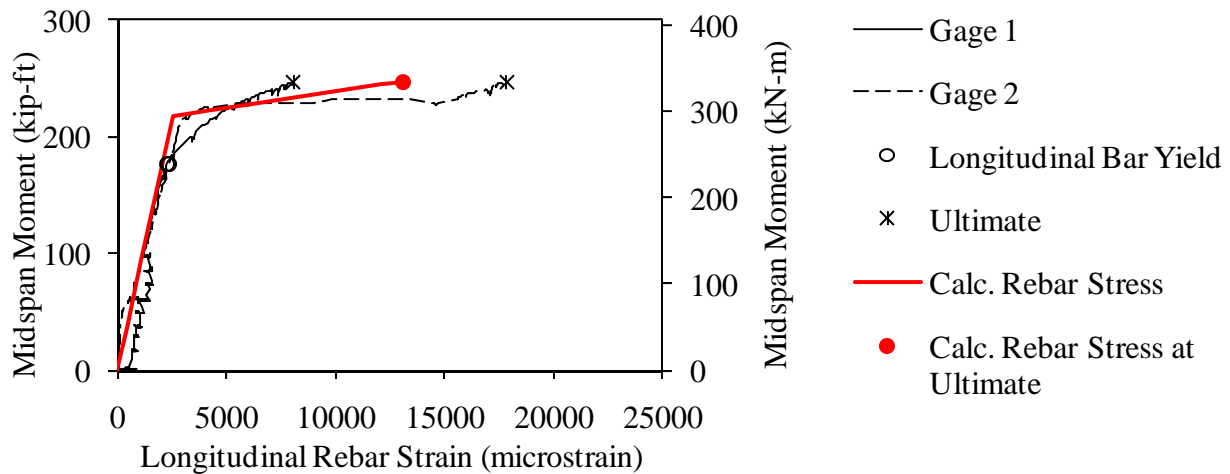**Figure 271. Graph. Load versus transverse rebar strain for Beam C8-ST.**

Figure 272. Graph. Measured and predicted midspan moment versus longitudinal rebar strain for Beam C8-ST.
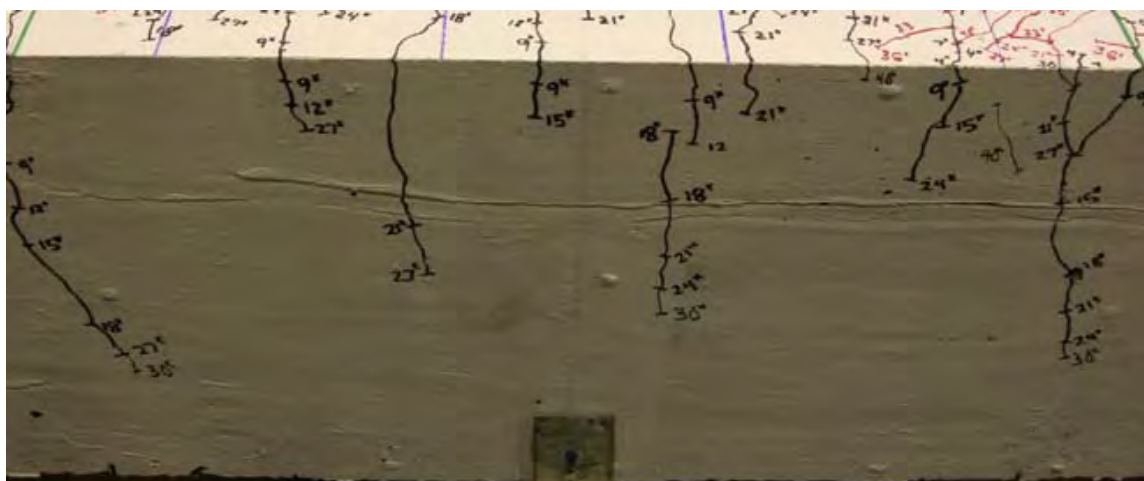
**Figure 273. Photo. Side face of Beam C8-ST before failure.**
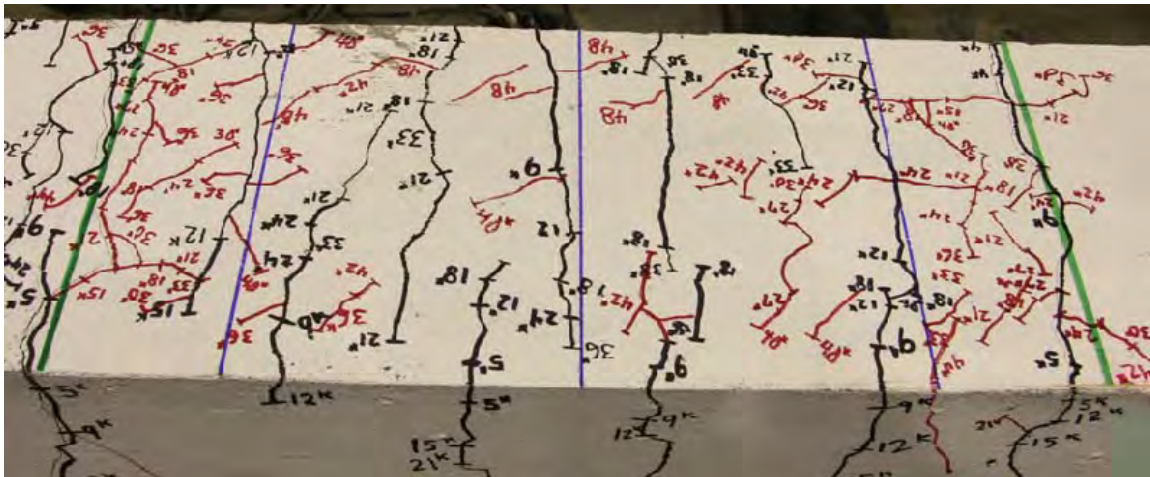
Figure 274. Photo. Top face of Beam C8-ST before failure.
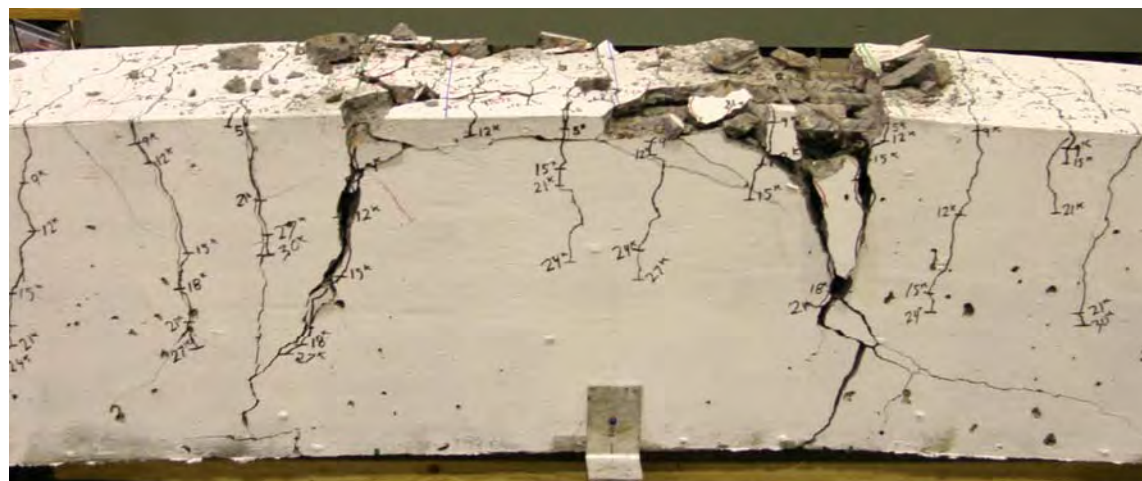
Figure 275. Photo. Beam C8-ST after failure.

D-64

Splice Beam A8-LT

Table 84. Test parameters for Splice Beam A8-LT.

Concrete Mix	Spliced Bar Size	Lap Length, inch (mm)	#3 (10M) Bar Transverse Reinforcement	Nominal Beam Cross-Section Dimensions (Width by Height), inch (mm)
Stalite	#8 (25M)	32 (810)	(4) at 8 in. (200mm)	18 by 18 (460 by 460)

Table 85. Test data for Splice Beam A8-LT.

| Event	Average Jack Load, kips (kN)	Average Beam End Deflection, inch (mm)	Longitudinal Rebar Strain, microstrain		Transverse Rebar Strain, microstrain	
			Gage 1	Gage 2	Gage 1	Gage 2
Flexural cracking	7 (31)	0.04 (1)	110	154	-7	0
Top splitting crack	15.1 (67)	0.12 (3.1)	635	776	-10	-4
Side splitting crack	N/A	N/A	N/A	N/A	N/A	N/A
Long. rebar yield	42.8 (190)	0.5 (12.8)	2007	2309	318	113
Ultimate	56.8 (253)	0.9 (22.7)	4504	3158	719	872

Notes:
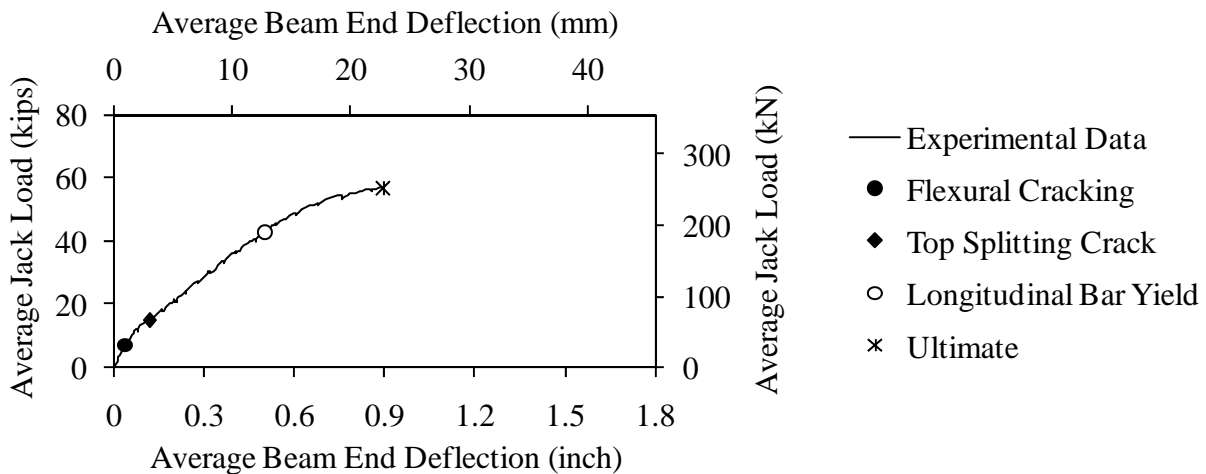
Figure 276. Graph. Load versus deflection for Beam A8-LT.
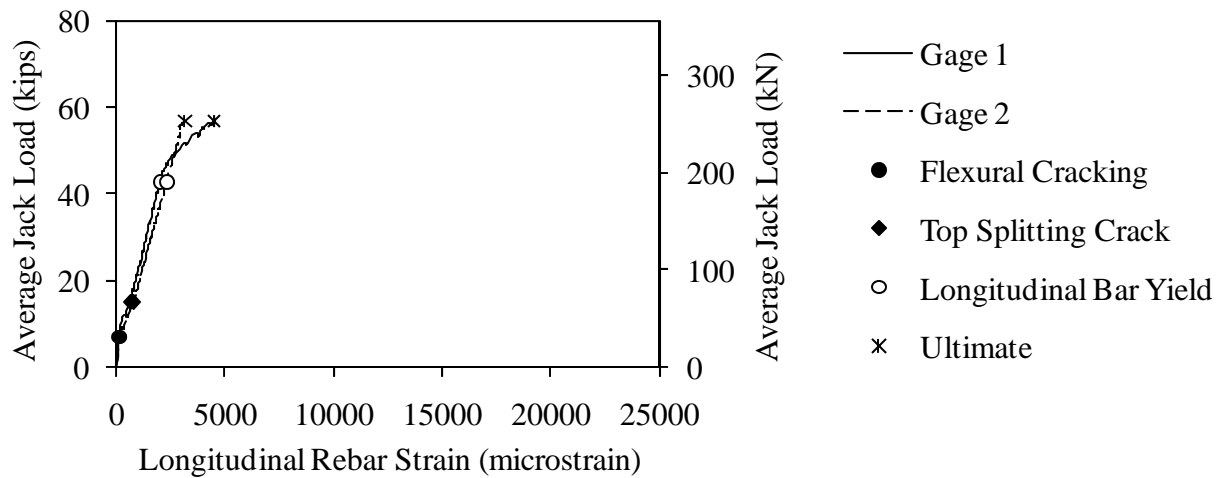
Figure 277. Graph. Load versus longitudinal rebar strain for Beam A8-LT.
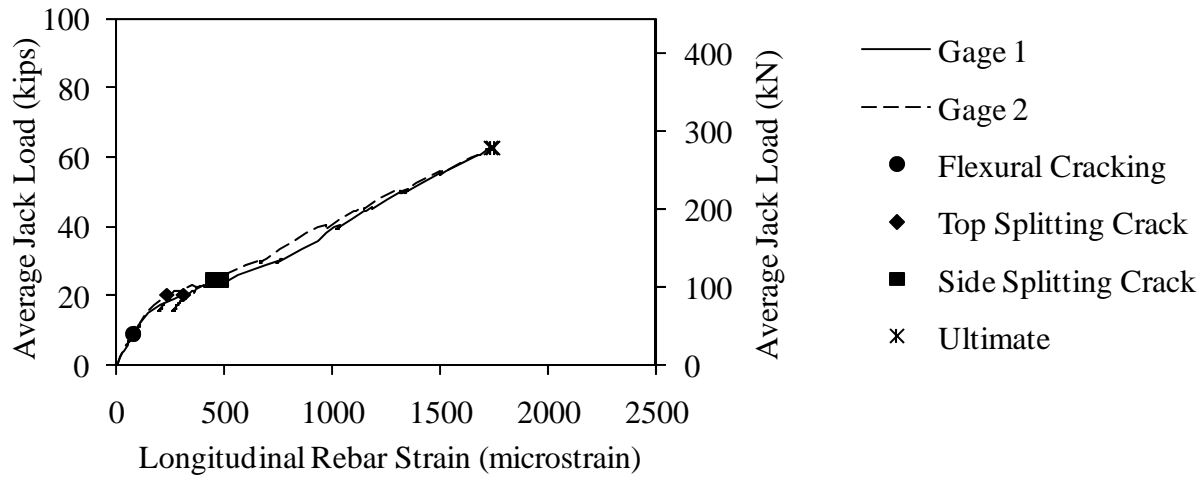

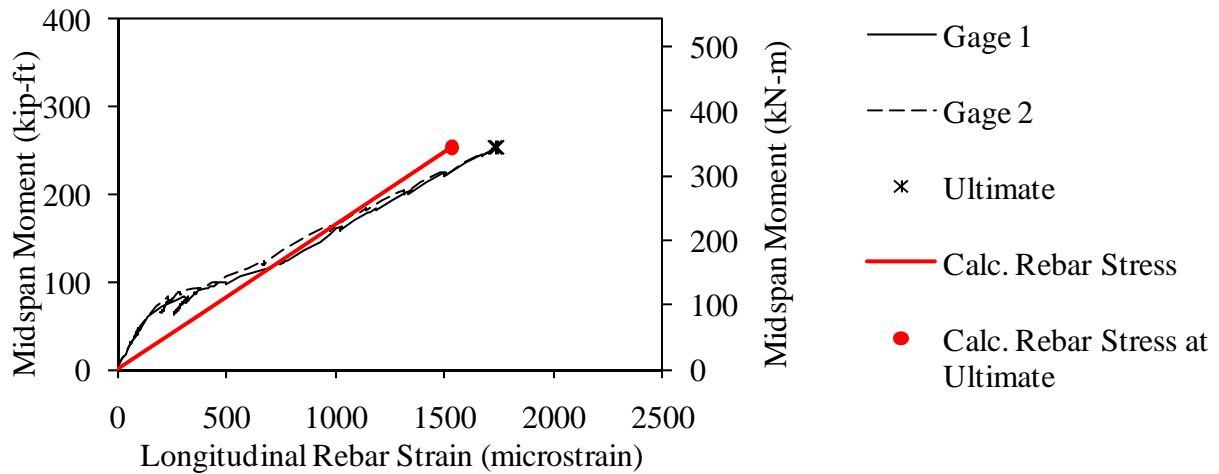**Figure 278. Graph. Load versus transverse rebar strain for Beam A8-LT.**

**Figure 279. Graph. Measured and predicted midspan moment versus longitudinal rebar strain for Beam A8-LT.**
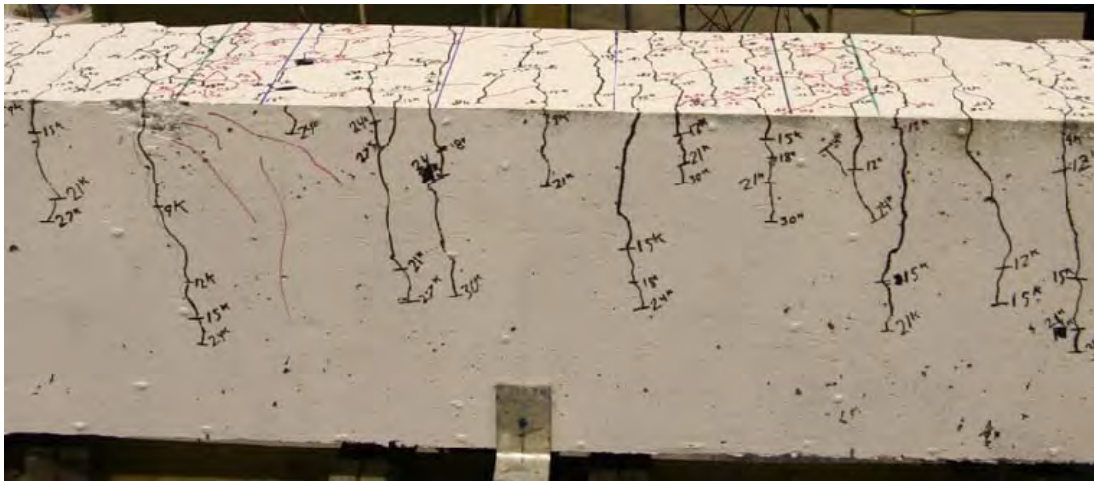
**Figure 280. Photo. Side face of Beam A8-LT before failure.**
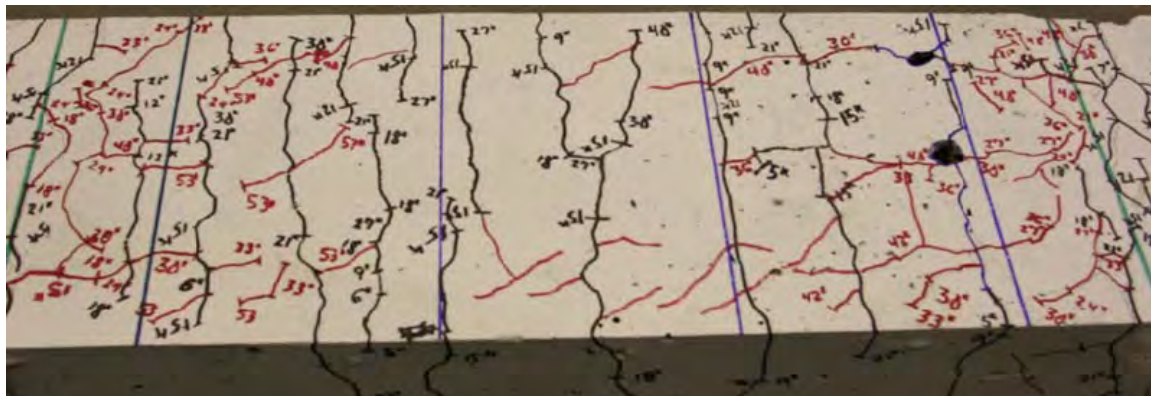
**Figure 281. Photo. Top face of Beam A8-LT before failure.**
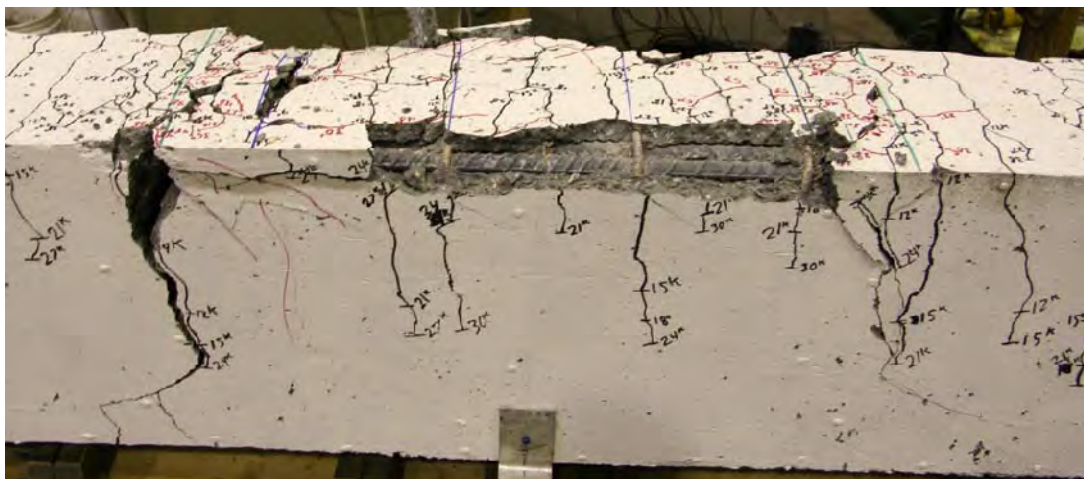
Figure 282. Photo. Beam A8-LT after failure.

Splice Beam B8-LT

<div align="center">

Table 86. Test parameters for Splice Beam B8-LT.

</div>

Concrete Mix	Spliced Bar Size	Lap Length, inch (mm)	#3 (10M) Bar Transverse Reinforcement	Nominal Beam Cross-Section Dimensions (Width by Height), inch (mm)
Utelite	#8 (25M)	32 (810)	(4) at 8 in. (200mm)	18 by 18 (460 by 460)

<div align="center">

Table 87. Test data for Splice Beam B8-LT.

</div>

Event	Average Jack Load, kips (kN)	Average Beam End Deflection, inch (mm)	Longitudinal Rebar Strain, microstrain		Transverse Rebar Strain, microstrain	
			Gage 1	Gage 2	Gage 1	Gage 2
Flexural cracking	4 (18)	0 (0)	1613	58	-11	-7
Top splitting crack	16.1 (72)	0.1 (2.6)	2281	678	-20	2
Side splitting crack	N/A	N/A	N/A	N/A	N/A	N/A
Long. rebar yield	N/A	N/A	N/A	N/A	N/A	N/A
Ultimate	62.5 (278)	1.66 (42.1)	9632	19009	1457	415

Notes:
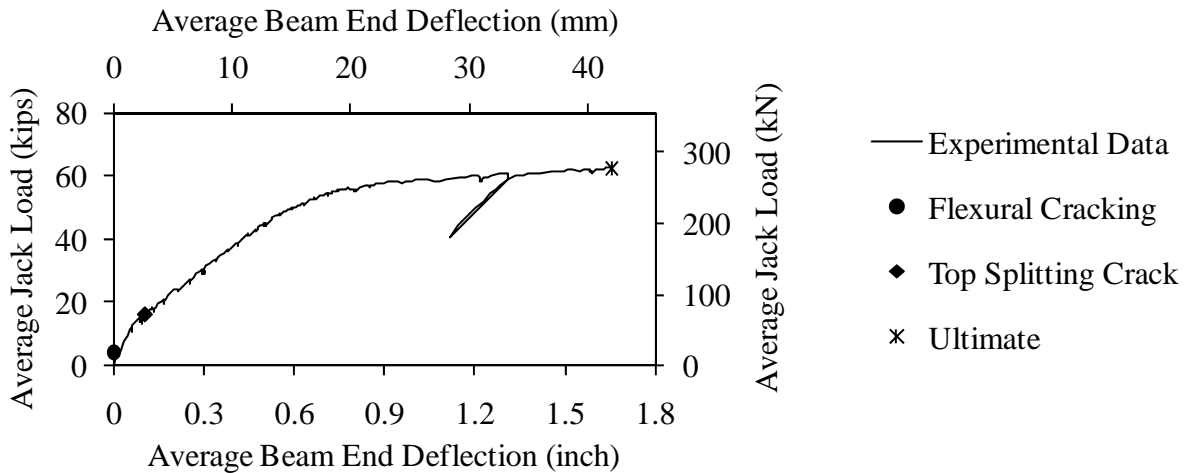
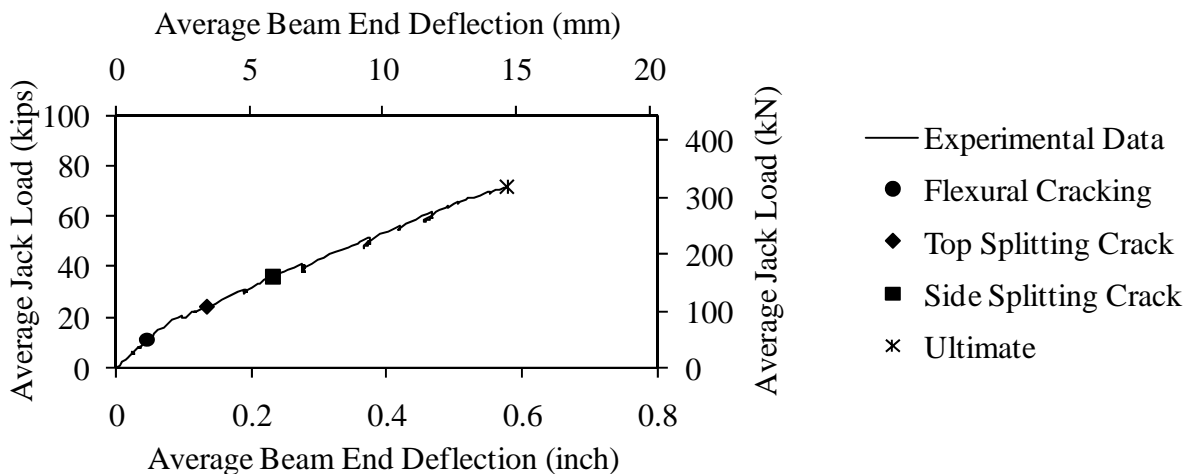**Figure 283. Graph. Load versus deflection for Beam B8-LT.**

Figure 284. Graph. Load versus longitudinal rebar strain for Beam B8-LT.
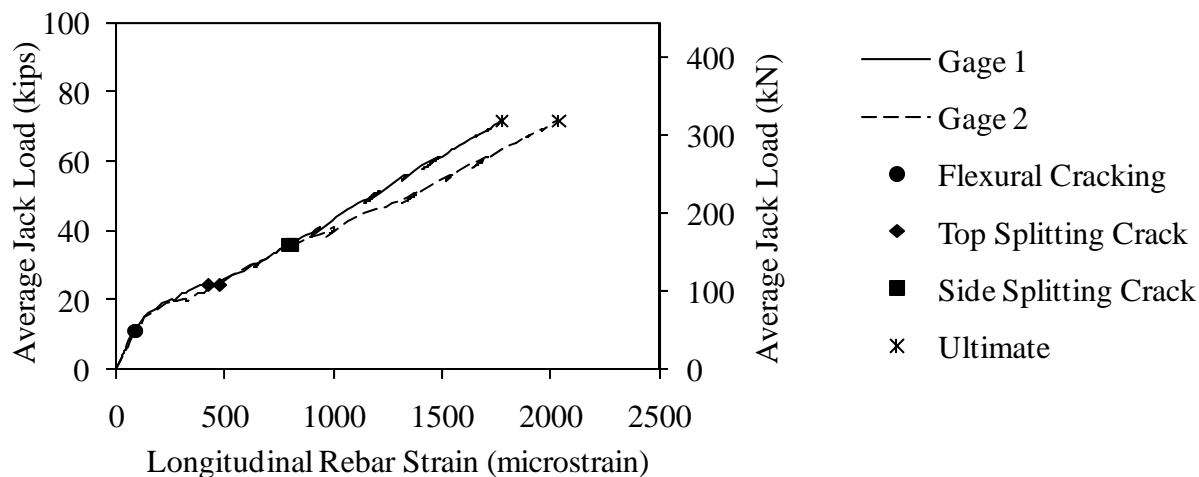

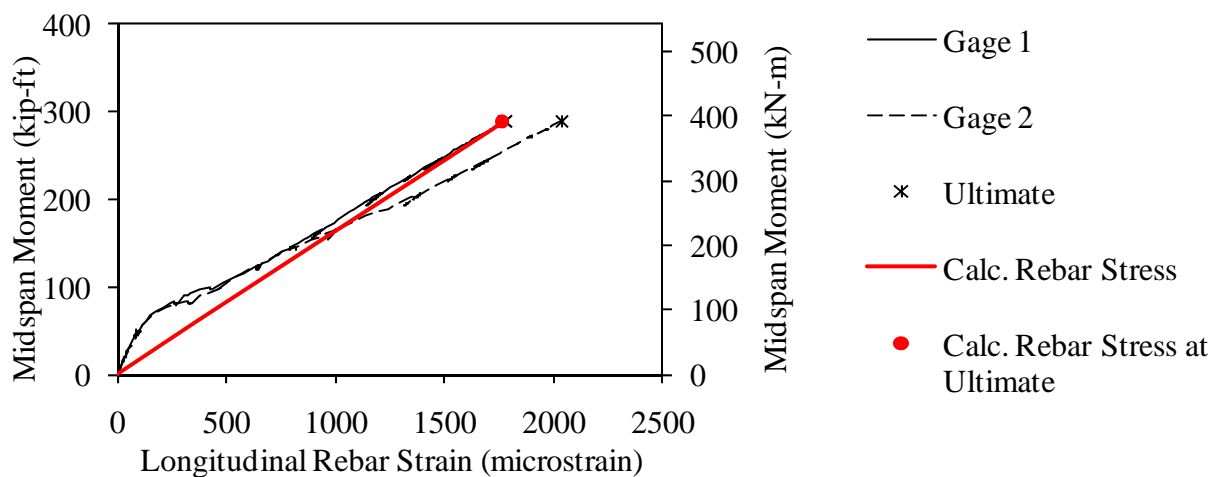**Figure 285. Graph. Load versus transverse rebar strain for Beam B8-LT.**

**Figure 286. Graph. Measured and predicted midspan moment versus longitudinal rebar strain for Beam B8-LT.**

**Figure 287. Photo. Side face of Beam B8-LT before failure.**
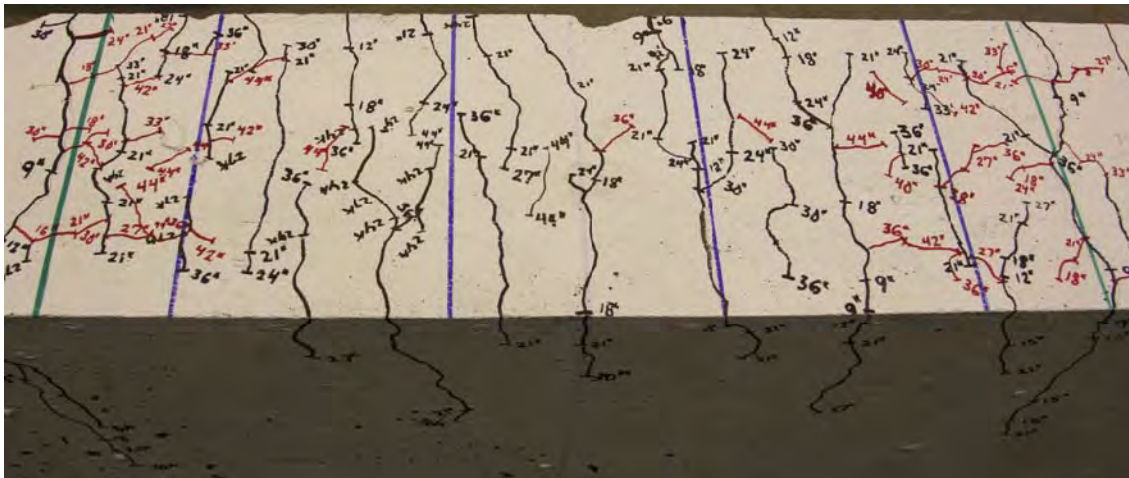
Figure 288. Photo. Top face of Beam B8-LT before failure.
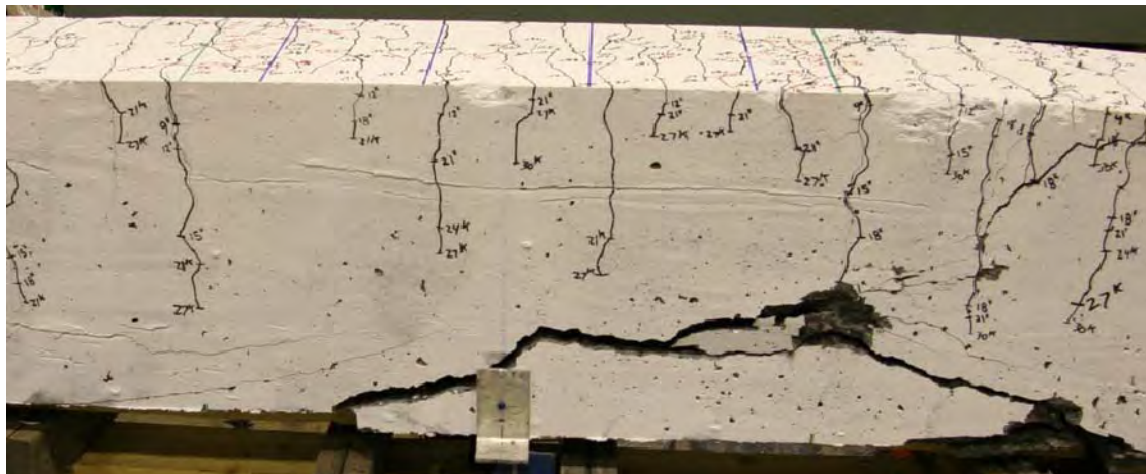
Figure 289. Photo. Beam B8-LT after failure.

D-70

Splice Beam C8-LT

Table 88. Test parameters for Splice Beam C8-LT.

Concrete Mix	Spliced Bar Size	Lap Length, inch (mm)	#3 (10M) Bar Transverse Reinforcement	Nominal Beam Cross-Section Dimensions (Width by Height), inch (mm)
Haydite	#8 (25M)	32 (810)	(4) at 8 in. (200mm)	18 by 18 (460 by 460)

Table 89. Test data for Splice Beam C8-LT.

| Event	Average Jack Load, kips (kN)	Average Beam End Deflection, inch (mm)	Longitudinal Rebar Strain, microstrain		Transverse Rebar Strain, microstrain	
			Gage 1	Gage 2	Gage 1	Gage 2
Flexural cracking	4 (18)	0.02 (0.5)	783	56	22	-7
Top splitting crack	15.3 (68)	0.1 (2.5)	851	615	106	-20
Side splitting crack	45.3 (202)	0.51 (12.9)	2489	2469	398	33
Long. rebar yield	43.6 (194)	0.48 (12.1)	2267	2366	333	32
Ultimate	61 (272)	1.35 (34.2)	8069	17838	1060	349

Notes:
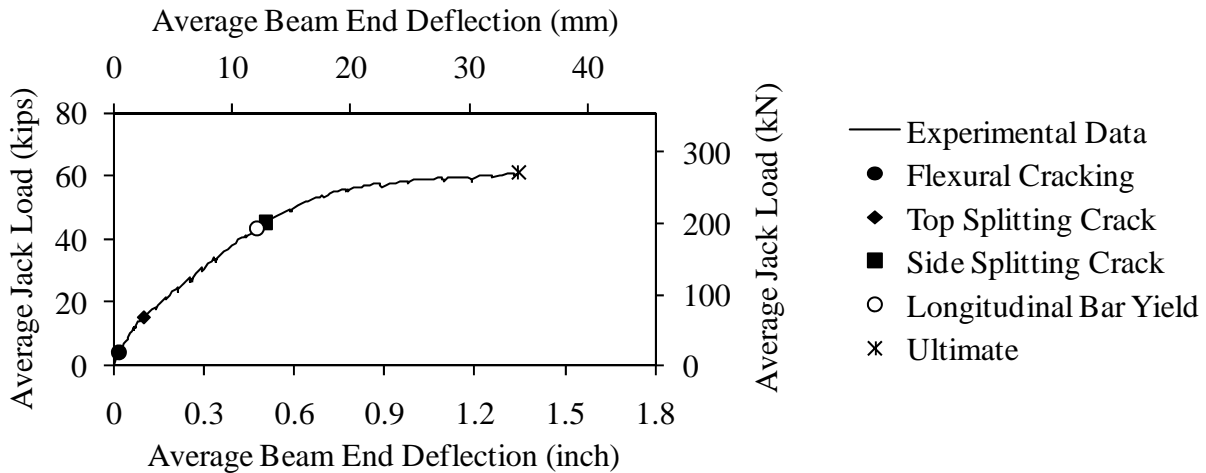
Figure 290. Graph. Load versus deflection for Beam C8-LT.

Figure 291. Graph. Load versus longitudinal rebar strain for Beam C8-LT.
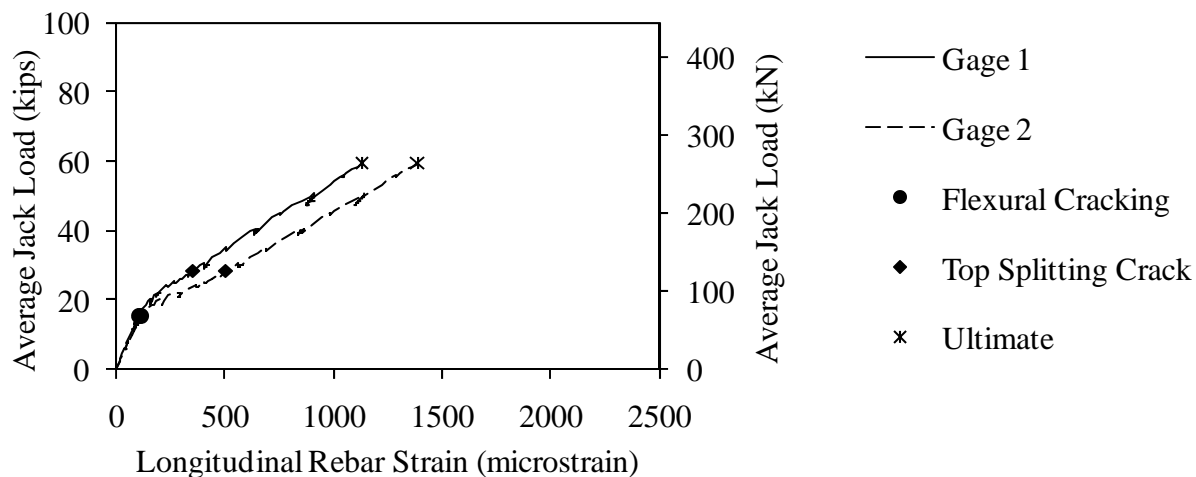

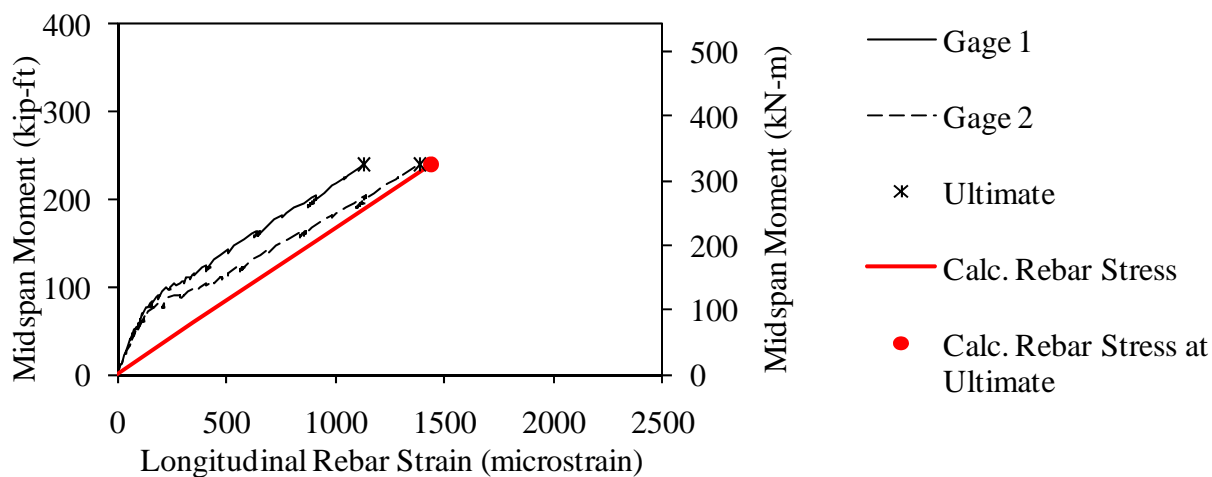**Figure 292. Graph. Load versus transverse rebar strain for Beam C8-LT.**

Figure 293. Graph. Measured and predicted midspan moment versus longitudinal rebar strain for Beam C8-LT.

Figure 294. Photo. Side face of Beam C8-LT before failure.
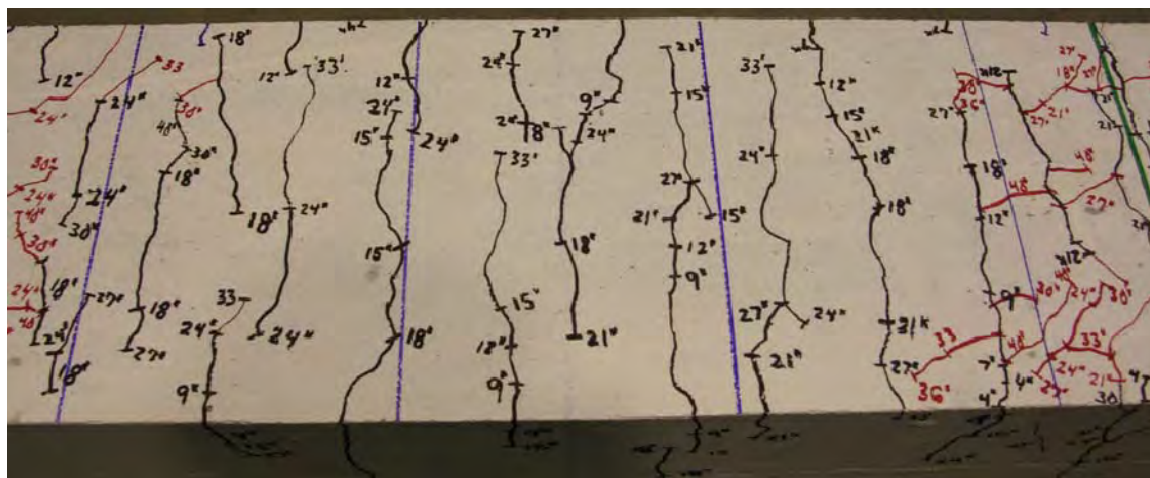
Figure 295. Photo. Top face of Beam C8-LT before failure.

Figure 296. Photo. Beam C8-LT after failure.

D-73

Splice Beam A11-SN

Table 90. Test parameters for Splice Beam A11-SN.

Concrete Mix	Spliced Bar Size	Lap Length, inch (mm)	#3 (10M) Bar Transverse Reinforcement	Nominal Beam Cross-Section Dimensions (Width by Height), inch (mm)
Stalite	#11 (40M)	32 (810)	None	18 by 18 (460 by 460)

Table 91. Test data for Splice Beam A11-SN.

Event	Average Jack Load, kips (kN)	Average Beam End Deflection, inch (mm)	Longitudinal Rebar Strain, microstrain		Transverse Rebar Strain, microstrain	
			Gage 1	Gage 2	Gage 1	Gage 2
Flexural cracking	9.2 (41)	0.04 (1)	82	78	N/A	N/A
Top splitting crack	20.4 (91)	0.1 (2.5)	306	230	N/A	N/A
Side splitting crack	24.5 (109)	0.13 (3.4)	488	447	N/A	N/A
Long. rebar yield	N/A	N/A	N/A	N/A	N/A	N/A
Ultimate	62.8 (279)	0.48 (12.2)	1732	1743	N/A	N/A

Notes:
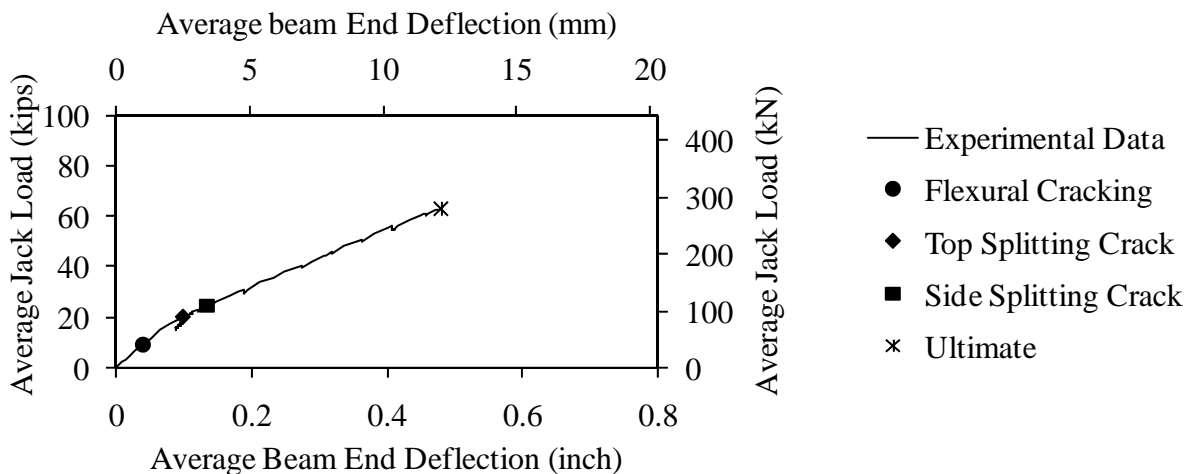
Figure 297. Graph. Load versus deflection for Beam A11-SN.

Figure 298. Graph. Load versus longitudinal rebar strain for Beam A11-SN.

Figure 299. Graph. Measured and predicted midspan moment versus longitudinal rebar strain for Beam A11-SN.
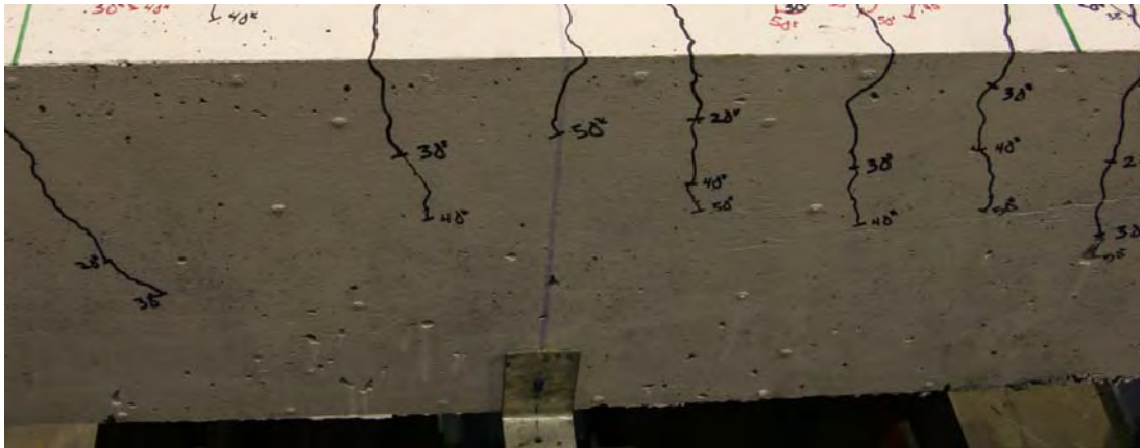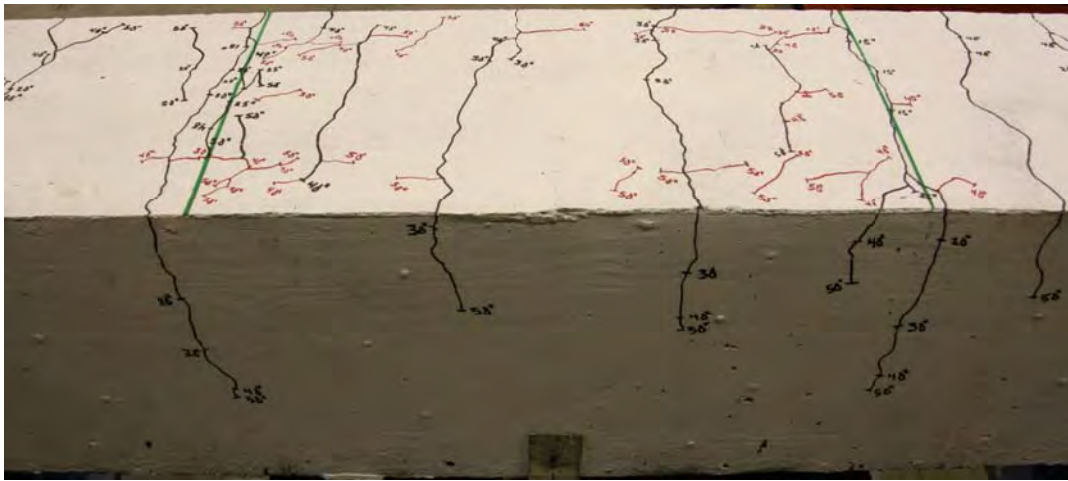
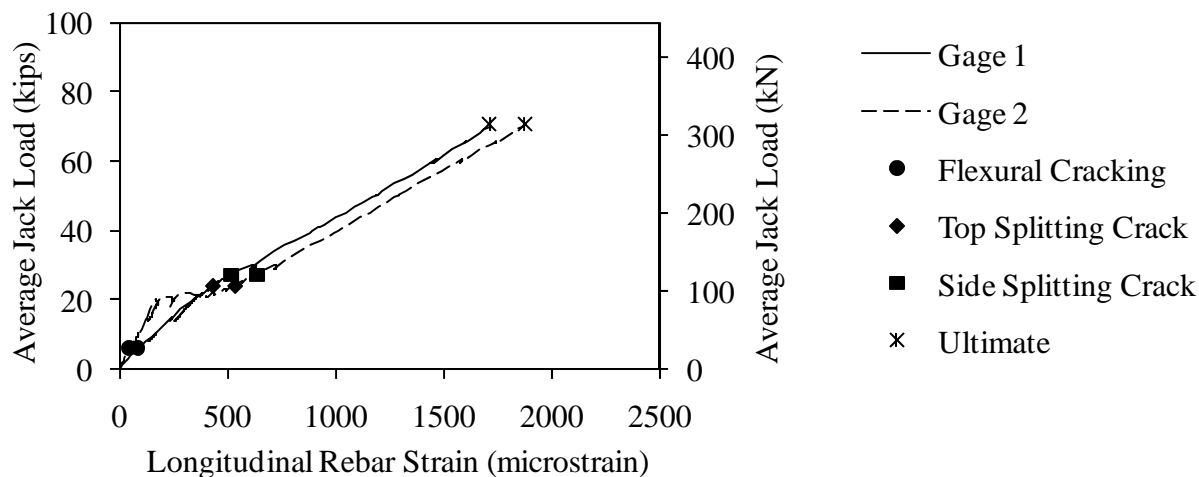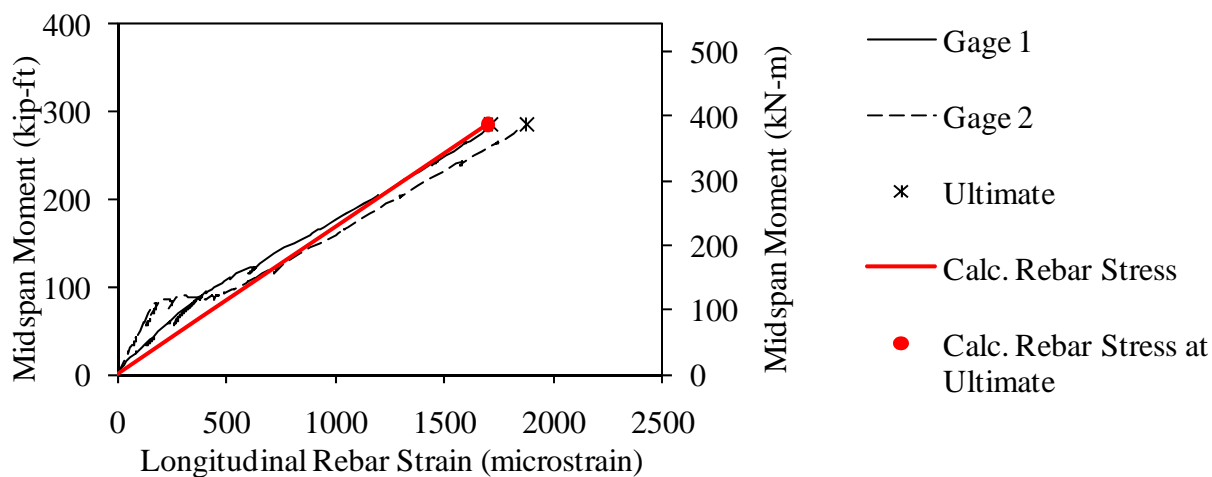**Figure 300. Photo. Side face of Beam A11-SN before failure.**
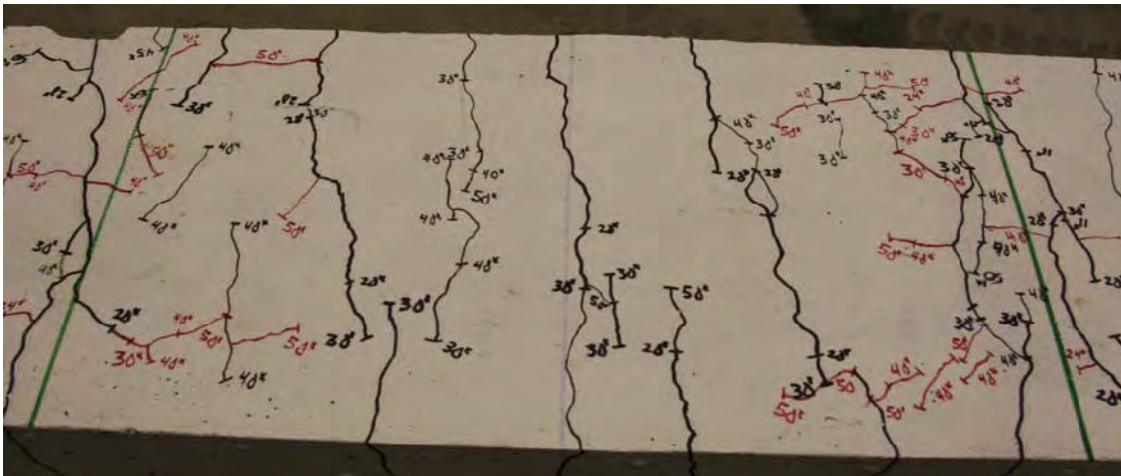
Figure 301. Photo. Top face of Beam A11-SN before failure.
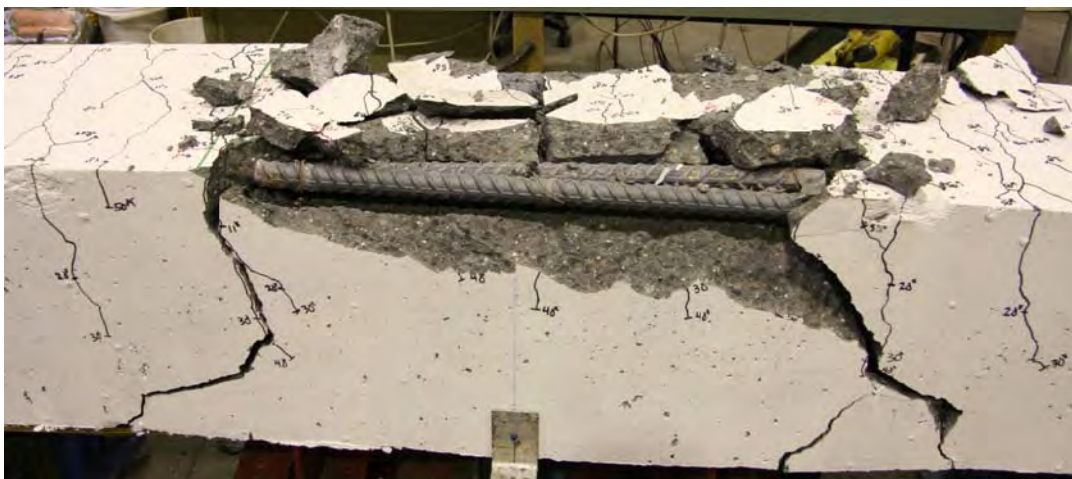
Figure 302. Photo. Beam A11-SN after failure.

Splice Beam B11-SN

Table 92. Test parameters for Splice Beam B11-SN.

Concrete Mix	Spliced Bar Size	Lap Length, inch (mm)	#3 (10M) Bar Transverse Reinforcement	Nominal Beam Cross-Section Dimensions (Width by Height), inch (mm)
Utelite	#11 (40M)	32 (810)	None	18 by 18 (460 by 460)

Table 93. Test data for Splice Beam B11-SN.

Event	Average Jack Load, kips (kN)	Average Beam End Deflection, inch (mm)	Longitudinal Rebar Strain, microstrain		Transverse Rebar Strain, microstrain	
			Gage 1	Gage 2	Gage 1	Gage 2
Flexural cracking	11.1 (50)	0.05 (1.2)	83	91	N/A	N/A
Top splitting crack	24.4 (108)	0.13 (3.4)	423	477	N/A	N/A
Side splitting crack	35.9 (160)	0.23 (5.9)	797	810	N/A	N/A
Long. rebar yield	N/A	N/A	N/A	N/A	N/A	N/A
Ultimate	71.5 (318)	0.58 (14.7)	1776	2037	N/A	N/A

Notes:

Figure 303. Graph. Load versus deflection for Beam B11-SN.

Figure 304. Graph. Load versus longitudinal rebar strain for Beam B11-SN.

Figure 305. Graph. Measured and predicted midspan moment versus longitudinal rebar strain for Beam B11-SN.
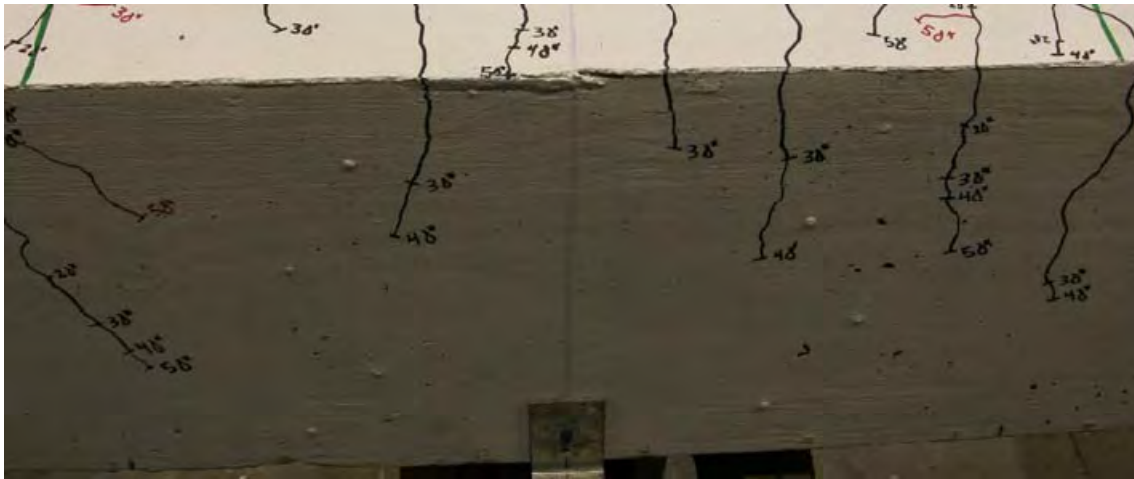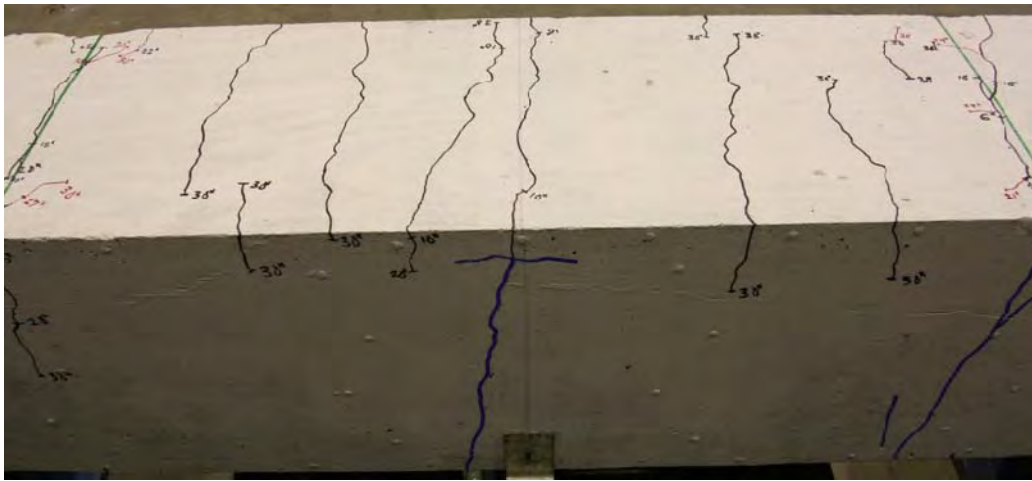
**Figure 306. Photo. Side face of Beam B11-SN before failure.**
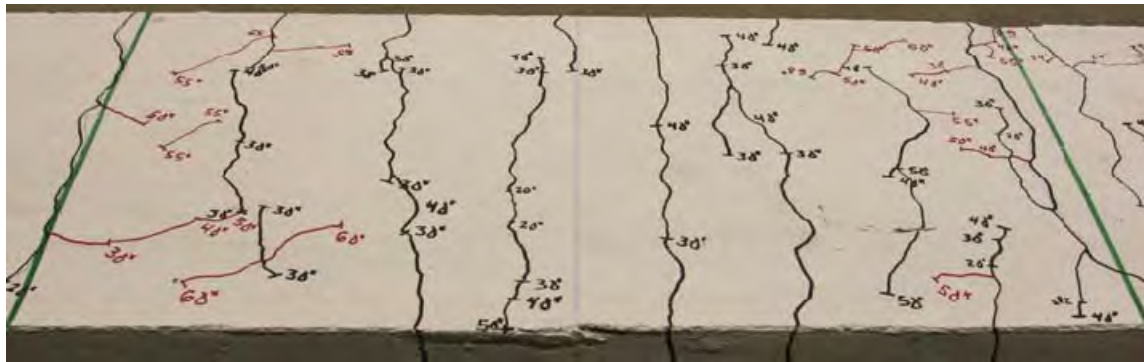
Figure 307. Photo. Top face of Beam B11-SN before failure.

Figure 308. Photo. Beam B11-SN after failure.

Splice Beam C11-SN

Table 94. Test parameters for Splice Beam C11-SN.

Concrete Mix	Spliced Bar Size	Lap Length, inch (mm)	#3 (10M) Bar Transverse Reinforcement	Nominal Beam Cross-Section Dimensions (Width by Height), inch (mm)
Haydite	#11 (40M)	32 (810)	None	18 by 18 (460 by 460)

Table 95. Test data for Splice Beam C11-SN.

| Event	Average Jack Load, kips (kN)	Average Beam End Deflection, inch (mm)	Longitudinal Rebar Strain, microstrain		Transverse Rebar Strain, microstrain	
			Gage 1	Gage 2	Gage 1	Gage 2
Flexural cracking	15.3 (68)	0.05 (1.4)	104	116	N/A	N/A
Top splitting crack	28.4 (126)	0.14 (3.5)	352	505	N/A	N/A
Side splitting crack	N/A	N/A	N/A	N/A	N/A	N/A
Long. rebar yield	N/A	N/A	N/A	N/A	N/A	N/A
Ultimate	59.5 (265)	0.39 (10)	1132	1387	N/A	N/A

Notes:
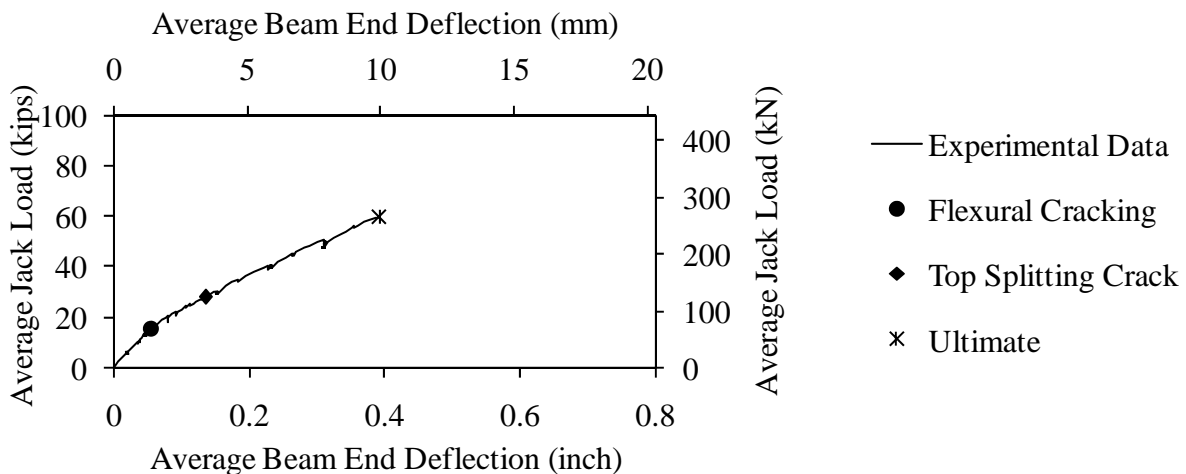
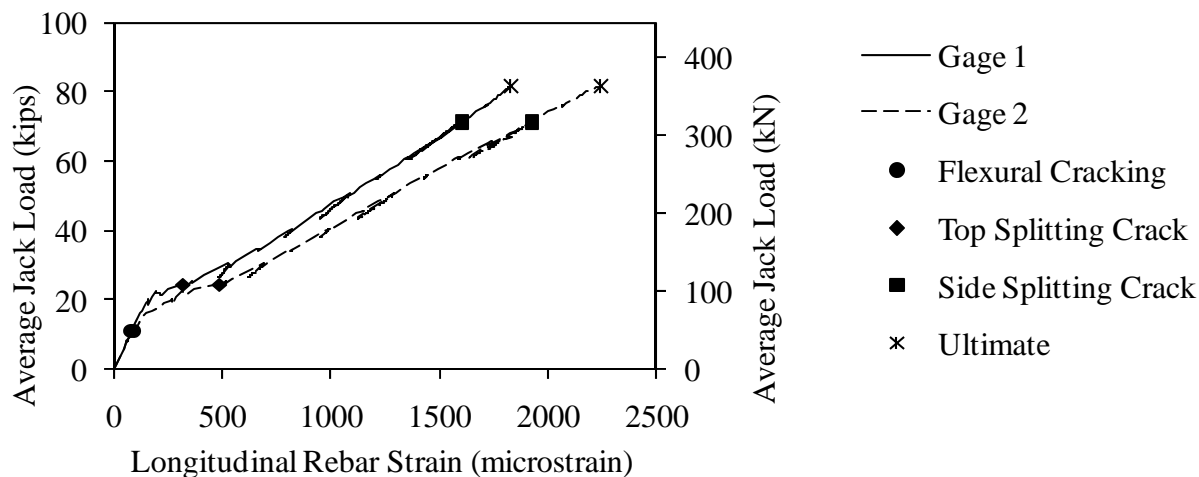**Figure 309. Graph. Load versus deflection for Beam C11-SN.**

Figure 310. Graph. Load versus longitudinal rebar strain for Beam C11-SN.
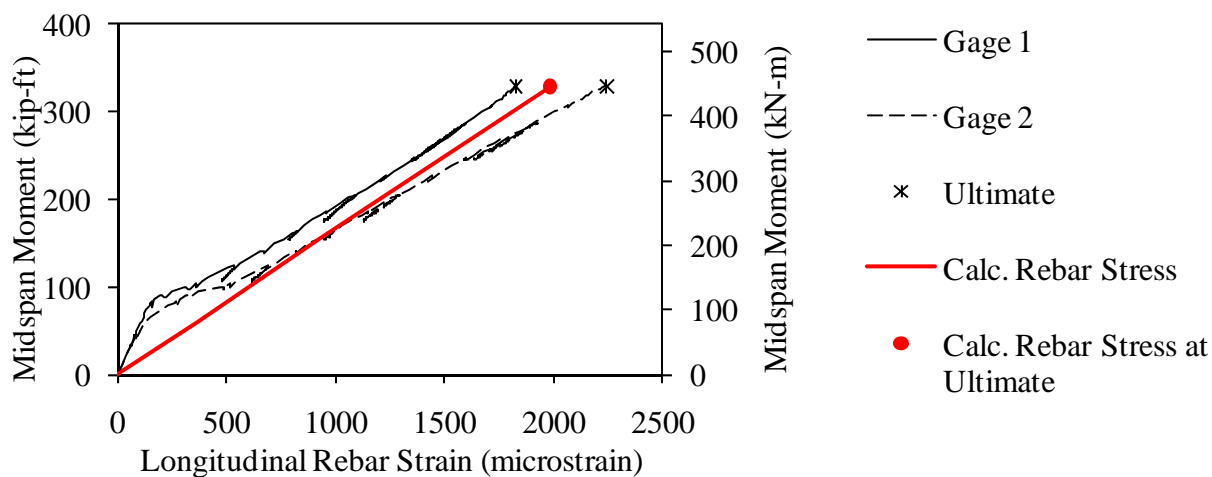

**Figure 311. Graph. Measured and predicted midspan moment versus longitudinal rebar strain for Beam C11-SN.**

**Figure 312. Photo. Side and top face of Beam C11-SN before failure.**
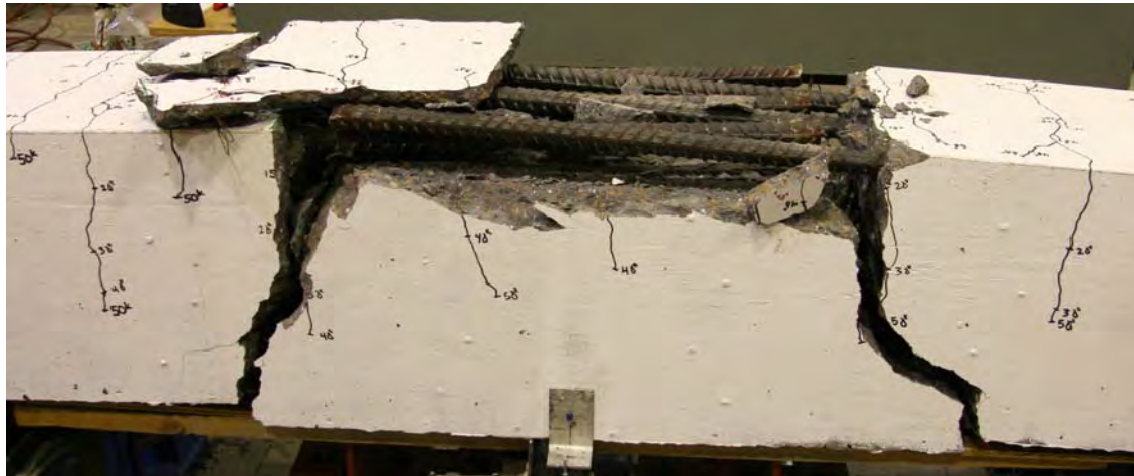
Figure 313. Photo. Beam C11-SN after failure.

Splice Beam A11-LN

Table 96. Test parameters for Splice Beam A11-LN.

Concrete Mix	Spliced Bar Size	Lap Length, inch (mm)	#3 (10M) Bar Transverse Reinforcement	Nominal Beam Cross-Section Dimensions (Width by Height), inch (mm)
Stalite	#11 (40M)	48 (1220)	None	18 by 18 (460 by 460)

Table 97. Test data for Splice Beam A11-LN.

| Event	Average Jack Load, kips (kN)	Average Beam End Deflection, inch (mm)	Longitudinal Rebar Strain, microstrain		Transverse Rebar Strain, microstrain	
			Gage 1	Gage 2	Gage 1	Gage 2
Flexural cracking	6 (26)	0.05 (1.4)	87	48	N/A	N/A
Top splitting crack	24.1 (107)	0.19 (4.8)	435	534	N/A	N/A
Side splitting crack	27.3 (121)	0.21 (5.4)	516	636	N/A	N/A
Long. rebar yield	N/A	N/A	N/A	N/A	N/A	N/A
Ultimate	70.6 (314)	0.6 (15.2)	1714	1877	N/A	N/A

Notes:
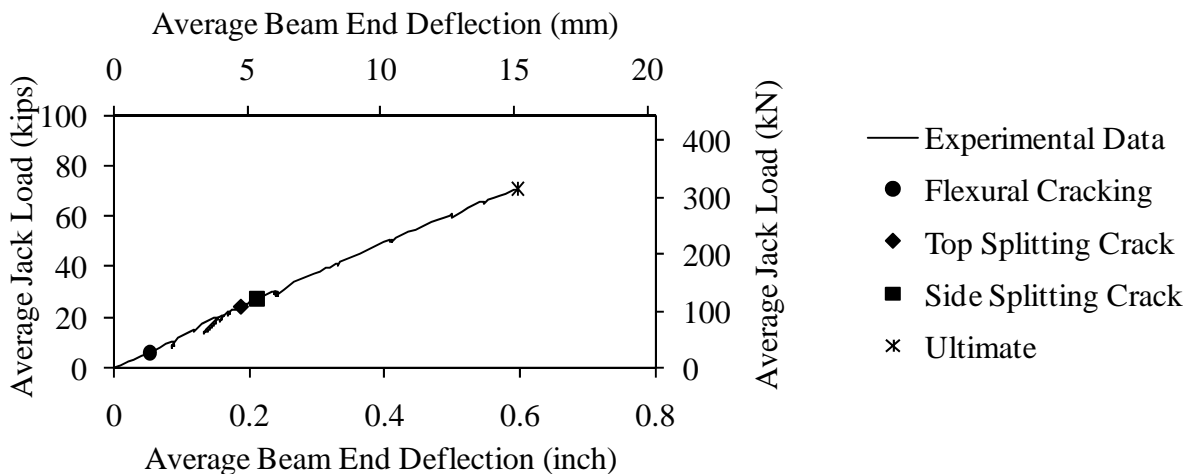
Figure 314. Graph. Load versus deflection for Beam A11-LN.
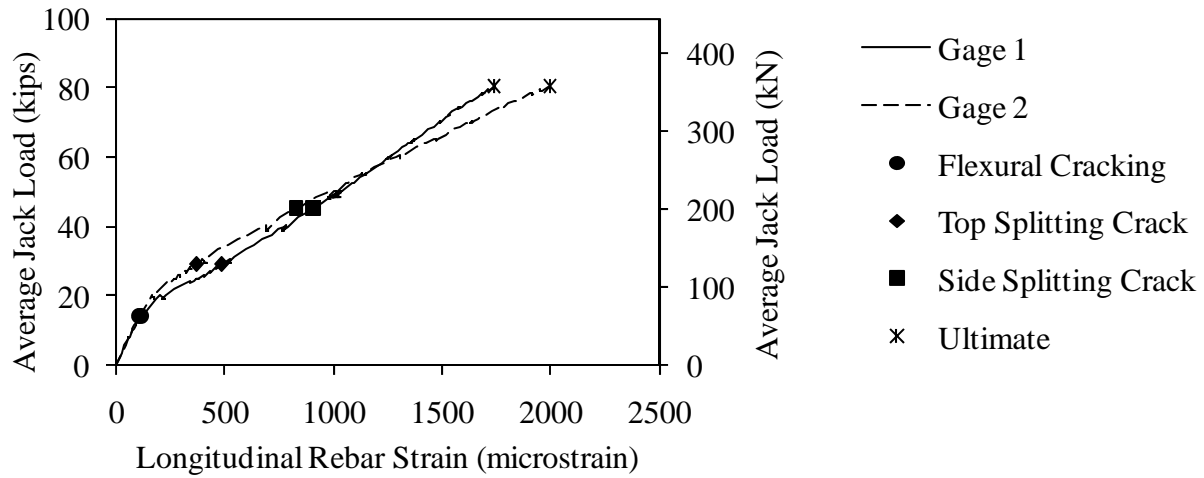
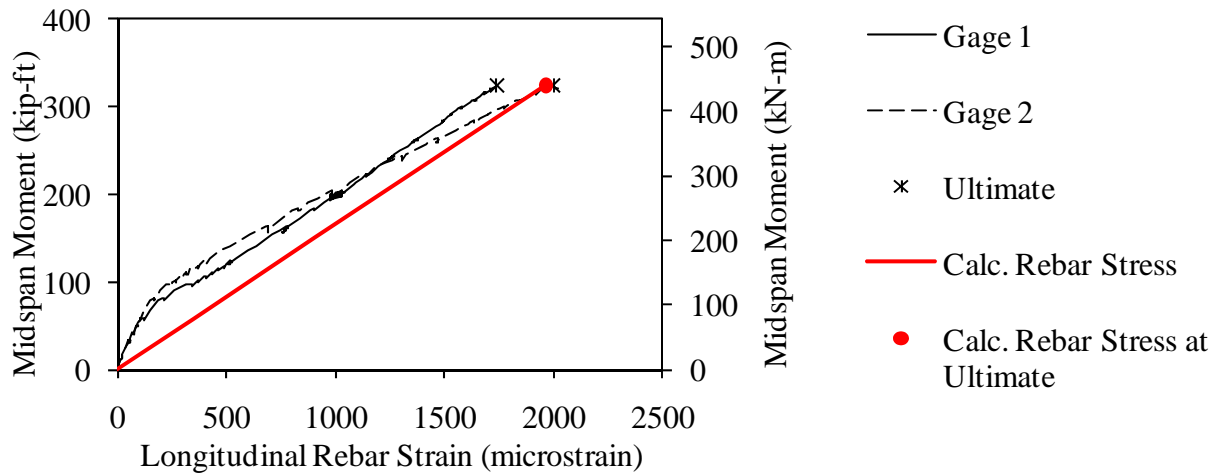**Figure 315. Graph. Load versus longitudinal rebar strain for Beam A11-LN.**

Figure 316. Graph. Measured and predicted midspan moment versus longitudinal rebar strain for Beam A11-LN.
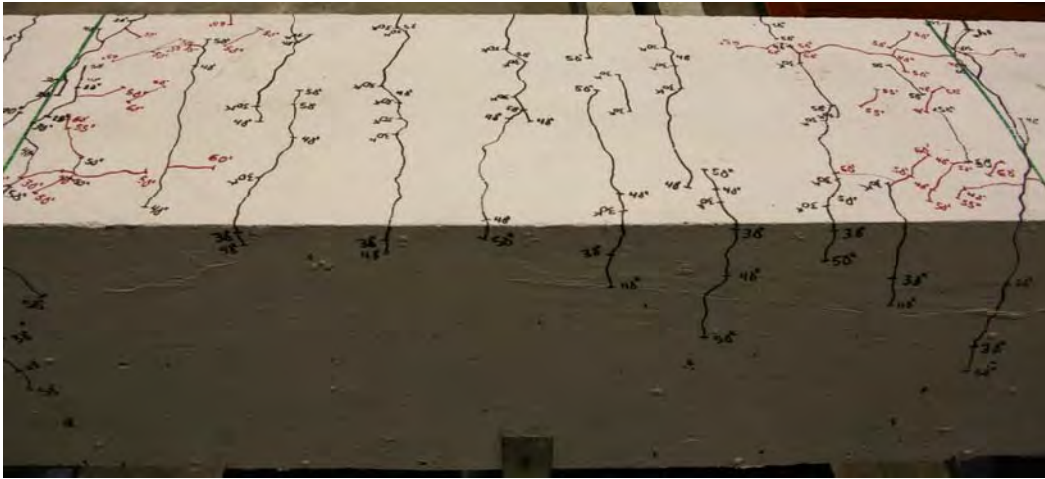
**Figure 317. Photo. Side and top face of Beam A11-LN before failure.**
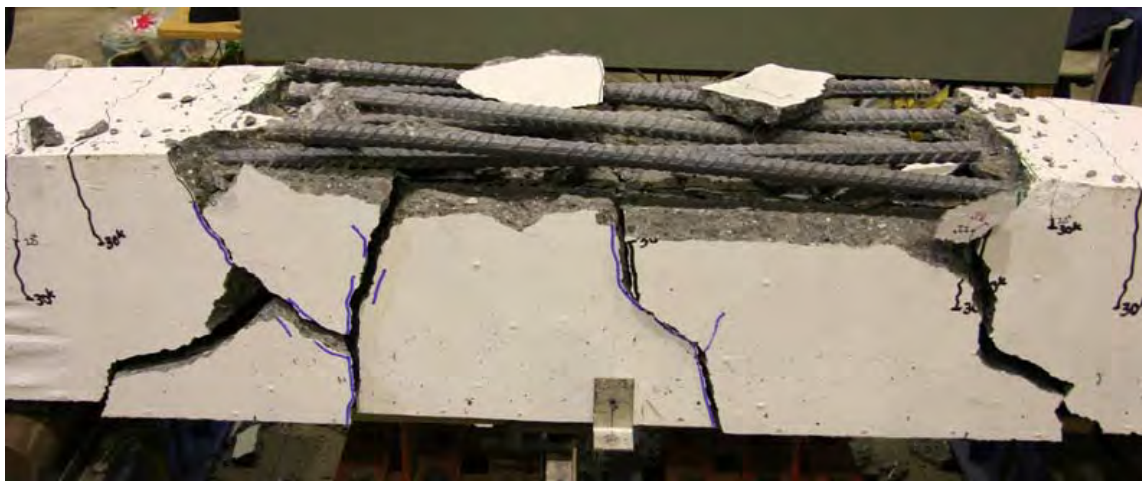
Figure 318. Photo. Beam A11-LN after failure.

Splice Beam B11-LN

Table 98. Test parameters for Splice Beam B11-LN.

Concrete Mix	Spliced Bar Size	Lap Length, inch (mm)	#3 (10M) Bar Transverse Reinforcement	Nominal Beam Cross-Section Dimensions (Width by Height), inch (mm)
Utelite	#11 (40M)	48 (1220)	None	18 by 18 (460 by 460)

Table 99. Test data for Splice Beam B11-LN.

Event	Average Jack Load, kips (kN)	Average Beam End Deflection, inch (mm)	Longitudinal Rebar Strain, microstrain		Transverse Rebar Strain, microstrain	
			Gage 1	Gage 2	Gage 1	Gage 2
Flexural cracking	11 (49)	0.04 (1)	82	94	N/A	N/A
Top splitting crack	24.2 (108)	0.1 (2.7)	319	485	N/A	N/A
Side splitting crack	71.4 (317)	0.49 (12.4)	1603	1925	N/A	N/A
Long. rebar yield	N/A	N/A	N/A	N/A	N/A	N/A
Ultimate	81.6 (363)	0.59 (15.1)	1828	2243	N/A	N/A

Notes:
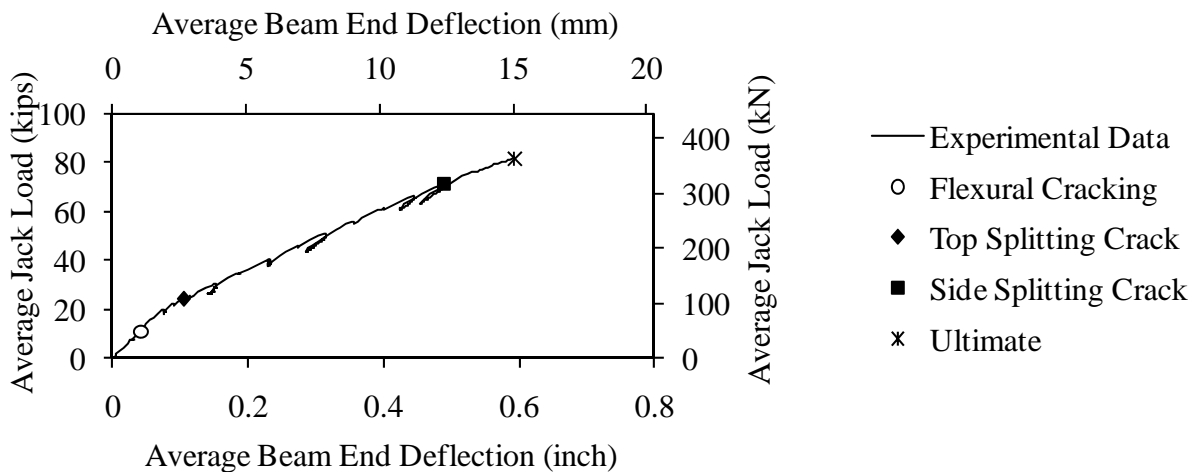
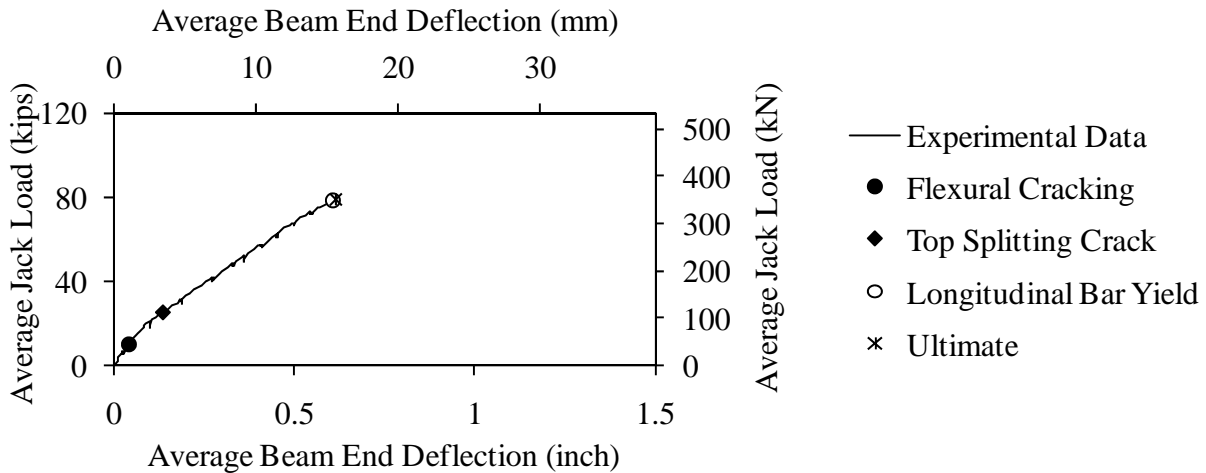**Figure 319. Graph. Load versus deflection for Beam B11-LN.**

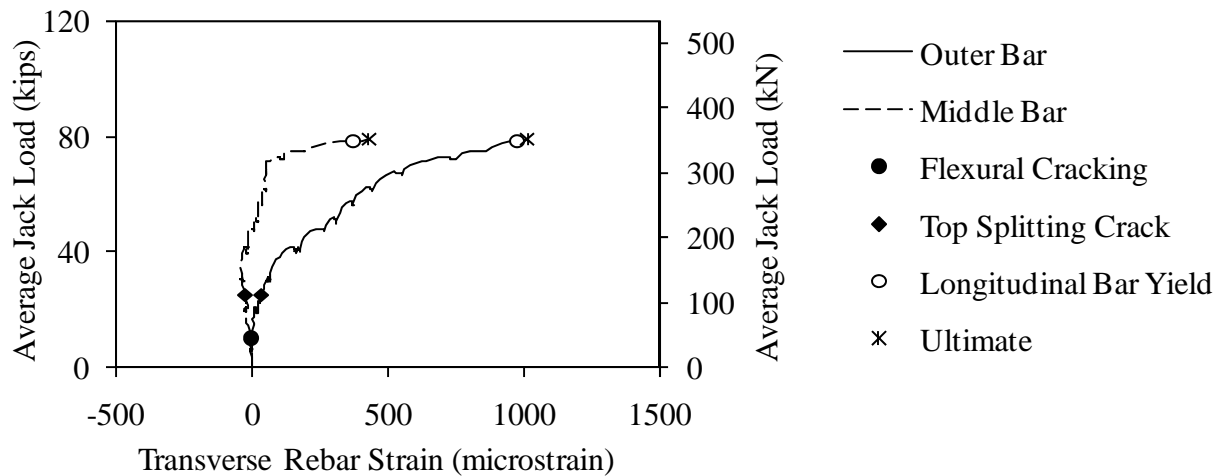**Figure 320. Graph. Load versus longitudinal rebar strain for Beam B11-LN.**
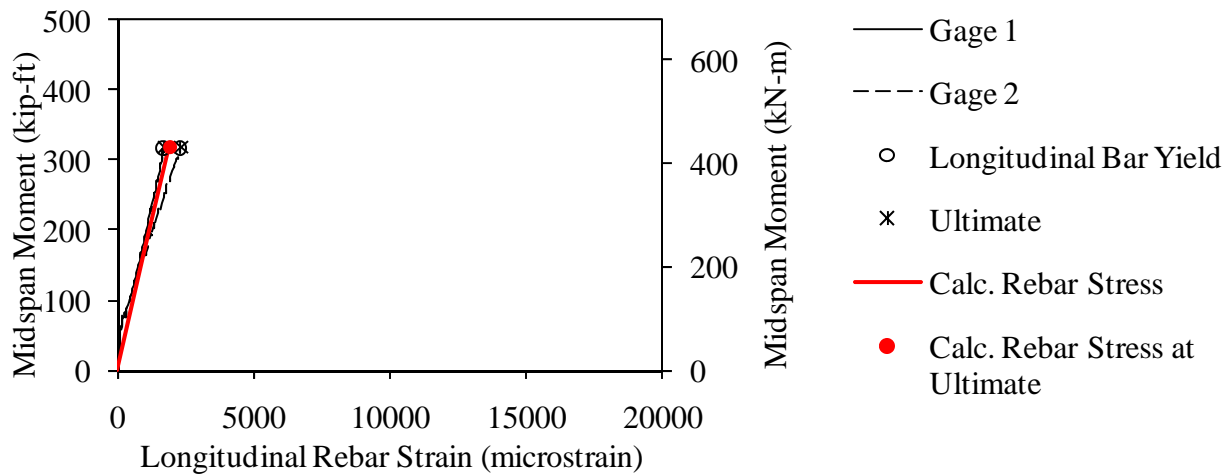

**Figure 321. Graph. Measured and predicted midspan moment versus longitudinal rebar strain for Beam B11-LN.**
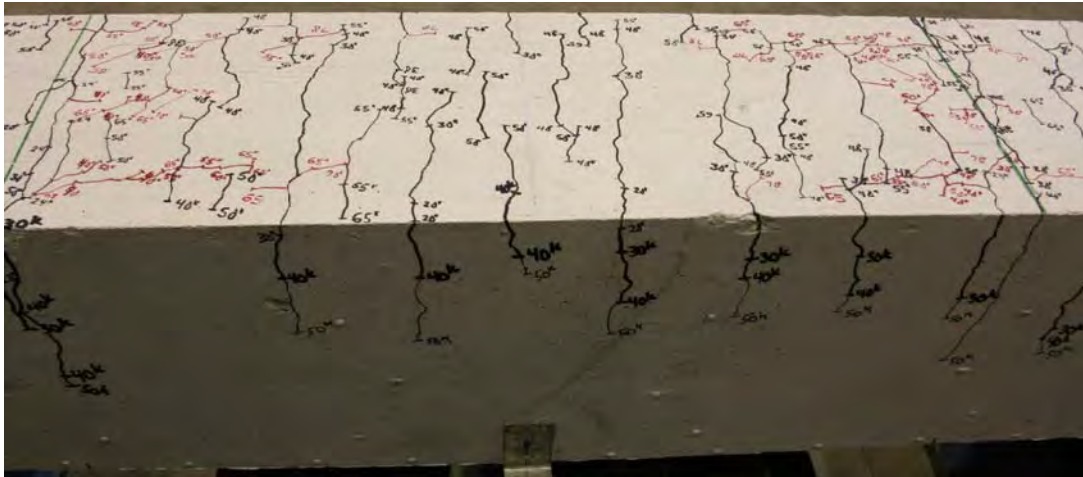
Figure 322. Photo. Side and top face of Beam B11-LN before failure.
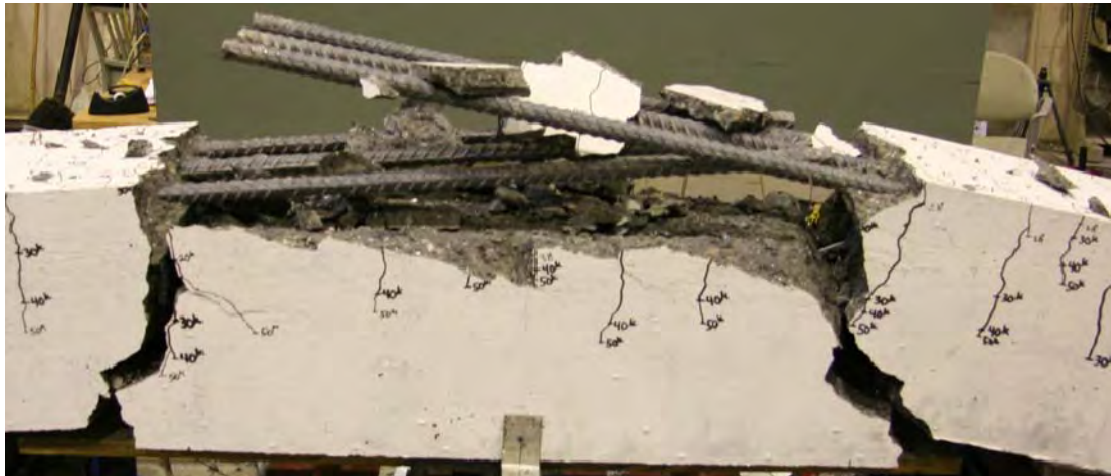
Figure 323. Photo. Beam B11-LN after failure.

Splice Beam C11-LN

Table 100. Test parameters for Splice Beam C11-LN.

Concrete Mix	Spliced Bar Size	Lap Length, inch (mm)	#3 (10M) Bar Transverse Reinforcement	Nominal Beam Cross-Section Dimensions (Width by Height), inch (mm)
Haydite	#11 (40M)	48 (1220)	None	18 by 18 (460 by 460)

Table 101. Test data for Splice Beam C11-LN.

Event	Average Jack Load, kips (kN)	Average Beam End Deflection, inch (mm)	Longitudinal Rebar Strain, microstrain		Transverse Rebar Strain, microstrain	
			Gage 1	Gage 2	Gage 1	Gage 2
Flexural cracking	14.1 (63)	0.06 (1.5)	113	106	N/A	N/A
Top splitting crack	29.2 (130)	0.15 (3.9)	488	367	N/A	N/A
Side splitting crack	45.3 (201)	0.28 (7.1)	905	826	N/A	N/A
Long. rebar yield	N/A	N/A	N/A	N/A	N/A	N/A
Ultimate	80.4 (357)	0.6 (15.3)	1741	1998	N/A	N/A

Notes:
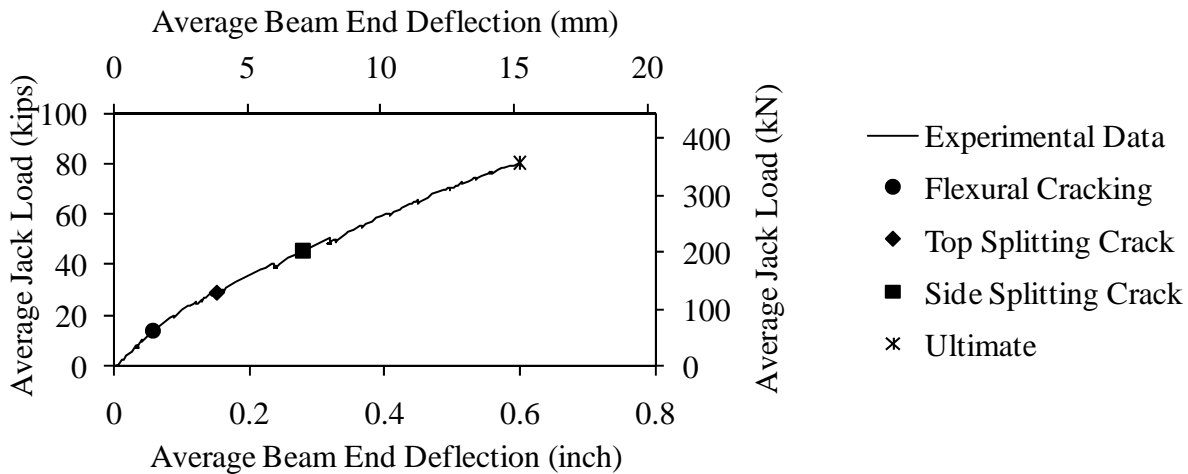
Figure 324. Graph. Load versus deflection for Beam C11-LN.

Figure 325. Graph. Load versus longitudinal rebar strain for Beam C11-LN.

Figure 326. Graph. Measured and predicted midspan moment versus longitudinal rebar strain for Beam C11-LN.

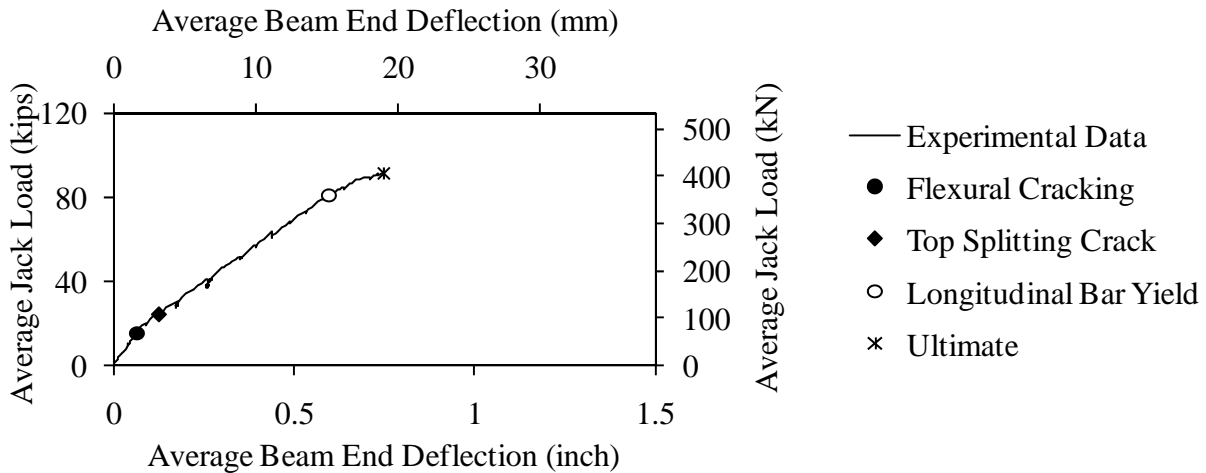**Figure 327. Photo. Side and top face of Beam C11-LN before failure.**
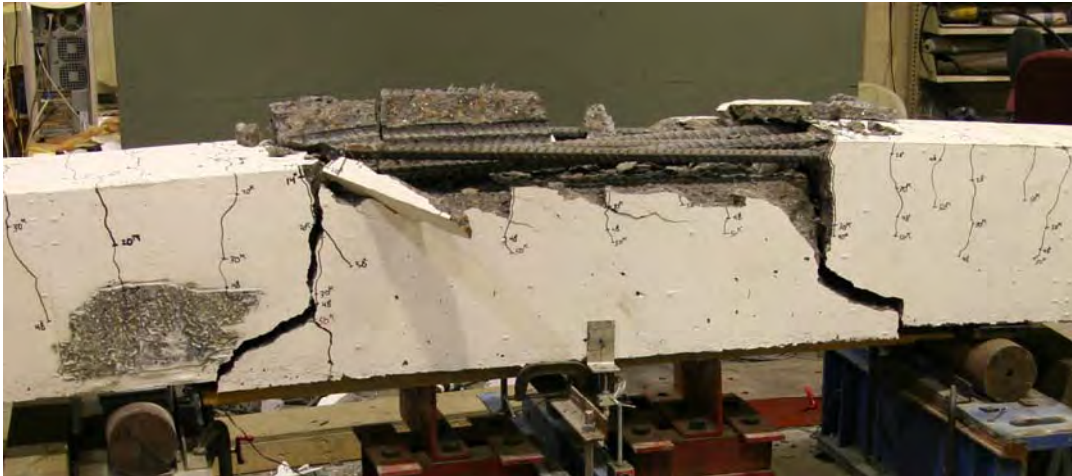
Figure 328. Photo. Beam C11-LN after failure.

Splice Beam A11-ST

Table 102. Test parameters for Splice Beam A11-ST.

Concrete Mix	Spliced Bar Size	Lap Length, inch (mm)	#3 (10M) Bar Transverse Reinforcement	Nominal Beam Cross-Section Dimensions (Width by Height), inch (mm)
Stalite	#11 (40M)	32 (810)	(4) at 8 in. (200mm)	18 by 18 (460 by 460)

Table 103. Test data for Splice Beam A11-ST.

Event	Average Jack Load, kips (kN)	Average Beam End Deflection, inch (mm)	Longitudinal Rebar Strain, microstrain		Transverse Rebar Strain, microstrain	
			Gage 1	Gage 2	Gage 1	Gage 2
Flexural cracking	10.3 (46)	0.04 (1.1)	74	85	-4	-6
Top splitting crack	24.9 (111)	0.13 (3.4)	462	450	33	-24
Side splitting crack	N/A	N/A	N/A	N/A	N/A	N/A
Long. rebar yield	78.4 (349)	0.61 (15.5)	1698	2309	978	374
Ultimate	78.9 (351)	0.62 (15.6)	1711	2333	1013	429

Notes:

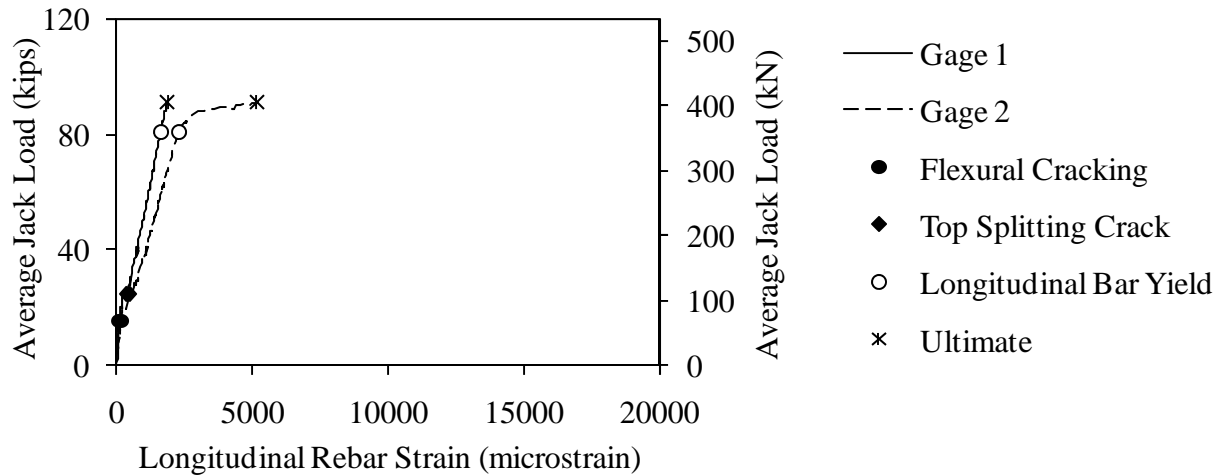**Figure 329. Graph. Load versus deflection for Beam A11-ST.**
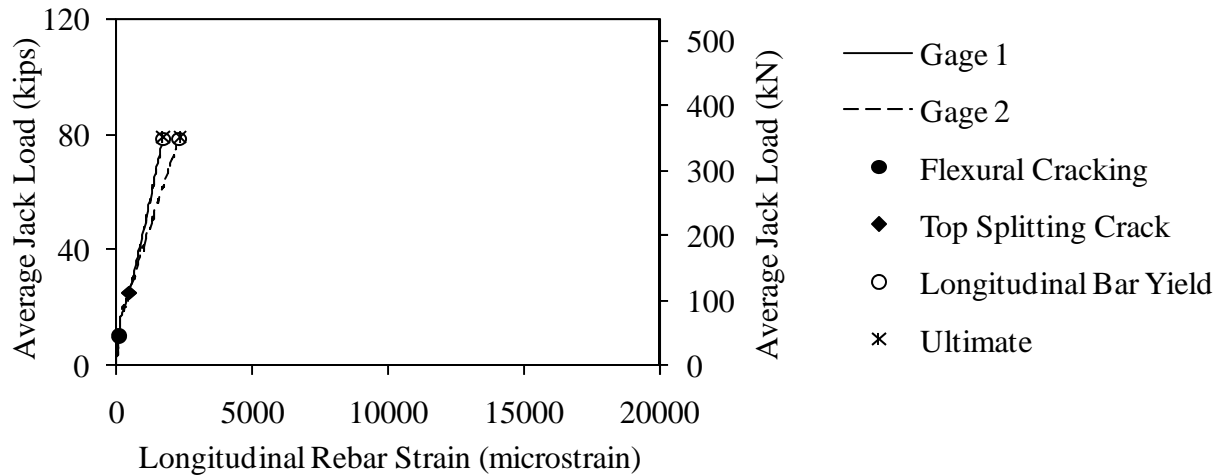
Figure 330. Graph. Load versus longitudinal rebar strain for Beam A11-ST.
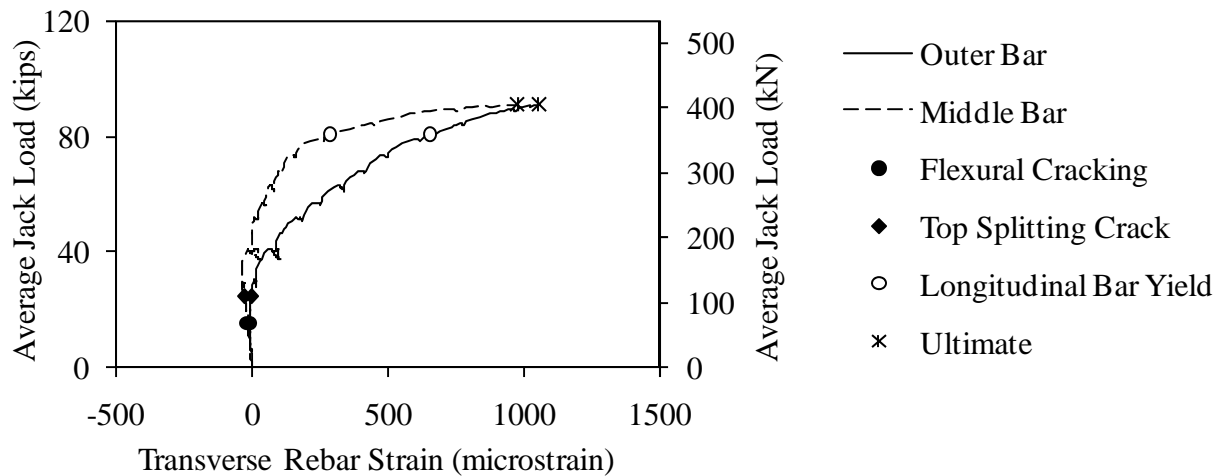

Figure 331. Graph. Load versus transverse rebar strain for Beam A11-ST.
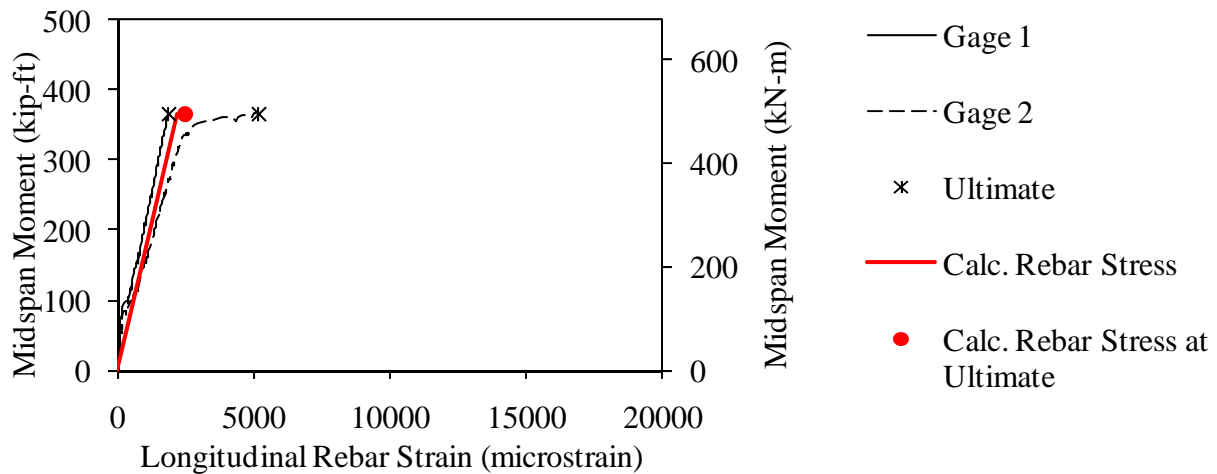

Figure 332. Graph. Measured and predicted midspan moment versus longitudinal rebar strain for Beam A11-ST.
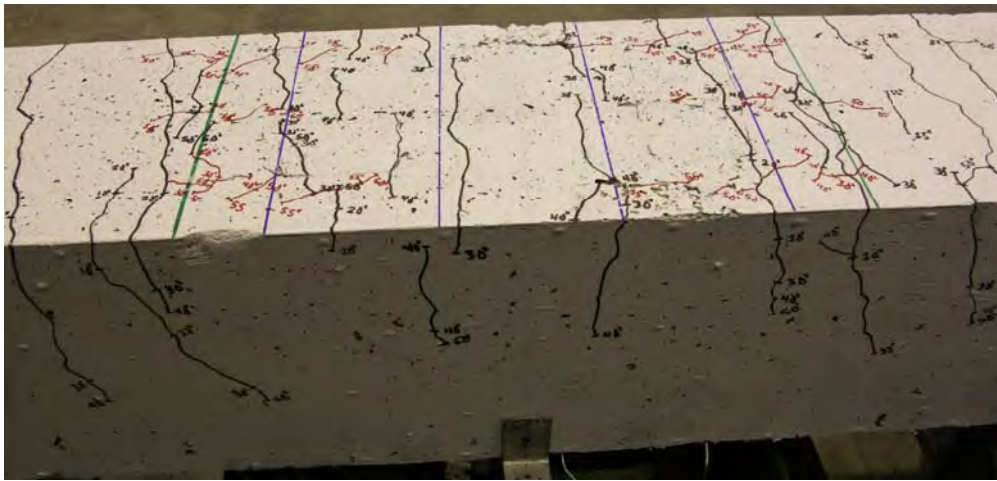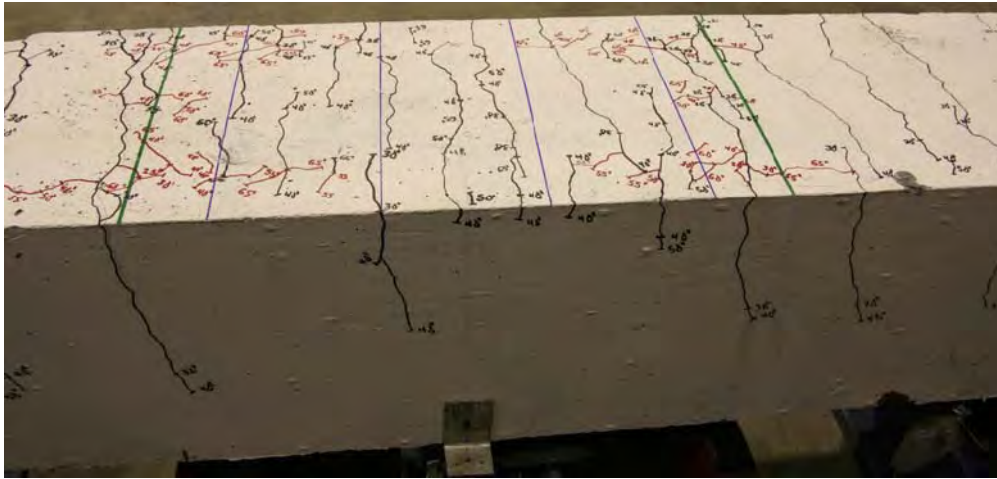
Figure 333. Photo. Side and top face of Beam A11-ST before failure.
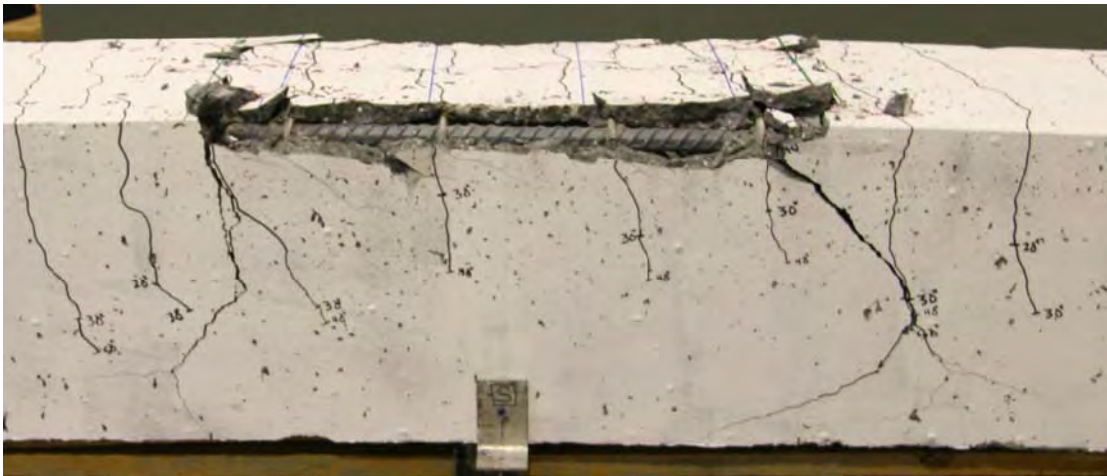
Figure 334. Photo. Beam A11-ST after failure.

Splice Beam B11-ST

Table 104. Test parameters for Splice Beam B11-ST.

Concrete Mix	Spliced Bar Size	Lap Length, inch (mm)	#3 (10M) Bar Transverse Reinforcement	Nominal Beam Cross-Section Dimensions (Width by Height), inch (mm)
Utelite	#11 (40M)	32 (810)	(4) at 8 in. (200mm)	18 by 18 (460 by 460)

Table 105. Test data for Splice Beam B11-ST.

| Event	Average Jack Load, kips (kN)	Average Beam End Deflection, inch (mm)	Longitudinal Rebar Strain, microstrain		Transverse Rebar Strain, microstrain	
			Gage 1	Gage 2	Gage 1	Gage 2
Flexural cracking	15.4 (68)	0.06 (1.6)	103	154	-7	-17
Top splitting crack	24.6 (109)	0.12 (3.2)	363	510	-2	-30
Side splitting crack	N/A	N/A	N/A	N/A	N/A	N/A
Long. rebar yield	80.5 (358)	0.6 (15.1)	1626	2300	656	287
Ultimate	91 (405)	0.75 (19)	1873	5180	1056	978

Notes:

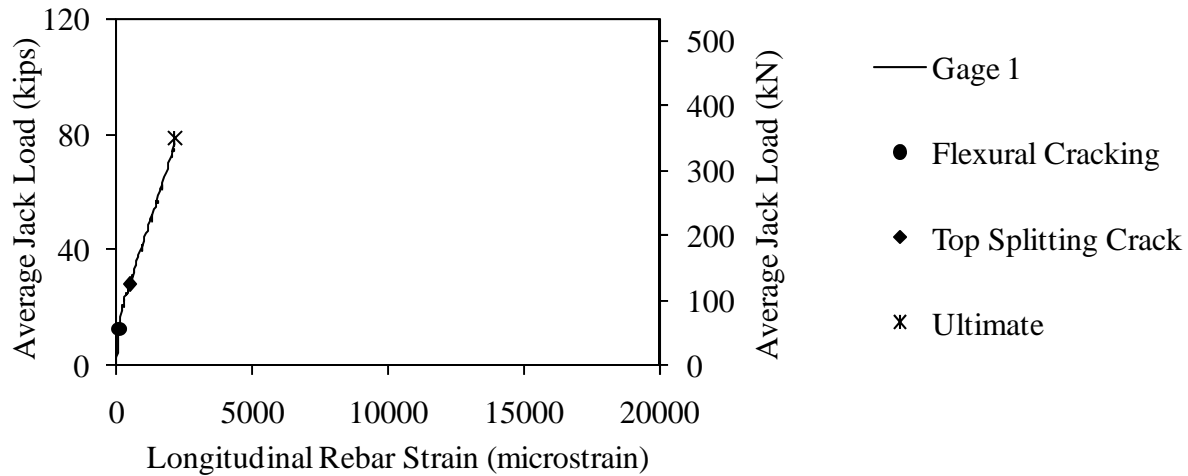**Figure 335. Graph. Load versus deflection for Beam B11-ST.**

Figure 336. Graph. Load versus longitudinal rebar strain for Beam B11-ST.
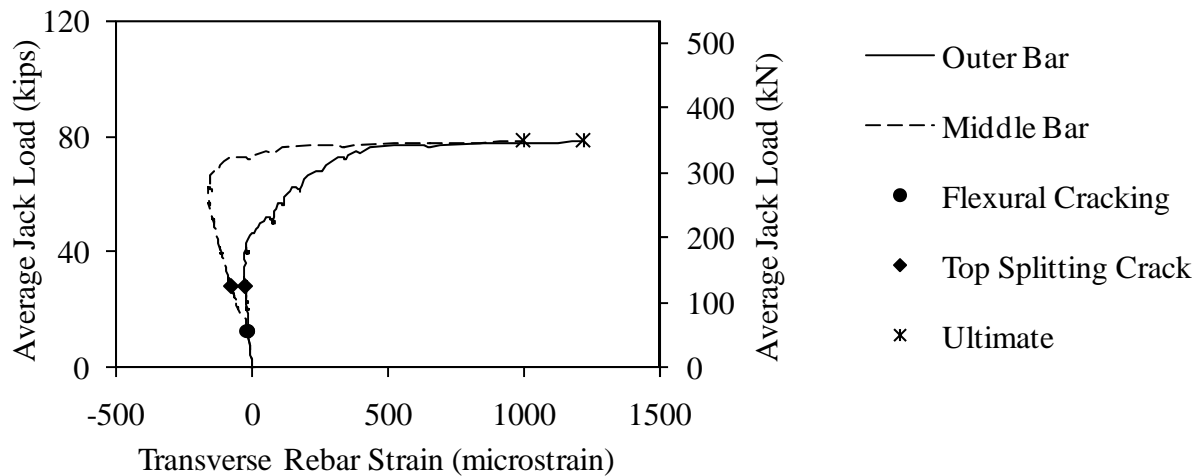

Figure 337. Graph. Load versus transverse rebar strain for Beam B11-ST.
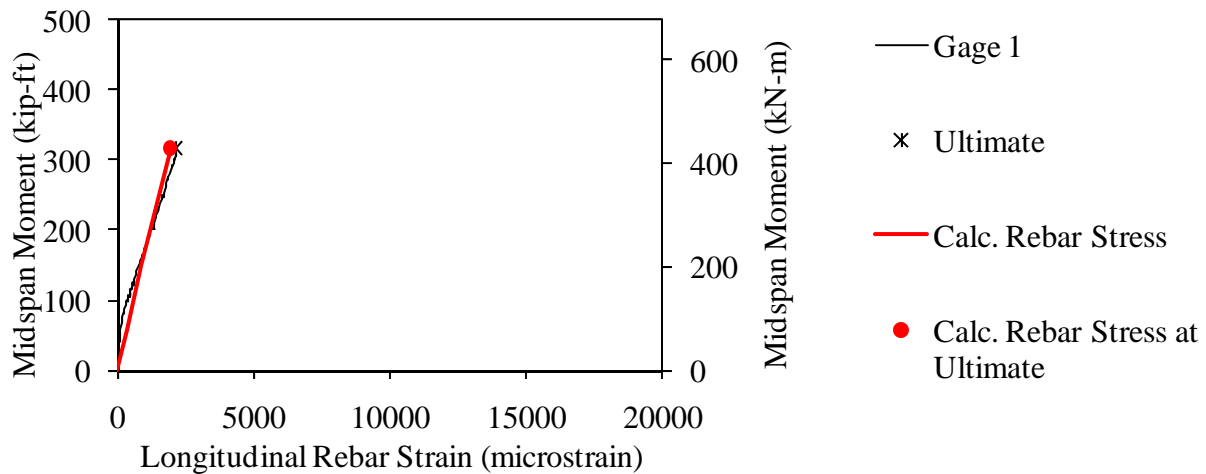

Figure 338. Graph. Measured and predicted midspan moment versus longitudinal rebar strain for Beam B11-ST.
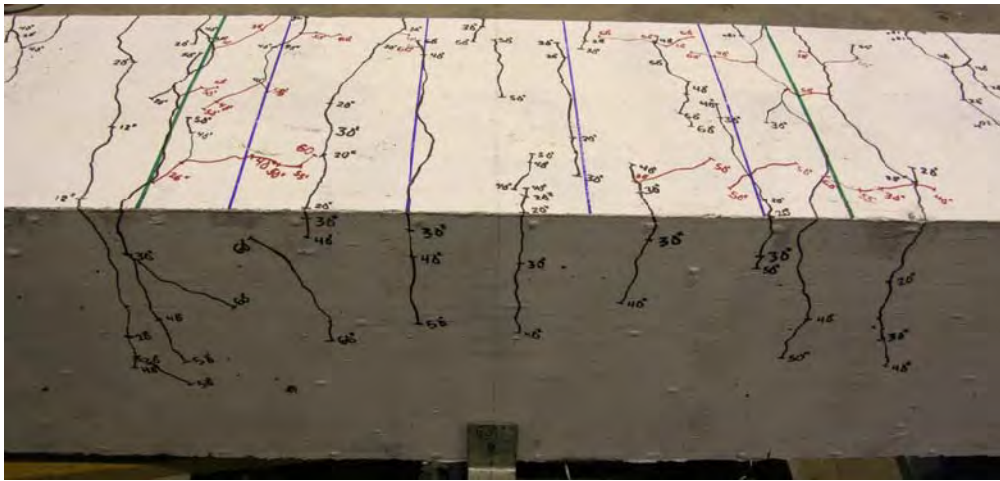
Figure 339. Photo. Side and top face of Beam B11-ST before failure.

Figure 340. Photo. Beam B11-ST after failure.

Splice Beam C11-ST

<p align="center">Table 106. Test parameters for Splice Beam C11-ST.</p>

Concrete Mix	Spliced Bar Size	Lap Length, inch (mm)	#3 (10M) Bar Transverse Reinforcement	Nominal Beam Cross-Section Dimensions (Width by Height), inch (mm)
Haydite	#11 (40M)	32 (810)	(4) at 8 in. (200mm)	18 by 18 (460 by 460)

<p align="center">Table 107. Test data for Splice Beam C11-ST.</p>

| Event	Average Jack Load, kips (kN)	Average Beam End Deflection, inch (mm)	Longitudinal Rebar Strain, microstrain Gage 1	Gage 2	Transverse Rebar Strain, microstrain Gage 1	Gage 2
Flexural cracking	12.6 (56)	0.05 (1.2)	0	104	-15	-19
Top splitting crack	28.2 (125)	0.14 (3.7)	0	492	-28	-76
Side splitting crack	N/A	N/A	N/A	N/A	N/A	N/A
Long. rebar yield	N/A	N/A	N/A	N/A	N/A	N/A
Ultimate	78.5 (349)	0.61 (15.4)	0	2144	1221	1000

Notes:
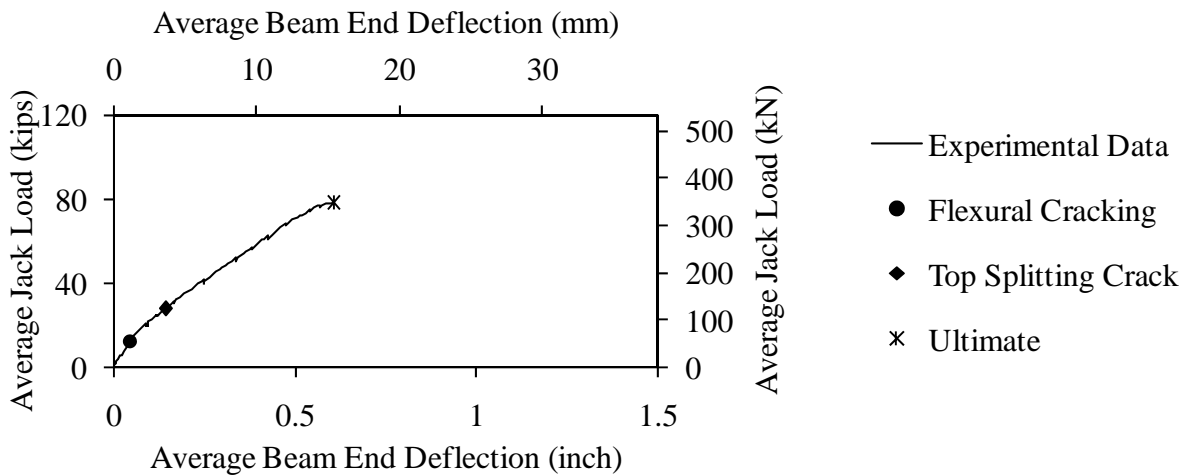
Figure 341. Graph. Load versus deflection for Beam C11-ST.

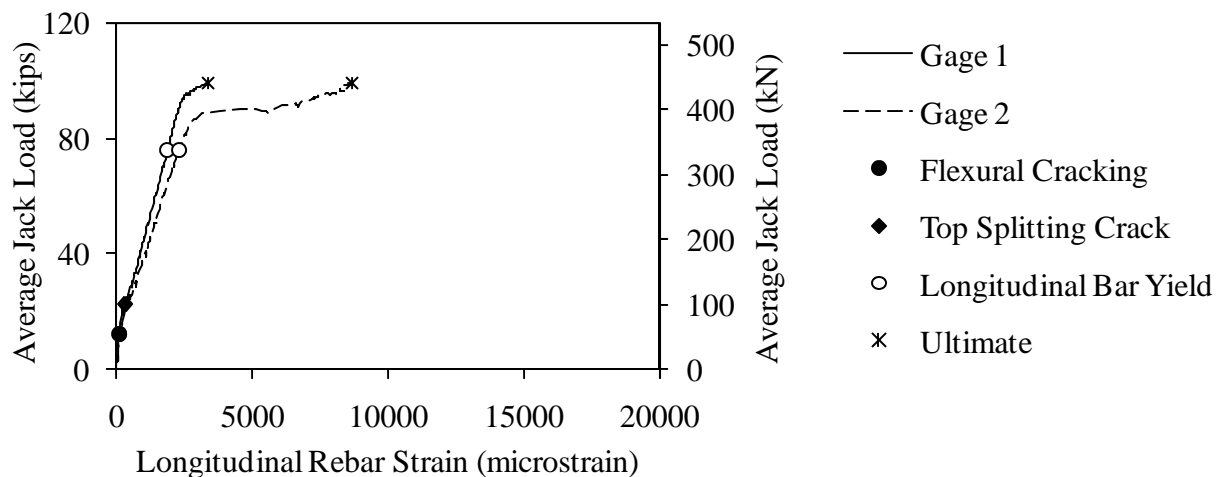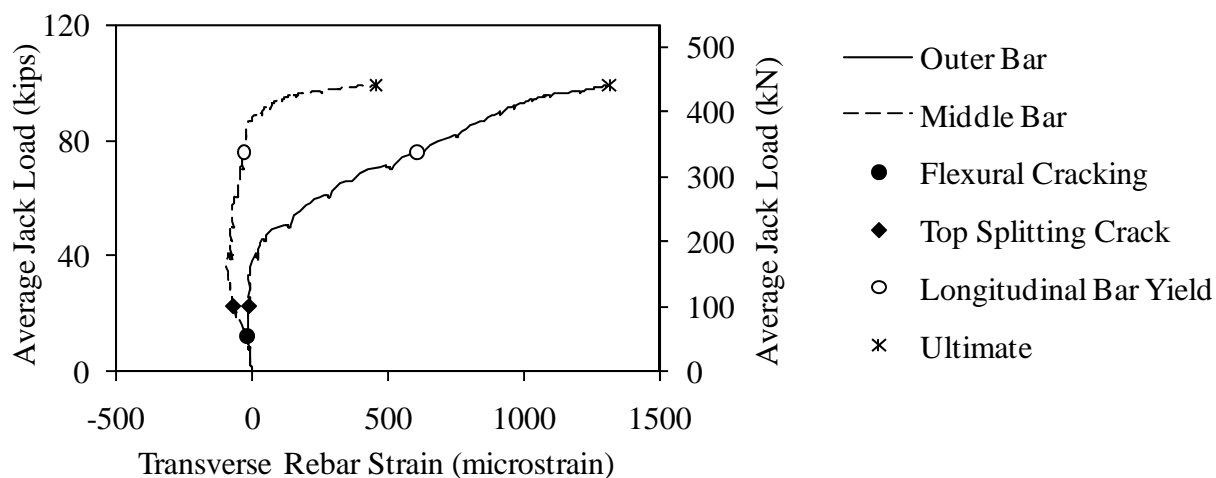**Figure 342. Graph. Load versus longitudinal rebar strain for Beam C11-ST.**

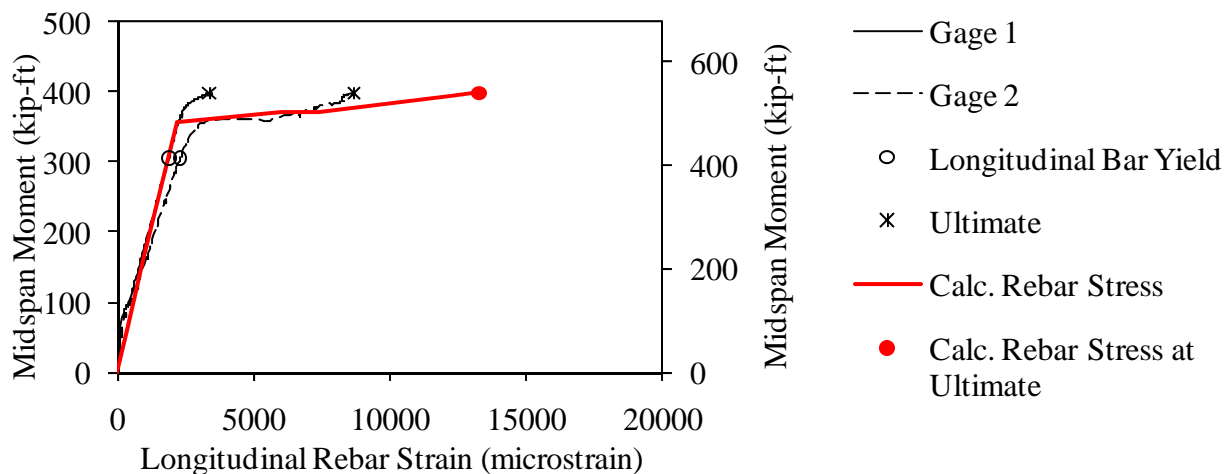**Figure 343. Graph. Load versus transverse rebar strain for Beam C11-ST.**

Figure 344. Graph. Measured and predicted midspan moment versus longitudinal rebar strain for Beam C11-ST.
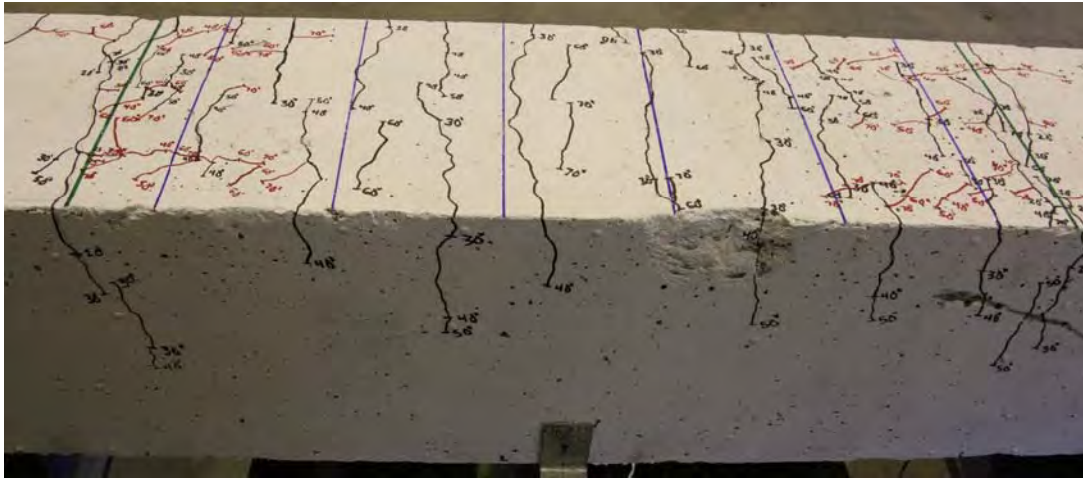
Figure 345. Photo. Side and top face of Beam C11-ST before failure.

Figure 346. Photo. Beam C11-ST after failure.

Splice Beam A11-LT

<p style="text-align:center">Table 108. Test parameters for Splice Beam A11-LT.</p>

Concrete Mix	Spliced Bar Size	Lap Length, inch (mm)	#3 (10M) Bar Transverse Reinforcement	Nominal Beam Cross-Section Dimensions (Width by Height), inch (mm)
Stalite	#11 (40M)	48 (1220)	(6) at 8 in. (200mm)	18 by 18 (460 by 460)

<p style="text-align:center">Table 109. Test data for Splice Beam A11-LT.</p>

| Event	Average Jack Load, kips (kN)	Average Beam End Deflection, inch (mm)	Longitudinal Rebar Strain, microstrain Gage 1	Gage 2	Transverse Rebar Strain, microstrain Gage 1	Gage 2
Flexural cracking	12.4 (55)	0.05 (1.2)	103	126	-19	-19
Top splitting crack	22.5 (100)	0.1 (2.6)	271	360	-13	-69
Side splitting crack	N/A	N/A	N/A	N/A	N/A	N/A
Long. rebar yield	76 (338)	0.56 (14.1)	1883	2305	606	-30
Ultimate	99.1 (441)	1.18 (29.9)	3380	8674	1315	458

Notes:
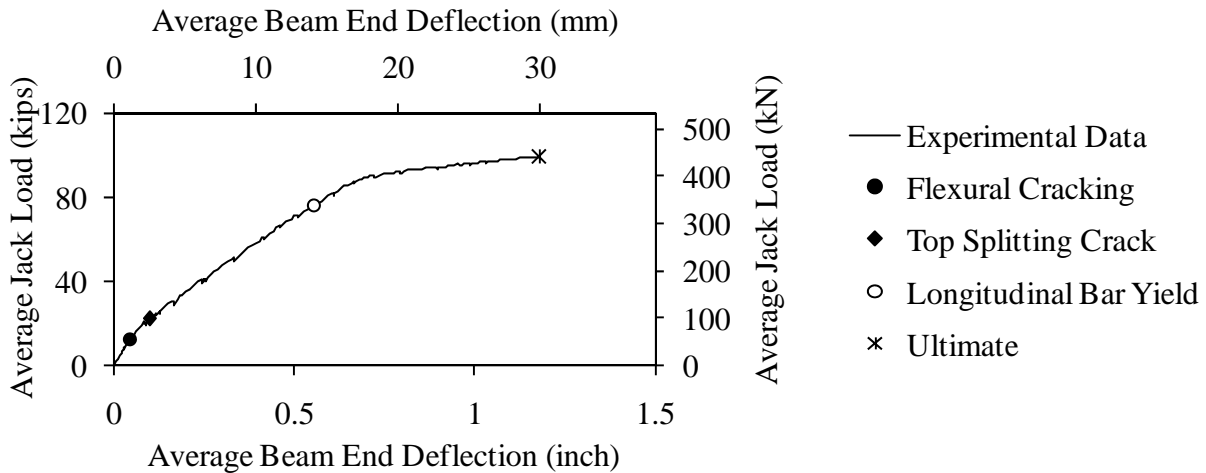
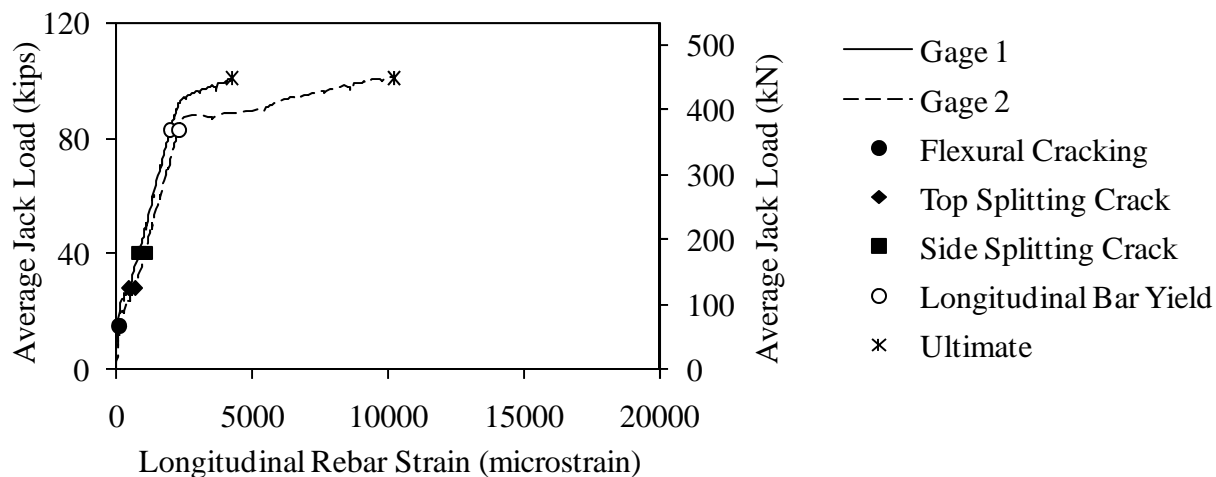**Figure 347. Graph. Load versus deflection for Beam A11-LT.**

Figure 348. Graph. Load versus longitudinal rebar strain for Beam A11-LT.
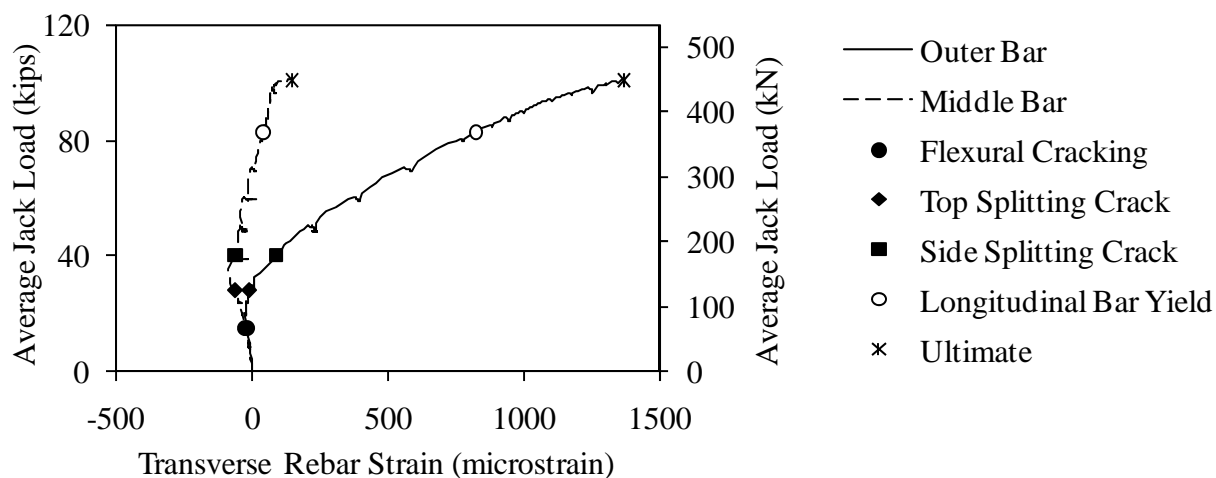

Figure 349. Graph. Load versus transverse rebar strain for Beam A11-LT.
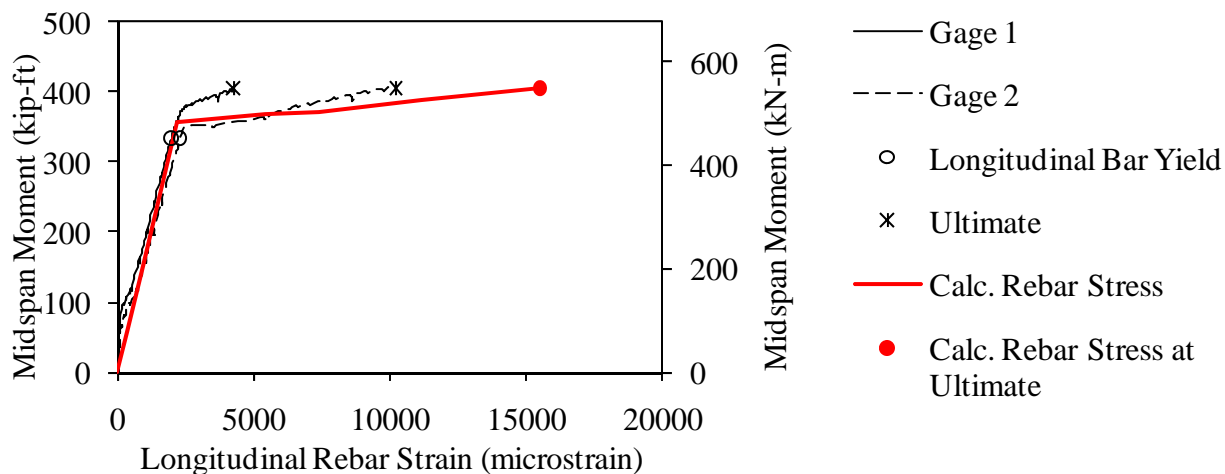

**Figure 350. Graph. Measured and predicted midspan moment versus longitudinal rebar strain for Beam A11-LT.**

**Figure 351. Photo. Side and top face of Beam A11-LT before failure.**

Figure 352. Photo. Beam A11-LT after failure.

Splice Beam B11-LT

<p style="text-align:center">Table 110. Test parameters for Splice Beam B11-LT.</p>

Concrete Mix	Spliced Bar Size	Lap Length, inch (mm)	#3 (10M) Bar Transverse Reinforcement	Nominal Beam Cross-Section Dimensions (Width by Height), inch (mm)
Utelite	#11 (40M)	48 (1220)	(6) at 8 in. (200mm)	18 by 18 (460 by 460)

<p style="text-align:center">Table 111. Test data for Splice Beam B11-LT.</p>

| Event	Average Jack Load, kips (kN)	Average Beam End Deflection, inch (mm)	Longitudinal Rebar Strain, microstrain		Transverse Rebar Strain, microstrain	
			Gage 1	Gage 2	Gage 1	Gage 2
Flexural cracking	15.2 (67)	0.06 (1.5)	63	130	-20	-24
Top splitting crack	28.3 (126)	0.15 (3.8)	435	675	-13	-63
Side splitting crack	40.3 (179)	0.25 (6.3)	824	1043	89	-61
Long. rebar yield	82.8 (368)	0.63 (15.9)	1982	2302	825	41
Ultimate	100.9 (449)	1.36 (34.5)	4264	10218	1369	147

Notes:
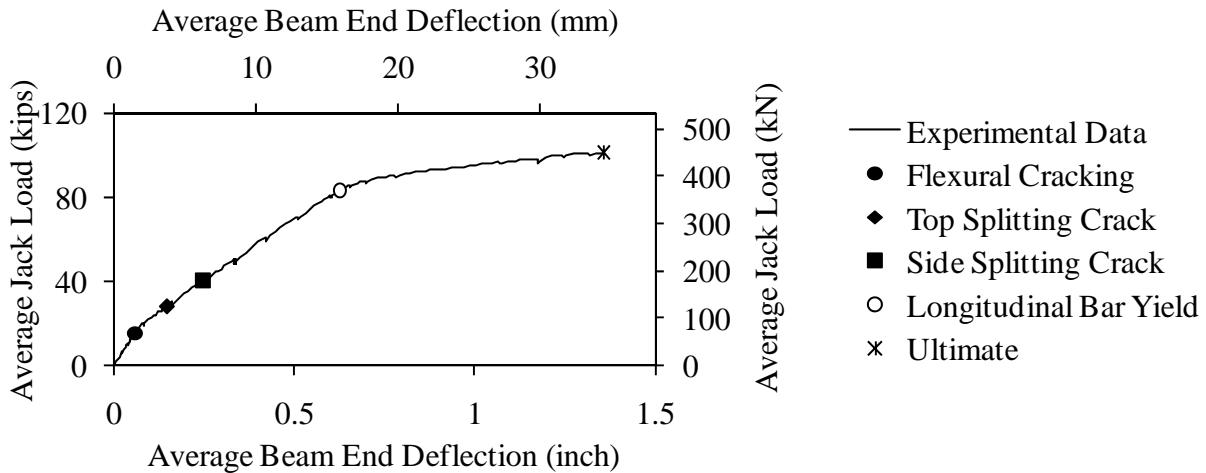
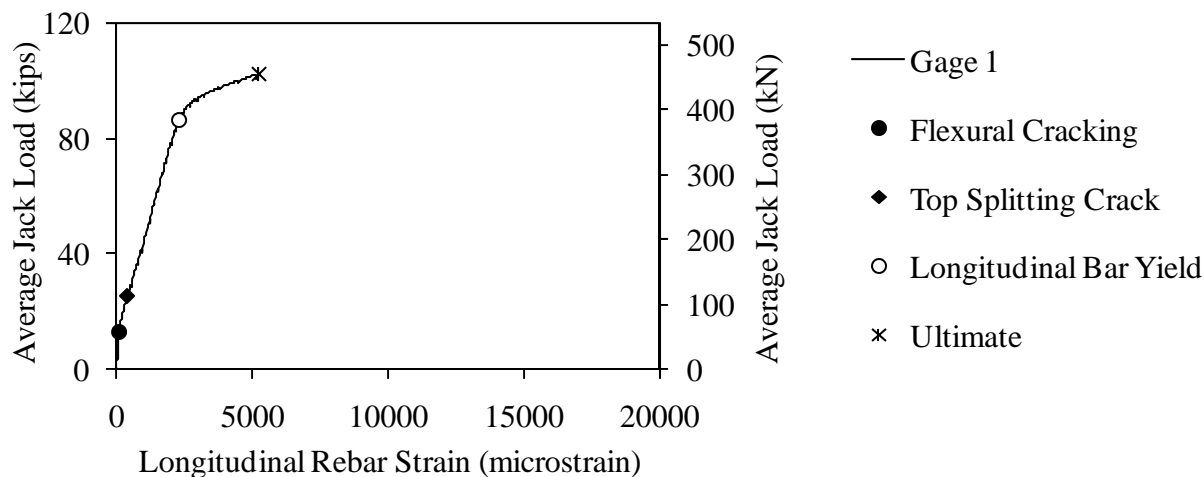**Figure 353. Graph. Load versus deflection for Beam B11-LT.**

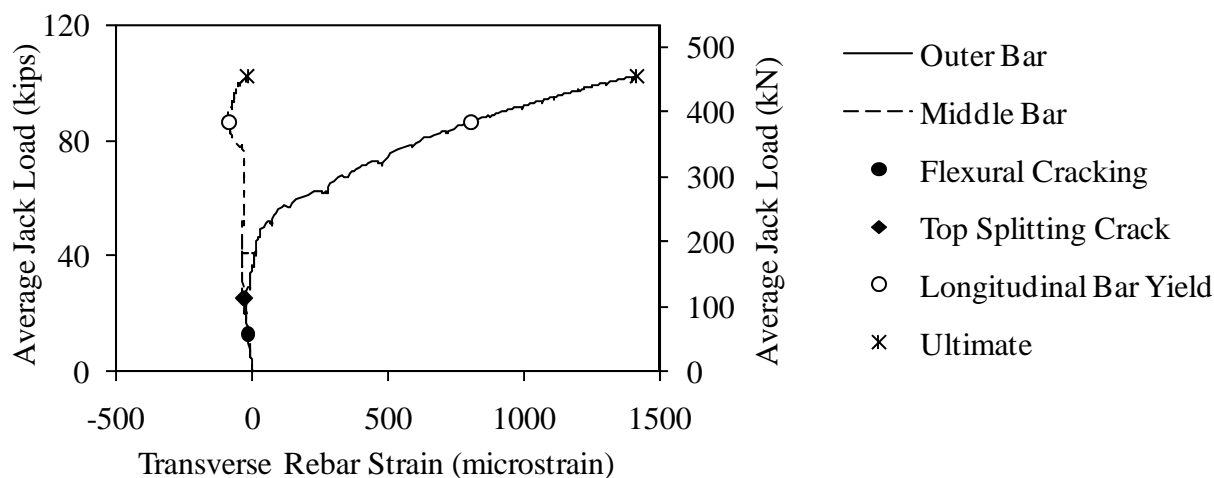**Figure 354. Graph. Load versus longitudinal rebar strain for Beam B11-LT.**

Figure 355. Graph. Load versus transverse rebar strain for Beam B11-LT.

Figure 356. Graph. Measured and predicted midspan moment versus longitudinal rebar strain for Beam B11-LT.
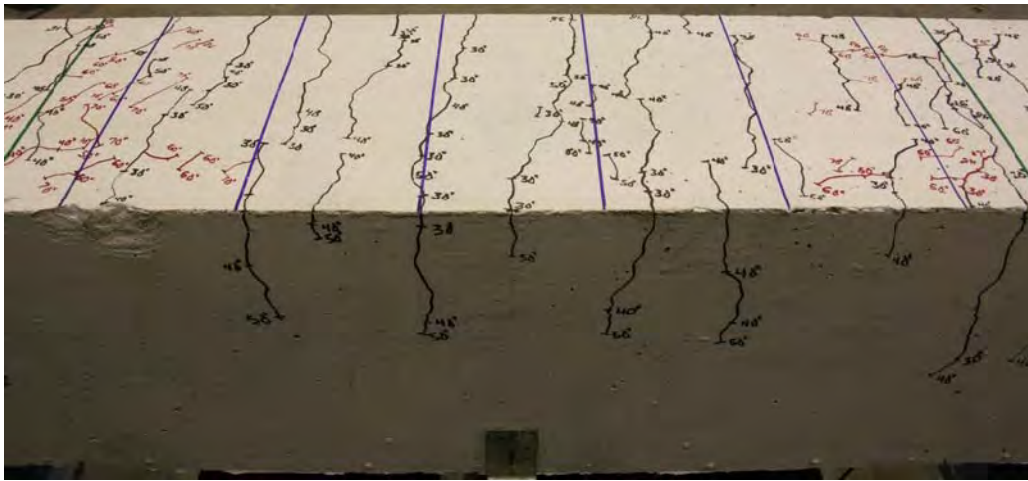
Figure 357. Photo. Side and top face of Beam B11-LT before failure.
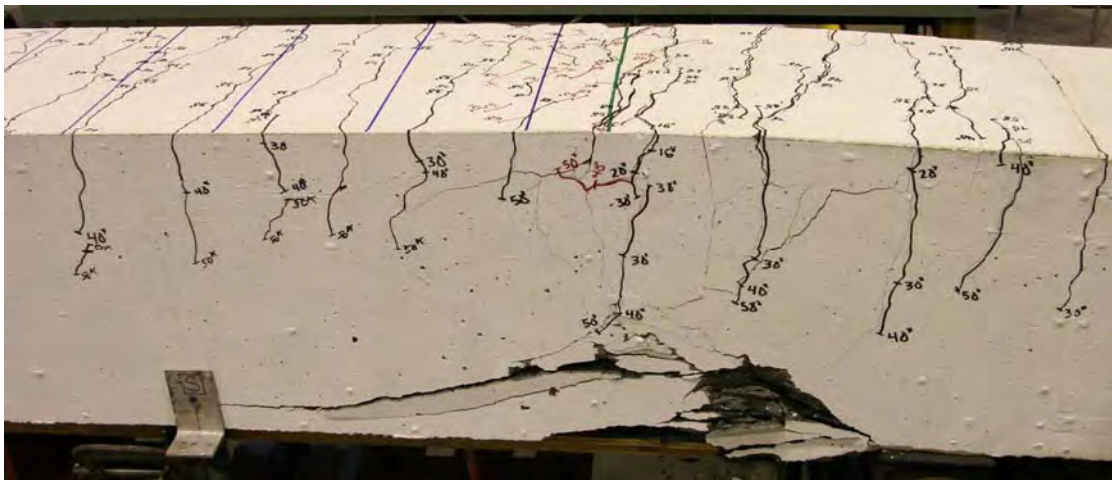
Figure 358. Photo. Beam B11-LT after failure.

Splice Beam C11-LT

<div align="center">

Table 112. Test parameters for Splice Beam C11-LT.

</div>

Concrete Mix	Spliced Bar Size	Lap Length, inch (mm)	#3 (10M) Bar Transverse Reinforcement	Nominal Beam Cross-Section Dimensions (Width by Height), inch (mm)
Haydite	#11 (40M)	48 (1220)	(6) at 8 in. (200mm)	18 by 18 (460 by 460)

<div align="center">

Table 113. Test data for Splice Beam C11-LT.

</div>

Event	Average Jack Load, kips (kN)	Average Beam End Deflection, inch (mm)	Longitudinal Rebar Strain, microstrain		Transverse Rebar Strain, microstrain	
			Gage 1	Gage 2	Gage 1	Gage 2
Flexural cracking	13 (58)	0.05 (1.3)	107	0	-15	-15
Top splitting crack	25.2 (112)	0.12 (3.1)	391	0	-23	-32
Side splitting crack	N/A	N/A	N/A	N/A	N/A	N/A
Long. rebar yield	86.2 (383)	0.68 (17.2)	2318	0	809	-85
Ultimate	102.2 (455)	1.39 (35.3)	5243	0	1417	-19

Notes:
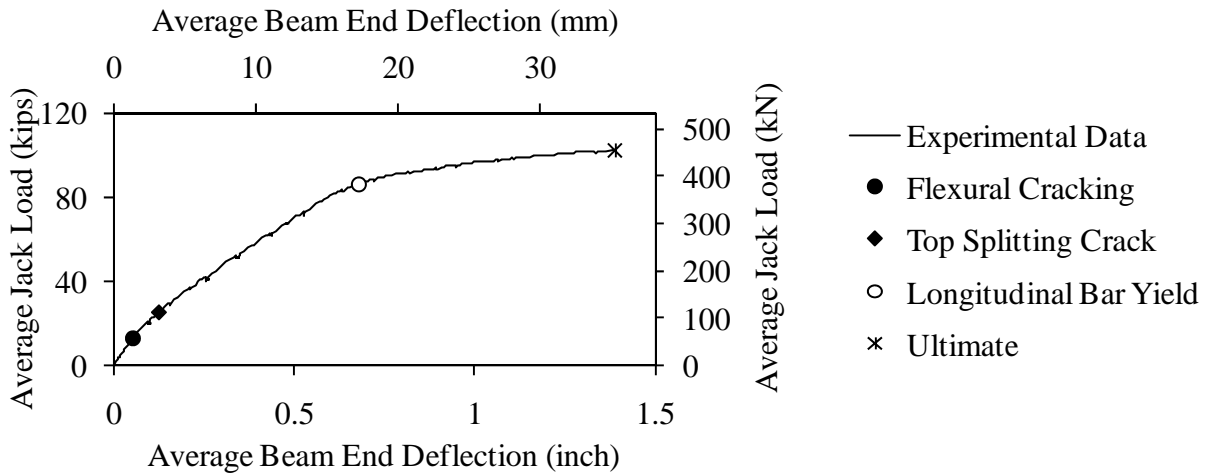
Figure 359. Graph. Load versus deflection for Beam C11-LT.

Figure 360. Graph. Load versus longitudinal rebar strain for Beam C11-LT.

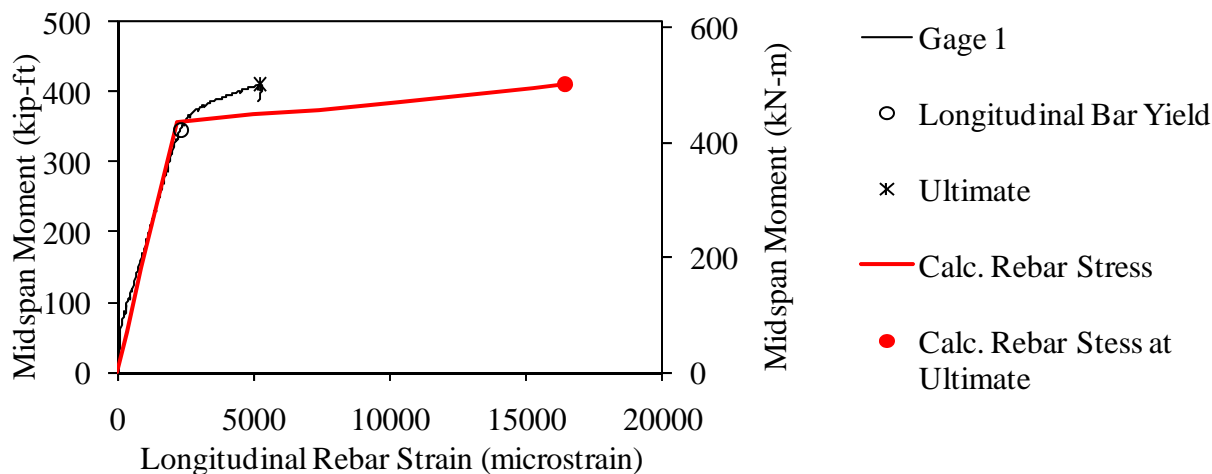**Figure 361. Graph. Load versus transverse rebar strain for Beam C11-LT.**

Figure 362. Graph. Measured and predicted midspan moment versus longitudinal rebar strain for Beam C11-LT.
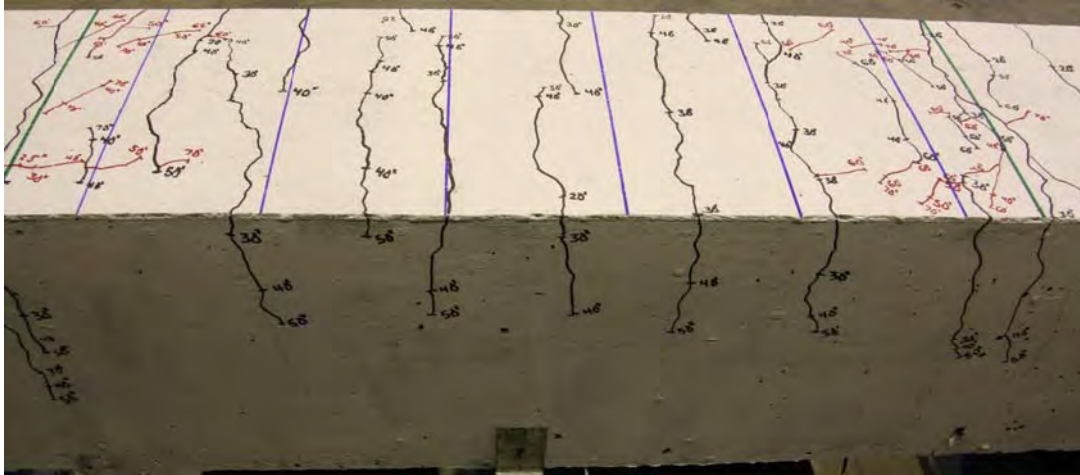
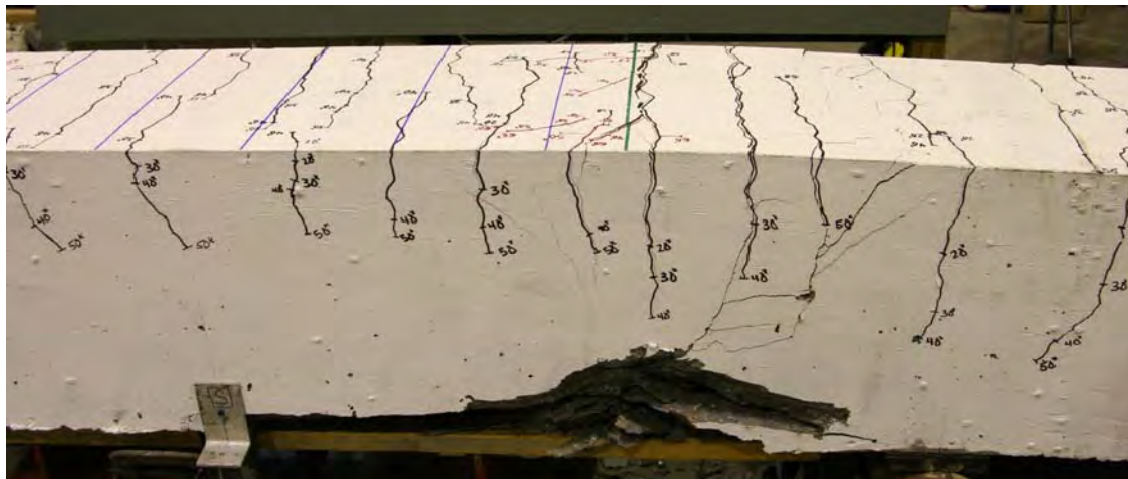**Figure 363. Photo. Side and top face of Beam C11-LT before failure.**

Figure 364. Photo. Beam C11-LT after failure.

Splice Beam D4-LN

Table 114. Test parameters for Splice Beam D4-LN.

Concrete Mix	Spliced Bar Size	Lap Length, inch (mm)	#3 (10M) Bar Transverse Reinforcement	Nominal Beam Cross-Section Dimensions (Width by Height), inch (mm)
Stalite (Deck)	#4 (13M)	16 (410)	None	18 by 18 (460 by 460)

Table 115. Test data for Splice Beam D4-LN.

| Event	Average Jack Load, kips (kN)	Average Beam End Deflection, inch (mm)	Longitudinal Rebar Strain, microstrain		Transverse Rebar Strain, microstrain	
			Gage 1	Gage 2	Gage 1	Gage 2
Flexural cracking	5.4 (24)	0.05 (1.2)	522	327	N/A	N/A
Top splitting crack	7.9 (35)	0.16 (4.1)	1311	1510	N/A	N/A
Side splitting crack	N/A	N/A	N/A	N/A	N/A	N/A
Long. rebar yield	11.7 (52)	0.33 (8.5)	2212	2418	N/A	N/A
Ultimate	12.9 (58)	0.43 (11)	2600	7249	N/A	N/A

Notes:
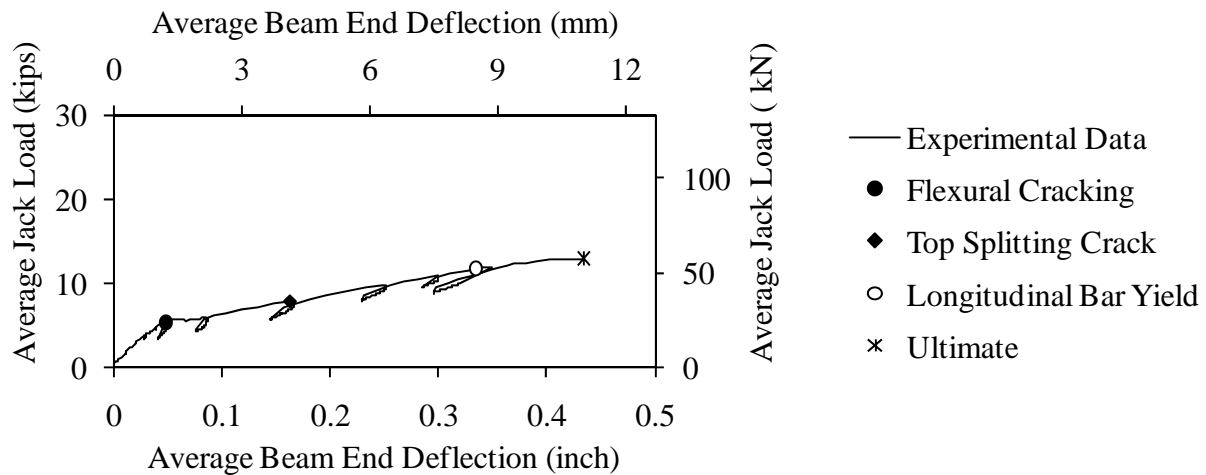
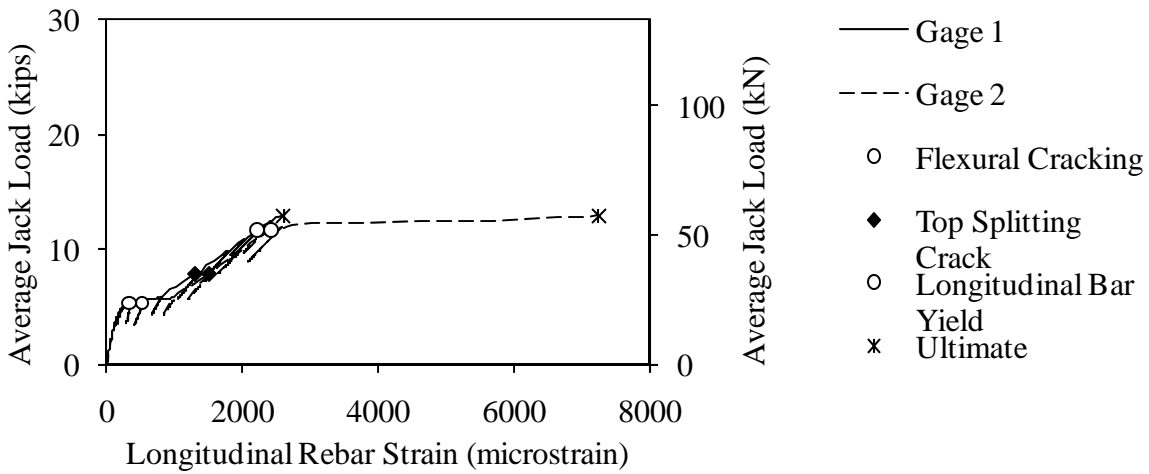**Figure 365. Graph. Load versus deflection for Beam D4-LN.**

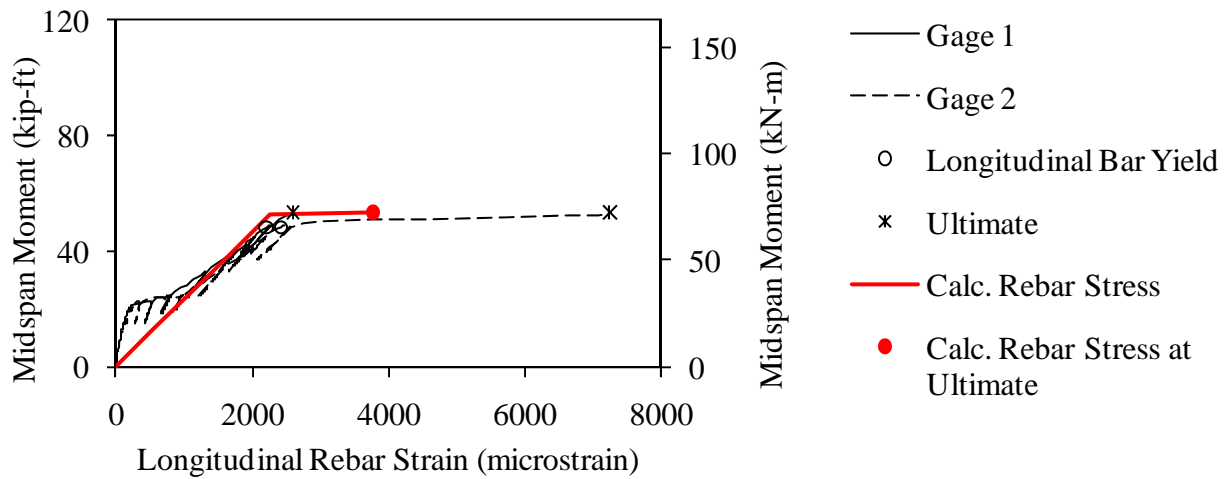**Figure 366. Graph. Load versus longitudinal rebar strain for Beam D4-LN.**

Figure 367. Graph. Measured and predicted midspan moment versus longitudinal rebar strain for Beam D4-LN.
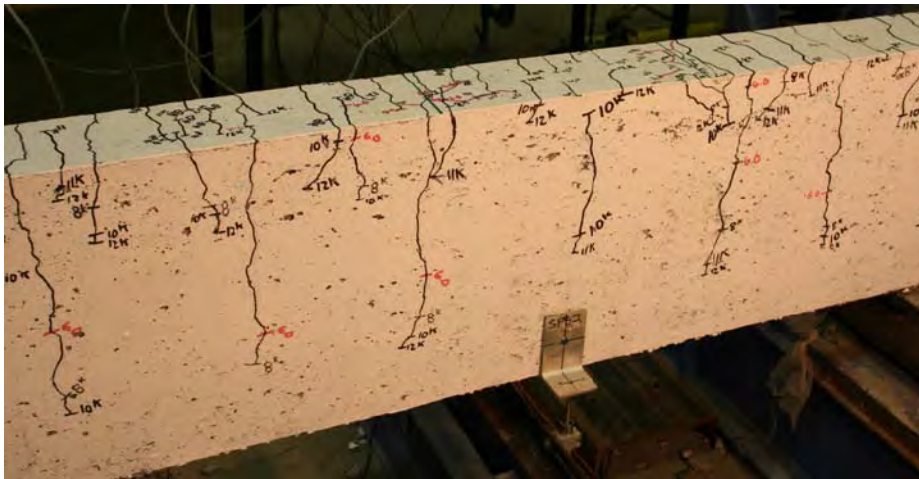
Figure 368. Photo. Side face of Beam D4-LN before failure.

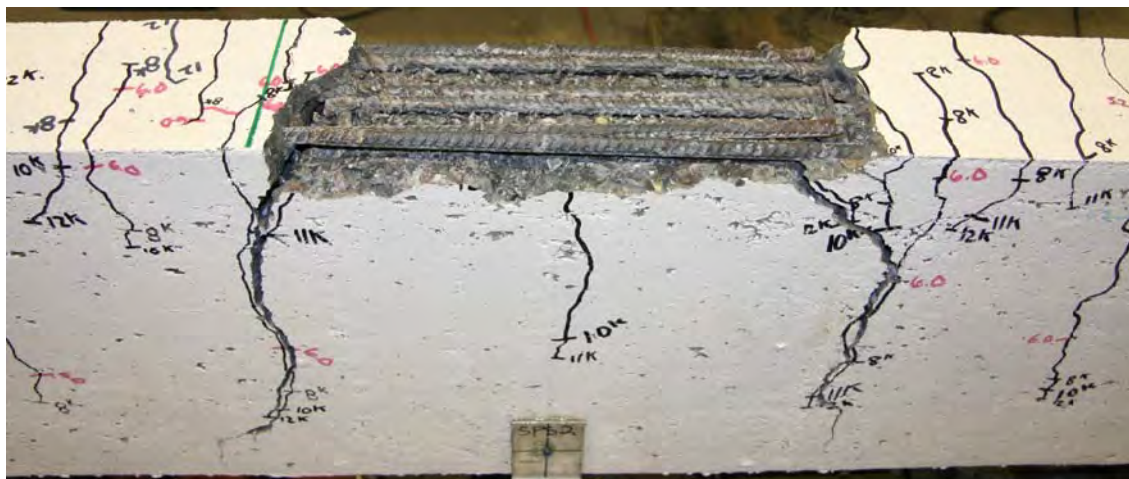**Figure 369. Photo. Top face of Beam D4-LN before failure.**

Figure 370. Photo. Beam D4-LN after failure.

Splice Beam D4-SN

Table 116. Test parameters for Splice Beam D4-SN.

Concrete Mix	Spliced Bar Size	Lap Length, inch (mm)	#3 (10M) Bar Transverse Reinforcement	Nominal Beam Cross-Section Dimensions (Width by Height), inch (mm)
Stalite (Deck)	#4 (13M)	12 (300)	None	18 by 18 (460 by 460)

Table 117. Test data for Splice Beam D4-SN.

| Event	Average Jack Load, kips (kN)	Average Beam End Deflection, inch (mm)	Longitudinal Rebar Strain, microstrain		Transverse Rebar Strain, microstrain	
			Gage 1	Gage 2	Gage 1	Gage 2
Flexural cracking	5.7 (25)	0.06 (1.5)	271	318	N/A	N/A
Top splitting crack	7.1 (32)	0.14 (3.5)	842	898	N/A	N/A
Side splitting crack	11.2 (50)	0.32 (8.1)	1734	1973	N/A	N/A
Long. rebar yield	N/A	N/A	N/A	N/A	N/A	N/A
Ultimate	13 (58)	0.42 (10.6)	2217	2489	N/A	N/A

Notes:
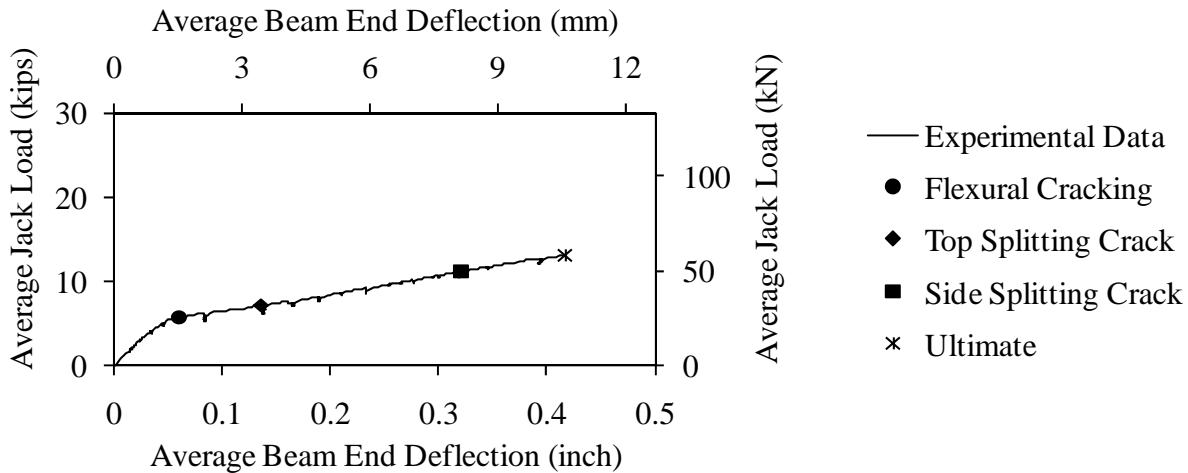
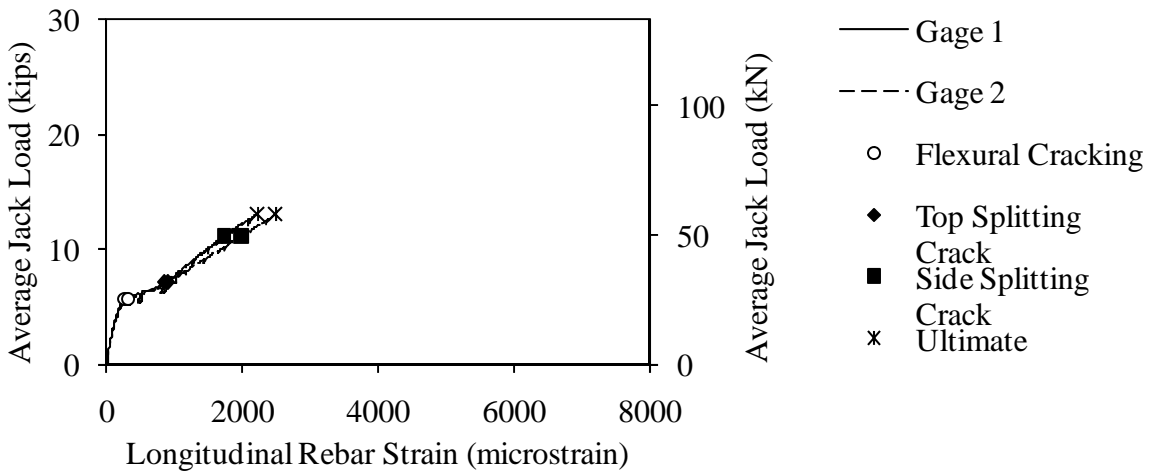**Figure 371. Graph. Load versus deflection for Beam D4-SN.**

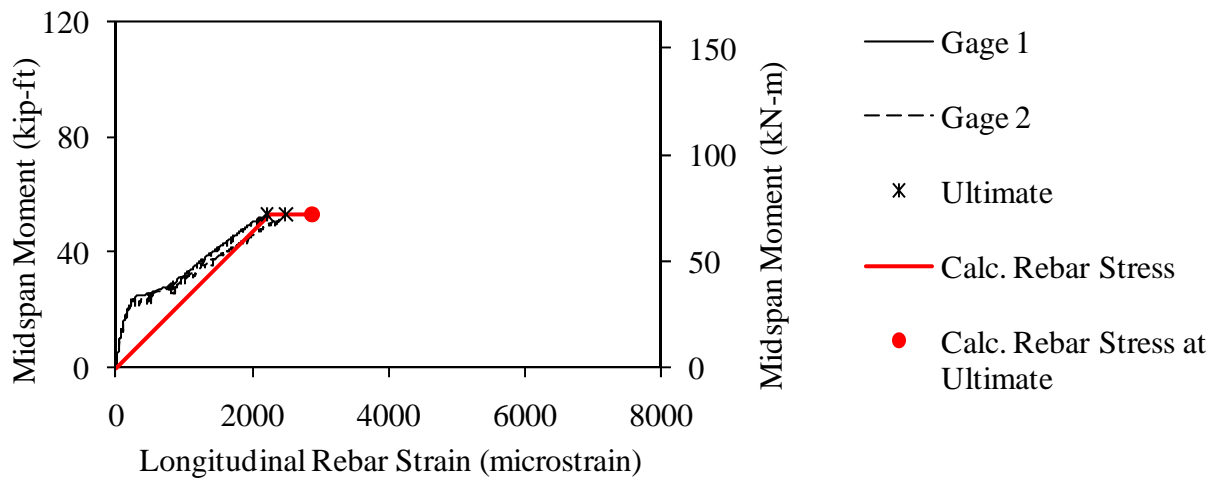**Figure 372. Graph. Load versus longitudinal rebar strain for Beam D4-SN.**

Figure 373. Graph. Measured and predicted midspan moment versus longitudinal rebar strain for Beam D4-SN.
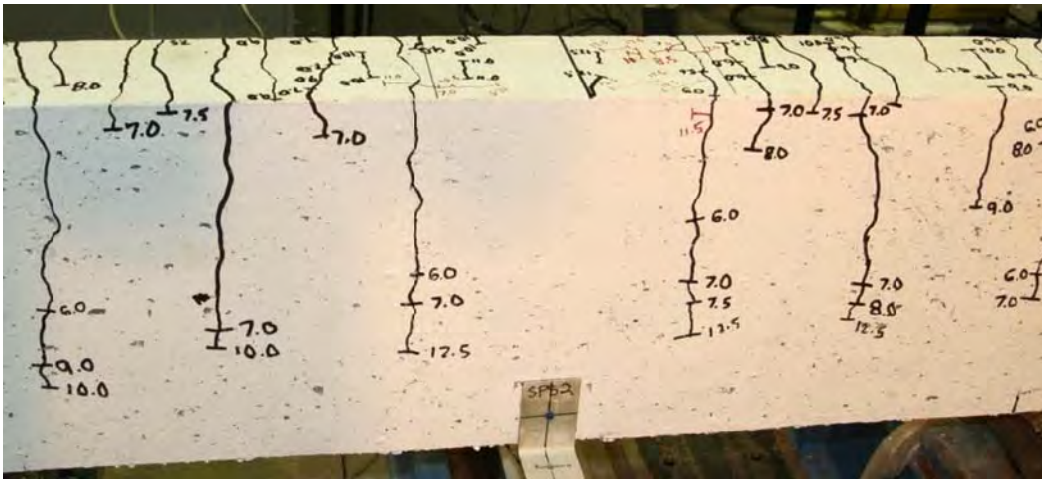
Figure 374. Photo. Side face of Beam D4-SN before failure.

Figure 375. Photo. Top face of Beam D4-SN before failure.

Figure 376. Photo. Beam D4-SN after failure.

Splice Beam D6-LN

<p style="text-align:center">Table 118. Test parameters for Splice Beam D6-LN.</p>

Concrete Mix	Spliced Bar Size	Lap Length, inch (mm)	#3 (10M) Bar Transverse Reinforcement	Nominal Beam Cross-Section Dimensions (Width by Height), inch (mm)
Stalite (Deck)	#6 (19M)	24 (610)	None	18 by 18 (460 by 460)

<p style="text-align:center">Table 119. Test data for Splice Beam D6-LN.</p>

| Event	Average Jack Load, kips (kN)	Average Beam End Deflection, inch (mm)	Longitudinal Rebar Strain, microstrain		Transverse Rebar Strain, microstrain	
			Gage 1	Gage 2	Gage 1	Gage 2
Flexural cracking	9 (40)	0.05 (1.3)	380	0	N/A	N/A
Top splitting crack	13.5 (60)	0.13 (3.4)	947	0	N/A	N/A
Side splitting crack	22.5 (100)	0.32 (8.2)	1837	0	N/A	N/A
Long. rebar yield	N/A	N/A	N/A	N/A	N/A	N/A
Ultimate	24 (107)	0.36 (9.1)	1995	0	N/A	N/A

Notes:
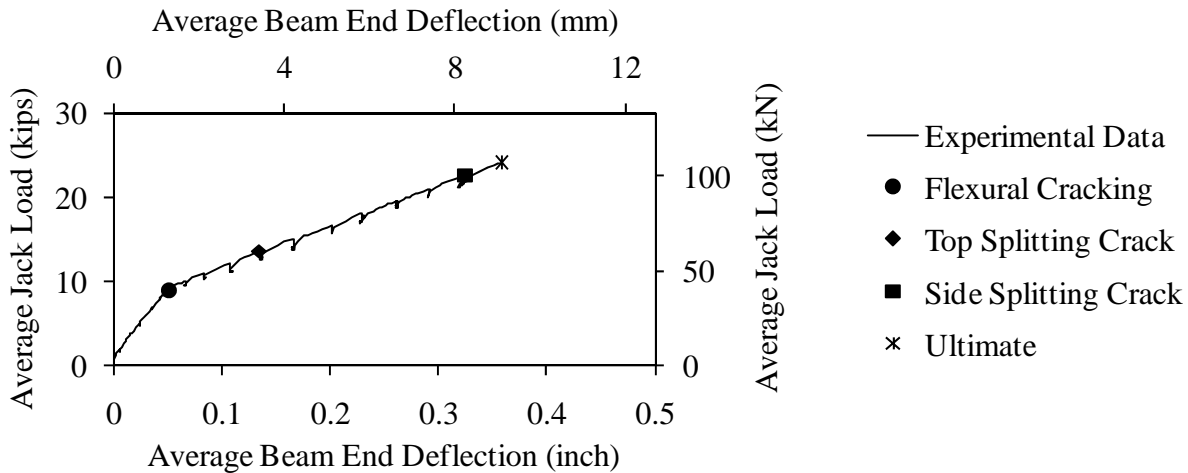
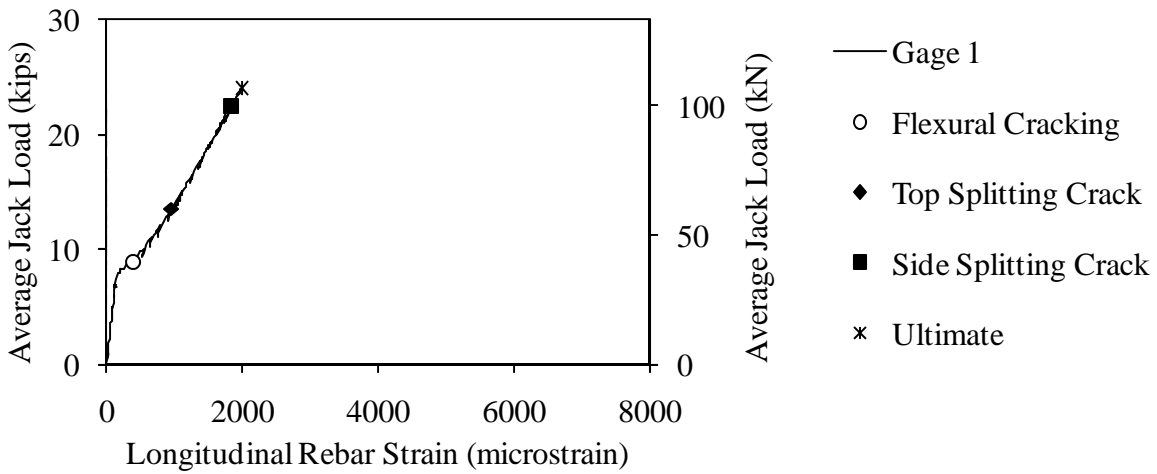**Figure 377. Graph. Load versus deflection for Beam D6-LN.**

Figure 378. Graph. Load versus longitudinal rebar strain for Beam D6-LN.
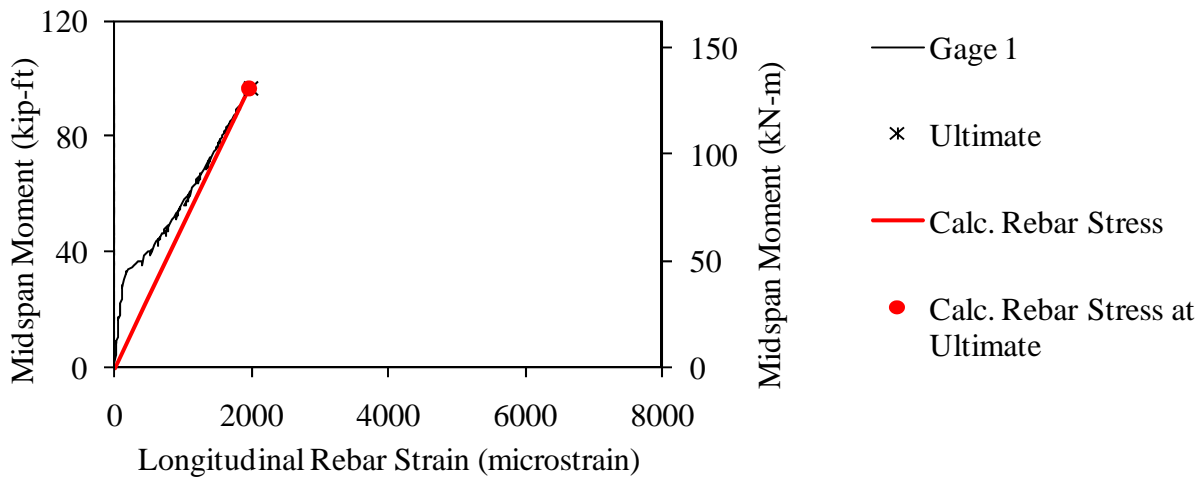

Figure 379. Graph. Measured and predicted midspan moment versus longitudinal rebar strain for Beam D6-LN.

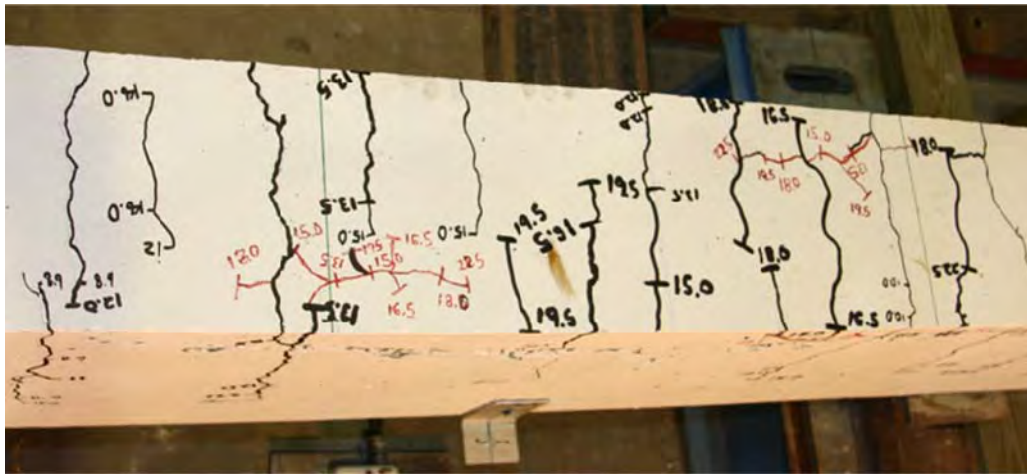**Figure 380. Photo. Side face of Beam D6-LN before failure.**

Figure 381. Photo. Top face of Beam D6-LN before failure.

Figure 382. Photo. Beam D6-LN after failure.

Splice Beam D6-SN

Table 120. Test parameters for Splice Beam D6-SN.

Concrete Mix	Spliced Bar Size	Lap Length, inch (mm)	#3 (10M) Bar Transverse Reinforcement	Nominal Beam Cross-Section Dimensions (Width by Height), inch (mm)
Stalite (Deck)	#6 (19M)	16 (410)	None	18 by 18 (460 by 460)

Table 121. Test data for Splice Beam D6-SN.

| Event	Average Jack Load, kips (kN)	Average Beam End Deflection, inch (mm)	Longitudinal Rebar Strain, microstrain		Transverse Rebar Strain, microstrain	
			Gage 1	Gage 2	Gage 1	Gage 2
Flexural cracking	9.6 (43)	0.06 (1.5)	235	415	N/A	N/A
Top splitting crack	12.1 (54)	0.11 (2.9)	807	800	N/A	N/A
Side splitting crack	N/A	N/A	N/A	N/A	N/A	N/A
Long. rebar yield	N/A	N/A	N/A	N/A	N/A	N/A
Ultimate	19.8 (88)	0.28 (7.1)	1570	1589	N/A	N/A

Notes:
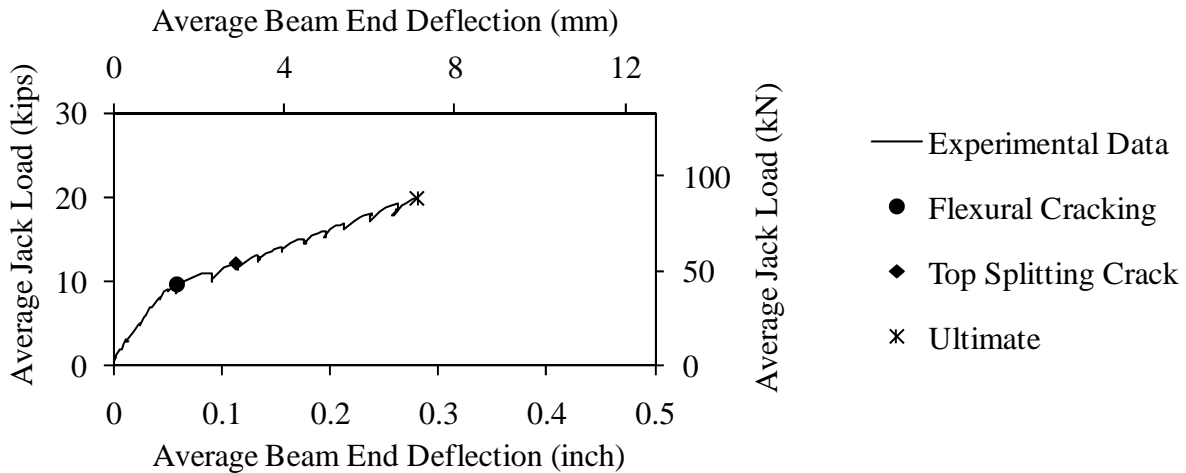
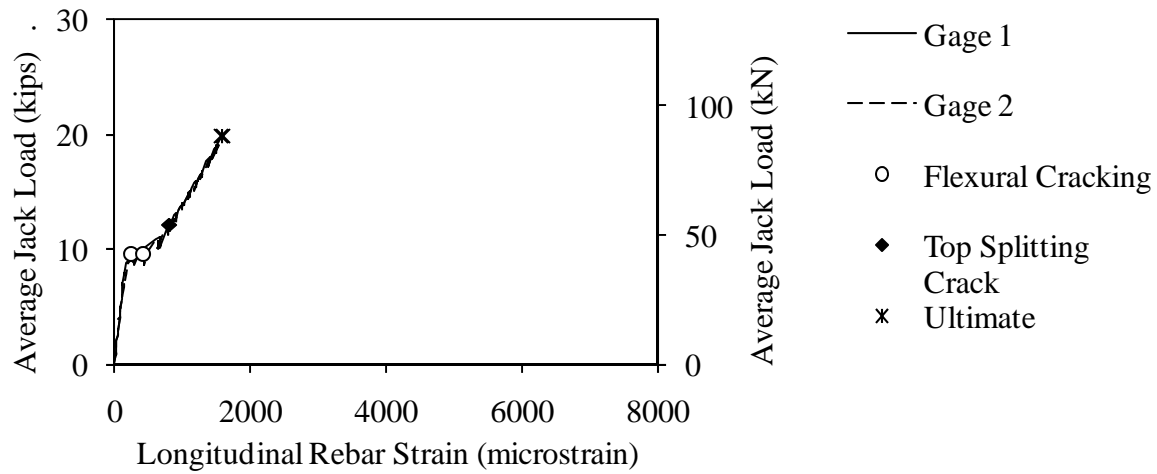**Figure 383. Graph. Load versus deflection for Beam D6-SN.**

Figure 384. Graph. Load versus longitudinal rebar strain for Beam D6-SN.
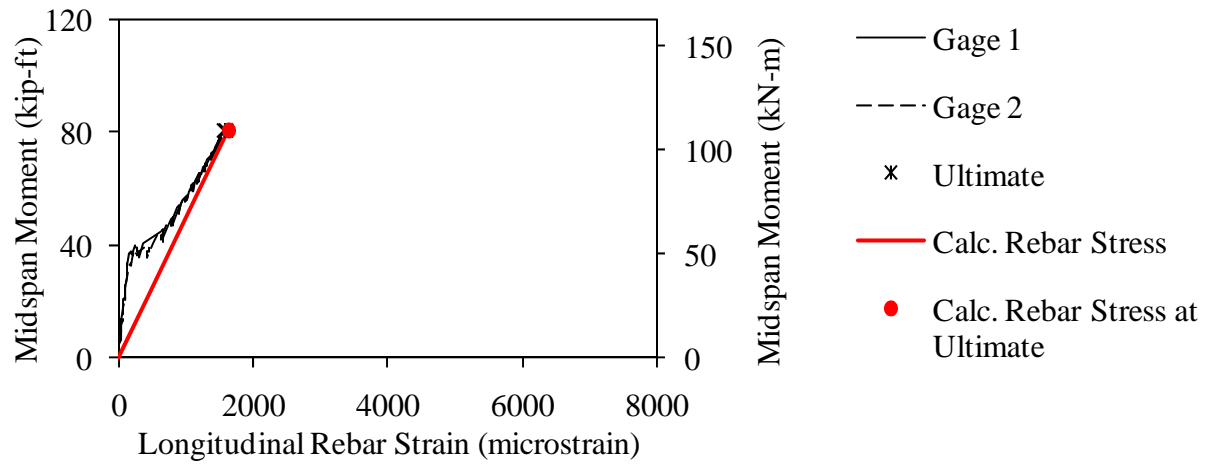

Figure 385. Graph. Measured and predicted midspan moment versus longitudinal rebar strain for Beam D6-SN.
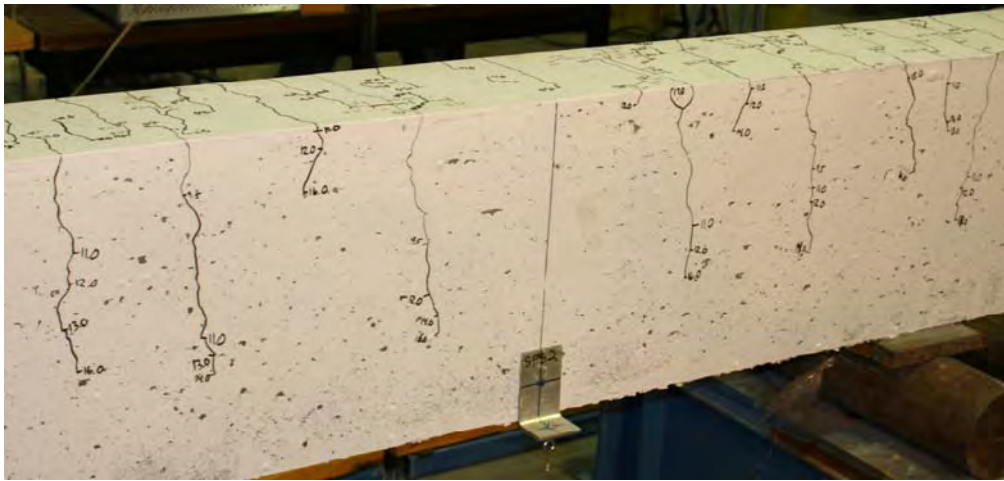
Figure 386. Photo. Side face of Beam D6-SN before failure.
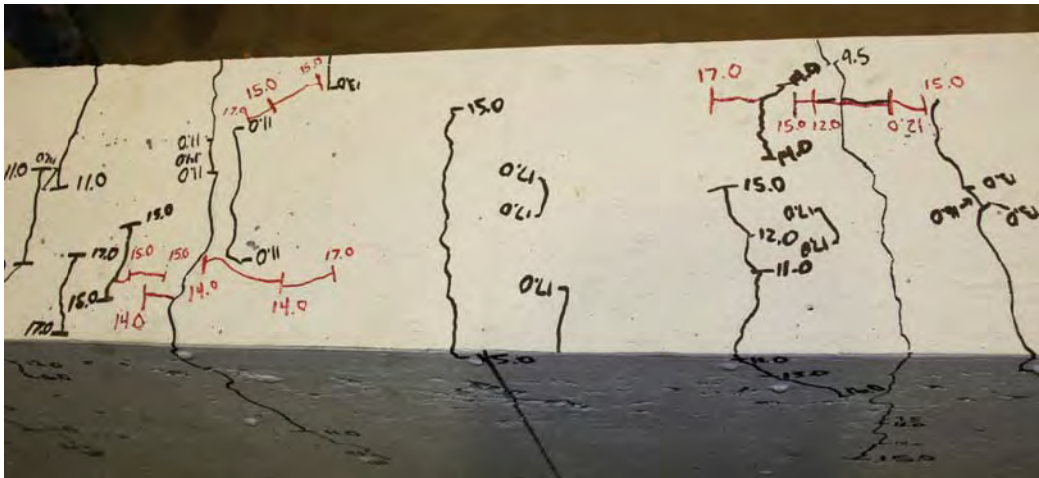

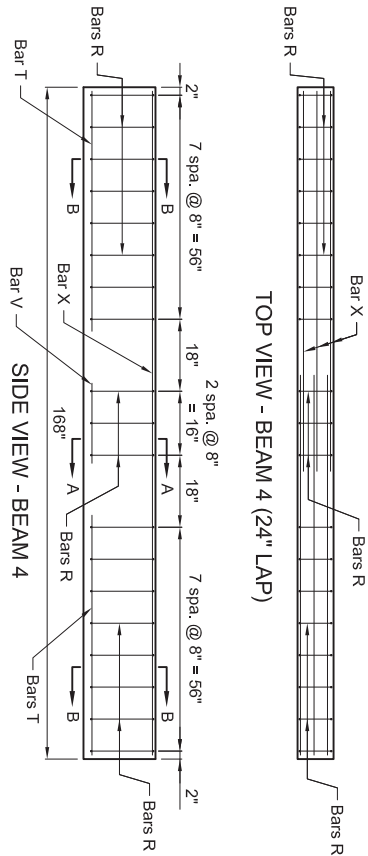**Figure 387. Photo. Top face of Beam D6-SN before failure.**
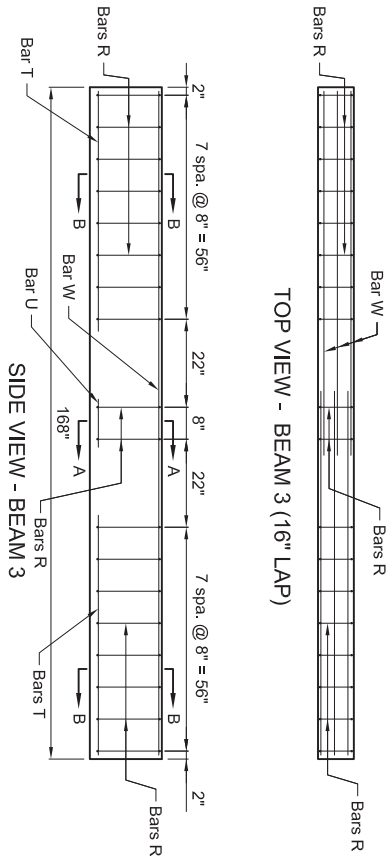

Figure 388. Photo. Beam D6-SN after failure.

APPENDIX E

This appendix contains the drawings of the TFHRC splice beams that were given to the beam fabricator.
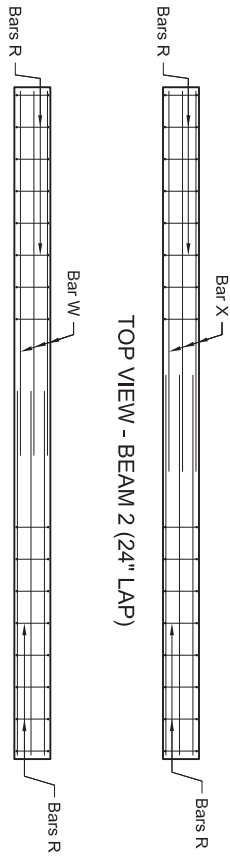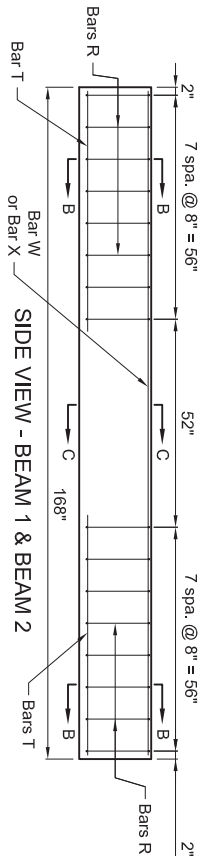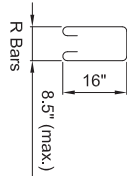
TOP VIEW - BEAM 4 (24" LAP)

Bars R — Bar X — Bars R
2" / 7 spa. @ 8" = 56" / 18" / 2 spa. @ 8" = 16" / 18" / 7 spa. @ 8" = 56" / 2"

SIDE VIEW - BEAM 4

Bar T — Bar X — Bar V — A — A — Bars R
168"
Bars R — Bars T — Bars R

TOP VIEW - BEAM 3 (16" LAP)

Bars R — Bar U — Bar W
2" / 7 spa. @ 8" = 56" / 22" / 8" / 22" / 7 spa. @ 8" = 56" / 2"

SIDE VIEW - BEAM 3

Bar T — Bar W — A — A — Bars R
168"
Bars R — Bars T — Bars R

TOP VIEW - BEAM 2 (24" LAP)

Bars R — Bar W

TOP VIEW - BEAM 1 (16" LAP)

Bars R — Bar X

SIDE VIEW - BEAM 1 & BEAM 2

Bar T — Bar W or Bar X — B — C — C — B
2" / 7 spa. @ 8" = 56" / 52" / 168" / 7 spa. @ 8" = 56" / 2"
Bars R — Bars T

Reinforcing Steel Schedule

T, U, V, W, and X Bars
Dim "A"
R Bars
16"
8.5" (max.)

Mark	Size	Dim "A"	No.	No. for (3) Sets	Extra
R Bars	#3	-	69	207	20
T Bars	#3	60"	16	48	4
U Bars	#3	12"	2	6	2
V Bars	#3	20"	2	6	2
W Bars	#6	91"	6	18	2
X Bars	#6	96"	6	18	2

Notes:
1) Dimensions in bending diagram are out-to-out of bars.
2) Reinforcing bars shown on the above schedule are for four beams shown on this sheet only.

Notes:

1) Concrete cover shown in section is crucial on top and sides. Cover dimension is from outer edge of bar to surface of concrete. Spacers to maintain cover shall not be used in the middle of the beam (between the regions with Bar R stirrups).

2) Orientation of longitudinal rib on reinforcing steel should be 45° from vertical. All bars should be oriented in the same manner.

3) Exact length of splice is crucial. Tolerance on splice length is ± 1/8".

4) Center of all three splices in beam should be aligned with each other and with the longitudinal centerline of beam.

5) Some of the mild steel reinforcement will have attached instrumentation. The location of the instrumented reinforcement is crucial. FHWA will provide details on the location of this reinforcement later. FHWA will also provide guidance on the correct location and placement of the the instrumented reinforcement during girder fabrication.

6) This drawing provides the details for one set of four beams. A total of twelve beams using these details are to be constructed. A different concrete mix will be used for each set of four beams.

7) Specimens are shown in test orientation. The spliced reinforcement shall be "bottom cast" (placed near the bottom of the form).

Sections Through Beams

SECTION A-A
Bar W or Bar X — Bar R
9" / 18"

SECTION B-B
Bar W or Bar X — Bar R

SECTION C-C
Bar W or Bar X
0.75" Cover / 0.75" Cover

| FHWA LWHPC | #6 Bar Splice Beams (Girder Mix) | Drawn by: GGG 11/9/2007 | Sheet 1 of 4 |

TOP VIEW - BEAM 4 (32" LAP)

TOP VIEW - BEAM 3 (24" LAP)

TOP VIEW - BEAM 2 (32" LAP)

TOP VIEW - BEAM 1 (24" LAP)

SIDE VIEW - BEAM 4

SIDE VIEW - BEAM 3

SIDE VIEW - BEAM 1 & BEAM 2
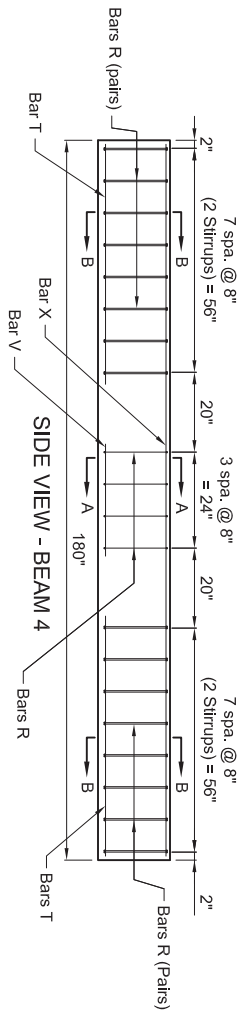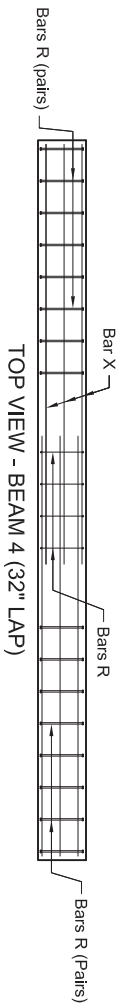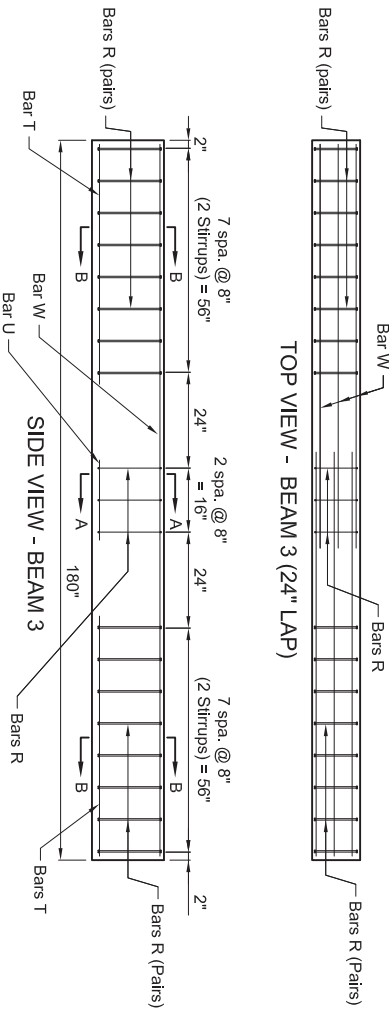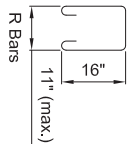
Bars R (pairs)
Bar T
Bar W or Bar X
Bar V
Bar X
Bar U
Bars R
Bars T
Bars R (Pairs)

2"
7 spa. @ 8" (2 Stirrups) = 56"
20"
3 spa. @ 8" = 24"
20"
2 spa. @ 8" = 16"
24"
24"
64"
180"

Notes:

1) Concrete cover shown in section is crutial on top and sides. Cover dimension is from outer edge of bar to surface of concrete. Spacers to maintain cover shall not be used in the middle of the beam (between the regions with Bar R stirrups).

2) Orientation of longitudinal rib on reinforcing steel should be 45° from vertical. All bars should be oriented in the same manner.

3) Exact lenth of splice is crucial. Tolerance on splice length is ± 1/8".

4) Center of all three splices in beam should be aligned with each other and with the longitudinal centerline of beam.

5) Some of the mild steel reinforcement will have attached instrumentation. The location of the instrumented reinforcement is crucial. FHWA will provide details on the location of this reinforcement later. FHWA will also provide guidance on the correct location and placement of the the instrumented reinforcement during girder fabrication.

6) This drawing provides the details for one set of four beams. A total of twelve beams using these details are to be constructed. A different concrete mix will be used for each set of four beams.

7) Specimens are shown in test orientation. The spliced reinforcement shall be "bottom cast" (placed near the bottom of the form.

Reinforcing Steel Schedule

T, U, V, W, and X Bars

R Bars
11" (max.)
16"
Dim "A"

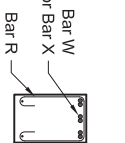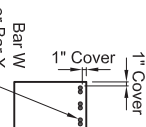| Mark	Size	Dim "A"	No.	No. for (3) Sets	Extra
R Bars	#3	-	128	384	30
T Bars	#3	60"	16	48	4
U Bars	#3	20"	2	6	2
V Bars	#3	28"	2	6	2
W Bars	#8	101"	6	18	2
X Bars	#8	105"	6	18	2

Notes:

1) Dimensions in bending diagram are out-to-out of bars.

2) Reinforcing bars shown on the above schedule are for four beams shown on this sheet only.

Sections Through Beams

SECTION A-A
Bar W or Bar X
Bar R
12"
18"

SECTION B-B
Bar W or Bar X
Bar R

SECTION C-C
Bar W or Bar X
1" Cover
1" Cover

FHWA LWHPC

#8 Bar Splice Beams (Girder Mix)

Drawn by: GGG 11/9/2007

Sheet 2 of 4

SIDE VIEW - BEAM 1 & BEAM 2

Bar T · Bars R (pairs)
3"
9 spa. @ 6" (2 Stirrups) = 54"
B
Bar W or Bar X
192"
C — 192" — C
78"
B
9 spa. @ 6" (2 Stirrups) = 54"
3"
Bars T · Bars R (Pairs)

TOP VIEW - BEAM 1 (32" LAP)

Bars R (pairs)
Bar W
Bars R (Pairs)

TOP VIEW - BEAM 2 (48" LAP)

Bars R (pairs)
Bar X
Bars R (Pairs)

SIDE VIEW - BEAM 3

Bars R (pairs) · Bar T
3"
9 spa. @ 6" (2 Stirrups) = 54"
B
Bar W · Bar V
27"
A — 192" — A
3 spa. @ 8" = 24"
27"
B
9 spa. @ 6" (2 Stirrups) = 54"
3"
Bars S · Bars T · Bars R (Pairs)

TOP VIEW - BEAM 3 (32" LAP)

Bars R (pairs)
Bar W
Bar U
Bars S
Bars R (Pairs)

SIDE VIEW - BEAM 4

Bars R (pairs) · Bar T
3"
9 spa. @ 6" (2 Stirrups) = 54"
19"
A — 192" — A
5 spa. @ 8" = 40"
19"
B
9 spa. @ 6" (2 Stirrups) = 54"
3"
Bar X · Bar W · Bars S · Bars T · Bars R (Pairs)

TOP VIEW - BEAM 4 (48" LAP)

Bars R (pairs)
Bar X
Bars S
Bars R (Pairs)

Notes:

1) Concrete cover shown in section is crutial on top and sides. Cover dimension is from outer edge of bar to surface of concrete. Spacers to maintain cover shall not be used in the middle of the beam (between the regions with Bar R stirrups).

2) Orientation of longitudinal rib on reinforcing steel should be 45° from vertical. All bars should be oriented in the same manner.

3) Exact lenth of splice is crutial. Tolerance on splice length is ± 1/8".

4) Center of all three splices in beam should be aligned with each other and with the longitudinal centerline of beam.

5) Some of the mild steel reinforcement will have attached instrumentation. The location of the instrumented reinforcement is crucial. FHWA will provide details on the location of this reinforcement later. FHWA will also provide guidance on the correct location and placement of the the instrumented reinforcement during girder fabrication.

6) This drawing provides the details for one set of four beams. A total of twelve beams using these details are to be constructed. A different concrete mix will be used for each set of four beams.

7) Specimens are shown in test orientation. The spliced reinforcement shall be "bottom cast" (placed near the bottom of the form).
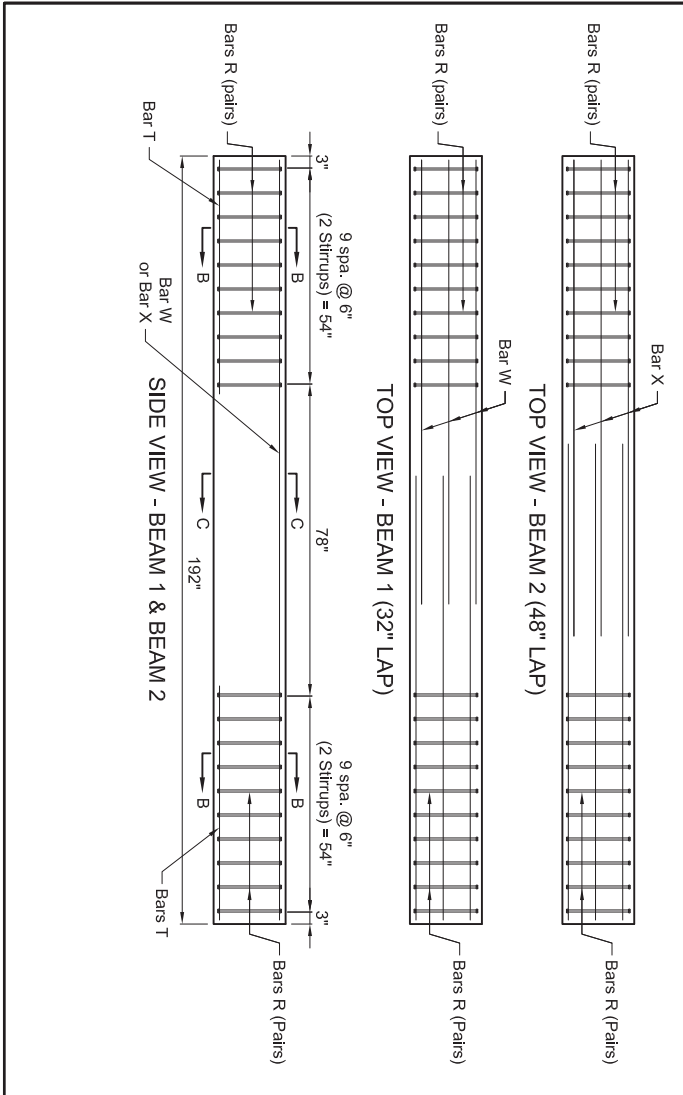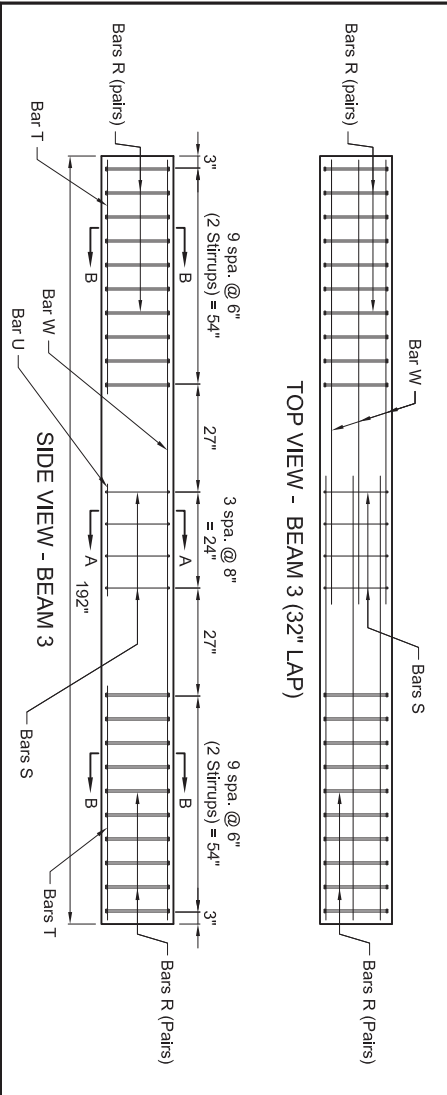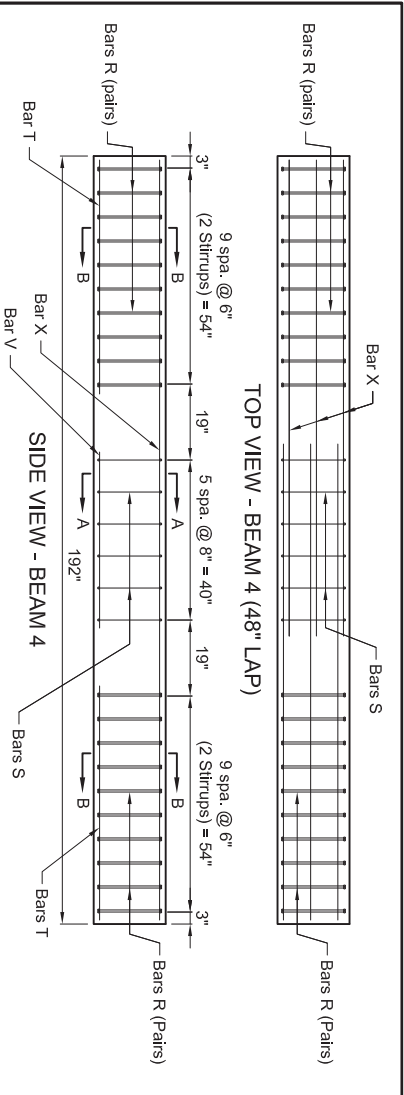
Reinforcing Steel Schedule

R Bars — 16" (max.)
S Bars — 16" (max.)

T, U, V, W, and X Bars — Dim "A"

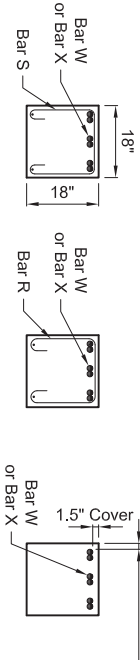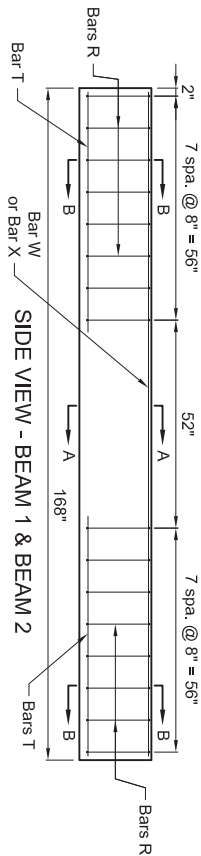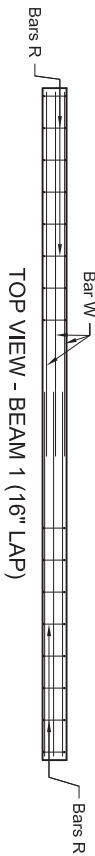| Mark	Size	Dim "A"	No.	No. for (3) Sets	Extra
R Bars	#4	-	160	480	20
S Bars	#3	-	10	30	10
T Bars	#3	60"	16	48	4
U Bars	#3	28"	2	6	2
V Bars	#3	44"	2	6	2
W Bars	#11	111"	6	18	2
X Bars	#11	119"	6	18	2

Notes:

1) Dimensions in bending diagram are out-to-out of bars.

2) Reinforcing bars shown on the above schedule are for four beams shown on this sheet only.
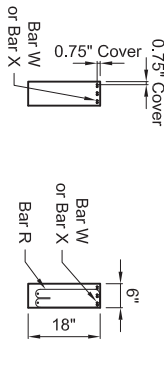
SECTION A-A

Bar W or Bar X · Bar S
18" × 18"

SECTION B-B

Bar W or Bar X · Bar R

SECTION C-C

Bar W or Bar X
1.5" Cover
1.5" Cover

Sections Through Beams

FHWA LWHPC

#11 Bar Splice Beams (Girder Mix)

Drawn by: GGG 11/9/2007

Sheet 3 of 4

Mild-#11, 11/30/2007 7:36:50 AM

E - 4

#6 Bar Beams

SECTION A-A

SECTION B-B

SIDE VIEW - BEAM 1 & BEAM 2

TOP VIEW - BEAM 1 (12" LAP)

TOP VIEW - BEAM 1 (16" LAP)

0.75" Cover

2"

7 spa. @ 8" = 56"

52"

168"

7 spa. @ 8" = 56"

6"

18"

Bars R, Bar T, Bar W or Bar X, Bars T

Reinforcing Steel Schedule

Mark	Size	Dim "A"	No.	No. for (3) Sets	Extra
R Bars	#3	-	32	96	20
T Bars	#3	60"	8	24	4
W Bars	#4	89"	3	9	2
X Bars		91"	3	9	2

T, U, V, W, and X Bars

16"

4.5" (max.)

Dim "A"

R Bars

Notes:
1) Dimensions in bending diagram are out-to-out of bars.
2) Reinforcing bars shown on the above schedule are for four beams shown on this sheet only.

#4 Bar Beams

SECTION A-A

SECTION B-B

SIDE VIEW - BEAM 1 & BEAM 2

TOP VIEW - BEAM 1 (12" LAP)

TOP VIEW - BEAM 2 (16" LAP)

0.75" Cover   0.75" Cover

2"

7 spa. @ 8" = 56"

52"

168"

7 spa. @ 8" = 56"

2"

9"

18"

Bars R, Bar T, Bar W or Bar X, Bars T

Reinforcing Steel Schedule

Mark	Size	Dim "A"	No.	No. for (3) Sets	Extra
R Bars	#3	-	32	96	20
T Bars	#3	60"	8	24	4
W Bars	#6	89"	3	9	2
X Bars	#6	91"	3	9	2

T, U, V, W, and X Bars

16"

4.5" (max.)

Dim "A"

R Bars

Notes:
1) Dimensions in bending diagram are out-to-out of bars.
2) Reinforcing bars shown on the above schedule are for four beams shown on this sheet only.

Notes:

1) Concrete cover shown in section is crucial on top and sides. Cover dimension is from outer edge of bar to surface of concrete. Spacers to maintain cover shall not be used in the middle of the beam (between the regions with Bar R stirrups).

2) Orientation of longitudinal rib on reinforcing steel should be 45° from vertical. All bars should be oriented in the same manner.

3) Exact lenth of splice is crucial. Tolerance on splice length is ± 1/8".

4) Center of all three splices in beam should be aligned with each other and with the longitudinal centerline of beam.

5) Some of the mild steel reinforcement will have attached instrumentation. The location of the instrumented reinforcement is crucial. FHWA will provide details on the location of this reinforcement later. FHWA will also provide guidance on the correct location and placement of the the instrumented reinforcement during girder fabrication.

6) This drawing provides the details for two sets of two beams. A total of six beams using these details of each set are to be constructed (for a total of twelve). Different concrete mixes will be used for each set of four beams.

7) Specimens are shown in test orientation. The spliced reinforcement shall be "bottom cast" (placed near the bottom of the form.
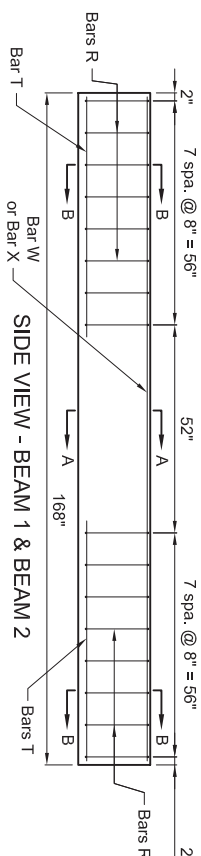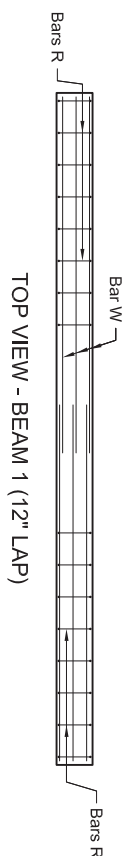

FHWA LWHPC
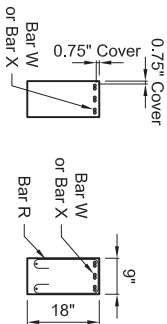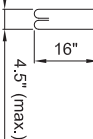
#4 & #6 Bar Splice Beams (Deck Mix)

Drawn by: GGG 11/9/2007

Sheet 4 of 4